

***o*-Phenylene Bridged Diamidophosphine Complexes of Groups 4 and 5
Metals for Dinitrogen Activation**

by

Fiona Millicent Hess

B. Sc., University of Cape Town, 1995

B. Sc.(HONS), University of Cape Town, 1996

M. Sc., University of Cape Town, 1999

A thesis submitted in partial fulfillment of

the requirements for the degree of

DOCTOR OF PHILOSOPHY

in

The Faculty of Graduate and Postdoctoral Studies

(CHEMISTRY)

THE UNIVERSITY OF BRITISH COLUMBIA

(Vancouver)

November 2014

© Fiona Millicent Hess, 2014

Abstract

A series of diamidophosphine donor sets (^{iprop}NPN, ^{tol}NPN and ^{ph}NPN) was prepared, whereby the arylamido groups have no *ortho* substituents. This allowed for the Buchwald-Hartwig arylation to be replaced by a directed *ortho* metalation (DOM) process, sourcing commercial diarylamines. Amido and chloro complexes of Zr, Ti, Hf and Ta with these new diamidophosphine donor sets were prepared.

Reduction of the zirconium dichlorides with KC₈ under N₂ gave the side-on dinitrogen complexes [^{iprop}NPNZr(THF)]₂(μ-η²:η²-N₂) and [^{tol}NPNZr(THF)]₂(μ-η²:η²-N₂) and of titanium dichloride gave the end-on complex [^{tol}NPNTi(THF)]₂(μ-η¹:η¹-N₂). Compared to previously reported sterically encumbered [^{mes}NPNZr(THF)]₂(μ-η²:η²-N₂), the zirconium complexes were more stable, with longer N-N bonds, less labile THF ligands and shorter Zr-O bond lengths. THF adduct displacement thus occurred less readily; for phosphine donors, displacement was at both zirconium centres i.e. [^{iprop}NPNZr(PPhMe₂)]₂(μ-η²:η²-N₂), compared to the ^{mes}NPN analogue with an open site at one of the zirconium centres i.e. [^{mes}NPNZr(PPhMe₂)](μ-η²:η²-N₂)[^{mes}NPNZr]. For titanium, four different pyridine adduct species were observed in solution, but only one species was isolated wherein each THF was displaced by two pyridine molecules i.e. [^{tol}NPNTi(Py)₂](μ-η¹:η¹-N₂). These new dinitrogen complexes were found to be unreactive with H₂; for zirconium, the lack of an open site at one of the metal centres may explain lack of reactivity, and for titanium, the end-on dinitrogen bonding mode is not amenable to hydrogenolysis.

The potassium salt of ^{tol}NPN with TaMe₃Cl₂ gave the trimethyl species ^{tol}NPNTaMe₃, but [^{tol}NPNTaMe₄][Li(THF)₄] was isolated from ^{tol}NPNTaCl₃ with MeLi. Tantalum hydrides from trimethyl species and H₂ were unstable and did not form dinitrogen complexes, but mass spectra of tantalum trichlorides with KHBET₃ and N₂ indicated dinitrogen hydrides [NPNTaH]₂(N₂) and further reaction with BEt₃. Reduction of tantalum trichlorides with KC₈ under N₂ gave mass spectra of dinitrogen complexes [NPNTaCl]₂(N₂), with no crystals isolated.

Preface

This dissertation is the original intellectual product of the author, F. Hess, except for the following contributions:

Chapter 2: The $[\text{ipropNPNLi}_2\cdot\text{diox}]_n$ **[2.6]** ligand was originally prepared by E. MacLachlan and the directed *ortho* metalation (DOM) process was first introduced by Y. Ohki. The x-ray crystal structure for $[\text{ipropNPNLi}_2\cdot\text{diox}]_n$ **[2.6]** was solved by E. MacLachlan and for $[\text{tolNPNLi}_2\cdot 0.5\text{TMEDA}\cdot\text{DME}]_2$ by Y. Ohki.

Chapter 3: The x-ray crystal structure for $\text{ipropNPNZr}(\text{NMe}_2)_2$ **[3.7]** was solved by E. MacLachlan and for $\text{tolNPNZrCl}_2(\text{HNMe}_2)$ **[3.4]** and $\text{tolNPNZr}(\text{NMe}_2)_2$ **[3.8]** by Y. Ohki.

Chapter 4: The x-ray crystal structure for iprop-PNPTaMe_3 was solved by D. Nied.

Chapter 5: The zirconium dinitrogen complex $[\text{tolNPNZr}(\text{THF})]_2(\mu\text{-}\eta^2\text{:}\eta^2\text{-N}_2)$ **[5.3]** was initially prepared by Y. Ohki.

The zirconium dinitrogen complex $[\text{ipropNPNZr}(\text{THF})]_2(\mu\text{-}\eta^2\text{:}\eta^2\text{-N}_2)$ **[5.1]** was presented orally at the *236th ACS National Meeting, Philadelphia, August 17-21 2008*, INOR-004. The zirconium **[5.1]** / **[5.3]** and titanium **[5.16]** / **[5.17]** / **[5.18]** dinitrogen complexes were presented orally at the *239th ACS National Meeting, San Francisco, March 21-25 2010*, INOR-1366 and the *93rd CSC Canadian Chemistry Conference and Exhibition, May 29 - June 25 2010*.

Table of Contents

| | |
|--|--------|
| Abstract | ii |
| Preface..... | iii |
| Table of Contents | iv |
| List of Tables..... | ix |
| List of Figures | xii |
| Glossary of Terms | xxiii |
| List of Compounds..... | xxx |
| Acknowledgements | xxxvi |
| Dedication | xxxvii |
| Chapter 1: Introduction | 1 |
| 1.1. Historical Context | 1 |
| 1.2. Dinitrogen Complexes | 7 |
| 1.2.1. Zirconium N ₂ Chemistry | 8 |
| 1.2.2. Hafnium N ₂ Chemistry | 11 |
| 1.2.3. Titanium N ₂ Chemistry | 12 |
| 1.2.4. Tantalum N ₂ Chemistry..... | 16 |
| 1.3. Project Objectives | 19 |
| Chapter 2: Ligand Synthesis | 24 |
| 2.1. Buchwald-Hartwig Arylamination..... | 30 |
| 2.1.1. Synthesis of ^{iprop} Ar ^{Br} ArNH [2.1]..... | 30 |
| 2.2. Directed <i>Ortho</i> -Metallation (DOM) Reaction..... | 34 |
| 2.2.1. Synthesis of [^{tol} Ar ^{Li} ArNLi·TMEDA] ₂ [2.2] and [^{ph} Ar ^{Li} ArNLi·1.5TMEDA] ₂ [2.3] .. | 34 |
| 2.3. Lithiated NPN Ligands | 39 |
| 2.3.1. Synthesis of [^{iprop} NPNLi ₂ ·diox] _n [2.6]..... | 39 |
| 2.3.2. Synthesis of [^{tol} NPNLi ₂ ·1.5TMEDA] ₂ [2.7] and [^{ph} NPNLi ₂ ·1.5TMEDA] ₂ [2.8].. | 45 |
| 2.4. Protonated NPN Ligands..... | 52 |

| | |
|--|-----|
| 2.5. Conclusions | 54 |
| Chapter 3: Group 4 Diamido-Phosphine Complexes | 55 |
| 3.1. Zirconium Diamido-Phosphine Complexes | 55 |
| 3.1.1. Salt Metathesis Route | 55 |
| 3.1.2. Protonolysis Route | 59 |
| Synthesis of ^{iprop} NPNZrCl ₂ (HNMe ₂) [3.3] and ^{tol} NPNZrCl ₂ (HNMe ₂) [3.4] | 60 |
| Synthesis of ^{iprop} NPNZrCl ₂ (THF) [3.5] and ^{tol} NPNZrCl ₂ (THF) [3.6] | 64 |
| Synthesis of ^{iprop} NPNZr(NMe ₂) ₂ [3.7] and ^{tol} NPNZr(NMe ₂) ₂ [3.8] | 68 |
| Synthesis of [^{iprop} NPNZrCl ₂] ₂ [3.9] and [^{tol} NPNZrCl ₂] ₂ [3.10] | 70 |
| 3.2. Titanium Diamido-Phosphine Complexes | 78 |
| Synthesis of ^{iprop} NPNTiCl ₂ (HNMe ₂) [3.11] and ^{tol} NPNTiCl ₂ (HNMe ₂) [3.12] | 79 |
| Synthesis of ^{iprop} NPNTiCl ₂ (THF) [3.13] and ^{tol} NPNTiCl ₂ (THF) [3.14] | 81 |
| Synthesis of ^{iprop} NPNTi(NMe ₂) ₂ [3.15] and ^{tol} NPNTi(NMe ₂) ₂ [3.16] | 85 |
| Synthesis of ^{iprop} NPNTiCl ₂ [3.17] and ^{tol} NPNTiCl ₂ [3.18] | 87 |
| 3.3. Hafnium Diamido-Phosphine Complexes | 89 |
| Synthesis of ^{iprop} NPNHf(NMe ₂) ₂ [3.19] | 89 |
| Synthesis of [^{iprop} NPNHfCl ₂] ₂ [3.20] | 91 |
| Synthesis of ^{iprop} NPNHfCl ₂ (THF) [3.21] | 94 |
| 3.4. Conclusions | 97 |
| Chapter 4: Tantalum Diamido-Phosphine Complexes | 98 |
| 4.1. Tantalum Chloride Complexes | 99 |
| 4.1.1. Synthesis of Tantalum Amido Complexes | 100 |
| 4.1.2. Synthesis of Tantalum Trichloro Complexes | 104 |
| 4.2. Tantalum Alkyl Complexes | 109 |
| 4.2.1. Salt Metathesis with TaCl ₂ Me ₃ | 110 |
| 4.2.2. Salt Metathesis with ^{tol} NPNTaCl ₃ [4.5] | 115 |
| Summary | 120 |

| | | |
|----------|--|-----|
| 4.3. | Tantalum Dinitrogen Complexes | 121 |
| 4.3.1. | Hydride Route | 121 |
| | Hydrogenation of $^{iprop}\text{NPNTaMe}_3$ [4.8]..... | 121 |
| | Reactions with KHBet_3 and N_2 | 121 |
| 4.3.2. | Reduction Route..... | 125 |
| | Reduction with 2 KC_8 and N_2 | 125 |
| | Reduction with 3.5 KC_8 and N_2 | 126 |
| 4.4. | Summary | 127 |
| | Chapter 5: Group 4 Dinitrogen Complexes..... | 129 |
| 5.1. | Zirconium Dinitrogen Complexes..... | 129 |
| 5.1.1. | Synthesis of $^{iprop}\text{NPNZr(THF)}_2(\mu\text{-}\eta^2\text{:}\eta^2\text{-N}_2)$ [5.1] and $^{tol}\text{NPNZr(THF)}_2(\mu\text{-}\eta^2\text{:}\eta^2\text{-N}_2)$ [5.3] | 129 |
| 5.2. | Reduction of $^{iprop}\text{NPNHfCl}_2(\text{THF})$ [3.21] with KC_8 and N_2 | 143 |
| 5.3. | Zirconium Dinitrogen Adducts | 144 |
| 5.3.1. | Nitrogen Atom Donors..... | 145 |
| 5.3.1.1. | Pyridine | 145 |
| 5.3.1.2. | 4,4'-Bipyridine | 149 |
| 5.3.2. | Phosphorus Atom Donors | 152 |
| 5.3.2.1. | PMe_3 and PPhMe_3 | 153 |
| 5.3.3. | Sulphur Atom Donors | 158 |
| 5.3.3.1. | THT | 158 |
| 5.4. | Titanium Dinitrogen Complexes..... | 163 |
| 5.4.1. | Synthesis of $^{iprop}\text{NPNTi(THF)}_2\text{N}_2$ [5.17] and $^{tol}\text{NPNTi(THF)}_2\text{N}_2$ [5.15]..... | 163 |
| 5.5. | Titanium Dinitrogen Adducts..... | 171 |
| 5.5.1. | Nitrogen Atom Donors..... | 171 |
| 5.5.1.1. | Pyridine | 171 |
| 5.6. | Titanium Hydrides for Alternative Dinitrogen Activation Route | 178 |

| | |
|---|-----|
| 5.7. Summary | 180 |
| Chapter 6: Group 4 Dinitrogen Complex Reactivity..... | 183 |
| 6.1. Reactivity of Zirconium Dinitrogen Complexes | 183 |
| 6.1.1. Reaction with Dihydrogen | 183 |
| 6.1.2. Reaction with Isocyanide | 187 |
| 6.1.3. Reaction with Phenylsilane | 194 |
| 6.1.4. Reaction with Ethylene | 196 |
| 6.1.5. Reaction with Carbon Monoxide | 198 |
| 6.1.6. Reaction with 4,4'-Dimethylbenzophenone..... | 201 |
| 6.1.7. Reaction with Carbon Dioxide..... | 203 |
| 6.1.8. Reaction with (Trimethylsilyl)diazomethane | 204 |
| 6.2. Titanium Dinitrogen Complex Reactivity | 205 |
| 6.2.1. Reaction with Dihydrogen | 205 |
| 6.2.2. Reaction with Carbon Monoxide | 206 |
| 6.2.3. Reaction with Ethylene | 206 |
| Chapter 7: Conclusions and Future Directions | 208 |
| 7.1. Summary | 208 |
| 7.2. Future Ligand Designs | 212 |
| 7.3. ^{naph} NPN and ^{2,6-<i>i</i>Pr₂} NPN Donor Sets | 214 |
| 7.3.1. Synthesis of ^{naph} Ar ^{Br} ArNH [7.1] and ^{2,6-<i>i</i>Pr₂} Ar ^{Br} ArNH [7.2]..... | 214 |
| 7.3.2. Synthesis of [^{2,6-<i>i</i>Pr₂} Ar ^{Li} ArNLi] _n [7.3] and [^{2,6-<i>i</i>Pr₂} Ar ^{Li} ArNLi·2THF] ₂ [7.3a] | 216 |
| 7.3.3. Synthesis of [^{naph} Ar ^{Li} ArNLi·2Et ₂ O] ₂ [7.4] and [^{naph} Ar ^{Li} ArNLi·2THF] ₂ [7.5]..... | 222 |
| 7.3.4. Synthesis of [^{naph} NPNLi ₂ ·diox] _n [7.6]..... | 223 |
| 7.3.5. Synthesis of [^{2,6-<i>i</i>Pr₂} NPNLi ₂ ·diox] _n [7.7] | 226 |
| 7.3.6. Synthesis of ^{naph} NPNH ₂ [7.8] and ^{2,6-<i>i</i>Pr₂} NPNH ₂ [7.9]..... | 229 |
| 7.4. Final Thoughts | 230 |
| Chapter 8: Experimental | 231 |

| | | |
|--------|---|-----|
| 8.1. | General Experimental..... | 231 |
| 8.2. | Starting Materials and Reagents..... | 232 |
| 8.3. | Synthetic Methods..... | 233 |
| | References | 368 |
| | Appendix A: Supporting NMR Spectroscopic Information..... | 388 |
| A. | DOSY $^{31}\text{P}\{^1\text{H}\}$ NMR Data for [$^{\text{iprop}}\text{NPNZrCl}_2$] $_2$ [3.9] at -40 °C..... | 388 |
| A.1. | DOSY $^{31}\text{P}\{^1\text{H}\}$ NMR Data for $^{\text{tol}}\text{NPNTaCl}_3$ [4.5] at -60 °C..... | 392 |
| A.2. | Variable Temperature $^{31}\text{P}\{^1\text{H}\}$ NMR Data for NPNTaCl $_3$ Complexes..... | 394 |
| A.2.1. | $^{\text{iprop}}\text{NPNTaCl}_3$ [4.4]..... | 395 |
| A.2.2. | $^{\text{tol}}\text{NPNTaCl}_3$ [4.5] | 395 |
| A.2.3. | $^{\text{Ph}}\text{NPNTaCl}_3$ [4.6] | 396 |
| | Appendix B: X-ray Crystal Structure Data | 397 |
| B.1. | X-ray Crystal Structure Analysis | 397 |
| B.2. | X-ray Crystal Structures..... | 398 |

List of Tables

| | |
|---|-----|
| Table 1 : Pre-column GC-MS data for Pd ₂ (dba) ₃ / <i>rac</i> -BINAP catalyst, 0.7 mol% Pd and Pd/ <i>rac</i> -BINAP (1:1.5)..... | 31 |
| Table 2 : Selected bond lengths (Å) and angles (°) for [^{tol} Ar ^{Li} ArNLi·TMEDA] ₂ [2.2]..... | 37 |
| Table 3 : Comparative bond lengths (Å) and angles (°) for the ^{iprop} NPNLi ₂ and ^{mes} NPNLi ₂ donor sets. ⁹⁷ | 40 |
| Table 4 : Comparative bond lengths (Å) and angles (°) for the ^{tol} NPNLi ₂ donor set. | 50 |
| Table 5 : Comparative bond lengths (Å) and angles (°) for ^{tol} NPNH ₂ [2.11] and ^{ph} NPNH ₂ [2.12] .. | 54 |
| Table 6 : Selected bond lengths (Å) and angles (°) for [^{tol} NPN] ₂ Zr [3.2] | 58 |
| Table 7 : Selected bond lengths (Å) and angles (°) for ^{tol} NPNZrCl ₂ (HNMe ₂) [3.4] ²⁶¹ and ^{mes} NPNZrCl ₂ (Py) ⁹⁷ | 64 |
| Table 8 : Selected bond lengths (Å) and angles (°) for ^{iprop} NPNZrCl ₂ (THF) [3.5] and ^{tol} NPNZrCl ₂ (THF) [3.6] ²⁶¹ | 67 |
| Table 9 : Selected bond lengths (Å) and angles (°) for ^{iprop} NPNZr(NMe ₂) ₂ [3.7] and ^{tol} NPNZr(NMe ₂) ₂ [3.8] ²⁶¹ | 70 |
| Table 10 : Selected bond lengths (Å) and angles (°) for [^{iprop} NPNZrCl ₂] ₂ [3.9] and ^{mes} NPNZrCl ₂ ⁹⁷ , 214 | 73 |
| Table 11 : Selected bond lengths (Å) and angles (°) for ^{iprop} NPNTi(NMe ₂) ₂ [3.15] | 86 |
| Table 12 : Selected bond lengths (Å) and angles (°) for ^{tol} NPNTiCl ₂ [3.18] and ^{Si} NPNTiCl ₂ ¹³⁷ .. | 88 |
| Table 13 : Selected bond lengths (Å) and angles (°) for ^{iprop} NPNHf(NMe ₂) ₂ [3.19] and ^{mes} NPNHf(NMe ₂) ₂ ⁹⁷ | 90 |
| Table 14 : Selected bond lengths (Å) and angles (°) for [^{iprop} NPNHfCl ₂] ₂ [3.20] and ^{mes} NPNHfCl ₂ ⁹⁷ | 92 |
| Table 15 : Selected bond lengths (Å) and angles (°) for ^{iprop} NPNHfCl ₂ (THF) [3.21] | 97 |
| Table 16 : Selected bond lengths (Å) and angles (°) for ^{tol} NPNTa(NMe ₂) ₃ [4.2] | 103 |
| Table 17: Comparative bond lengths (Å) and angles (°) for related ^{Si} NPN and P ₂ N ₂ tantalum complexes..... | 103 |
| Table 18 : Selected bond lengths (Å) and angles (°) for ^{Ph} NPNTaCl ₃ [4.6]..... | 105 |
| Table 19 : ³¹ P{ ¹ H} NMR data for NPNTaCl ₃ complexes at -70 °C..... | 106 |
| Table 20 : Selected bond lengths (Å) and angles (°) for ^{iprop-P} NPNTaMe ₃ | 114 |
| Table 21 : Selected bond lengths (Å) and angles (°) for [^{tol} NPNTaMe ₄][Li(THF) ₄] [4.14] with comparative Ta-Me bond lengths (Å) | 117 |
| Table 22: Inter-ligand bond angle analysis for seven coordinate geometries of [^{tol} NPNTaMe ₄][Li(THF) ₄] [4.14] | 118 |

| | |
|---|-----|
| Table 23 : Selected bond lengths (Å) and angles (°) for [^{iprop} NPNZr(THF)] ₂ (μ-η ² :η ² -N ₂) [5.1] compared to [^{mes} NPNZr(THF)] ₂ (μ-η ² :η ² -N ₂), [^{Si} NPNZr(THF)] ₂ (μ-η ² :η ² -N ₂) and [^{CY5} NPN ^{DMP} Zr(THF)] ₂ (μ-η ² :η ² -N ₂) | 137 |
| Table 24 : ¹ H and ¹³ C{ ¹ H} NMR Data for the Py ligand in [5.4] and [5.5] in C ₆ D ₆ | 147 |
| Table 25 : Selected bond lengths (Å) and angles (°) for [^{tol} NPNTi(THF)] ₂ (μ-η ¹ :η ¹ -N ₂) [5.15] compared to [PNPTiCl] ₂ (μ-η ¹ :η ¹ -N ₂) ¹⁸² and [P ₂ N ₂ Ti] ₂ (μ-η ¹ :η ¹ -N ₂) ¹³⁷ | 166 |
| Table 26 : Selected bond lengths (Å) and angles (°) for <i>trans</i> -[^{tol} NPNTi(Py) ₂] ₂ (μ-η ¹ :η ¹ -N ₂) [5.19] | 174 |
| Table 27 : ³¹ P{ ¹ H} and ¹⁵ N{ ¹ H} NMR data for reactions of xylolNC and ¹ BuNC with [5.1], [5.2] and [5.3] | 187 |
| Table 28 : Screening studies with zirconium dinitrogen complexes | 212 |
| Table 29 : Selected bond lengths (Å) and angles (°) for ^{2,6-iPr2} ArBrArNH [7.2] and ^{naph} Ar ^{Br} ArNH [7.1] | 216 |
| Table 30 : GC-MS data for lithiation of ^{2,6-iPr2} ArBrArNH [7.2]..... | 216 |
| Table 31 : Selected bond lengths (Å) and angles (°) for [^{2,6-iPr2} Ar ^{Li} ArNLi·2THF] ₂ [7.3a]..... | 221 |
| Table 32 : ³¹ P{ ¹ H} NMR spectroscopic data for the thermal / light decomposition study of ^{iprop} NPNTaMe ₃ [4.8]..... | 294 |
| Table 33: Fryzuk Research Group x-ray data processing code (mf#)..... | 398 |
| Table 34: Crystal Data and Structure Refinement for [^{tol} Ar ^{Li} ArNLi·TMEDA] ₂ [2.2], [^{tol} NPNLi ₂ ·1.5TMEDA] ₂ [2.7] and [^{tol} NPNLi ₂ ·0.5TMEDA·DME] ₂ | 399 |
| Table 35: Crystal Data and Structure Refinement for ^{tol} NPNH ₂ [2.11], ^{ph} NPNH ₂ [2.12] and [^{tol} NPN] ₂ Zr [3.2]..... | 400 |
| Table 36: Crystal Data and Structure Refinement for ^{tol} NPNZrCl ₂ (HNMe ₂) [3.4], ^{iprop} NPNZrCl ₂ (THF) [3.5] and ^{tol} NPNZrCl ₂ (THF) [3.6]..... | 401 |
| Table 37: Crystal Data and Structure Refinement for ^{iprop} NPNZr(NMe ₂) ₂ [3.7], ^{tol} NPNZr(NMe ₂) ₂ [3.8] and [^{iprop} NPNZrCl ₂] ₂ [3.9]..... | 402 |
| Table 38: Crystal Data and Structure Refinement for ^{iprop} NPNTi(NMe ₂) ₂ [3.15], ^{tol} NPNTiCl ₂ [3.18] and ^{iprop} NPNHf(NMe ₂) ₂ [3.19]..... | 403 |
| Table 39: Crystal Data and Structure Refinement for [^{iprop} NPNHfCl ₂] ₂ [3.20], ^{iprop} NPNHfCl ₂ (THF) [3.21] and ^{tol} NPNTa(NMe ₂) ₃ [4.2]..... | 404 |
| Table 40: Crystal Data and Structure Refinement for ^{Ph} NPNTaCl ₃ [4.6], ^{iprop-P} NPNTaMe ₃ and [^{tol} NPNTaMe ₄][Li(THF) ₄] [4.14] | 405 |
| Table 41: Crystal Data and Structure Refinement for [^{iprop} NPNZr(THF)] ₂ (μ-η ² :η ² -N ₂) [5.1], [^{tol} NPNTi(THF)] ₂ (μ-η ¹ :η ¹ -N ₂) [5.15] and <i>trans</i> -[^{tol} NPNTi(Py) ₂] ₂ (μ-η ¹ :η ¹ -N ₂) [5.19] | 406 |

| | |
|--|-----|
| Table 42: Crystal Data and Structure Refinement for $^{\text{naph}}\text{Ar}^{\text{Br}}\text{ArNH}$ [7.1], $^{2,6\text{-}i\text{Pr}^2}\text{ArBrArNH}$ [7.2] and $^{2,6\text{-}i\text{Pr}^2}\text{ArLiArNLi}\cdot 2\text{THF}$] ₂ [7.3a] | 407 |
|--|-----|

List of Figures

| | |
|--|----|
| Figure 1: Chatt cycle for mononuclear molybdenum complexes ($\text{Mo}^0\text{-Mo}^{\text{VI}}$) ²⁶ | 3 |
| Figure 2: Schrock's $[\text{HIPTN}_3\text{N}]\text{Mo}(\text{N}_2)$ catalyst, HIPT = hexa-iso-propyl-terphenyl ^{45, 51} | 4 |
| Figure 3: Idealised catalytic cycle for the combination of dinitrogen with substrates | 5 |
| Figure 4: Activated dinitrogen bonding modes for dinuclear complexes | 7 |
| Figure 5: Steric effect of ligand on N_2 bonding modes | 8 |
| Figure 6: Selected examples of zirconium dinitrogen complexes | 9 |
| Figure 7: Dinitrogen bonding modes for titanium dinitrogen complexes | 13 |
| Figure 8: End-on dinitrogen $[\text{PNPTiCl}]_2(\mu\text{-}\eta^1\text{:}\eta^1\text{-N}_2)^{182}$ and $[\text{P}_2\text{N}_2\text{Ti}]_2(\mu\text{-}\eta^1\text{:}\eta^1\text{-N}_2)^{137}$ complexes | 15 |
| Figure 9: Dinitrogen bonding modes for titanium dinitrogen complexes | 15 |
| Figure 10: Tantalum dinitrogen alkylidene complexes obtained by reduction of precursor chlorides ⁷²⁻⁷⁵ | 16 |
| Figure 11: Tantalum dinitrogen cyclopentadienyl complexes obtained by reduction of precursor chlorides ^{76-78, 183, 184} | 17 |
| Figure 12: Tantalum $^{\text{Si}}\text{NPN}$ dinitrogen complexes obtained by the hydride route | 18 |
| Figure 13: $^{\text{Si}}\text{NPN}$ vs. <i>o</i> -phenylene NPN ligand | 19 |
| Figure 14: Reactivity of $^{\text{mes}}\text{NPN}$ containing zirconium dinitrogen complexes ⁹⁷ | 20 |
| Figure 15: $^{\text{Si}}\text{NPN}$ vs. <i>o</i> -phenylene NPN ligand | 21 |
| Figure 16: Donor variation for the PNP, P_2N_2 and NPN donor sets | 24 |
| Figure 17: Variation in organic groups of phosphine donors | 25 |
| Figure 18: NPN donor sets with different backbones | 26 |
| Figure 19: Summary of NPN donor sets with reduced steric bulk at the amido units | 26 |
| Figure 20: Synthesis of $^{\text{mes}}\text{NPN}$ precursors | 27 |
| Figure 21: General DOM mechanism | 29 |
| Figure 22: Synthesis of $^{\text{iprop}}\text{Ar}^{\text{Br}}\text{ArNH}$ [2.1] under $\text{Pd}_2\text{dba}_3/\text{rac-BINAP}$ /toluene catalytic conditions. | 31 |
| Figure 23: Potential formation of $o\text{-(}^{\text{iprop}}\text{ArNH)}_2\text{C}_6\text{H}_4$ | 32 |
| Figure 24: Potential formation of $^{\text{iprop}}\text{ArN(C}_6\text{H}_4\text{Br)}_2$ | 32 |
| Figure 25: $^7\text{Li}\{^1\text{H}\}$ (top) and ^1H NMR (bottom) spectra of $[\text{tolAr}^{\text{Li}}\text{ArNLi}\cdot\text{TMEDA}]_2$ [2.2] in C_6D_6 and THF-d_8 | 35 |
| Figure 26: Synthesis of $[\text{tolAr}^{\text{Li}}\text{ArNLi}\cdot\text{TMEDA}]_2$ [2.2] and $[\text{phAr}^{\text{Li}}\text{ArNLi}\cdot 1.5\text{TMEDA}]_2$ [2.3] | 36 |
| Figure 27: ORTEP representation of the solid state molecular structure of $[\text{tolAr}^{\text{Li}}\text{ArNLi}\cdot\text{TMEDA}]_2$ [2.2] | 37 |

| | |
|---|----|
| Figure 28: Synthesis of $^{\text{tol}}\text{Ar}^{\text{D}}\text{ArND}$ [2.4] and $^{\text{ph}}\text{Ar}^{\text{D}}\text{ArND}$ [2.5]..... | 38 |
| Figure 29: ^2H NMR spectrum of $^{\text{tol}}\text{Ar}^{\text{D}}\text{ArND}$ [2.4] in C_6H_6 | 38 |
| Figure 30: Synthesis of $[\text{ipropNPNLi}_2\cdot\text{diox}]_n$ [2.6]..... | 39 |
| Figure 31: ORTEP representation of the solid-state molecular structure of $[\text{ipropNPNLi}_2\cdot\text{diox}]_n$ [2.6] ⁹⁷ | 41 |
| Figure 32: ^1H NMR spectra for the $^{\text{iprop}}\text{NPNLi}_2$ donor set: 1,4-dioxane, mixed 1,4-dioxane/THF and THF adducts | 42 |
| Figure 33: Chain and monomeric forms of the $^{\text{iprop}}\text{NPNLi}_2$ donor set | 42 |
| Figure 34: $^{31}\text{P}\{^1\text{H}\}$ NMR spectra for the $^{\text{iprop}}\text{NPNLi}_2$ donor set: 1,4-dioxane, mixed 1,4-dioxane/THF and THF adducts | 44 |
| Figure 35: $^7\text{Li}\{^1\text{H}\}$ NMR spectra for the $^{\text{iprop}}\text{NPNLi}_2$ donor set: 1,4-dioxane, mixed 1,4-dioxane/THF and THF adducts | 44 |
| Figure 36: Synthesis of $[\text{tolNPNLi}_2\cdot 1.5\text{TMEDA}]_2$ [2.7] | 45 |
| Figure 37: $^{31}\text{P}\{^1\text{H}\}$ NMR spectra of the $^{\text{tol}}\text{NPNLi}_2$ donor set: TMEDA, mixed TMEDA/THF and THF adducts | 46 |
| Figure 38: $^7\text{Li}\{^1\text{H}\}$ NMR spectra of the $^{\text{tol}}\text{NPNLi}_2$ donor set: TMEDA, mixed TMEDA/THF and THF adducts | 46 |
| Figure 39: ^1H NMR spectra of the $^{\text{tol}}\text{NPNLi}_2$ donor set: TMEDA, mixed TMEDA/THF and THF adducts | 48 |
| Figure 40: Structural forms of the $^{\text{tol}}\text{NPNLi}_2$ donor set..... | 48 |
| Figure 41: ORTEP representation of the solid state molecular structure of $[\text{tolNPNLi}_2\cdot 1.5\text{TMEDA}]_2$ [2.7] and $^{\text{tol}}\text{NPNLi}_2\cdot 0.5\text{TMEDA}\cdot 1\text{DME}$ ²⁶¹ | 49 |
| Figure 42: $^{31}\text{P}\{^1\text{H}\}$ NMR spectrum of $^{\text{tol}}\text{NPNPPh}$ [2.9] | 51 |
| Figure 43: Synthesis of $^{\text{tol}}\text{NPNPPh}$ [2.9]..... | 52 |
| Figure 44: Synthesis of $^{\text{iprop}}\text{NPNH}_2$ [2.10], $^{\text{tol}}\text{NPNH}_2$ [2.11] and $^{\text{ph}}\text{NPNH}_2$ [2.12] | 53 |
| Figure 45: ORTEP representations of the solid state molecular structures of $^{\text{tol}}\text{NPNH}_2$ [2.11] and $^{\text{ph}}\text{NPNH}_2$ [2.12] | 53 |
| Figure 46: Salt metathesis and protonolysis routes for zirconium complexes | 55 |
| Figure 47: Formation of $[\text{ipropNPN}]_2\text{Zr}$ [3.1] and $[\text{tolNPN}]_2\text{Zr}$ [3.2] | 56 |
| Figure 48: $^{31}\text{P}\{^1\text{H}\}$ (top) and ^1H NMR (bottom) spectra of $[\text{ipropNPN}]_2\text{Zr}$ [3.1] in C_6D_6 | 57 |
| Figure 49: ORTEP representation of the solid state molecular structure of $[\text{tolNPN}]_2\text{Zr}$ [3.2]..... | 58 |
| Figure 50: Reaction of $^{\text{Si}}\text{NPNLi}_2\cdot 2\text{THF}$, $^{\text{mes}}\text{NPNLi}_2\cdot\text{diox}$ and $[\text{ipropNPNLi}_2\cdot\text{diox}]_n$ [2.6] with $\text{ZrCl}_4(\text{THF})_2$ | 59 |
| Figure 51: Protonolysis with $\text{ZrCl}_2(\text{NMe}_2)_2(\text{DME})$ or $\text{Zr}(\text{NMe}_2)_4$ | 60 |

| | |
|--|----|
| Figure 52: $^{31}\text{P}\{^1\text{H}\}$ (top) and ^1H NMR (bottom) spectra of $^{101}\text{NPNZrCl}_2(\text{HNMe}_2)$ [3.4] in C_6D_6 . | 61 |
| Figure 53: Proton transfer for $^{101}\text{NPNZrCl}_2(\text{HNMe}_2)$ [3.4]..... | 61 |
| Figure 54: Possible origin of the minor impurity trichloride $^{\text{iprop}}\text{NPN}(\text{H})\text{ZrCl}_3$ | 62 |
| Figure 55: Isomers of $\text{NPNZrCl}_2(\text{HNMe}_2)$ | 63 |
| Figure 56: ORTEP representation of the solid state molecular structure of $^{101}\text{NPNZrCl}_2(\text{HNMe}_2)$ [3.4] | 63 |
| Figure 57: Isomers of $\text{NPNZrCl}_2(\text{THF})$ | 65 |
| Figure 58: $^{31}\text{P}\{^1\text{H}\}$ (top), partial $^{13}\text{C}\{^1\text{H}\}$ (middle) and ^1H NMR (bottom) spectra of $^{\text{iprop}}\text{NPNZrCl}_2(\text{THF})$ [3.5] in C_6D_6 | 66 |
| Figure 59: ORTEP representations of the solid state molecular structures of $^{\text{iprop}}\text{NPNZrCl}_2(\text{THF})$ [3.5] and $^{101}\text{NPNZrCl}_2(\text{THF})$ [3.6] | 67 |
| Figure 60: Protonolysis of $^{101}\text{NPNH}_2$ [2.11] with $\text{ZrCl}_2(\text{NMe}_2)_2(\text{DME})$ in THF at 60 °C | 68 |
| Figure 61: $^{31}\text{P}\{^1\text{H}\}$ (top) and ^1H NMR (bottom) spectra of $^{101}\text{NPNZr}(\text{NMe}_2)_2$ [3.8]..... | 69 |
| Figure 62: ORTEP representation of the solid state molecular structure of $^{\text{iprop}}\text{NPNZr}(\text{NMe}_2)_2$ [3.7] and $^{101}\text{NPNZr}(\text{NMe}_2)_2$ [3.8]..... | 69 |
| Figure 63: $^{31}\text{P}\{^1\text{H}\}$ NMR spectra of $^{\text{iprop}}\text{NPNZr}(\text{NMe}_2)_2$ [3.7] (bottom) and after 2, 5 and 7 equiv of TMSCl (middle three) and $^{\text{iprop}}\text{NPNZrCl}_2(\text{THF})$ [3.5] after excess THF (top) in C_6D_6 at 25 °C | 71 |
| Figure 64: $^{31}\text{P}\{^1\text{H}\}$ (top) and ^1H NMR (bottom) spectra of $[\text{iprop}\text{NPNZrCl}_2]_2$ [3.9] and $[\text{101}\text{NPNZrCl}_2]_2$ [3.10] in C_6D_6 at 25 °C | 72 |
| Figure 65: ORTEP representation of the solid state molecular structure of $[\text{iprop}\text{NPNZrCl}_2]_2$ [3.9] | 73 |
| Figure 66: $^{31}\text{P}\{^1\text{H}\}$ NMR spectra of $[\text{101}\text{PNZrCl}_2]_2$ [3.10] in toluene- d_8 at 93 and -71 °C | 74 |
| Figure 67: $^{31}\text{P}\{^1\text{H}\}$ NMR spectra of $[\text{iprop}\text{NPNZrCl}_2]_2$ [3.9] in toluene- d_8 from 93 to -60 °C (δ 4.54 at 25 °C used as reference for spectra at other temperatures) | 75 |
| Figure 68: $^{31}\text{P}\{^1\text{H}\}$ NMR spectra of different samples $[\text{iprop}\text{NPNZrCl}_2]_2$ [3.9] in toluene- d_8 at -60 °C | 75 |
| Figure 69: ^1H NMR spectrum of $[\text{iprop}\text{NPNZrCl}_2]_2$ [3.9] in toluene- d_8 at -60 °C, 25 °C and 93 °C | 76 |
| Figure 70: Chloro-bridged isomers for $[\text{NPNZrCl}_2]_2$, [3.9] and [3.10]..... | 77 |
| Figure 71: Protonolysis with $\text{TiCl}_2(\text{NMe}_2)_2$ or $\text{Ti}(\text{NMe}_2)_4$ | 79 |
| Figure 72: Possible isomers for $\text{NPNTiCl}_2(\text{HNMe}_2)$ [3.11] and [3.12] | 79 |
| Figure 73: $^{31}\text{P}\{^1\text{H}\}$ NMR spectrum of $^{101}\text{NPNTiCl}_2(\text{HNMe}_2)$ [3.12]..... | 80 |
| Figure 74: ^1H NMR spectrum of $^{101}\text{NPNTiCl}_2(\text{HNMe}_2)$ [3.12] | 80 |

| | |
|--|----|
| Figure 75: ^1H NMR spectrum of $^{\text{tol}}\text{NPNTiCl}_2(\text{THF})$ [3.14] in C_6D_6 | 81 |
| Figure 76: $^{31}\text{P}\{^1\text{H}\}$ NMR spectra of $^{\text{iprop}}\text{NPNTiCl}_2(\text{THF})$ [3.13] and $^{\text{tol}}\text{NPNTiCl}_2(\text{THF})$ [3.14] in C_6D_6 | 82 |
| Figure 77: ^1H NMR of $^{\text{iprop}}\text{NPNTiCl}_2(\text{THF})$ [3.13] before and after THF spike in C_6D_6 | 82 |
| Figure 78: Possible isomeric structures for $^{\text{iprop}}\text{NPNTiCl}_2(\text{THF})$ [3.13] and $^{\text{tol}}\text{NPNTiCl}_2(\text{THF})$ [3.14] | 83 |
| Figure 79: $^{31}\text{P}\{^1\text{H}\}$ (top) and ^1H NMR (bottom) spectra of $^{\text{iprop}}\text{NPNTiCl}_2(\text{HNMe}_2)/(\text{THF})$ [3.11]/[3.13] | 83 |
| Figure 80: Equilibrium structures for $^{\text{iprop}}\text{NPNTiCl}_2(\text{THF})$ [3.13] and $^{\text{iprop}}\text{NPNTiCl}_2(\text{HNMe}_2)$ [3.11] | 84 |
| Figure 81: $^{31}\text{P}\{^1\text{H}\}$ NMR spectrum of $^{\text{iprop}}\text{NPNTi}(\text{NMe}_2)_2$ [3.15]..... | 85 |
| Figure 82: Partial $^{13}\text{C}\{^1\text{H}\}$ (top) and ^1H NMR (bottom) spectra of $^{\text{iprop}}\text{NPNTi}(\text{NMe}_2)_2$ [3.15] | 85 |
| Figure 83: ORTEP representation of the solid state molecular structure of $^{\text{iprop}}\text{NPNTi}(\text{NMe}_2)_2$ [3.15] | 86 |
| Figure 84: $^{31}\text{P}\{^1\text{H}\}$ NMR spectra of $^{\text{iprop}}\text{NPNTi}(\text{NMe}_2)_2$ [3.15] (bottom) and + 2, 4 and 6 equiv of TMSCl in C_6D_6 | 87 |
| Figure 85: ORTEP representation of the solid state molecular structure of $^{\text{tol}}\text{NPNTiCl}_2$ [3.18]... | 88 |
| Figure 86: Protonolysis of $^{\text{iprop}}\text{NPNH}_2$ [2.10] with $\text{Hf}(\text{NMe}_2)_4$ | 89 |
| Figure 87: ORTEP representation of the solid state molecular structure of $^{\text{iprop}}\text{NPNHf}(\text{NMe}_2)_2$ [3.19] | 90 |
| Figure 88: $^{31}\text{P}\{^1\text{H}\}$ (top) and ^1H NMR (bottom) spectrum of $[\text{ipropNPNHfCl}_2]_2$ [3.20] in C_6D_6 at 25 $^\circ\text{C}$ | 91 |
| Figure 89: ORTEP representation of the solid state molecular structure of $[\text{ipropNPNHfCl}_2]_2$ [3.20] | 92 |
| Figure 90: $^{31}\text{P}\{^1\text{H}\}$ NMR spectra of $[\text{ipropNPNHfCl}_2]_2$ [3.20] in toluene- d_8 from 93 to -81 $^\circ\text{C}$ (δ 7.89 at 93 $^\circ\text{C}$ used as reference for spectra at other temperatures) | 93 |
| Figure 91: ^1H NMR spectra of $[\text{ipropNPNHfCl}_2]_2$ [3.20] in toluene- d_8 at 25 $^\circ\text{C}$ and -71 $^\circ\text{C}$ | 94 |
| Figure 92: $^{31}\text{P}\{^1\text{H}\}$ (top) and ^1H NMR (bottom) spectra of $^{\text{iprop}}\text{NPNHfCl}_2(\text{THF})$ [3.21] in C_6D_6 . | 95 |
| Figure 93: Partial $^{13}\text{C}\{^1\text{H}\}$ NMR spectrum of $^{\text{iprop}}\text{NPNHfCl}_2(\text{THF})$ [3.21] in C_6D_6 | 95 |
| Figure 94: Isomers of $^{\text{iprop}}\text{NPNHfCl}_2(\text{THF})$ [3.21]..... | 95 |
| Figure 95: ORTEP representation of the solid state molecular structure of $^{\text{iprop}}\text{NPNHfCl}_2(\text{THF})$ [3.21] | 96 |
| Figure 96: Schematic representation of target NPN tantalum complexes..... | 98 |
| Figure 97: Salt metathesis and protonolysis routes for tantalum complexes | 99 |

| | |
|---|-----|
| Figure 98: Protonolysis route for synthesis of NPNTaCl ₃ complexes [4.4], [4.5] and [4.6]..... | 100 |
| Figure 99: ¹ H (top) and ³¹ P{ ¹ H} NMR (bottom) spectra of ^{tol} NPNTa(NMe ₂) ₃ [4.2] in C ₆ D ₆ , “hex” in the ¹ H NMR spectrum refers to residual hexanes | 101 |
| Figure 100: Partial ¹³ C{ ¹ H} NMR spectrum of ^{tol} NPNTa(NMe ₂) ₃ [4.2] in C ₆ D ₆ | 102 |
| Figure 101: ORTEP representation of the solid state molecular structure of ^{tol} NPNTa(NMe ₂) ₃ [4.2] | 102 |
| Figure 102: ¹ H (top) and ³¹ P{ ¹ H} NMR (bottom) spectra for ^{tol} NPNTaCl ₃ [4.5] in C ₆ D ₆ at room temperature..... | 104 |
| Figure 103: ORTEP representation of the solid state molecular structure for ^{Ph} NPNTaCl ₃ [4.6]. | 105 |
| Figure 104: ³¹ P{ ¹ H} NMR spectra for ^{tol} NPNTaCl ₃ [4.5] in toluene- <i>d</i> ₈ and THF- <i>d</i> ₈ at -70 °C. . | 107 |
| Figure 105: Partial ¹ H NMR spectra for ^{tol} NPNTaCl ₃ [4.5] in toluene- <i>d</i> ₈ and THF- <i>d</i> ₈ at -70 °C. | 107 |
| Figure 106: Implausible equilibria for solvated NPNTaCl ₃ complexes | 108 |
| Figure 107: Possible configurational isomers for solvated NPNTaCl ₃ complexes | 109 |
| Figure 108: Synthesis of ^{tol} NPNTaMe ₃ [4.7]..... | 110 |
| Figure 109: ¹ H (top) and ³¹ P{ ¹ H} NMR (bottom) spectra for ^{tol} NPNTaMe ₃ [4.7] in C ₆ D ₆ | 110 |
| Figure 110: ¹ H- ³¹ P HMBC NMR spectrum for ^{tol} NPNTaMe ₃ [4.7] in C ₆ D ₆ | 111 |
| Figure 111: ³¹ P{ ¹ H} NMR spectra for reaction of [^{iprop} NPNLi ₂ ·diox] _n [2.6] with TaMe ₃ Cl ₂ in toluene- <i>d</i> ₈ (successive spectra offset by δ 2 units, 0 min = time the sample was placed inside the spectrometer at -80 °C) | 112 |
| Figure 112: ¹ H NMR spectrum for reaction of [^{iprop} NPNLi ₂ ·diox] _n [2.6] with TaMe ₃ Cl ₂ in toluene- <i>d</i> ₈ at -80 °C, CH-iprop = methine, Me-iprop = methyl of the isopropyl group..... | 113 |
| Figure 113: <i>o</i> -Phenylene bridged NPNTaMe ₃ complexes | 113 |
| Figure 114: ORTEP representation of the solid state molecular structure for ^{iprop-P} NPNTaMe ₃ . | 114 |
| Figure 115: ³¹ P{ ¹ H} NMR spectra of ^{tol} NPNTaCl ₃ [4.5] + 1, 2, 3 and 4 equiv of MeLi at room temperature in toluene- <i>d</i> ₈ | 115 |
| Figure 116: ¹ H NMR spectrum for species tol _{4MeLi} in toluene- <i>d</i> ₈ after 4 equiv of MeLi. | 116 |
| Figure 117: ORTEP representation of the solid state molecular structure for [^{tol} NPNTaMe ₄][Li(THF) ₄] [4.14]. | 117 |
| Figure 118: Possible seven-coordinate geometries for the [^{tol} NPNTaMe ₄] ⁻ anion of [4.14]. Pentagonal bipyramid: Me1, Me2 axial and Me3, Me4, N, N, P pentagonal. Capped octahedron: Me1, P axial and Me3, Me4, N, N equatorial of octahedron with Me2 cap of trigonal face Me1, N, N. Capped trigonal prism: Me1, Me3, Me4 and Me2, N, N trigonal bases with P cap of | |

| | |
|--|-----|
| quadrilateral face Me ₃ , Me ₄ , N, N. 4:3 Piano stool: Me ₁ , Me ₂ , Me ₃ , Me ₄ tetragonal base and N, N, P trigonal cap..... | 119 |
| Figure 119: Potential tantalum methyl species for the salt metathesis of ^{tol} NPNTaCl ₃ [4.5] with MeLi..... | 120 |
| Figure 120: Partial ³¹ P{ ¹ H} (top) and partial ¹ H NMR (bottom) spectra for ^{iprop} NPNTaCl ₃ [4.4] + KHBet ₃ (Ar) + N ₂ in C ₆ D ₆ | 122 |
| Figure 121: Potential species indicated by mass spectral data..... | 123 |
| Figure 122: ³¹ P{ ¹ H} (top) and partial ¹ H NMR (bottom) spectra for ^{tol} NPNTaCl ₃ [4.5] + KHBet ₃ + N ₂ in C ₆ D ₆ | 123 |
| Figure 123: Schematic of potential reactions of NPNTaCl ₃ with KHBet ₃ under Ar and N ₂ | 124 |
| Figure 124: ³¹ P{ ¹ H} NMR spectrum for reaction of ^{tol} NPNTaCl ₃ [4.5] with 2.2 KC ₈ under N ₂ in C ₆ D ₆ | 125 |
| Figure 125: Reduction of NPNTaCl ₃ complexes with 2.2 KC ₈ under N ₂ | 126 |
| Figure 126: ³¹ P{ ¹ H} NMR spectra for ^{tol} NPNTaCl ₃ [4.5] + 3.5 KC ₈ under N ₂ in C ₆ D ₆ | 127 |
| Figure 127: Synthesis of [^{iprop} NPNZr(THF)] ₂ (μ-η ² :η ² -N ₂) [5.1] and [^{tol} NPNZr(THF)] ₂ (μ-η ² :η ² -N ₂) [5.3]..... | 129 |
| Figure 128: ³¹ P{ ¹ H} (bottom) and ¹ H NMR (top) spectra of [^{iprop} NPNZr(THF)] ₂ (μ-η ² :η ² -N ₂) [5.1]..... | 130 |
| Figure 129: ³¹ P{ ¹ H} (bottom) and ¹ H NMR (top) spectra of [^{tol} NPNZr(THF)] ₂ (μ-η ² :η ² -N ₂) [5.3]..... | 131 |
| Figure 130: Potential mechanism for the formation of zirconium dinitrogen complexes..... | 132 |
| Figure 131: Experimental set-up of the glass liner for the Parr reactor with the KC ₈ ampoule.. | 134 |
| Figure 132: ORTEP representation of the solid state molecular structure of [^{iprop} NPNZr(THF)] ₂ (μ-η ² :η ² -N ₂) [5.1]..... | 136 |
| Figure 133: ³¹ P{ ¹ H} and ¹⁵ N{ ¹ H} NMR spectra for [^{iprop} NPNZr(THF)] ₂ (μ-η ² :η ² - ¹⁵ N ₂) [5.2] in C ₆ D ₆ | 139 |
| Figure 134: Infrared spectra for [^{iprop} NPNZr(THF)] ₂ (μ-η ² :η ² -N ₂) [5.1] and [^{iprop} NPNZr(THF)] ₂ (μ-η ² :η ² - ¹⁵ N ₂) [5.2]..... | 140 |
| Figure 135: Theoretical vibrational modes for a Zr ₂ N ₂ core ¹⁴¹ | 141 |
| Figure 136: UV-Vis spectra for [^{iprop} NPNZr(THF)] ₂ (μ-η ² :η ² -N ₂) [5.1]..... | 142 |
| Figure 137: Reduction of ^{iprop} NPNHfCl ₂ (THF) [3.21] with KC ₈ and N ₂ | 144 |
| Figure 138: Comparison of zirconium dinitrogen complexes P ₂ N ₂ (silyl methyls omitted for clarity) with NPN(L _n)..... | 145 |

| | |
|--|-----|
| Figure 139: ORTEP representations of the solid state molecular structures of related $[\text{Si}^{\text{NPNZr}}(\text{Py})]_2(\mu\text{-}\eta^2\text{:}\eta^2\text{-N}_2)^{137}$ and $[\text{mes}^{\text{NPNZr}}(\text{Py})]_2(\mu\text{-}\eta^2\text{:}\eta^2\text{-N}_2)^{92, 97}$ complexes | 146 |
| Figure 140: Synthesis of $[\text{tol}^{\text{NPNZr}}(\text{Py})]_2(\mu\text{-}\eta^2\text{:}\eta^2\text{-N}_2)$ [5.4] and $[\text{tol}^{\text{NPNZr}}(\text{Py-}d_5)]_2(\mu\text{-}\eta^2\text{:}\eta^2\text{-N}_2)$ [5.5] | 146 |
| Figure 141: $[\text{tol}^{\text{NPNZr}}(\text{Py})]_2(\mu\text{-}\eta^2\text{:}\eta^2\text{-N}_2)$ [5.4] with excess pyridine | 147 |
| Figure 142: $^{31}\text{P}\{^1\text{H}\}$ NMR (top) spectrum of [5.4] and partial ^1H NMR spectra of [5.4] (middle) and [5.5] (bottom) in C_6D_6 | 148 |
| Figure 143: Partial ^1H NMR spectra with variation in free pyridine for $[\text{tol}^{\text{NPNZr}}(\text{Py})]_2(\mu\text{-}\eta^2\text{:}\eta^2\text{-N}_2)$ [5.4] in C_6D_6 | 148 |
| Figure 144: $^{31}\text{P}\{^1\text{H}\}$ NMR (bottom) and partial ^1H NMR (top) spectra of $[\text{iprop}^{\text{NPNZr}}(\text{THF})]_2(\mu\text{-}\eta^2\text{:}\eta^2\text{-N}_2)$ [5.1] after 1 and 2 equiv of 4,4'-bipyridine in C_6D_6 | 150 |
| Figure 145: Reaction of $[\text{iprop}^{\text{NPNZr}}(\text{THF})]_2(\mu\text{-}\eta^2\text{:}\eta^2\text{-N}_2)$ [5.1] with one and two equiv of 4,4'-bipyridine | 150 |
| Figure 146: Chain vs. Dimer structure for $[\text{iprop}^{\text{NPNZr}}(4,4'\text{-bipy})]_2(\mu\text{-}\eta^2\text{:}\eta^2\text{-N}_2)$ [5.6] | 152 |
| Figure 147: Reaction of $[\text{mes}^{\text{NPNZr}}(\text{THF})]_2(\mu\text{-}\eta^2\text{:}\eta^2\text{-N}_2)$ with PMe_3 and PPhMe_2 | 152 |
| Figure 148: Reaction of the zirconium dinitrogen THF adducts [5.1] and [5.3] with PMe_3 and PPhMe_2 | 153 |
| Figure 149: $^{31}\text{P}\{^1\text{H}\}$ (a, b and c-1) and ^1H NMR (c-2) spectra of mixtures of $[\text{iprop}^{\text{NPNZr}}(\text{THF})](\mu\text{-}\eta^2\text{:}\eta^2\text{-N}_2)[\text{iprop}^{\text{NPNZr}}(\text{PMe}_3)]$ [5.7] and $[\text{iprop}^{\text{NPNZr}}(\text{THF})]_2(\mu\text{-}\eta^2\text{:}\eta^2\text{-N}_2)$ [5.1] in C_6D_6 | 155 |
| Figure 150: $^{31}\text{P}\{^1\text{H}\}$ spectra of $[\text{iprop}^{\text{NPNZr}}(\text{PMe}_3)]_2(\mu\text{-}\eta^2\text{:}\eta^2\text{-N}_2)$ [5.8] (top), $[\text{tol}^{\text{NPNZr}}(\text{PMe}_3)]_2(\mu\text{-}\eta^2\text{:}\eta^2\text{-N}_2)$ [5.9] (middle) and $[\text{iprop}^{\text{NPNZr}}(\text{PPhMe}_2)]_2(\mu\text{-}\eta^2\text{:}\eta^2\text{-N}_2)$ [5.10] (bottom) | 156 |
| Figure 151: $^{31}\text{P}\{^1\text{H}\}$ NMR spectra of $[\text{tol}^{\text{NPNZr}}(\text{PPhMe}_2)]_2(\mu\text{-}\eta^2\text{:}\eta^2\text{-N}_2)$ [5.11] at 25 and -25 °C in C_6D_6 | 157 |
| Figure 152: ^1H NMR spectra of $[\text{tol}^{\text{NPNZr}}(\text{PMe}_3)]_2(\mu\text{-}\eta^2\text{:}\eta^2\text{-N}_2)$ [5.9] (top) and $[\text{iprop}^{\text{NPNZr}}(\text{PPhMe}_2)]_2(\mu\text{-}\eta^2\text{:}\eta^2\text{-N}_2)$ [5.10] (bottom), with excess free phosphine in C_6D_6 | 157 |
| Figure 153: $^{31}\text{P}\{^1\text{H}\}$ (bottom) and ^1H NMR (top) spectra of exchanging $[\text{tol}^{\text{NPNZr}}(\text{THF})]_2(\mu\text{-}\eta^2\text{:}\eta^2\text{-N}_2)$ [5.3] and $[\text{tol}^{\text{NPNZr}}(\text{THT})]_2(\mu\text{-}\eta^2\text{:}\eta^2\text{-N}_2)$ [5.14] in C_6D_6 | 159 |
| Figure 154: Exchange between THF ([5.3] and [5.1]) and potential THT ([5.14] and [5.12]) adducts | 160 |
| Figure 155: $^{31}\text{P}\{^1\text{H}\}$ (bottom) and ^1H NMR (top) spectra of 30 equiv of THT with $[\text{iprop}^{\text{NPNZr}}(\text{PMe}_3)]_2(\mu\text{-}\eta^2\text{:}\eta^2\text{-N}_2)$ [5.8] + trace THF in C_6D_6 | 160 |
| Figure 156: $^{31}\text{P}\{^1\text{H}\}$ (bottom) and ^1H NMR (top) spectra of $[\text{tol}^{\text{NPNZr}}(\text{THT})]_2(\mu\text{-}\eta^2\text{:}\eta^2\text{-N}_2)$ [5.14] in C_6D_6 | 161 |

| | |
|--|-----|
| Figure 157: Phosphine displacement with neat THT, <i>in situ</i> from $[\text{}^{\text{tol}}\text{NPNTi}(\text{THF})]_2(\mu\text{-}\eta^2\text{:}\eta^2\text{-N}_2)$ [5.3] | 162 |
| Figure 158: Synthesis of $[\text{}^{\text{tol}}\text{NPNTi}(\text{THF})]_2(\mu\text{-}\eta^1\text{:}\eta^1\text{-N}_2)$ [5.15] | 163 |
| Figure 159: $^{31}\text{P}\{^1\text{H}\}$ (bottom) and ^1H NMR (top) spectra of $[\text{}^{\text{tol}}\text{NPNTi}(\text{THF})]_2(\mu\text{-}\eta^1\text{:}\eta^1\text{-N}_2)$ [5.15] in C_6D_6 | 164 |
| Figure 160: $^{31}\text{P}\{^1\text{H}\}$ (bottom) and ^1H NMR (top) spectra of crude brown solid after THF centrifuge in C_6D_6 | 165 |
| Figure 161: ORTEP representation of solid state molecular structure of $[\text{}^{\text{tol}}\text{NPNTi}(\text{THF})]_2(\mu\text{-}\eta^1\text{:}\eta^1\text{-N}_2)$ [5.15] ³³² | 165 |
| Figure 162: $^{31}\text{P}\{^1\text{H}\}$ (bottom) and ^1H NMR (top) spectra of crude brown solid for $^{\text{iprop}}\text{NPNTiCl}_2$ [3.17] reduction in C_6D_6 | 167 |
| Figure 163: Potential phosphinimide formation during the reduction of NPNTiCl_2 [3.17] and [3.18] | 168 |
| Figure 164: $^{31}\text{P}\{^1\text{H}\}$ NMR spectra of $[\text{}^{\text{tol}}\text{NPNTi}(\text{THF})]_2(\mu\text{-}\eta^1\text{:}\eta^1\text{-N}_2)$ [5.15] + species a before (bottom) and after THF spike (top) in C_6D_6 | 169 |
| Figure 165: $^{31}\text{P}\{^1\text{H}\}$ (bottom) and ^1H NMR (top) spectra of species a in C_6D_6 | 169 |
| Figure 166: Formation of $[\text{}^{\text{tol}}\text{NPNTi}(\text{THF})]_2(\mu\text{-}\eta^1\text{:}\eta^1\text{-N}_2)$ [5.16] | 170 |
| Figure 167: $^{31}\text{P}\{^1\text{H}\}$ NMR spectra after pyridine addition to $[\text{}^{\text{tol}}\text{NPNTi}(\text{THF})]_2(\mu\text{-}\eta^1\text{:}\eta^1\text{-N}_2)$ [5.15] in C_6D_6 | 171 |
| Figure 168: Synthesis of <i>trans</i> - $[\text{}^{\text{tol}}\text{NPNTi}(\text{Py})]_2(\mu\text{-}\eta^1\text{:}\eta^1\text{-N}_2)$ [5.19] from $[\text{}^{\text{tol}}\text{NPNTi}(\text{THF})]_2(\mu\text{-}\eta^1\text{:}\eta^1\text{-N}_2)$ [5.15] | 172 |
| Figure 169: Potential pyridine adducts observed in the C_6D_6 solution with two or four Py per titanium centre | 173 |
| Figure 170: ORTEP representation of solid state molecular structure of <i>trans</i> - $[\text{}^{\text{tol}}\text{NPNTi}(\text{Py})]_2(\mu\text{-}\eta^1\text{:}\eta^1\text{-N}_2)$ [5.19] ³³² | 174 |
| Figure 171: $^{31}\text{P}\{^1\text{H}\}$ NMR spectra of <i>trans</i> - $[\text{}^{\text{tol}}\text{NPNTi}(\text{Py})]_2(\mu\text{-}\eta^1\text{:}\eta^1\text{-N}_2)$ [5.19] (bottom) and with a 20 μL Py-d_5 spike (top) in C_6D_6 | 175 |
| Figure 172: ^1H NMR spectra of <i>trans</i> - $[\text{}^{\text{tol}}\text{NPNTi}(\text{Py})]_2(\mu\text{-}\eta^1\text{:}\eta^1\text{-N}_2)$ [5.19] (bottom) and with a 20 μL Py-d_5 spike (top) and with a 20 μL Py spike (middle) in C_6D_6 | 177 |
| Figure 173: Synthesis of $[\text{}^{\text{tol}}\text{NPNTi}(2,2'\text{-bipy})]_2(\mu\text{-}\eta^1\text{:}\eta^1\text{-N}_2)$ [5.20] | 177 |
| Figure 174: $^{31}\text{P}\{^1\text{H}\}$ (bottom) and ^1H NMR (top) spectra of $[\text{}^{\text{tol}}\text{NPNTi}(2,2'\text{-bipy})]_2(\mu\text{-}\eta^1\text{:}\eta^1\text{-N}_2)$ [5.20] in C_6D_6 | 178 |
| Figure 175: Synthesis of $[\text{}^{\text{tol}}\text{NPNTiH}_2]_2$ [5.21] | 179 |

| | |
|--|-----|
| Figure 176: $^{31}\text{P}\{^1\text{H}\}$ (bottom), partial ^1H (middle two) and partial $^1\text{H}\{^{31}\text{P}\}$ NMR (top) spectra of $[\text{}^{101}\text{NPNTiH}_2]_2$ [5.21] in C_6D_6 | 180 |
| Figure 177: Hydrogenation with P_2N_2 (silyl methyls omitted for clarity) and NPN amido-phosphine N_2 complexes | 184 |
| Figure 178: Failed hydrogenations with $\text{NPN}(\text{L}_n)$ zirconium N_2 complexes | 185 |
| Figure 179: Reaction of 2:2 dinitrogen complexes $\text{NPN}(\text{L}_n)$, $[\text{}^{101}\text{NPNZr}(\text{THF})_2(\mu\text{-}\eta^2\text{:}\eta^2\text{-N}_2)]$ [5.3] and $[\text{}^{101}\text{NPNZr}(\text{PMe}_3)_2(\mu\text{-}\eta^2\text{:}\eta^2\text{-N}_2)]$ [5.9] with molecular hydrogen..... | 186 |
| Figure 180: $^{31}\text{P}\{^1\text{H}\}$ (top) and ^1H NMR (bottom) spectra of complex [5.1] + 2 equiv of xylylNC (species a) in C_6D_6 , x denotes residual toluene and <i>n</i> -hexane solvents..... | 188 |
| Figure 181: $^{31}\text{P}\{^1\text{H}\}$ (top) and $^{15}\text{N}\{^1\text{H}\}$ NMR (bottom) spectra of complex [5.2] + 2 equiv of xylylNC (species a-1) in C_6D_6 | 189 |
| Figure 182: Proposed reaction of complexes [5.1], [5.2] and [5.3] with 2 equiv of xylylNC or $^t\text{BuNC}$. Note: (i) the N-N bond is depicted intact, as insufficient data to evaluate if N-N cleavage occurred, (ii) isocyanide insertion is depicted as N-inside, but may be N-outside ³⁵⁴ and (iii) the P atoms of the ligands are depicted in a <i>trans</i> arrangement (as in the precursors), but could be <i>cis</i> | 190 |
| Figure 183: $^{31}\text{P}\{^1\text{H}\}$ (top) and ^1H NMR (bottom) spectra of complex [5.1] + 2 equiv of $^t\text{BuNC}$ (species c) in C_6D_6 | 191 |
| Figure 184: $^{31}\text{P}\{^1\text{H}\}$ NMR spectra of complex [5.2] with 1, 2, 3 and 4 xylylNC (species a-1 and e-1) (top) and ^1H NMR spectrum with 4 xylylNC (species e-1) (bottom) in C_6D_6 | 192 |
| Figure 185: $^{31}\text{P}\{^1\text{H}\}$ and partial $^{15}\text{N}\{^1\text{H}\}$ NMR spectra of complex [5.2] with 4 xylylNC (species e-1) in C_6D_6 | 193 |
| Figure 186: Hydrosilylation with P_2N_2 and $^{\text{Si}}\text{NPN}$ dinitrogen complexes | 194 |
| Figure 187: Hydrosilylation with the $^{\text{mes}}\text{NPN}$ containing dinitrogen complex | 195 |
| Figure 188: $^{31}\text{P}\{^1\text{H}\}$ NMR spectrum of $[\text{}^{\text{iprop}}\text{NPNZr}(\text{THF})_2(\mu\text{-}\eta^2\text{:}\eta^2\text{-N}_2)]$ [5.1] + PhSiH_3 in C_6D_6 | 195 |
| Figure 189: Hydrosilylation with $[\text{}^{\text{iprop}}\text{NPNZr}(\text{THF})_2(\mu\text{-}\eta^2\text{:}\eta^2\text{-N}_2)]$ [5.1] with PhSiH_3 | 196 |
| Figure 190: $^{31}\text{P}\{^1\text{H}\}$ (top) and ^1H NMR (bottom) of $[\text{}^{\text{iprop}}\text{NPNZr}(\text{THF})_2(\mu\text{-}\eta^2\text{:}\eta^2\text{-N}_2)]$ [5.1] after 1 atm $\text{H}_2\text{C}=\text{CH}_2$ | 197 |
| Figure 191: Partial ^1H NMR of $[\text{}^{\text{iprop}}\text{NPNZr}(\text{THF})_2(\mu\text{-}\eta^2\text{:}\eta^2\text{-N}_2)]$ [5.1] after 1atm $\text{H}_2\text{C}=\text{CH}_2$ in C_6D_6 | 197 |
| Figure 192: Theoretical products for reaction of $[\text{}^{\text{iprop}}\text{NPNZr}(\text{THF})_2(\mu\text{-}\eta^2\text{:}\eta^2\text{-N}_2)]$ [5.1] with large excess CO..... | 198 |

| | |
|--|-----|
| Figure 193: Theoretical products for reaction of $[\text{ipropNPNZr}(\text{THF})_2(\mu\text{-}\eta^2\text{:}\eta^2\text{-N}_2)]$ [5.1] with 1 equiv of CO | 199 |
| Figure 194: $^{31}\text{P}\{^1\text{H}\}$ NMR spectra of $[\text{ipropNPNZr}(\text{THF})_2(\mu\text{-}\eta^2\text{:}\eta^2\text{-N}_2)]$ [5.1] after 1 atm CO in C_6D_6 | 200 |
| Figure 195: $^{31}\text{P}\{^1\text{H}\}$ spectrum of $[\text{ipropNPNZr}(\text{THF})_2(\mu\text{-}\eta^2\text{:}\eta^2\text{-N}_2)]$ [5.1] after 1 equiv of CO ... | 201 |
| Figure 196: Theoretical products for reaction of $[\text{ipropNPNZr}(\text{THF})_2(\mu\text{-}\eta^2\text{:}\eta^2\text{-N}_2)]$ [5.1] with $\text{Ar}_2\text{C=O}$ | 202 |
| Figure 197: $^{31}\text{P}\{^1\text{H}\}$ NMR spectrum of $[\text{ipropNPNZr}(\text{THF})_2(\mu\text{-}\eta^2\text{:}\eta^2\text{-N}_2)]$ [5.1] after 1 equiv of $\text{Ar}_2\text{C=O}$ in C_6D_6 | 203 |
| Figure 198: Theoretical products for $[\text{ipropNPNZr}(\text{THF})_2(\mu\text{-}\eta^2\text{:}\eta^2\text{-N}_2)]$ [5.1] with 1 equiv of $\text{N}_2\text{CHSiMe}_3$ | 204 |
| Figure 199: $^{31}\text{P}\{^1\text{H}\}$ NMR spectrum of $[\text{ipropNPNZr}(\text{THF})_2(\mu\text{-}\eta^2\text{:}\eta^2\text{-N}_2)]$ [5.1] + 1 equiv of $\text{N}_2\text{CHSiMe}_3$ in C_6D_6 | 205 |
| Figure 200: $^{31}\text{P}\{^1\text{H}\}$ (bottom) and partial ^1H NMR (top) spectra for $[\text{tolNPNTi}]_2(\text{H}_2\text{C=CH}_2)$ [5.22] in C_6D_6 | 207 |
| Figure 201: NPN donor set variation of arylamido groups | 212 |
| Figure 202: Potential reactivity of bulky NPN zirconium N_2 complexes with dihydrogen | 213 |
| Figure 203: Potential NPN ligand design for side-on titanium N_2 complexes..... | 214 |
| Figure 204: Synthesis of $^{\text{naph}}\text{Ar}^{\text{Br}}\text{ArNH}$ [7.1] and $^{2,6\text{-iPr}_2}\text{Ar}^{\text{Br}}\text{ArNH}$ [7.2]..... | 215 |
| Figure 205: Solid state molecular structures of $^{2,6\text{-iPr}_2}\text{ArBrArNH}$ [7.2] and $^{\text{naph}}\text{Ar}^{\text{Br}}\text{ArNH}$ [7.1]. | 216 |
| Figure 206: Lithiation of $^{2,6\text{-iPr}_2}\text{ArBrArNH}$ [7.2] | 217 |
| Figure 207: Synthesis of $[\text{^{2,6-iPr}_2Ar}^{\text{Li}}\text{ArNLi}]_n$ [7.3] and $[\text{^{2,6-iPr}_2Ar}^{\text{Li}}\text{ArNLi}\cdot 2\text{THF}]_2$ [7.3a]..... | 217 |
| Figure 208: $^7\text{Li}\{^1\text{H}\}$ (bottom) and ^1H NMR (top) of $[\text{^{2,6-iPr}_2Ar}^{\text{Li}}\text{ArNLi}]_n$ [7.3] in C_6D_6 | 218 |
| Figure 209: $^7\text{Li}\{^1\text{H}\}$ (bottom) and ^1H NMR (top) of $[\text{^{2,6-iPr}_2Ar}^{\text{Li}}\text{ArNLi}\cdot 2\text{THF}]_2$ [7.3a] in $\text{THF-}d_8$ | 219 |
| Figure 210: Solid state molecular structure of dimeric $[\text{^{2,6-iPr}_2Ar}^{\text{Li}}\text{ArNLi}\cdot 2\text{THF}]_2$ [7.3a] in two different orientations, with the carbon atoms of the THF adducts omitted for clarity | 220 |
| Figure 211: Synthesis of $[\text{^naphAr}^{\text{Li}}\text{ArNLi}\cdot 2\text{Et}_2\text{O}]_2$ [7.4] and $[\text{^naphAr}^{\text{Li}}\text{ArNLi}\cdot 2\text{THF}]_2$ [7.5] | 222 |
| Figure 212: Synthesis of $[\text{^naphNPNLi}_2\cdot \text{diox}]_n$ [7.6] | 223 |
| Figure 213: $^{31}\text{P}\{^1\text{H}\}$ NMR spectrum of $[\text{^naphNPNLi}_2\cdot \text{diox}]_n$ [7.6] in toluene- d_8 | 224 |
| Figure 214: $^7\text{Li}\{^1\text{H}\}$ NMR spectrum of $[\text{^naphNPNLi}_2\cdot \text{diox}]_n$ [7.6] in toluene- d_8 | 224 |
| Figure 215: Structural forms for $[\text{^naphNPNLi}_2\cdot \text{diox}]_n$ [7.6], $[\text{^naphNPNLi}_2\cdot 1.5\text{diox}]_n$ [7.6a] and $[\text{^naphNPNLi}_2\cdot \text{diox}\cdot 2\text{THF}]_n$ [7.6b]..... | 225 |
| Figure 216: $^{31}\text{P}\{^1\text{H}\}$ NMR spectrum of $[\text{^naphNPNLi}_2\cdot \text{diox}\cdot 2\text{THF}]_n$ [7.6b] in C_6D_6 | 226 |

| | |
|--|-----|
| Figure 217: Potential P-Li coupled P-N and P-C side-products for one-pot reaction (a) | 227 |
| Figure 218: Synthesis of $[^{2,6-i\text{Pr}_2\text{NPNLi}_2\cdot\text{diox}]_n$ [7.7], $[^{2,6-i\text{Pr}_2\text{NPNLi}_2\cdot 1.5\text{diox}]_n$ [7.7a], $^{2,6-i\text{Pr}_2\text{NPNLi}_2\cdot 2\text{Et}_2\text{O}}$ [7.7b] or $^{2,6-i\text{Pr}_2\text{NPNLi}_2\cdot 3\text{Et}_2\text{O}}$ [7.7c] | 228 |
| Figure 219: $^{31}\text{P}\{^1\text{H}\}$ NMR spectra of crude reaction mixtures for $[^{2,6-i\text{Pr}_2\text{NPNLi}_2\cdot\text{diox}]_n$ [7.7] in C_6D_6 | 228 |
| Figure 220: Synthesis of $^{\text{naph}}\text{NPNH}_2$ [7.8]..... | 229 |
| Figure 221: Synthesis of $^{2,6-i\text{Pr}_2}\text{NPNH}_2$ [7.9]..... | 229 |
| Figure 222: DOSY $^{31}\text{P}\{^1\text{H}\}$ NMR spectrum and diffusion coefficients (D) for $[\text{ipropNPNZrCl}_2]_2$ [3.9] in toluene- d_8 at $-40\text{ }^\circ\text{C}$ | 388 |
| Figure 223: Diffusion coefficients (D) from DOSY $^{31}\text{P}\{^1\text{H}\}$ NMR spectrum of $^{\text{tol}}\text{NPNTaCl}_3$ [4.5] in toluene- d_8 at $-60\text{ }^\circ\text{C}$ | 392 |
| Figure 224: Variable temperature $^{31}\text{P}\{^1\text{H}\}$ NMR spectra for $^{\text{iprop}}\text{NPNTaCl}_3$ [4.4] in C_7D_8 from $25\text{ }^\circ\text{C}$ to $-70\text{ }^\circ\text{C}$ | 395 |
| Figure 225: Variable temperature $^{31}\text{P}\{^1\text{H}\}$ NMR spectra for $^{\text{tol}}\text{NPNTaCl}_3$ [4.5] in C_7D_8 from $25\text{ }^\circ\text{C}$ to $-69\text{ }^\circ\text{C}$ | 396 |
| Figure 226: Variable temperature $^{31}\text{P}\{^1\text{H}\}$ NMR spectra for $^{\text{Ph}}\text{NPNTaCl}_3$ [4.6] in C_7D_8 from $25\text{ }^\circ\text{C}$ to $-69\text{ }^\circ\text{C}$ | 396 |

Glossary of Terms

| | |
|--|--|
| $^{\circ}\text{C}$ | degrees Celsius |
| <i>ca</i> | approximately |
| \AA | Ångström (10^{-10} m) |
| N_2 , $\text{N}\equiv\text{N}$ | dinitrogen |
| $\text{PhN}=\text{NPh}$ | diazobenzene |
| N_2^{2-} , $(\text{N}=\text{N})^{2-}$ | diazenido |
| N_2^{4+} , $(\text{N}-\text{N})^{4+}$ | hydrazido |
| NH_3 | ammonia |
| H_2 | dihydrogen |
| Ar | argon |
| CDCl_3 | deuterated chloroform |
| C_6D_6 | deuterated benzene |
| C_7D_8 | deuterated toluene |
| $\text{THF-}d_8$ | deuterated tetrahydrofuran |
| THF | tetrahydrofuran |
| ^1H | proton |
| ^{31}P | phosphorus-31 |
| $\{^1\text{H}\}$ | proton decoupled |
| NMR | nuclear magnetic resonance |
| MHz | megahertz |
| ^{13}C | carbon-13 |
| ^7Li | lithium-7 |
| ^2H | deuterium |
| ^{15}N | nitrogen-15 |
| δ | delta |
| $\eta^1\text{-N}_2$ | terminal end-on-bound N_2 |
| $\mu\text{-}\eta^1\text{:}\eta^1\text{-N}_2$ | bridging end-on-bound N_2 |
| $\mu\text{-}\eta^2\text{:}\eta^2\text{-N}_2$ | bridging side-on-bound N_2 |
| $\mu\text{-}\eta^1\text{:}\eta^2\text{-N}_2$ | bridging side-on-end-on-bound N_2 |
| ppm | parts per million |
| Hz | Hertz, seconds $^{-1}$ |
| kcalmol^{-1} | kilocalorie per mole |
| r.t. | room temperature |

| | |
|-------------------|---|
| % | percentage, fraction or ratio with 100 denominator |
| GC | gas chromatography |
| UV-Vis | Ultraviolet-Visible |
| LMCT | Ligand-to-Metal Charge Transfer |
| equiv | equivalent(s) |
| av | average |
| d | doublet |
| $^nJ_{AB}$ | coupling constant between nuclei A and B over n bonds |
| CH ₃ | methyl group |
| hep | heptet |
| CH | methine group |
| CH ₂ | methylene |
| ArH | phenyl proton |
| C _{ipso} | <i>ipso</i> -carbon |
| ArC | aromatic carbon |
| Anal. | analysis |
| Calcd. | calculated |
| EI | electron impact |
| MS | mass spectrometry |
| m/z | mass-to-charge ratio |
| [M] ⁺ | parent ion |
| hr | hour(s) |
| min | minute(s) |
| R.T. | retention time |
| conc. | concentration |
| ppt | precipitate |
| bs | broad singlet |
| t | triplet |
| qt | quartet |
| s | singlet |
| m | multiplet |
| DOM | directed ortho-metalation |
| DMG | direct metalation group |
| ORTEP | Oak Ridge thermal ellipsoid plot |

| | |
|---|---|
| KAAP | KBR Advanced Ammonia Process (KBR = Kellogg, Brown & Root) |
| D ₂ O | deuterium oxide |
| diox | 1,4-dioxane |
| C ₆ H ₆ | benzene |
| P(OPh) ₃ | triphenyl phosphate |
| H ₃ PO ₄ | phosphoric acid |
| MeNO ₂ | nitromethane |
| NH ₄ NO ₃ | ammonium nitrate |
| LiCl | lithium chloride |
| D ₂ O | deuterium oxide |
| H ₂ O | water |
| CO ₂ | carbon dioxide |
| CaH ₂ | calcium hydride |
| C | carbon |
| H | hydrogen or proton |
| N | nitrogen |
| S | sulphur |
| P | phosphorus |
| Fe | iron |
| Mo | molybdenum |
| Ru | ruthenium |
| Cr | chromium |
| Si | silicon |
| Al | aluminium |
| B | boron |
| Me ₃ SiI | iodotrimethylsilane |
| dba | trans, trans-dibenzylidene acetone |
| PdCl ₂ | palladium dichloride |
| Pd | palladium |
| <i>rac</i> -BINAP | <i>rac</i> -2,2'-bis(diphenylphosphino)-1,1'-binaphthalene |
| DPPF | 1,1'-bis(diphenylphosphino)ferrocene |
| Pd ₂ dba ₂ | tris(dibenzylideneacetone)dipalladium(0) |
| PdCl ₂ (CH ₃ CN) ₂ | dichloro-bis(acetonitrile)palladium(II) |
| PdCl ₂ (DPPF) | dichloro(1,1'-bis(diphenylphosphino)ferrocene)palladium(II) |

| | |
|---|---|
| CH ₃ CN | acetonitrile |
| Na ^t OBu | sodium tertiary butoxide |
| <i>o</i> -C ₆ H ₄ Br ₂ | 1,2-dibromobenzene |
| C ₆ H ₄ BrI | 1-bromo-2-iodobenzene |
| K ^t OBu | potassium tertiary butoxide |
| Br ₂ | bromine |
| TMEDA | N,N,N',N'-tetramethylethylenediamine |
| Et ₂ O | diethylether |
| Bu ₂ O | dibutylether |
| PPhCl ₂ | p,p-dichlorophenylphosphine |
| NMe ₃ .HCl | trimethylamine hydrochloride |
| tol ₂ NH | di-p-tolylamine |
| Ph ₂ NH | diphenylamine |
| ^{ph} NPNPPh | bis-(N-phenyl-2-(phenylamine)-phenylphosphine- P-phenyl-phosphonous diamide |
| DME | dimethoxyethane |
| P ⁱ Pr ₂ Cl | diisopropylchlorophosphine |
| PR ₂ Cl | dialkylchlorophosphine or diarylchlorophosphine |
| P ^t Bu ₃ | tri-tert-butylphosphine |
| PCy ₃ | tricyclohexylphosphine |
| PMe ₃ | trimethylphosphine |
| PPhMe ₂ | dimethylphenylphosphine |
| ^{naph} ArNH ₂ | 1-naphthylamine |
| ^{4-iPr} ArNH ₂ | 4-isopropylaniline |
| ^{4-iPr} ArNHLi | 4-isopropylphenylamidolithium |
| ^{2,6-iPr²} ArNH ₂ | 2,6-diisopropylaniline |
| Cp* | η^5 -C ₅ Me ₅ , pentamethylcyclopentadienyl |
| Cp | cyclopentadienyl |
| η^5 -C ₅ Me ₄ H | tetramethylcyclopentadienyl |
| ^{mes} NPNLi ₂ | bis-(N-mesityl-2-(4-methylphenyl)amidolithium)-phenylphosphine |
| ^{Si} NPNLi ₂ | bis-(N-phenyl-(N-dimethyl-methylenesilane)amidolithium)-phenylphosphine |
| ^{iprop} NPNLi ₂ | bis-(N-4-isopropyl-phenyl-2-phenylamidolithium)-phenylphosphine |

| | |
|---|--|
| $\text{Ph,mes}^{\text{NPNLi}}_2$ | bis-(N-mesityl-2-phenylamidolithium)-phenylphosphine |
| $\text{tol}^{\text{NPNLi}}_2$ | bis-[bis-(N-tolyl-2-(4-methylphenyl)amidolithium)-phenyl phosphine |
| $\text{ph}^{\text{NPNLi}}_2$ | bis-[bis-(N-phenyl-2-phenylamidolithium)-phenylphosphine |
| $\text{naph}^{\text{NPNLi}}_2$ | bis-(N-1-naphthyl-2-phenylamidolithium)-phenylphosphine |
| $2,6\text{-iPr}^2\text{NPNLi}_2$ | bis-(N-2,6-diisopropyl-phenyl-2-phenylamidolithium)-phenylphosphine |
| $\text{mes}^{\text{Ar}^{\text{Br}}\text{ArNH}}$ | N-mesityl-2-bromo-4-methylaniline |
| $\text{mes}^{\text{Ar}^{\text{Br-Ph}}\text{ArNH}}$ | N-mesityl-2-bromo-4-aniline |
| NBS | N-bromosuccinimide |
| $o\text{-(PhNH)}_2\text{C}_6\text{H}_4$ | N,N'-bis-phenyl-1,6-benzenediamine |
| $o\text{-(}^{\text{iprop}}\text{ArNH)}_2\text{C}_6\text{H}_4$ | N,N'-bis-4-isopropyl-phenyl-1,6-benzenediamine |
| $\text{iprop}^{\text{ArArNH}}$ | N-(4-isopropylphenyl)-aniline |
| $\text{iprop}^{\text{ArN(C}_6\text{H}_4\text{Br)}_2}$ | 2-bromo-N-(2-bromophenyl)-N-phenyl-benzenamine |
| $\text{iprop}^{\text{Ar}^{\text{Li}}\text{ArNLi}}$ | bis-(N-4-isopropyl-phenyl-2-lithiophenylamidolithium) |
| $[(\text{tol-Li}^{\text{Ar}})_2\text{NLi} \cdot \text{TMEDA}]_n$ | poly-(bis-(2-lithio-4-methyl-phenyl)-amido lithium \cdot TMEDA) |
| $\text{Si}^{\text{NPNLi}}_2 \cdot 2\text{THF}$ | bis-(N-phenyl-(N-dimethyl-methylenesilane)amidolithium)-phenylphosphine \cdot 2THF |
| $\text{iprop}^{\text{NPNLi}}_2 \cdot 2\text{THF}$ | bis-(N-4-isopropyl-phenyl-2-phenylamidolithium)-phenyl phosphine \cdot 2THF |
| $\text{iprop}^{\text{NPNLi}}_2 \cdot 4\text{THF}$ | bis-(N-4-isopropyl-phenyl-2-phenylamidolithium)-phenyl phosphine \cdot 4THF |
| $[\text{iprop}^{\text{NPNLi}}_2 \cdot 2\text{THF} \cdot \text{diox}]_n$ | poly-[bis-(N-4-isopropyl-phenyl-2-phenylamidolithium)-phenyl phosphine \cdot 2THF \cdot 1,4-dioxane] |
| $\text{tol}^{\text{NPNZrCl}_2(\text{Et}_2\text{O})}$ | dichloro-(bis-(N-tolyl-2-(4-methyl)-phenylamido)-phenylphosphine) (diethylether) zirconium(IV) |
| $o\text{-C}_6\text{H}_4\text{BrF}$ | 1-bromo-2-fluoro-benzene |
| $n\text{-BuLi}$ | <i>n</i> -butyllithium |
| tert-BuLi | <i>tert</i> -butyllithium |
| $\text{naph}^{\text{Ar}^{\text{Cl}}\text{ArNH}}$ | N-1-naphthyl-2-chloroaniline |
| DPEPhos | bis-(2-(diphenylphosphino)phenyl)ether |
| $\text{naph}^{\text{Ar}^{\text{H}}\text{ArNH}}$ | N-(1-naphthyl)-aniline |
| $\text{mes}^{\text{NPNH}_2}$ | bis-(N-mesityl-2-(4-methyl-phenylamine))-phenylphosphine |
| $\text{Ph,mes}^{\text{NPNH}_2}$ | bis-(N-mesityl-2-(phenylamine))-phenylphosphine |

| | |
|--|---|
| $[\text{Ph}^{\text{mes}}\text{NPNLi}_2\cdot\text{diox}]_n$ | poly-[bis-(N-mesityl-2-phenylamidolithium)-phenylphosphine·1,4-dioxane] |
| MesBr | 2-bromo-1,3,5-trimethylbenzene |
| PCy ₃ | tricyclohexylphosphine |
| PPh ₃ | triphenylphosphine |
| PNP | diphosphine amido |
| P ₂ N ₂ | diphosphine diamido |
| NPN | phosphine diamido |
| NPN(P) | diphosphine diamido |
| NPN(O) | phosphine diamido alkoxy |
| Ar ₂ NH | diarylamine |
| $[\text{Ar}_2\text{NLi}]_n$ | poly-[diarylamidolithium] |
| $[\text{Ar}_2\text{NLi}\cdot\text{TMEDA}]_2$ | bis-(diarylamidolithium·N,N,N',N'-tetramethylethylenediamine) |
| Ph-naph ArNH_2 | 2-phenylnaphthalen-1-amine |
| $\text{Ph-naph Ar}^{\text{Br}}\text{ArNH}$ | N-(2-bromophenyl)-2-phenylnaphthalen-1-amine |
| ZrCl ₄ (THF) ₂ | tetrachloro-bis(tetrahydrofuran)zirconium(IV) |
| ZrCl ₄ | tetrachlorozirconium(IV) |
| Zr(NMe ₂) ₄ | tetrakis(dimethylamino)zirconium(IV) |
| ZrCl ₂ (NMe ₂) ₂ (DME) | dichloro-bis-(dimethylamino)(1,2-dimethoxyethane)zirconium(IV) |
| TMSCl | chlorotrimethylsilane |
| KC ₈ | potassium graphite |
| P ^t Bu ₃ | tris-tert-butylphosphine |
| dmpe | 1,2-Bis(dimethylphosphino)ethane |
| THT | tetrahydrothiophene |
| xylylNC | 2,6-dimethylphenylisocyanide |
| ^t BuNC | <i>tert</i> -butylisocyanide |
| PhSiH ₃ | phenylsilane |
| TiCl ₄ | tetrachlorotitanium(IV) |
| Ti(NMe ₂) ₄ | tetrakis(dimethylamino)titanium(IV) |
| Hf(NMe ₂) ₄ | tetrakis(dimethylamino)hafnium(IV) |
| [TaCl ₅] ₂ | pentachlorotantalum(V) |
| Ta(NMe ₂) ₅ | pentakis(dimethylamino)tantalum(V) |
| $[\text{TaCl}_3(\text{PMe}_3)_2]_2$ | Trichloro-bis-(trimethylphosphine) tantalum(III) dimer |

| | |
|--|--|
| $[\text{}^{\text{iprop}}\text{NPNTaCl}(\text{PMe}_3)]_2$ | Chloro[(bis-N-4-isopropyl-phenyl-2-phenylamido)-phenylphosphine](trimethylphenylphosphine) tantalum (III) dimer |
| $[\text{}^{\text{iprop}}\text{NPNTaCl}]_2$ | Chloro[(bis-N-4-isopropyl-phenyl-2-phenylamido)-phenylphosphine] tantalum (III) dimer |
| $[\text{}^{\text{iprop}}\text{NPNTaCl}]_x$ | Chloro[(bis-N-4-isopropyl-phenyl-2-phenylamido)-phenylphosphine] tantalum (III) if $x = 1$, or dimer (if $x = 2$), etc. |
| $[\text{}^{\text{iprop}}\text{NPNTaCl}_4]$ | Tetrachloro[(bis-N-4-isopropyl-phenyl-2-phenylamido)-phenylphosphine]tantalum(V) anion |
| $[\text{}^{\text{iprop}}\text{NPNTaCl}_2]$ | Dichloro[(bis-N-4-isopropyl-phenyl-2-phenylamido)-phenylphosphine] tantalum(V) cation |
| $[\text{}^{\text{tol}}\text{NPNTaCl}_4]$ | Tetrachloro[(bis-(N-tolyl-2-(4-methyl)-phenylamido)-phenylphosphine]tantalum(V) anion |
| $[\text{}^{\text{tol}}\text{NPNTaCl}_2]$ | Dichloro[(bis-(N-tolyl-2-(4-methyl)-phenylamido)-phenylphosphine] tantalum(V) cation |
| $\text{}^{\text{Si}}\text{NP}(\text{C})\text{NTa}(\text{NMe}_2)_2$ | [(N-phenyl-(N-dimethyl-methylenesilane-phenylphosphino))-(N-phenyl-(N-dimethyl-silane)-methane]-bis-(dimethylamido)tantalum (V) |
| $[\{\text{}^{\text{iprop}}\text{NPNTaMe}_2\}_2]\text{Cl}_2$ | bis-[Dimethyl-[(bis-N-4-isopropyl-phenyl-2-phenylamido)-phenylphosphine] tantalum (V)] dichloride (or species \mathbf{u}_{ipr}) |
| $[\{\text{}^{\text{tol}}\text{NPNTaMe}_2\}_2]\text{Cl}_2$ | bis-[Dimethyl-[(bis-N-tolyl-2-(4-methyl)-phenylamido)-phenylphosphine] tantalum (V)] dichloride (or species \mathbf{u}_{tol}) |
| $\text{}^{\text{tol}}\text{NPNTaBn}_3$ | Tribenzyl-[(bis-N-tolyl-2-(4-methyl)-phenylamido)-phenylphosphine] tantalum (V) |
| KHBet_3 | potassium triethylborohydride |
| KH | potassium hydride |

List of Compounds

$^{iprop}Ar^{Br}ArNH$ [2.1]: N-4-isopropyl-phenyl-2-bromoaniline

$[^{tol}Ar^{Li}ArNLi \cdot TMEDA]_2$ [2.2]: bis-(N-4-methyl-phenyl-(2-lithio-4-methyl-phenyl)-amido lithium TMEDA)

$[^{ph}Ar^{Li}ArNLi \cdot 1.5TMEDA]_2$ [2.3]: bis-[N-phenyl-(2-lithio-phenyl)amidolithium \cdot 1.5TMEDA]

$^{tol}Ar^DArND$ [2.4]: N-4-methyl-phenyl-(2-deuterio-4-methyl-phenyl)-deuterioamine

$^{ph}Ar^DArND$ [2.5]: N-phenyl-(2-deuterio-phenyl)-deuterioamine

$[^{iprop}NPnLi_2 \cdot diox]_n$ [2.6]: poly-[bis-(N-4-isopropyl-phenyl-2-phenylamidolithium)-phenyl phosphine dioxane]

$[^{tol}NPnLi_2 \cdot 1.5TMEDA]_2$ [2.7]: bis-[bis-(N-tolyl-2-(4-methylphenyl)amidolithium)-phenyl phosphine \cdot 1.5 TMEDA]

$[^{ph}NPnLi_2 \cdot 1.5TMEDA]_2$ [2.8]: bis-[bis-(N-phenyl-2-phenylamidolithium)-phenylphosphine \cdot 1.5TMEDA]

$^{tol}NPnPPh$ [2.9]: bis-(N-tolyl-2-(4-methyl-phenylamine))-phenylphosphine- P- phenyl -phosphonous diamide

$^{iprop}NPnNH_2$ [2.10]: bis-(N-4-isopropyl-phenyl-2-phenylamine)-phenylphosphine

$^{tol}NPnNH_2$ [2.11]: bis-(N-tolyl-2-(4-methyl-phenylamine))-phenylphosphine

$^{ph}NPnNH_2$ [2.12]: bis-(N-phenyl-2-(phenylamine))-phenylphosphine

$[^{iprop}NPn]_2Zr$ [3.1]: bis-[bis-(N-4-isopropyl-phenyl-2-phenylamido)-phenylphosphine] zirconium(IV)

$[^{tol}NPn]_2Zr$ [3.2]: bis-[bis-(N-tolyl-2-(4-methyl)-phenylamido)-phenylphosphine]zirconium(IV)

$^{iprop}NPnZrCl_2(HNMe_2)$ [3.3]: Dichloro-(bis-(N-4-isopropyl-phenyl-2-phenylamido)-phenyl phosphine)(dimethylamine) zirconium(IV)

$^{tol}NPnZrCl_2(HNMe_2)$ [3.4]: Dichloro-(bis-(N-tolyl-2-(4-methyl)-phenylamido)-phenyl phosphine)(dimethylamine) zirconium(IV)

$^{iprop}NPnZrCl_2(THF)$ [3.5]: Dichloro-(bis-(N-4-isopropyl-phenyl-2-phenylamido)-phenyl phosphine)(tetrahydrofuran) zirconium(IV)

$^{tol}NPnZrCl_2(THF)$ [3.6]: Dichloro-(bis-(N-tolyl-2-(4-methyl)-phenylamido)-phenylphosphine) (tetrahydrofuran) zirconium(IV)

$^{iprop}NPnZr(NMe_2)_2$ [3.7]: (bis-(N-4-tolyl-2-(4-methyl)-phenylamido)-phenylphosphine)-bis-(dimethylamido) zirconium (IV)

$^{tol}NPnZr(NMe_2)_2$ [3.8]: (bis-(N-4-tolyl-2-(4-methyl)-phenylamido)-phenylphosphine)-bis-(dimethylamido) zirconium (IV)

$[^{iprop}NPnZrCl_2]_2$ [3.9]: bis-[Dichloro-(bis-(N-4-isopropyl-phenyl-2-phenylamido)-phenyl

- phosphine) zirconium(IV)]
- [^{tol}NPNTiCl₂]₂ [3.10]:** bis-[Dichloro-(bis-(N-tolyl-2-(4-methyl)-phenylamido)-phenyl phosphine) zirconium(IV)]
- ^{iprop}NPNTiCl₂(HMe₂) [3.11]:** Dichloro-(bis-(N-4-isopropyl-phenyl-2-phenylamido)-phenyl phosphine)(dimethylamine) titanium (IV)
- ^{tol}NPNTiCl₂(HMe₂) [3.12]:** Dichloro-(bis-(N-tolyl-2-(4-methyl)-phenylamido)-phenyl phosphine)(dimethylamine) titanium (IV)
- ^{iprop}NPNTiCl₂(THF) [3.13]:** Dichloro-(bis-(N-4-isopropyl-phenyl-2-phenylamido)-phenyl phosphine)(tetrahydrofuran) titanium (IV)
- ^{tol}NPNTiCl₂(THF) [3.14]:** Dichloro-(bis-(N-tolyl-2-(4-methyl)-phenylamido)-phenylphosphine) (tetrahydrofuran) titanium (IV)
- ^{iprop}NPNTi(NMe₂)₂ [3.15]:** (bis-(N-4-tolyl-2-(4-methyl)-phenylamido)-phenylphosphine)-bis-(dimethylamido) titanium (IV)
- ^{tol}NPNTi(NMe₂)₂ [3.16]:** (bis-(N-4-tolyl-2-(4-methyl)-phenylamido)-phenylphosphine)-bis-(dimethylamido) zirconium (IV)
- ^{iprop}NPNTiCl₂ [3.17]:** Dichloro-(bis-(N-4-isopropyl-phenyl-2-phenylamido)-phenylphosphine) titanium (IV)
- ^{tol}NPNTiCl₂ [3.18]:** Dichloro-(bis-(N-tolyl-2-(4-methyl)-phenylamido)-phenylphosphine) titanium (IV)
- ^{iprop}NPNTi(NMe₂)₂ [3.19]:** (bis-(N-4-tolyl-2-(4-methyl)-phenylamido)-phenylphosphine)-bis-(dimethylamido) hafnium (IV)
- [^{iprop}NPNTiCl₂]₂ [3.20]:** bis-[Dichloro-(bis-(N-4-isopropyl-phenyl-2-phenylamido)-phenyl phosphine) hafnium(IV)]
- ^{iprop}NPNTiCl₂(THF) [3.21]:** Dichloro-(bis-(N-4-isopropyl-phenyl-2-phenylamido)-phenyl phosphine)(tetrahydrofuran) hafnium (IV)
- ^{iprop}NPNTa(NMe₂)₃ [4.1]:** [(bis-N-4-isopropyl-phenyl-2-phenylamido)-phenyl phosphine]-tris-(dimethylamido)tantalum (V)
- ^{tol}NPNTa(NMe₂)₃ [4.2]:** [(bis-N-tolyl-2-(4-methyl)-phenylamido)-phenyl phosphine]-tris-(dimethylamido)tantalum (V)
- ^{Ph}NPNTa(NMe₂)₃ [4.3]:** [(bis-N-bis-phenylamido)-phenylphosphine]-tris-(dimethylamido)tantalum (V)
- ^{iprop}NPNTaCl₃ [4.4]:** Trichloro-[(bis-N-4-isopropyl-phenyl-2-phenylamido)-phenyl phosphine] tantalum (V)
- ^{tol}NPNTaCl₃ [4.5]:** Trichloro-[(bis-N-tolyl-2-(4-methyl)-phenylamido)-phenyl

phosphine] tantalum (V)

^{Ph}**NPNTaCl₃ [4.6]:** Trichloro-[(bis-N-bis-phenylamido)-phenylphosphine]
tantalum (V)

^{tol}**NPNTaMe₃ [4.7]:** Trimethyl-[(bis-N-tolyl-2-(4-methyl)-phenylamido)-phenyl
phosphine] tantalum (V)

^{iprop}**NPNTaMe₃ [4.8]:** Trimethyl-[(bis-N-4-isopropyl-phenyl-2-phenylamido)-phenyl
phosphine] tantalum (V)

^{tol}**NPNTaMe₄Li(Et₂O) [4.13]:** Tetramethyl-[(bis-N-tolyl-2-(4-methyl)-phenylamido)-phenyl
phosphine] tantalum (V) lithium diethylether (**or species tol_{4MeLi}**)

[^{tol}**NPNTaMe₄][Li(THF)₄] [4.14]:** Tetramethyl-[(bis-N-tolyl-2-(4-methyl)-phenylamido)-phenyl
phosphine] tantalum (V) lithium tetrakis-tetrahydrofuran

^{tol}**NPNTaMe₄Li(THF) [4.15]:** Tetramethyl-[(bis-N-tolyl-2-(4-methyl)-phenylamido)-phenyl
phosphine] tantalum (V) lithium tetrahydrofuran (**or species tol_{4MeLi}**)

[^{iprop}**NPNTaH**]₂(N₂) [4.17]: Bis-{[(bis-N-4-isopropyl-phenyl-2-phenylamido)-phenyl
phosphine] tantalum (V) hydride}(dinitrogen)

[^{iprop}**NPNTaH**]₂(NBt₃)₂(N₂)₂ [4.17a]: Bis-{[(bis-N-4-isopropyl-phenyl-2-phenylamido)-phenyl
phosphine] tantalum (V) hydride}(hexaethyl-diboron- μ - η^1 : η^1 -N,N'-hydrazine)(bis-
dinitrogen)

[^{tol}**NPNTaH**]₂(N₂) [4.18]: Bis-{[(bis-N-tolyl-2-(4-methyl)-phenylamido)-phenyl
phosphine] tantalum (V) hydride}(dinitrogen)

[^{tol}**NPNTaH**]₂(NBt₃)₂(N₂)₂ [4.18a]: Bis-{[(bis-N-tolyl-2-(4-methyl)-phenylamido)-phenyl
phosphine] tantalum (V) hydride} (hexaethyl-diboron- μ - η^1 : η^1 -N,N'-hydrazine)(bis-
dinitrogen)

[^{iprop}**NPNTaCl**]₂(N₂) [4.19]: Bis-{[(bis-N-4-isopropyl-phenyl-2-phenylamido)-phenyl
phosphine] tantalum (V) chloride}(dinitrogen)

[^{tol}**NPNTaCl**]₂(N₂) [4.20]: Bis-{[(bis-N-tolyl-2-(4-methyl)-phenylamido)-phenyl
phosphine] tantalum (V) chloride}(dinitrogen)

[^{iprop}**NPNZr(THF)**]₂(μ - η^2 : η^2 -N₂) [5.1]: Bis{[bis-(N-4-isopropyl-phenyl-2-phenylamido)-
phenylphosphine](tetrahydrofuran) zirconium(IV)}(μ - η^2 : η^2 -dinitrogen)

[^{iprop}**NPNZr(THF)**]₂(μ - η^2 : η^2 -¹⁵N₂) [5.2]: Bis{[bis-(N-4-isopropyl-phenyl-2-phenylamido)-
phenylphosphine](tetrahydrofuran) zirconium(IV)}(μ - η^2 : η^2 -dinitrogen-15)

[^{tol}**NPNZr(THF)**]₂(μ - η^2 : η^2 -N₂) [5.3]: Bis{[(bis-N-tolyl-2-(4-methyl)-phenylamido)-phenyl
phosphine](tetrahydrofuran) zirconium(IV)}(μ - η^2 : η^2 -dinitrogen)

[^{tol}**NPNZr(Py)**]₂(μ - η^2 : η^2 -N₂) [5.4]: bis{[(bis-N-tolyl-2-(4-methyl)-phenylamido)-phenyl

- phosphine](pyridine) zirconium(IV)}(μ - η^2 : η^2 -dinitrogen)
- [^{tol}NPNZr(Py-*d*₅)]₂(μ - η^2 : η^2 -N₂) [5.5]: bis{[(bis-N-tolyl-2-(4-methyl)-phenylamido)-phenyl phosphine](pyridine-*d*₅) zirconium(IV)}(μ - η^2 : η^2 -dinitrogen)
- [^{iprop}NPNZr(4,4'-bipy)]₂(μ - η^2 : η^2 -N₂) [5.6]: bis{[bis-(N-4-isopropyl-phenyl-2-phenylamido)-phenylphosphine](4,4'-bipyridine)zirconium(IV)}(μ - η^2 : η^2 -dinitrogen)
- {[^{iprop}NPNZr]₂(4,4'-bipy)(μ - η^2 : η^2 -N₂)}_n [5.6a]: poly-{bis{[bis-(N-4-isopropyl-phenyl-2-phenylamido)-phenylphosphine]zirconium(IV)}(4,4'-bipyridine)(μ - η^2 : η^2 -dinitrogen)}
- [^{iprop}NPNZr(THF)](μ - η^2 : η^2 -N₂)[^{iprop}NPNZr(PMe₃)] [5.7]: {[bis-(N-4-isopropyl-phenyl-2-phenylamido)-phenylphosphine](tetrahydrofuran) zirconium(IV)}{[bis-(N-4-isopropyl-phenyl-2-phenylamido)-phenylphosphine](trimethylphosphine) zirconium(IV)}(μ - η^2 : η^2 -dinitrogen)
- [^{iprop}NPNZr(PMe₃)]₂(μ - η^2 : η^2 -N₂) [5.8]: Bis{[bis-(N-4-isopropyl-phenyl-2-phenylamido)-phenylphosphine](trimethylphosphine) zirconium(IV)}(μ - η^2 : η^2 -dinitrogen)
- [^{tol}NPNZr(PMe₃)]₂(μ - η^2 : η^2 -N₂) [5.9]: Bis{[(bis-N-tolyl-2-(4-methyl)-phenylamido)-phenyl phosphine](trimethylphosphine) zirconium(IV)}(μ - η^2 : η^2 -dinitrogen)
- [^{iprop}NPNZr(PPMe₂)]₂(μ - η^2 : η^2 -N₂) [5.10]: Bis{[bis-(N-4-isopropyl-phenyl-2-phenylamido)-phenylphosphine](dimethylphenylphosphine) zirconium(IV)}(μ - η^2 : η^2 -dinitrogen)
- [^{tol}NPNZr(PPhMe₂)]₂(μ - η^2 : η^2 -N₂) [5.11]: Bis{[(bis-N-tolyl-2-(4-methyl)-phenylamido)-phenyl phosphine](dimethylphenylphosphine) zirconium(IV)}(μ - η^2 : η^2 -dinitrogen)
- [^{iprop}NPNZr(THT)]₂(μ - η^2 : η^2 -N₂) [5.12]: Bis{[bis-(N-4-isopropyl-phenyl-2-phenylamido)-phenylphosphine](tetrahydrothiophene) zirconium(IV)}(μ - η^2 : η^2 -dinitrogen)
- [^{tol}NPNZr(THT)]₂(μ - η^2 : η^2 -N₂) [5.14]: Bis{[bis-(N-4-isopropyl-phenyl-2-phenylamido)-phenyl phosphine](tetrahydrothiophene) zirconium(IV)}(μ - η^2 : η^2 -dinitrogen)
- [^{tol}NPNTi(THF)]₂(μ - η^1 : η^1 -N₂) [5.15]: Bis{[(bis-N-tolyl-2-(4-methyl)-phenylamido)-phenyl phosphine](tetrahydrofuran) titanium(IV)}(μ - η^1 : η^1 -dinitrogen)
- [^{tol}NPNTi(THF)]₂(μ - η^1 : η^1 -N₂) [5.16]: Bis{[(bis-N-tolyl-2-(4-methyl)-phenylamido) phenylphosphine](bis-tetrahydrofuran) titanium(IV)}(μ - η^1 : η^1 -dinitrogen)
- [^{iprop}NPNTi(THF)]₂(μ - η^1 : η^1 -N₂) [5.17]: Bis{[bis-(N-4-isopropyl-phenyl-2-phenylamido)-phenylphosphine](tetrahydrofuran) titanium(IV)}(μ - η^1 : η^1 -dinitrogen)
- cis*-[^{tol}NPNTi(Py)]₂(μ - η^1 : η^1 -N₂) [5.18]: Bis{[(bis-N-tolyl-2-(4-methyl)-phenylamido)-phenyl phosphine]*cis*-(pyridine) titanium(IV)}(μ - η^1 : η^1 -dinitrogen)
- trans*-[^{tol}NPNTi(Py)]₂(μ - η^1 : η^1 -N₂) [5.18a]: Bis{[(bis-N-tolyl-2-(4-methyl)-phenylamido)-phenyl phosphine]*trans*-(pyridine) titanium(IV)}(μ - η^1 : η^1 -dinitrogen)
- trans*-[^{tol}NPNTi(Py)]₂(μ - η^1 : η^1 -N₂) [5.19]: Bis{[(bis-N-tolyl-2-(4-methyl)-phenylamido)-phenyl

- phosphine]*trans*-(bis-pyridine) titanium(IV)}(μ - η^1 : η^1 -dinitrogen)
- cis*-[^{tol}NPNTi(Py)₂]₂(μ - η^1 : η^1 -N₂) [5.19a]: Bis{[(bis-N-tolyl-2-(4-methyl)-phenylamido)-phenyl phosphine]*cis*-(bis-pyridine) titanium(IV)}(μ - η^1 : η^1 -dinitrogen)
- trans*-[^{tol}NPNTi(Py-*d*₅)₂]₂(μ - η^1 : η^1 -N₂) [5.19b]: Bis{[(bis-N-tolyl-2-(4-methyl)-phenylamido)-phenylphosphine]*trans*-(bis-pyridine-deuterium) titanium(IV)}(μ - η^1 : η^1 -dinitrogen)
- [^{tol}NPNTi(2,2'-bipy)₂]₂(μ - η^1 : η^1 -N₂) [5.20]: Bis{[(bis-N-tolyl-2-(4-methyl)-phenylamido)-phenyl phosphine](2,2'-bipyridine) titanium(IV)}(μ - η^1 : η^1 -dinitrogen)
- [^{tol}NPNTiH₂]₂ [5.21]: Bis-{[(bis-N-tolyl-2-(4-methyl)-phenylamido)-phenyl phosphine] titanium (IV) hydride }
- [^{iprop}NPNZr(THF)](xylylNC-N₂)[^{iprop}NPNZr(xylylNC)] [6.1]: {[bis-(N-4-isopropyl-phenyl-2-phenylamido)-phenylphosphine](tetrahydrofuran) zirconium(IV)}{[bis-(N-4-isopropyl-phenyl-2-phenylamido)-phenylphosphine](2,6-dimethylphenylisocyanide) zirconium(IV)}(N-(2,6-dimethylphenyl)methanimine-hydrazide)
- [^{iprop}NPNZr(THF)](xylylNC-¹⁵N₂)[^{iprop}NPNZr(xylylNC)] [6.2]: {[bis-(N-4-isopropyl-phenyl-2-phenylamido)-phenylphosphine](tetrahydrofuran) zirconium(IV)}{[bis-(N-4-isopropyl-phenyl-2-phenylamido)-phenylphosphine](2,6-dimethylphenylisocyanide) zirconium(IV)}(N-(2,6-dimethylphenyl)methanimine-hydrazide-15N)
- [^{tol}NPNZr(THF)](xylylNC-N₂)[^{tol}NPNZr(xylylNC)] [6.3]: {[bis-(N-tolyl-2-(4-methyl)-phenylamido)-phenylphosphine](tetrahydrofuran) zirconium(IV)}{[(bis-N-tolyl-2-(4-methyl)-phenylamido)-phenylphosphine](2,6-dimethylphenylisocyanide) zirconium(IV)}(N-(2,6-dimethylphenyl)methanimine-hydrazide)
- [^{iprop}NPNZr(THF)](^tBuNC-N₂)[^{iprop}NPNZr(^tBuNC)] [6.4]: {[bis-(N-4-isopropyl-phenyl-2-phenylamido)-phenylphosphine](tetrahydrofuran) zirconium(IV)}{[bis-(N-4-isopropyl-phenyl-2-phenylamido)-phenylphosphine](*tert*-butylisocyanide) zirconium(IV)}(N-(*tert*-butyl)methanimine-hydrazide)
- [^{tol}NPNZr(THF)](^tBuNC-N₂)[^{tol}NPNZr(^tBuNC)] [6.5]: {[bis-(N-tolyl-2-(4-methyl)-phenyl amido)-phenylphosphine](tetrahydrofuran) zirconium(IV)}{[(bis-N-tolyl-2-(4-methyl)-phenylamido)-phenylphosphine](*tert*-butylisocyanide) zirconium(IV)}(N-(*tert*-butyl)methanimine-hydrazide)
- ^{naph}Ar^{Br}ArNH [7.1]: N-1-Naphthyl-2-bromoaniline
- ^{2,6-iPr2}Ar^{Br}ArNH [7.2]: N-2,6-Diisopropylphenyl-2-bromoaniline
- [^{2,6-iPr2}Ar^{Li}ArNLi]_n [7.3]: poly-{bis-(N-2,6-diisopropyl-phenyl-2-lithiophenylamidolithium)}
- [^{2,6-iPr2}Ar^{Li}ArNLi·2THF]₂ [7.3a]: Di-{bis-(N-2,6-diisopropyl-phenyl-2-lithiophenylamidolithium)·bis-tetrahydrofuran }

$[\text{}^{\text{naph}}\text{Ar}^{\text{Li}}\text{ArNLi}\cdot 2\text{Et}_2\text{O}]_2$ **[7.4]**: Di-{bis-(N-2-naphthyl-2-lithiophenylamidolithium)·bis-diethyl ether}

$[\text{}^{\text{naph}}\text{Ar}^{\text{Li}}\text{ArNLi}\cdot 2\text{THF}]_2$ **[7.5]**: Di-{bis-(N-2-naphthyl-2-lithiophenylamidolithium)·bis-tetrahydrofuran}

$[\text{}^{\text{naph}}\text{NPnLi}_2\cdot \text{diox}]_n$ **[7.6]**: poly-{bis-(N-1-naphthyl-2-phenylamidolithium)-phenylphosphine·dioxane}

$[\text{}^{\text{naph}}\text{NPnLi}_2\cdot 1.5\text{diox}]_n$ **[7.6a]**: poly{di-[bis-(N-1-naphthyl-2-phenylamidolithium)-phenyl phosphine]·tris-dioxane}

$[\text{}^{\text{naph}}\text{NPnLi}_2\cdot \text{diox}\cdot 2\text{THF}]_n$ **[7.6b]**: poly-{bis-(N-1-naphthyl-2-phenylamidolithium)-phenyl phosphine·dioxane·bis-tetrahydrofuran}

$[\text{}^{2,6-i\text{Pr}2}\text{NPnLi}_2\cdot \text{diox}]_n$ **[7.7]**: poly-{bis-(N-2,6-diisopropyl-phenyl-2-phenylamidolithium)-phenyl phosphine·dioxane}

$[\text{}^{2,6-i\text{Pr}2}\text{NPnLi}_2\cdot 1.5\text{diox}]_n$ **[7.7a]**: poly-{di-[bis-(N-2,6-diisopropyl-phenyl-2-phenylamidolithium)-phenylphosphine]·tris-dioxane}

$\text{}^{2,6-i\text{Pr}2}\text{NPnLi}_2\cdot 2\text{Et}_2\text{O}$ **[7.7b]**: bis-(N-2,6-diisopropyl-phenyl-2-phenylamidolithium)-phenyl phosphine·bis-diethylether

$\text{}^{2,6-i\text{Pr}2}\text{NPnLi}_2\cdot 3\text{Et}_2\text{O}$ **[7.7c]**: bis-(N-2,6-diisopropyl-phenyl-2-phenylamidolithium)-phenyl phosphine·tris-diethylether

$\text{}^{\text{naph}}\text{NPnH}_2$ **[7.8]**: bis-(N-1-naphthyl-2-phenylamine)-phenylphosphine

$\text{}^{2,6-i\text{Pr}2}\text{NPnH}_2$ **[7.9]**: bis-(N-2,6-diisopropyl-phenyl-2-phenylamine)-phenylphosphine

Acknowledgements

Within this allotted space, I am unable to give thanks in a fair and equitable way to all those persons who have helped me in so many ways through the different stages of my journey of scientific and personal discovery to the final completion of this thesis document.

I will thus limit myself to those of direct relevance to the production, interpretation and presentation of this body of work. To my research supervisor, Prof. Michael Fryzuk, for his unwavering support and guidance for the lifetime of the project and to Prof. Laurel Schafer, whose crucial assistance at two important pivotal occasions was invaluable.

To the Fryzuk Group Research Members for advice on laboratory matters and friendly scientific discourse and the Technical, Mechanical and Analytic Support Services at the UBC Chemistry Department.

Dedication

A major navigational prize of the 18th century was the location of the southern continent Antarctica. This goal inspired Captain James Cook's expeditions of discovery in the Pacific Ocean. Towards the end of his first voyage from 1768 to 1771 on the ship *Endeavor*, he navigated the east coast of New Holland (a.k.a. Australia) through the treacherous Great Barrier Reef. Below is an excerpt from his diary days before he passed through the *Endeavour Strait* between the mainland and Prince of Wales, in the process proving that New Guinea and New Holland were not a continuous landmass.

"...our depth of water in the Channell was from 30 to 7 fathom very erregular soundings and foul ground until we had got quite within the Reef where we anchor'd in 19 fathom a Corally & Shelly bottom happy once more to encounter those shoals which but two days ago our utmost wishes were crowned by geting clear of, such are the Vicissitudes attending this kind of service and must always attend an unknown Navigation: Was it not for the pleasure which naturly results to a Man from being the first discoverer, even was it nothing more than sands and Shoals, this service would be insupportable especially in far distant parts, like this, short of Provisions and almost every other necessary. The world will hardly admit of an excuse for a man leaving a Coast unexplored he has once discover'd, if dangers are his excuse he is than charged with *Timorousness* and want of Perseverance and at once pronounced the unfitest man in the world to be employ'd as a discoverer; if on the other hand he boldy incounters all the dangers and obstacles he meets and is unfortunate enough not to succeed he is than charged with *Temerity* and want of conduct..."

On repairing his ship at Batavia before his return trip to Europe, he had the following to say about the condition of the keel of *Endeavour* "... so that it was a Matter of Surprise to every one who saw her bottom how we had kept her above water; and yet in these conditions we had

sailed some hundreds of Leagues in as dangerous a Navigation as in any part of the world, happy in being ignorant of the continual danger we were in.”

These insights from Captain Cook should resonate with anyone pursuing new journeys of scientific discovery. First and foremost, one has to create a vision and thereafter have the excitement and resolution to follow through with requisite scientific rigour, mindful always of the fact that even negative results can lead to the advancement of knowledge. The personal delight in contributing towards concepts and discoveries greater than the individual, with potential gargantuan scientific consequences should be muted by the humbleness displayed in a quote by Sir Isaac Newton “If I have seen further it is by standing on the shoulders of giants”.

Chapter 1: Introduction

1.1. Historical Context

Nitrogen is essential for life and the conversion of N_2 to ammonia is a crucial step in the nitrogen cycle.¹⁻³ Atmospheric nitrogen can enter into the cycle via biological fixation (nitrogenase enzymes), lightning mediated oxidation and industrial fixation.

Earlier competing industrial nitrogen fixation technologies such as the Birkelan-Eyde process (also known as Norwegian Arc), the Frank-Caro cyanamide process and by-product ammonia recovery from coke ovens all proved inferior to the Haber-Bosch process.³⁻⁵ The Haber-Bosch process, whereby ammonia is produced from nitrogen and hydrogen gasses was developed by Fritz Haber in 1905-1909⁶⁻⁸ and commercialised by Carl Bosch for BASF, with the first plant being built in Oppau in 1913.⁵ Haber received the Nobel Prize in 1918 for his invention, and later in 1931 Bosch (joint with Friedrich Bergius) received the Nobel Prize for his contributions towards the development of industrial chemical high pressure methods.

Although the Haber-Bosch process is highly efficient, it is energy intensive due to the high temperatures (400-500 °C) and pressures (130 to 300 atm) of operation.^{4, 9, 10} The predominant solid state pre-catalyst is composed of iron oxide (magnetite or wustite) with traces of oxide promoters (Al, Mg, Si, Ca and K). More recently, catalysts with ruthenium on graphite or boron nitride allow for slightly lower operating pressures (KAAP process).^{4, 11}

To this day, ammonia production via the Haber-Bosch process remains the only economically viable industrial process,^{9, 12} with an annual global production estimated at over 100 to 130 million metric tons.¹³⁻¹⁵ Ammonium salts, nitrates and urea for fertilizer utilization accounts for the largest ammonia consumption, with an estimated annual 70 million metric tons³ and approximately 87% of US domestic ammonia use in 2010 was for fertilizers.¹⁵ Ammonia and nitric acid (derived from ammonia via the Ostwald process^{16, 17}) are essential building blocks for nitrogen-containing chemical classes such as amines, amides and nitriles, which are precursors to

compounds with applications in diverse industries such explosives,^{18, 19} pharmaceuticals²⁰ and synthetic fibres.²¹

As with industrial fixation, the biological fixation process needs the intervention of a transition metal catalyst, located within the MoFe protein of the nitrogenase enzymes complex.^{10, 22-33} Vanadium and ‘iron-only’ variations of dinitrogenase proteins also exist and the V and Fe ions are thought to occupy similar positions to the Mo atom.^{27, 34-36} The high energy requirement for the conversion is reflected in the large number of adenosine triphosphate (ATP) molecules consumed by the Fe protein (dinitrogenase reductase) during the natural process (16 ATP ~ 468.6 kJ.mol⁻¹).^{10, 28, 37} Biotic ammonia production is higher than industrial fixation with an estimated annual production of 170 million metric tons.^{10, 38}

In contrast to the heterogeneous solid-gas Haber-Bosch process, biological fixation takes place in a homogeneous aqueous medium at mild temperatures (290 K) and pressures (0. 8 atm). The FeMo cofactor (7Fe-9S-Mo-C-homocitrate) within the MoFe protein has been associated with substrate binding^{5, 26, 33} and the Thorneley-Lowe model⁵ depicts increasingly more oxidised electronic states of the MoFe cofactor from the most reduced (E₀) to the most oxidised (E₇), as a series of 8 electrons and 8 protons are sequentially added to N₂ to liberate 2 NH₃ + H₂.^{26, 29, 31, 39}

It is of considerable interest to develop a low temperature and pressure alternative for the Haber-Bosch process. While steady-state assays⁴⁰ of natural nitrogenases are able to replicate catalytic conversion of N₂ to NH₃, strategies focusing on biosynthesis of the MoFe protein^{41, 42} or biomimetic transition metal clusters^{31, 43-45} have yielded no successful results.

In a more traditional chemical approach, the isolation of the first discrete N₂ complex [Ru(NH₃)₅(N₂)]²⁺ in 1965⁴⁶⁻⁴⁸ paved the way for the development in 1976 of the Chatt cycle (Figure 1), which is a hypothetical model for nitrogenase action with mononuclear dinitrogen complexes.^{26, 30}

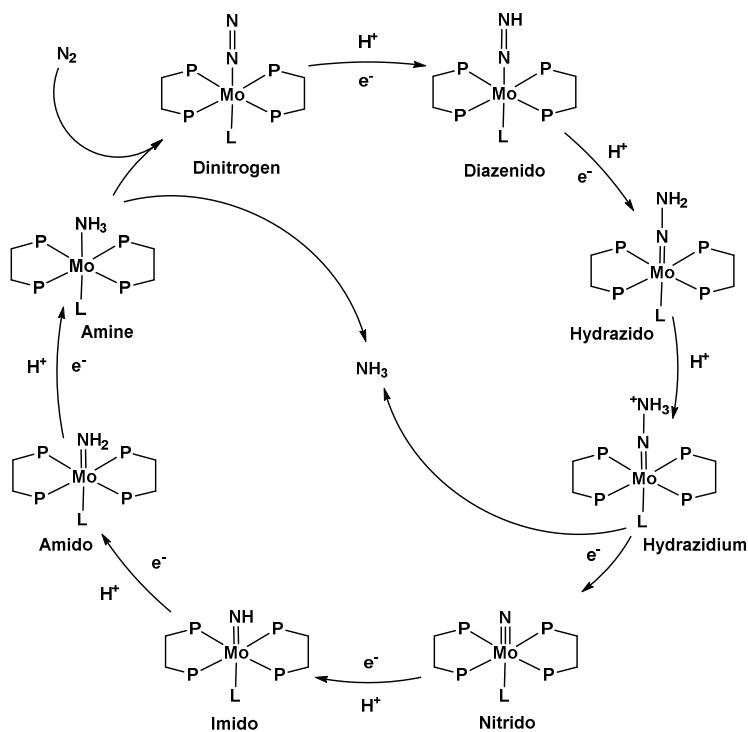


Figure 1: Chatt cycle for mononuclear molybdenum complexes ($\text{Mo}^0\text{-Mo}^{\text{VI}}$)²⁶

While the rationale for this approach is not based on direct mimicry of nitrogenase,^{27, 49} many researchers use the metals implicated in nitrogenase enzymes as a starting point, thus accounting for focussed investigations of molybdenum⁵⁰⁻⁵⁴ (or tungsten⁵⁵⁻⁵⁸), iron⁵⁹⁻⁶³ (or ruthenium⁵³) and vanadium⁶⁴⁻⁶⁶ (or niobium⁶⁷⁻⁷¹ and tantalum⁷²⁻⁸¹) containing systems, and with sulphur-binding thiolate ligands.^{61, 62, 82, 83} The first homogeneous transition metal complex to generate NH_3 via fixation of N_2 , however, was a titanium complex reported by Vol'pin and Shur in 1964⁸⁴⁻⁸⁷ and this served to cement group 4 metals as suitable dinitrogen activator candidates.

A landmark breakthrough was achieved by Schrock et al (Figure 2) with the first homogeneous mononuclear catalyst exhibiting four turnovers of NH_3 with respect to one molybdenum atom at room temperature and pressure.⁵¹ The oxidation states in the Schrock system ($\text{Mo}^{\text{III}}\text{-Mo}^{\text{VI}}$) are not as reduced as proposed in the Chatt cycle ($\text{Mo}^0\text{-Mo}^{\text{VI}}$) and the reductant CrCp_2^* performs an equivalent role as the nitrogenase reductase (Fe protein) in the natural process.

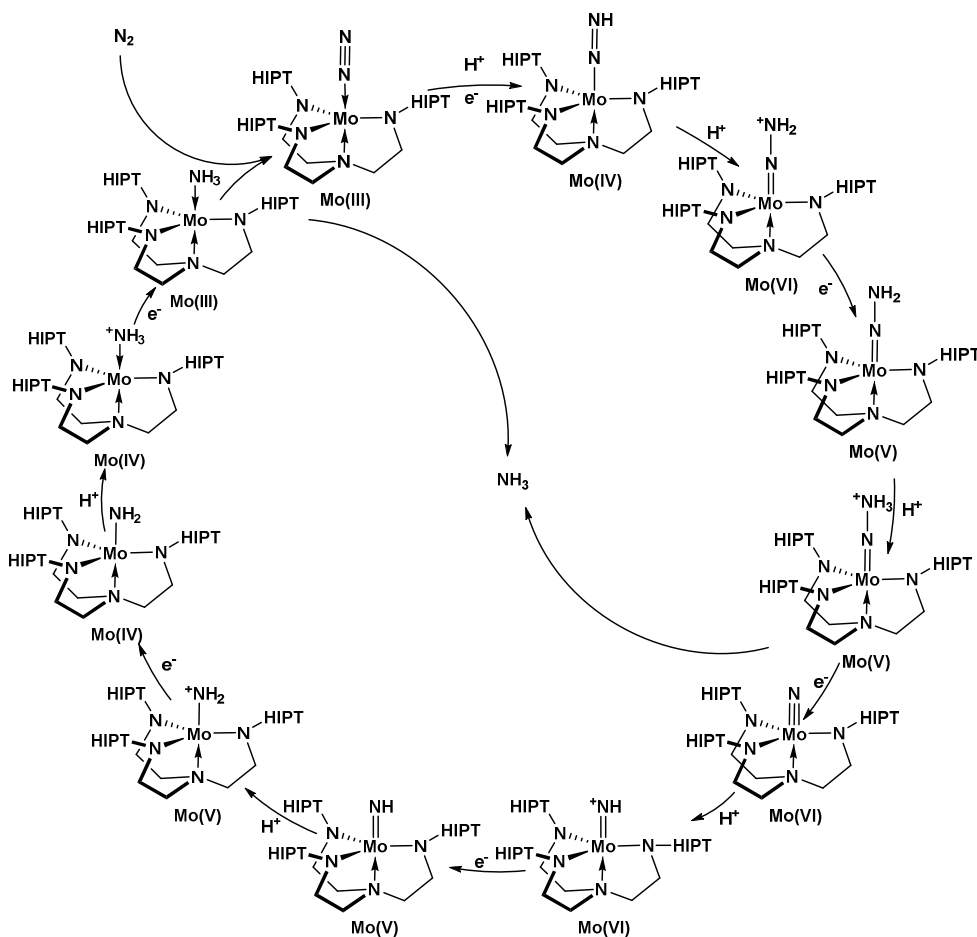


Figure 2: Schrock's $[\text{HIPTN}_3\text{N}]\text{Mo}(\text{N}_2)$ catalyst, HIPT = hexa-iso-propyl-terphenyl^{45, 51}

Unfortunately, while catalytic, the highly favoured competitive reaction of electrons with protons is a likely factor inhibiting the Schrock system from achieving the higher turnover levels requisite for industrially viable processes. Subsequently, a molybdenum complex with a PNP pincer ligand developed by Nishibayashi *et al*⁵⁰ and a iron complex with a tripodal phosphine borane ligand developed by Peters *et al*^{88, 89} has been reported to catalyse ammonia generation from nitrogen in the presence of a protic source and a reductant, but conversions were still too low for industrial consideration.

The development of a homogeneous equivalent of the Haber-Bosch process remains a lofty prize for chemists. Since the first partial hydrogenation reported for a zirconium dinitrogen complex with a P_2N_2 macrocycle by Fryzuk and workers in 1997,⁹⁰ a handful of dinitrogen

complexes have shown reactivity with hydrogen gas, in some cases associated with the liberation of ammonia, but none of these systems have demonstrated catalytic ability (see chapter six for more discussion).^{63, 90-101} The substituted cyclopentadienyl trinuclear titanium complexes reported recently by Shima and co-workers are unique in that molecular hydrogen is first converted into a metal hydride complex before activating N_2 and forming N-H bonds.¹⁰⁰

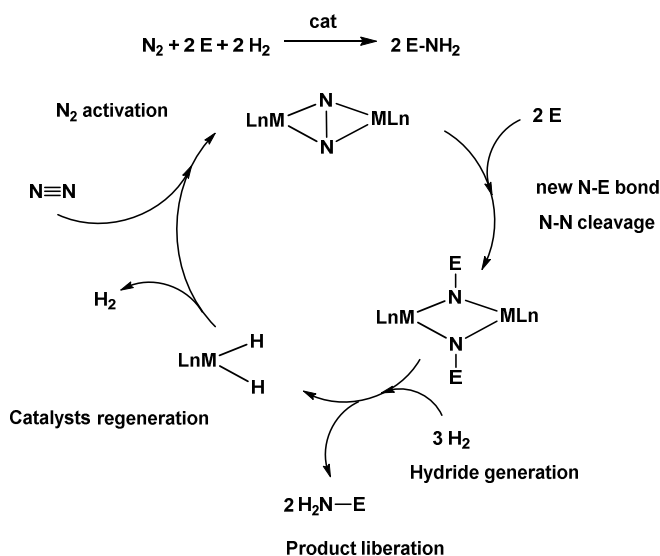


Figure 3: Idealised catalytic cycle for the combination of dinitrogen with substrates

Another desirable goal of N_2 fixation studies in homogeneous solution chemistry would be to move “beyond nature” and directly combine dinitrogen with substrates without intermediate ammonia production.^{27, 54} A catalytic process (Figure 3) for the transformation of dinitrogen into functionalised nitrogen compounds would require the following, namely;

- (i) activation of the dinitrogen molecule
- (ii) formation of new N-element bonds
- (iii) cleavage of the N-N bond
- (iv) liberation of the product with the new N-element
- (v) regeneration of the activated dinitrogen metal complex.

Transition metal dinitrogen complexes are often labile and the coordinated dinitrogen unit typically undergoes displacement, however, under certain conditions, it should be possible to

functionalise the coordinated dinitrogen before it can be displaced. The nature of the ligand L_n plays a crucial role, as at earlier stages of the catalytic cycle strong L_nM -nitrogen bonds are needed to avoid displacement, however, at later stages weaker L_nM -nitrogen bonds are needed to ensure reaction with substrates and the liberation of products. The steric and electronic interactions between L_n and the metal centres need to be robust and able to respond to the varying L_nM -nitrogen conditions. As activated dinitrogen complexes can be formed from metal hydrides,^{68, 80, 100, 102} this provides a mechanism for catalyst regeneration, whereby the introduction of a hydride source to the nitrogen-substrate bound product liberates the protonated final product and generates the associated metal hydride. For ammonia production, the ability of a recently reported trinuclear titanium polyhydride complex¹⁰⁰ to simultaneously activate N_2 and form new N-H bonds via molecular hydrogen as a proton source may represent the groundwork towards the development of a homogeneous catalysts analogue to the heterogeneous Haber-Bosch process.

New N-C bonds can be accessed from N_2 complexes via condensation reactions of protonated N_2 complexes with aldehydes or ketones or via reaction with electrophilic reagents (i.e. organohalides) or via cycloaddition of alkynes across the metal-N bond.^{27, 54, 79, 103, 104} N_2 compounds also react with isocyanates¹⁰⁵ and CO_2 ¹⁰⁶ to form new C-N bonds. New N-Si bonds can be formed by reaction with Me_3SiI ⁵⁸ or via hydrosilylation¹⁰⁷⁻¹⁰⁹ with silanes. Similarly, new N-B and N-Al bonds are formed via hydroboration^{110, 111} and hydroalumination.¹¹² The complete cleavage of N_2 can occur immediately on complex formation,^{52, 113, 114} or during further reduction or heating of the N_2 complex.^{93, 115-117} One of the elusive challenges that remain is to develop strategies to liberate the functionalised nitrogen products with concomitant regeneration of the activated dinitrogen species. The first noteworthy example is the catalytic formation of silylamines in 1972,¹¹⁸ with Hidai and co-workers reporting a discreet molybdenum dinitrogen complex in 1989 capable of a turnover number of 25 mol / Mo atoms.¹¹⁹ This result was greatly improved upon by Nishibayashi to 226 mol / Mo atoms, using a molybdenum dinitrogen complex

with ferrocenyl linked phosphine ligands.¹²⁰ Dinitrogen complexes from iron carbonyl and ferrocenes can also catalyse this transformation under ambient conditions, but the active catalytic species has yet to be isolated.¹²¹ Numerous other organo-nitrogen compounds have been formed from N_2 via *in situ* generated titanium dinitrogen complexes.¹²²

1.2. Dinitrogen Complexes

The bonding of N_2 to transition metals is explained using the Dewar-Chatt-Duncanson model.^{123, 124} The activated N_2 unit may bind in a side-on, end-on or hybrid side-on/end-on fashion (Figure 4) and mono, di and polynuclear complexes can be formed. Note that in an idealised catalytic cycle (Figure 3), the activated dinitrogen is depicted as side-on rather than end-on, as the lone pair in the side-on mode is more available and is considered more conducive to further reactivity with substrates.¹²⁵ The degree of back-donation on activation can be correlated with the degree of elongation of the N-N bond length obtained via X-ray diffraction data.

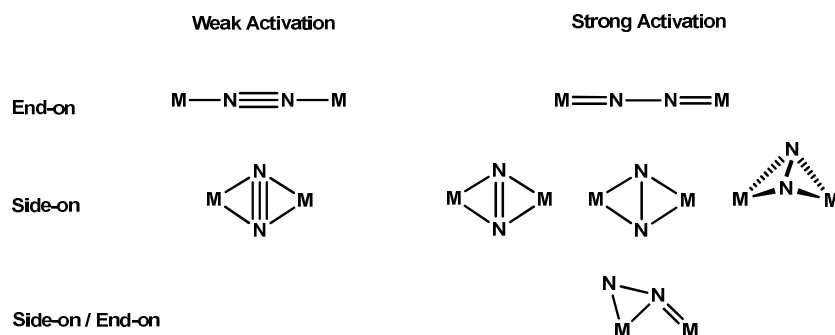


Figure 4: Activated dinitrogen bonding modes for dinuclear complexes

For weak activation, the N-N bond length is similar to that of free $N \equiv N$ (1.10 Å), for moderate activation the N-N bond length is similar to $PhN=NPh$ (1.26 Å) and for strong activation the N-N bond length is similar to that of hydrazine (1.47 Å). The formal oxidation state of the N_2 unit varies accordingly, with the moderately activated diazenido ($N=N$)⁻² unit, strongly activated hydrazido ($N-N$)⁻⁴ unit and the completely cleaved bridging or terminal nitride

$(=N-)^{3-} / (\equiv N)^{3-}$. Spectroscopy can be helpful to distinguish between the end-on and side-on N-N binding modes.¹²⁶

Again, the nature of the ligand can have a profound effect on the type of N₂ bonding observed, as is illustrated in the below-mentioned series of cyclopentadienyl titanium complexes (Figure 5). For pentamethyl-substitution, a dinuclear complex with one end-on unit is reported;¹²⁷ increasing the steric bulk of one group to iso-propyl results in a mononuclear complex with two end-on N₂ ligands.¹²⁸ Reducing the steric bulk by removing two methyl groups leads to a side-on dinuclear complex instead.¹²⁹

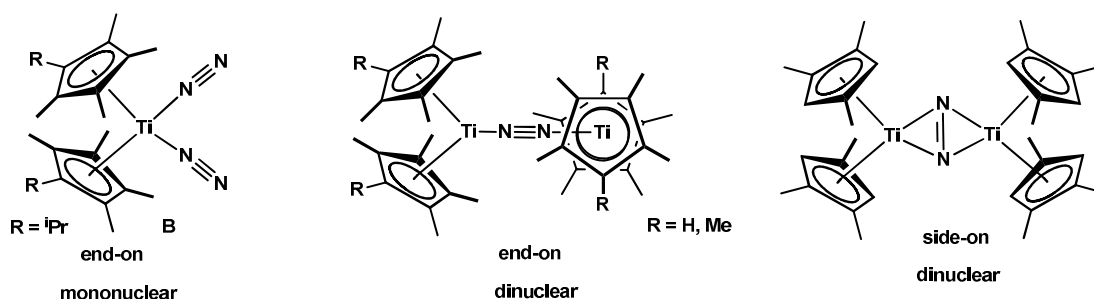


Figure 5: Steric effect of ligand on N₂ bonding modes

1.2.1. Zirconium N₂ Chemistry

The first report of a zirconium dinitrogen complex was made by Bercaw and Manriquez^{130, 131} in 1974 for an end-on bridged dinuclear zirconocene (A in Figure 6). This bright green complex contained two additional terminal side-on dinitrogen ligands and the two different bonding modes were confirmed later with x-ray crystallography.¹³² Since then a wide variety of zirconium dinitrogen complexes have been reported, mostly containing substituted cyclopentadienyl, amide or phosphorus ligands (Figure 6). Mixed heterobimetallic zirconium and tungsten containing complexes were also prepared, which coordinated dinitrogen in a bridging end-on fashion.^{133, 134} The first side-on zirconium dinitrogen complex, which contained a planar Zr₂N₂ core, was reported for an amidodiphosphine complex [PNPZrCl]₂(μ-η²:η²-N₂) by Fryzuk *et al* in 1990 (F).¹³⁵ Changing the anionic chloride donor to an aryloxy group resulted in a butterfly

distortion of the Zr_2N_2 core (G)¹³⁶ and when the donor was changed to cyclopentadienyl group a bridging side-on bonding mode was observed (D).⁷⁵ Resonance Raman spectroscopy was shown to be a useful for discriminating between the side-on and end-on modes.¹²⁶ Of the Fryzuk groups side-on diamidophosphine (NPN) zirconium dinitrogen complexes, $[\text{Si}^i\text{NPNZr}(\text{THF})]_2(\mu\text{-}\eta^2\text{:}\eta^2\text{-N}_2)$,^{137, 138} $[\text{Si}^i\text{NPNZr}(\text{Py})]_2(\mu\text{-}\eta^2\text{:}\eta^2\text{-N}_2)$,^{137, 138} and $[\text{CY}^5\text{NPN}^{\text{DMP}}\text{Zr}(\text{THF})]_2(\mu\text{-}\eta^2\text{:}\eta^2\text{-N}_2)$ ^{139, 140} have planar Zr_2N_2 cores and $[\text{mes}^i\text{NPNZr}(\text{THF})]_2(\mu\text{-}\eta^2\text{:}\eta^2\text{-N}_2)$, $[\text{mes}^i\text{NPNZr}(\text{Py})]_2(\mu\text{-}\eta^2\text{:}\eta^2\text{-N}_2)$ and $[\text{mes}^i\text{NPNZr}(\text{PPhMe}_2)](\mu\text{-}\eta^2\text{:}\eta^2\text{-N}_2)[\text{mes}^i\text{NPNZr}]$ ^{92, 97} complexes display a butterfly distortion. Vibrational spectroscopic studies have been conducted of this butterfly distortion of the planar Zr_2N_2 core complexes.^{136, 141}

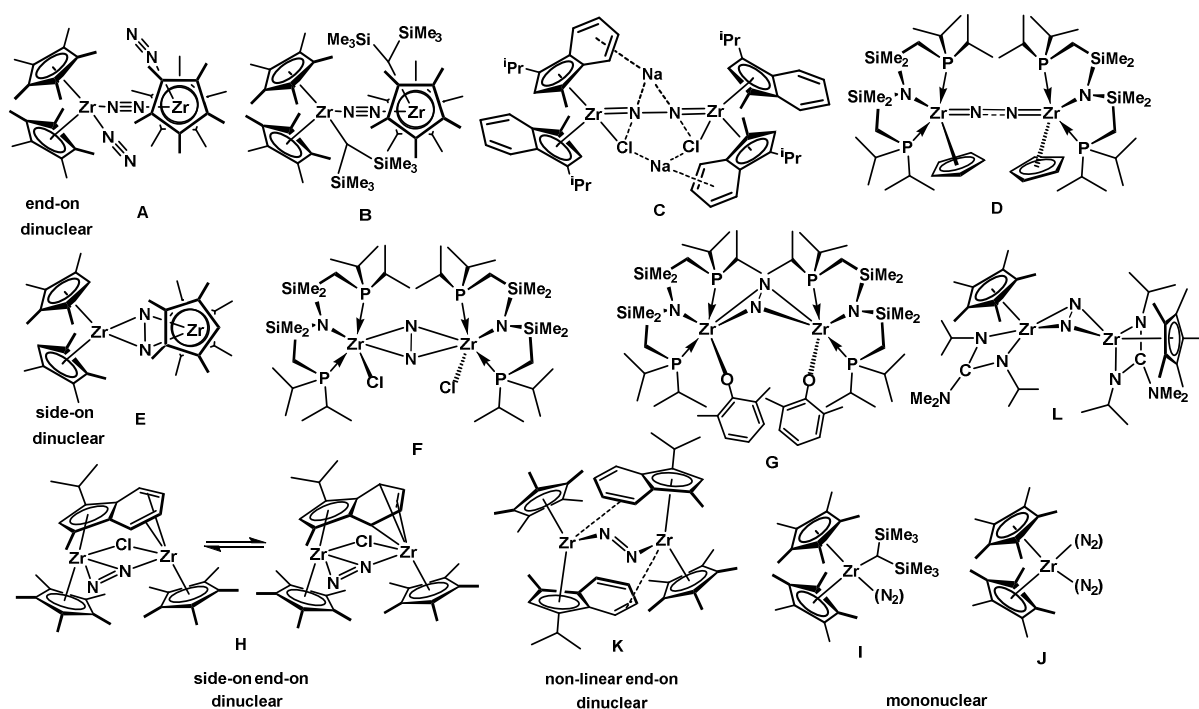


Figure 6: Selected examples of zirconium dinitrogen complexes

Subtle changes to the substitution of cyclopentadienyl groups were found to lead to dramatic changes in the dinitrogen bonding mode. For example, removing one of the methyl groups from the pentamethylcyclopentadienyl moiety led to the coordination of one planar bridging side-on dinitrogen group (E).^{93, 94} The *ansa*-zirconocene with *tert*-butyl and methyl

substituents display a butterfly distorted Zr_2N_2 core,¹⁴² whereas *tert*-butyl and TMS substituents result in a planar Zr_2N_2 core.¹⁴³ The mixed pentamethylcyclopentadienyl / guanidinate side-on zirconium dinitrogen complexes (L) also exhibit a distortion from linearity.¹⁴⁴ The bis-indenyl dinitrogen complex results in a side-on mode with two weakly coordinated sodium chlorides (C),⁹⁸ however, with a mixed indenyl / pentamethylcyclopentadienyl system, a side-on end-on mode was observed (H).¹⁴⁵ The formation of the side-on, end-on mode observed for complex (H) is strongly dependant on method of preparation and requires the reduction of the precursor dichloride in the presence of dinitrogen. If, however, the mixed indenyl / pentamethylcyclopentadienyl sandwich complex was isolated by reduction of the self-same dichloride under argon, subsequent exposure to dinitrogen led to the isolation of a non-linear end-on bridged complex (K).¹⁴⁵

While crystal structures of mononuclear zirconium dinitrogen complexes have not yet been reported, a presence of a bis-dinitrogen binuclear intermediate (J) is postulated during the splitting of water by the tris-dinitrogen zirconocene (A).¹⁴⁶ Pentamethyl zirconocene with a bulky alkyl ($-\text{CH}(\text{SiMe}_3)_2$) ligand was reported to form a brown ‘side-on’ dinitrogen complex (I).¹⁴⁷ Even more interesting, low temperature ($-30\text{ }^\circ\text{C}$) re-crystallisation of this brown mononuclear zirconocene dinitrogen led to the purple dinuclear end-on dinitrogen zirconocene (B).¹⁴⁷ Conversion of the brown mononuclear complex (I) to the purple dinuclear one (B) was also observed on prolonged exposure to reduced pressure. This purple dinuclear complex (B) was also not characterised crystallographically, but is surmised to have a similar structure to the related titanocene dinitrogen complex with an aryl ligand characterised by Teuben *et al.*¹⁴⁸ The green side-on dinitrogen complexes $[(\text{Cp-Me}_5)(\text{Cp-1,2-Me}_2,4\text{-R})\text{Zr}]_2(\mu\text{-}\eta^2\text{:}\eta^2\text{-N}_2)$ with $\text{R} = \text{Me}$ or Ph were isolated as isomeric *syn:anti* mixtures, with preference given to the *anti* isomers.⁹⁶ Isomeric exchange between these isomers is confirmed with increasing temperature above $50\text{ }^\circ\text{C}$, with a mechanism involving inter-conversion between an end-on and side-on dinitrogen ligand. The

forest green side-on dinitrogen zirconocene (E) was also observed to undergo transformation in excess dinitrogen to an intense purple complex, which is favoured at lower temperatures. Electronic and infrared spectra of the purple solutions suggest that the bridged dinitrogen unit was side-on, with two additional terminal side-on dinitrogen ligands, similar to the structure reported for A.⁹⁶

Reduced zirconium species have a high affinity for reducing dinitrogen, forming strongly activated dinitrogen transition metal complexes with some of the longest N-N bonds having been reported for the butterfly distorted side-on mixed cyclopentadienyl / amidinate¹⁴⁴ and planar side-on amidodiphosphine (PNP),¹³⁵ diamidodiphosphine (NNP)¹⁴⁹ and diamidodiphosphine (P₂N₂)^{90, 150} zirconium complexes, with bond lengths of 1.518(2) Å, 1.548(7) Å, 1.576(9) Å and 1.465(19) Å, respectively.

1.2.2. Hafnium N₂ Chemistry

Hafnium and zirconium have similar covalent radii and display similar chemical behaviour,¹⁵¹ but fewer dinitrogen complexes with hafnium have been reported, in part due to the hafnium dichlorides being more difficult to reduce.¹⁵² To date, a few cyclopentadienyl based hafnium dinitrogen complexes have been prepared, via reduction of either the precursor chlorides or iodides.^{99, 134, 144} The dinitrogen ligand was postulated to be end-on for a dinuclear hafnocene complex¹⁵³ and characterised end-on in the case of the mixed tungsten / hafnium dinuclear complex.¹³⁴ Varying the substitution on the cyclopentadienyl group led to the side-on dinitrogen dinuclear hafnocene dinitrogen complexes⁹⁹ and recently mixed cyclopentadienyl / guanidinate and cyclopentadienyl / amidinate dinitrogen complexes¹⁴⁴ were reported. The side-on dinuclear hafnocene dinitrogen complexes proved to be highly activated and reactive with H₂,⁹⁹ CO,¹⁵⁴⁻¹⁵⁶ CO₂,^{106, 157} methyl triflate¹⁵⁸ and phenyl isocyanate¹⁰⁵ substrates. While no solid state molecular structure was obtained, a mass spectrum confirmed the formation of a [P₂N₂Hf]₂(N₂) complex, as well as [P₂N₂Hf]₂ and P₂N₂Hf(C₇H₈) side-products with Hf-arene bonds.¹⁵⁹

1.2.3. Titanium N₂ Chemistry

Titanium dinitrogen complexes form an integral part of the early history and development of transition metal dinitrogen complexes. The first reports of the ability of transition metals to fix dinitrogen and facilitate conversion with appropriate substrates into functionalised nitrogen containing compounds was made by Vol'pin and Shur in 1964^{84-86, 160} for the observation of ammonia by exposing *in situ* reduced titanocene species 'Cp₂Ti' to dinitrogen and quenching with dilute acid. This discovery fueled the speculation that a putative 'Cp₂Ti(N₂)' species was involved in this transformation. One year later in 1965 the first transition metal dinitrogen complex was serendipitously reported by Allen and Senoff¹⁶¹ while studying ruthenium ammonia complexes.

The first reports of the isolation of titanocene-based dinitrogen complexes were made by Shilov *et al*,¹⁶² van Tamelen *et al*¹⁶³ and Brintzinger *et al*¹⁶⁴ between 1969 to 1971 and a titanium (II) dimer [Cp₂Ti]₂, implicated in the genesis of these complexes, was isolated by Bercaw and Britzinger in 1971.¹⁶⁴ Elucidation of the solid state molecular structure of the dinitrogen complexes proved evasive and the topic of extensive debate until crystals obtained for [Cp*₂Ti]₂(μ-η¹:η¹-N₂) in 1976 by Bercaw *et al*¹⁶⁵ revealed that the dinitrogen was bound end-on between two titanium atoms with N-N bond lengths of 1.155(14) Å and 1.165(14) Å (see C in Figure 7). A notable contribution was also made by Pez and workers, who in 1976 isolated a cyclopentadienyl-based titanium (II) dimer¹⁶⁶ and a tetrameric titanium dinitrogen complex.¹⁶⁷ The side-on, end-on bound dinitrogen unit to three of the titanium centres of the tetramer was crystallographically characterised in 1982 (G).¹⁶⁸

Since then numerous end-on titanocene dinitrogen complexes have been isolated,^{127, 129, 148, 169-171} as well as other end-on dinitrogen titanium complexes with amido,¹⁷² guanidinate,¹⁷³ benzamidinate,¹⁷⁴ pyridine¹⁷⁵ and multidentate NON¹⁷⁶ and NNP¹⁴⁹ ligand systems. The N-N bond for the cyclopentadienyl based end-on dinitrogen titanium complexes are generally classed

as moderately activated with bond lengths in the range of 1.15-1.20 Å, whereas the non-titanocene based dinitrogen complexes tend to be more strongly activated with N-N bond lengths ranging from 1.25 to 1.30 Å.¹⁷⁷ This trend is also present in the side-on bridged dinitrogen complexes, where a titanocene side-on dinitrogen complex (E) is moderately activated with a N-N length of 1.22 Å¹²⁹ and a titanium side-on bis-dinitrogen amido based complex (F) is strongly activated (1.38 Å).¹⁷² Cyclopentadienyl chloro titanium centres have been reported to form heterobimetallic bridged end-on dinitrogen structures with phosphine chloro tungsten centres.¹³³ Complete cleavage and functionalisation of the N-N bond during reduction has also been reported for titanium complexes with pyrrolide¹⁷⁸ and NPN^{137, 138} ligand systems.

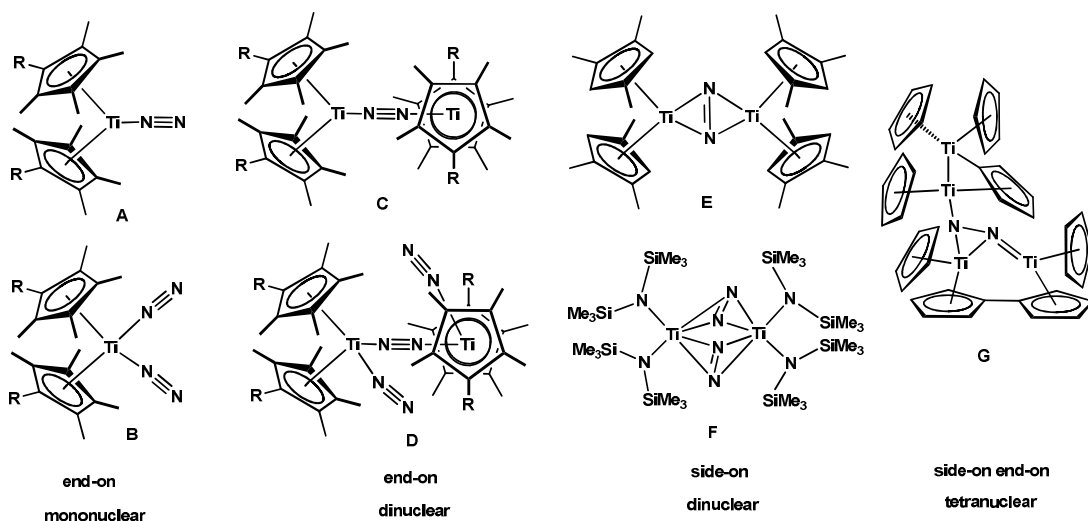


Figure 7: Dinitrogen bonding modes for titanium dinitrogen complexes

The chemistry of the titanocene dinitrogen complexes has been comprehensively reviewed recently and classified according to the mode of dinitrogen coordination.^{179, 180} A wide variety of different dinitrogen bonding modes have been elucidated, from mono-¹⁸¹ and bis-dinitrogen¹²⁸ mononuclear complexes (A and B in Figure 7) to dinuclear end-on (C) or side-on bridged (E)¹²⁹ and mixed terminal / end-on bridged (D).^{129, 180} The size and number of substituents on the cyclopentadienyl ring play a major role in determining the observed structural diversity. The

dinuclear side-on bridging mode is preferred with the sterically least hindered $\eta^5\text{-C}_5\text{H}_2\text{-1,2,4-Me}_3$ ligand.¹²⁹ With the more bulky $\eta^5\text{-C}_5\text{Me}_4\text{R}$, R = H, Me, Et, Ar and $-(\text{SiMe}_2)_{0.5}$ ^{127, 129, 132, 180} the dinuclear end-on bridged mode is observed, and in the case of R = Et, additional terminal side-on dinitrogen can coordinate.¹⁸⁰ It may be that the size of the substituent may play a larger role in promoting an end-on rather than side-on bonding mode compared with increasing substitution of the cyclopentadienyl ligand, as the 1,3 di-substituted $\eta^5\text{-C}_5\text{H}_3\text{-1,3-(SiMe}_3)_2$ ¹⁶⁹ and ansa ($\eta^5\text{-C}_5\text{H}_2\text{-2-SiMe}_3\text{-4-}^t\text{Bu})_2\text{-SiMe}_2$ ¹²⁹ ligands also exhibit an end-on bonding mode.

As the R group for the $\eta^5\text{-C}_5\text{Me}_4\text{R}$ ligands become more bulky, bridging of the dinitrogen unit no longer occurs and for R = ^iPr , two terminal end-on dinitrogen ligands are coordinated to a single titanium centre,¹²⁸ with only one terminal dinitrogen unit when R = SiMe_2Ph .¹⁸¹ Electronic effects of the substituted cyclopentadienyl complement the steric effects, where the smallest, least substituted and hence more electrophilic titanocenes form more highly activated bridging dinitrogen complexes, with decreasing electrophilicity leading to weakly activated monomeric species.¹⁷⁹

The Fryzuk group's mixed amidophosphine ligands attached to titanium metal centres are also capable of activating dinitrogen. Brown end-on bridged $[\text{PNPTiCl}]_2(\mu\text{-}\eta^1\text{:}\eta^1\text{-N}_2)$ ¹⁸² and $[\text{P}_2\text{N}_2\text{Ti}]_2(\mu\text{-}\eta^1\text{:}\eta^1\text{-N}_2)$ ¹³⁷ complexes were obtained with N-N bond lengths of 1.275(7) Å and 1.255(7) Å, respectively, which falls into the range of a strongly activated N_2^{4+} unit (Figure 8).

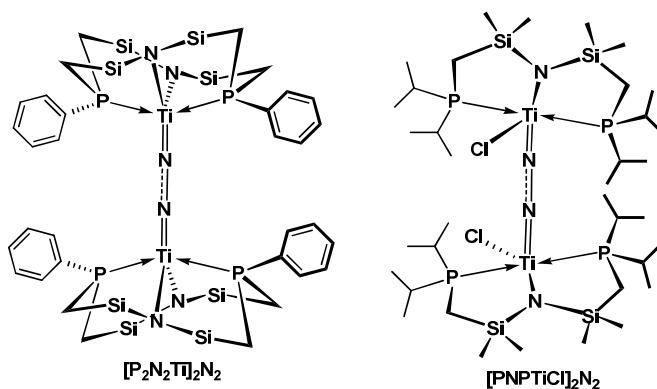


Figure 8: End-on dinitrogen $[\text{PNPTiCl}]_2(\mu\text{-}\eta^1\text{:}\eta^1\text{-N}_2)^{182}$ and $[\text{P}_2\text{N}_2\text{Ti}]_2(\mu\text{-}\eta^1\text{:}\eta^1\text{-N}_2)^{137}$ complexes

However, the reduction of $^{\text{Si}}\text{NPNTiCl}_2$ with KC_8 under N_2 led to the formation of a bridged phosphinimide titanium complex.^{137, 138} A corresponding reaction with $^{15}\text{N}_2$ confirmed that the source of the nitrogen of the phosphinimide was an activated dinitrogen molecule, which implies that facile cleavage of coordinated dinitrogen occurred, with the associated formation of phosphorus-nitrogen bonds.

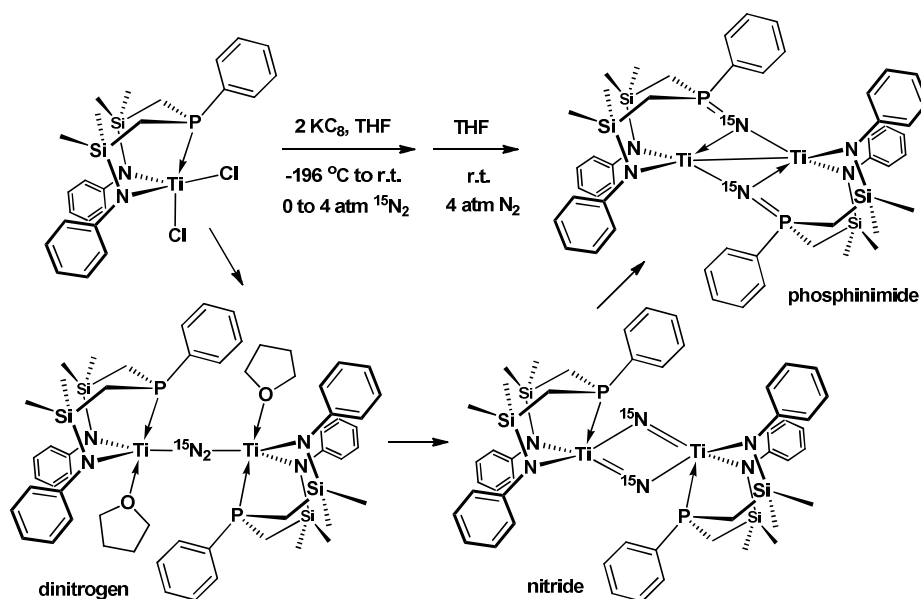


Figure 9: Dinitrogen bonding modes for titanium dinitrogen complexes

The forest green phosphinimide complex $\{[^{\text{Si}}\text{N}(\text{P}=\text{N})\text{N}]\text{Ti}\}_2$ was shown to transform into an olive green intermediate with an upfield shifted $^{31}\text{P}\{^1\text{H}\}$ NMR spectral signal. It was not possible to isolate this intermediate, but its identity was speculated to be the dinitrogen complex $[\text{SiNPNTi}]_2(\text{N}_2)$.

While this phosphinimide complex represents a novel $\text{P}=\text{N}$ functionalisation, the $^{\text{Si}}\text{NPN}$ ligand is unfortunately transformed during the process. The new o-phenylene bridged NPN ligands synthesized for this project ($^{\text{iprop}}\text{NPN}$ and $^{\text{tol}}\text{NPN}$) have a more rigid back-bone, which may inhibit phosphinimide formation and stabilise a dinitrogen complex.

1.2.4. Tantalum N₂ Chemistry

The first group 5 dinitrogen complexes were formed by reduction of a neopentylidene tantalum bis(trimethylphosphine)trichloride with sodium mercury amalgam in the presence of N₂.⁷²⁻⁷⁴ The activated bridging N₂ unit was coordinated in an end-on bonding mode (Figure 10). Reduction of alkylidene tantalum complexes ^{Si}PNPTaCl₂(=CHR), R = ^tBu, Ph with sodium mercury amalgam and N₂ were later also reported to form end-on bridged N₂ complexes (Figure 10).⁷⁵

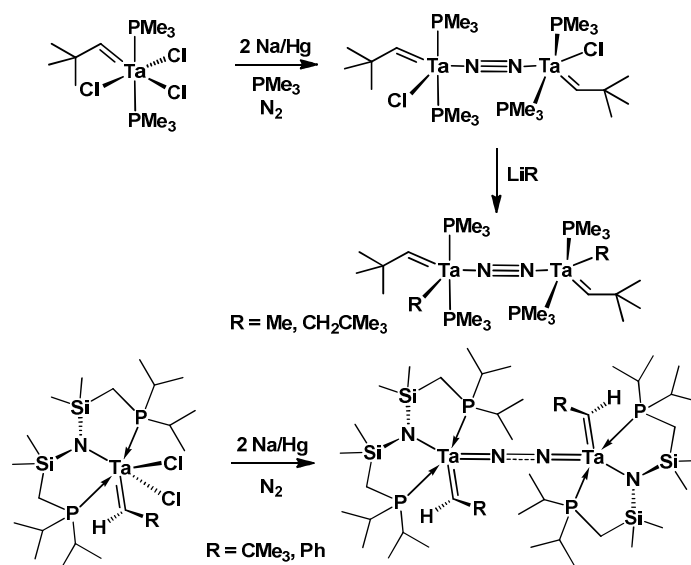


Figure 10: Tantalum dinitrogen alkylidene complexes obtained by reduction of precursor chlorides⁷²⁻⁷⁵

Reduction of substituted cyclopentadienyl^{76, 77} and mixed pentamethylcyclopentadienyl-guanidinate⁷⁸ tantalum chloride complexes under N₂ also leads to end-on bridged N₂ complexes (Figure 11). Further reaction with H₂ and PhSiH₃ was reported for the mixed pentamethylcyclopentadienyl-guanidinate system,⁷⁸ as well as complete cleavage of N₂ to form a bridging nitrido complex.⁷⁸ The tetrachloride $[\text{Cp}^*\text{TaCl}_2]_2(\text{N}_2)$ has proved to be a convenient salt metathesis precursor for the mixed pentamethylcyclopentadienyl-amidate system.¹⁸³ In one case a Ta(III) dimer $[\text{Cp}^*\text{TaCl}_2]_2$ ^{76, 184} was implicitly identified as an intermediate formed during the reduction process. A Ta(III) hydroxide was also reported to be the active species in the reduction

of N_2 to yield hydrazine.¹⁸⁵ Alternative routes for the preparation of tantalum N_2 complexes exist, where the nitrogen sources were hydrazine⁷⁶ or substituted hydrazines^{71, 186-189} and not molecular N_2 . Heterobimetallic tantalum-tungsten N_2 complexes have also been prepared by reaction of a pre-activated tungsten N_2 complex with Cp^*TaCl_4 .¹³³

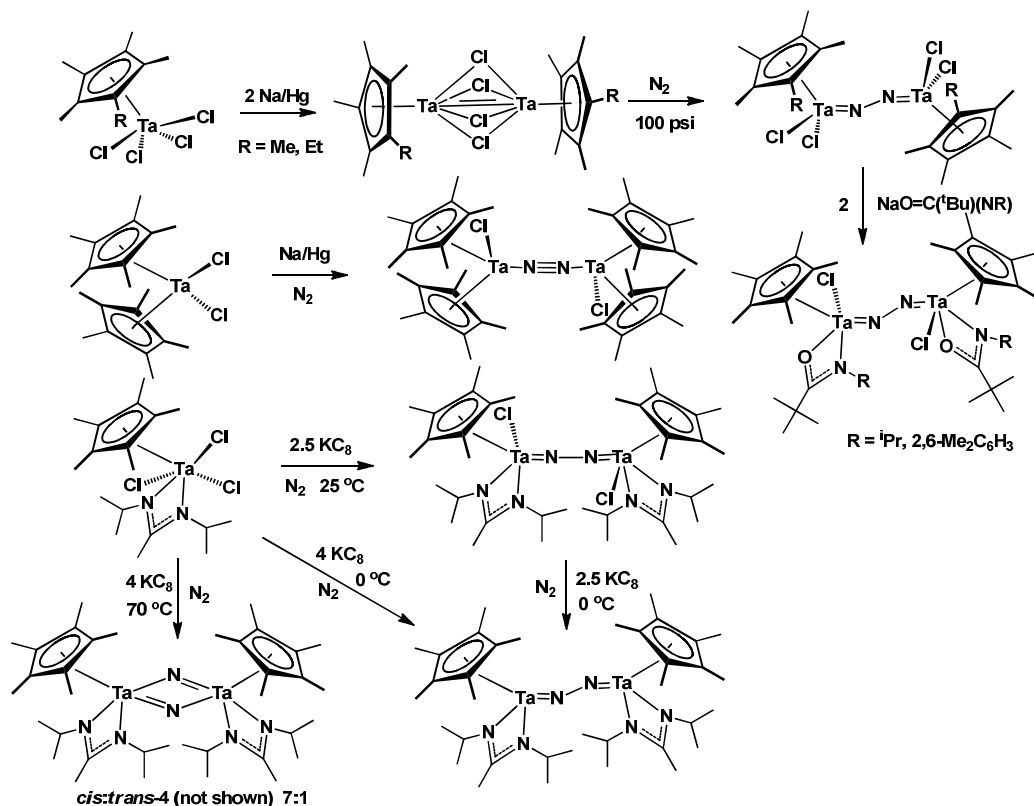


Figure 11: Tantalum dinitrogen cyclopentadienyl complexes obtained by reduction of precursor chlorides^{76-78, 183, 184}

Dinitrogen activation can also be achieved in specific cases from transition metal hydrides.¹⁹⁰ For example, silica-grafted single site organometallic tantalum hydrides have been reported to completely cleave N_2 .¹⁹¹ The seminal $[\text{SiNPNTaH}]_2(\text{N}_2)$ complex was formed from a precursor tetrahydride $[\text{SiNPNTaH}_2]_2$ (Figure 12), where the side-on, end-on bonding mode for a bridging N_2 unit was described for the first time.⁷⁹⁻⁸¹ A wide range of reactivity was displayed with this complex, namely:

- i) reaction with alkyl halides⁷⁹ and 1,2-cumulenes¹⁹² to form new N-C bonds

- ii) hydroboration^{110, 111} to form new N-B bonds
- iii) hydrosilylation¹⁰⁷⁻¹⁰⁹ to form new N-Si bonds
- iv) hydroalumination¹¹² to form new N-Al bonds
- v) reaction with Schwartz's reagent to form new N-Zr bonds and fully cleave the N-N bond¹¹⁵
- vi) formation of aluminum, gallium and boron Lewis adducts¹⁹³
- vii) reaction with propene¹⁹⁴ to form Ta-alkyl N₂ complexes with conversion to end-on bonding mode
- viii) displacement of N₂ when reacted with phenylacetylene¹⁹⁵ or carbon disulphide¹⁹⁶

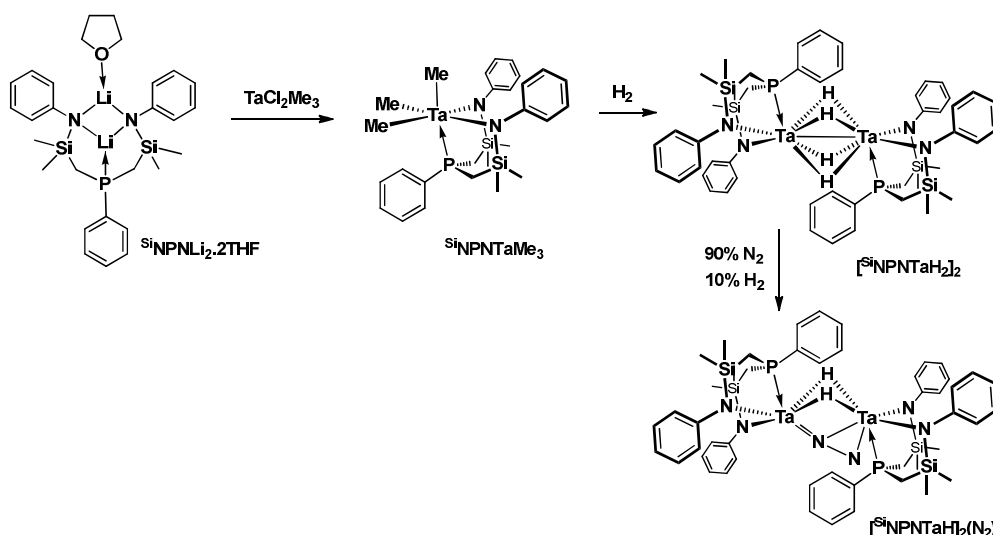


Figure 12: Tantalum $^{\text{Si}}\text{NPN}$ dinitrogen complexes obtained by the hydride route

Despite the rich new types of chemical reactivity discovered for this novel $[\text{SiNPnTaH}]_2(\text{N}_2)$ complex, numerous types of ligand degradation pathways have also been reported. For example, the reaction of the hydroalumination product of $[\text{SiNPnTaH}]_2(\text{N}_2)$ with diisobutylaluminum hydride reacts further to fully cleave the N₂ bond, but the amide of the ligand decoordinates from Ta and migrates to the Al centre.¹¹² Similarly, reaction with Schwartz's reagent $\text{Cp}_2\text{Zr}(\text{Cl})\text{H}$ leads to complete cleavage of N₂, but the P atom of the ligand decoordinates and forms a phosphinimide with one of the cleaved N atoms.¹¹⁵ C-H activation has been reported for the phenyl ring of the P atom in the reaction with butylsilane¹⁰⁸ and loss of H₂ after

hydroboration with 9-borabicyclononane (9-BBN) leads to cleavage of N_2 , with associated scission of the ligand's Si-N bond and migration of the Si atom to the cleaved N atom.^{110, 111}

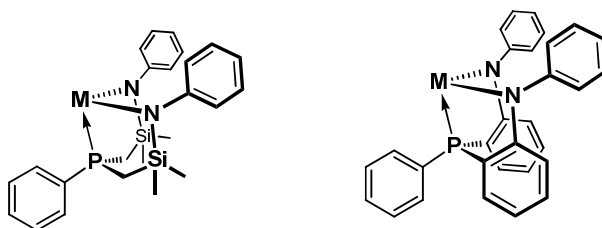


Figure 13: ^{Si}NPN vs. *o*-phenylene NPN ligand

These facile ^{Si}NPN ligand rearrangements hamper further development of this research area, mostly due to the labile N-Si bond and the flexible backbone. Replacing $P-CH_2-SiMe_2-N$ with an *o*-phenylene bridge (Figure 13) would eliminate this problem, making the ligand more rigid while maintaining the relative amine basicity.¹⁹⁷

1.3. Project Objectives

Previous Fryzuk Group researchers observed some interesting chemical reactivity for the side-on dinitrogen zirconium complexes containing the *o*-phenylene-bridged ^{mes}NPN ligand (Figure 14).^{92, 97} For example, displacement of the labile THF solvent with more bulky phosphine ligands led to the formation of dinuclear dinitrogen complexes where one of the zirconium centres had an open coordination site, which may provide a ready reactive centre with substrates. These zirconium dinitrogen complexes reacted with substrates such as dihydrogen, a silane, an aldehyde, a ketone, an imine, ethylene, carbon monoxide and a phosphine oxide. In some cases new nitrogen-hydrogen, nitrogen-silicon and nitrogen-carbon bonds were created. In other cases zirconium oxides were obtained with inconclusive results regarding the fate of the activated nitrogen atoms.

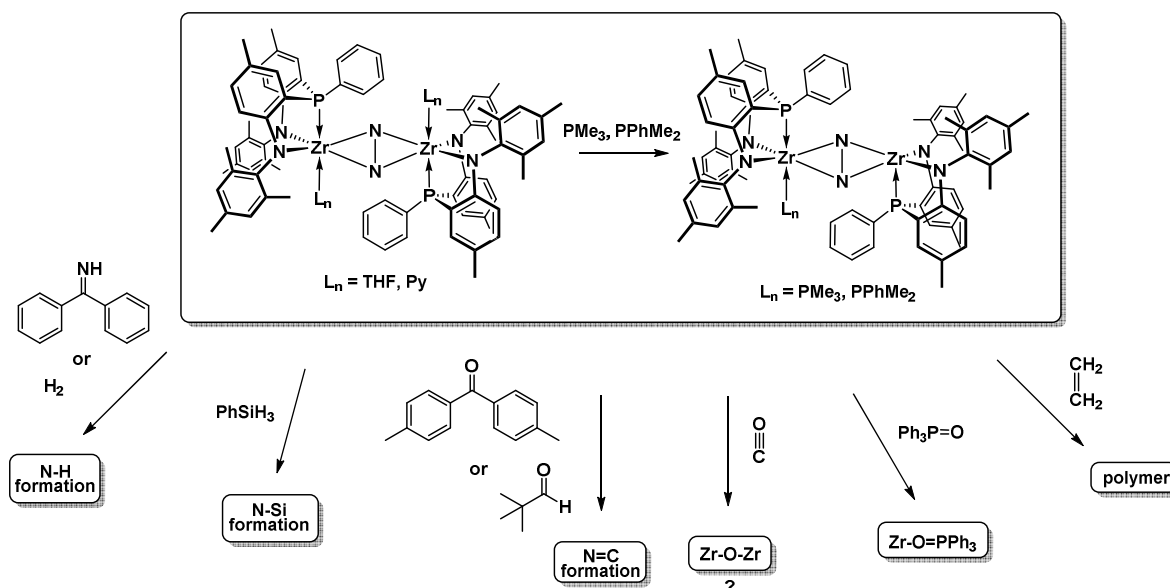


Figure 14: Reactivity of ^{mes}NPN containing zirconium dinitrogen complexes⁹⁷

The overall objective of this project is to investigate the effect of reduced steric bulk in the ortho position of the aromatic amine of this arene-bridged NPN donor set and to probe reactivity studies with the expected zirconium dinitrogen complexes. The mesityl group (^{mes}NPN) would be replaced by 4-isopropyl phenyl (^{iprop}NPN), p-tolyl (^{tol}NPN) and phenyl (^{ph}NPN) groups, thereby reducing the steric bulk and providing a range of similar complexes with potentially different solubility, and perhaps different reactivity. A secondary aim of the project is to expand the Fryzuk group's *o*-phenylene-bridged NPN donor set into other group 4 metals (titanium and hafnium) and group 5 metals (tantalum). One of the intrinsic problems with group 4 (Ti, Zr, Hf) dinitrogen complexes is that only 4 electrons can be supplied at a time, making it impossible to cleave the N_2 bond. For nitride formation with the NPN donor set, group 5 and higher transition metals are needed, based purely on reducing power.

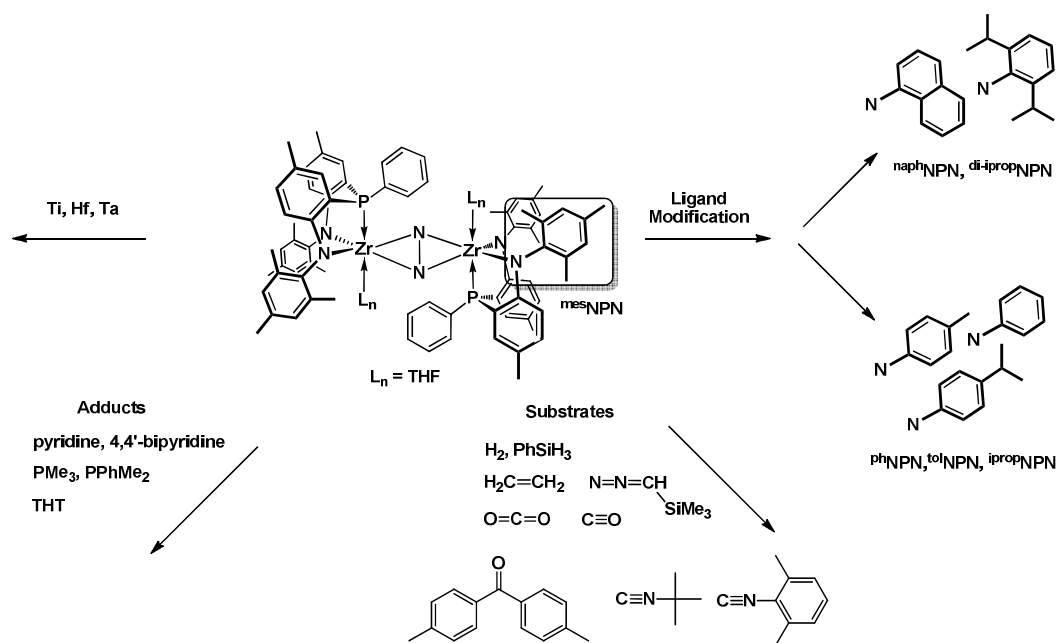


Figure 15: SiNPN vs. *o*-phenylene NPN ligand

For future work, a project was initiated to increase the steric bulk at the ortho position of the aromatic amine with 2,6-diisopropyl phenyl ($\text{di-}i\text{propNPN}$) or naphthyl (naphNPN), as this may encourage the formation of activated dinitrogen complexes with open sites at one or both of the zirconium centres.

In chapter 2, the synthesis of the $i\text{propNPN}$ donor set is described, modelled on the previously reported mesNPN donor set, with a modification for the synthesis of the intermediate *o*-bromo-diarylamine using a Buchwald-Hartwig arylamination. A new method starting with commercially available diarylamines is introduced for the synthesis of the tolNPN and phNPN donor sets, using a directed *ortho* metalation (DOM) process, which is specific to arylamido groups that have no *ortho* substituents.

In chapter 3, the synthesis of zirconium, titanium and hafnium amido and dichloro complexes containing $i\text{propNPN}$ and tolNPN ligands is described. For zirconium, complexation was evaluated via salt metathesis with $\text{ZrCl}_4(\text{THF})_2$ and protonolysis with $\text{Zr}(\text{NMe}_2)_4$ and $\text{ZrCl}_2(\text{NMe}_2)_2\text{DME}$ and for titanium with $\text{Ti}(\text{NMe}_2)_4$ or $\text{TiCl}_2(\text{NMe}_2)_2$.

In chapter 4, the synthesis of tantalum trichloro complexes containing ^{iprop}NPN, ^{tol}NPN and ^{Ph}NPN ligands is described via protonolysis with Ta(NMe₂)₅ followed by reaction with TMSCl. The trimethyl species ^{tol}NPNTaMe₃ [4.7] was isolated by reaction of the potassium salt of the ^{tol}NPN ligand and TaMe₃Cl₂. The ionic species [^{tol}NPNTaMe₄][Li(THF)₄] was isolated on reaction of the trichloride with MeLi, indicating ^{tol}NPNTaMe₃ [4.7] reacts further with MeLi.

The synthesis of tantalum hydrides was attempted by reacting tantalum trimethyl species with H₂ and tantalum trichlorides with KHBet₃. *In situ* introduction of N₂ was performed for both of these above-mentioned hydride routes in attempts to isolate tantalum dinitrogen complexes, as well as reduction of tantalum trichlorides with KC₈ under N₂.

In Chapter 5, reduction with KC₈ under N₂ was investigated for the zirconium, hafnium and titanium dichloride complexes prepared in chapter 3, with the aim of forming activated dinitrogen complexes. Reaction of titanium dichloride with KHBet₃ under N₂ was also evaluated.

In Chapter 6, screening tests (predominantly ³¹P{¹H} NMR experiments) were conducted with the new zirconium and titanium dinitrogen complexes to evaluate potential for reactivity of the activated dinitrogen ligand. The former complex was reacted with dihydrogen, organo isocyanide, phenylsilane, ethylene, carbon monoxide, 4,4'-dimethylbenzophenone, carbon dioxide and (trimethylsilyl)-diazomethane and the latter with dihydrogen, ethylene and carbon monoxide.

In Chapter 7, the pertinent findings from this study dealing with the synthesis of the new sterically less hindered *o*-phenylene-bridged ^{iprop}NPN, ^{tol}NPN and ^{Ph}NPN donor sets and complexes with zirconium, hafnium, titanium and tantalum are summarised, as well as the new zirconium and titanium dinitrogen complexes. Preliminary results for the synthesis of ^{naph}NPN and ^{2,6-*i*Pr₂}NPN donor sets is presented.

For the overall project, it was found that reducing the steric bulk of the amido substituents led to more strongly activated zirconium side-on dinitrogen complexes, with less labile THF adducts. This inhibited displacement with other neutral donors, or formation of open coordination sites at the zirconium centres and reaction with molecular hydrogen did not occur. Future projects should focus on increasing the steric bulk of the amido substituents instead.

The more rigid *o*-phenylene-bridge resulted in the isolation of stable end-on titanium dinitrogen complexes, which had not been possible with the flexible ^{Si}NPN donor set. These complexes displayed no reactivity with molecular hydrogen and other small molecules such as CO, and future ligand design should focus on being able to achieve side-on dinitrogen binding.

Hafnium complexes with these ligands failed to reduce dinitrogen. For tantalum, the alkyl / hydride route for accessing dinitrogen complexes failed; neither was it possible to isolate the dinitrogen complexes formed via reduction or hydrogenation of precursor trichlorides.

Chapter 2: Ligand Synthesis

The Fryzuk suite of mixed ‘hard’ amido and ‘soft’ phosphine ligand donor sets (PNP, P_2N_2 and NPN in Figure 16) provide a flexible platform for variation in ligand design. For example, the amido donor in the PNP donor set has been replaced by a cyclopentadienyl¹⁹⁸ donor (**A**) and an N-heterocyclic carbene donor with a saturated backbone^{199, 200} (**B**). In the NPN donor set, it was replaced by an aryloxy²⁰¹ donor (**G**).

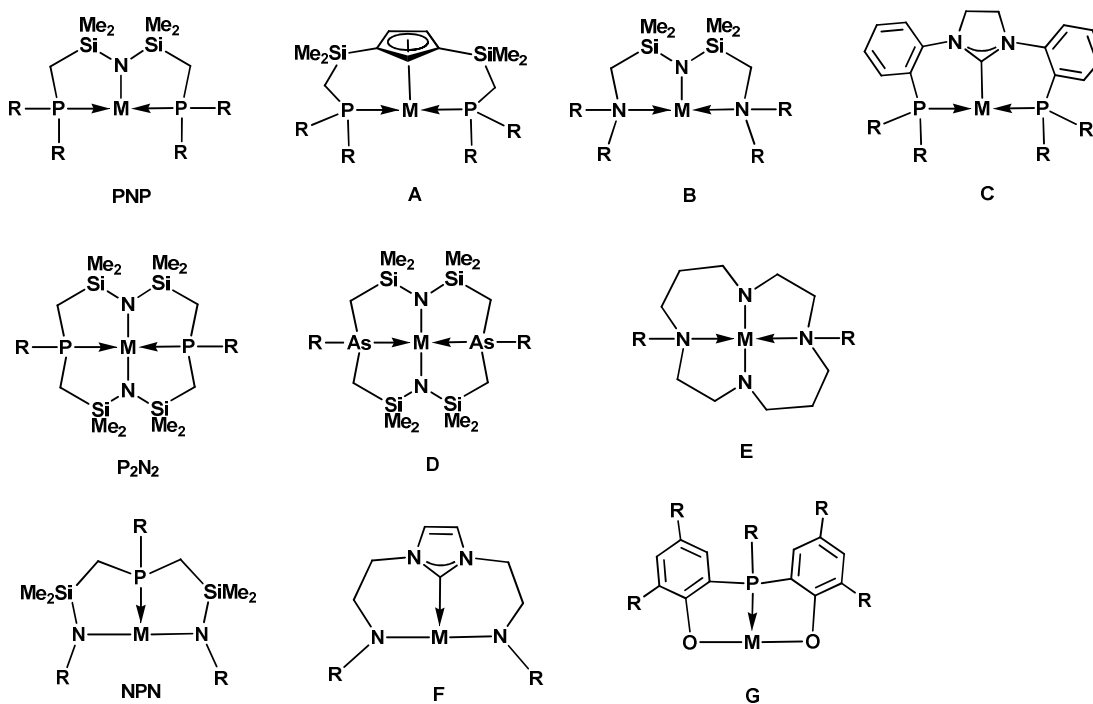


Figure 16: Donor variation for the PNP, P_2N_2 and NPN donor sets

The neutral phosphine donor was replaced by amine²⁰²⁻²⁰⁴ (**B** and **E**), arsine^{205, 206} (**D**) and an N-heterocyclic carbene with an unsaturated backbone²⁰⁷ (**F**). Another degree of variance is the organic fragments bonded to the donor groups. Phosphine donors with methyl^{208, 209} (**I**) in Figure 17), *i*-propyl^{135, 209} (**H**), *t*-butyl²⁰⁹ (**J**), cyclohexyl^{116, 210} (**L**) and phenyl^{80, 211, 212} (**K**) groups have been employed.

The organic spacer between the donor groups can be varied to contain two (**B**, **D** and **G**) or three (**A**, **C** and **F**) or a mixture of two and three (**E**) atoms. The methylene and SiMe₂ groups introduce flexibility into the backbone (**A**, **B**, **D** and **E**), whereas the *o*-phenylene and N-heterocyclic carbene groups impart planarity to provide a more rigid structure (**C**, **F** and **G**). The number of atoms in the spacer would affect the bite angles between the ligand donor atoms and the metal centre and the spacer flexibility could affect the range of reactivity possible for the metal complexes.

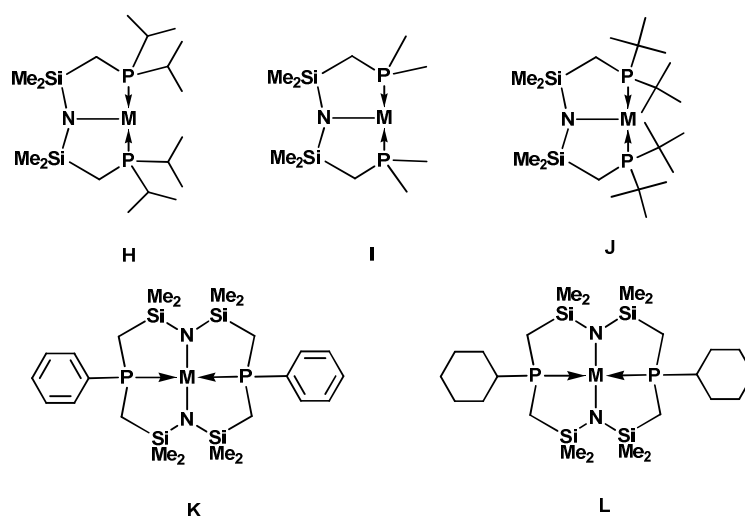


Figure 17: Variation in organic groups of phosphine donors

For the NPN donor set (Figure 18), the degree of aromaticity in the backbone was further varied via the introduction of a thiophene²¹³ (denoted ^SNPN) and a cyclopentenyl^{139, 140} (denoted ^{CY5}NPN) bridge. Despite extensive new reactivity observed with the ^{Si}NPN based group 4 and 5 dinitrogen complexes (see discussion in Chapter 1), further investigations were often hampered by ligand rearrangement, mostly due to the labile N-Si bond and the flexible backbone. Replacing -CH₂-SiMe₂- with an *o*-phenylene bridge (^{mes}NPN)^{92, 97, 214} may mitigate this problem, making the ligand more rigid while maintaining the relative amine basicity. The pK_a of diphenylamine (25)²¹⁵ and bis(trimethylsilyl)amine (26)²¹⁶ are similar, whereas secondary alkylamines (36) are more basic.²¹⁶

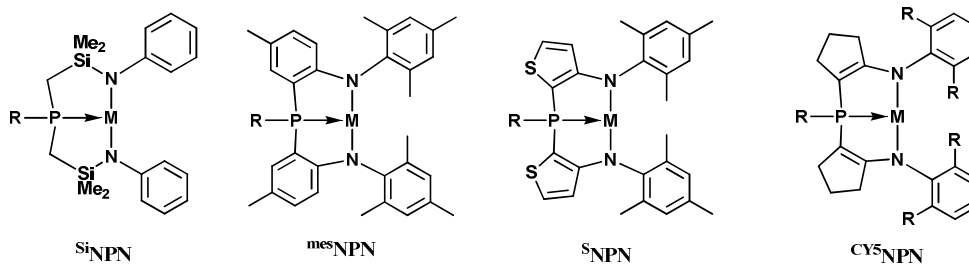


Figure 18: NPN donor sets with different backbones

In donor sets that contain terminal amido groups, i.e. the NPN donor set, the terminal organic fragment can also be varied. The Si^{NPN} donor set with flexible spacers contain terminal phenyl groups, whereas the mes^{NPN} , S^{NPN} and CY5^{NPN} donor sets contain sterically hindered mesityl,^{92, 213, 214} 2,6-dimethylphenyl and 2,6-diisopropylphenyl^{139, 140} groups (Figure 18).

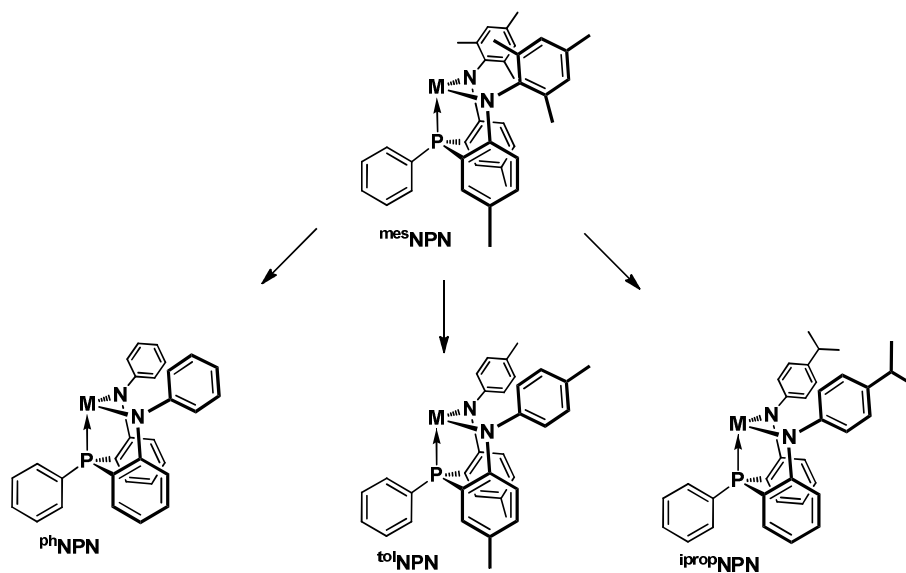


Figure 19: Summary of NPN donor sets with reduced steric bulk at the amido units

For this project, the key aim in ligand design was to reduce the steric bulk at the *ortho* position of the terminal aryl amido group for the *o*-phenylene bridged NPN donor set, which would reduce steric crowding in the vicinity of the metal centre. This could be achieved by replacement of the *N*-mesityl group with *N*-4-isopropylphenyl ($\text{iprop}^{\text{NPN}}$), *N*-4-methylphenyl

(^{tol}NPN), and *N*-phenyl (^{ph}NPN) (Figure 19). The ^{iprop}NPN, ^{tol}NPN and ^{ph}NPN ligands are expected to have similar chemical characteristics, but with decreasing relative solubilities.

The initial synthesis of the ^{mes}NPN donor set involved the formation of an intermediate *ortho*-brominated diarylamine (^{mes}Ar^{Br}ArNH) in a two-step process via a copper-catalysed C-N coupling, followed by bromination with NBS (see route **A** in Figure 20).^{97, 214} A modification of the original method allows for the one-step synthesis of ^{mes}Ar^{Br-Ph}ArNH in a 53% yield via a Buchwald-Hartwig arylation (see route **B** in Figure 20), using a palladium catalyst (2.0 mol% Pd) with a bidentate phosphine ligand Pd/DPPF (1:3).⁹⁷

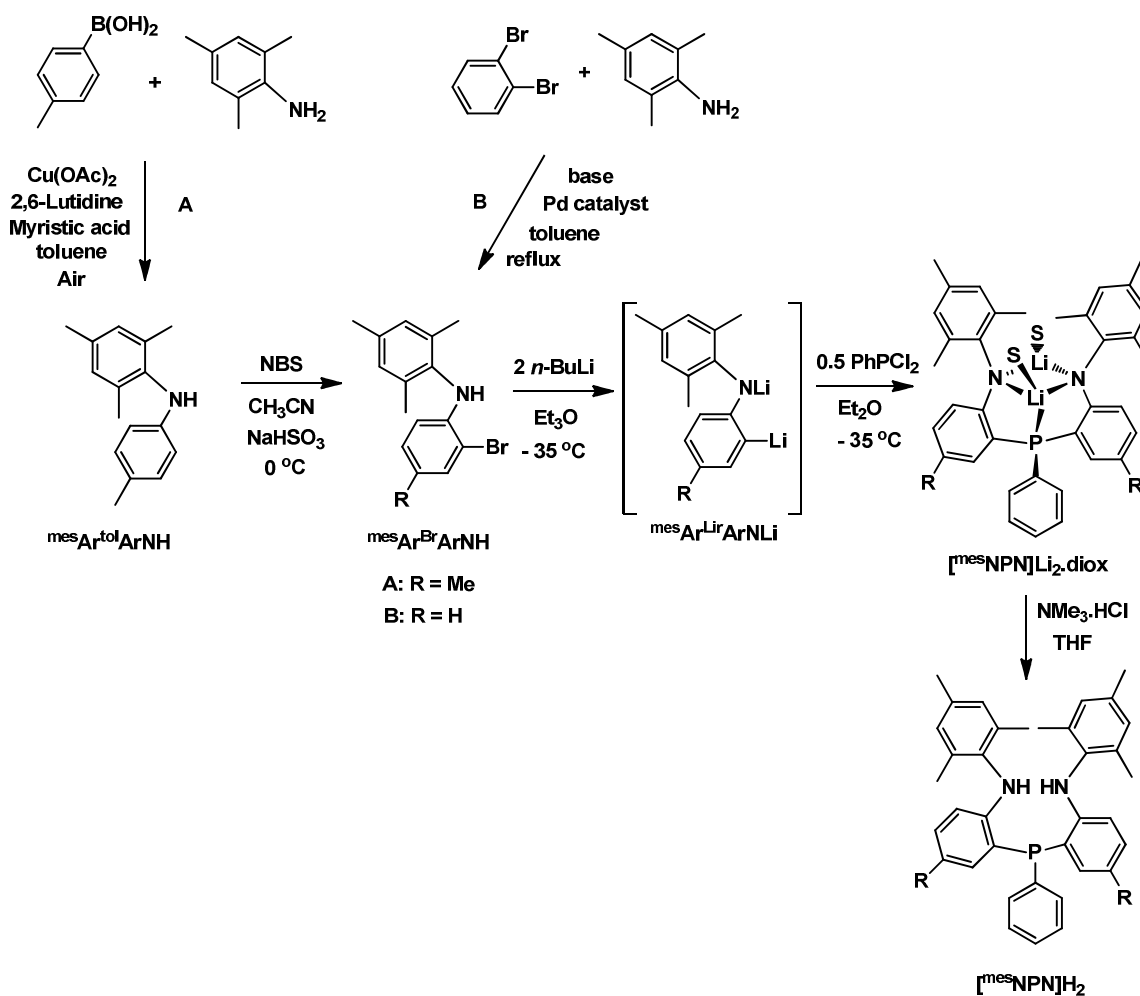


Figure 20: Synthesis of ^{mes}NPN precursors

Preliminary work on the ^{iprop}NPN donor set demonstrated that ^{iprop}Ar^{Br}ArNH [**2.1**] (Figure 22) could be prepared in 62% yield using a palladium catalyst (1.7 mol% Pd) with a bidentate phosphine ligand Pd/*rac*-BINAP (1:3).⁹⁷ These reactions were conducted at 80 °C to 85 °C over three to five days. While the effectiveness and versatility of mono-bromo-aryl substrates in the Buchwald-Hartwig reaction is well established,^{217, 218} there is less precedent using dihalo-arenes. Other reasonable examples include the reaction of C₆H₄BrI with aniline to form *N*-(2-Br-C₆H₄)-(C₆H₅)NH²¹⁹ and of *o*-C₆H₄Br₂ with *o*-nitroaniline to form *N*-(2-Br-C₆H₄)-(2-NO₂-C₆H₄)NH.²²⁰ However, *o*-C₆H₄Br₂ has also been reported to react with aniline at both halogen centres to form *o*-(PhNH)₂C₆H₄^{221, 222} and it can react with mono- and diarylanilines to form carbazoles.^{223, 224}

Mono-halo-arenes and halogenated anilines may also be used as substrates, for example 2-chloroaniline reacts with iodo- or bromoaryl substrates to give *ortho*-chlorinated diarylamines.²²⁴ However, under certain conditions carbazoles can be obtained from 2-chloroaniline and aryl bromides.²²⁵ In arylaminations involving mono-halo-arenes and halo-substituted anilines, it is desirable that the halogen on the arene be more reactive than on the aniline (I > Br > F)²²⁶, as demonstrated in the synthesis of the amido PNP pincer ligand precursors.²²⁷ Difficulties can be encountered when the same halogen is present on both the arene and the aniline, for example the reaction of *o*-bromo-aniline with MesBr is reported not to form the desired ^{mes}Ar^{Br}ArNH in the presence of a palladium catalyst.²²⁸

The type of ligand used during these palladium-catalysed reactions is of crucial importance. Bidentate diphosphines such as *rac*-BINAP^{220, 228} and DPEPhos²²⁴ favour *ortho*-halogenated diarylamines. However, the aforementioned *o*-(PhNH)₂C₆H₄ and carbazole products were obtained when bulky mono-phosphine donors (P^tBu₃ and PCy₃) were used.

The synthetic utility for making these new *o*-phenylene bridged diamidophosphine ligand precursors would be greatly enhanced if one could avoid the Buchwald-Hartwig arylamination

step altogether (with associated column chromatography purification). An alternative method, where the phosphorous atom is first attached to the arene backbone by reacting PhPCl_2 with *o*-Li- $\text{C}_6\text{H}_4\text{F}$,²²⁹ followed by aromatic nucleophilic substitution of the appropriate primary lithium amide, was briefly evaluated. However, this was abandoned as there were indications that the *in situ* generated *o*-Li- $\text{C}_6\text{H}_4\text{F}$ became involved in side reactions.²³⁰

It would be attractive to start with a commercially available secondary diaryl amine instead, and to this purpose, the directed *ortho* metalation (DOM), also known as heteroatom-facilitated *o*-lithiation, was investigated.²³¹⁻²³⁹ Reactions typically associated with aromatic benzene rings involve electrophilic substitution such as the Friedel-Crafts reaction as this is promoted by the delocalised pi-electron system. DOM reactions, however, involve nucleophilic substitution, which is disfavoured due to the inherent difficulty in removing a proton from the self-same pi-electron system.

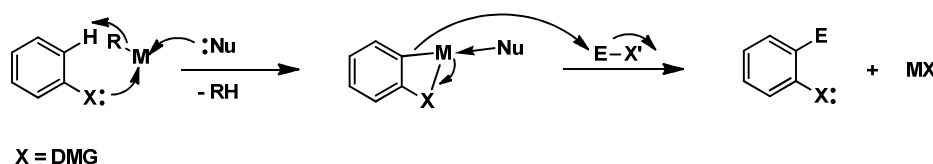


Figure 21: General DOM mechanism

The DOM reaction involves the initial coordination of an organometallic compound, usually RLi , to the lone pair of the directing metalation group (DMG) (Figure 21).²³²⁻²³⁴ DMGs typically contain oxygen, sulphur or nitrogen, decreasing in their ability to act as *ortho*-directors. The proton *ortho* to the DMG is deprotonated to form the *ortho*-lithiated species. This species can then be further reacted with the desired electrophile. The reaction is almost exclusively *ortho*-directing, but *meta*-directed examples have been reported.^{240, 241}

The application of the DOM reaction to amines is well established.^{232, 235, 242, 243} The first equivalent of *n*-BuLi is expected to react quickly with the N-H proton of the diarylamine

(Ar₂NH) to form an insoluble [Ar₂NLi]_n ladder aggregate.²⁴⁴ Addition of TMEDA serves two functions; firstly, it would solubilise the [Ar₂NLi]_n aggregate by disrupting the Li-N network to form a dimeric [Ar₂NLi·TMEDA]₂ species,²⁴⁵⁻²⁴⁷ and secondly, it would increase the basicity of the amido DMG group to promote coordination of the second *n*-BuLi.²³³ After deprotonation and *ortho*-lithiation, a dimeric [Ar^{*o*-Li}ArNLi·2TMEDA]₂ structure was observed with two TMEDA molecules per Ar^{*o*-Li}ArNLi units.²⁴⁶

The utility of the DOM reaction has potential to extend beyond a more efficient NPN ligand synthesis. Experimental evidence indicates that addition of 3 equiv of *n*-BuLi to tol₂NH with TMEDA gives the trilithio-diarylamide [(^{tol-Li}Ar)₂NLi·TMEDA]_n in high yield. This may replace the less efficient bromination step during the synthesis of a new class of diphosphine amido (PNP) ligands^{227, 248} that has proven to be highly efficient catalysts in carbon-carbon bond-forming reactions.^{249, 250}

2.1. Buchwald-Hartwig Arylamination

2.1.1. Synthesis of ^{iprop}Ar^{Br}ArNH [2.1]

^{iprop}Ar^{Br}ArNH [2.1] was obtained via the Buchwald-Hartwig amination in yields ranging from 26 - 37%, using a Pd/*rac*-BINAP (1:1.5) catalyst at 80 °C in toluene for 1 day (Figure 22). The lower catalyst loading (0.7 mol% Pd) and shorter reaction times were deemed to be sufficient, and is consistent with typical literature procedures.²²⁴ No significant increase in yield was observed for 3 days compared to 1 day. GC-MS analysis of the pre-column mixture did, however, indicate a higher 51% yield (Table 1, (i)), hence losses were incurred during inefficient column work-up procedures.

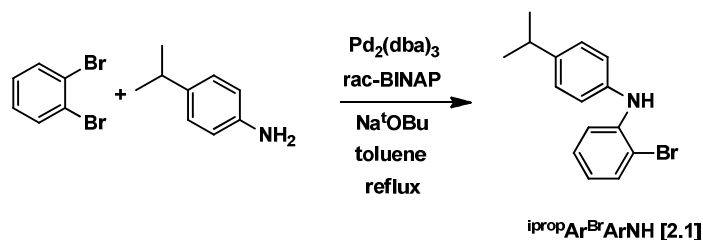


Figure 22: Synthesis of $\text{iprop-Ar}^{\text{Br}}\text{ArNH [2.1]}$ under $\text{Pd}_2\text{dba}_3/\text{rac-BINAP}/\text{toluene}$ catalytic conditions.

The GC-MS analysis of all reaction mixtures indicated a large amount of unreacted $4\text{-}^i\text{Pr-ArNH}/o\text{-C}_6\text{H}_4\text{Br}_2$ as well as a *ca* 4% iprop-ArArNH (Table 1). When a reaction with 1.8 mol% Pd, Pd/DPPF (1:3) was monitored over a 5 day period, the pre-column GC-MS yield decreased from 52.2% to 28.3, and the iprop-ArArNH side-product increased to 15.8%, with a larger amount of unidentified material. This suggests a catalyst decomposition pathway may exist where one or more products are more reactive than the reactants. iprop-ArArNH may be explained by protonation of a four-membered C_2NPd -palladacycle²⁵¹ formed by base-catalysed oxidative addition of Pd(BINAP) or Pd(DPPF) to $\text{iprop-Ar}^{\text{Br}}\text{ArNH [2.1]}$.

Table 1 : Pre-column GC-MS data for $\text{Pd}_2(\text{dba})_3/\text{rac-BINAP}$ catalyst, 0.7 mol% Pd and Pd/*rac*-BINAP (1:1.5).

| R.T. (min) | [M] ⁺ (m/z) | M | Relative concentrations (wt %) | | |
|------------|------------------------|---|--------------------------------|---------------------|---------------------|
| | | | (i) | (ii) | (iii) |
| 11.3 | 234 | $o\text{-C}_6\text{H}_4\text{Br}_2$ | 51.4 ^(a) | 51.6 ^(a) | 40.1 ^(a) |
| | 135 | $4\text{-}^i\text{Pr-ArNH}$ | | | |
| 16.6 | 211 | iprop-ArArNH | 3.9 | 4.1 | 3.8 |
| 18.0 | 291 | $\text{iprop-Ar}^{\text{Br}}\text{ArNH}$ | 41.6 | 37.8 | 22.11 |
| 22.6 | 344 | $o\text{-(}^i\text{prop-ArNH)}_2\text{C}_6\text{H}_4$ | 1.2 | - | - |
| - | - | unidentified | 1.8 | 6.5 | 33.3 |

(i) $4\text{-}^i\text{Pr-ArNH}_2/o\text{-C}_6\text{H}_4\text{Br}_2/\text{Na}^t\text{OBu}$ (1:0.9:1.3), (ii) $4\text{-}^i\text{Pr-ArNH}_2/o\text{-C}_6\text{H}_4\text{Br}_2/\text{Na}^t\text{OBu}$ (1:0.5:1.3), (iii) $4\text{-}^i\text{Pr-ArNH}_2/o\text{-C}_6\text{H}_4\text{Br}_2/\text{K}^t\text{OBu}$ (1:2.1:1.2), ^(a) combined $o\text{-C}_6\text{H}_4\text{Br}_2 + 4\text{-}^i\text{Pr-ArNH}_2$

Certain reaction conditions for the synthesis of $\text{iprop-Ar}^{\text{Br}}\text{ArNH [2.1]}$ were varied, all at a reaction temperature of 80 °C:

(i) Effect of ligand (*rac*-BINAP vs DPPF): When the ligand was changed from *rac*-BINAP to Pd/DPPF (1:3) with a slightly higher catalyst loading of 1.8 mol% Pd, the pre-column GC-MS

data indicates a 52.2% yield (isolated yield 33%), which shows no observable improvement over the $\text{Pd}_2(\text{dba})_3/\text{rac-BINAP}$ catalyst system (Table 1, (i)).

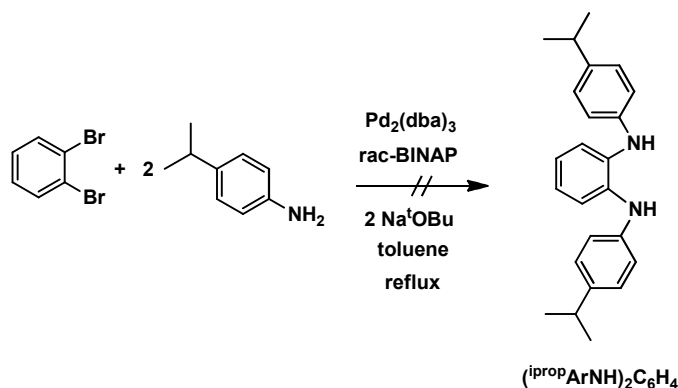


Figure 23: Potential formation of $o\text{-(ipropArNH)}_2\text{C}_6\text{H}_4$

(ii) Effect of increased $4\text{-}i\text{PrArNH}$: Increasing the amount of $4\text{-}i\text{PrArNH}$ could favour formation of the bis-diarylamine side-product, $o\text{-(ipropArNH)}_2\text{C}_6\text{H}_4$ (Figure 23). There are no significant changes in the composition of the pre-column mixture (Table 1, (ii) compared to (i)); most notably only a trace amount of $o\text{-(ipropArNH)}_2\text{C}_6\text{H}_4$ is observed to form. This agrees with literature evidence that a bulky mono-phosphine ligand such as P^tBu_3 is required to promote coordination of a second $4\text{-}i\text{PrArNH}$ molecule to form the bis-arylamine species.²²¹

(iii) Effect of increased $o\text{-C}_6\text{H}_4\text{Br}_2$: Another possible side-reaction may be the formation of $\text{ipropArN}(o\text{-C}_6\text{H}_4\text{Br})_2$ due to competition between the primary and secondary amine (Figure 24). However, no $[\text{M}]^+$ of 971 m/z is ever observed for this reaction, even when $o\text{-C}_6\text{H}_4\text{Br}_2$ is doubled (see Table 1, (iii)).

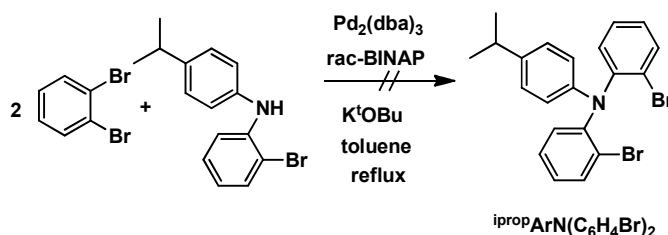


Figure 24: Potential formation of $\text{ipropArN}(\text{C}_6\text{H}_4\text{Br})_2$

(iv) Effect of bases: The lower yield and greater amount of unidentified material observed for data in Table 1, (iii) is not due to increased *o*-C₆H₄Br₂ and could be attributed to changing the base from Na^tOBu to K^tOBu. As reported previously, Na^tOBu is the base of choice.

(v) Effect of increased catalyst loading: After reaction for 3 days, a second aliquot of Pd₂(dba)₃/*rac*-BINAP was added, maintaining Pd/*rac*-BINAP (1:1.5). However, after further reaction for 2 days, no additional benefit could be observed, with the final isolated yield being 37%.

(vi) Effect of increased Pd/*rac*-BINAP ratio: When the Pd/*rac*-BINAP ratio was increased from 1:1.5 to 1:3, together with an increased catalyst loading, a lower isolated yield of 21% was obtained. Mechanistic studies of the Pd₂dba₃/*rac*-BINAP system have revealed that in solution a mixture of mono- and bis-BINAP complexes exists, viz. Pd(BINAP)(dba), Pd(BINAP)₂(dba) and Pd(BINAP)₂, with the bis-BINAP species predominating.²⁵² The active catalyst Pd(BINAP) is formed from Pd(BINAP)₂ / Pd(BINAP)₂(dba) in a pre-equilibrium step. It may be that the equilibrium was shifted too far towards the bis-BINAP complexes.

It was later found that increasing the oil bath temperature from 80 °C to 130-140 °C with a Pd/DPPF (1:3) catalyst and a higher loading (6 mol% Pd) led to a significantly increased pre-column GC-MS yield of 82% with a shorter reaction time of 7 hrs. This agrees with what was reported for the reaction of N-2,4,6-trimethylphenylamine with *o*-dibromobenzene.²²⁸ The main disadvantage of this method remains the column purification step, which impedes the ability to scale-up the reaction. Further increase in yield may be possible by changing to a higher boiling solvent such as Bu₂O, but it would be more difficult to remove the solvent during subsequent work-up procedures.

2.2. Directed *Ortho*-Metallation (DOM) Reaction

2.2.1. Synthesis of $[\text{tol-Ar}^{\text{Li}}\text{ArNLi}\cdot\text{TMEDA}]_2$ [2.2] and $[\text{ph-Ar}^{\text{Li}}\text{ArNLi}\cdot 1.5\text{TMEDA}]_2$ [2.3]

Tol₂NH and Ph₂NH react with two equiv of *n*-BuLi and TMEDA in *n*-hexanes to give the white solids $[\text{tol-Ar}^{\text{Li}}\text{ArNLi}\cdot\text{TMEDA}]_2$ [2.2] and $[\text{ph-Ar}^{\text{Li}}\text{ArNLi}\cdot 1.5\text{TMEDA}]_2$ [2.3] (Figure 26). High yields of 75% to 90% were obtained, irrespective if one or two equiv of TMEDA were used. The $^7\text{Li}\{^1\text{H}\}$ NMR spectrum of $[\text{tol-Ar}^{\text{Li}}\text{ArNLi}\cdot\text{TMEDA}]_2$ [2.2] displays a peak at δ 0.73 in C₆D₆ (Figure 25), but no signal could be observed for $[\text{ph-Ar}^{\text{Li}}\text{ArNLi}\cdot 1.5\text{TMEDA}]_2$ [2.3] as it is only sparingly soluble in C₆D₆.

The ^1H NMR spectrum of the isolated solid $[\text{tol-Ar}^{\text{Li}}\text{ArNLi}\cdot\text{TMEDA}]_2$ [2.2] in C₆D₆ has a single peak at δ 1.76 for coordinated TMEDA (δ 2.04 for CH₃ and δ 2.18 for CH₂ for free TMEDA) (Figure 25) with relative integration indicating only one TMEDA per $\text{tol-Ar}^{\text{Li}}\text{ArNLi}$, which is corroborated by a solid state molecular structure (see later discussion). The $^7\text{Li}\{^1\text{H}\}$ NMR spectrum of [2.2] exhibits a more shielded signal at δ -1.16 in THF-*d*₈ compared to C₆D₆ (Figure 25), which suggests that the THF solvated species may have increased basicity. In THF-*d*₈ (Figure 25), the TMEDA in [2.2] displays two peaks at δ 2.16 for CH₃ and δ 2.101 for CH₂ indicating free TMEDA. The residual THF signals at δ 1.73 and δ 3.58 suggest exchange between completely solvated (coordinated) THF and large excess THF solvent (free THF at δ 1.73 and δ 3.58). A dimeric $[\text{tol-Ar}^{\text{Li}}\text{ArNLi}\cdot 2\text{THF}]_2$ species may be formed on solvation of $[\text{tol-Ar}^{\text{Li}}\text{ArNLi}\cdot\text{TMEDA}]_2$ [2.2] in THF (Figure 26). As lithium ions in solvated lithium amide structures may have two THF ligands,²⁴⁵ solvated species with a molecular formulae $[\text{tol-Ar}^{\text{Li}}\text{ArNLi}\cdot 4\text{THF}]_n$ may also be possible, wherein the dimer structure could possibly disaggregate into monomers.

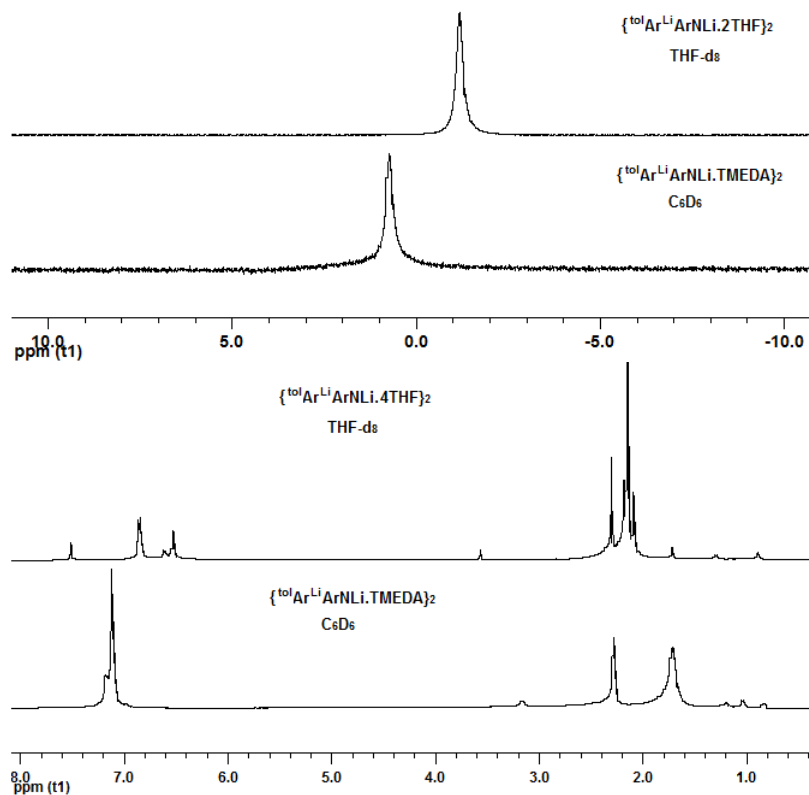


Figure 25: $^7\text{Li}\{^1\text{H}\}$ (top) and ^1H NMR (bottom) spectra of $[\text{tol-Ar}^{\text{Li}}\text{ArNLi} \cdot \text{TMEDA}]_2$ [2.2] in C_6D_6 and THF-d_8

The $^7\text{Li}\{^1\text{H}\}$ NMR spectrum of solvated $[\text{ph-Ar}^{\text{Li}}\text{ArNLi} \cdot 1.5\text{TMEDA}]_2$ [2.3] displays a singlet at δ -0.91 in THF-d_8 . Relative integration of free TMEDA in the ^1H NMR spectrum of solvated [2.3] in THF-d_8 indicates 1.5 TMEDA per $\text{ph-Ar}^{\text{Li}}\text{ArNLi}$ unit and elemental analysis of this solid also confirms 1.5 TMEDA. A possible hybrid structure is proposed for $[\text{ph-Ar}^{\text{Li}}\text{ArNLi} \cdot 1.5\text{TMEDA}]_2$ [2.3] between dimeric $[\text{ph-Ar}^{\text{Li}}\text{ArNLi} \cdot \text{TMEDA}]_2$ and monomeric $\text{ph-Ar}^{\text{Li}}\text{ArNLi} \cdot 2\text{TMEDA}$ resonance structures (Figure 26). Lithium ions in solvated lithium amide structures may have two donor ligands, i.e., bidentate TMEDA.²⁴⁶

As the cyclic ether tetrahydropyran performed better than TMEDA in the DOM of phenol,²³⁶ a reaction was conducted with 1,4-dioxane instead of TMEDA. However, no *ortho*-lithiated product was observed, which emphasizes the importance of being able to depolymerise the $[\text{Ar}_2\text{NLi}]_n$ aggregate.²⁴⁴

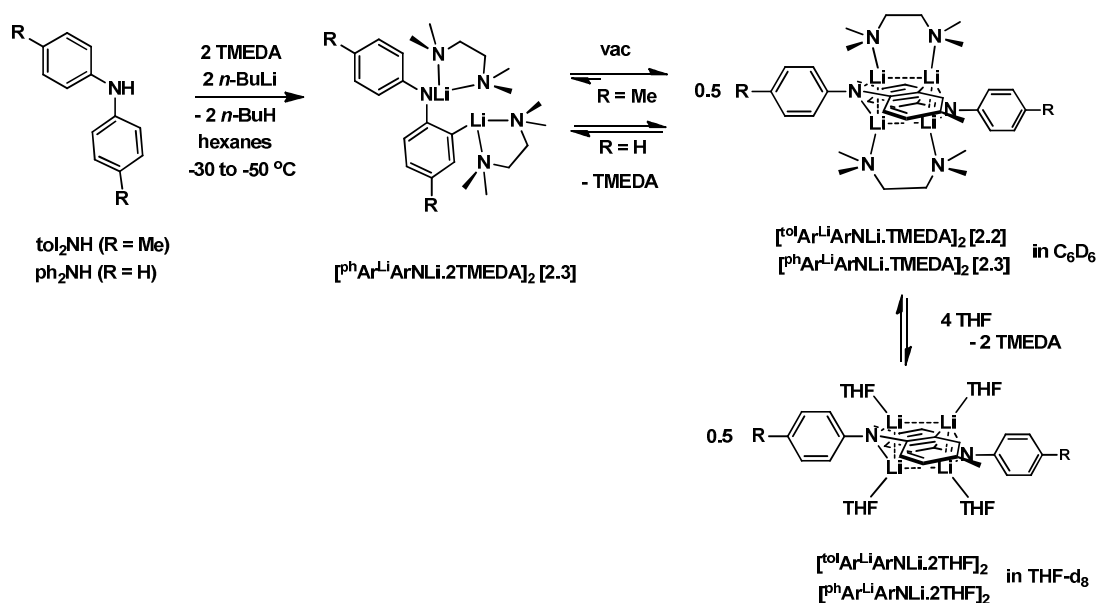


Figure 26: Synthesis of $[\text{Ar}^{\text{Li}}\text{ArNLi} \cdot \text{TMEDA}]_2$ [2.2] and $[\text{Ar}^{\text{Li}}\text{ArNLi} \cdot 1.5\text{TMEDA}]_2$ [2.3]

The solid state molecular structure of $[\text{Ar}^{\text{Li}}\text{ArNLi} \cdot \text{TMEDA}]_2$ [2.2] was obtained (Figure 27). Each dimeric $[\text{Ar}^{\text{Li}}\text{ArNLi} \cdot \text{TMEDA}]_2$ unit has a core containing four lithium, four carbon and two nitrogen atoms. Two of the lithiums (Li1 and 'Li1) are three-coordinate and the other two (Li8 and 'Li8) are five-coordinate. The four lithium atoms form a rhombus with an average $\text{Li} \cdots \text{Li}$ distance of 2.277 Å (Table 2), which is shorter than the sum of the van der Waals radii between two lithium atoms (3.64 Å). The diagonal $\text{Li8} \cdots \text{Li8}$ distance of 2.1176(6) Å may also represent a non-bonding close contact.

One of the nitrogen atoms of the TMEDA is bonded to a three-coordinate lithium N19-Li1 2.032(3) Å and the other to a five-coordinate lithium N19a-Li8 2.052(3) Å. The amido nitrogen atoms are bonded to two lithium atoms, one three- and one five-coordinate i.e. N8-Li1 (2.006(3) Å) and N8-'Li8 (1.985(3) Å), with neither of these lithium atoms bonded to the same TMEDA molecule. These bond lengths compare well with those reported for other lithium amides.^{245, 246, 253}

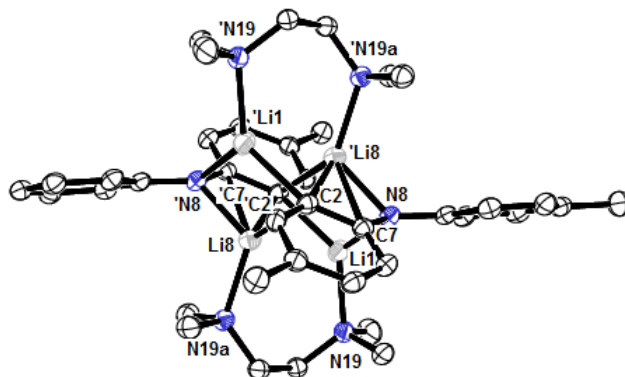


Figure 27: ORTEP representation of the solid state molecular structure of $[\text{tol-Ar}^{\text{Li}}\text{ArNLi} \cdot \text{TMEDA}]_2$ [2.2]

The C2- Li1 , C2- Li8 and C2- Li8 bond lengths for the *ortho*-carbon are 2.169(4), 2.601(3) and 2.666(3) Å, which compares with average Li-C bond lengths of 2.67 Å reported for a ferrocenyllithium and other aryllithium compounds.^{246, 254-259} The C7- Li8 bond length for the *ipso*-carbon adjacent to the nitrogen atom is longer at 2.238(3) Å, but still shorter than the weak $\text{Li} \cdots \text{C}$ intermolecular association reported for $\text{Ph}(\text{naphthyl})\text{NLi} \cdot \text{TMEDA}$ at 3.12 and 3.15 Å.²⁴⁶

Table 2 : Selected bond lengths (Å) and angles (°) for $[\text{tol-Ar}^{\text{Li}}\text{ArNLi} \cdot \text{TMEDA}]_2$ [2.2]

| $[\text{tol-Ar}^{\text{Li}}\text{ArNLi} \cdot \text{TMEDA}]_2$ | | | |
|--|------------|-----------------------|-------------|
| $\text{Li1} \cdots \text{Li8}$ | 2.282(4) | N19-Li1-Li8 | 103.61(15) |
| $\text{Li1} \cdots \text{Li8}$ | 2.271(4) | N19-Li1-Li8 | 164.70(18) |
| Li1-N8 | 2.006(3) | N19-Li1-N8 | 117.93(16) |
| Li1-N19 | 2.032(3) | N19-Li1-C2 | 131.71(16) |
| Li1-C2 | 2.169(4) | | |
| $\text{Li8} \cdots \text{Li1}$ | 2.271(4) | N19a-Li8-Li1 | 97.04(14) |
| $\text{Li8} \cdots \text{Li1}$ | 2.282(4) | N19a-Li8-Li1 | 152.118(17) |
| Li8-N8 | 1.985(3) | N19a-Li8-N8 | 117.89(16) |
| Li8-N19a | 2.052(3) | N19a-Li8-C2 | 121.74(15) |
| Li8-C2 | 2.601(3) | N19a-Li8-C2 | 126.69(15) |
| Li8-C2 | 2.666(3) | N19a-Li8-C7 | 122.08(14) |
| $\text{Li8} \cdots \text{C7}$ | 2.238(3) | N19a-Li8-Li8 | 150.9(2) |
| $\text{Li8} \cdots \text{Li8}$ | 2.1176(6) | | |
| Li8-N8-Li1 | 76.93(13) | Li8-Li8-N8 | 87.61(14) |
| Li1-Li8-N8 | 124.82(16) | Li1-Li8-N8 | 51.92(11) |
| Li1-Li8-Li1 | 109.03(14) | Li1-Li8-Li8 | 54.69(12) |
| Li8-Li1-Li8 | 70.97(14) | Li1-Li8-Li8 | 54.34(12) |

Compounds $[\text{}^{\text{tol}}\text{Ar}^{\text{Li}}\text{ArNLi}\cdot\text{TMEDA}]_2$ [**2.2**] and $[\text{}^{\text{ph}}\text{Ar}^{\text{Li}}\text{ArNLi}\cdot 1.5\text{TMEDA}]_2$ [**2.3**] were deuterolyzed with D_2O in THF (Figure 28) and parent ions were observed at 199 m/z and 171 m/z in their respective electron impact mass spectra.

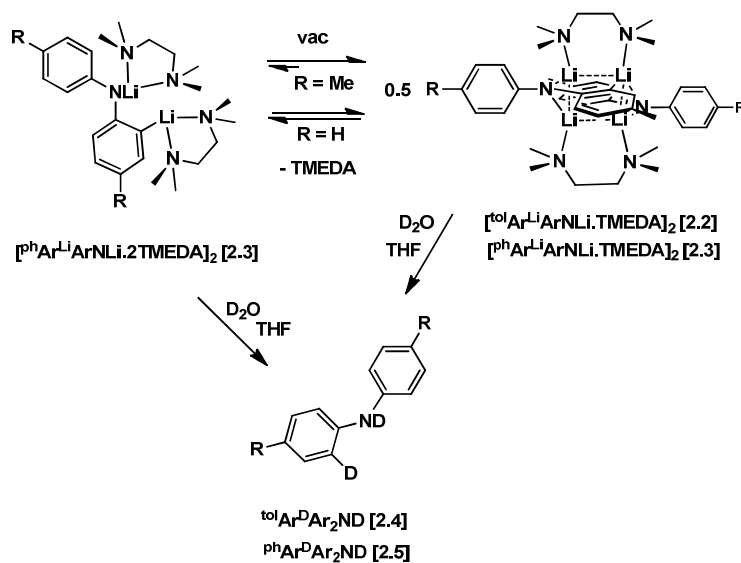


Figure 28: Synthesis of $\text{}^{\text{tol}}\text{Ar}^{\text{D}}\text{ArND}$ [**2.4**] and $\text{}^{\text{ph}}\text{Ar}^{\text{D}}\text{ArND}$ [**2.5**]

The ^2H NMR spectrum of $\text{}^{\text{tol}}\text{Ar}^{\text{D}}\text{ArND}$ [**2.4**] in benzene displays two peaks in a 1:1 ratio at δ 4.91 (N-D) and δ 6.85 (Ar-D) (Figure 29) and of $\text{}^{\text{ph}}\text{Ar}^{\text{D}}\text{ArND}$ [**2.5**] at δ 4.97 (N-D) and δ 6.85 (Ar-D).

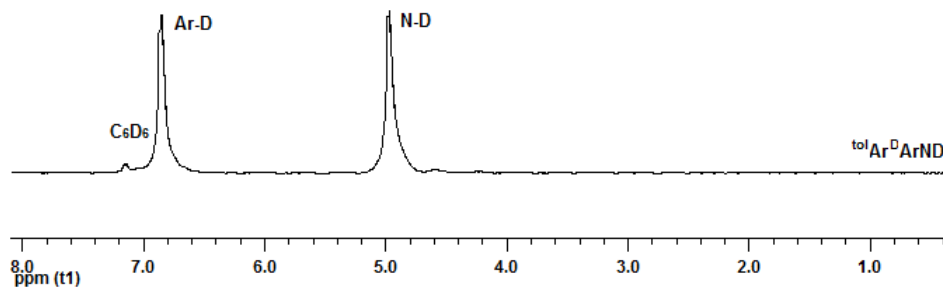


Figure 29: ^2H NMR spectrum of $\text{}^{\text{tol}}\text{Ar}^{\text{D}}\text{ArND}$ [**2.4**] in C_6H_6

2.3. Lithiated NPN Ligands

2.3.1. Synthesis of $[\text{ipropNPNLi}_2\cdot\text{diox}]_n$ [2.6]

The synthesis of $[\text{ipropNPNLi}_2\cdot\text{diox}]_n$ [2.6] was reported in a preliminary study, together with the solid state molecular structure.⁹⁷ However, NMR spectroscopic data was only given for the THF adduct $\text{ipropNPNLi}_2\cdot 2\text{THF}$. $[\text{ipropNPNLi}_2\cdot\text{diox}]_n$ [2.6] is obtained from $\text{ipropAr}^{\text{Br}}\text{ArNH}$ [2.1] in a two-step one-pot process (Figure 30). In the first step, [2.1] reacts with *n*-BuLi in Et₂O to form an aryllithium lithioamido intermediate ($\text{ipropAr}^{\text{Li}}\text{ArNLi}$). Although $\text{ipropAr}^{\text{Li}}\text{ArNLi}$ is not isolated, the solid state molecular structure of analogous $[\text{2,6diipropAr}^{\text{Li}}\text{ArNLi}\cdot 2\text{THF}]_2$ [7.3a] reported in chapter 7 suggests a dimer with two solvent molecules per $\text{ipropAr}^{\text{Li}}\text{ArNLi}$ unit. It is imperative that exactly two equiv of *n*-BuLi are used in order to avoid undesired side reactions in the subsequent PPhCl₂ quenching step.

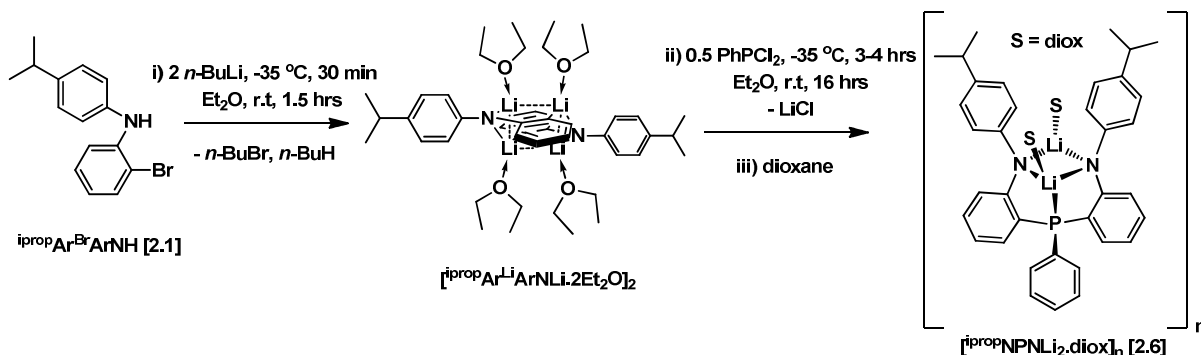


Figure 30: Synthesis of $[\text{ipropNPNLi}_2\cdot\text{diox}]_n$ [2.6]

The second step involves quenching the aryllithium moiety with the electrophile PPhCl₂. The PPhCl₂ was added as a dilute ethereal solution (0.04 to 0.25 M) with a controlled addition rate of 1-2 cm³/min. The reaction temperature should ideally be maintained between -30 to -40 °C during the PPhCl₂ addition; while lower temperatures than -40 °C are acceptable, higher temperatures are to be avoided (*vide infra*). The final product $[\text{ipropNPNLi}_2\cdot\text{diox}]_n$ [2.6] is isolated in 78 - 93% yields as the 1,4-dioxane adduct, which is an improvement on the previously

reported yield of 66%.⁹⁷ Deviation from these reaction conditions leads to a greater concentration of side-products, which form a tar-like residue that inhibits precipitation of [^{iprop}NPNLi₂·diox]_n [**2.6**]. Heating the crude material to 60 °C helps to dissolve these tarry side-products and allows the isolation of pure [**2.6**] as a fluffy yellow powder. Compound [**2.6**] is stable indefinitely at room temperature in the absence of air or moisture, both in solution and as a solid.

The solid-state molecular structure of [^{iprop}NPNLi₂·diox]_n [**2.6**] (Figure 31)⁹⁷ shows that one 1,4-dioxane molecule bridges two ^{iprop}NPNLi₂ units, forming a one-dimensional chain. The Li22 is coordinated to P1 in a distorted tetrahedral geometry and the other Li23 atom has a distorted trigonal geometry. The Li22-Li23 distance of 2.217(10) Å for the N₂Li₂ diamond core is shorter than the sum of the van der Waals radii between two lithium atoms (3.64 Å). The bond lengths and angles are similar to those reported for the [^{Ph,mes}NPNLi₂·diox]_n chain structure⁹⁷ and monomeric ^{mes}NPNLi₂·2THF^{97, 214} (Table 3).

Table 3 : Comparative bond lengths (Å) and angles (°) for the ^{iprop}NPNLi₂ and ^{mes}NPNLi₂ donor sets.⁹⁷

| | [^{iprop} NPNLi ₂ ·diox] _n | [^{Ph,mes} NPNLi ₂ ·diox] _n | ^{mes} NPNLi ₂ ·2THF |
|----------------------|---|--|---|
| P1-Li22 | 2.278(7) | 2.284(8) | 2.410(3) |
| Li22-O27 | 1.868(8) | 1.892(9) | 1.908(3) |
| L23-O24 | 1.867(8) | 1.910(9) | 1.932(3) |
| N8-Li22 | 2.050(9) | 2.056(9) | 2.078(3) |
| N8-Li23 | 1.974(9) | 2.022(9) | 2.046(4) |
| N8a-Li22 | 2.079(8) | 2.065(9) | 2.076(3) |
| N8a-Li23 | 1.978(9) | 2.014(10) | 2.051(3) |
| Li22...Li23 | 2.217(10) | 2.274(12) | 2.418(4) |
| N8-Li22-N8a | 102.11(3) | 103.7(4) | 103.71(15) |
| N8-Li23-N8a | 109.5(4) | 106.7(3) | 105.76(15) |
| Li22-N8-Li23 | 73.1(3) | 74.8(2) | 75.26(13) |
| Li22-N8a-Li23 | 73.8(3) | 74.7(4) | 75.21(13) |
| P1-Li22-N8 | 81.0(3) | 81.1(2) | 80.56(11) |
| P1-Li22-N8a | 81.3(3) | 81.8(2) | 81.55(11) |
| P1-Li22-O27 | 125.0(4) | 136.6(3) | 138.07(16) |
| P1-Li22-Li23 | 80.9(3) | 77.4(3) | 77.01(11) |
| O24-Li23-N8 | 131.3(4) | 122.9(5) | 123.57(16) |
| O24-Li23-N8a | 120.0(4) | 126.3(5) | 126.96(17) |
| O27-Li22-N8 | 123.4(5) | 118.8(4) | 115.48(16) |
| O27-Li22-N8a | 126.7(5) | 123.8(5) | 126.13(16) |

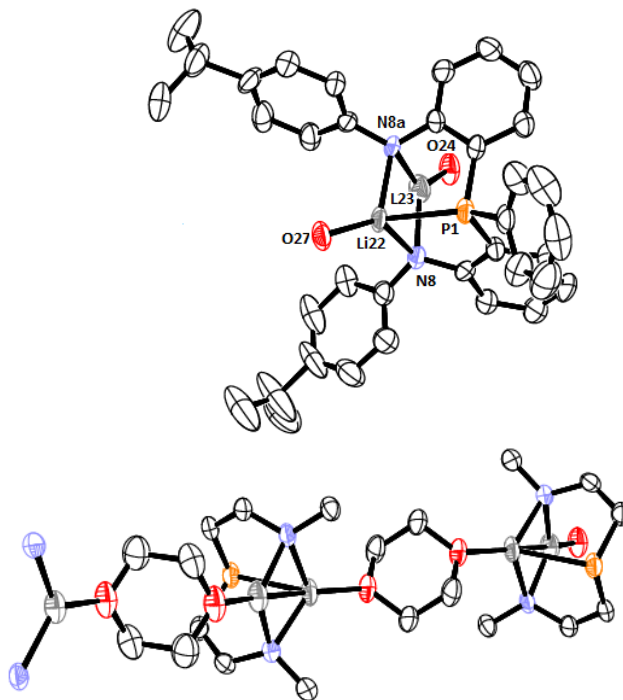


Figure 31: ORTEP representation of the solid-state molecular structure of $[\text{ipropNPnLi}_2 \cdot \text{diox}]_n$ [2.6]⁹⁷

The Li22-O27 and Li23-O24 bond lengths are shorter for $[\text{ipropNPnLi}_2 \cdot \text{diox}]_n$ [2.6] than $[\text{Ph,mesNPnLi}_2 \cdot \text{diox}]_n$ and $\text{mesNPnLi}_2 \cdot 2\text{THF}$. The less bulky 4-*iso*-propyl amido group thus enhances coordination of the oxygen donor, leading to a more strongly bound 1,4-dioxane. The P1-Li22 bond length is longer for $\text{mesNPnLi}_2 \cdot 2\text{THF}$ compared to $[\text{Ph,mesNPnLi}_2 \cdot \text{diox}]_n$ and $[\text{ipropNPnLi}_2 \cdot \text{diox}]_n$ [2.6], and the THF adduct would be expected to have a weaker P-Li bond.

In the previously reported synthesis of the THF adduct $\text{ipropNPnLi}_2 \cdot 2\text{THF}$, values for bound THF were observed at δ 3.10 and δ 1.06 in the ^1H NMR spectrum (δ 3.58 and δ 1.73 for free THF).⁹⁷ $\text{ipropNPnLi}_2 \cdot 2\text{THF}$ is expected to have a monomeric structure similar to what was observed in the solid state molecular structure of $\text{mesNPnLi}_2 \cdot 2\text{THF}$,^{97, 214} where the P-Li coupling is maintained (Figure 33). The signal for 1,4-dioxane in the ^1H NMR spectrum of $[\text{ipropNPnLi}_2 \cdot \text{diox}]_n$ [2.6] in C_6D_6 is at δ 3.09 (free 1,4-dioxane at δ 3.53) and the relative

integration of the peak indicates that only one molecule of 1,4-dioxane is present (Figure 32), which is consistent with the previously reported solid state molecular structure.⁹⁷

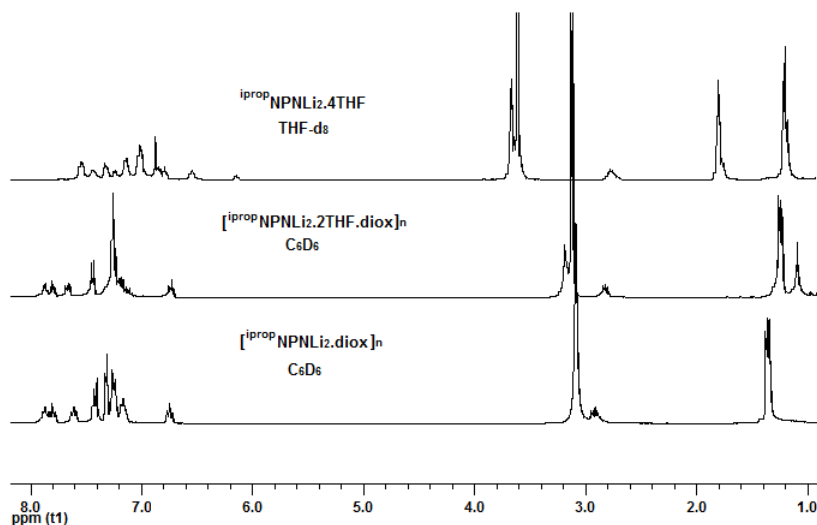


Figure 32: ^1H NMR spectra for the ipropNPNLi_2 donor set: 1,4-dioxane, mixed 1,4-dioxane/THF and THF adducts

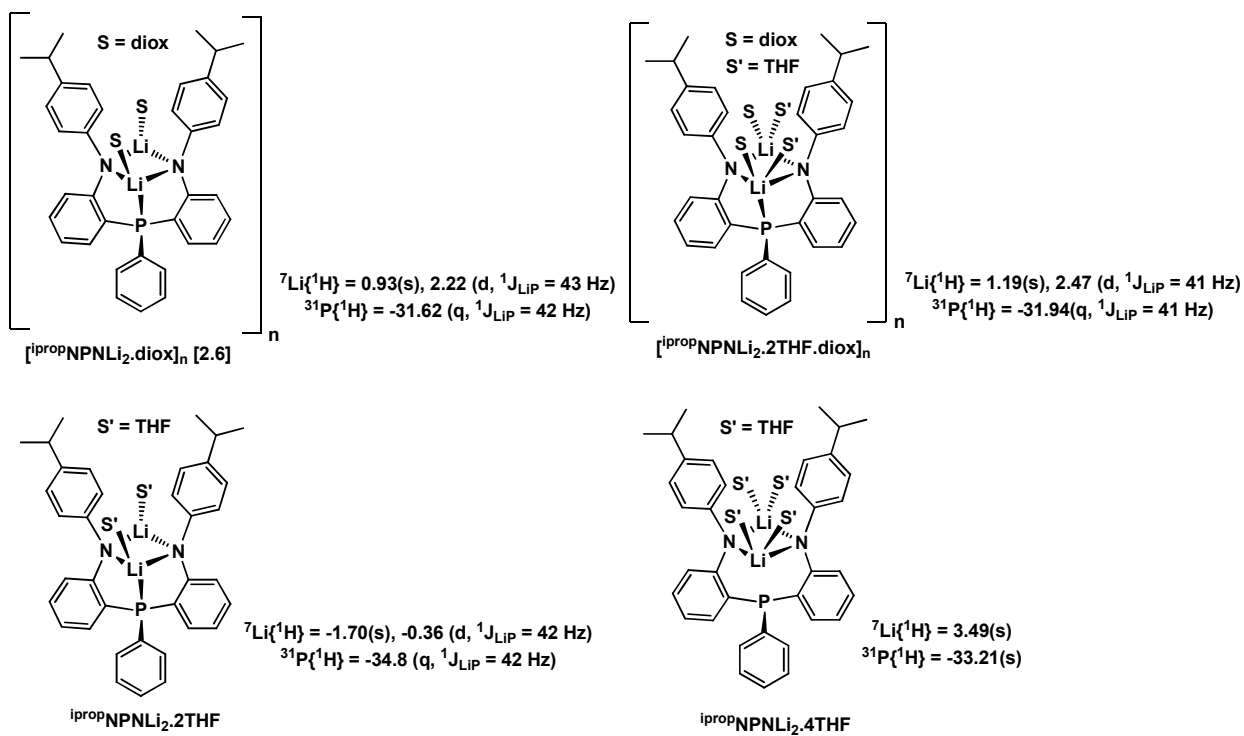


Figure 33: Chain and monomeric forms of the ipropNPNLi_2 donor set

When two equiv of THF are added to $[\text{ipropNPNLi}_2\cdot\text{diox}]_n$ **[2.6]** in C_6D_6 , both the 1,4-dioxane and THF remain bound to lithium (Figure 32), forming a mixed THF/1,4-dioxane adduct, $[\text{ipropNPNLi}_2\cdot 2\text{THF}\cdot\text{diox}]_n$.

The ^1H NMR spectrum in THF-d_8 spiked with THF has a peak for 1,4-dioxane at δ 3.58 and THF peaks at δ 3.64 and δ 1.80 (Figure 32). This indicates that 1,4-dioxane is no longer bound and that the THF is weakly coordinated or exchange occurs between bound THF and a large excess free THF. A monomeric $\text{ipropNPNLi}_2\cdot 4\text{THF}$ species may be formed in excess THF (Figure 33), similar in structure to that reported for dimeric *N*-lithiocarbazole.²⁶⁰

The $^{31}\text{P}\{^1\text{H}\}$ NMR spectrum of $[\text{ipropNPNLi}_2\cdot\text{diox}]_n$ **[2.6]** in C_6D_6 displays a quartet at δ -31.62 ($^1J_{\text{PLi}} = 42$ Hz) and the $^7\text{Li}\{^1\text{H}\}$ NMR spectrum shows a singlet at δ 0.93 and a doublet at δ 2.62 ($^1J_{\text{LiP}} = 43$ Hz) (Figure 34 and Figure 35). The quartet in the $^{31}\text{P}\{^1\text{H}\}$ NMR spectrum and the doublet in the $^7\text{Li}\{^1\text{H}\}$ NMR spectrum are due to coupling of one of the Li atoms (Li22) to the P atom (P1). These values are similar to what was obtained for $\text{ipropNPNLi}_2\cdot 2\text{THF}$ and other NPNLi_2 derivatives.^{79, 80, 97, 114, 214}

As the peaks in the $^7\text{Li}\{^1\text{H}\}$ NMR spectrum for $[\text{ipropNPNLi}_2\cdot\text{diox}]_n$ **[2.6]** are shifted δ 2.7 downfield compared to $\text{ipropNPNLi}_2\cdot 2\text{THF}$ ⁹⁷ in C_6D_6 (Figure 35), the oxygen of the monomeric species (THF adduct) may be more strongly bound to Li than in the chain structure (1,4-dioxane adduct). The peaks in the $^{31}\text{P}\{^1\text{H}\}$ NMR spectrum of $\text{ipropNPNLi}_2\cdot 2\text{THF}$ ⁹⁷ have also shifted 3.18 ppm upfield (Figure 34), indicating that the P atom is more weakly bound, reminiscent of the longer Li-P bond length obtained for $\text{mesNPNLi}_2\cdot 2\text{THF}$. The Li22-Li23 distance of 2.217(10) Å for the N_2Li_2 diamond core is shorter than the sum of the Van Der Waals Radii for two lithium atoms (3.64 Å). The bond lengths and angles are similar to those reported for the $[\text{Ph},\text{mesNPNLi}_2\cdot\text{diox}]_n$ chain structure^[22] and monomeric $\text{mesNPNLi}_2\cdot 2\text{THF}$ ^[22, 23] (Table 3).

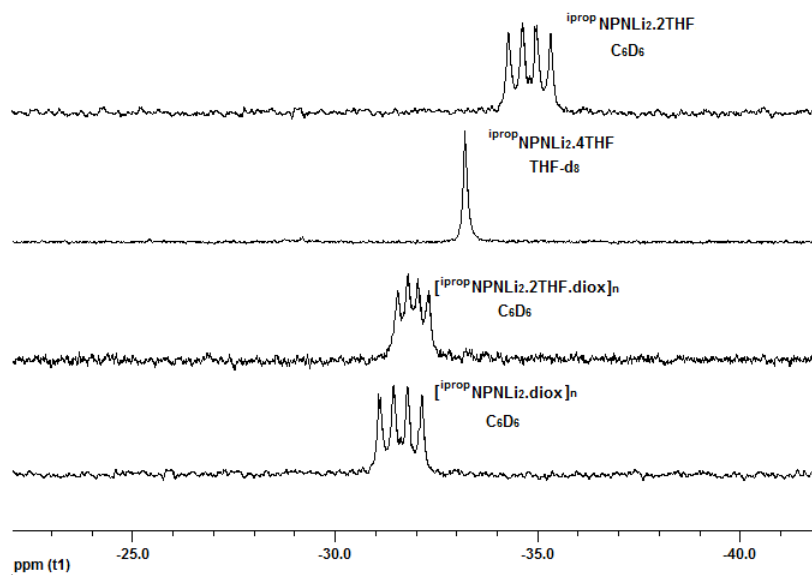


Figure 34: $^{31}\text{P}\{^1\text{H}\}$ NMR spectra for the ipropNPNLi_2 donor set: 1,4-dioxane, mixed 1,4-dioxane/THF and THF adducts

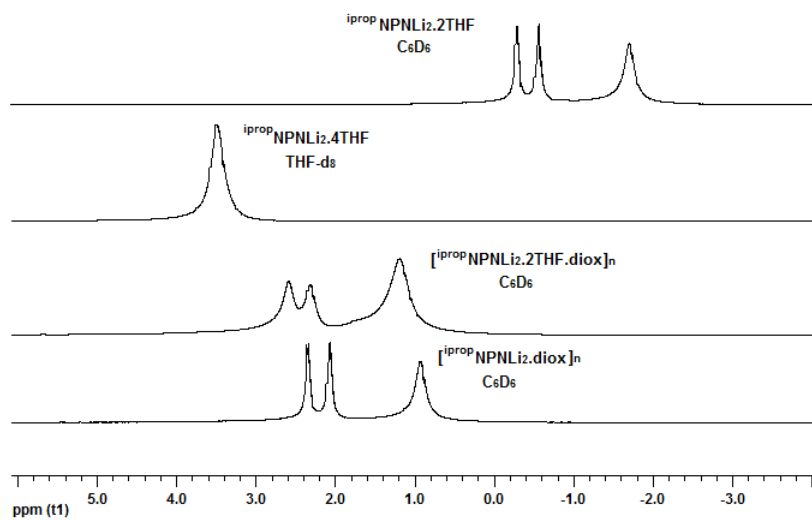


Figure 35: $^7\text{Li}\{^1\text{H}\}$ NMR spectra for the ipropNPNLi_2 donor set: 1,4-dioxane, mixed 1,4-dioxane/THF and THF adducts

For the mixed THF/1,4-dioxane adduct, $[\text{ipropNPNLi}_2 \cdot 2\text{THF} \cdot \text{diox}]_n$, the $^{31}\text{P}\{^1\text{H}\}$ and $^7\text{Li}\{^1\text{H}\}$ NMR spectra are indistinguishable from $[\text{ipropNPNLi}_2 \cdot \text{diox}]_n$ [2.6] and the P-Li coupling has remained intact (Figure 34 and Figure 35).

When $[\text{ipropNPNLi}_2 \cdot \text{diox}]_n$ [2.6] is dissolved in $\text{THF-}d_8$, the $^{31}\text{P}\{^1\text{H}\}$ NMR spectrum displays a singlet at δ -33.21 and the $^7\text{Li}\{^1\text{H}\}$ NMR spectrum shows a singlet at δ 3.49 (Figure 34 and Figure 35), indicating that for $\text{ipropNPNLi}_2 \cdot 4\text{THF}$ the coupling between the P donor and Li is disrupted (Figure 33). The $^7\text{Li}\{^1\text{H}\}$ NMR spectral peak for $\text{ipropNPNLi}_2 \cdot 4\text{THF}$ in $\text{THF-}d_8$ is shifted significantly downfield (Figure 35) which is in agreement with the more weakly bound THF and lack of P-Li coupling.

2.3.2. Synthesis of $[\text{tolNPNLi}_2 \cdot 1.5\text{TMEDA}]_2$ [2.7] and $[\text{phNPNLi}_2 \cdot 1.5\text{TMEDA}]_2$ [2.8]

To generate the $^{\text{tol}}\text{NPN}$ and $^{\text{ph}}\text{NPN}$ donor sets, PPhCl_2 is added slowly at low temperature to $[\text{tolAr}^{\text{Li}}\text{ArNLi} \cdot \text{TMEDA}]_2$ [2.2] or $[\text{phAr}^{\text{Li}}\text{ArNLi} \cdot 1.5\text{TMEDA}]_2$ [2.3] in THF (Figure 36).

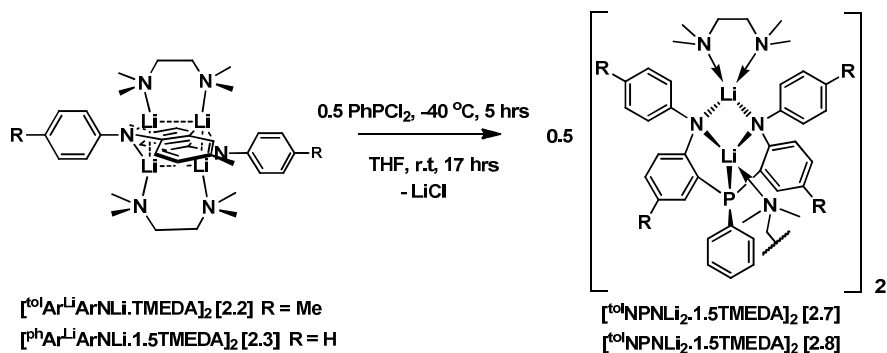


Figure 36: Synthesis of $[\text{tolNPNLi}_2 \cdot 1.5\text{TMEDA}]_2$ [2.7]

Upon work-up, $[\text{tolNPNLi}_2 \cdot 1.5\text{TMEDA}]_2$ [2.7] and $[\text{phNPNLi}_2 \cdot 1.5\text{TMEDA}]_2$ [2.8] can be obtained in moderate yields as fluffy yellow powders, which are stable indefinitely at room temperature in the absence of air and moisture, both as a solid and in solution. The solid-state molecular structure of $[\text{tolNPNLi}_2 \cdot 1.5\text{TMEDA}]_2$ [2.7] confirms a structure with two $^{\text{tol}}\text{NPNLi}_2$ units and 1.5 TMEDA per $^{\text{tol}}\text{NPNLi}_2$ unit (Figure 41). It was not possible to obtain acceptable

elemental analysis for $[\text{}^{\text{tol}}\text{NPNLi}_2 \cdot 1.5\text{TMEDA}]_2$ [2.7] or $[\text{}^{\text{ph}}\text{NPNLi}_2 \cdot 1.5\text{TMEDA}]_2$ [2.8] and it may be that the degree of TMEDA coordination can vary, resulting in different structures. Loss of 0.5 equiv of TMEDA may lead to the formation of $[\text{}^{\text{tol}}\text{NPNLi}_2 \cdot \text{TMEDA}]_n$ chains or even more condensed structures.

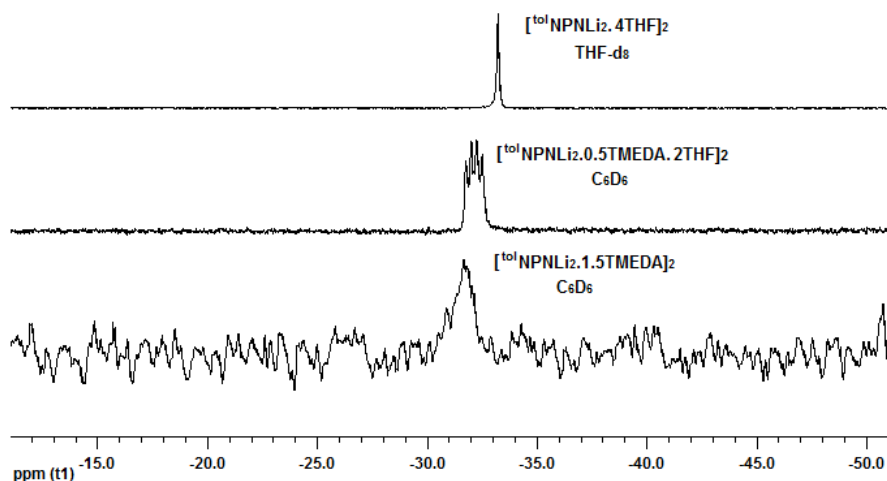


Figure 37: $^{31}\text{P}\{^1\text{H}\}$ NMR spectra of the $^{\text{tol}}\text{NPNLi}_2$ donor set: TMEDA, mixed TMEDA/THF and THF adducts

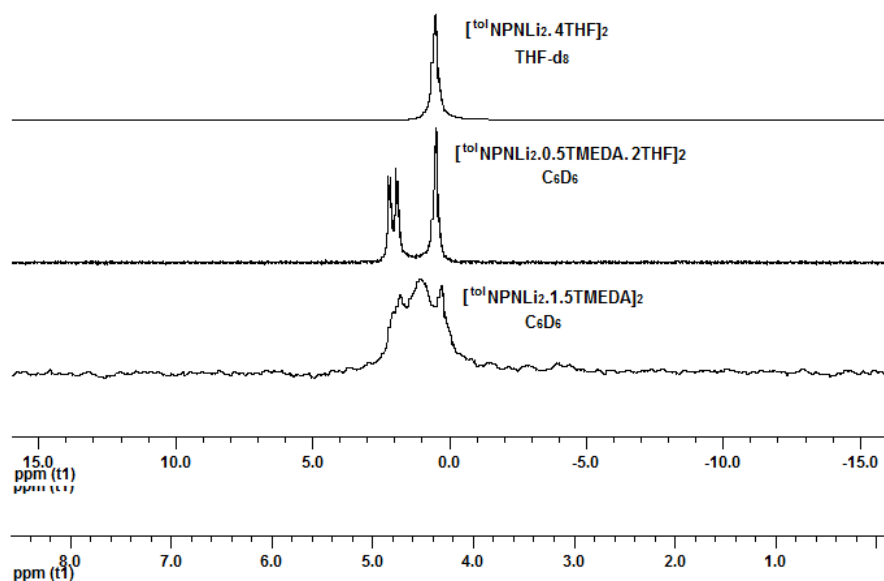


Figure 38: $^7\text{Li}\{^1\text{H}\}$ NMR spectra of the $^{\text{tol}}\text{NPNLi}_2$ donor set: TMEDA, mixed TMEDA/THF and THF adducts

The $^{31}\text{P}\{^1\text{H}\}$ NMR spectra of $[\text{tolNPNLi}_2 \cdot 1.5\text{TMEDA}]_2$ **[2.7]** (Figure 37) and $[\text{phNPNLi}_2 \cdot 1.5\text{TMEDA}]_2$ **[2.8]** in C_6D_6 have broad singlets at δ -31.66 and δ -31.96, respectively, which may be masking any Li-P coupling. The $^7\text{Li}\{^1\text{H}\}$ NMR spectrum of **[2.7]** shows a broad singlet at δ 0.29 which may also be masking any Li-P coupling (Figure 38). For **[2.8]**, the $^7\text{Li}\{^1\text{H}\}$ NMR spectrum does exhibit a singlet at δ 0.09 and a doublet at δ 1.67 ($^1J_{\text{LiP}} = 40$ Hz), confirming Li-P coupling.

The ^1H NMR spectrum of $[\text{tolNPNLi}_2 \cdot 1.5\text{TMEDA}]_2$ **[2.7]** in C_6D_6 (Figure 39) shows a very broad peak for TMEDA at δ 1.92 (free TMEDA at δ 2.18 for CH_2 and δ 2.04 CH_3) that overlaps the tolyl region; unfortunately, poor solubility makes NMR spectroscopic characterisation difficult. Similarly, the TMEDA signals in the ^1H NMR spectrum of **[2.8]** in C_6D_6 appear as a broad peak at δ 1.63, and two sharp peaks at δ 1.57 and δ 1.47.

These broad peaks in the $^7\text{Li}\{^1\text{H}\}$ NMR, $^{31}\text{P}\{^1\text{H}\}$ NMR and ^1H NMR spectra of $[\text{tolNPNLi}_2 \cdot 1.5\text{TMEDA}]_2$ **[2.7]** and $[\text{phNPNLi}_2 \cdot 1.5\text{TMEDA}]_2$ **[2.8]** are not due to an impurity, as when the samples are spiked with THF, typical spectra are obtained for $[\text{tolNPNLi}_2 \cdot 4\text{THF}]_2$ or $[\text{tolNPNLi}_2 \cdot 0.5\text{TMEDA} \cdot 2\text{THF}]_2$ (Figure 37, Figure 38 and Figure 39). Clearly, Li / TMEDA exchange or a more complex Li coordination model may exist for **[2.7]** and **[2.8]** in C_6D_6 than the solid state molecular structure of **[2.7]** in Figure 41 would suggest.

The $^{31}\text{P}\{^1\text{H}\}$ NMR spectrum of $[\text{tolNPNLi}_2 \cdot 1.5\text{TMEDA}]_2$ **[2.7]** in $\text{C}_6\text{D}_6 + 4\text{THF}$ (Figure 37) shows a quartet at δ -32.8 ($^1J_{\text{PLi}} = 41$ Hz) and the $^7\text{Li}\{^1\text{H}\}$ NMR spectrum (Figure 38) displays a singlet at δ 0.49 and a doublet at δ 2.06 ($^1J_{\text{LiP}} = 41$ Hz). These values are indistinguishable from those obtained for $[\text{ipropNPNLi}_2 \cdot \text{diox}]_n$ **[2.6]**.

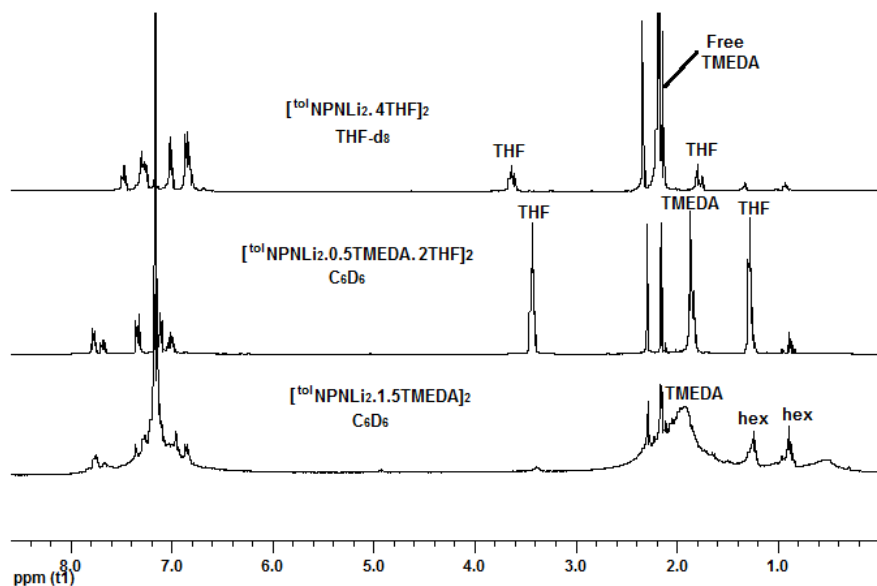


Figure 39: ^1H NMR spectra of the $^{\text{tol}}\text{NPNLi}_2$ donor set: TMEDA, mixed TMEDA/THF and THF adducts

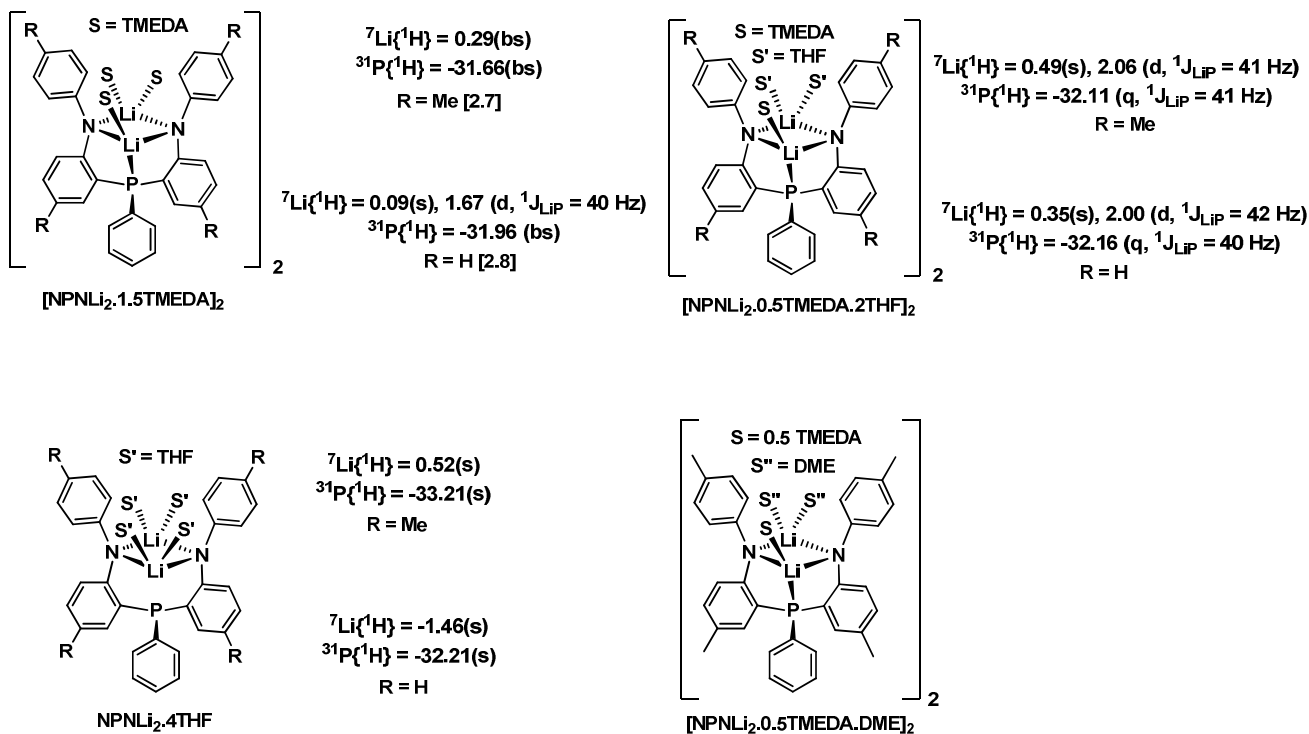


Figure 40: Structural forms of the $^{\text{tol}}\text{NPNLi}_2$ donor set

Similarly, $[\text{P}^{\text{h}}\text{NPnLi}_2 \cdot 1.5\text{TMEDA}]_2$ **[2.8]** in $\text{C}_6\text{D}_6 + 8\text{THF}$ displays a quartet at $\delta -32.16$ ($^1J_{\text{PLi}} = 40$ Hz) in the $^{31}\text{P}\{^1\text{H}\}$ NMR spectrum and a singlet at $\delta 0.35$ and a doublet at $\delta 2.00$ ($^1J_{\text{LiP}} = 42$ Hz) in the $^7\text{Li}\{^1\text{H}\}$ NMR spectrum, indicating that the P-Li coupling remains intact. The ^1H NMR spectra of **[2.7]** and **[2.8]** of these samples suggest that both TMEDA and THF are bound to the Li centres, potentially forming $[\text{P}^{\text{h}}\text{NPnLi}_2 \cdot 0.5\text{TMEDA} \cdot 2\text{THF}]_2$ and $[\text{P}^{\text{h}}\text{NPnLi}_2 \cdot 0.5\text{TMEDA} \cdot 2\text{THF}]_2$ (Figure 40), similar to the solid state molecular structure of $[\text{P}^{\text{h}}\text{NPnLi}_2 \cdot 0.5\text{TMEDA} \cdot \text{DME}]_2$ (Figure 41).²⁶¹

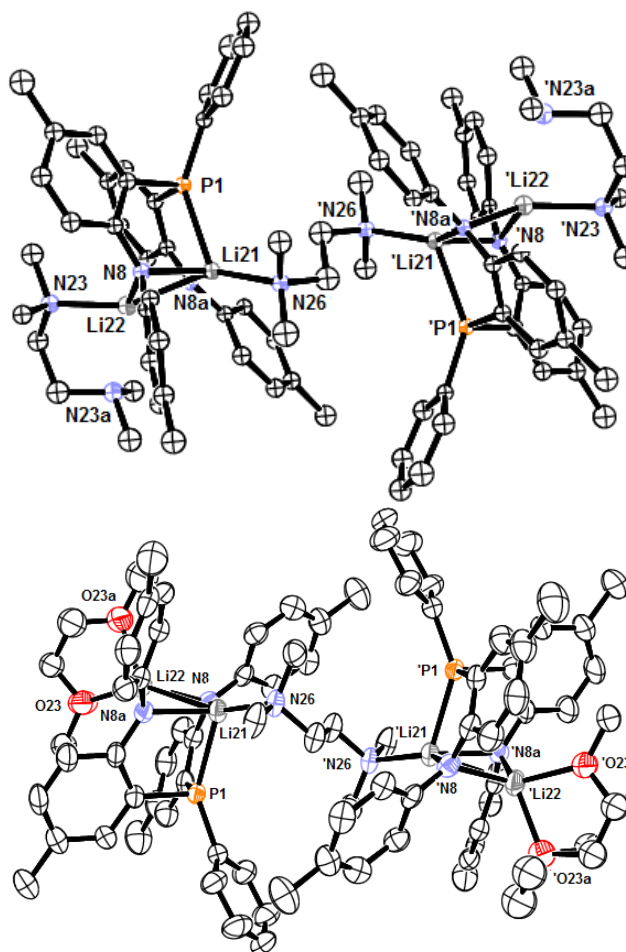


Figure 41: ORTEP representation of the solid state molecular structure of $[\text{P}^{\text{h}}\text{NPnLi}_2 \cdot 1.5\text{TMEDA}]_2$ **[2.7]** and $[\text{P}^{\text{h}}\text{NPnLi}_2 \cdot 0.5\text{TMEDA} \cdot 1\text{DME}]_2$ ²⁶¹

In THF- d_8 the Li-P coupling of solvated [2.7] and [2.8] is disrupted, with singlets at δ -33.21 (Figure 37) and δ -32.61 in the $^{31}\text{P}\{^1\text{H}\}$ NMR spectrum, respectively, and at δ 0.52 (Figure 38) and δ -1.46 in the $^7\text{Li}\{^1\text{H}\}$ NMR spectrum. Their ^1H NMR spectra in THF- d_8 indicate that TMEDA is free and the THF is either weakly coordinated or exchanging between bound THF and the large excess of free THF. The P atom and TMEDA are most likely de-coordinated from lithium, which is solvated with THF, forming monomeric $^{\text{tol}}\text{NPNLi}_2 \cdot 4\text{THF}$ or $^{\text{ph}}\text{NPNLi}_2 \cdot 4\text{THF}$ structures (Figure 40).

Table 4 : Comparative bond lengths (Å) and angles (°) for the $^{\text{tol}}\text{NPNLi}_2$ donor set.

| $[\text{tolNPNLi}_2 \cdot 1.5\text{TMEDA}]_2$ | | $[\text{tolNPNLi}_2 \cdot \text{DME} \cdot 0.5\text{TMEDA}]_2^{261}$ | |
|---|----------|--|-----------|
| P1-Li21 | 2.272(7) | P1-Li21 | 2.296(13) |
| Li22-N23 | 2.078(7) | Li22-O23 | 2.016(15) |
| Li22...N23a | 2.430(8) | Li22-O23a | 2.059(16) |
| Li21-N26 | 2.065(7) | Li21-N26 | 2.52(14) |
| N8-Li21 | 2.069(8) | N8-Li21 | 2.89(13) |
| N8-Li22 | 2.169(7) | N8-Li22 | 2.081(16) |
| N8a-Li21 | 2.046(7) | N8a-Li21 | 2.52(14) |
| N8a-Li22 | 2.082(8) | N8a-Li22 | 2.82(15) |
| Li21...Li22 | 2.723(9) | Li21...Li22 | 2.750(18) |
| N8-Li21-N8a | 102.1(3) | N8-Li21-N8a | 99.4(6) |
| N8-Li22-N8a | 97.7(3) | N8-Li22-N8a | 100.4(6) |
| Li21-N8-Li22 | 76.5(3) | Li21-N8-Li22 | 78.2(5) |
| Li21-N8a-Li22 | 78.9(3) | Li21-N8a-Li22 | 77.9(6) |
| P1-Li21-N8 | 80.7(2) | P1-Li21-N8 | 79.8(4) |
| P1-Li21-N8a | 81.3(2) | P1-Li21-N8a | 81.1(5) |
| P1-Li21-N26 | 121.2(3) | P1-Li21-N26 | 116.0(6) |
| P1-Li21-Li22 | 89.0(3) | P1-Li21-Li22 | 86.9(5) |
| N23-Li22-N8 | 108.0(3) | O23-Li22-N8 | 111.2(7) |
| N23-Li22-N8a | 137.1(4) | O23-Li22-N8a | 124.7(8) |
| N23a-Li22-N8 | 137.5(3) | O23a-Li22-N8 | 126.2(7) |
| N23a-Li22-N8a | 103.1(3) | O23a-Li22-N8a | 114.6(7) |
| N26-Li21-N8 | 120.5(3) | N26-Li21-N8 | 122.6(7) |
| N26-Li21-N8a | 133.4(4) | N26-Li21-N8a | 136.4(7) |

X-ray analysis of single crystals of $[\text{tolNPNLi}_2 \cdot 1.5\text{TMEDA}]_2$ [2.7] reveals two $^{\text{tol}}\text{NPNLi}_2$ units with one bridging and one non-bridging TMEDA (Figure 41). The Li-N bonds lengths for N8, N8a, N23 and N26 range from 2.046(7) to 2.169(7) Å (Table 4) and are comparable to typical reported Li-N bond lengths of 1.9 to 2.10 Å.^{245, 246, 253} The other nitrogen atom N23a of the non-bridging TMEDA is located too far away from Li22 at 2.430(8) Å to be covalently bonded, but may be weakly interacting. It is unclear why one of the TMEDA molecules bridges and the

other does not. In an analogous system with DME instead of THF, a solid state molecular structure was obtained showing that the bridging TMEDA between the two $^{tol}\text{NPNLi}_2$ units remains, with the other lithium atom bonded to the bidentate DME (Figure 41).²⁶¹ The structural parameters for $[\text{tolNPNLi}_2 \cdot 0.5\text{TMEDA} \cdot \text{DME}]_2$ (Table 4) show no marked differences compared to $[\text{tolNPNLi}_2 \cdot 1.5\text{TMEDA}]_2$ [2.7].

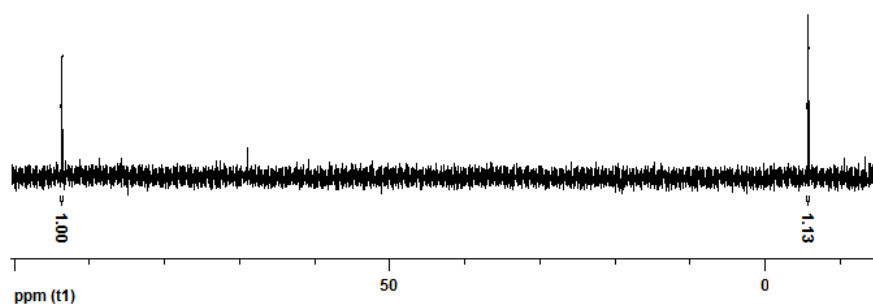


Figure 42: $^{31}\text{P}\{^1\text{H}\}$ NMR spectrum of $^{tol}\text{NPNPPh}$ [2.9]

The lower yields obtained when PPhCl_2 quenches the TMEDA adduct precursors $[\text{tolAr}^{\text{Li}}\text{ArNLi} \cdot \text{TMEDA}]_2$ [2.2] and $[\text{phAr}^{\text{Li}}\text{ArNLi} \cdot 1.5\text{TMEDA}]_2$ [2.3] compared to the 1,4-dioxane adduct may be correlated with the observation of a prominent side-product. For the reaction of $[\text{tolAr}^{\text{Li}}\text{ArNLi} \cdot \text{TMEDA}]_2$ [2.2] with PPhCl_2 , the crude reaction mixture for [2.7] displayed, amongst others, peaks at δ -5.7 and δ 93.8 in a 1:1 ratio for this side-product in the $^{31}\text{P}\{^1\text{H}\}$ NMR spectrum. In Et_2O solvent, these peaks dominate and $^{tol}\text{NPNPPh}$ [2.9] was isolated (Figure 42). The P-N bonds of [2.9] are susceptible to hydrolysis and [2.9] reacts slowly with excess H_2O to form $^{tol}\text{NPNH}_2$ [2.11] (Figure 43). The incorporation of the *ortho* C2 carbon in the $\text{Li}_2\text{N}_2\text{C}_4$ core of $[\text{tolAr}^{\text{Li}}\text{ArNLi} \cdot \text{TMEDA}]_2$ [2.2] may inhibit C-P bond formation. Exploratory reactions with the trithio-diarylamide $[(\text{tol-LiAr})_2\text{NLi} \cdot \text{TMEDA}]_n$ species indicated only one C-P bond formation in combination with P-N bond formation, even when quenching with three equiv of $\text{P}^i\text{Pr}_2\text{Cl}$.

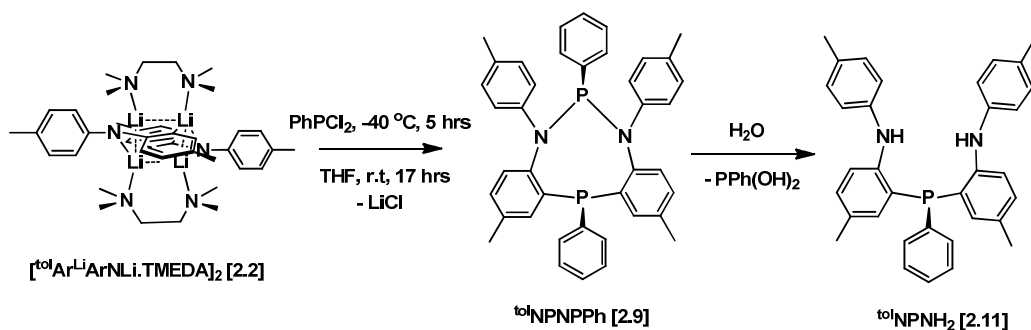


Figure 43: Synthesis of $\text{tol}^{\text{NPNPPh}}$ [2.9]

The formation of $\text{tol}^{\text{NPNPPh}}$ [2.9] would be favoured by a combination of enhanced N-P bond formation relative to C-P bond formation and a stoichiometric excess of PPhCl_2 . Due to the possibility of more than one TMEDA molecule per dilithio-diarylamide unit, if the TMEDA content of the $[\text{tol}^{\text{ArLi}}\text{ArNLi} \cdot \text{TMEDA}]_2$ [2.2] or $[\text{ph}^{\text{ArLi}}\text{ArNLi} \cdot 1.5\text{TMEDA}]_2$ [2.3] reactants are not accurately ascertained prior to PPhCl_2 addition, conditions for excess PPhCl_2 may be attained. As $[\text{tol}^{\text{ArLi}}\text{ArNLi} \cdot \text{TMEDA}]_2$ [2.2] is less soluble in Et_2O than THF, the less solvated Et_2O adduct may further disfavour C-P bond formation.

2.4. Protonated NPN Ligands

Protonation of $[\text{iprop}^{\text{NPNLi}_2} \cdot \text{diox}]_n$ [2.6], $[\text{tol}^{\text{NPNLi}_2} \cdot 1.5\text{TMEDA}]_2$ [2.7] and $[\text{ph}^{\text{NPNLi}_2} \cdot 1.5\text{TMEDA}]_2$ [2.8] with excess $\text{NMe}_3 \cdot \text{HCl}$ gives $\text{iprop}^{\text{NPNH}_2}$ [2.10], $\text{tol}^{\text{NPNH}_2}$ [2.11] and $\text{ph}^{\text{NPNH}_2}$ [2.12] in yields up to 90% (Figure 44). The reaction can be performed in either THF or toluene. Although an excess $\text{NMe}_3 \cdot \text{HCl}$ is used, two equiv are sufficient. H_2O can also be used as the source of protons.

The $^{31}\text{P}\{^1\text{H}\}$ NMR spectra of [2.10], [2.11] and [2.12] display signals at δ -31.35, δ -29.39 and δ -30.80. These values are not significantly different from those obtained for the lithiated version of the ligands. The ^1H NMR spectra exhibit a characteristic doublet at δ 6.38

($^4J_{\text{HP}} = 6 \text{ Hz}$), δ 6.21 ($^4J_{\text{PH}} = 5 \text{ Hz}$) and δ 6.30 ($^4J_{\text{PH}} = 5 \text{ Hz}$) for the N-H proton of **[2.10]**, **[2.11]** and **[2.12]**, respectively.

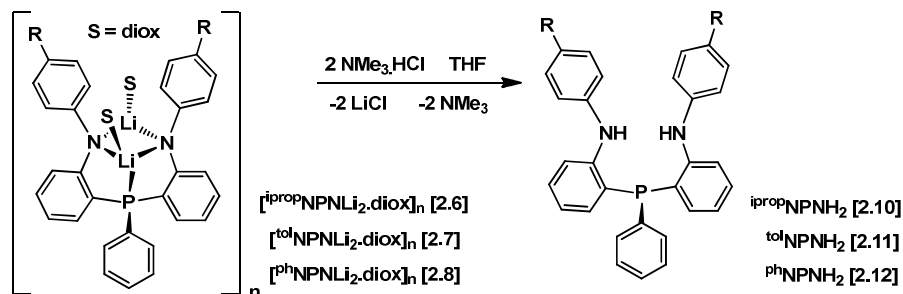


Figure 44: Synthesis of ipropNPNH_2 **[2.10]**, tolNPNH_2 **[2.11]** and phNPNH_2 **[2.12]**

ipropNPNH_2 **[2.10]** is a translucent oil and it is more convenient to weigh its precursor, the solid dilithio derivative **[2.6]**. Thus **[2.10]** is often not isolated, but prepared *in situ* and reacted further with the desired precursor metal dimethyamido complex (see Chapter 3 and Chapter 4). tolNPNH_2 **[2.11]** and phNPNH_2 **[2.12]** are white solids that are isolated prior to protonolysis with the metal dimethyamido complexes.

Single crystals and solid state molecular structures of tolNPNH_2 **[2.11]** and phNPNH_2 **[2.12]**²⁶¹ were obtained (Figure 45) and the P-C and N-C bond lengths and C-P-C and C-N-C bond angles (Table 5) are not significantly different from those reported for PPh_3 ,²⁶² HNPh_2 ²⁶³ and $\text{Ph}_{\text{mes}}\text{NPNH}_2$ ⁹⁷.

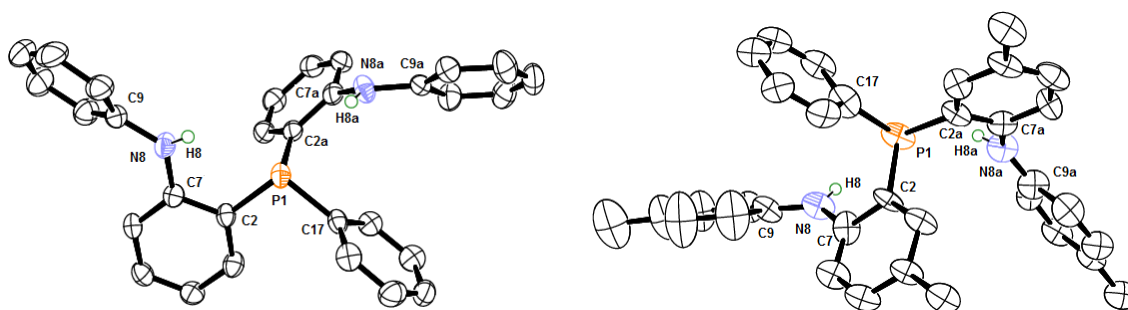


Figure 45: ORTEP representations of the solid state molecular structures of tolNPNH_2 **[2.11]** and phNPNH_2 **[2.12]**

Table 5 : Comparative bond lengths (Å) and angles (°) for ^{tol}NPNH₂ [2.11] and ^{ph}NPNH₂ [2.12]

| | ^{tol} NPNH ₂ | | ^{ph} NPNH ₂ ²⁶¹ |
|--------------------|----------------------------------|--------------------|--|
| P1-C2 | 1.805(10) | P1-C2 | 1.843(2) |
| P1-C2a | 1.815(9) | P1-C2a | 1.833(2) |
| P1-C17 | 1.820(12) | P1-C17 | 1.835(2) |
| N8-C7 | 1.399(12) | N8-C7 | 1.409(3) |
| N8a-C7a | 1.423(12) | N8a-C7a | 1.403(3) |
| N8-C9 | 1.369(14) | N8-C9 | 1.410(3) |
| N8a-C9a | 1.370(12) | N8a-C9a | 1.411(3) |
| C2-P1-C17 | 104.6(5) | C2-P1-C17 | 102.39(11) |
| C2a-P1-C17 | 98.2(5) | C2a-P1-C17 | 103.42(10) |
| C2-P1-C2a | 101.6(4) | C2-P1-C2a | 101.73(10) |
| C7-N8-C9 | 128.0(9) | C7-N8-C9 | 125.5(2) |
| C7a-N8a-C9a | 125.7(9) | C7a-N8a-C9a | 127.0(2) |

2.5. Conclusions

A modification for the synthesis of the new ^{iprop}NPN donor set was presented, whereby an *o*-bromo-diarylamine intermediate was prepared using a Buchwald-Hartwig arylation of *o*-dibromo-benzene. It was found that increasing the external temperature of the oil-bath from 80 °C to 130-140 °C significantly improved the yield, however, a short-coming of this method is the chromatographic work-up necessitated by the remaining unreacted *o*-dibromobenzene.

The ^{tol}NPN and ^{ph}NPN donor sets were prepared using a directed *ortho* metalation (DOM) method specific to arylamido groups that have no *ortho* substituents, starting with commercially available diarylamines. While column chromatography is eliminated, the Li₂N₂C₄ cores of the *ortho*-lithiated diaryl lithium amide intermediates [^{tol}Ar^{Li}ArN^{Li}·TMEDA]₂ [2.2] and [^{ph}Ar^{Li}ArN^{Li}·1.5TMEDA]₂ [2.3] possess aryl-lithium associations, inhibiting C-P and favouring N-P bond formation during the PPhCl₂ quenching. The moderate yields obtained for [^{tol}NPNLi₂·1.5TMEDA]₂ [2.7] and [^{ph}NPNLi₂·1.5TMEDA]₂ [2.8] are offset by the fact that the synthesis of [^{tol}Ar^{Li}ArN^{Li}·TMEDA]₂ [2.2] and [^{ph}Ar^{Li}ArN^{Li}·TMEDA]₂ [2.3] are nearly quantitative and can be prepared in large scale.

Chapter 3: Group 4 Diamido-Phosphine Complexes

The use of group 4 metal halides as precursors for the formation of dinitrogen complexes is well established.^{154, 178, 179, 264} This chapter deals with the synthesis and characterisation of zirconium, titanium and hafnium chloro complexes with the new *o*-phenylene-bridged ligand systems, ^{iprop}NPN and ^{tol}NPN, the syntheses of which were described in the previous chapter.

3.1. Zirconium Diamido-Phosphine Complexes

Two different routes were investigated for the synthesis of the zirconium dichloro complexes. Given that the ligand precursors are isolated as dilithio salts (see Chapter 2), the salt metathesis route is most attractive as it only requires reaction of this lithiated form with zirconium tetrachloride $\text{ZrCl}_4(\text{THF})_2$ (Figure 46). The protonolysis route is multi-step and requires reaction of the protonated form of the ligand with tetrakis(-dimethylamido)zirconium(IV) $\text{Zr}(\text{NMe}_2)_4$. Starting with zirconium dichloride bis(-dimethylamido) complex $\text{ZrCl}_2(\text{NMe}_2)_2(\text{DME})$ instead can eliminate the subsequent TMSCl chlorination step from the latter route (Figure 46).

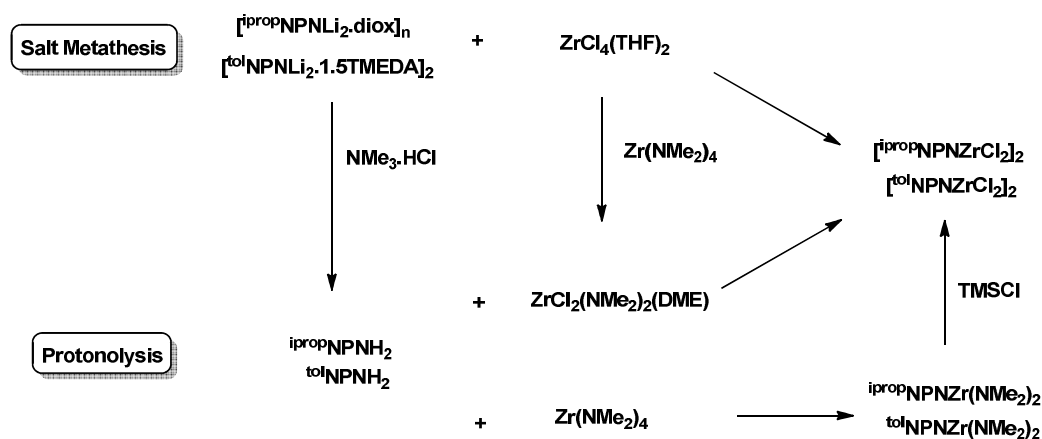
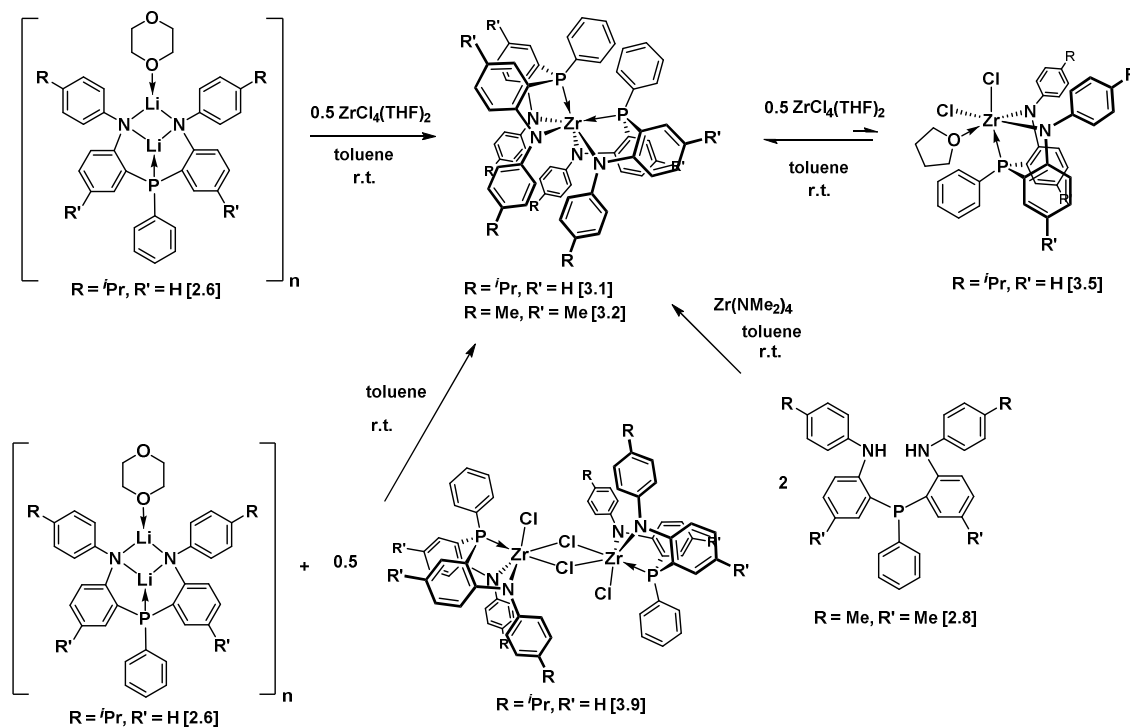


Figure 46: Salt metathesis and protonolysis routes for zirconium complexes

3.1.1. Salt Metathesis Route

Addition of one equiv of $[\text{ipropNPNLi}_2\cdot\text{diox}]_n$ [2.6] to a toluene solution of $\text{ZrCl}_4(\text{THF})_2$ at room temperature forms $[\text{ipropNPN}]_2\text{Zr}$ [3.1], which displays a singlet in the $^{31}\text{P}\{^1\text{H}\}$ NMR



If the reaction of one equiv of each of [ⁱpropNPNLi₂·diox]_n [**2.6**] and ZrCl₄(THF)₂ is allowed to continue, a mixture of 77% [ⁱpropNPN]₂Zr [**3.1**] and 23% ⁱpropNPNZrCl₂(THF) [**3.5**] can be observed after 24 days. In order to confirm that ⁱpropNPNZrCl₂(THF) [**3.5**] forms via conproportionation of [ⁱpropNPN]₂Zr [**3.1**] with ZrCl₄(THF)₂, one equiv of both solids were dissolved in toluene-*d*₈ at room temperature and the reaction monitored via ³¹P{¹H} NMR spectroscopy. After 6 days, 14% ⁱpropNPNZrCl₂(THF) [**3.5**] was observed, which increased to 28% after 18 days.

Single peaks in the $^{31}\text{P}\{^1\text{H}\}$ NMR spectra of $[\text{ipropNPN}]_2\text{Zr}$ **[3.1]** and $[\text{tolNPN}]_2\text{Zr}$ **[3.2]** may indicate that the two NPN ligands are symmetrically bonded to the central Zr atom in solution, with either trans- or cis-disposed phosphorus donors. The ^1H and $^{13}\text{C}\{^1\text{H}\}$ NMR spectra however, show considerable complexity, suggestive of chiral structures and therefore cis-disposed phosphines (Figure 48).

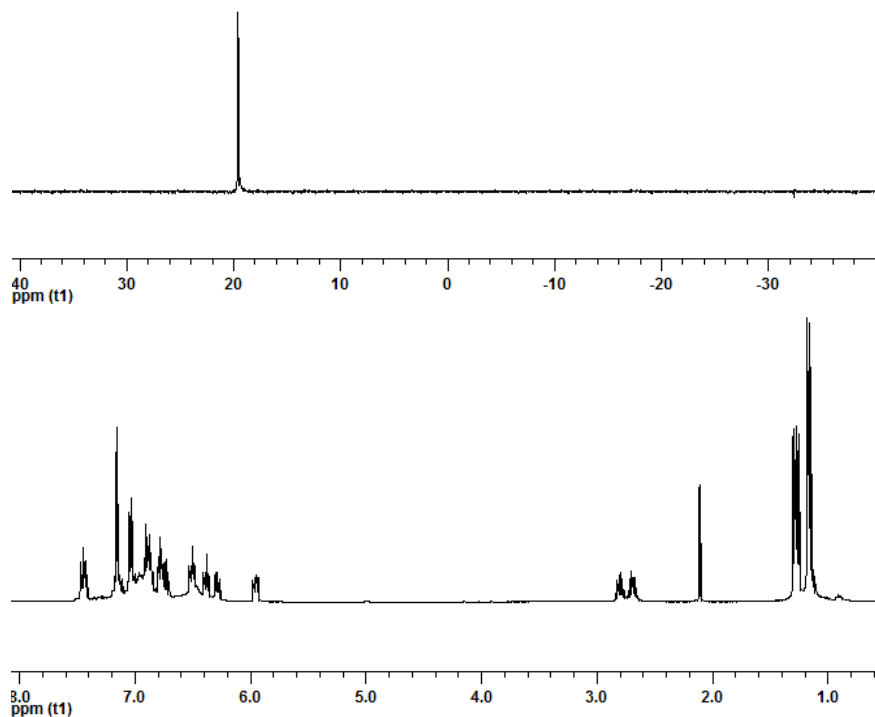


Figure 48: $^{31}\text{P}\{^1\text{H}\}$ (top) and ^1H NMR (bottom) spectra of $[\text{ipropNPN}]_2\text{Zr}$ **[3.1]** in C_6D_6

In the solid state both $^{\text{tol}}\text{NPN}$ ligands of $[\text{tolNPN}]_2\text{Zr}$ **[3.2]** are coordinated in a facial manner and the geometry about the Zr centre is best described as trigonal prismatic, with the P1, N8 and N8a atoms forming one basal plane and the P1a, N8b and N8c atoms the other (Figure 49). Overall this molecule is chiral (C_2 point group) and the two P atoms (P1 and P1a) are in a *cis* configuration. The Zr1-P1 bond length 2.6977(11) Å agrees well with the average Zr-P bond lengths reported for $^{\text{mes}}\text{NPN}$ containing zirconium complexes^{97, 125, 214} and is significantly longer than the Zr1-P1a bond length of 2.4455(10) Å (Table 2).

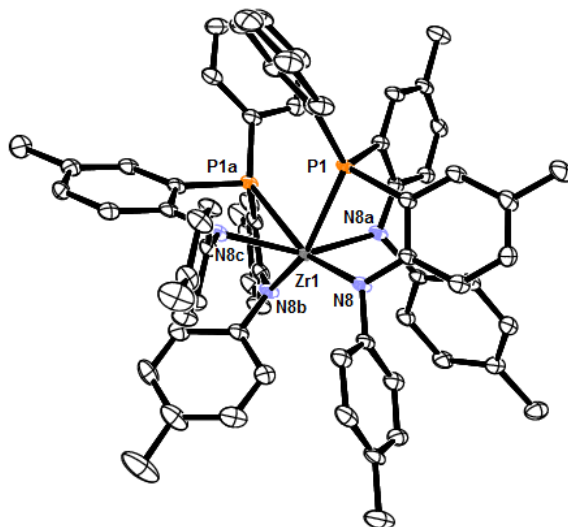


Figure 49: ORTEP representation of the solid state molecular structure of [^{tol}NPN]₂Zr [3.2]

For both of the NPN Ligands, one of the Zr-amido bond lengths are significantly shorter at 1.869(3) Å for Zr1-N8 and 2.038(3) Å for Zr1-N8b and the other are longer at 2.464(4) Å for Zr1-N8a and 2.407(4) Å for Zr1-N8c (Table 2). While they all fall within the range of Zr-N bond lengths reported for zirconium complexes with the ^{mes}NPN ligand,^{97, 125, 214} there is no explanation for why there is such a wide range from Zr-imido (Zr1-N8) to Zr-amine (Zr-N8a and Zr-N8c) bond character. The average P-Zr-N ligand bite angle of 73.9° is typical, but the average N-Zr-N ligand bite angle of 89.7° is smaller than those observed for monodentate ^{mes}NPN zirconium complexes ^{mes}NPNZrCl₂ (113.96(9)°) and ^{mes}NPNZrCl₂(Py) (97.87(6)°). This may be due to reduced steric bulk at the *ortho* position of the arylamido groups of the ^{tol}NPN ligand compared to ^{mes}NPN.

Table 6 : Selected bond lengths (Å) and angles (°) for [^{tol}NPN]₂Zr [3.2]

| [^{tol} NPN] ₂ Zr [3.2] | | | |
|---|------------|-------------|------------|
| Zr1-P1 | 2.6977(11) | P1-Zr1-P1a | 76.29(3) |
| Zr1-P1a | 2.4455(10) | P1-Zr1-N8 | 72.44(11) |
| Zr1-N8 | 1.869(3) | P1-Zr1-N8a | 70.57(8) |
| Zr1-N8a | 2.464(4) | P1a-Zr1-N8b | 82.98(10) |
| Zr1-N8b | 2.038(3) | P1a-Zr1-N8c | 69.53(8) |
| Zr1-N8c | 2.407(4) | N8-Zr1-N8b | 127.84(15) |
| P1-Zr1-N8b | 159.22(10) | N8-Zr1-N8a | 92.03(15) |
| P1a-Zr1-N8 | 145.00(11) | N8b-Zr1-N8c | 87.33(13) |
| N8a-Zr1-N8c | 154.04(12) | | |

With the bulkier *o*-phenylene bridged ^{mes}NPN precursor ligand,⁹⁷ salt metathesis generated a mixture of products (Figure 50); interestingly, metathesis using the classic ^{Si}NPN ligand yields the dichloride ^{Si}NPNZrCl₂(THF) in toluene at 60 °C (Figure 50).^{137, 138} While there is no evidence for bis-(ligand) complex formation in this latter reaction, the higher reaction temperature may facilitate a facile disproportionation of a potential [^{Si}NPN]₂Zr intermediate and ZrCl₄(THF).

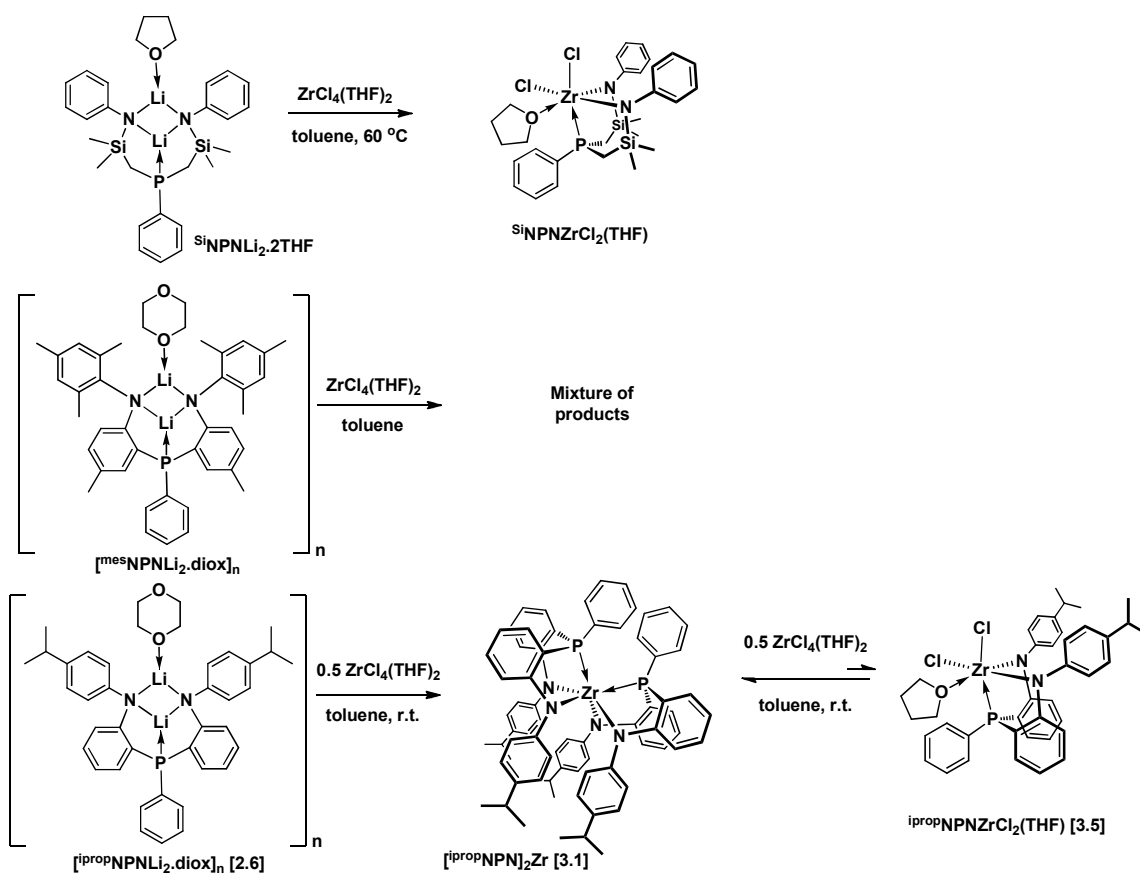


Figure 50: Reaction of $\text{SiNPNLi}_2 \cdot 2\text{THF}$, $\text{mesNPNLi}_2 \cdot \text{diox}$ and $[\text{ipropNPNLi}_2 \cdot \text{diox}]_n$ [2.6] with $\text{ZrCl}_4(\text{THF})_2$

Increasing the reaction temperature for the salt metathesis with $[\text{ipropNPNLi}_2 \cdot \text{diox}]_n$ [2.6] may speed up the conversion to $\text{ipropNPNZrCl}_2(\text{THF})$ [3.5], however, this route was abandoned for the alternative protonolysis method.

3.1.2. Protonolysis Route

Protonolysis involves reaction of the protonated form of the NPN ligand with zirconium

dimethylamido precursors, liberating dimethylamine. Two different precursors, namely $\text{Zr}(\text{NMe}_2)_4$ and $\text{ZrCl}_2(\text{NMe}_2)_2(\text{DME})$, were investigated (Figure 51).

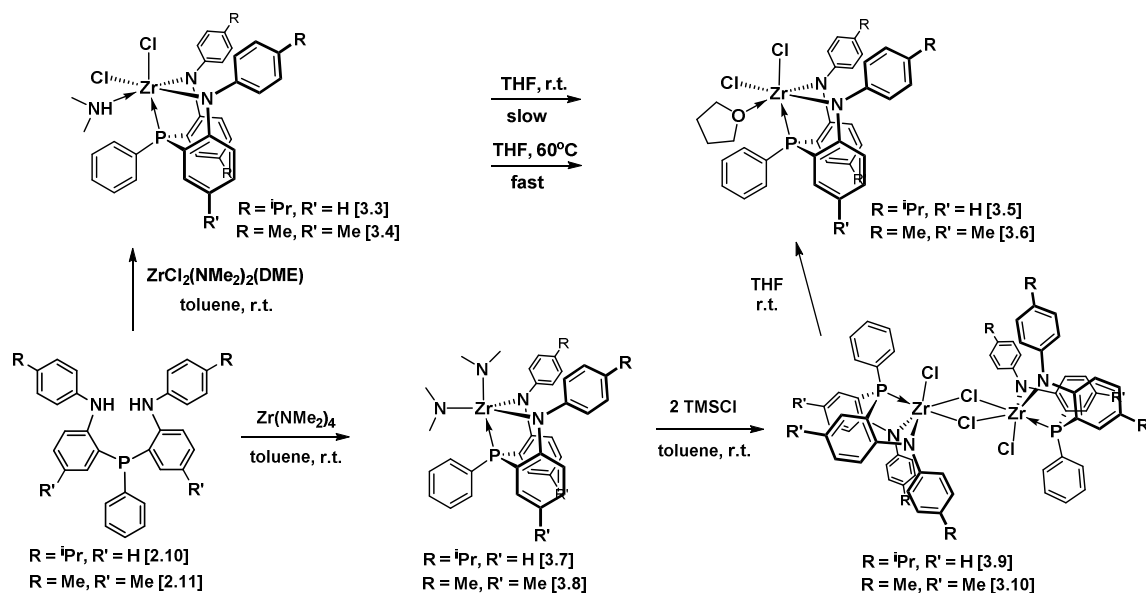


Figure 51: Protonolysis with $\text{ZrCl}_2(\text{NMe}_2)_2(\text{DME})$ or $\text{Zr}(\text{NMe}_2)_4$

Both routes led to the isolation of the desired zirconium mono(ligand) dichloride complexes, however, as will be discussed below, the route starting with $\text{Zr}(\text{NMe}_2)_4$ is preferred.

Synthesis of $^{i\text{prop}}\text{NPNZrCl}_2(\text{HNMe}_2)$ [3.3] and $^{tol}\text{NPNZrCl}_2(\text{HNMe}_2)$ [3.4]

The reaction of $^{\text{mes}}\text{NPNH}_2$ with $\text{Zr}(\text{NMe}_2)_4$ is well established,^{97, 214} but no reaction was observed when $^{\text{mes}}\text{NPNH}_2$ was reacted with $\text{ZrCl}_2(\text{NMe}_2)_2(\text{DME})$ at room temperature in toluene. A modest conversion to 14% $^{\text{mes}}\text{NPNZrCl}_2$ was observed in THF. Reaction of $^{i\text{prop}}\text{NPNH}_2$ [2.10] and $^{tol}\text{NPNH}_2$ [2.11] with $\text{ZrCl}_2(\text{NMe}_2)_2(\text{DME})$ in toluene at room temperature gave the orange solids $^{i\text{prop}}\text{NPNZrCl}_2(\text{HNMe}_2)$ [3.3] and $^{tol}\text{NPNZrCl}_2(\text{HNMe}_2)$ [3.4], respectively. The less bulky $^{i\text{prop}}\text{NPN}$ and ^{tol}NPN ligands appear to favour HNMe_2 adduct formation.

The $^{31}\text{P}\{^1\text{H}\}$ NMR spectra display singlets at δ 9.06 and δ 8.20 for [3.3] and [3.4] (Figure 52), respectively. In the ^1H NMR spectra [3.3] and [3.4] display broad peaks at δ 2.57 and δ 2.39 (N-H) and doublets at δ 2.08 and δ 2.01 (N-CH₃), respectively, which indicates coordinated HNMe_2 (Figure 52). The $^{13}\text{C}\{^1\text{H}\}$ NMR spectra display peaks at δ 41.8 and δ 42.2 (N-CH₃). The

elemental analysis suggests that some HNMe_2 may be liberated under prolonged reduced pressure from $^{\text{iprop}}\text{NPNZrCl}_2(\text{HNMe}_2)$ [3.3].

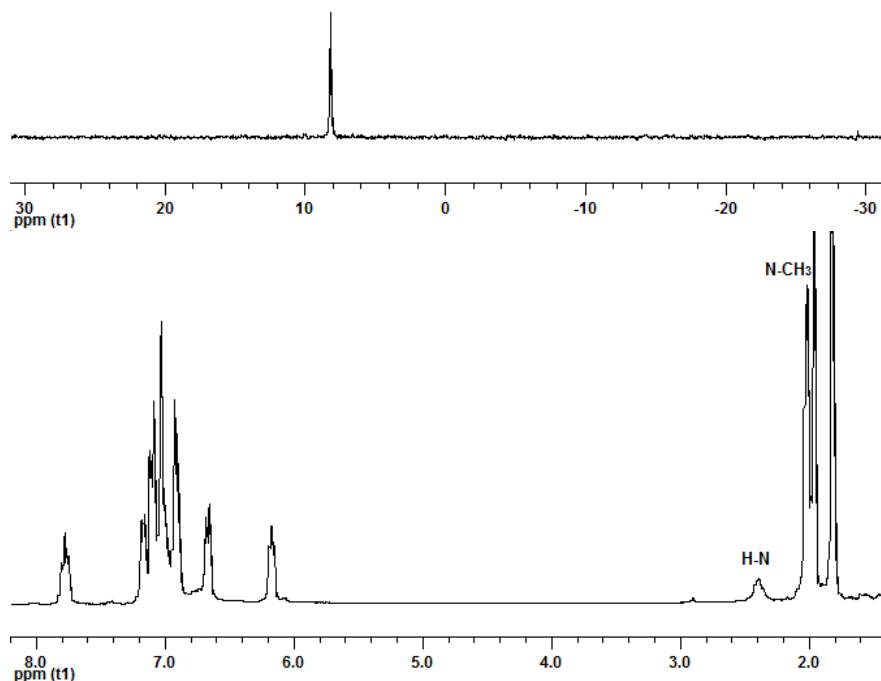


Figure 52: $^{31}\text{P}\{^1\text{H}\}$ (top) and ^1H NMR (bottom) spectra of $^{101}\text{NPNZrCl}_2(\text{HNMe}_2)$ [3.4] in C_6D_6

The mass spectrum for $^{101}\text{NPNZrCl}_2(\text{HNMe}_2)$ [3.4] shows the expected fragment ion $[\text{M} - \text{HNMe}_2]^+$ at 660 m/z. There is a small peak at 704 m/z that could correspond to the parent M^+ ion. This is unusual as neutral donors such as THF and HNMe_2 can be liberated at the early stages of analysis and as a result, fragment ions are observed as the most abundant ions in the mass spectrum. However, it is possible that proton transfer occurs from HNMe_2 to the ^{101}NPN ligand during analysis to generate a tautomeric form of the complex (Figure 53).

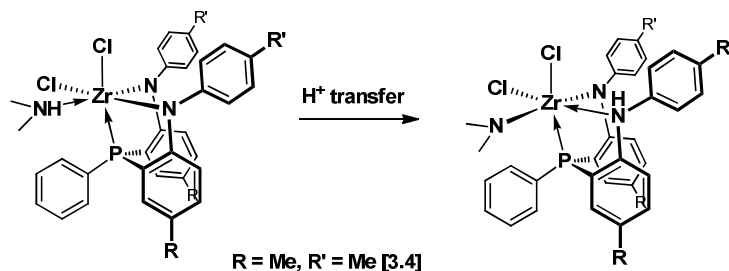


Figure 53: Proton transfer for $^{101}\text{NPNZrCl}_2(\text{HNMe}_2)$ [3.4]

In addition to the fragment ion $[M - \text{HNMe}_2]^+$ for $^{\text{iprop}}\text{NPNZrCl}_2(\text{HNMe}_2)$ [**3.3**], the mass spectrum also shows trace amounts of an ion at 724 m/z, which may be due to the presence of a zirconium trichloride species $^{\text{iprop}}\text{NPN}(\text{H})\text{ZrCl}_3$ (Figure 54) perhaps formed by the reaction of $^{\text{iprop}}\text{NPNH}_2$ [**2.10**] with $\text{ZrCl}_3(\text{NMe}_2)$, which may be an impurity formed during the synthesis of $\text{ZrCl}_2(\text{NMe}_2)_2(\text{DME})$. These minor species were not observable by $^{31}\text{P}\{^1\text{H}\}$ NMR spectroscopy.

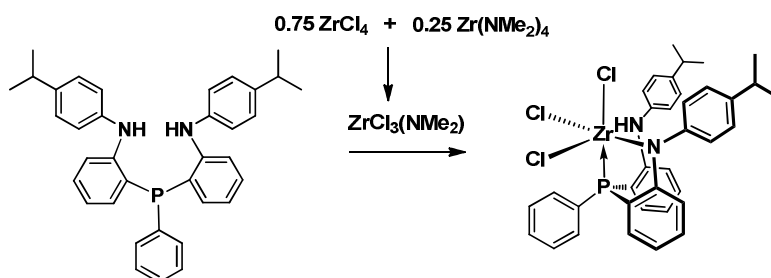


Figure 54: Possible origin of the minor impurity trichloride $^{\text{iprop}}\text{NPN}(\text{H})\text{ZrCl}_3$

The NPN ligand is usually coordinated in a facial conformation, which could result in two isomers for $^{\text{iprop}}\text{NPNZrCl}_2(\text{HNMe}_2)$ [**3.3**] and $^{\text{tol}}\text{NPNZrCl}_2(\text{HNMe}_2)$ [**3.4**] (Figure 55). The chlorides are arranged *cis* relative to each in both possibilities, with both chlorides *cis* and HNMe_2 *trans* to the P atom in one case and in the other case one of the chlorides and HNMe_2 is *cis* and the other chloride *trans* relative to the P atom. The latter case implies a chiral structure, which would require two different R and R' environments for substituents of the NPN ligand. The $^{31}\text{P}\{^1\text{H}\}$ NMR spectra of [**3.3**] and [**3.4**] display a singlet resonance, which indicates that in solution either only one of the two aforementioned isomers is formed or both isomers are exchanging fast on the NMR timescale. Because one set of R and R' environments is observed in the ^1H NMR spectra, either (i) the exclusive occurrence of the *trans* isomer is indicated in solution; (ii) an equilibrium (which may be slow) shifted significantly towards the left such that the concentration of the *cis* isomer is below NMR detection limits or (iii) fast exchange between appreciable concentrations of both isomers.

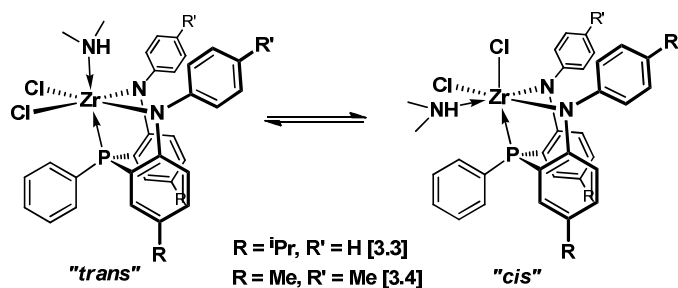


Figure 55: Isomers of $\text{NPNZrCl}_2(\text{HNMe}_2)$

The solid state molecular structure of $^{\text{tol}}\text{NPNZrCl}_2(\text{HNMe}_2)$ [3.4] was determined from single crystals grown by slow evaporation from a benzene solution at room temperature.²⁶¹ The geometry around the Zr atom is octahedral and the $^{\text{tol}}\text{NPN}$ ligand is bound facially, with one of the chlorides (Cl1) *trans* to the P1 atom and the other chloride (Cl2) *cis* (Figure 56). This *cis* isomeric form corresponds to that observed for the solid state molecular structure of $^{\text{mes}}\text{NPNZrCl}_2(\text{Py})$.⁹⁷ The P1-Zr1-Cl1 angle is more linear at $170.63(3)^\circ$ than N8-Zr1-Cl2 and N8a-Zr1-N21 (Table 7).

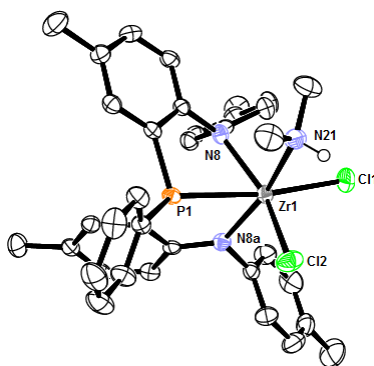


Figure 56: ORTEP representation of the solid state molecular structure of $^{\text{tol}}\text{NPNZrCl}_2(\text{HNMe}_2)$ [3.4]

The zirconium amido (Zr1-N8, Zr1-N8a), phosphine (Zr1-P1) and chloride (Zr1-Cl1, Zr1-Cl2) bond lengths (Table 7) agree well with previously reported $^{\text{mes}}\text{NPNZrCl}_2(\text{Py})$ ⁹⁷ and other NPN-containing zirconium dichloride complexes.^{97, 139, 140, 213, 214} The Zr1-N21 bond length of $2.438(3) \text{ \AA}$ for the neutral donor HNMe_2 is longer than for the zirconium amido bond lengths. As with the bis-(ligand) $[^{\text{tol}}\text{NPN}]_2\text{Zr}$ [3.2], the N8-Zr1-N8a ligand bite angle for $^{\text{tol}}\text{NPNZrCl}_2(\text{HNMe}_2)$ [3.4] with the less bulky tolyl arylamido group is smaller at $91.71(9)^\circ$ than

the corresponding ^{mes}NPNZrCl₂(Py) complex at 97.97(6)°. No intramolecular hydrogen bonding was observed between the HNMe₂ and Cl groups, with N-H···Cl distances (av 2.94 Å) being longer than sum of the van der Waals radii for nitrogen and hydrogen (2.75 Å).

Table 7 : Selected bond lengths (Å) and angles (°) for ^{tol}NPNZrCl₂(HNMe₂) [3.4]²⁶¹ and ^{mes}NPNZrCl₂(Py)⁹⁷

| | ^{tol} NPNZrCl ₂ (HNMe ₂) [3.4] ²⁶¹ | ^{mes} NPNZrCl ₂ (Py) ⁹⁷ |
|-------------|---|--|
| Zr1-P1 | 2.7631(8) | 2.7131(5) |
| Zr1-N8 | 2.139(2) | 2.1695(16) |
| Zr1-N8a | 2.098(2) | 2.1082(15) |
| Zr1-N21 | 2.438(3) | 2.3889(16) |
| Zr1-Cl1 | 2.4484(9) | 2.4419(5) |
| Zr1-Cl2 | 2.4938(9) | 2.5257(5) |
| P1-Zr1-Cl1 | 170.63(3) | 176.657(18) |
| N8-Zr1-Cl2 | 150.54(7) | 151.42(4) |
| N8a-Zr1-N21 | 160.99(9) | 155.53(6) |
| P1-Zr1-N8 | 67.54(6) | 67.54(6) |
| P1-Zr1-N8a | 73.59(7) | 73.45(4) |
| P1-Zr1-N21 | 88.01(7) | 88.36(4) |
| P1-Zr1-Cl2 | 85.76(3) | 82.143(17) |
| Cl1-Zr1-N8 | 107.56(7) | 104.55(4) |
| Cl1-Zr1-N8a | 115.11(7) | 113.11(5) |
| Cl1-Zr1-N21 | 83.57(7) | 88.83(4) |
| Cl1-Zr1-Cl2 | 96.96(3) | 99.060(19) |
| N8-Zr1-N8a | 91.71(9) | 97.87(6) |
| N8-Zr1-N21 | 85.47(10) | 86.23(6) |
| Cl2-Zr1-N8a | 92.44(7) | 87.27(4) |
| Cl2-Zr1-N21 | 81.22(7) | 78.30(4) |

The fact that the *cis* isomer is isolated in the solid state, but not apparently observed in solution may be explained by either (i) fast exchange between both isomers or (ii) an equilibrium shifted significantly towards the *trans* isomer such that the concentration of the *cis* isomer is below NMR detection limits.

Synthesis of ^{iprop}NPNZrCl₂(THF) [3.5] and ^{tol}NPNZrCl₂(THF) [3.6]

The orange-yellow solids ^{iprop}NPNZrCl₂(THF) [3.5] and ^{tol}NPNZrCl₂(THF) [3.6] were obtained by addition of THF to the dimethylamine adducts [3.3] and [3.4] or to dichloro dimers [3.9] and [3.10] (see later discussion). Displacement of dimethylamine is sluggish at room temperature in neat THF. Monitoring via ³¹P{¹H} NMR spectroscopy, 28% conversion to [3.5] occurred after 5 min, increasing to 62% overnight, with complete conversion after *ca* 2 weeks; and placement of the system under reduced pressure did not improve matters. For [3.6], 44% unreacted ^{tol}NPNZrCl₂(HNMe₂) [3.4] remained after 21 hrs. In hot THF (60 °C), conversions of

[3.3] and [3.4] to their respective THF adducts [3.5] and [3.6] occurred within one to six hours, in agreement with the previously reported formation of [3.6], where the THF solution was also heated.²⁶¹

$^{31}\text{P}\{^1\text{H}\}$ NMR spectra of $^{\text{iprop}}\text{NPNZrCl}_2(\text{THF})$ [3.5] and $^{\text{tol}}\text{NPNZrCl}_2(\text{THF})$ [3.6] display singlets at δ 6.48 (Figure 58) and 6.07, respectively. The ^1H NMR spectra respectively of [3.5] and [3.6] have signals at δ 3.87 and 1.03 (Figure 58), and at δ 3.83 and 1.10, attributable to coordinated THF. In the corresponding $^{13}\text{C}\{^1\text{H}\}$ NMR spectra, there are signals at δ 74.4 and 25.1 (Figure 58), and at δ 72.9 and 25.2 that are assigned to the THF carbons of [3.5] and [3.6], respectively.

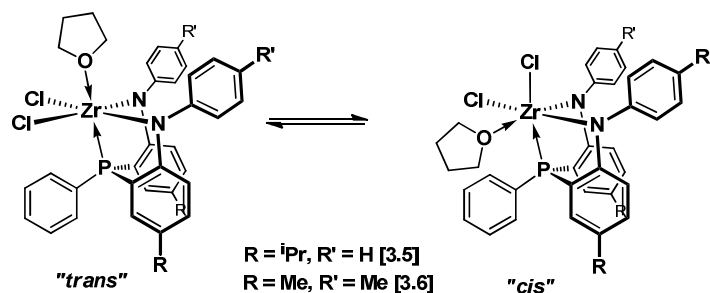


Figure 57: Isomers of $\text{NPNZrCl}_2(\text{THF})$

As with $^{\text{iprop}}\text{NPNZrCl}_2(\text{HNMe}_2)$ [3.3] and $^{\text{tol}}\text{NPNZrCl}_2(\text{HNMe}_2)$ [3.4], two isomers are possible for $^{\text{iprop}}\text{NPNZrCl}_2(\text{THF})$ [3.5] and $^{\text{tol}}\text{NPNZrCl}_2(\text{THF})$ [3.6] (Figure 57), but only one set of R and R' signals were observed in their respective ^1H NMR spectra.

Single crystals of both $^{\text{iprop}}\text{NPNZrCl}_2(\text{THF})$ [3.5] and $^{\text{tol}}\text{NPNZrCl}_2(\text{THF})$ [3.6]²⁶¹ verify that in the solid state the isomer with the THF *cis* to the P atom was obtained (Figure 59). Again, a similar argument to the one used for $^{\text{tol}}\text{NPNZrCl}_2(\text{HNMe}_2)$ [3.4] can be invoked to explain the incongruence between the *cis* solid state structure and the inferred *trans* solution structure. Upon cooling a toluene- d_8 solution of $^{\text{iprop}}\text{NPNZrCl}_2(\text{THF})$ to -60°C , no changes were observed in the $^{31}\text{P}\{^1\text{H}\}$ NMR and ^1H NMR spectra.

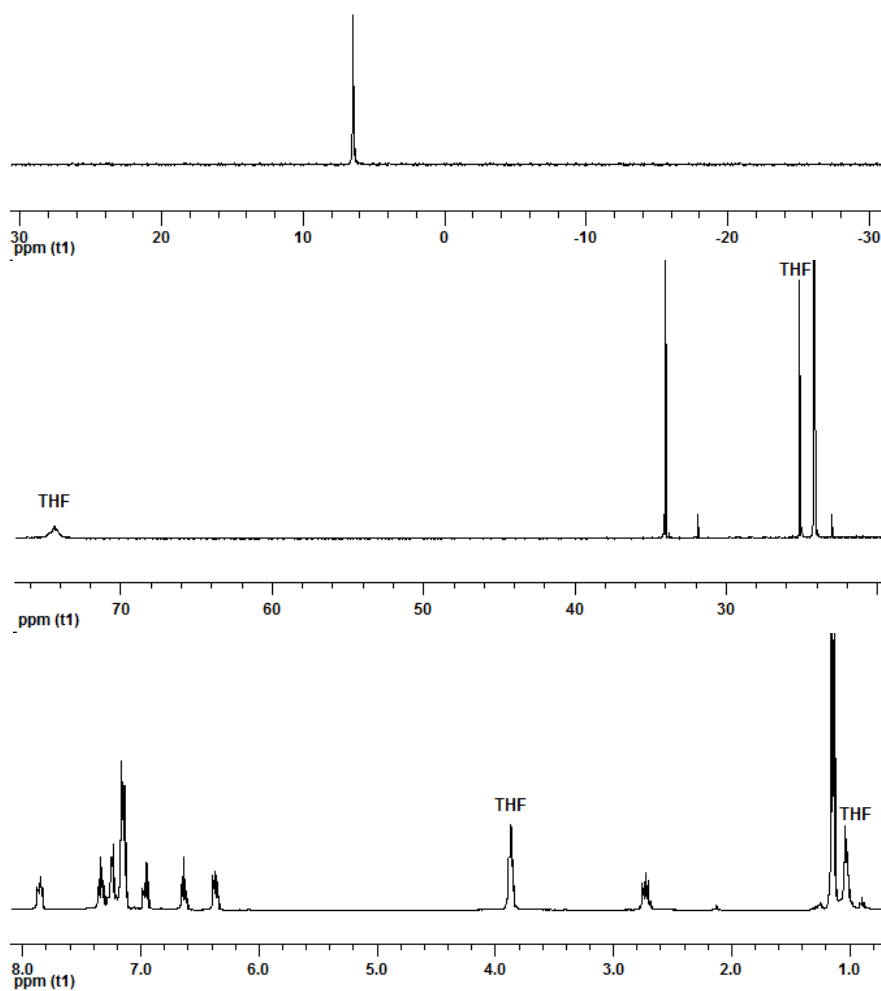


Figure 58: $^{31}\text{P}\{^1\text{H}\}$ (top), partial $^{13}\text{C}\{^1\text{H}\}$ (middle) and ^1H NMR (bottom) spectra of $^{\text{iprop}}\text{NPNZrCl}_2(\text{THF})$ [3.5] in C_6D_6

Both $^{\text{iprop}}\text{NPNZrCl}_2(\text{THF})$ [3.5] and $^{\text{tol}}\text{NPNZrCl}_2(\text{THF})$ [3.6] display distorted octahedral geometries, with the P1-Zr1-Cl1 and N8-Zr1-O1 angles for [3.5] being less linear than for [3.6] (Table 8). The zirconium chloride bond lengths (Zr1-Cl1 and Zr1-Cl2) for [3.5] and [3.6] (Table 8) are all similar to those obtained for $^{\text{mes}}\text{NPNZrCl}_2$, $^{97} \text{mes}\text{NPNZrCl}_2(\text{Py})$ ⁹⁷ and $^{\text{tol}}\text{NPNZrCl}_2(\text{HNMe}_2)$ [3.4] (Table 7). So too are the Zr1-P1, Zr1-N8 and Zr1-N8a bond lengths and angles (Table 8). The Zr1-O1 bond lengths of [3.5] and [3.6] (Table 8) are shorter compared to those obtained for $[\text{Si}^{\text{NPNZr}}(\text{THF})]_2(\text{N}_2)$ ^{137, 138} at 2.305(1) Å and $[\text{mes}^{\text{NPNZr}}(\text{THF})]_2(\text{N}_2)$ at 2.371(2) Å.^{92, 97}

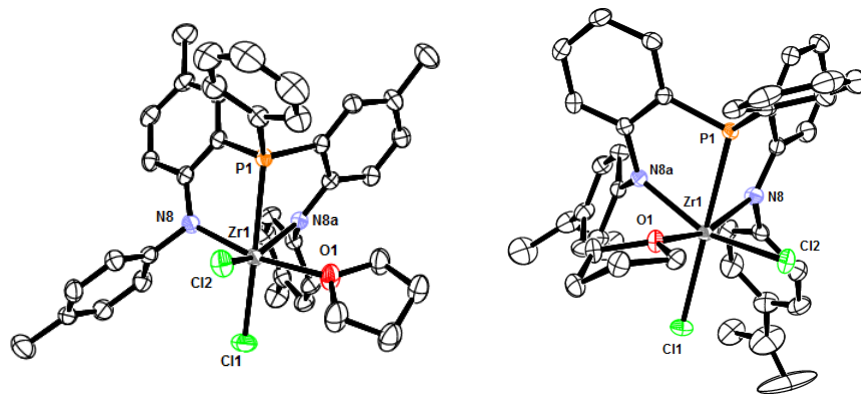


Figure 59: ORTEP representations of the solid state molecular structures of $\text{ipropNPNZrCl}_2(\text{THF})$ [3.5] and $\text{tolNPNZrCl}_2(\text{THF})$ [3.6]

Table 8 : Selected bond lengths (\AA) and angles ($^\circ$) for $\text{ipropNPNZrCl}_2(\text{THF})$ [3.5] and $\text{tolNPNZrCl}_2(\text{THF})$ [3.6]²⁶¹

| | $\text{ipropNPNZrCl}_2(\text{THF})$ [3.5] | $\text{tolNPNZrCl}_2(\text{THF})$ [3.6] ²⁶¹ |
|-------------|---|--|
| Zr1-P1 | 2.6945(6) | 2.7316(10) |
| Zr1-N8a | 2.1540(17) | 2.128(3) |
| Zr1-N8 | 2.0853(17) | 2.088(3) |
| Zr1-O1 | 2.2862(14) | 2.254(2) |
| Zr1-Cl1 | 2.4469(6) | 2.4098(10) |
| Zr1-Cl2 | 2.4653(6) | 2.4596(10) |
| P1-Zr1-Cl1 | 168.92(2) | 174.02(3) |
| N8a-Zr1-Cl2 | 149.27(5) | 149.42(7) |
| N8-Zr1-O1 | 155.55(6) | 161.70(10) |
| P1-Zr1-N8a | 70.54(5) | 67.70(7) |
| P1-Zr1-N8 | 72.79(5) | 73.94(7) |
| P1-Zr1-O1 | 82.80(4) | 87.82(7) |
| P1-Zr1-Cl2 | 82.00(2) | 86.80(3) |
| Cl1-Zr1-N8a | 113.12(5) | 106.32(7) |
| Cl1-Zr1-N8 | 116.61(5) | 106.80(8) |
| Cl1-Zr1-O1 | 87.53(4) | 91.19(7) |
| Cl1-Zr1-Cl2 | 91.53(2) | 98.91(4) |
| N8a-Zr1-N8 | 92.93(7) | 91.32(10) |
| N8a-Zr1-O1 | 79.96(6) | 80.18(9) |
| Cl2-Zr1-N8 | 91.82(5) | 97.75(8) |
| Cl2-Zr1-O1 | 83.25(4) | 82.33(7) |

Protonolysis of tolNPNH_2 [2.11] with $\text{ZrCl}_2(\text{NMe}_2)_2(\text{DME})$ in THF instead of toluene may avoid HNMe_2 formation and lead directly to the THF adduct; however, reaction at 60°C gave a mixture that contained amongst others $\text{tolNPNZrCl}_2(\text{THF})$ [3.6], $\text{tolNPNZr}(\text{NMe}_2)_2$ [3.8] and unreacted tolNPNH_2 [2.11]. Possible explanations for [3.8] is a conproportionation between $\text{tolNPNZrCl}_2(\text{THF})$ [3.6] and $\text{ZrCl}_2(\text{NMe}_2)_2(\text{DME})$, or $\text{ZrCl}_2(\text{NMe}_2)(\text{DME})$ may be in equilibrium with $\text{ZrCl}_x(\text{NMe}_2)_{4-x}$ species i.e. $x = 0$ and 4 (Figure 60).

While reaction of the protonated NPN ligands with $\text{ZrCl}_2(\text{NMe}_2)_2(\text{DME})$ may utilise less steps compared to $\text{Zr}(\text{NMe}_2)_4$, traces of $\text{ZrCl}_3(\text{NMe}_2)$ in $\text{ZrCl}_2(\text{NMe}_2)_2(\text{DME})$ led to the occasional observation of the zirconium trichloride species $^{\text{iprop}}\text{NPN}(\text{H})\text{ZrCl}_3$ (see earlier discussion). A different method for the synthesis of $\text{ZrCl}_2(\text{NMe}_2)_2(\text{DME})$ from $\text{Zr}(\text{NMe}_2)_4$, TMSCl and DME ²⁶⁵ instead of reaction of ZrCl_4 with $\text{Zr}(\text{NMe}_2)_4$ ²⁶⁶ may be considered in future.

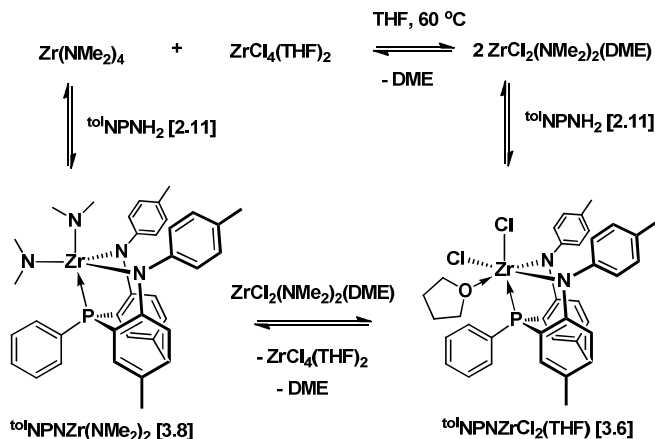


Figure 60: Protonolysis of $^{\text{tol}}\text{NPNH}_2$ [2.11] with $\text{ZrCl}_2(\text{NMe}_2)_2(\text{DME})$ in THF at 60 °C

Synthesis of $^{\text{iprop}}\text{NPNZr}(\text{NMe}_2)_2$ [3.7] and $^{\text{tol}}\text{NPNZr}(\text{NMe}_2)_2$ [3.8]

Reaction of one equiv of $^{\text{iprop}}\text{NPNH}_2$ [2.10] or $^{\text{tol}}\text{NPNH}_2$ [2.11] with $\text{Zr}(\text{NMe}_2)_4$ in toluene at room temperature gave the lemon yellow solids $^{\text{iprop}}\text{NPNZr}(\text{NMe}_2)_2$ [3.7] or $^{\text{tol}}\text{NPNZr}(\text{NMe}_2)_2$ [3.8] in high yield. Their $^{31}\text{P}\{^1\text{H}\}$ NMR spectra display singlets at δ -10.60 and δ -10.16, similar to $^{\text{mes}}\text{NPNZr}(\text{NMe}_2)_2$ ^{97, 214} at δ -11.5. There are two different methyl environments for the NMe_2 groups, with peaks at δ 2.48 / 2.80 and δ 2.56 / 2.87 in their ^1H NMR spectra (Figure 61) and at δ 40.7 / 41.5 and δ 40.8 / 41.6 in their $^{31}\text{C}\{^1\text{H}\}$ NMR spectra, for [3.7] and [3.8] respectively. This agrees with what has been observed for $^{\text{mes}}\text{NPNZr}(\text{NMe}_2)_2$ ^{97, 214} and other $\text{NPNZr}(\text{NMe}_2)_2$ ^{213, 267} complexes.

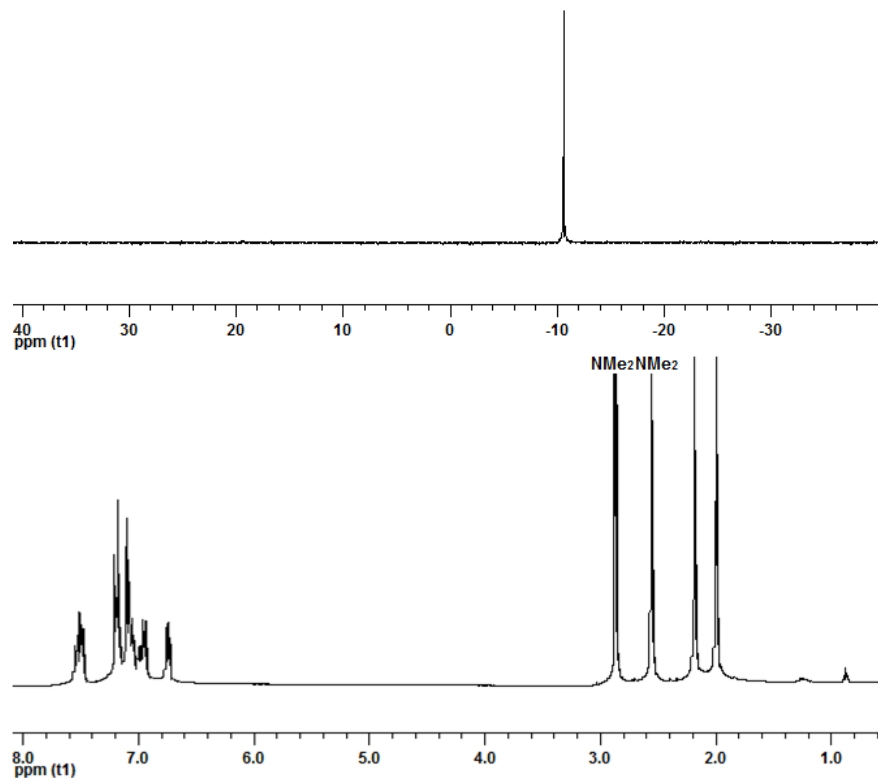


Figure 61: $^{31}\text{P}\{^1\text{H}\}$ (top) and ^1H NMR (bottom) spectra of $^{\text{tol}}\text{NPNZr}(\text{NMe}_2)_2$ [3.8]

Single crystals of $^{\text{iprop}}\text{NPNZr}(\text{NMe}_2)_2$ [3.7]⁹⁷ [3.7] and $^{\text{tol}}\text{NPNZr}(\text{NMe}_2)_2$ [3.8]²⁶¹ were obtained and their solid state molecular structures display a distorted trigonal bipyramidal geometry around the zirconium centre (Figure 62), as observed in other $\text{NPNZr}(\text{NMe}_2)_2$ complexes.^{139, 140}

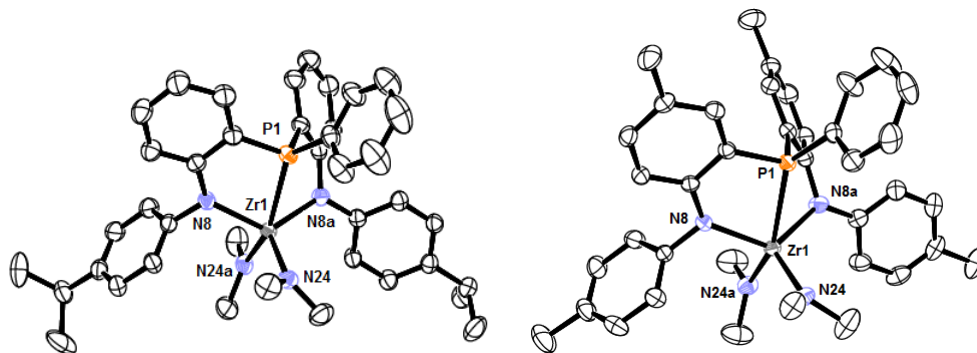


Figure 62: ORTEP representation of the solid state molecular structure of $^{\text{iprop}}\text{NPNZr}(\text{NMe}_2)_2$ [3.7] and $^{\text{tol}}\text{NPNZr}(\text{NMe}_2)_2$ [3.8]

The ^{iprop}NPN and ^{tol}NPN ligands are bonded facially with one NMe₂ (N24a) and the P atom forming the apexes and the other NMe₂ (N24) and the two N atoms of the ligand (N24 and N24a) in the trigonal plane. The Zr-NMe₂ bond lengths for ^{iprop}NPNZr(NMe₂)₂ [3.7] and ^{tol}NPNZr(NMe₂)₂ [3.8] (Table 9) are typical of zirconium amido complexes^{139, 140, 213, 268, 269} and the two different NMe₂ environments observed in solution are clearly reflected in the solid state. The P1-Zr1-N8 and P1-Zr1-N8a bite angles for the five-coordinate [3.7] and [3.8] complexes are similar to the octahedral ^{iprop}NPN and ^{tol}NPN zirconium complexes discussed in this chapter (Table 2, Table 7 and Table 8), but the N8-Zr1-N8a bite angles of 125.17(8)° and 123.16(17)° are much larger.

Table 9 : Selected bond lengths (Å) and angles (°) for ^{iprop}NPNZr(NMe₂)₂ [3.7] and ^{tol}NPNZr(NMe₂)₂ [3.8]²⁶¹

| | ^{iprop} NPNZr(NMe ₂) ₂ [3.7] ⁹⁷ | ^{tol} NPNZr(NMe ₂) ₂ [3.8] ²⁶¹ |
|--------------|--|---|
| Zr1-P1 | 2.7355(7) | 2.7509(6) |
| Zr1-N8 | 2.158(2) | 2.1570(18) |
| Zr1-N8a | 2.157(2) | 2.1376(18) |
| Zr1-N24 | 2.027(2) | 2.0153(18) |
| Zr1-N24a | 2.053(2) | 2.0418(19) |
| P1-Zr1-N8 | 70.71(6) | 70.39(5) |
| P1-Zr1-N8a | 72.06(6) | 72.10(5) |
| P1-Zr1-N24 | 100.36(6) | 99.50(6) |
| P1-Zr1-N24a | 155.07(6) | 154.11(6) |
| N24-Zr1-N8 | 109.76(9) | 111.11(7) |
| N24-Zr1-N8a | 115.41(8) | 115.97(8) |
| N24a-Zr1-N8 | 98.60(9) | 98.75(7) |
| N24a-Zr1-N8a | 98.62(8) | 96.89(8) |
| N8-Zr1-N8a | 125.17(8) | 123.16(7) |
| N24-Zr1-N24a | 104.49(9) | 106.37(8) |

Synthesis of [^{iprop}NPNZrCl₂]₂ [3.9] and [^{tol}NPNZrCl₂]₂ [3.10]

Monitoring the addition of TMSCl to ^{iprop}NPNZr(NMe₂)₂ [3.7] with ³¹P{¹H} NMR spectroscopy, an intermediate with a sharp peak at δ 0.09 is observed after 2 equiv of TMSCl (Figure 63); *ca* 7 equiv of TMSCl are required for complete conversion to [^{iprop}NPNZrCl₂]₂ [3.9], and also observed for [^{tol}NPNZrCl₂]₂ [3.10]. More often, the dimeric complexes with bridging dichlorides [3.9] and [3.10] were not isolated; after addition of TMSCl the toluene solvent was replaced with THF at room temperature, giving ^{iprop}NPNZrCl₂(THF) [3.5] and ^{tol}NPNZrCl₂(THF) [3.6].

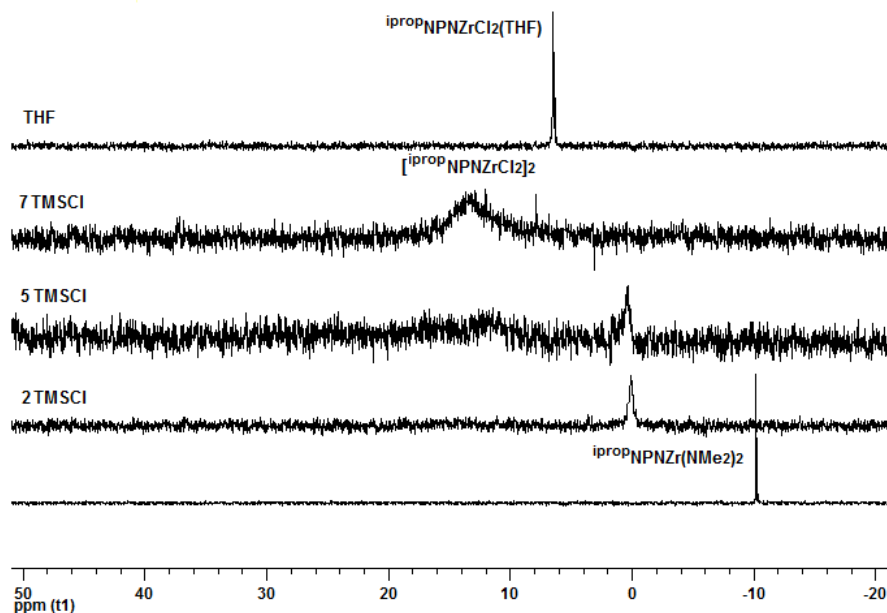


Figure 63: $^{31}\text{P}\{^1\text{H}\}$ NMR spectra of $\text{ipropNPNZr}(\text{NMe}_2)_2$ [3.7] (bottom) and after 2, 5 and 7 equiv of TMSCl (middle three) and $\text{ipropNPNZrCl}_2(\text{THF})$ [3.5] after excess THF (top) in C_6D_6 at 25°C

These bridging dichloride complexes [3.9] and [3.10] are not very soluble in benzene, improving marginally in toluene. Their $^{31}\text{P}\{^1\text{H}\}$ NMR spectra at room temperature in C_6D_6 exhibit very broad peaks at δ 11.23 and δ 9.95, respectively, with spurious sharp peaks observed at δ 4.54, δ 33.90 and δ 7.54 (Figure 64). The corresponding ^1H NMR spectra indicates that no impurities, other than solvent, are present in the samples (Figure 64) and elemental analysis results also reflect sample purity.

It was not possible with either EI-MS or MALDI-TOF mass spectrometry to obtain the parent ions $[\text{M}]^+$ for $[\text{ipropNPNZrCl}_2]_2$ [3.9] and $[\text{tolNPNZrCl}_2]_2$ [3.10]. For [3.9], the largest fragment ion was observed at 688 m/z indicating survival of the monomer $[\text{M} - \text{ipropNPNZrCl}_2]^+$. For [3.10], a larger fragment ion corresponding to $[\text{M} - \text{ZrCl}_4]^+$ was observed at 1087 m/z, as well as the monomer fragment ion $[\text{M} - \text{tolNPNZrCl}_2]^+$ at 660 m/z.

$^{\text{mes}}\text{NPNZrCl}_2$, $^{97, 214} \text{CY}^5\text{NPNZrCl}_2$, $^{139, 140}$ and thiophene-based $^{\text{S}}\text{NPNZrCl}_2$ 213 are monomers in the solid state. However, a NPNZrCl_2 complex with a $-\text{CH}_2\text{CH}_2-$ backbone 267 has been

postulated to be dimeric, along with confirmed chloro-bridged solid state structures reported for a Zr(III) dimeric derivative $[\text{NPN}(\text{P})\text{ZrCl}_2]_2$,¹⁴⁹ and a zirconium trichloride phosphine dimer.²⁷⁰

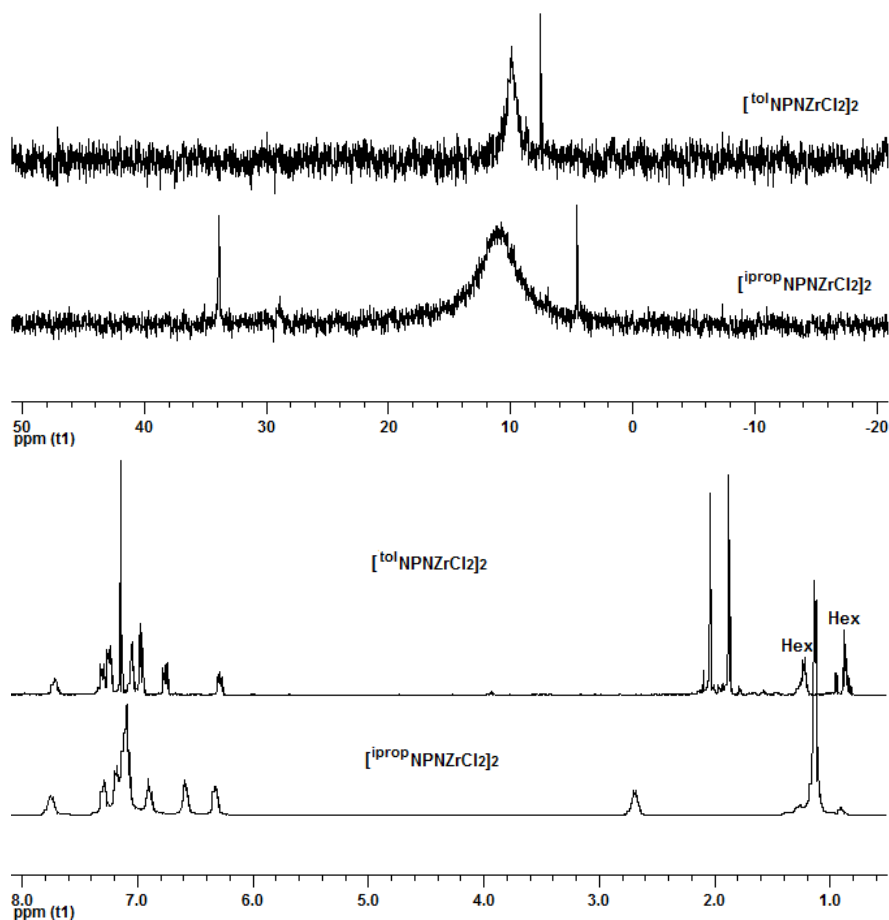


Figure 64: $^{31}\text{P}\{^1\text{H}\}$ (top) and ^1H NMR (bottom) spectra of $[\text{ipropNPNZrCl}_2]_2$ [3.9] and $[\text{tolNPNZrCl}_2]_2$ [3.10] in C_6D_6 at 25 °C

Single crystals of $[\text{ipropNPNZrCl}_2]_2$ [3.9] reveal a chloro-bridged dimer (Figure 65). The coordination environment around the Zr atom can best be described as distorted octahedral, with the P1-Zr1-Cl2 , N8-Zr1-Cl2' and N8a-Zr1-Cl1 angles deviating significantly from 180° (Table 10). The terminal chlorides of the opposing Zr centres are situated *trans* to each other and the ipropNPN ligands are facially bound such that the phosphorus atom (P1) on one zirconium atom (Zr1) is orientated *trans* to the other P1' atom attached to the Zr1' atom.

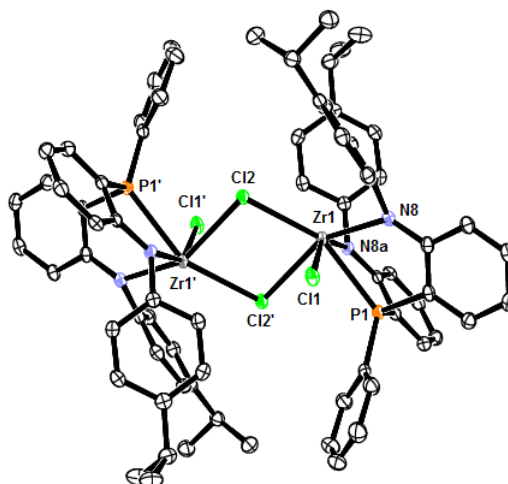


Figure 65: ORTEP representation of the solid state molecular structure of $[\text{ipropNPNZrCl}_2]_2$ [3.9]

The terminal chlorides (Cl1, Cl1') have shorter bonds to zirconium than the bridging chlorides (Cl2, Cl2') and both types have longer Zr-Cl bond lengths than reported for $\text{CY}^5\text{NPNZrCl}_2$,^{139, 140} mesNPNZrCl_2 (Table 10),^{97, 214} $\text{tolNPNZrCl}_2(\text{HNMe}_2)$ [3.4], $\text{ipropNPNZrCl}_2(\text{THF})$ [3.5] and $\text{tolNPNZrCl}_2(\text{THF})$ [3.6] (Table 7 and Table 8). The Zr-Cl terminal bonds in $[\text{ZrCl}_3(\text{PBU}_3)_2]_2$ are also shorter than the bridged Zr-Cl bonds,²⁷⁰ though the inverse was observed for $[\text{NPN}(\text{P})\text{ZrCl}_2]_2$.¹⁴⁹

Table 10 : Selected bond lengths (Å) and angles (°) for $[\text{ipropNPNZrCl}_2]_2$ [3.9] and mesNPNZrCl_2 ^{97, 214}

| | $[\text{ipropNPNZrCl}_2]_2$ [3.9] | mesNPNZrCl_2 ^{97, 214} |
|--------------|-----------------------------------|--|
| Zr1-P1 | 2.6661(9) | 2.7228(8) |
| Zr1-N8a | 2.1400(16) | 2.071(2) |
| Zr1-N8 | 2.1219(17) | 2.060(2) |
| Zr1-Cl1 | 2.5037(8) | 2.4098(8) |
| Zr1-Cl2 | 2.6278(10) | 2.4279(8) |
| Zr1-Cl2' | 2.6506(10) | |
| P1-Zr1-Cl2 | 152.840(17) | 178.63(3) |
| N8a-Zr1-Cl1 | 145.23(4) | |
| N8-Zr1-Cl2' | 152.14(4) | |
| P1-Zr1-N8a | 70.36(5) | 70.38(7) |
| P1-Zr1-N8 | 71.57(4) | 72.73(7) |
| P1-Zr1-Cl1 | 75.71(4) | 85.02(3) |
| P1-Zr1-Cl2' | 81.348(19) | |
| Cl2-Zr1-N8a | 124.41(5) | 109.43(7) |
| Cl2-Zr1-N8 | 124.72(4) | 106.25(7) |
| Cl2-Zr1-Cl1 | 84.34(3) | 96.24(3) |
| Cl2-Zr1-Cl2' | 78.259(19) | |
| N8a-Zr1-N8 | 92.83(6) | 113.97(9) |
| Cl1-Zr1-N8 | 83.42(4) | 111.40(7) |
| Cl2'-Zr1-N8a | 83.94(4) | 117.49(7) |
| Cl1-Zr1-Cl2' | 83.69(2) | |
| Zr1-Cl2-Zr1' | 101.741(19) | |

In order to further explore the solution behaviour of these dichloride complexes, variable temperature NMR experiments were conducted. When $[\text{tolNPNZrCl}_2]_2$ **[3.10]** is heated to 93 °C there is a single sharp peak at δ 6.86 in the $^{31}\text{P}\{^1\text{H}\}$ NMR spectrum (Figure 66). When the temperature is lowered to -71 °C, four peaks are observed at δ 14.05, δ 7.54, δ 5.14 and further downfield at δ 33.85.

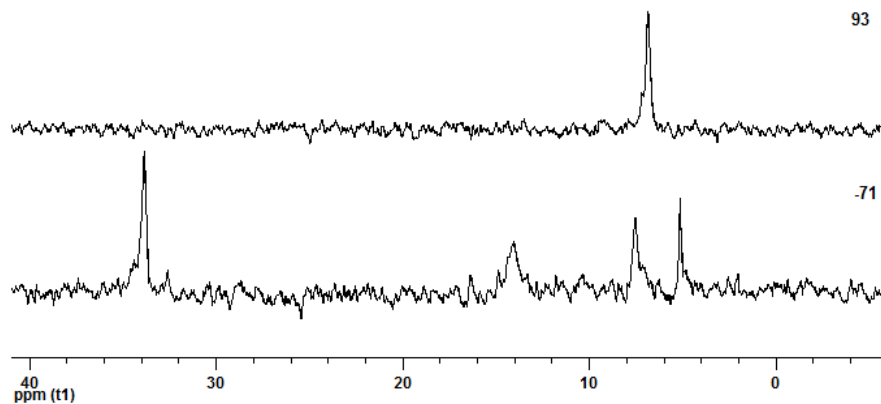


Figure 66: $^{31}\text{P}\{^1\text{H}\}$ NMR spectra of $[\text{tolNPNZrCl}_2]_2$ **[3.10]** in toluene- d_8 at 93 and -71 °C

For $[\text{ipropNPNZrCl}_2]_2$ **[3.9]**, on heating to 93 °C a broader peak is observed at δ 7.80 with a small peak at δ 4.54 (Figure 67). As the sample cools, the peak at δ 7.80 continues to broaden even more at room temperature, gradually shifting downfield and a third peak is observed at δ 7.29. With further cooling down to -60 °C, the broad peak sharpens and shifts to δ 12.90, and together with δ 7.29 and δ 4.54, these signals mirrors those observed for **[3.10]** at low temperature (Figure 66).

Unlike $[\text{tolNPNZrCl}_2]_2$ **[3.10]** (Figure 66), more than one signal is observed at ca δ 33 for $[\text{ipropNPNZrCl}_2]_2$ **[3.9]** at low temperature, which starts growing in below 7 °C (Figure 67). When the experiment was repeated with a different sample $[\text{ipropNPNZrCl}_2]_2$ **[3.9]**, the peak at δ 7.29 was not observed at low temperatures (Figure 68). We were unable to rationalise this temperature dependent behaviour other than to suggest that different diastereomeric forms with bridging chlorides may be forming at low temperatures, as discussed below.

$[\text{ipropNPNZrCl}_2]_2$ [3.9] and $[\text{tolNPNZrCl}_2]_2$ [3.10] compounds both displayed complex solution behaviour compared to monomeric $^{\text{mes}}\text{NPNZrCl}_2$. An authentic sample of $^{\text{mes}}\text{NPNZrCl}_2$ was cooled down to $-50\text{ }^\circ\text{C}$ in toluene- d_8 , with no changes observed for the single sharp peak at δ -1.86 the $^{31}\text{P}\{^1\text{H}\}$ NMR spectrum.

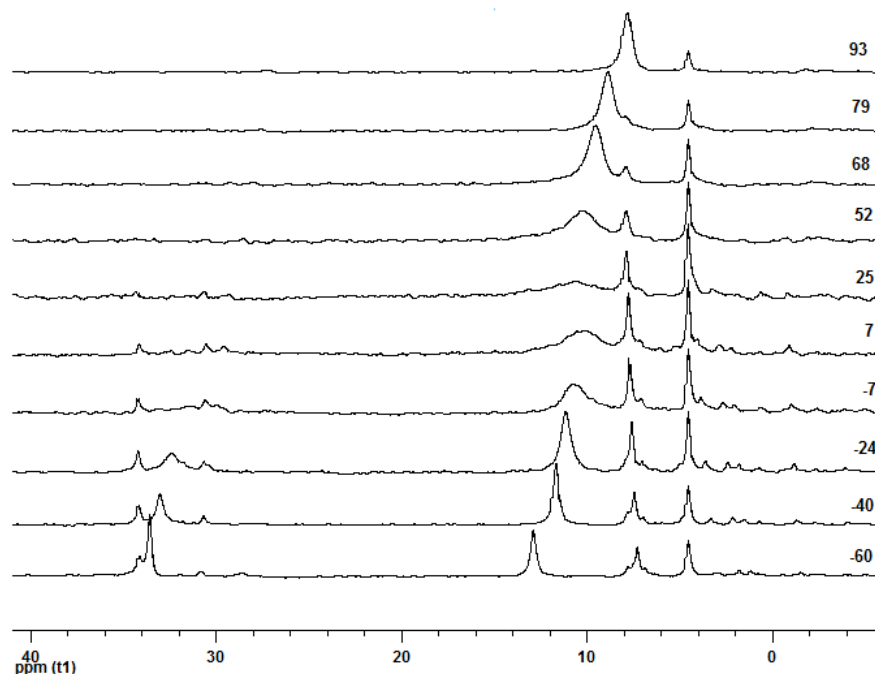


Figure 67: $^{31}\text{P}\{^1\text{H}\}$ NMR spectra of $[\text{ipropNPNZrCl}_2]_2$ [3.9] in toluene- d_8 from 93 to $-60\text{ }^\circ\text{C}$ (δ 4.54 at $25\text{ }^\circ\text{C}$ used as reference for spectra at other temperatures)

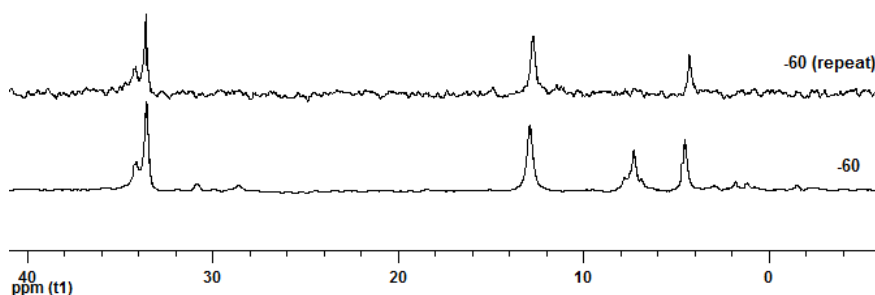


Figure 68: $^{31}\text{P}\{^1\text{H}\}$ NMR spectra of different samples $[\text{ipropNPNZrCl}_2]_2$ [3.9] in toluene- d_8 at $-60\text{ }^\circ\text{C}$

Changes are also observed for the ^1H NMR spectra, as illustrated for $[\text{ipropNPNZrCl}_2]_2$ [3.9] at $-60\text{ }^\circ\text{C}$, $25\text{ }^\circ\text{C}$ and $93\text{ }^\circ\text{C}$ (Figure 69). On cooling to $-60\text{ }^\circ\text{C}$, new peaks are observed in the phenyl region at δ 8.45, 8.19 (downfield) and δ 5.98, 5.88, 5.65 and 5.28 (upfield). At least seven

different methine signals are observed, indicating multiple *i*-propyl environments, with one signal significantly downfield at δ 3.69 (Figure 69).

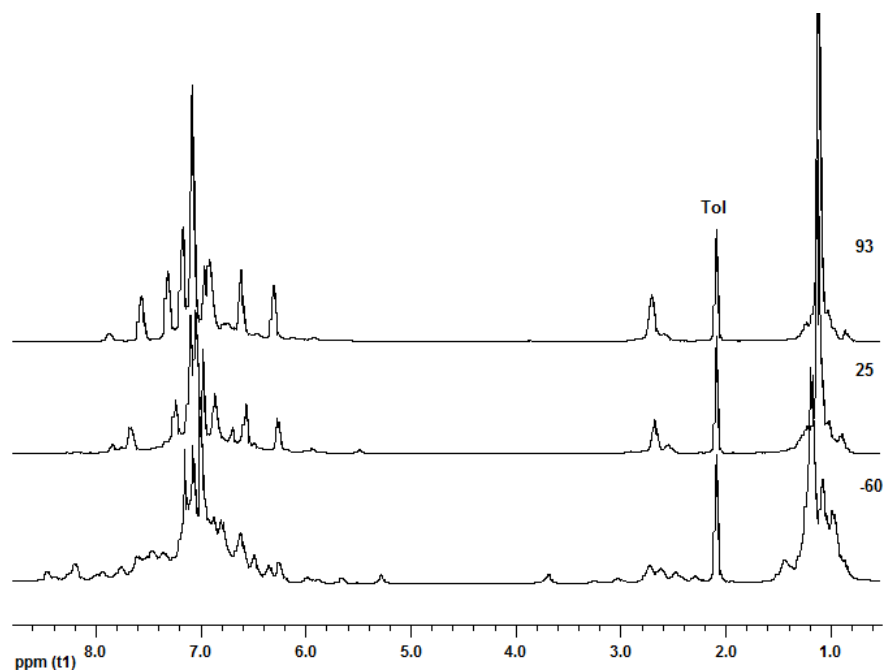


Figure 69: ^1H NMR spectrum of $[\text{ipropNPNZrCl}_2]_2$ [3.9] in toluene- d_8 at -60°C , 25°C and 93°C

To rationalize the observation of multiple species in solution at low temperatures, different dinuclear chloro-bridged species can be envisioned (Figure 70). Isomer A depicts the solid state molecular structure of $[\text{ipropNPNZrCl}_2]_2$ [3.9] (Figure 65) and Isomer C correlates with the solid state molecular structure obtained for the hafnium congener $[\text{ipropNPNHfCl}_2]_2$ [3.20] (see later discussion and Figure 89).

The possibility cannot be discounted that the N atoms of the ipropNPN / tolNPN ligands may also form bridging amido structures,²⁷¹ although these are not explicitly shown below. Furthermore, monomeric ipropNPNZrCl_2 / tolNPNZrCl_2 species may be in equilibrium with the proposed dimers. It may be that the dimers dissociate to generate monomers that recombine to give the isomeric forms proposed in Figure 70.

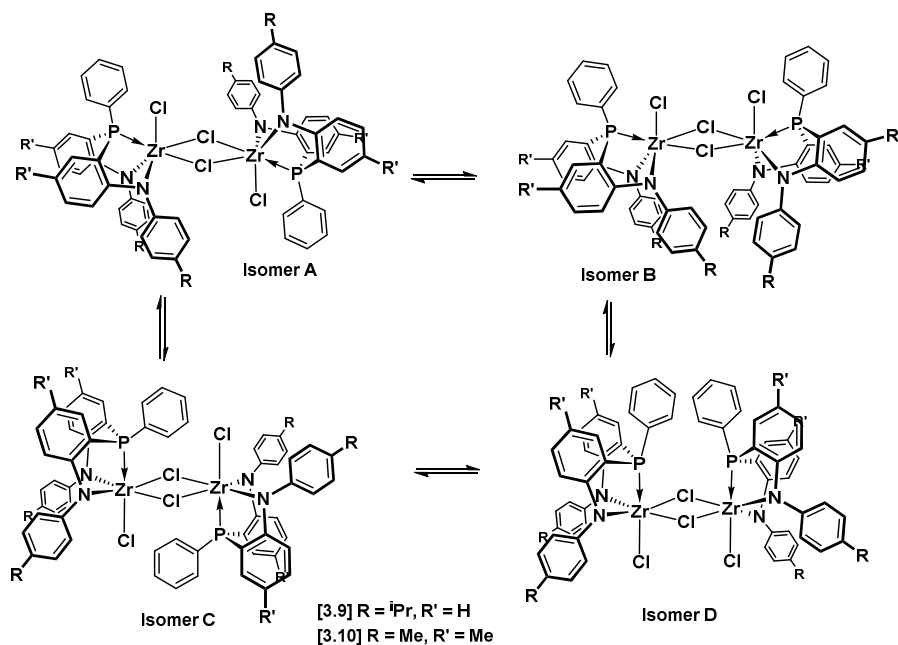


Figure 70: Chloro-bridged isomers for [NPNZrCl₂]₂, [3.9] and [3.10]

Diffusion ordered NMR spectroscopy (DOSY)^{272, 273} is a technique that can be used to determine the diffusion coefficients of dissolved species and hence particle size. More specifically, according to the Stokes-Einstein equation, the spherical radius of a particle (*r*) in a liquid is inversely proportional to the diffusion coefficient (*D*).

$$r = \frac{kT}{6\pi\eta D}$$

Thus the *D* values for dimers are expected to be half that obtained for a monomer. A DOSY ³¹P{¹H} NMR experiment was conducted for a sample of [^{*i*prop}NPNZrCl₂]₂ [3.9] at -40 °C in order to investigate the particle size of the isomeric species observed. It was not possible to attain the rigorous experimental conditions required to determine the absolute diffusion coefficient values, and analysis was further hampered by low solubility and broad peaks. However, a qualitative comparison between the peaks could still be made, as all the particles can be evaluated during a single experiment. The *D* values obtained for the six peaks at δ 34.4, δ 33.3, δ 31.0, δ 12.0, δ 7.7 and δ 4.8 were determined to be 5.99, 7.12, 7.72, 6.55, 7.16 and 8.11 × 10⁻⁹ m²s⁻¹, respectively (see Appendix A).

Assuming that the smallest D value represents a dimer, doubling this value gave $5.99 \times 2 = 11.98 \times 10^{-9} \text{ m}^2\text{s}^{-1}$, which is significantly larger than the largest D value obtained in this experiment. This suggests that none of the species present can be correlated to a monomer. The D values obtained are consistent with the presence of species of similar size to the dimer in solution, however, uncertainty remains as the equation is based on the assumption of spherical particles. Repeating this experiment spiking with ^{13}C -NPNZrCl₂ may in future provide a better reference D value for a monomer. However, if the monomer is present in very small concentrations but undergoes fast exchange, then the DOSY experiment will not be affected.

These DOSY NMR experiments with the zirconium dichlorides failed to provide conclusive evidence for the presences of a monomeric species. However, if an experiment mixing a solution of [$^{i\text{prop}}\text{NPNZrCl}_2$]₂ [3.9] with [$^{tol}\text{NPNZrCl}_2$]₂ [3.10] was shown to produce a mixed dimer such as [$^{i\text{prop}}\text{NPN}(\text{Cl})\text{Zr}(\mu\text{-Cl})_2\text{Zr}(\text{Cl})\text{NPN}^{tol}$], more credence could be placed on a mechanism whereby a dimer dissociates into monomers before recombining into a different dimer.

3.2. Titanium Diamido-Phosphine Complexes

The protonolysis method using both TiCl₂(NMe₂) and Ti(NMe₂)₄ was investigated (Figure 71) and the most notable difference from the zirconium system is that dimeric chloride-bridged structures were not observed.

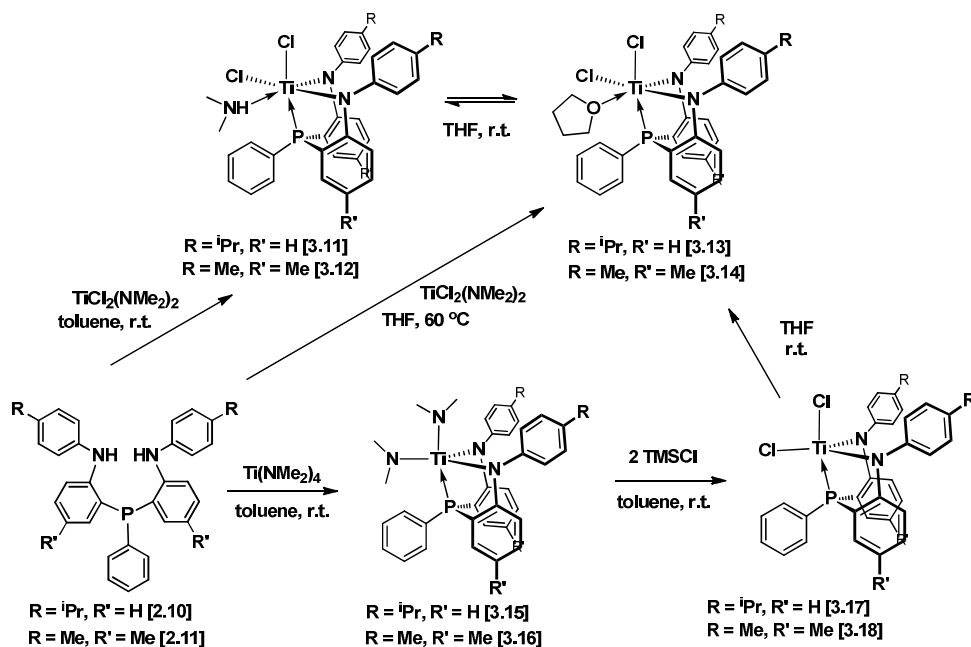


Figure 71: Protonolysis with $\text{TiCl}_2(\text{NMe}_2)_2$ or $\text{Ti}(\text{NMe}_2)_4$

Synthesis of $^{\text{iPr}}\text{NPNTiCl}_2(\text{HNMe}_2)$ [3.11] and $^{\text{tol}}\text{NPNTiCl}_2(\text{HNMe}_2)$ [3.12]

The purplish-black solids $^{\text{iPr}}\text{NPNTiCl}_2(\text{HNMe}_2)$ [3.11] and $^{\text{tol}}\text{NPNTiCl}_2(\text{HNMe}_2)$ [3.12] were obtained from $^{\text{iPr}}\text{NPNH}_2$ [2.10] or $^{\text{tol}}\text{NPNH}_2$ [2.11] and $\text{TiCl}_2(\text{NMe}_2)_2$ in toluene at room temperature. As with zirconium, two isomers are possible for [3.11] and [3.12] (Figure 72). The observance of one set of R and R' signals in their respective ^1H NMR spectra suggests a similar scenario for the *cis* and *trans* isomers as outlined for the zirconium congeners. Unfortunately single crystals were not obtained in order to determine the preferred isomer in the solid state.

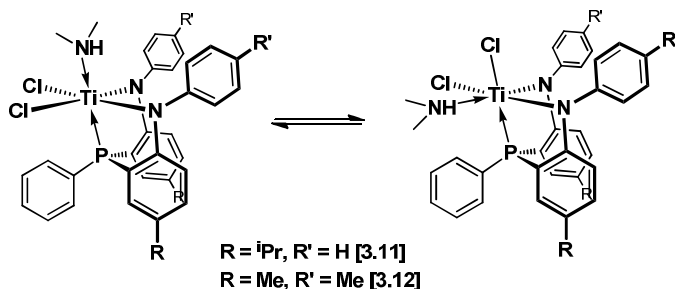


Figure 72: Possible isomers for $\text{NPNTiCl}_2(\text{HNMe}_2)$ [3.11] and [3.12]

Their $^{31}\text{P}\{^1\text{H}\}$ NMR spectra display singlets at δ 27.83 and δ 26.35 (see Figure 73 for [3.12]) and their ^1H NMR (see Figure 74 for [3.12]) and $^{13}\text{C}\{^1\text{H}\}$ NMR spectra display characteristic signals for coordinated HNMe_2 .

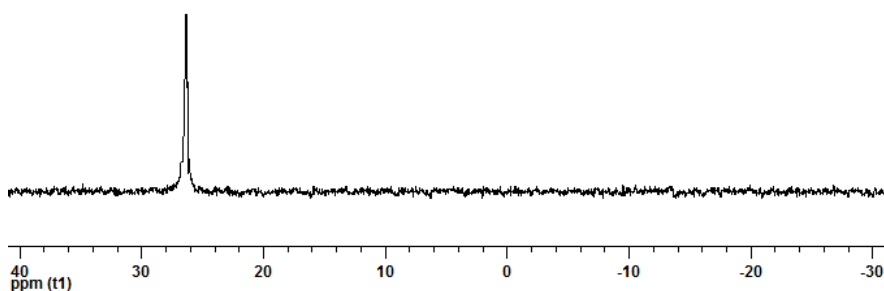


Figure 73: $^{31}\text{P}\{^1\text{H}\}$ NMR spectrum of $^{10}\text{lNPNTiCl}_2(\text{HNMe}_2)$ [3.12]

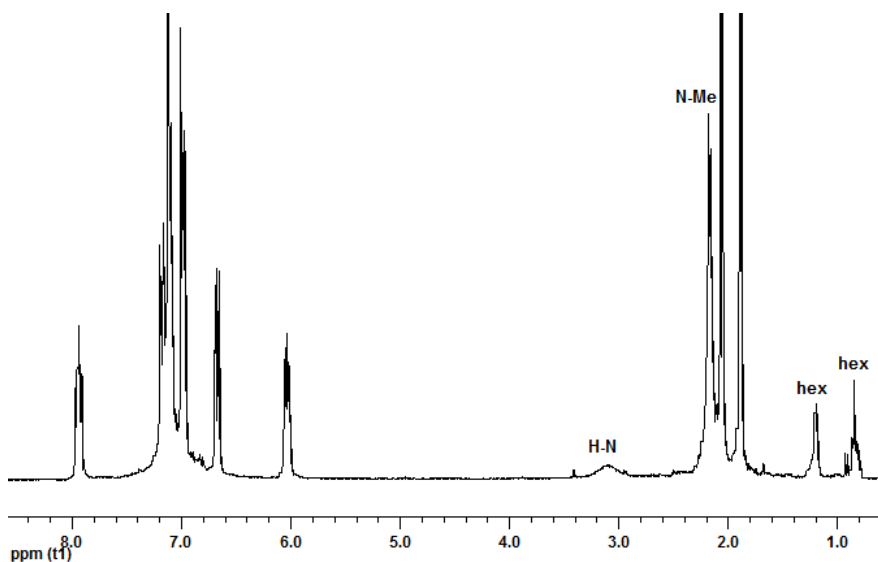


Figure 74: ^1H NMR spectrum of $^{10}\text{lNPNTiCl}_2(\text{HNMe}_2)$ [3.12]

Relative integration of the broad N-H peaks in the ^1H NMR spectra for [3.11] and [3.12] indicates less than 1 equiv of coordinated HNMe_2 , some of which may have been liberated while drying the sample under reduced pressure.

Synthesis of ^{iprop}NPNTiCl₂(THF) [3.13] and ^{tol}NPNTiCl₂(THF) [3.14]

Unlike the zirconium system (see earlier discussion), it was possible to cleanly obtain ^{tol}NPNTiCl₂(THF) [3.14] by reacting ^{tol}NPNH₂ [2.11] with TiCl₂(NMe₂)₂ in THF at 60 °C in 97% isolated yield (Figure 71). While not directly tested, the facile conversion of HNMe₂ adducts of titanium dichloride to THF adducts is implicit from the aforementioned reaction.

Reaction of ^{Si}NPNLi₂·2THF with TiCl₄(THF)₂ in toluene at room temperature yields ^{Si}NPNTiCl₂ with no evidence for THF adduct formation.¹³⁷ However, ^{iprop}NPNTiCl₂ [3.17] and ^{tol}NPNTiCl₂ [3.18] react with THF at room temperature to form THF adducts that can be isolated as purple-black solids of formula ^{iprop}NPNTiCl₂(THF) [3.13] and ^{tol}NPNTiCl₂(THF) [3.14], respectively.

In solution, [3.13] and [3.14] display a sharp singlet in their ³¹P{¹H} NMR spectra at δ 30.34 and δ 24.04 (Figure 76), respectively, and the ¹H NMR spectra display THF peaks at δ 1.37 and δ 3.72 for [3.13] (Figure 77) and δ 1.35 and δ 3.65 for [3.14] (Figure 75).

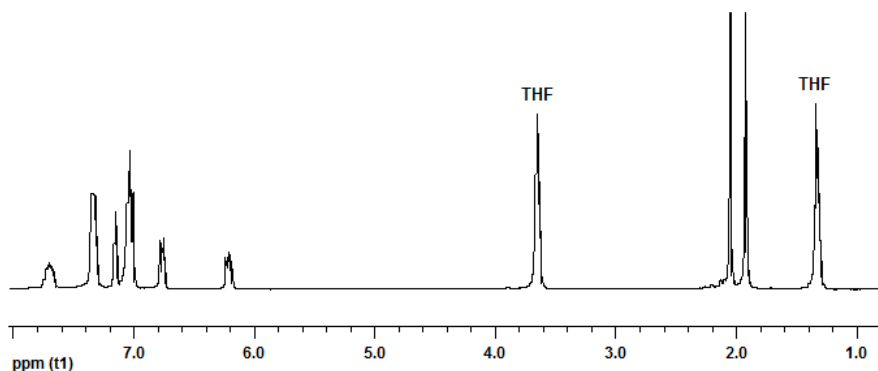


Figure 75: ¹H NMR spectrum of ^{tol}NPNTiCl₂(THF) [3.14] in C₆D₆

Given close agreement between the ³¹P{¹H} NMR δ values for the ^{iprop}NPN and ^{tol}NPN containing zirconium adducts of THF and HNMe₂, as well as the titanium HNMe₂ adducts, it is unusual that ^{iprop}NPNTiCl₂(THF) [3.13] has a value shifted significantly downfield compared to ^{tol}NPNTiCl₂(THF) [3.14].

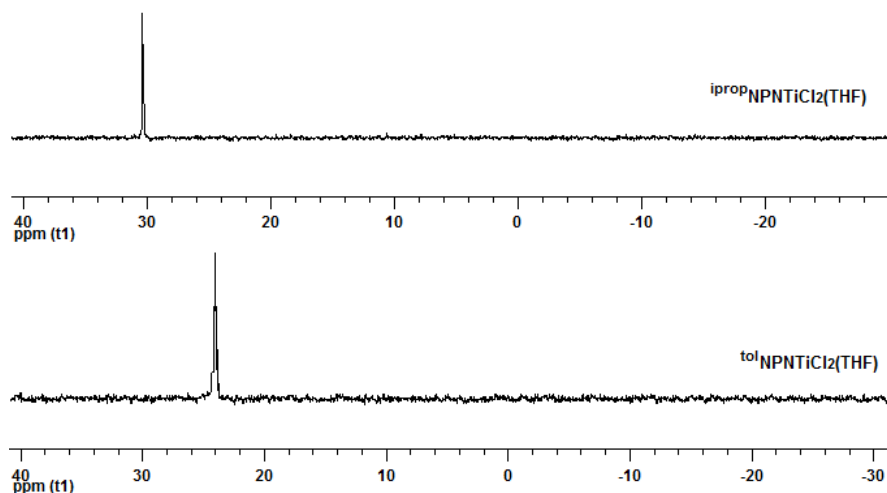


Figure 76: $^{31}\text{P}\{^1\text{H}\}$ NMR spectra of $^{\text{iprop}}\text{NPNTiCl}_2(\text{THF})$ [3.13] and $^{\text{tol}}\text{NPNTiCl}_2(\text{THF})$ [3.14] in C_6D_6

For $^{\text{iprop}}\text{NPNTiCl}_2(\text{THF})$ [3.13], partial 0.25 equiv of THF coordination is suggested by the relative integration of the ^1H NMR spectrum (Figure 77). Loss of THF may have occurred while drying the sample *in vacuo*. Two methine CH signals were also observed for this sample of [3.13], indicating two distinct *iso*-propyl environments of the ligand (Figure 77). As both signals remain after the sample was spiked with excess THF (Figure 77), the possibility of an equilibrium co-existence of [3.13] with a solvent-free $^{\text{tol}}\text{NPNTiCl}_2$ [3.18] species can be eliminated.

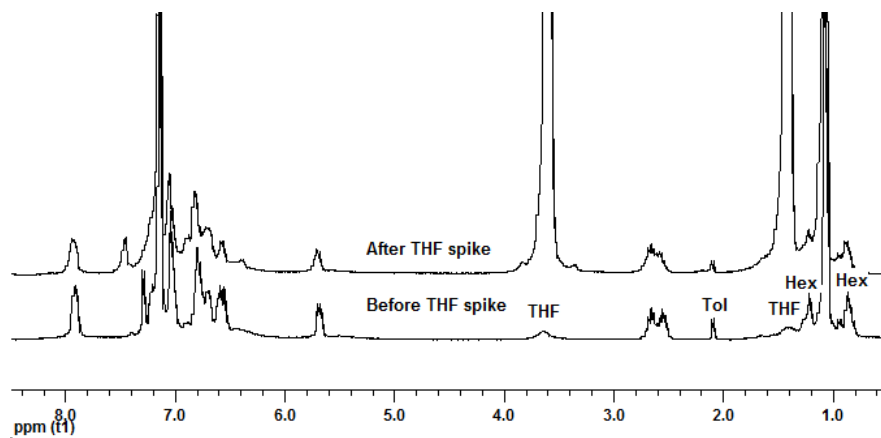


Figure 77: ^1H NMR of $^{\text{iprop}}\text{NPNTiCl}_2(\text{THF})$ [3.13] before and after THF spike in C_6D_6

As with the zirconium congeners, $^{\text{iprop}}\text{NPNTiCl}_2(\text{THF})$ [3.13] and $^{\text{tol}}\text{NPNTiCl}_2(\text{THF})$ [3.14] can exist in two different isomeric forms (Figure 78).

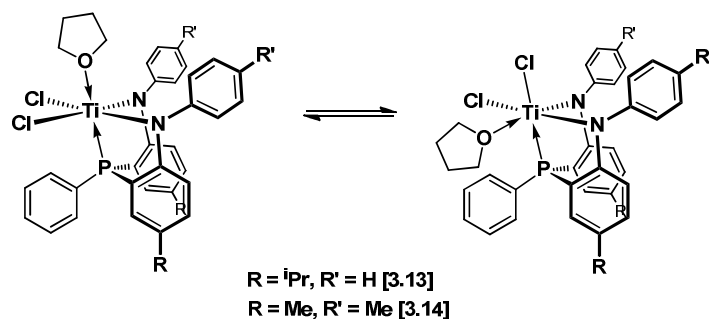


Figure 78: Possible isomeric structures for $^{iPr}NPNTiCl_2(THF)$ [3.13] and $^{tol}NPNTiCl_2(THF)$ [3.14]

For [3.14], the observation of a single set of *p*-tolyl methyl signals in solution allows the previously developed *cis* / *trans* arguments to apply. However, for [3.13], the observation of two different 4-isopropyl signals suggests that the chiral isomer with the THF group *cis* to the P atom may be dominant in solution (though the presence of an amine impurity cannot be discounted). Unfortunately single crystals for [3.13] and [3.14] were not obtained to verify structures formed in the solid state.

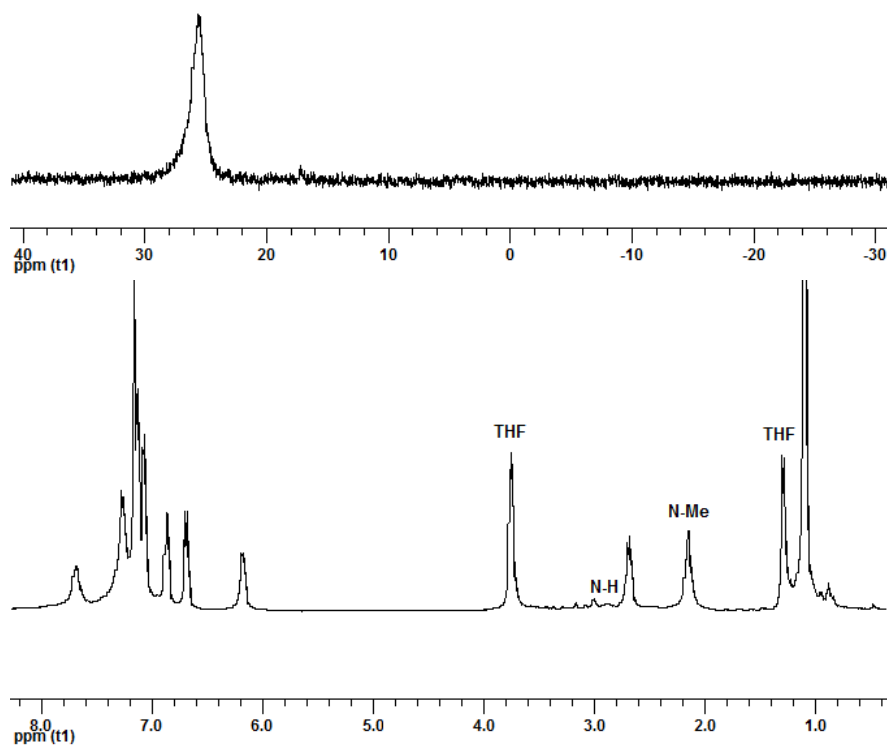


Figure 79: $^{31}P\{^1H\}$ (top) and 1H NMR (bottom) spectra of $^{iPr}NPNTiCl_2(HNMe_2)/(THF)$ [3.11]/[3.13]

Under certain conditions a mixture of coordinated THF and HNMe₂ [3.11] / [3.13] was obtained (Figure 79). The ³¹P{¹H} NMR spectrum has a single broad peak at δ 25.83 which is upfield relative to both pure [3.11] and [3.13]. The ¹H NMR spectrum indicates partial coordination of both THF and HNMe₂ (Figure 79), with peaks at δ 3.75 and 1.29 (THF) and δ 2.89 and 2.15 (N-H and N-CH₃).

The occurrence of only one 4-isopropyl suggests that the more symmetric isomers with THF and HNMe₂ *trans* to the P atom were formed (Figure 80).

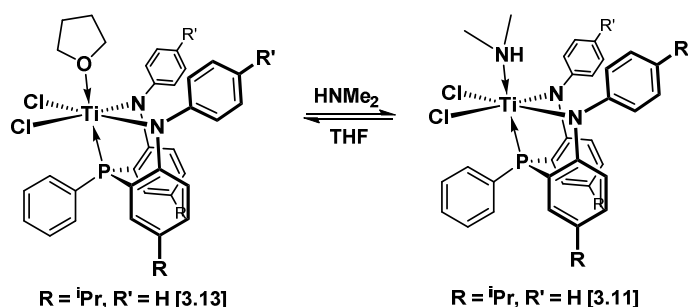


Figure 80: Equilibrium structures for ^{iprop}NPNTiCl₂(THF) [3.13] and ^{iprop}NPNTiCl₂(HNMe₂) [3.11]

In an attempt to grow single crystals of [3.11] / [3.13] from THF / *n*-hexanes, an example of crystal picking led to the identification of TiCl₃(NMe₂)(THF)₂ being present in the sample. A mass spectrum of the sample also confirmed the presence of an ion corresponding to [TiCl₃(NMe₂)]⁺. It is possible that this was generated during the reaction of TiCl₄ with Ti(NMe₂)₄. Despite the fact that elemental analysis for TiCl₂(NMe₂)₂ indicated sample purity and only one peak was observed at δ 2.97 in the ¹H NMR spectrum, the mass spectrum did indicate a peak at 198 m/z (10%) for [TiCl₃(NMe₂)]⁺ in addition to the parent ion at 206 m/z (65%). For [3.12], elemental analysis suggests that some TiCl₃(NMe₂) may also be present.

So, while protonolysis of TiCl₂(NMe₂)₂ by the NPNH₂ ligands in warm THF represents an efficient one-step process for the formation of the titanium dichloride species, the method for the synthesis of TiCl₂(NMe₂)₂ requires care to avoid the presence of titanium trichloride impurities.

Synthesis of ^{iprop}NPNTi(NMe₂)₂ [3.15] and ^{tol}NPNTi(NMe₂)₂ [3.16]

Reaction of ^{iprop}NPNH₂ [2.10] or ^{tol}NPNH₂ [2.11] with Ti(NMe₂)₄ in toluene at room temperature gave the brick red solids ^{iprop}NPNTi(NMe₂)₂ [3.15] and ^{tol}NPNTi(NMe₂)₂ [3.16], with singlets observed in their ³¹P{¹H} NMR spectra at δ -2.05 (Figure 81) and δ -2.35, respectively.

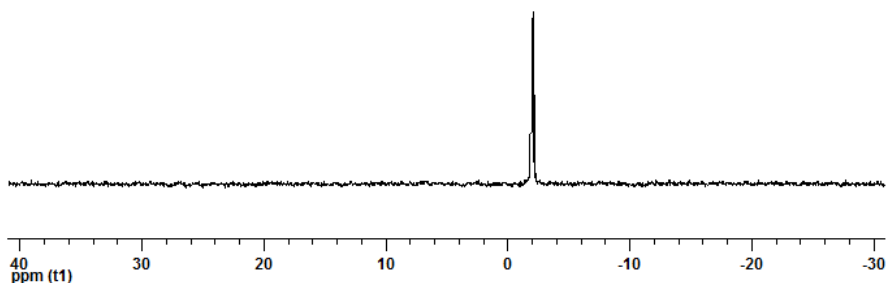


Figure 81: ³¹P{¹H} NMR spectrum of ^{iprop}NPNTi(NMe₂)₂ [3.15]

Their ¹H and ¹³C{¹H} NMR spectra display characteristic signals indicative of two different coordinated NMe₂ environments (Figure 82).

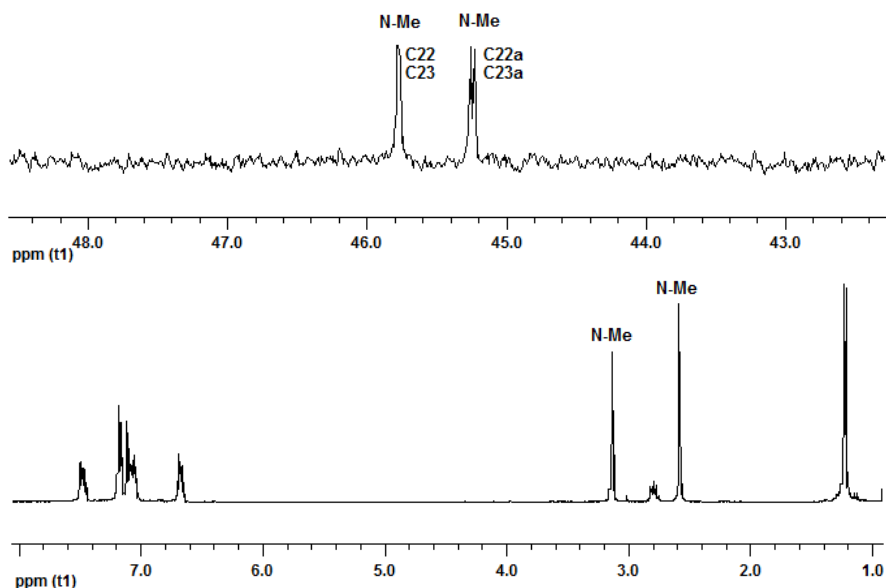


Figure 82: Partial ¹³C{¹H} (top) and ¹H NMR (bottom) spectra of ^{iprop}NPNTi(NMe₂)₂ [3.15]

The solid state molecular structure for ^{iprop}NPNTi(NMe₂)₂ [3.15] was determined from single crystals grown by slow evaporation from a benzene solution (Figure 83) and confirms two

different environments for the NMe₂ groups, one *cis* (N24) and one *trans* (N24a) to the P atom of the NPN ligand. This corresponds to what was observed in the zirconium complexes [3.7] and [3.8] (Figure 62).

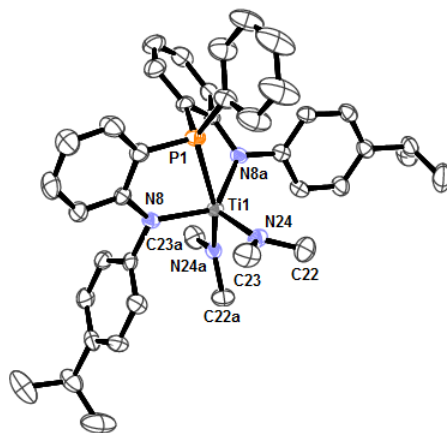


Figure 83: ORTEP representation of the solid state molecular structure of ^{iprop}NPNTi(NMe₂)₂ [3.15]

Similarly, the geometry about the Ti centre can be described as distorted trigonal bipyramidal, with an axial P1-Ti1-N24a angle of 159.80(9)°. The ligand is arranged facially with the two N8 and N8a ligand atoms in the trigonal plane, together with one of the NMe₂ (N24) groups. The ligand Ti1-P1, Ti1-N8 and Ti1-N8a bond lengths (Table 11) are comparable to those observed for ^{Si}NPNTiCl₂,¹³⁷ [(P₂N₂)Ti]₂(N₂),¹³⁷ [(PNP)TiCl]₂(N₂)¹⁸² and other (NN)TiCl(NR₂)²⁷⁴ and (NNN)TiL_n²⁷⁵ complexes. The NMe₂ bond lengths Ti1-N24 and Ti1-N24a are 1.880(3) Å and 1.921(3) Å and compare well with other titanium dimethylamido complexes.^{269, 275-277}

Table 11 : Selected bond lengths (Å) and angles (°) for ^{iprop}NPNTi(NMe₂)₂ [3.15]

| ^{iprop} NPNTi(NMe ₂) ₂ [3.15] | | | |
|---|------------|----------------|----------|
| Ti1-P1 | 2.5939(11) | N24-C22 | 1.454(4) |
| Ti1-N8 | 2.033(3) | N24-C23 | 1.452(4) |
| Ti1-N8a | 2.028(3) | N24a-C22a | 1.443(4) |
| Ti1-N24 | 1.880(3) | N24a-C24a | 1.460(4) |
| Ti1-N24a | 1.921(3) | Ti1-N24-C22 | 124.0(3) |
| P1-Ti1-N8 | 74.83(8) | Ti1-N24-C23 | 124.7(2) |
| P1-Ti1-N8a | 73.99(8) | Ti1-N24a-C22a | 127.9(2) |
| P1-Ti1-N24 | 98.42(9) | Ti1-N24a-C23a | 121.1(2) |
| P1-Ti1-N24a | 159.80(9) | C22-N24-C23 | 111.2(3) |
| N24-Ti1-N8 | 115.93(13) | C22a-N24a-C23a | 110.1(3) |
| N24-Ti1-N8a | 108.20(12) | | |
| N24a-Ti1-N8 | 97.49(12) | | |
| N24a-Ti1-N8a | 98.01(11) | | |
| N8-Ti1-N8a | 128.66(12) | | |
| N24-Ti1-N24a | 101.72(12) | | |

The Ti-N-C bond angles for one amido groups (N24) are the same, but differ by 6.8° for the other amido group (N24a) (Table 11). This structural feature most likely persists in solution, as evidenced by the $^{13}\text{C}\{^1\text{H}\}$ NMR spectra, wherein a singlet is observed for the carbons (C22 and C23) on the N24 amido group and two singlets for carbons (C22a and C23a) on the N24a amido group (Figure 82).

Synthesis of *iprop*NPNTiCl₂ [3.17] and *tol*NPNTiCl₂ [3.18]

After addition of 2 equiv of TMSCl to *iprop*NPNTi(NMe₂)₂ [3.15], a 68% conversion to *iprop*NPNTiCl₂ [3.17] was observed via $^{31}\text{P}\{^1\text{H}\}$ NMR spectroscopy, with an unidentified intermediate visible at δ 17.35 (Figure 84). The conversion is almost complete after 4 equiv of TMSCl, with only 7% unreacted [3.15]. Reaction of *iprop*NPNTi(NMe₂)₂ [3.15] and *tol*NPNTi(NMe₂)₂ [3.16] with *ca* 6 equiv of TMSCl in toluene gave *iprop*NPNTiCl₂ [3.17] and *tol*NPNTiCl₂ [3.18] in 80% and 99% yields, respectively, both as purple solids. Their $^{31}\text{P}\{^1\text{H}\}$ NMR spectra display peaks at δ 24.85 and δ 24.41, respectively.

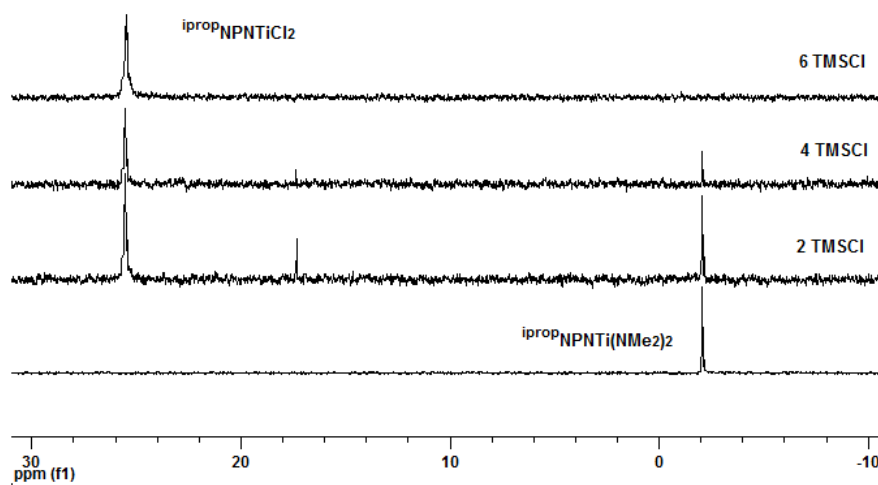


Figure 84: $^{31}\text{P}\{^1\text{H}\}$ NMR spectra of *iprop*NPNTi(NMe₂)₂ [3.15] (bottom) and + 2, 4 and 6 equiv of TMSCl in C₆D₆

When a solution of [3.18] in toluene-*d*₈ is cooled down to -70°C , no change is observed in the $^{31}\text{P}\{^1\text{H}\}$ NMR spectrum. The solid state molecular structure of *tol*NPNTiCl₂ [3.18],

obtained by x-ray crystallographic analysis of single crystals grown via vapour diffusion of *n*-hexanes into a toluene solution in the freezer, confirms a monomeric structure (Figure 85).

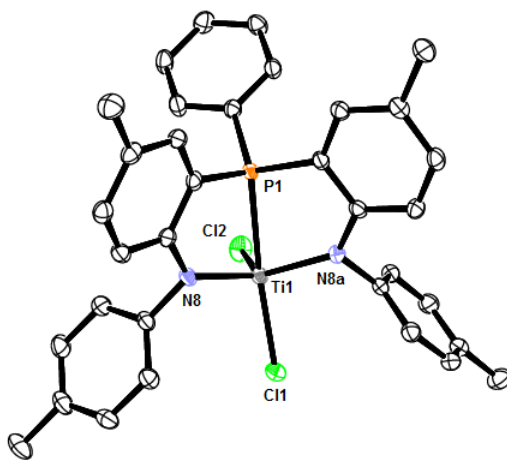


Figure 85: ORTEP representation of the solid state molecular structure of ^{tol}NPNTiCl₂ [3.18]

The geometry about the Ti centre mirrors that observed for ^{iprop}NPNTi(NMe₂)₂ [3.15] as distorted trigonal bipyramidal, with an axial P1-Ti1-Cl1 angle of 162.05(2)° (Table 12) that is slightly larger than [3.15] at 159.80(9)°, but significant more bent than ^{mes}NPNZrCl₂ complex at 178.63(3)°^{97, 214} or ^{Si}NPNTiCl₂ at 176.08(5)°¹³⁷. Compared to the classical ^{Si}NPN ligand containing ^{Si}NPNTiCl₂ complex (Table 12), ^{tol}NPNTiCl₂ [3.18] has a shorter Ti1-P1 bond length, smaller P1-Ti1-N8 / P1-Ti1-N8a bite angles and a wider N8-Ti1-N8a bite angle.

Table 12 : Selected bond lengths (Å) and angles (°) for ^{tol}NPNTiCl₂ [3.18] and ^{Si}NPNTiCl₂¹³⁷

| | ^{tol} NPNTiCl ₂ [3.18] | ^{Si} NPNTiCl ₂ ¹³⁷ |
|-------------|--|---|
| Ti1-P1 | 2.5809(6) | 2.6084(12) |
| Ti1-N8a | 1.9519(15) | 1.936(4) |
| Ti1-N8 | 1.9586(15) | 1.914(3) |
| Ti1-Cl1 | 2.2968(5) | 2.2937(12) |
| Ti1-Cl2 | 2.2545(6) | 2.2874(12) |
| P1-Ti1-Cl1 | 162.05(2) | 176.08(5) |
| P1-Ti1-Cl2 | 93.70(2) | 87.80(4) |
| P1-Ti1-N8a | 73.87(5) | 75.85(11) |
| P1-Ti1-N8 | 74.96(5) | 80.64(10) |
| Cl1-Ti1-N8a | 96.94(5) | 100.45(12) |
| Cl1-Ti1-N8 | 99.72(5) | 100.11(11) |
| Cl1-Ti1-Cl2 | 104.18(2) | 95.21(5) |
| N8a-Ti1-N8 | 126.34(6) | 116.45(14) |
| Cl2-Ti1-N8 | 110.61(5) | 117.58(11) |
| Cl2-Ti1-N8a | 113.95(5) | 119.42(11) |

The Ti-Cl1 and Ti1-Cl2 bond lengths of 2.2545(6) Å and 2.2968(5) Å and the ligand-metal bond lengths of Ti1-P1, Ti1-N8 and Ti1-N8a (Table 12) are comparable to those observed for SiNPNTiCl_2 ,¹³⁷ $[(\text{PNP})\text{TiCl}]_2(\text{N}_2)$ ¹⁸² and $(\text{NN})\text{TiCl}(\text{NR}_2)$ ²⁷⁴ complexes.

3.3. Hafnium Diamido-Phosphine Complexes

The hafnium dichloride complexes were accessed using the protonolysis method with $\text{Hf}(\text{NMe}_2)_4$ and $^{\text{iprop}}\text{NPNH}_2$ [2.10] and as with zirconium, the hafnium dichlorides were dimeric (Figure 86).

Synthesis of $^{\text{iprop}}\text{NPNHf}(\text{NMe}_2)_2$ [3.19]

The lemon yellow solid $^{\text{iprop}}\text{NPNHf}(\text{NMe}_2)_2$ [3.19] was obtained in 57% yield from the reaction of $^{\text{iprop}}\text{NPNH}_2$ [2.10] with $\text{Hf}(\text{NMe}_2)_4$ in toluene at room temperature. The $^{31}\text{P}\{^1\text{H}\}$ NMR spectrum displayed a singlet at δ -3.12, and as expected, two unique environments are indicated for the NMe_2 groups, with peaks at δ 2.56 and δ 2.90 in the ^1H NMR spectra and at δ 40.5 and δ 41.1 in the $^{13}\text{C}\{^1\text{H}\}$ NMR spectrum.

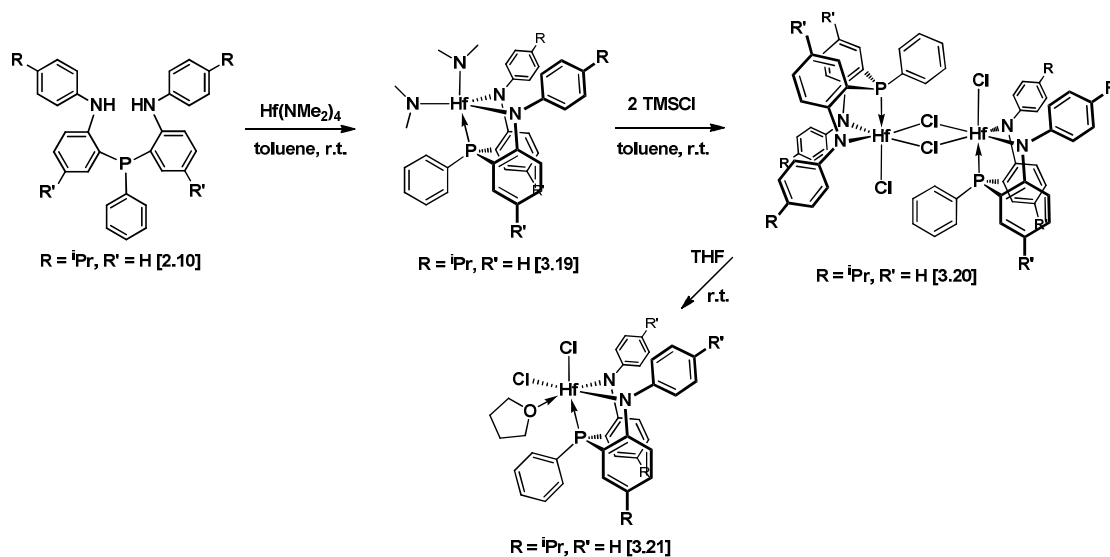


Figure 86: Protonolysis of $^{\text{iprop}}\text{NPNH}_2$ [2.10] with $\text{Hf}(\text{NMe}_2)_4$

The solid state molecular structure of **3.19** was obtained via x-ray crystallographic analysis of single crystals grown by vapour diffusion of *n*-hexanes into a toluene solution at -30

°C (Figure 87). A distorted trigonal bipyramidal geometry was observed for the atoms bonding to the hafnium centre, as was reported for the zirconium [3.7] and [3.8] (Figure 62) and titanium [3.15] congeners (Figure 83) and $^{\text{mes}}\text{NPNZr}(\text{NMe}_2)_2$.⁹⁷

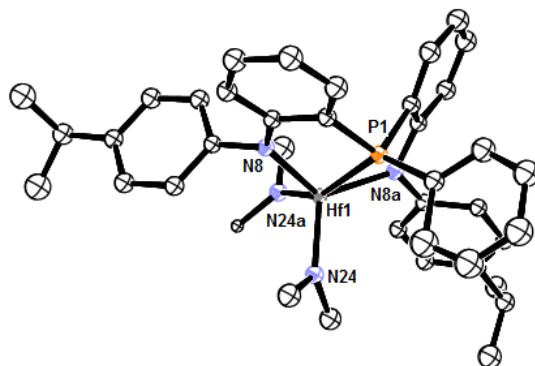


Figure 87: ORTEP representation of the solid state molecular structure of $^{\text{iprop}}\text{NPNHf}(\text{NMe}_2)_2$ [3.19]

The apexes are defined by the P1 and N24a atoms and the N8, N8a and N24 atoms form the trigonal plane. The Hf1-P1, Hf1-N8 and Hf-N8a bond lengths and hafnium-amido Hf1-N24 and Hf1-N24a bond lengths (Table 13) compare well with those obtained for other NPN^{97} and PNP^{209} hafnium complexes and the axial P1-Hf1-N24a angle at $155.76(9)^\circ$ is more distorted compared $^{\text{mes}}\text{NPNHf}(\text{NMe}_2)_2$ (Table 13). As with the other group 4 $^{\text{iprop}}\text{NPN}$ / $^{\text{tol}}\text{NPN}$ containing complexes, the N8-Hf1-N8a bite angle for [3.19] at $125.86(11)^\circ$ is larger than for $^{\text{mes}}\text{NPNHf}(\text{NMe}_2)_2$.

Table 13 : Selected bond lengths (Å) and angles (°) for $^{\text{iprop}}\text{NPNHf}(\text{NMe}_2)_2$ [3.19] and $^{\text{mes}}\text{NPNHf}(\text{NMe}_2)_2$ ⁹⁷

| | $^{\text{iprop}}\text{NPNHf}(\text{NMe}_2)_2$ [3.19] | $^{\text{mes}}\text{NPNHf}(\text{NMe}_2)_2$ ⁹⁷ |
|--------------|--|---|
| Hf1-P1 | 2.7089(10) | 2.7717(9) |
| Hf1-N8 | 2.136(3) | 2.156(3) |
| Hf1-N8a | 2.132(3) | 2.137(3) |
| Hf1-N24 | 2.007(3) | 2.019(3) |
| Hf1-N24a | 2.037(3) | 2.066(3) |
| P1-Hf1-N8 | 71.15(8) | 70.74(8) |
| P1-Hf1-N8a | 72.79(9) | 73.01(8) |
| P1-Hf1-N24 | 100.52(9) | 95.16(10) |
| P1-Hf1-N24a | 155.76(9) | 163.71(12) |
| N24-Hf1-N8 | 110.03(12) | 119.44(12) |
| N24-Hf1-N8a | 115.21(12) | 108.79(13) |
| N24a-Hf1-N8 | 98.77(12) | 98.05(12) |
| N24a-Hf1-N8a | 97.95(12) | 104.70(13) |
| N8-Hf1-N8a | 125.86(11) | 120.89(11) |
| N24-Hf1-N24a | 103.67(12) | 100.75(15) |

Synthesis of [*i*propNPNHfCl₂]₂ [3.20]

ⁱpropNPNHf(NMe₂)₂ [3.19] reacts with *ca* 6 equiv of TMSCl to give the yellow solid [ⁱpropNPNHfCl₂]₂ [3.20] in 62% yield; a single sharp peak at δ 3.80 at room temperature in the ³¹P{¹H} NMR spectrum (Figure 88) is observed. This is in contrast to the broad peaks observed for the zirconium congeners [3.9] and [3.10] (Figure 64).

Single crystals of [ⁱpropNPNHfCl₂]₂ [3.20] were grown from a saturated toluene solution at -30 °C and the solid state molecular structure (as with zirconium) reveals a dimeric structure (Figure 89), in contrast to penta-coordinate monomeric ^{mes}NPNHfCl₂.⁹⁷ Due to the similar covalent radii of Zr (175 ± 7 × 10⁻¹² m) and Hf (175 ± 10 × 10⁻¹² m)²⁷⁸ and their relative positions in the periodic table, similar chemical behaviour is often observed. However, the solid state molecular structure obtained for [ⁱpropNPNHfCl₂]₂ [3.20] has a different isomeric form with the terminal chloride atoms (Cl1 and Cl1') *trans* to the P1 atom compared to the zirconium congener [ⁱpropNPNZrCl₂]₂ [3.9] (Figure 65), where the terminal Cl1 and Cl1' atoms are *cis* to the P atom.

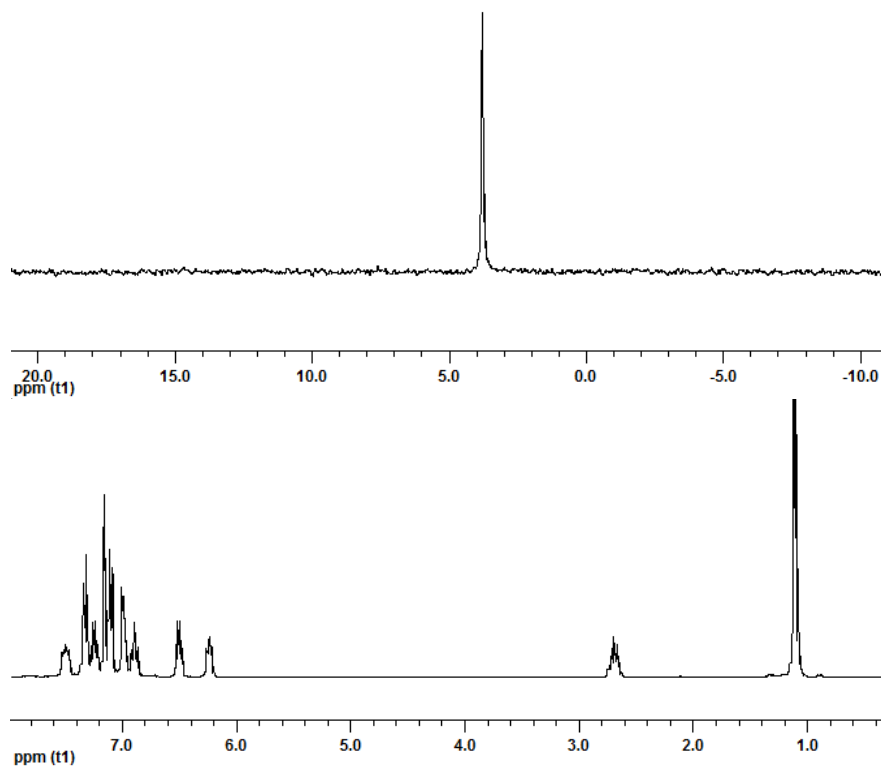


Figure 88: ³¹P{¹H} (top) and ¹H NMR (bottom) spectrum of [ⁱpropNPNHfCl₂]₂ [3.20] in C₆D₆ at 25 °C

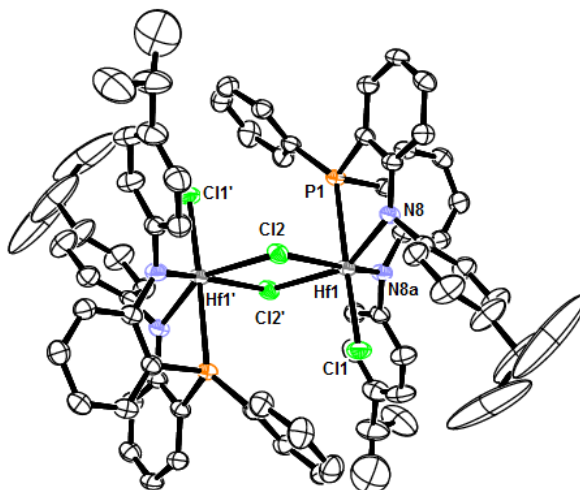


Figure 89: ORTEP representation of the solid state molecular structure of [^{iprop}NPNHfCl₂]₂ [3.20]

The Hf1-P1, Hf1-N8 and Hf-N8a bond lengths 2.7487(12) Å, 2.062(4) Å and 2.080(4) Å (Table 14) are typical^{97, 209} and the terminal chloride bond length Hf1-Cl11 of 2.3923(12) Å is similar to those obtained for ^{mes}NPNHfCl₂⁹⁷ and PNP⁺HfCl₃.²⁰⁹ The bridging chloride bond lengths Hf1-Cl12 and Hf1-Cl12' of 2.5403(12) Å and 2.6335(11) Å are longer than those for the terminal chloride (Hf1-Cl11) as well as those in ^{mes}NPNHfCl₂.⁹⁷

Table 14 : Selected bond lengths (Å) and angles (°) for [^{iprop}NPNHfCl₂]₂ [3.20] and ^{mes}NPNHfCl₂⁹⁷

| | [^{iprop} NPNHfCl ₂] ₂ [3.20] | ^{mes} NPNHfCl ₂ ⁹⁷ |
|----------------|---|---|
| Hf1-P1 | 2.7487(12) | 2.709(3) |
| Hf1-N8a | 2.062(4) | 2.082(10) |
| Hf1-N8 | 2.080(4) | 2.078(10) |
| Hf1-Cl12 | 2.5403(12) | 2.393(4) |
| Hf1-Cl11 | 2.3923(12) | 2.402(3) |
| Hf1-Cl12' | 2.6335(11) | |
| P1-Hf1-Cl11 | 176.40(4) | 176.60(11) |
| N8a-Hf1-Cl12 | 149.41(11) | |
| N8-Hf1-Cl12' | 164.24(12) | |
| P1-Hf1-N8a | 68.03(11) | 72.0(3) |
| P1-Hf1-N8 | 75.57(11) | 73.7(3) |
| P1-Hf1-Cl12 | 86.50(4) | 86.12(11) |
| P1-Hf1-Cl12' | 95.19(4) | |
| Cl11-Hf1-N8a | 112.81(11) | 118.1(3) |
| Cl11-Hf1-N8 | 100.84(11) | 112.3(3) |
| Cl11-Hf1-Cl12 | 93.68(4) | 97.27(12) |
| Cl11-Hf1-Cl12' | 88.36(4) | |
| N8a-Hf1-N8 | 100.36(15) | 115.3(4) |
| Cl12-Hf1-N8 | 88.76(12) | 112.3(3) |
| Cl12'-Hf1-N8a | 87.57(11) | 118.1(3) |
| Cl12-Hf1-Cl12' | 77.82(4) | |
| Hf1-Cl12-Hf1' | 102.18(4) | |

The three *trans* angles for octahedral $[\text{ipropNPNHfCl}_2]_2$ **[3.20]** (Table 14) are less distorted compared to $[\text{ipropNPNZrCl}_2]_2$ **[3.9]** (Table 10) and the hafnium atom is more weakly bonded to phosphorus (P1) and more strongly bonded to the terminal (Cl1) and bridged (Cl2, Cl2') chloride atoms compared to the isomer isolated for $[\text{ipropNPNZrCl}_2]_2$ **[3.9]** (comparing bond lengths in Table 10 to Table 14).

In order to probe the solution behaviour of $[\text{ipropNPNHfCl}_2]_2$ **[3.20]** for the occurrence of other isomeric forms, variable temperature NMR spectroscopy was employed. When $[\text{ipropNPNHfCl}_2]_2$ **[3.20]** in toluene- d_8 was cooled down from 93° to -81°, the peak at δ 5.39 in the $^{31}\text{P}\{^1\text{H}\}$ NMR spectra gradually sharpens and shifts upfield to δ 0.08 (Figure 90).

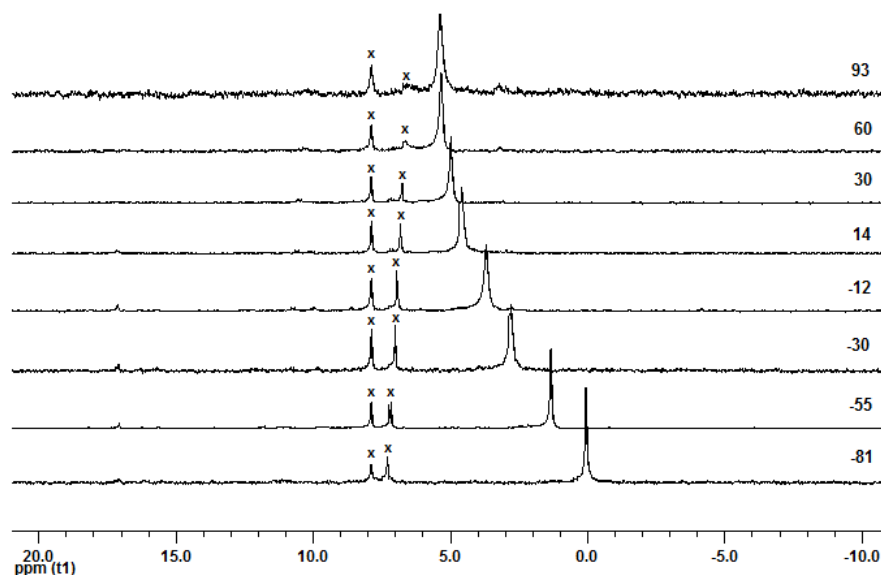


Figure 90: $^{31}\text{P}\{^1\text{H}\}$ NMR spectra of $[\text{ipropNPNHfCl}_2]_2$ **[3.20]** in toluene- d_8 from 93 to -81 °C (δ 7.89 at 93 °C used as reference for spectra at other temperatures)

The two smaller peaks observed at δ 7.89 and δ 7.30 may be considered to be impurities, as they were not observed in a pure sample of **[3.20]** at room temperature (see Figure 88). Some differences are also noted for the P-Ph peaks in the ^1H NMR spectrum of **[3.20]** at low temperature (Figure 91).

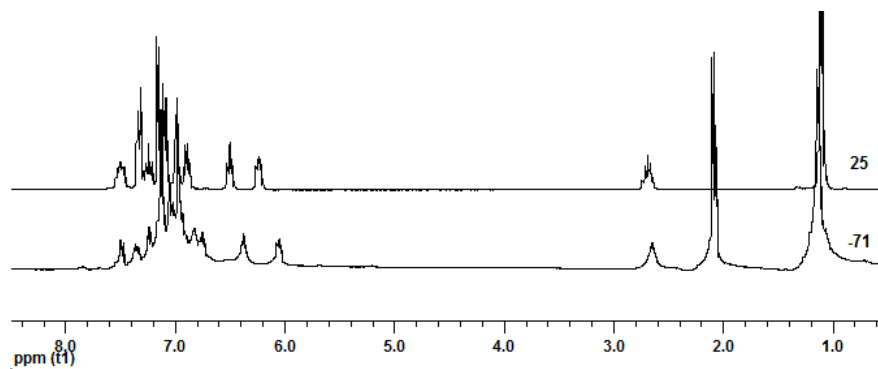


Figure 91: ^1H NMR spectra of $[\text{ipropNPNHfCl}_2]_2$ [3.20] in toluene- d_8 at 25 °C and -71 °C

It is noteworthy that one of the signals observed for the zirconium congener isomers $[\text{ipropNPNZrCl}_2]_2$ [3.9] at δ 7.80 (Figure 67) and $[\text{tolNPNZrCl}_2]_2$ [3.10] at δ 6.86 [3.10] (Figure 66) has a gradual downfield shift with decreasing temperature, contrasting the upfield shift observed for $[\text{ipropNPNHfCl}_2]_2$ [3.20] (Figure 90). Compared to $[\text{ipropNPNZrCl}_2]_2$ [3.9], the solution behaviour for $[\text{ipropNPNHfCl}_2]_2$ [3.20] appears less complex and it may be that the heavier, slightly smaller hafnium atom slows down the ability of the hafnium dichloride dimer [3.20] to dissociate into a monomer and re-associate into different isomeric forms compared to the zirconium congeners [3.9] and [3.10] (see DOSY NMR discussion on pgs 78-79).

Synthesis of $^{\text{iprop}}\text{NPNHfCl}_2(\text{THF})$ [3.21]

$^{\text{iprop}}\text{NPNHfCl}_2(\text{THF})$ [3.21] is formed by dissolution of $[\text{ipropNPNHfCl}_2]_2$ [3.20] in THF at room temperature, typically directly after TMSCl addition to $^{\text{iprop}}\text{NPNHf}(\text{NMe}_2)_2$ [3.19]. The yellow solid was isolated in 76% yield; in solution the $^{31}\text{P}\{^1\text{H}\}$ NMR spectrum displays a single sharp peak at δ 5.44 and the ^1H NMR spectrum shows broad coordinated THF peaks at δ 3.92 and δ 0.93 (Figure 92).

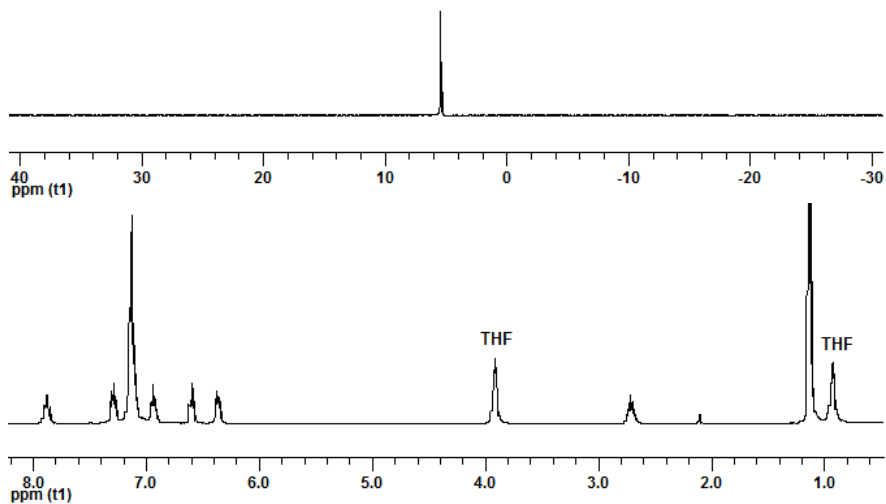


Figure 92: $^{31}\text{P}\{^1\text{H}\}$ (top) and ^1H NMR (bottom) spectra of $\text{ipropNPNHfCl}_2(\text{THF})$ [3.21] in C_6D_6

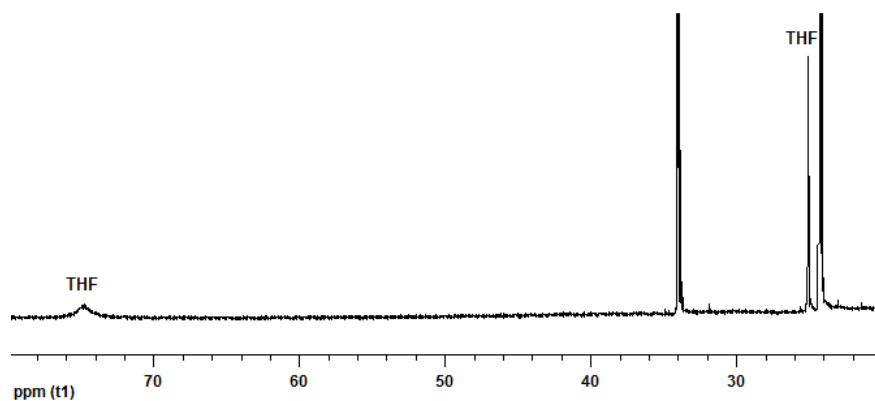


Figure 93: Partial $^{13}\text{C}\{^1\text{H}\}$ NMR spectrum of $\text{ipropNPNHfCl}_2(\text{THF})$ [3.21] in C_6D_6

The $^{13}\text{C}\{^1\text{H}\}$ NMR spectrum displays a sharp singlet at δ 25.1 and a broad singlet at δ 74.5 for coordinated THF (Figure 93). As with the corresponding zirconium (Figure 57) and titanium (Figure 78) systems, two different isomers can be expected for [3.21] (Figure 94).

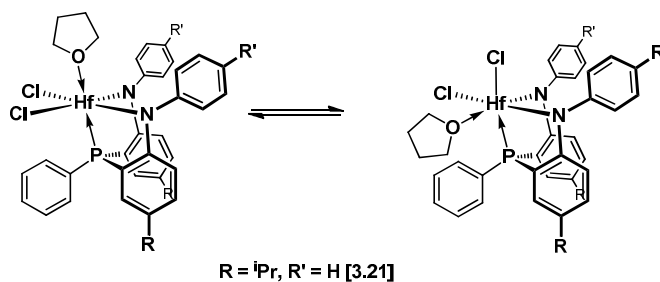


Figure 94: Isomers of $\text{ipropNPNHfCl}_2(\text{THF})$ [3.21]

As only one methine signal is observed for the isopropyl groups, the more symmetric isomer with THF *trans* to the P atom is likely formed in solution. The broad THF resonance at δ 74.5 in the $^{13}\text{C}\{^1\text{H}\}$ NMR spectrum of **[3.21]** may indicate some fluxionality, but low temperature solution NMR spectroscopic experiments were not conducted to further elucidate the solution behaviour of **[3.21]**.

Single crystals of $^{\text{iprop}}\text{NPNHfCl}_2(\text{THF})$ **[3.21]** were obtained via vapour diffusion of *n*-hexanes into a toluene solution in the freezer. The solid state molecular structure for **[3.21]** (Figure 95) is similar to those determined for zirconium complexes **[3.5]** and **[3.6]**, where the chiral isomer having THF *cis* to the P atom of the ligand is observed.

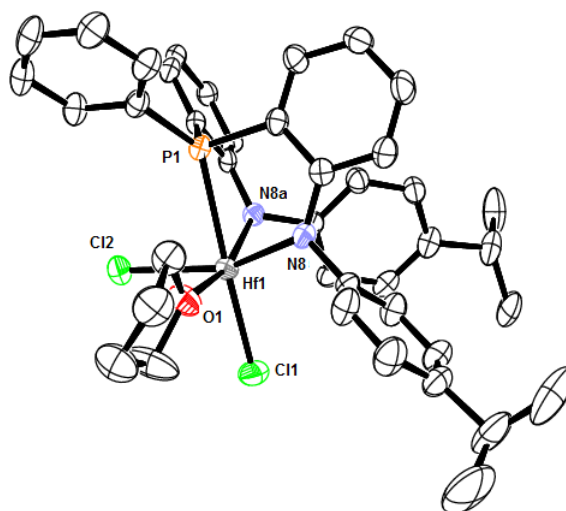


Figure 95: ORTEP representation of the solid state molecular structure of $^{\text{iprop}}\text{NPNHfCl}_2(\text{THF})$ **[3.21]**

Complex **[3.21]** has distorted octahedral geometry, with the N8-Hf1-Cl2 and N8a-Hf1-O1 *trans* angles of $153.65(15)^\circ$ and $161.6(2)^\circ$ more distorted than the P1-Hf1-Cl1 angle of $178.08(6)^\circ$. The Hf1-P1, Hf1-N8, Hf1-N8a, Hf1-Cl1 and Hf1-Cl2 bond lengths (Table 15) are comparable with the other hafnium complexes mentioned in this chapter and the Hf1-O1 bond length of $2.210(5)$ Å is typical for THF ligands bonded to hafnium.^{279, 280}

Table 15 : Selected bond lengths (Å) and angles (°) for ^{iprop}NPNHfCl₂(THF) [3.21]

| ^{iprop} NPNHfCl ₂ (THF) [3.21] | |
|--|------------|
| Hf1-P1 | 2.6821(17) |
| Hf1-N8 | 2.131(5) |
| Hf1-N8a | 2.084(5) |
| Hf1-O1 | 2.210(5) |
| Hf1-Cl1 | 2.3955(18) |
| Hf1-Cl2 | 2.4428(19) |
| P1-Hf1-Cl1 | 178.08(6) |
| N8-Hf1-Cl2 | 153.65(15) |
| N8a-Hf1-O1 | 161.6(2) |
| P1-Hf1-N8 | 74.37(15) |
| P1-Hf1-N8a | 71.21(14) |
| P1-Hf1-O1 | 90.36(15) |
| P1-Hf1-Cl2 | 82.98(6) |
| Cl1-Hf1-N8 | 104.27(15) |
| Cl1-Hf1-N8a | 107.62(15) |
| Cl1-Hf1-O1 | 90.82(15) |
| Cl1-Hf1-Cl2 | 98.66(7) |
| N8-Hf1-N8a | 92.2(2) |
| N8-Hf1-O1 | 83.4(2) |
| Cl2-Hf1-N8a | 93.12(15) |
| Cl2-Hf1-O1 | 83.50(15) |

3.4. Conclusions

Salt metathesis and protonolysis routes were evaluated for the complexation of the NPN donor set with group 4 metals. In the case of zirconium, the salt metathesis route proceeded via a two step mechanism. Due to the lack of substituents in the *ortho* position of the amido moieties of the ^{iprop}NPN and ^{tol}NPN ligands, a facile bis-(ligand) complex formation was followed by a sluggish conproportionation with ZrCl₄(THF)₂. Protonolysis proved to be the superior method, with tetrakis(dimethylamido) metal(IV) complexes being the preferred precursors; dichloride bis(dimethylamido) metal(IV) complexes are also effective, but care should be employed to avoid trichloride impurities and HNMe₂ adducts are not always easily displaced by THF. The titanium(IV) dichlorides are monomers in the solid state but the zirconium(IV) and hafnium(IV) dichlorides form chloro-bridged dimers, with complex solution behaviour. Again, the dimer formation may be facilitated by the lack of steric bulk at the *ortho* position of the amido moieties, as the analogous ^{mes}NPN containing zirconium(IV) and hafnium(IV) dichlorides do not form dimers in the solid state, and do not readily coordinate a solvent molecule to form octahedral complexes.

Chapter 4: Tantalum Diamido-Phosphine Complexes

From the discussion of group 5 dinitrogen complexes in chapter 1, one could access tantalum dinitrogen complexes via reduction of precursor chloride complexes or hydrogenation of precursor alkyl (methyl) complexes in the presence of N_2 (Figure 96). In addition, Kawaguchi and co-workers^{68, 70} demonstrated that the reaction of a tripodal triaryloxide niobium trichloride complex with $KHBEt_3$ completely cleaved the N_2 bond to form a niobium nitride complex, via a niobium tetrahydride intermediate. Thus tantalum hydride complexes could conceivably be accessed from NPN tantalum trichloride complexes via reduction of the trichloride in the presence of H_2 or reaction of the trichloride with hydride reagents (Figure 96).

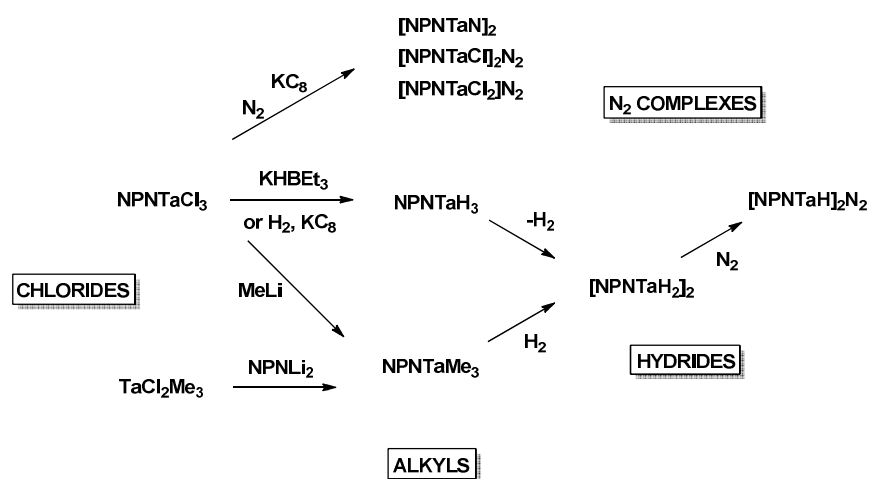


Figure 96: Schematic representation of target NPN tantalum complexes

The hydrogenation route is well established for ^{Si}NPN tantalum trimethyl complexes,^{79, 80} and although the reduction of ^{Si}PNP tantalum-alkylidene chloride complexes under N_2 was successful,⁷⁵ all subsequent attempts to form tantalum trichloride complexes with the related P_2N_2 , ^{Si}NPN or ^{mes}NPN Fryzuk donor sets have thus far failed.

The main aim of this study is to investigate the potential for the sterically less hindered ⁱpropNPN, ^{tol}NPN and ^{Ph}NPN *o*-phenylene bridged ligands developed in this project (see chapter 2) to form tantalum chloride, alkyl, hydride and ultimately N_2 complexes.

4.1. Tantalum Chloride Complexes

Salt metathesis and protonolysis routes were investigated for obtaining tantalum chloride complexes, utilising lithium salts or protonated forms of the NPN ligand, respectively (Figure 46). Tantalum(V) trichlorides or tantalum(III) chlorides could be accessed via salt metathesis, with tantalum pentachloride $[\text{TaCl}_5]_2$ or $[\text{TaCl}_3(\text{PMe}_3)_2]_2$ precursors, respectively (Figure 46).⁷⁴ Although NPN tantalum chloride formation was observed in both cases, difficulties were encountered and these routes were abandoned. Tantalum trichloride complexes may be accessed by reaction of $[\text{TaCl}_5]_2$ with protonated ligands, liberating HCl(g) ,²⁸² but this route was not investigated.

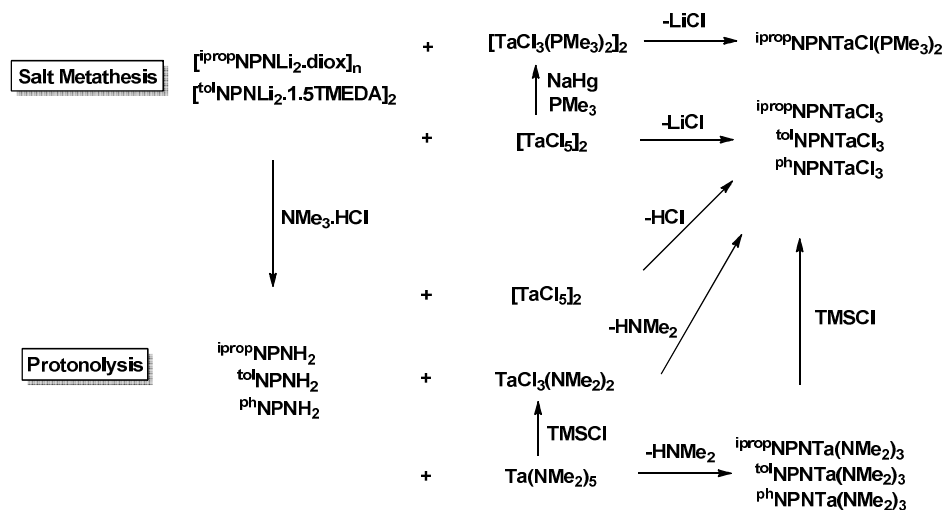


Figure 97: Salt metathesis and protonolysis routes for tantalum complexes

Protonolysis of $\text{TaCl}_3(\text{NMe}_2)_2(\text{THF})$ with ipropNPNH_2 [2.10] did form the expected tantalum(V) trichloride complex ipropNPNTaCl_3 [4.4] (Figure 98), but only as a minor species in a mixture of other inseparable side-products.

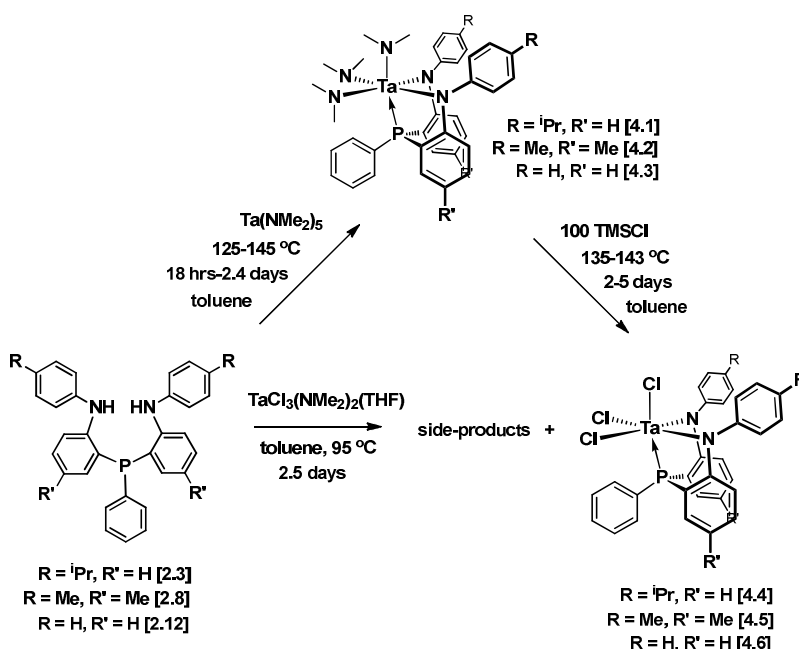


Figure 98: Protonolysis route for synthesis of NPNTaCl₃ complexes [4.4], [4.5] and [4.6]

Protonolysis with $\text{Ta(NMe}_2)_5$ proved superior to $\text{TaCl}_3(\text{NMe}_2)_2(\text{THF})$ as no unwanted side-products were obtained, but is sluggish, requiring high reaction temperatures. This became the preferred mode for accessing the NPN tantalum chloride complexes. It should be noted that this route is not general for all variations of the NPN donor set. When this promising new protonolysis route was explored for $^{\text{Si}}\text{NPNH}_2$ with $\text{Ta(NMe}_2)_5$ in toluene at 145 °C, a $^{\text{Si}}\text{NP(C)NTa(NMe}_2)_2$ species²⁸³ was obtained instead of the expected $^{\text{Si}}\text{NPNTa(NMe}_2)_3$ complex. This result serves to emphasize the difficulties encountered in trying to obtain tantalum trichloride complexes with the $^{\text{Si}}\text{NPN}$ ligand, which has eluded synthetic attempts since the $^{\text{Si}}\text{NPN}$ ligand was first generated in 1998.⁸⁰

4.1.1. Synthesis of Tantalum Amido Complexes

Orange $^{\text{iprop}}\text{NPNTa(NMe}_2)_3$ [4.1], yellow-orange $^{\text{tol}}\text{NPNTa(NMe}_2)_3$ [4.2], and yellow $^{\text{Ph}}\text{NPNTa(NMe}_2)_3$ [4.3] were obtained by reaction of the corresponding protonated ligands $^{\text{iprop}}\text{NPNH}_2$ [2.10], $^{\text{tol}}\text{NPNH}_2$ [2.11], and $^{\text{Ph}}\text{NPNH}_2$ [2.12] with $\text{Ta(NMe}_2)_5$ in toluene under reduced pressure at temperatures of 125 °C to 145 °C over *ca* 1 to 2 days (Figure 98). The

solution $^{31}\text{P}\{^1\text{H}\}$ NMR spectra of these isolated solids display singlets at δ 13.00, δ 12.48, and δ 13.04, respectively (see Figure 99 for [4.2]).

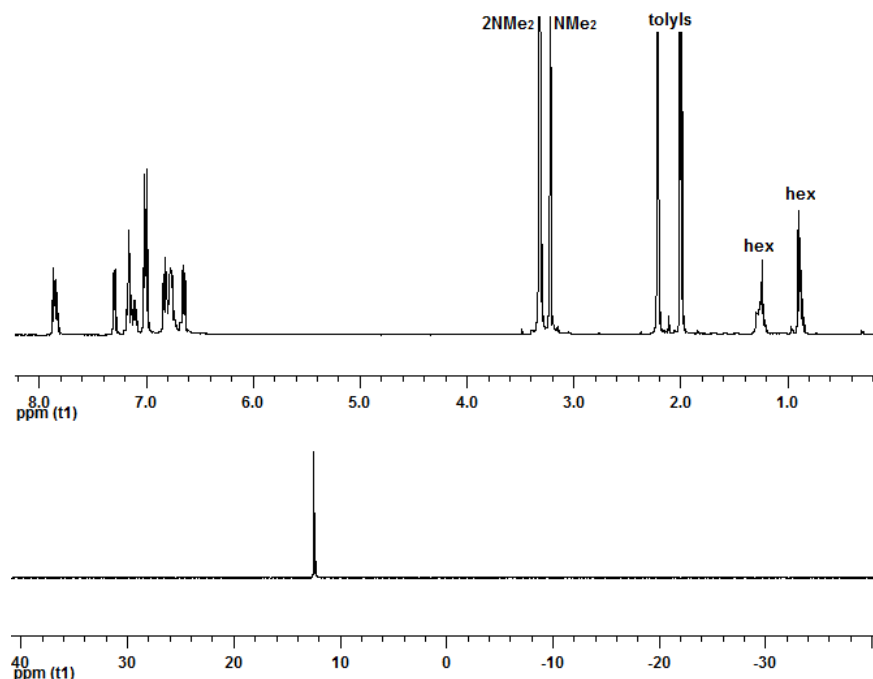


Figure 99: ^1H (top) and $^{31}\text{P}\{^1\text{H}\}$ NMR (bottom) spectra of $^{10}\text{lNPNTa}(\text{NMe}_2)_3$ [4.2] in C_6D_6 , “hex” in the ^1H NMR spectrum refers to residual hexanes

The ^1H NMR spectra reveal that two of the NMe_2 groups have identical environments with singlets at δ 3.44, 3.32, and 3.29, respectively, for [4.1], [4.2], and [4.3] and the other NMe_2 group appears upfield with singlets at 3.28, 3.22, and 3.14 (Figure 99). The $^{13}\text{C}\{^1\text{H}\}$ NMR spectra display two different NMe_2 environments; doublets at δ 48.3 ($^3J_{\text{PC}} = 3$ Hz), δ 48.3 ($^3J_{\text{PC}} = 2$ Hz), and δ 48.2 ($^3J_{\text{PC}} = 3$ Hz), respectively, for [4.1], [4.2], and [4.3] and less well-resolved doublets upfield at δ 47.7 ($^3J_{\text{PC}} = 1$ Hz), δ 48.0 ($^3J_{\text{PC}} = 1$ Hz), and δ 47.8 ($^3J_{\text{PC}} = 2$ Hz), respectively, with smaller $^3J_{\text{PC}}$ couplings (Figure 100). ^1H - ^{13}C HMBC spectra correlate the downfield doublets with larger $^3J_{\text{PC}}$ couplings in the $^{13}\text{C}\{^1\text{H}\}$ NMR spectra to the downfield singlets in the ^1H NMR spectra representing the two identical amido groups.

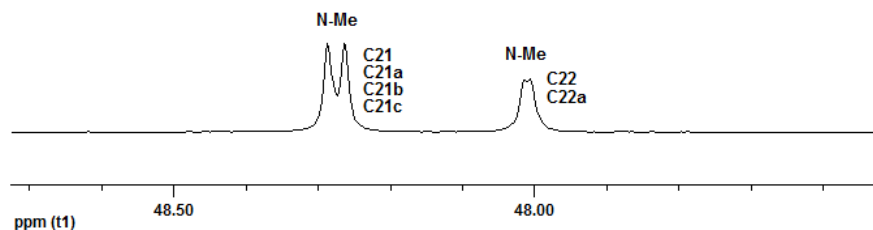


Figure 100: Partial $^{13}\text{C}\{^1\text{H}\}$ NMR spectrum of $^{10\text{l}}\text{NPNTa}(\text{NMe}_2)_3$ [4.2] in C_6D_6

Suitable single crystals of $^{10\text{l}}\text{NPNTa}(\text{NMe}_2)_3$ [4.2] were obtained and the solid state molecular structure reveals an octahedral geometry about the central tantalum atom with distorted P1-Ta1-N22, N8-Ta1-N21 and N8a-Ta1-N21a angles av 161° (Table 10). The $^{10\text{l}}\text{NPN}$ ligand is facially bound (Figure 101). As alluded to in the NMR spectroscopic data discussion, two of the NMe_2 groups (N21 and N21a) have similar environments with larger *cis* $^3J_{\text{PC}}$ couplings. The other NMe_2 group (N22) is *trans* to the P atom of the ligand (P1) with a smaller $^3J_{\text{PC}}$ coupling.

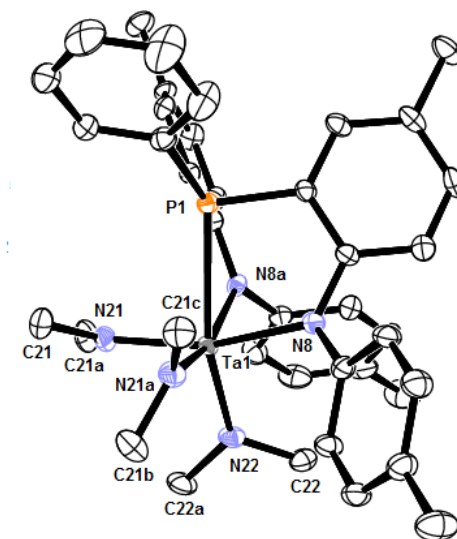


Figure 101: ORTEP representation of the solid state molecular structure of $^{10\text{l}}\text{NPNTa}(\text{NMe}_2)_3$ [4.2]

The Ta1-N21, Ta1-N21a, and Ta1-N22 bond lengths of 2.009(5) Å, 1.990(6) Å, and 1.991(5) Å for the NMe_2 groups (Table 10) are very similar to those reported for $\text{Ta}(\text{NMe}_2)_5$ at 1.965(5) - 2.038(8) Å,^{284, 285} $\text{Ta}(\text{NEt}_2)_5$ at 1.917(9) - 2.238(9) Å²⁸⁶ and other tantalum(V)

complexes containing NMe₂ groups, ranging from 1.94(2) to 2.09(2).²⁸⁷⁻²⁹² The Ta1-P1, Ta1-N8 and Ta1-N8a bond lengths of ^{tol}NPNTa(NMe₂)₃ [4.2] (Table 10) fall within the range of bond lengths reported for P₂N₂TaMe₃,²⁹³ ^{Si}NPNTaMe₃^{79, 80} and [^{Si}NPNTaH]₂N₂^{79, 80} complexes (Table 1).

Table 16 : Selected bond lengths (Å) and angles (°) for ^{tol}NPNTa(NMe₂)₃ [4.2]

| ^{tol} NPNTa(NMe ₂) ₃ [4.2] | | | |
|--|------------|---------------------|------------|
| Ta1-P1 | 2.6643(17) | P1-Ta1-N8 | 73.94(13) |
| Ta1-N8 | 2.191(5) | P1-Ta1-N8a | 68.89(14) |
| Ta1-N8a | 2.157(5) | P1-Ta1-N21 | 89.82(16) |
| Ta1-N21 | 2.009(5) | P1-Ta1-N21a | 92.99(16) |
| Ta1-N21a | 1.990(6) | N22-Ta1-N8 | 99.0(2) |
| Ta1-N22 | 1.991(5) | N22-Ta1-N8a | 93.0(2) |
| | | N22-Ta1-N21 | 98.7(2) |
| N8-Ta1-N8a | 91.14(19) | N22-Ta1-N21a | 105.2(2) |
| N8-Ta1-N21a | 85.3(2) | P1-Ta1-N22 | 160.00(17) |
| N21-Ta1-N8a | 89.6(2) | N8-Ta1-N21 | 162.2(2) |
| N21-Ta1-N21a | 88.4(2) | N8a-Ta1-N21a | 161.8(2) |

When comparing the P-Ta-N bite angles of the new *o*-phenylene bridged ^{tol}NPN ligand (Table 10) with tantalum complexes containing the silyl-methylene bridged ^{Si}NPN and P₂N₂ ligands (Table 1), one of the angles (P1-Ta1-N8) is within the observed range of 70.3(1) - 86.2(2)° and the other (P1-Ta1-N8a) is smaller at 68.89(14)°. The N8-Ta1-N8a bite angle for ^{tol}NPNTa(NMe₂)₃ [4.2] at 91.14(19)° is significantly smaller compared to the complexes with the ^{Si}NPN ligand as well as the P₂N₂ macro-cycle (Table 1). Smaller ligand bite angles are to be expected with the more the rigid *o*-phenylene backbone.

Table 17: Comparative bond lengths (Å) and angles (°) for related ^{Si}NPN and P₂N₂ tantalum complexes.

| | ^{Si} NPNTaMe ₃ ⁷⁹ | P ₂ N ₂ TaMe ₃ ²⁹³ | [^{Si} NPNTaH] ₂ N ₂ ⁷⁹ |
|-------------------|--|--|---|
| Ta1-P1 | 2.7713(13) | 2.6180(8) | 2.573(5) |
| | | 2.6088(9) | 2.596(5) |
| Ta1-N8 | 2.025(4) | 2.141(3) | 2.079(4) |
| | | | 2.031(4) |
| Ta1-N8a | 2.078(4) | 2.210(2) | 2.069(4) |
| | | | 2.049(4) |
| P1-Ta1-N8 | 81.72(11) | 84.58(7) | 78.8(2) |
| | | 73.86(7) | 77.5(2) |
| P1-Ta1-N8a | 70.3(1) | 74.60(7) | 86.2(2) |
| | | 78.39(7) | 76.3(2) |
| N8-Ta1-N8a | 113.0(2) | 96.39(9) | 108.2(2) |
| | | | 107.2(2) |

4.1.2. Synthesis of Tantalum Trichloro Complexes

The synthesis of dark brown tantalum trichloride complexes $^{i\text{prop}}\text{NPNTaCl}_3$ [4.4], $^{t\text{ol}}\text{NPNTaCl}_3$ [4.5] and $^{\text{Ph}}\text{NPNTaCl}_3$ [4.6] required reaction with an excess of *ca* 100 equiv of TMSCl in toluene heated to 140 °C for at least 2 days. A high yield is achievable for this reaction, as was seen for $^{t\text{ol}}\text{NPNTaCl}_3$ [4.5] with 86%. However, the presence of impurities required multiple re-crystallisation events to effect complete removal, leading to lower yields for $^{i\text{prop}}\text{NPNTaCl}_3$ [4.4] and $^{\text{Ph}}\text{NPNTaCl}_3$ [4.6], respectively.

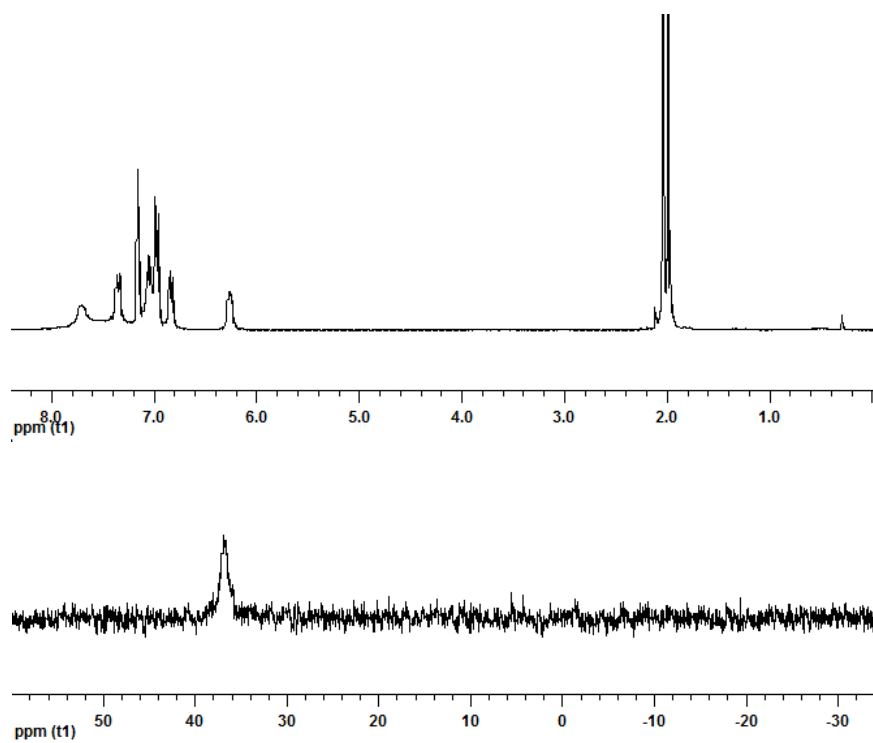


Figure 102: ^1H (top) and $^{31}\text{P}\{^1\text{H}\}$ NMR (bottom) spectra for $^{t\text{ol}}\text{NPNTaCl}_3$ [4.5] in C_6D_6 at room temperature

The $^{31}\text{P}\{^1\text{H}\}$ NMR spectra in C_6D_6 at room temperature for [4.4], [4.5] and [4.6] display broad peaks at δ 37.82, δ 36.77 and δ 36.04, respectively (Figure 102). Their corresponding ^1H NMR spectra at room temperature display broad peaks in the phenyl region (Figure 102) and it was not possible to obtain acceptable $^{13}\text{C}\{^1\text{H}\}$ NMR spectra under those conditions.

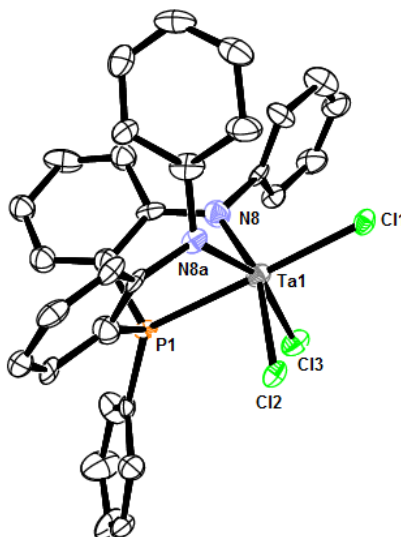


Figure 103: ORTEP representation of the solid state molecular structure for $^{\text{Ph}}\text{NPNTaCl}_3$ [4.6]

The solid state molecular structure of $^{\text{Ph}}\text{NPNTaCl}_3$ [4.6] shows the expected octahedral geometry about the tantalum centre (Figure 103) with an almost linear P1-Ta1-Cl1 angle of $178.52(13)^\circ$; however, the N8-Ta1-Cl2 and N8a-Ta1-Cl3 angles are severely distorted at 158° (Table 18). The NPN ligand for $^{\text{Ph}}\text{NPNTaCl}_3$ [4.6] is facially coordinated with P1-Ta1-N8, P1-Ta1-N8a and N8-Ta1-N8a bite angles (Table 18) of similar magnitude to those obtained for $^{\text{tol}}\text{NPNTa}(\text{NMe}_2)_3$ [4.2] (Table 10), however, the Ta1-P1, Ta1-N8 and Ta1-N8a bond lengths are all shorter, indicating that the ligand is more strongly bonded to $^{\text{Ph}}\text{NPNTaCl}_3$ [4.6] compared to $^{\text{tol}}\text{NPNTa}(\text{NMe}_2)_3$ [4.2].

Table 18 : Selected bond lengths (\AA) and angles ($^\circ$) for $^{\text{Ph}}\text{NPNTaCl}_3$ [4.6]

| $^{\text{Ph}}\text{NPNTaCl}_3$ [4.6] | | | |
|--------------------------------------|-----------|--------------------|------------|
| Ta1-P1 | 2.568(4) | P1-Ta1-N8 | 72.6(4) |
| Ta1-N8 | 2.017(12) | P1-Ta1-N8a | 76.9(4) |
| Ta1-N8a | 2.008(13) | P1-Ta1-Cl2 | 85.10(13) |
| Ta1-Cl1 | 2.351(4) | P1-Ta1-Cl3 | 82.98(13) |
| Ta1-Cl2 | 2.384(4) | Cl1-Ta1-N8 | 107.5(4) |
| Ta1-Cl3 | 2.403(4) | Cl1-Ta1-N8a | 101.6(4) |
| | | Cl1-Ta1-Cl2 | 94.98(14) |
| N8-Ta1-N8a | 89.5(5) | Cl1-Ta1-Cl3 | 98.51(14) |
| N8-Ta1-Cl3 | 84.8(4) | P1-Ta1-Cl1 | 178.52(13) |
| Cl2-Ta1-N8a | 91.3(4) | N8-Ta1-Cl2 | 156.8(4) |
| Cl2-Ta1-Cl3 | 86.51(13) | N8a-Ta1-Cl3 | 159.8(4) |

The tantalum chloride bond lengths Ta1-Cl1, Ta1-Cl2 and Ta1-Cl3 for $^{\text{Ph}}\text{NPNTaCl}_3$ [4.6] (Table 18) compare well with those reported for $[\text{TaCl}_5]_2$,²⁹⁴ $[\text{TaCl}_6]^{-1295}$ and other tantalum chloride complexes with nitrogen^{288, 296} or phosphorus²⁹⁷ donor atoms.

When the trichloro complexes [4.4], [4.5] and [4.6] are cooled down from room temperature to $-70\text{ }^\circ\text{C}$ in either toluene- d_8 or THF- d_8 , the broad peaks displayed in their $^{31}\text{P}\{^1\text{H}\}$ NMR spectra separate into two sharp peaks, with a major isomer at *ca* δ 36 and a minor isomer at *ca* δ 40 (Table 19). In all cases, the equilibrium is shifted more towards the minor isomer in toluene- d_8 than THF- d_8 , as is illustrated most prominently for $^{\text{tol}}\text{NPNTaCl}_3$ [4.5], where 14% is observed in THF- d_8 and 32% in toluene- d_8 (Figure 104).

Table 19 : $^{31}\text{P}\{^1\text{H}\}$ NMR data for NPNTaCl₃ complexes at $-70\text{ }^\circ\text{C}$.

| Isomer | Solvent | $^{\text{iprop}}\text{NPNTaCl}_3$ [4.4] δ (%) | $^{\text{tol}}\text{NPNTaCl}_3$ [4.5] δ (%) | $^{\text{Ph}}\text{NPNTaCl}_3$ [4.6] δ (%) |
|--------|----------------|---|---|--|
| Major | Toluene- d_8 | 36.16 (85) | 35.89 (68) | 35.25 (81) |
| Minor | Toluene- d_8 | 39.93 (15) | 40.64 (32) | 40.57 (19) |
| Major | THF- d_8 | 37.68 (89) | 35.82 (86) | 35.74 (84) |
| Minor | THF- d_8 | 41.66 (11) | 40.57 (14) | 41.65 (16) |

The isomeric mixtures for complexes [4.4], [4.5] and [4.6] are significantly less soluble in toluene- d_8 than THF- d_8 , with the observation of un-dissolved solids for the former. The above suggests that the isomers may differ in relative solubility in a given solvent, with the major isomer being relatively less soluble in toluene- d_8 compared to THF- d_8 .

Characterisation of both isomers in toluene- d_8 was attempted, but the low solubility of complexes [4.4], [4.5] and [4.6] in toluene- d_8 , accentuated at low temperatures, hampered characterisation of either. Complete ^1H and $^{13}\text{C}\{^1\text{H}\}$ NMR spectroscopic data for only the major isomers of [4.4], [4.5] and [4.6] were obtainable in THF- d_8 at $-70\text{ }^\circ\text{C}$ (Figure 105).

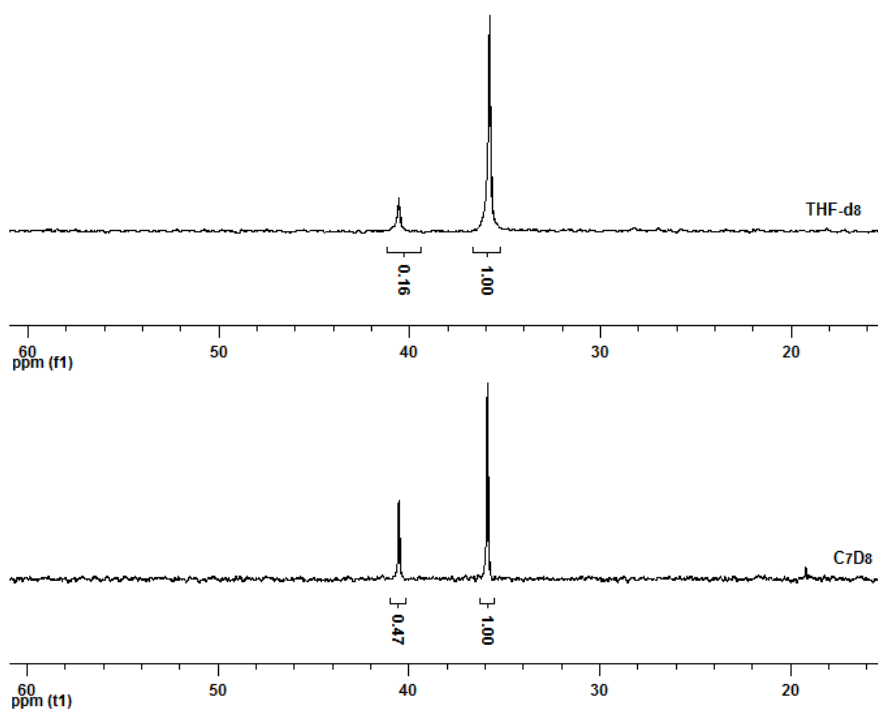


Figure 104: $^{31}\text{P}\{^1\text{H}\}$ NMR spectra for $^{101}\text{NPNTaCl}_3$ [4.5] in toluene- d_8 and THF- d_8 at -70°C .

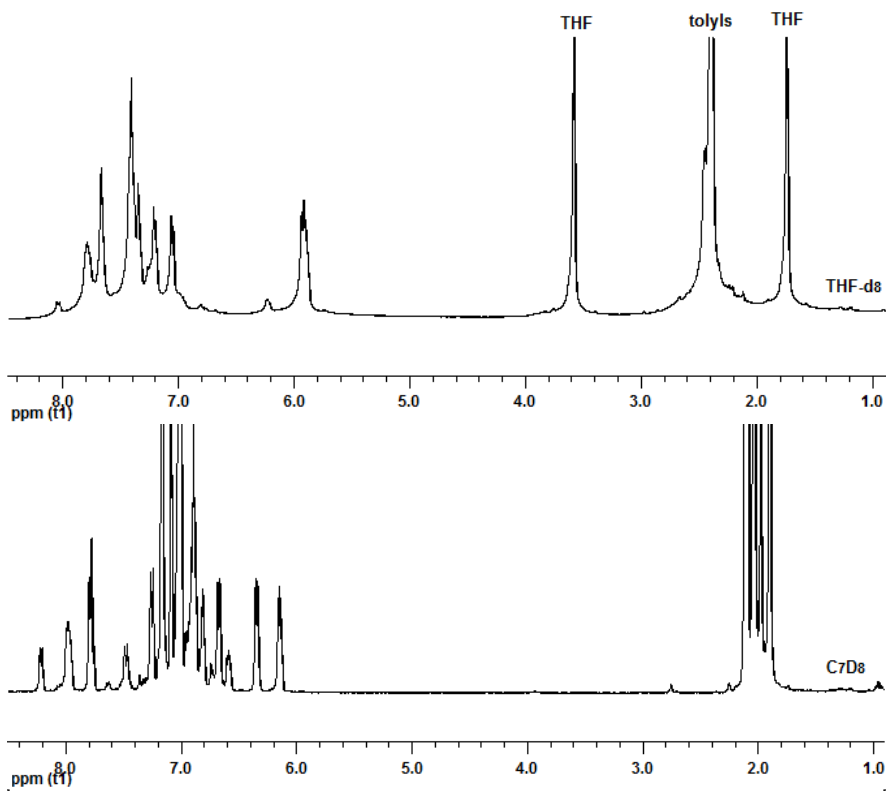


Figure 105: Partial ^1H NMR spectra for $^{101}\text{NPNTaCl}_3$ [4.5] in toluene- d_8 and THF- d_8 at -70°C .

Tantalum(V) is capable of seven-^{289, 293, 296, 298, 299} and eight-coordinate complexes,^{295, 297} but the possibility of an equilibrium with seven-coordinate THF adducts $\text{NPNTaCl}_3(\text{THF})$ can be discounted as this phenomenon is observed in both toluene- d_8 and THF- d_8 . It is also unlikely that NPNTaCl_3 monomers in the solid state form more condensed chloro-bridged dimeric structures $[\text{NPNTaCl}_3]_2$ in the solvated phase (Figure 106).

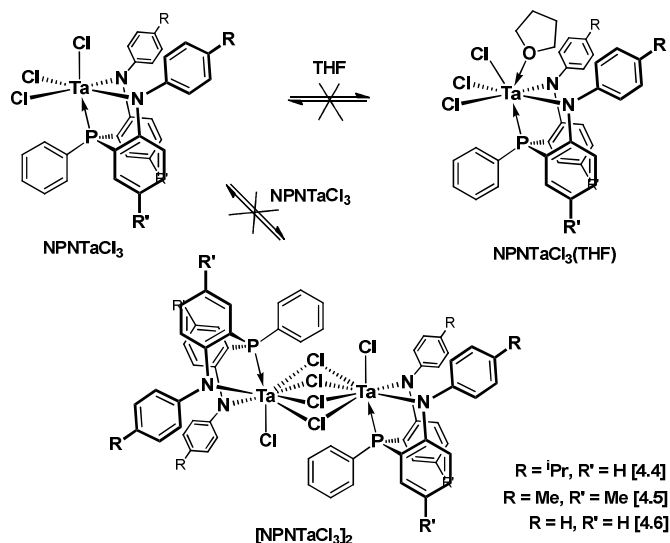


Figure 106: Implausible equilibria for solvated NPNTaCl_3 complexes

A $^3\text{P}\{^1\text{H}\}$ DOSY NMR²⁷² experiment was conducted on a sample of $^{101}\text{NPNTaCl}_3$ [4.5] at $-60\text{ }^\circ\text{C}$ in toluene- d_8 and the relative D values obtained for the peaks at δ 35.89 and δ 40.64 are 4.11 and $3.41 \times 10^{-9} \text{ m}^2\text{s}^{-1}$, respectively (see Appendix A). As with the experiment for $[\text{i}^\text{prop}\text{NPNZrCl}_2]_2$ [3.9] in chapter 3, only a qualitative comparison between peaks obtained in a single experiment can be made. According to the Stokes-Einstein equation (see chapter 3), a dimer is expected to have a D value half that of the monomer. The *ca* 20% difference between the two D values suggests that both species are similar in size. As the crystals obtained from a solution exhibiting both isomers reveal a monomeric structure (Figure 103), an assumption could be made that both species observed in solution may be monomers.

While a large majority of six-coordinate complexes are octahedral, substantial deviations from this idealised structure are possible, most notable towards trigonal prismatic³⁰⁰⁻³⁰⁴ and less commonly a bicapped tetrahedron.³⁰⁵⁻³⁰⁷

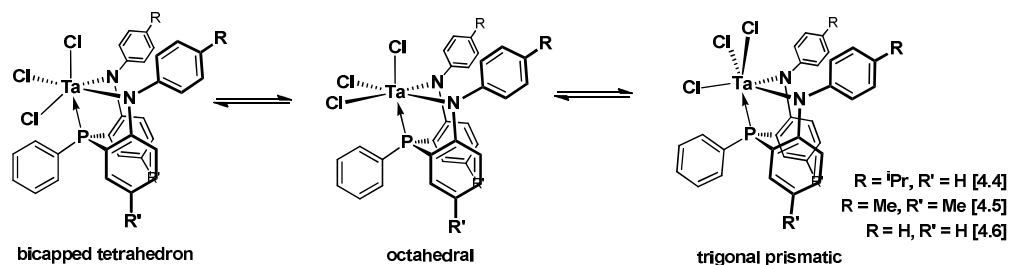


Figure 107: Possible configurational isomers for solvated NPNTaCl₃ complexes

The free energy of inter-conversion ΔG^\ddagger between the two isomers at room temperature was determined in toluene-*d*₈ to be 13.0 ± 0.3 kcal.mol⁻¹, 12.8 ± 0.3 kcal.mol⁻¹ and 12.8 ± 0.3 kcal.mol⁻¹ for ^{*i*prop}NPNTaCl₃ [4.4], ^{*tol*}NPNTaCl₃ [4.5] and ^{*Ph*}NPNTaCl₃ [4.6], respectively (see Appendix A). This low energy barrier may refer to either an octahedral-trigonal prismatic or an octahedral-bicapped tetrahedron structural transition (Figure 107). From the available data, it was not possible to distinguish between these two alternatives.

4.2. Tantalum Alkyl Complexes

There are two possible salt metathesis routes for obtaining NPN tantalum trialkyl complexes. One of the routes requires a reaction between TaCl₂Me₃ and the lithiated form of the NPN ligand (Figure 96) and it is routinely used for the synthesis of ^{*Si*}NPNTaMe₃.^{79, 80} The other route involves a reaction between NPNTaCl₃ complexes and alkyl lithium compounds (or other alkyl organometallic reagents) and is un-established within the Fryzuk group. In addition, there is precedent for the formation of trialkyltantalum complexes from pentaalkyltantalum precursor complexes and protonated ligands,³⁰⁸ which was not explored here.

4.2.1. Salt Metathesis with TaCl₂Me₃

In this study, TaCl₂Me₃ was reacted with [ⁱpropNPNLi₂·diox]_n [2.6], [^{tol}NPNLi₂·1.5TMEDA]₂ [2.7] and ^{tol}NPNK₂·2THF, where ^{tol}NPNK₂·2THF was not isolated, but formed *in situ* by reaction of ^{tol}NPNH₂ [2.11] with 2 equiv of KH in THF.

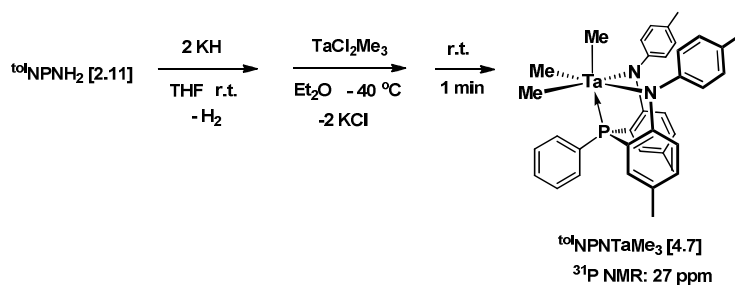


Figure 108: Synthesis of ^{tol}NPNTaMe₃ [4.7]

The synthesis of ^{tol}NPNTaMe₃ [4.7] was successfully achieved under very specific conditions with ^{tol}NPNK₂·2THF and TaCl₂Me₃ reacted at -40 °C over a short period of time (*ca* 1 min) with exactly 1 equiv of TaMe₃Cl₂ in the absence of light (Figure 108).

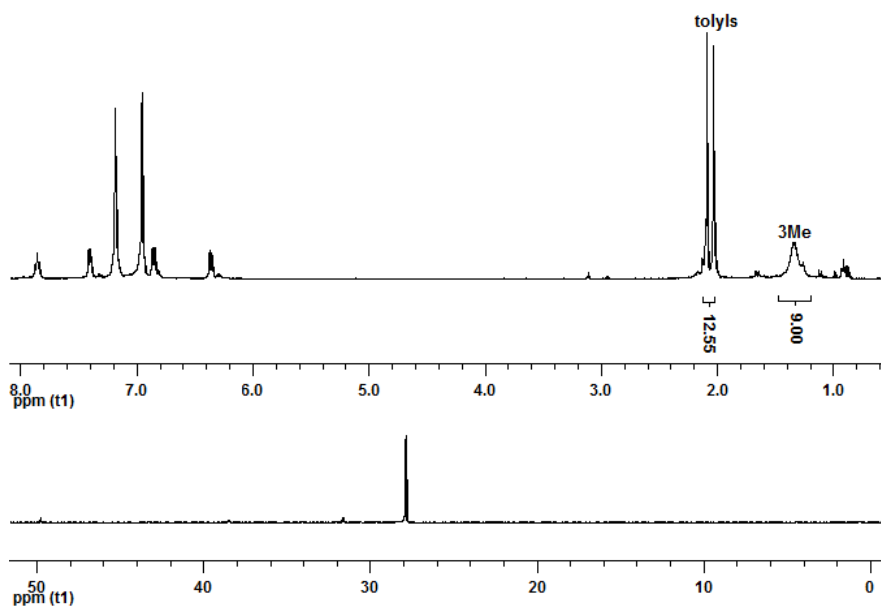


Figure 109: ¹H (top) and ³¹P{¹H} NMR (bottom) spectra for ^{tol}NPNTaMe₃ [4.7] in C₆D₆

The $^{31}\text{P}\{^1\text{H}\}$ NMR spectrum displayed a single peak at δ 27.88 for $^{101}\text{NPNTaMe}_3$ [4.7] (Figure 109) and the ^1H NMR spectrum displayed a broad peak at δ 1.34 (Figure 110) that integrates to three methyl groups per ^{101}NPN ligand. The ^1H - ^{31}P HMBC spectrum (Figure 110) indicates a correlation between this broad peak at δ 1.34 and the $^{31}\text{P}\{^1\text{H}\}$ NMR spectral peak at δ 27.88 (Figure 110). In the above-mentioned reaction, traces of a side-product (to be referred to as **species u_{tol}**) were observed, displaying a downfield shifted signal at δ 49.67 in $^{31}\text{P}\{^1\text{H}\}$ NMR spectrum and a doublet signal at δ 1.66 ($^3J_{\text{PH}} = 10$ Hz) in the ^1H NMR spectrum, which were strongly correlated in the ^1H - ^{31}P HMBC spectrum (Figure 110).

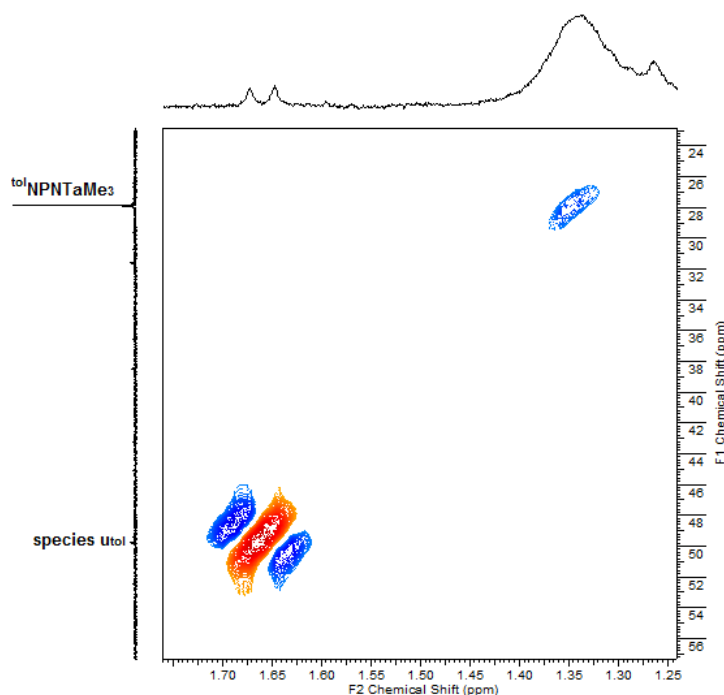


Figure 110: ^1H - ^{31}P HMBC NMR spectrum for $^{101}\text{NPNTaMe}_3$ [4.7] in C_6D_6

When the salt metathesis with $[\text{ipropNPnLi}_2\cdot\text{diox}]_n$ [2.6] was monitored as a function of temperature (see experimental section for more details), ipropNPNTaMe_3 [4.8] formation dominates at low temperature with a signal at δ 29.53 in $^{31}\text{P}\{^1\text{H}\}$ NMR spectrum, but at higher temperatures the downfield shifted side-product predominates (to be referred to as **species u_{ipr}**), displaying a signal at 50.95 (Figure 111). This suggests that while the trimethyl species is

kinetically preferred, there is a facile pathway favouring a thermodynamically stable side-product (species **u_{tol}** or species **u_{ipr}**, respectively).

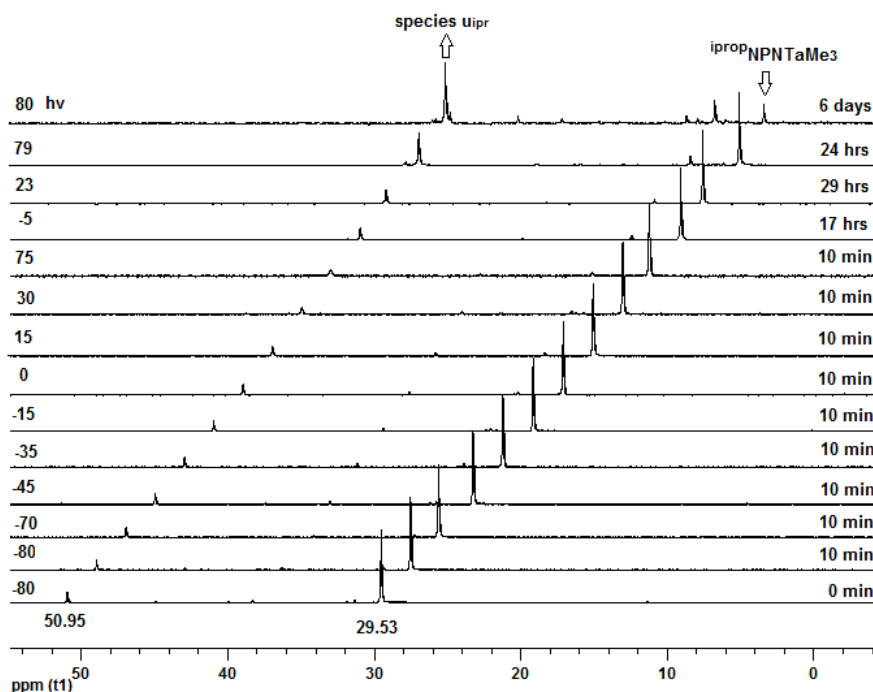


Figure 111: $^{31}\text{P}\{^1\text{H}\}$ NMR spectra for reaction of $[\text{ipropNPNLi}_2\text{diox}]_n$ [2.6] with TaMe_3Cl_2 in toluene- d_8 (successive spectra offset by $\delta 2$ units, 0 min = time the sample was placed inside the spectrometer at -80°C)

In the corresponding ^1H NMR spectra of the temperature dependent experiment (Figure 112), the Ta-methyl signal for ipropNPNTaMe_3 [4.8] was observed concurrent with the methyl doublet of the isopropyl group of the ipropNPN donor set at $\delta 1.15$ ($^3J_{\text{HH}} = 7\text{Hz}$). A doublet at $\delta 1.44$ ($^3J_{\text{PH}} = 10\text{Hz}$) was closely associated with the downfield shifted side-product **species **u_{ipr}****.

During the later stages of the $^{31}\text{P}\{^1\text{H}\}$ NMR monitored temperature experiment, the sample was exposed to heat and ambient light, leading to the observation of numerous additional side-products, potentially associated with radical decomposition processes.

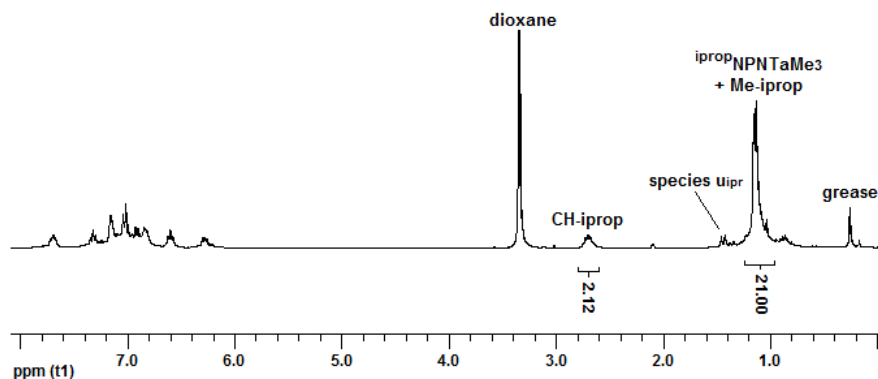


Figure 112: ^1H NMR spectrum for reaction of $[\text{ipropNPNTaLi}_2\text{diox}]_n$ [2.6] with TaMe_3Cl_2 in $\text{toluene-}d_8$ at -80°C , CH-iprop = methine, Me-iprop = methyl of the isopropyl group

Salt metathesis with the lithiated NPN donor sets seemed to favour the formation of the side-product (**species** u_{tol} or u_{ipr}) compared to the potassium analogue, given similar conditions. Excess TaCl_2Me_3 and introduction of hydrogen also promoted the observance of this side-product. A different side product **species** v_{tol} is also observed when the metathesis with the potassium salt $^{\text{tol}}\text{NPNK}_2 \cdot 2\text{THF}$ is prolonged at -40°C .

Subsequent to this study, complete spectroscopic analysis of $^{\text{tol}}\text{NPNTaMe}_3$ [4.7], as well as two related trimethyl complexes $^{\text{iprop-P}}\text{NPNTaMe}_3$ and $^{\text{mes}}\text{NPNTaMe}_3$ (Figure 113), have been elucidated (personal communication by Dr Dominik Nied), where the phenyl group on the phosphorus atom was replaced with an isopropyl group ($^{\text{iprop-P}}\text{NPN}$) and the steric bulk in the *ortho* position of the amido phenyl group was increased ($^{\text{mes}}\text{NPN}$).

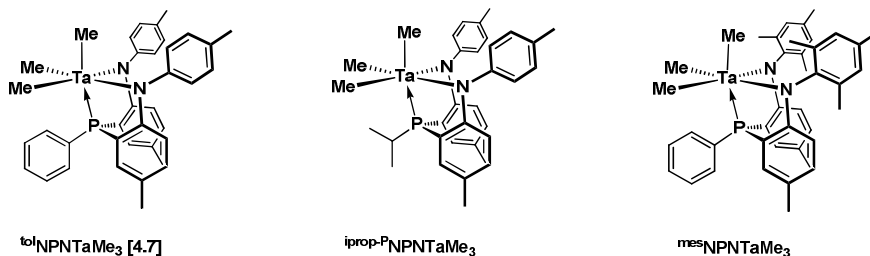


Figure 113: *o*-Phenylene bridged NPNTaMe_3 complexes

Suitable crystals for the solid state molecular structures of $^{\text{iprop-P}}\text{NPNTaMe}_3$ (Figure 114) and $^{\text{mes}}\text{NPNTaMe}_3$ were also obtained by Dr Dominik Nied.

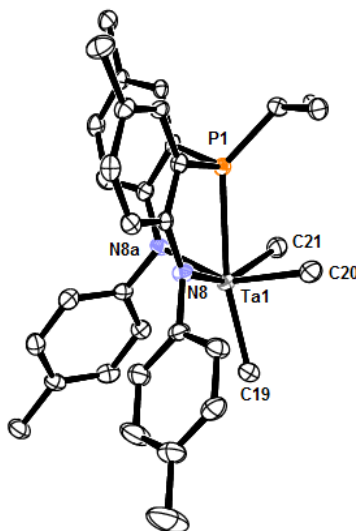


Figure 114: ORTEP representation of the solid state molecular structure for iprop-PNPNTaMe_3

The coordinated atoms in iprop-PNPNTaMe_3 are in a distorted octahedral arrangement around the tantalum centre with the iprop-PNPN ligand in a facial bonding mode and the P1-Ta1-C19, N8-Ta1-C21 and N8a-Ta1-C20 angles ranging between $168.36(10)^\circ$ and $150.44(13)^\circ$. The Ta1-P1, Ta1-N8 and Ta1-N8a bond lengths and P1-Ta1-N8, P1-Ta1-N8a and N8-Ta1-N8a bite angles for iprop-PNPNTaMe_3 (Table 20) are within the variance observed for the other *o*-phenylene-bridged NPN tantalum complexes reported in this chapter (Table 10, Table 18, Table 22 and Table 3).

Table 20 : Selected bond lengths (Å) and angles ($^\circ$) for iprop-PNPNTaMe_3

| iprop-PNPNTaMe_3 | | | |
|---------------------------|-----------|--------------------|------------|
| Ta1-P1 | 2.6576(9) | P1-Ta1-N8 | 73.42(8) |
| Ta1-N8 | 2.058(3) | P1-Ta1-N8a | 71.57(8) |
| Ta1-N8a | 2.058(3) | P1-Ta1-C20 | 80.00(10) |
| Ta1-C19 | 2.189(4) | P1-Ta1-C21 | 79.20(10) |
| Ta1-C20 | 2.217(4) | C19-Ta1-N8 | 112.36(13) |
| Ta1-C21 | 2.218(4) | C19-Ta1-N8a | 117.05(12) |
| | | C19-Ta1-C20 | 90.14(14) |
| N8-Ta1-N8a | 93.23(12) | C19-Ta1-C21 | 93.75(14) |
| N8-Ta1-C20 | 86.14(14) | P1-Ta1-C19 | 168.36(10) |
| C21-Ta1-N8a | 82.71(13) | N8-Ta1-C21 | 152.15(13) |
| C21-Ta1-C20 | 84.22(15) | N8a-Ta1-C20 | 150.44(13) |

The tantalum-alkyl bond lengths *trans* to the N atoms of the NPN ligand (Ta1-C20 and Ta1-C21) are longer than the one *trans* to the P atom (Ta1-C19) for iprop-PNPNTaMe_3 (Table 20)

but all are of a similar magnitude to the tantalum alkyl bond lengths reported for $^{51}\text{NPNTaMe}_3$,⁷⁹

$^{80}\text{P}_2\text{N}_2\text{TaMe}_3$,²⁹³ $\text{Ta}(\text{PMe}_3)_2\text{Cl}_2\text{Me}_3$,²⁹⁸ $[\text{tol}^{\text{NPNTaMe}_4}][\text{Li}(\text{THF})_4]$ [4.14] (Table 3) and

$^{51}\text{NP}(\text{C})\text{NTa}(\text{NMe}_2)_2$.²⁸³

4.2.2. Salt Metathesis with $^{\text{tol}}\text{NPNTaCl}_3$ [4.5]

Reaction of $^{\text{tol}}\text{NPNTaCl}_3$ [4.5] with MeLi (in Et₂O) at room temperature protected from light in toluene-*d*₈ leads to the observation of four different species with signals displayed at δ 50.85, δ 49.40, δ 43.42 and δ 27.58 in $^{31}\text{P}\{^1\text{H}\}$ NMR spectra, whose relative concentrations are affected by the amount of MeLi added (Figure 115).

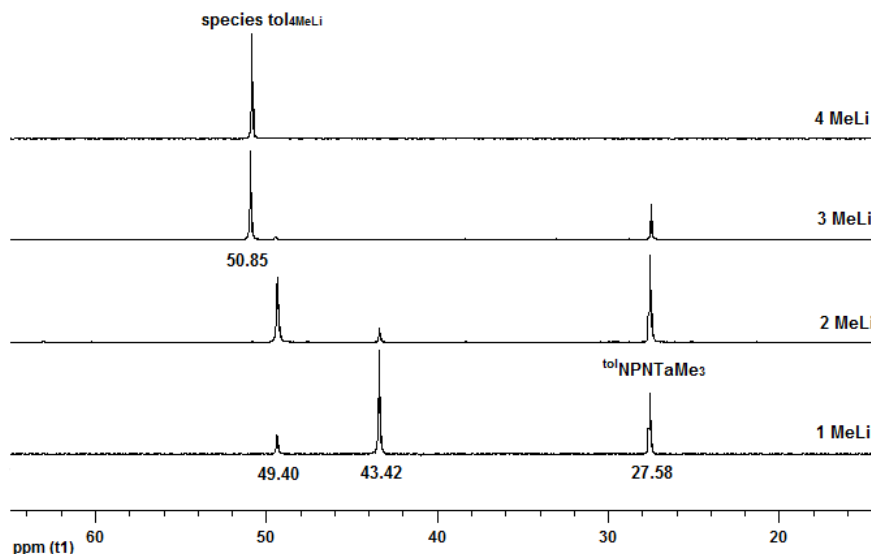


Figure 115: $^{31}\text{P}\{^1\text{H}\}$ NMR spectra of $^{\text{tol}}\text{NPNTaCl}_3$ [4.5] + 1, 2, 3 and 4 equiv of MeLi at room temperature in toluene-*d*₈.

The dominant peak after 1-2 equiv of MeLi (δ 27.58) represents $^{\text{tol}}\text{NPNTaMe}_3$ [4.7], however, after 3 equiv of MeLi most of it had been converted into the final product (δ 50.85). Isolation of the final product (referred to as **species tol₄MeLi**) is achieved upon reaction with 4 equiv of MeLi. **Species tol₄MeLi** and the other two unidentified species (δ 49.40 and 43.42) observed during the addition of MeLi are all downfield of both $^{\text{tol}}\text{NPNTaCl}_3$ [4.5] and $^{\text{tol}}\text{NPNTaMe}_3$ [4.7] and they are not likely to be $^{\text{tol}}\text{NPNTaCl}_{(3-x)}\text{Me}_x$ species. The corresponding ^1H NMR spectrum for 4 equiv of

MeLi i.e. **species** $\text{tol}_{4\text{MeLi}}$ has a doublet at δ 0.84 ($^3J_{\text{PH}} = 11$ Hz) integrating for two methyl groups and two broad peaks at δ 0.34 and δ 1.68 integrating for two separate methyl signals (Figure 116).

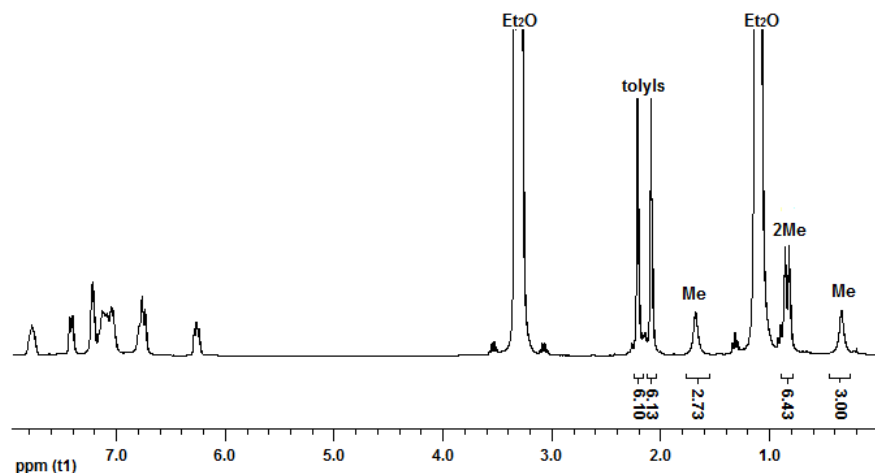


Figure 116: ^1H NMR spectrum for species $\text{tol}_{4\text{MeLi}}$ in toluene- d_8 after 4 equiv of MeLi.

After 7 days at room temperature and protected from light, the reaction solution with 4 equiv of MeLi in toluene- d_8 / Et_2O darkened. On removal of the solvent, a green toluene-insoluble solid was obtained. Dissolution in a THF/toluene solvent mixture and crystallisation at -40 °C over 53 days led to the isolation of the ionic tetramethyl species $[\text{}^{\text{tol}}\text{NPNTaMe}_4][\text{Li}(\text{THF})_4]$ **[4.14]**, which was characterised via X-ray crystallography (Figure 117) and elemental analysis. The four methyl groups in **[4.14]** are equivalent and do not correspond to the two pairs of inequivalent methyl groups observed for the precursor **species** $\text{tol}_{4\text{MeLi}}$.

The tantalum-carbon bond lengths for the tetramethyl anion of $[\text{}^{\text{tol}}\text{NPNTaMe}_4][\text{Li}(\text{THF})_4]$ **[4.14]** (Table 3) are comparable to other seven coordinate trimethyl complexes $\text{P}_2\text{N}_2\text{TaMe}_3^{293}$ and $\text{Ta}(\text{PMe}_3)_2\text{Cl}_2\text{Me}_3^{309}$ as well as the neutral six-coordinate $^{\text{Si}}\text{NPNTaMe}_3^{79, 80}$ complex (Table 3).

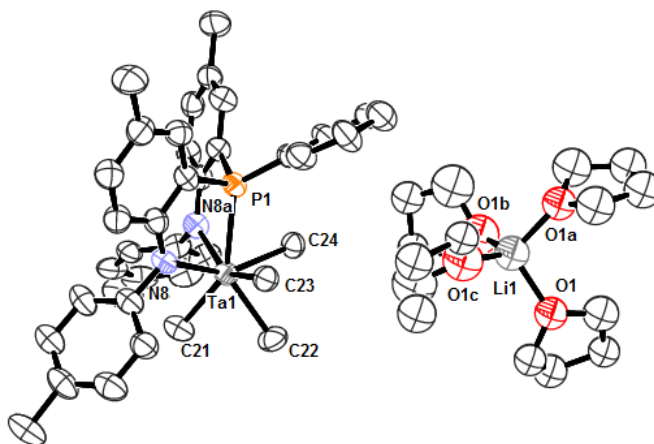


Figure 117: ORTEP representation of the solid state molecular structure for $[\text{tollNPNTaMe}_4][\text{Li}(\text{THF})_4]$ [4.14].

Table 21 : Selected bond lengths (Å) and angles (°) for $[\text{tollNPNTaMe}_4][\text{Li}(\text{THF})_4]$ [4.14] with comparative Ta-Me bond lengths (Å)

| | $[\text{tollNPNTaMe}_4][\text{Li}(\text{THF})_4]$ [4.14] | SiNPNTaMe_3 ⁷⁹ | $\text{P}_2\text{N}_2\text{TaMe}_3$ ²⁹³ | $\text{Ta}(\text{PMe}_3)_2\text{Cl}_2\text{Me}_3$ ³⁰⁹ |
|-------------|--|------------------------------------|--|--|
| Ta1-C21 | 2.213(9) | 2.224(5) | 2.239(3) | 2.219(3) |
| Ta1-C22 | 2.213(9) | 2.228(5) | 2.272(3) | 2.233(2) |
| Ta1-C23 | 2.242(8) | 2.204(5) | 2.252(4) | 2.240(3) |
| Ta1-C24 | 2.241(7) | | | |
| Ta1-P1 | 2.560(2) | | | |
| Ta1-N8 | 2.179(6) | | | |
| Ta1-N8a | 2.206(6) | | | |
| Li1-O1 | 1.94(3) | | | |
| Li1-O1a | 1.88(2) | | | |
| Li1-O1b | 1.94(3) | | | |
| Li1-O1c | 1.83(2) | | | |
| O1-Li1-O1a | 104.5(11) | | | |
| O1-Li1-O1b | 114.6(11) | | | |
| O1-Li1-O1c | 111.7(15) | | | |
| O1a-Li1-O1b | 104.1(14) | | | |
| O1a-Li1-O1c | 114.8(11) | | | |
| O1b-Li1-O1c | 107.1(13) | | | |

The Ta1-P1 bond length of $[\text{tollNPNTaMe}_4][\text{Li}(\text{THF})_4]$ [4.14] is 2.560(2) Å and of similar length to that reported for PhNPNTaCl_3 [4.6] (Table 18) and shorter than for $\text{tollNPNTa}(\text{NMe}_2)_3$ [4.2], $\text{P}_2\text{N}_2\text{TaMe}_3$,²⁹³ $[\text{SiNPNTaH}]_2\text{N}_2$, and SiNPNTaMe_3 ^{79, 80} (Table 10 and Table 1). The N8-Ta1-N8a bite angle of 93.2(3)° for [4.14] is similar to the other *o*-phenylene bridged NPN ligands (Table 18 and Table 10) and smaller than the silyl-bridged NPN tantalum containing complexes (Table 1). The Ta1-N8 and Ta1-N8a bond lengths (Table 3) and P1-Ta1-N8 and P1-Ta1-N8a

ligand bite angles (Table 22) of **[4.14]** are within the range reported for the other NPN tantalum complexes (Table 18, Table 10 and Table 1).

It is often difficult to distinguish between the four most common seven coordinate geometries (Figure 118) and, therefore, a numerical method^{309, 310} was applied to the seven-coordinate $[\text{Ta}^{\text{IV}}\text{NPNTaMe}_4]^-$ anion of **[4.14]**. This method involves comparison of the 21 inter-ligand bond angles of the idealised structures with the experimental data, listed in descending order of magnitude (Table 22).

Table 22: Inter-ligand bond angle analysis for seven coordinate geometries of $[\text{Ta}^{\text{IV}}\text{NPNTaMe}_4][\text{Li}(\text{THF})_4]$ **[4.14]**

| $[\text{Ta}^{\text{IV}}\text{NPNTaMe}_4]^-$ anion of [4.14] | | | Idealised structure angles ^{309, 310} | | | | Absolute difference from idealised angles | | | |
|--|---|-----------|--|----------------------|--------------------------|--------------------|---|----------------------|--------------------------|--------------------|
| No. | inter-ligand bond angle atom-Ta-atom | angle | pentagonal bipyramid | capped octahedron | capped trigonal prism | 4:3 piano stool | pentagonal bipyramid | capped octahedron | capped trigonal prism | 4:3 piano stool |
| 1 | N8-Ta1-C24 | 148.1(2) | 180.0 | 160.0 | 164.0 | 170.0 | 31.9 | 11.9 | 15.9 | 21.9 |
| 2 | C21-Ta1-P1 | 146.9(3) | 144.0 | 160.0 | 164.0 | 153.6 | 2.9 | 13.1 | 17.1 | 6.7 |
| 3 | N8a-Ta1-C23 | 145.5(2) | 144.0 | 160.0 | 144.2 | 153.6 | 1.5 | 14.5 | 1.3 | 8.1 |
| 4 | C22-Ta1-P1 | 137.4(3) | 144.0 | 130.0 | 144.2 | 130.8 | 6.6 | 7.4 | 6.8 | 6.6 |
| 5 | N8a-Ta1-C22 | 132.0(3) | 144.0 | 130.0 | 119.0 | 130.8 | 12.0 | 2.0 | 13.0 | 1.2 |
| 6 | C21-Ta1-C23 | 127.7(3) | 144.0 | 130.0 | 119.0 | 120.0 | 16.3 | 2.3 | 8.7 | 7.7 |
| 7 | N8-Ta1-C22 | 127.4(3) | 90.0 | 108.9 | 118.8 | 120.0 | 37.4 | 18.5 | 8.6 | 7.4 |
| 8 | C21-Ta1-C24 | 123.2(3) | 90.0 | 108.9 | 118.8 | 108.8 | 33.2 | 14.3 | 4.4 | 14.4 |
| 9 | N8a-Ta1-N8 | 93.2(3) | 90.0 | 108.9 | 99.0 | 108.8 | 3.2 | 15.7 | 5.8 | 15.6 |
| 10 | C24-Ta1-C23 | 90.7(3) | 90.0 | 83.1 | 99.0 | 89.4 | 0.7 | 7.6 | 8.3 | 1.3 |
| 11 | N8-Ta1-C21 | 85.9(3) | 90.0 | 83.1 | 83.7 | 89.4 | 4.1 | 2.8 | 2.2 | 3.5 |
| 12 | N8a-Ta1-C21 | 84.2(3) | 90.0 | 83.1 | 83.7 | 83.1 | 5.8 | 1.1 | 0.5 | 1.1 |
| 13 | N8a-Ta1-C24 | 78.8(3) | 90.0 | 82.0 | 80.3 | 83.1 | 11.2 | 3.2 | 1.5 | 4.3 |
| 14 | N8-Ta1-C23 | 78.5(3) | 90.0 | 82.0 | 80.3 | 83.1 | 11.5 | 3.5 | 1.8 | 4.6 |
| 15 | C22-Ta1-C24 | 76.9(3) | 90.0 | 82.0 | 78.8 | 75.5 | 13.1 | 5.1 | 1.9 | 1.4 |
| 16 | C22-Ta1-C21 | 75.6(4) | 90.0 | 82.0 | 78.6 | 75.5 | 14.4 | 6.4 | 3.0 | 0.1 |
| 17 | C22-Ta1-C23 | 75.5(3) | 72.0 | 82.0 | 75.2 | 75.5 | 3.5 | 6.5 | -0.3 | 0.0 |
| 18 | C24-Ta1-P1 | 74.9(2) | 72.0 | 82.0 | 75.2 | 75.5 | 2.9 | 7.1 | 0.3 | 0.6 |
| 19 | C23-Ta1-P1 | 73.6(2) | 72.0 | 70.0 | 75.0 | 73.3 | 1.6 | 3.6 | 1.4 | 0.3 |
| 20 | N8-Ta1-P1 | 73.23(16) | 72.0 | 70.0 | 75.0 | 73.3 | 1.2 | 3.2 | 1.8 | -0.1 |
| 21 | N8a-Ta1-P1 | 71.96(16) | 72.0 | 70.0 | 71.5 | 70.0 | 0.0 | 2.0 | 0.5 | 2.0 |
| | | | | | | Sum: | 215.1 | 151.8 | 104.4 | 108.7 |
| | | | | | | Average: | 10.2 | 7.2 | 5.0 | 5.2 |

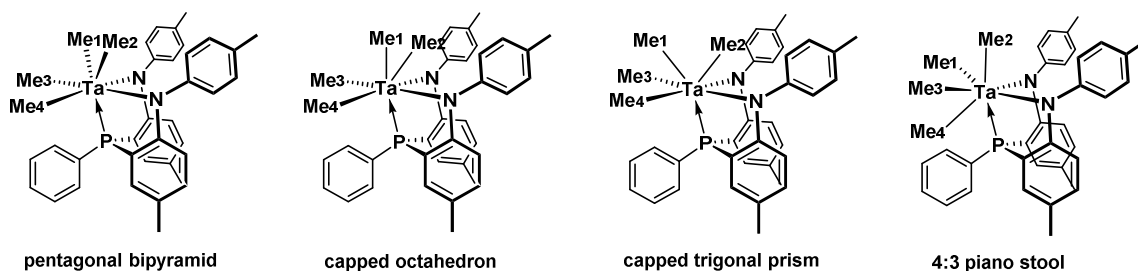


Figure 118: Possible seven-coordinate geometries for the $[\text{tolNPNTaMe}_4]^-$ anion of **[4.14]**. **Pentagonal bipyramid:** Me1, Me2 axial and Me3, Me4, N, N, P pentagonal. **Capped octahedron:** Me1, P axial and Me3, Me4, N, N equatorial of octahedron with Me2 cap of trigonal face Me1, N, N. **Capped trigonal prism:** Me1, Me3, Me4 and Me2, N, N trigonal bases with P cap of quadrilateral face Me3, Me4, N, N. **4:3 Piano stool:** Me1, Me2, Me3, Me4 tetragonal base and N, N, P trigonal cap.

When the angles for the $[\text{tolNPNTaMe}_4]^-$ anion of **[4.14]** were evaluated in this manner with the idealised angles for the pentagonal bipyramid, capped octahedron, capped trigonal prism and tetragonal base-trigonal cap (or 4:3 piano stool) geometries,^{309, 310} the least variance was observed for the capped trigonal prism (Table 22). Capped trigonal prisms were also reported for related $\text{P}_2\text{N}_2\text{TaMe}_3$ ²⁹³ and $\text{Ta}(\text{PMe}_3)_2\text{Cl}_2\text{Me}_3$ ³⁰⁹ structures.

Considering a capped trigonal prismatic geometry for the $[\text{tolNPNTaMe}_4]^-$ anion of **[4.14]**, one end of the prism is defined by three methyl groups C22-C23-C24 and the other by the two nitrogen atoms and the fourth methyl group N8-N8a-C21 (Figure 117). The phosphorus atom P1 forms the cap on one of the rectangular prism faces N8-N8a-C23-C24. The $\text{Li}(\text{THF})_4$ cation forms a regular tetrahedral structure (Table 3). If one considers a mirror plane containing C21, C22 and P1 dissecting N8-N8a and C23-C24 planes for the $[\text{tolNPNTaMe}_4]^-$ anion of **[4.14]**, then there are two equiv Me's (C23 & C24) and two inequiv Me's (C21 & C22) which matches the Ta-Me signals reflected in the ^1H NMR trace of the ethereal species observed prior to crystallisation (Figure 116).

All further attempts at isolation of $[\text{tolNPNTaMe}_4][\text{Li}(\text{THF})_4]$ **[4.14]** by reaction of tolNPNTaCl_3 **[4.5]** directly with 4 equiv of MeLi at -40°C failed, giving a light yellow hydrocarbon soluble solid **species** tol_4MeLi , which could be an alkyl-bridged lithium-tantalum complex $\text{tolNPNTaMe}_4\text{Li}(\text{Et}_2\text{O})$ **[4.13]**, or the THF analogue $\text{tolNPNTaMe}_4\text{Li}(\text{THF})$ **[4.15]**

(Figure 119 and see experimental section for further details). Furthermore, dissolution of $[\text{tol}^{\text{NPNTaMe}_4}][\text{Li}(\text{THF})_4]$ **[4.14]** crystals in $\text{THF-}d_8$ resulted in a different species with only two methyl groups per $\text{tol}^{\text{NPNTa}}$ unit.

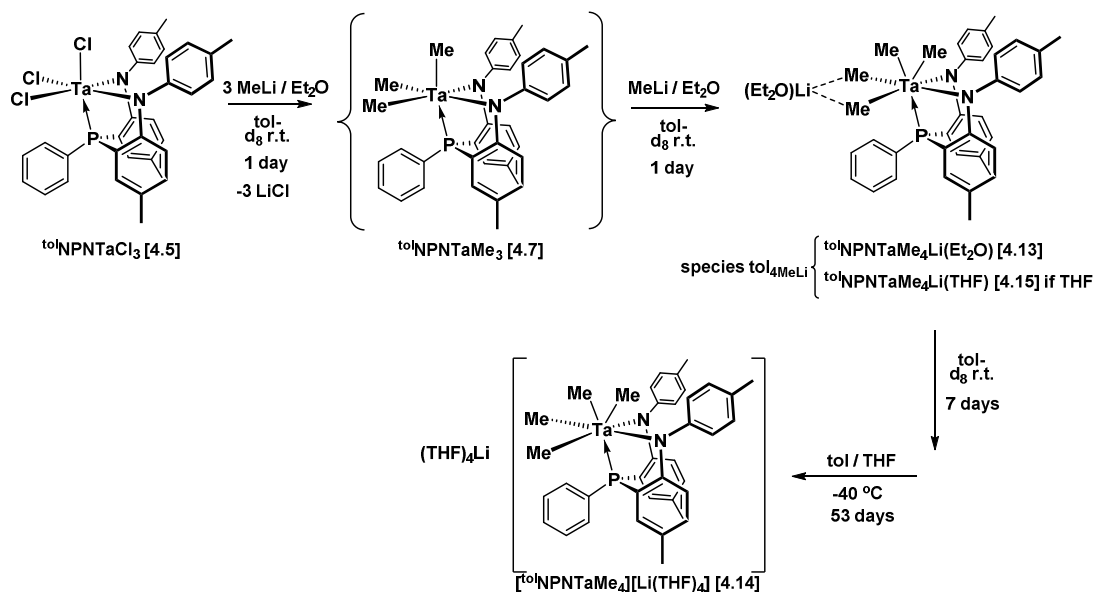


Figure 119: Potential tantalum methyl species for the salt metathesis of $\text{tol}^{\text{NPNTaCl}_3}$ **[4.5]** with MeLi

Preliminary reactions of $\text{tol}^{\text{NPNTaCl}_3}$ **[4.5]** with BnMgCl ($\text{Bn} = \text{CH}_2\text{Ph}$) suggest that the trialkyl species $\text{tol}^{\text{NPNTaBn}_3}$ can be isolated.

Summary

The synthesis of $\text{tol}^{\text{NPNTaMe}_3}$ **[4.7]** was successfully achieved with the potassium salt $\text{tol}^{\text{NPNK}_2} \cdot 2\text{THF}$ and TaCl_2Me_3 under specific conditions. The use of lithium salts of the NPN donor set or deviation from the specified conditions favoured the formation of undesired side-products. While the trimethyl species $\text{tol}^{\text{NPNTaMe}_3}$ **[4.7]** was observed during the reaction of $\text{tol}^{\text{NPNTaCl}_3}$ **[4.5]** with MeLi, the formation of a tetramethyl species $\text{tol}^{\text{NPNTaMe}_4\text{Li}(\text{Et}_2\text{O})}$ **[4.13]** with a bridged Li-Me-Ta structure was observed, which converts slowly in THF at -40°C into the ionic species $[\text{tol}^{\text{NPNTaMe}_4}][\text{Li}(\text{THF})_4]$ **[4.14]**. These tantalum methyl species were light and

thermally sensitive and may be prone to reductive elimination of methyl groups to give dimethyl species.

4.3. Tantalum Dinitrogen Complexes

In this study, investigation of the hydride route involved reaction of the *in situ* prepared $^{i\text{prop}}\text{NPNTaMe}_3$ [4.8] complex with hydrogen and the reaction of NPNTaCl_3 complexes with KHBet_3 . Having successfully obtained pure NPNTaCl_3 complexes, it was also possible to attempt the more traditional method for obtaining activated N_2 complexes via reduction in the presence of N_2 (see chapter one) and in this study reactions were conducted with 2.2 and 3.5 equiv of KC_8 .

4.3.1. Hydride Route

Hydrogenation of $^{i\text{prop}}\text{NPNTaMe}_3$ [4.8]

$[\text{}^{i\text{prop}}\text{NPnLi}_2\cdot\text{diox}]_n$ [2.6] was combined with TaMe_3Cl_2 at low temperature in the absence of light and allowed to warm to 0 °C before addition of H_2 . Based on a preceding control experiment, it is assumed that the predominant species formed prior to H_2 addition at 0 °C is $^{i\text{prop}}\text{NPNTaMe}_3$ [4.8]. However, this reaction was not ideal as the purity of the tantalum trimethyl complex was not independently verified but prepared *in situ*. Analysis after H_2 addition revealed the exclusive formation of **species \mathbf{u}_{ipr}** , based on $^{31}\text{P}\{^1\text{H}\}$ NMR and ^1H NMR spectral data. Further work involving hydrogenation of pure *o*-phenylene bridged NPNTaMe_3 complexes revealed that partial and complete tantalum hydride formation is achievable, but complicated due to thermal instability of the resulting hydrides (personal communication Dr. Dominik Nied).

Reactions with KHBet_3 and N_2

Two different reactions were attempted. In one instance, 3 equiv of KHBet_3 was added to $^{i\text{prop}}\text{NPNTaCl}_3$ [4.4] under an argon atmosphere at -115 °C in order to generate the intermediate

tantalum hydride species, followed by introduction of N₂ at -40 °C. In the other instance, 3 equiv of KHBet₃ were added to ¹⁰¹NPNTaCl₃ [4.5] under an N₂ atmosphere at -40 °C.

For the case where generation of the tantalum hydride species was attempted prior to exposure to N₂, a complex mixture of species was obtained, with numerous peaks in the ³¹P{¹H} NMR spectra between δ 31 and δ 49 (Figure 120) and further downfield at δ 189 and δ 192.

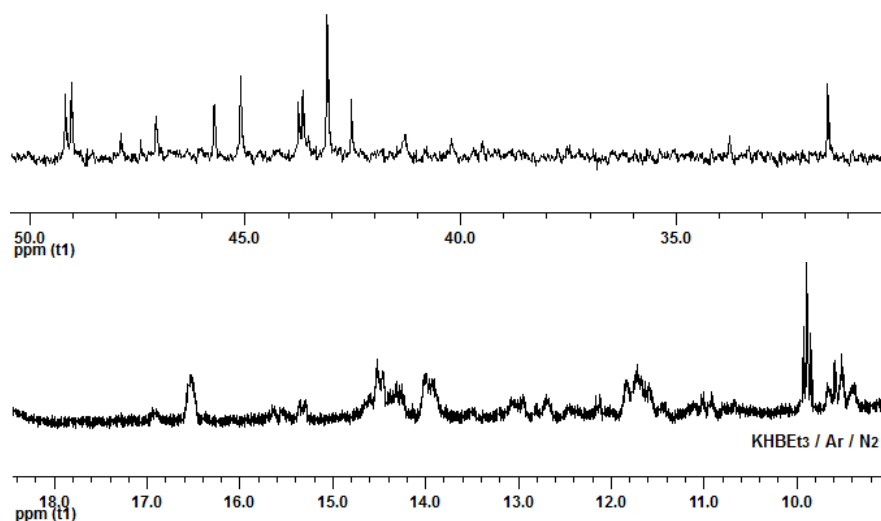


Figure 120: Partial ³¹P{¹H} (top) and partial ¹H NMR (bottom) spectra for ^{iprop}NPNTaCl₃ [4.4] + KHBet₃ (Ar) + N₂ in C₆D₆

The corresponding ¹H NMR spectra (Figure 120) contains numerous peaks of varying multiplicities in the expected tantalum-hydride region between δ 9.5 and δ 21.6. For comparison, [^{Si}NPNTaH₂]₂ displays a peak at δ 10.6 and [^{Si}NPNTaH](N₂) a doublet of doublets at δ 10.85 (²J_{PH} = 20.3 Hz and 14.3 Hz).^{79, 80} The question arises as to whether these may be various tantalum hydride species or if some are mixed hydride-dinitrogen species. The mass spectrum of the mixture after exposure to N₂ contained a parent ion at 1697 m/z, which is consistent with the molecular formula [^{iprop}NPNTaH]₂(NBet₃)₂(N₂)₂ [4.17a] and a fragment ion at 1444 m/z, which is consistent with the formulation for [^{iprop}NPNTaH]₂(N₂) [4.17] (Figure 121). The mass spectrum contained no evidence of peaks at 1419 m/z or 711 m/z for either a potential tetrahydride [^{iprop}NPNTaH₂]₂ or trihydride ^{iprop}NPNTaH₃ species. Given that these hydride complexes were

subsequently found to be thermally sensitive (Dr. Dominik Nied, personal communication), the complexity of these reactions is somewhat understandable.

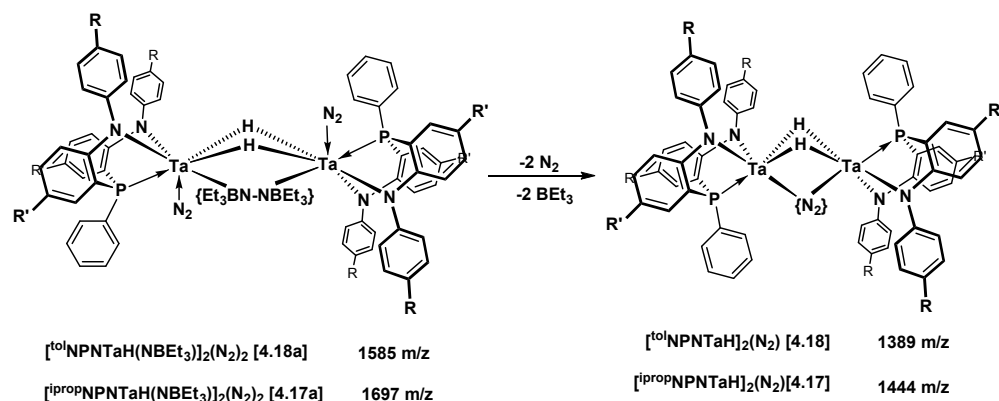


Figure 121: Potential species indicated by mass spectral data

The plausibility of the formation of a BEt_3 adduct with the activated N_2 ligand is substantiated by the reported reaction of $[\text{}^{\text{Si}}\text{NPNTaH}]_2(\text{N}_2)$ with $\text{B}(\text{C}_6\text{F}_5)_3$ to form a Lewis adduct.¹⁹³ It may be that the BEt_3 was not removed during evacuation before the sample was exposed to N_2 . Due to the complex nature of the sample, it was not possible to crystallise any single product.

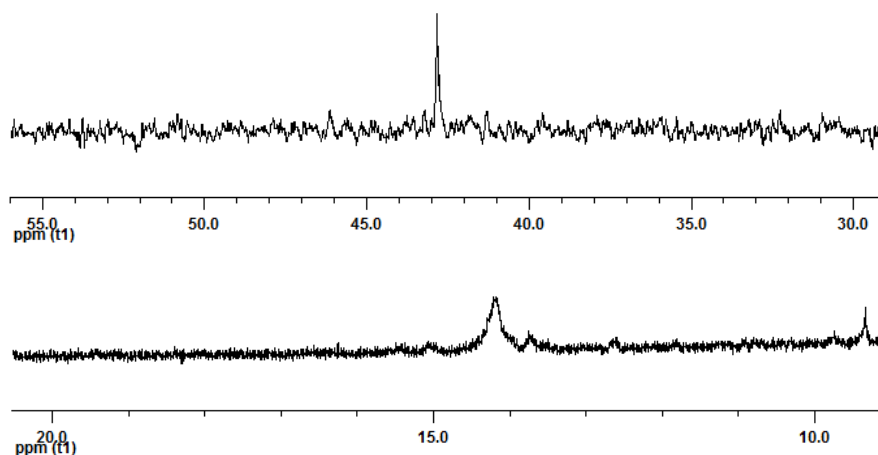


Figure 122: $^{31}\text{P}\{^1\text{H}\}$ (top) and partial ^1H NMR (bottom) spectra for $^{\text{tol}}\text{NPNTaCl}_3$ [4.5] + $\text{KHBET}_3 + \text{N}_2$ in C_6D_6

When the hydride generation was attempted in the presence of N_2 , a single product with a peak in the $^{31}\text{P}\{^1\text{H}\}$ NMR spectrum at δ 42.83 and a broad peak in the ^1H NMR spectrum at δ

14.20 (Figure 122) was obtained. A mass spectrum of the sample displayed a parent ion at 1585 m/z, which is consistent with a molecular formula of $[\text{}^{101}\text{NPNTaH}]_2(\text{NBEt}_3)_2(\text{N}_2)_2$ [**4.18a**] and a fragment ion at 1389 m/z for $[\text{}^{101}\text{NPNTaH}]_2(\text{N}_2)$ [**4.18**] (Figure 121). All attempts at obtaining a crystalline solid failed due to high solubility in *n*-hexanes and *n*-pentanes.

From on the above results, it is preferable to react NPNTaCl₃ complexes with KHBet₃ in the presence of N₂, as numerous hydride species are observed under argon. However, for *in situ* hydride generation under N₂, it may be unavoidable that BEt₃ liberated during the hydride formation would form an adduct with the activated N₂ unit, based on mass spectral evidence (Figure 123).

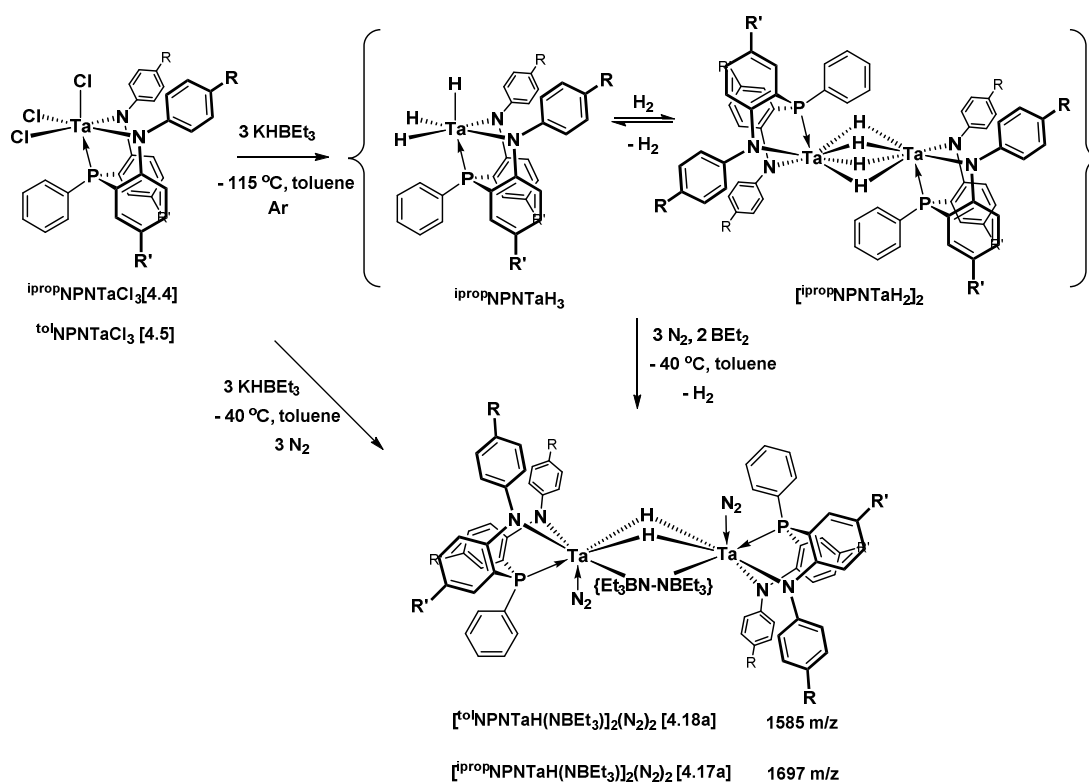


Figure 123: Schematic of potential reactions of NPNTaCl₃ with KHBet₃ under Ar and N₂

Future work should include (i) using the ^{ph}NPN ligand in order to reduce solubility and promote the isolation of any product species, (ii) reaction with alternate hydrides such as KH

under N_2 , that may avoid Lewis adduct formation and (iii) reduction with KC_8 in the presence of H_2 / N_2 .

4.3.2. Reduction Route

Reduction with 2 KC_8 and N_2

Reduction of $^{i\text{prop}}NPNTaCl_3$ [4.4] and $^{tol}NPNTaCl_3$ [4.5] with 2 equiv of KC_8 under 4 atm N_2 gave brown solids and their respective $^{31}P\{^1H\}$ NMR spectra indicated a major peak at δ 8.05 and δ 10.86, respectively. Considering reactions with $^{tol}NPNTaCl_3$ [4.5], minor peaks in varying amounts were observed downfield between δ 18.46 and δ 34.40, as well as the unreacted trichloride at δ 36.77 (Figure 124).

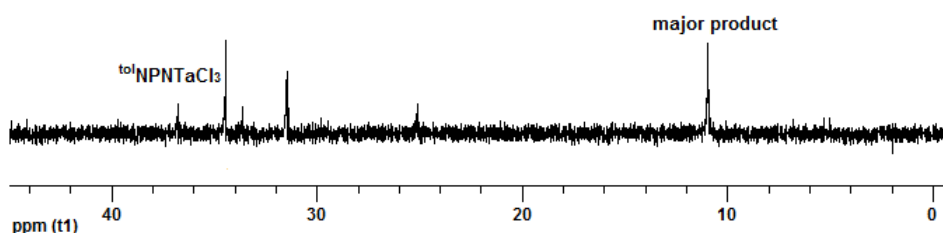


Figure 124: $^{31}P\{^1H\}$ NMR spectrum for reaction of $^{tol}NPNTaCl_3$ [4.5] with 2.2 KC_8 under N_2 in C_6D_6

It was not possible to crystallise pure products from the crude reduction mixtures, but the mass spectra of these mixtures suggest the formation of dichloride N_2 complexes occurred. For reduction with $^{i\text{prop}}NPNTaCl_3$ [4.4], a parent ion was observed at 1512 m/z corresponding to the chemical formulae $[^{i\text{prop}}NPNTaCl]_2(N_2)$ [4.19], with fragment ions at 1498 m/z and 1484 m/z indicating loss of one and two N atoms, respectively. Similarly a parent ion was observed at 1456 m/z for $[^{tol}NPNTaCl]_2(N_2)$ [4.20], with fragment ions at 1442 m/z and 1428 m/z indicating loss of one and two N atoms (Figure 125). It should be noted that while the end-on N_2 bonding mode depicted in Figure 125 is projected based on reported tantalum complexes³¹¹ this would need to be verified via x-ray crystallography.

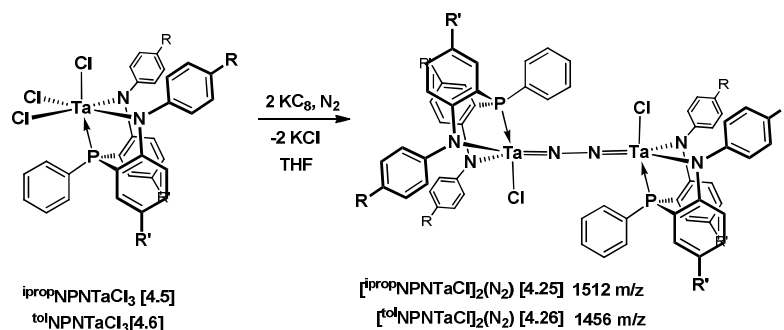


Figure 125: Reduction of NPNTaCl₃ complexes with 2.2 KC₈ under N₂

The persistence of unreacted trichloride species, despite reaction with 2 equiv of KC₈, implies competition with reduction intermediates. In a different study, it was shown that 2.5 equiv of KC₈ were required to reduce cyclopentadienyl-guanidinate tantalum trichloride complexes to their corresponding dichloride N₂ complexes.⁷⁸ Future work would involve investigations into the amount KC₈ needed to optimise the reduction of ^{iprop}NPNTaCl₃ [4.4] and ^{tol}NPNTaCl₃ [4.5] in order to reduce side-product formation and unreacted material. The use of a selective four electron reductant such as 3,6-bis(trimethylsilyl)-1,4-cyclohexadiene (BTCD)³¹² may be considered, which has been shown to reduce [TaCl₅]₂ to a tantalum trichloride complex.³¹³

Reduction with 3.5 KC₈ and N₂

One of the required fundamental steps for the design of a catalytic cycle converting N₂ to amines or other nitrogen-containing compounds is the scission of the N≡N triple bond, which requires addition of 6 electrons. The reduction of tantalum trichlorides with greater than 3 equiv of KC₈ in the presence of N₂ could potentially result in tantalum nitride complexes. The reduction of cyclopentadienyl-guanidinate tantalum trichloride complexes with an excess of 4 equiv of KC₈ was reported to form either tantalum nitride complexes or chloride-free N₂ complexes, depending on the temperature of the product work-up conditions.⁷⁸

When $^{101}\text{NPNTaCl}_3$ [4.5] was reacted with 3.5 equiv of KC_8 under 4 atm N_2 , the crude product isolated after THF filtration contained a single peak in the $^{31}\text{P}\{^1\text{H}\}$ NMR spectrum at δ 1.49. Subsequent suspension in *n*-hexanes at -40°C led to the isolation of a mixture with three major peaks at δ 11.18, δ 14.29 and δ 17.36, indicating the sensitivity of the initially observed species.

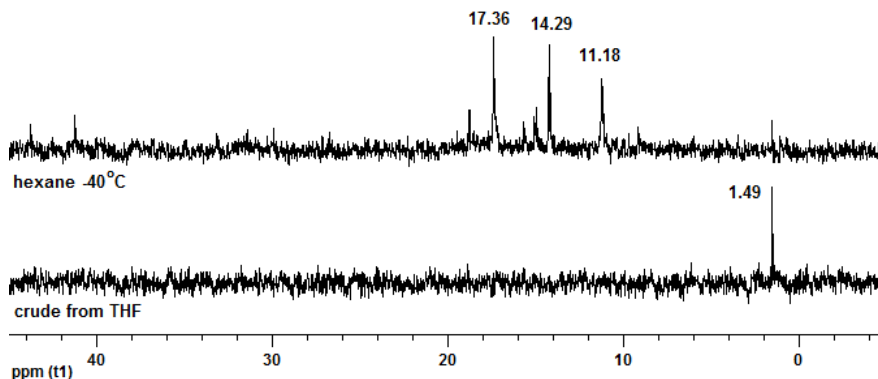


Figure 126: $^{31}\text{P}\{^1\text{H}\}$ NMR spectra for $^{101}\text{NPNTaCl}_3$ [4.5] + 3.5 KC_8 under N_2 in C_6D_6

Further work on this system would include identification of the products obtained as well as an investigation of the effect of varying the amount of KC_8 (between 3 to 4 equiv) and temperature of work-up conditions on the product selectivity.

4.4. Summary

In conclusion, the isolation of *o*-phenylene bridged diamidophosphine containing NPNTaCl_3 complexes was achieved via addition of a chlorinating agent (TMSCl) to $\text{NPNTa}(\text{NMe}_2)_3$ complexes, that was obtained by protonolysis of the NPNH_2 ligands with $\text{Ta}(\text{NMe}_2)_5$. These NPNTaCl_3 complexes exist as two different monomeric isomers in solution.

The corresponding NPNTaMe_3 complexes were obtained by salt metathesis of the potassium form of the NPN ligand with TaMe_3Cl_2 under well-constrained reaction conditions. Deviation from these conditions, or attempts to perform the salt metathesis with NPNTaCl_3 complexes and MeLi , resulted in the isolation of undesired side-products. Crystals of the ionic

species $[\text{}^{101}\text{NPNTaMe}_4][\text{Li}(\text{THF})_4]$ were obtained, indicating reaction of the NPNTaMe_3 complexes with MeLi . Unfortunately, all subsequent attempts to replicate the synthesis of this species failed.

Hydride formation from NPNTaMe_3 complexes and H_2 was verified in a later study (personal communication Dominik Nied). However, these complexes were found to be unstable in the presence of N_2 . Mass spectral evidence for the reaction of NPNTaCl_3 complexes with KBet_3 under N_2 suggests that activated N_2 complexes with BEt_3 adducts may have formed i.e. $[\text{NPNTaH}]_2(\text{NBet}_3)_2(\text{N}_2)_2$, though peaks corresponding to $[\text{NPNTaH}]_2(\text{N}_2)$ were also observed.

The formation of $[\text{NPNTaCl}]_2(\text{N}_2)$ complexes was also detected using mass spectrometry during the reduction of NPNTaCl_3 complexes with 2 equiv of KC_8 under N_2 . With 3.5 equiv of KC_8 , different species were observed via $^{31}\text{P}\{^1\text{H}\}$ NMR spectroscopy, and further investigation would be needed in order to verify if a tantalum nitride had been formed.

Crystallisation of the tantalum N_2 complexes above detected via mass spectrometry was hampered by complex reaction mixtures or enhanced solubility of the products. Based on the promising mass spectrometry results, future work should focus on the reduction of NPNTaCl_3 complexes or reaction with different less innocuous hydride reagents i.e. KH instead of KHBet_3 . Modification of the NPN ligands in order to lower solubility may enhance the possibility of isolating the desired N_2 complexes.

Chapter 5: Group 4 Dinitrogen Complexes

5.1. Zirconium Dinitrogen Complexes

5.1.1. Synthesis of $[\text{ipropNPNZr}(\text{THF})]_2(\mu\text{-}\eta^2\text{:}\eta^2\text{-N}_2)$ [5.1] and $[\text{tolNPNZr}(\text{THF})]_2(\mu\text{-}\eta^2\text{:}\eta^2\text{-N}_2)$ [5.3]

The new side-on bridged zirconium dinitrogen complexes $[\text{ipropNPNZr}(\text{THF})]_2(\mu\text{-}\eta^2\text{:}\eta^2\text{-N}_2)$ [5.1] and $[\text{tolNPNZr}(\text{THF})]_2(\mu\text{-}\eta^2\text{:}\eta^2\text{-N}_2)$ [5.3] were prepared by reduction of $\text{ipropNPNZrCl}_2(\text{THF})$ [3.5] and $\text{tolNPNZrCl}_2(\text{THF})$ [3.6], respectively, with KC_8 at -196°C in THF under 4 atm N_2 (Figure 127).³¹⁴ Reduction of the chloro-bridged dimer $[\text{ipropNPNZrCl}_2]_2$ [3.9] also yielded dinitrogen complex [5.1]. Elemental analysis for both [5.1] and [5.3] support the proposed molecular formulas.

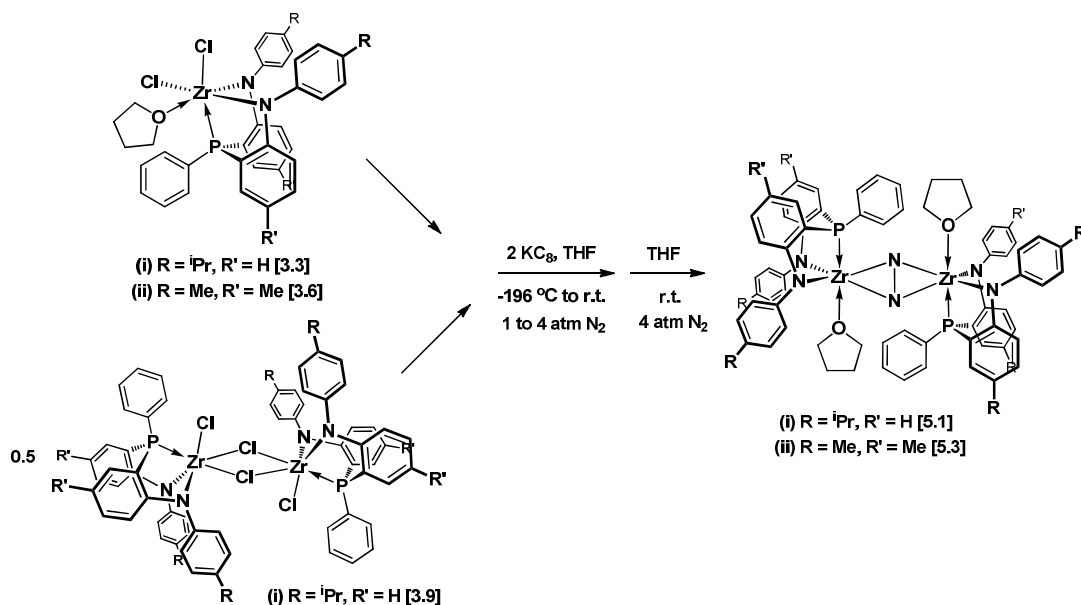


Figure 127: Synthesis of $[\text{ipropNPNZr}(\text{THF})]_2(\mu\text{-}\eta^2\text{:}\eta^2\text{-N}_2)$ [5.1] and $[\text{tolNPNZr}(\text{THF})]_2(\mu\text{-}\eta^2\text{:}\eta^2\text{-N}_2)$ [5.3]

Maintaining the concentration of the precursor dichlorides within the range of *ca* 0.3–1.2 g per 10 cm³ THF gave favourable yields of 60 to 78%. When the concentration is increased to *ca* 3 g per 10 cm³ THF, a lower yield of 25% was obtained, with a greater amount of side-

products. When too dilute i.e. 0.04 g per 10 cm³ THF (see control experiment for reduction at 600 psi N₂), a complex mixture of side-products was observed. Scaling the reaction up without reducing the concentration (*ca* 2 g per 20 cm³ THF) also resulted in a low yield of 19%. During typical reaction work-ups, an *n*-hexanes -soluble brown material has to be washed away from the purple product, which becomes more pronounced in the lower-yielding reactions. Multiple toluene filtrations through celite, or use of a centrifuge, are required in order to remove finely suspended insoluble material present in the reaction mixture.

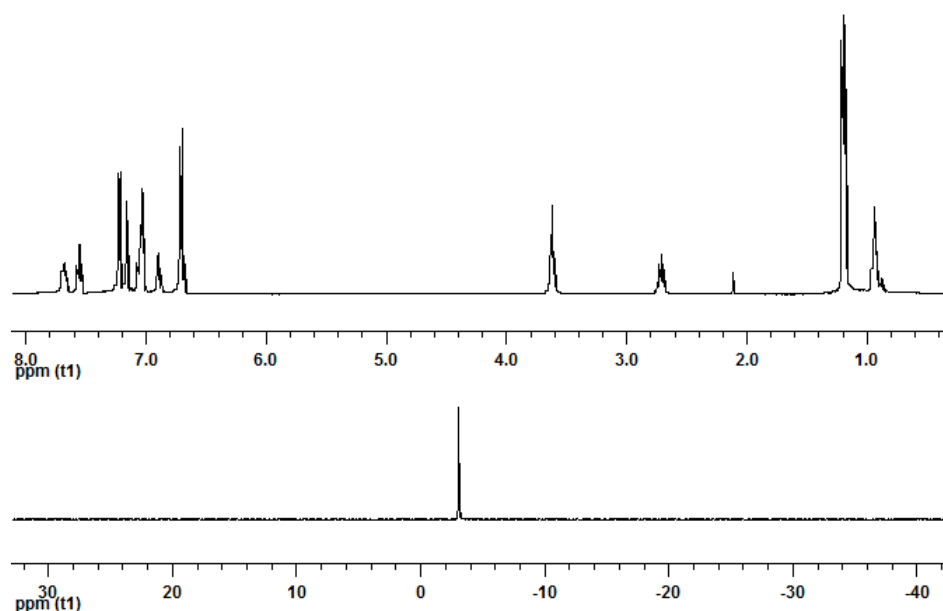


Figure 128: ³¹P{¹H} (bottom) and ¹H NMR (top) spectra of [^{iprop}NPNZr(THF)]₂(μ-η²:η²-N₂) [**5.1**]

The ³¹P{¹H} NMR spectra for [^{iprop}NPNZr(THF)]₂(μ-η²:η²-N₂) [**5.1**] and [^{tol}NPNZr(THF)]₂(μ-η²:η²-N₂) [**5.3**] display peaks at δ -3.05 and δ -3.93, respectively (Figure 128 and Figure 129), which are upfield compared to that reported for the [^{mes}NPNZr(THF)]₂(μ-η²:η²-N₂) complex at δ 5.0^{92, 125} and closer to that reported for the [^{Si}NPNZr(THF)]₂(μ-η²:η²-N₂) complex at -5.57.¹³⁸ This may indicate that the phosphorus atoms are less strongly bound to the zirconium atom in the sterically less hindered ^{iprop}NPN and ^{tol}NPN donor sets relative to ^{mes}NPN (as well as ^{Si}NPN, which contains unsubstituted phenyl groups). The new complexes [**5.1**] and

[**5.3**] are purple in colour, as was also observed for [$^{Si}NPNZr(THF)_2(\mu-\eta^2:\eta^2-N_2)$], rather than the blue-green colour reported for [$^{mes}NPNZr(THF)_2(\mu-\eta^2:\eta^2-N_2)$].

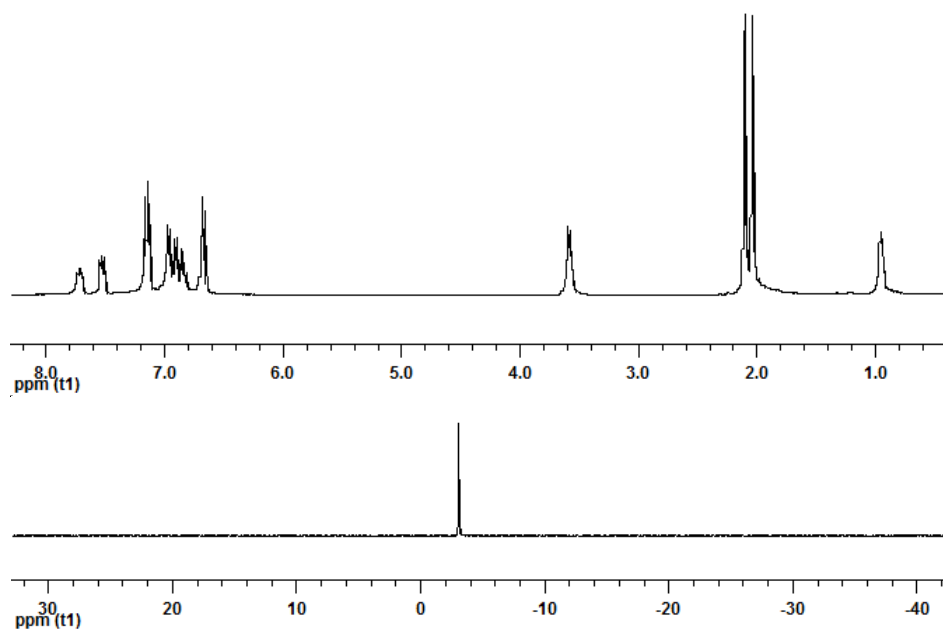


Figure 129: $^{31}P\{^1H\}$ (bottom) and 1H NMR (top) spectra of [$^{tob}NPNZr(THF)_2(\mu-\eta^2:\eta^2-N_2)$] [**5.3**]

It was not possible to obtain the parent ion for [**5.1**] or [**5.3**] with electron impact mass spectrometry, however, a fragment ion $[M - 2THF]^+$ for [$^{iprop}NPNZr(THF)_2(\mu-\eta^2:\eta^2-N_2)$] [**5.1**] was observed at 1264 m/z using Matrix-Assisted Laser Desorption / Ionisation (MALDI) mass spectrometry with a 2-amino-4-methyl-5-nitropyridine matrix. A mass spectrum (EI) of the product of [**5.1**] with 4,4'-dimethylbenzophenone (see chapter 6) also displayed fragment ions at 1264 m/z and 1249 m/z, indicating the dinitrogen complex [$^{iprop}NPNZr]_2(N_2)$ and less one N atom [$^{iprop}NPNZr]_2(N)$.

Unlike previously prepared [$^{mes}NPNZr(THF)_2(\mu-\eta^2:\eta^2-N_2)$], the THF in complexes [**5.1**] and [**5.3**] are not labile under reduced pressure. Their 1H NMR spectra display THF signals at δ 3.62 and δ 0.93 for [**5.1**] and at δ 3.58 and δ 0.93 for [**5.3**] (Figure 128 and Figure 129). For

comparison, these signals are reported for $[\text{mesNPNZr(THF)}]_2(\mu\text{-}\eta^2\text{:}\eta^2\text{-N}_2)$ to be not significantly different from free THF at δ 3.54 and δ 1.69. This would indicate that THF is more strongly bound to zirconium in the sterically less hindered ipropNPN and tolNPN dinitrogen complexes [5.1] and [5.3]. Similarly, the $[\text{SiNPNZr(THF)}]_2(\mu\text{-}\eta^2\text{:}\eta^2\text{-N}_2)$ complex displays THF signals at δ 3.21 and δ 0.55, which may also reflect a less labile THF group.

The mechanism for the formation of these zirconium dinitrogen complexes is not well established. Being a one electron reductant, reaction of KC_8 with zirconium dichloride precursors $\text{NPNZrCl}_2(\text{THF})$ may result in a Zr(III) species NPNZrCl(THF)_n (Figure 130). Reduction of related $\text{PNPZrCl}_2\text{Cp}$ with the one-electron reductant Na/Hg led to the isolation of a Zr(III) species.^{315, 316} A Zr(III) species may be stable enough to react further with more KC_8 to form a Zr(II) species NPNZr(THF)_n , or another possibility is that the Zr(III) species disproportionates to reform the precursor Zr(IV) species $\text{NPNZrCl}_2(\text{THF})_n$ and a Zr(II) species NPNZr(THF)_n .

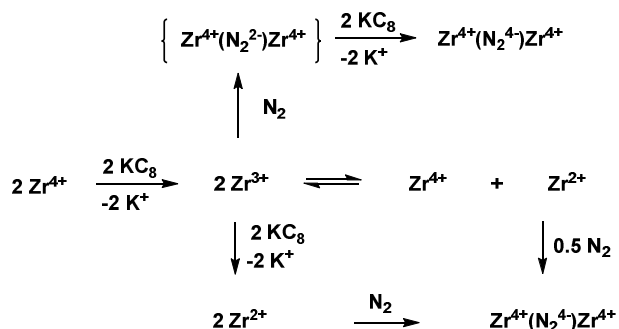


Figure 130: Potential mechanism for the formation of zirconium dinitrogen complexes

A Zr(III) species may conceivably reduce N_2 to form an intermediate dinuclear $[\text{NPNZrCl(THF)}_n]_2(\text{N}_2^{2-})$ complex, which would have to undergo another one-electron reduction event with 2 equiv of KC_8 to lead to the experimentally observed $[\text{NPNZr(THF)}]_2(\text{N}_2^{4-})$ complex. Alternatively, N_2 may be reduced directly by a Zr(II) species to form $[\text{NPNZr(THF)}]_2(\text{N}_2^{4-})$. Assuming that reduction of Zr(IV) to a Zr(III) species is easier than Zr(III) to a Zr(II) species, then complete consumption of Zr(IV) is expected after reaction of

$^{\text{iprop}}\text{NPNZrCl}_2(\text{THF})$ [3.5] with 1 equiv of KC_8 if no disproportionation of Zr(III) occurs. The fact that greater than 40% $^{\text{iprop}}\text{NPNZrCl}_2(\text{THF})$ [3.5] was recovered from a reaction with 1 equiv of KC_8 may add some credence to the proposal that disproportionation of a Zr(III) species occurs and that a Zr(II) species may be implicated in the reduction of N_2 .

The success of this reduction reaction depends on efficient intimate contact between insoluble KC_8 and dissolved zirconium dichloride species, with sufficient gas-liquid interface in order to promote solubility of N_2 . For example, when stirring is arrested during the early stages of the reaction, a purple solid was obtained that displayed a single peak at δ -9.64 in the $^{31}\text{P}\{^1\text{H}\}$ NMR spectrum and the ^1H NMR spectrum displayed very broad signals which may indicate the presence of a reduced paramagnetic zirconium species. When the reduction was conducted in the absence of N_2 , a dark brown-purple solid was obtained that displayed no signal in the $^{31}\text{P}\{^1\text{H}\}$ NMR spectrum and also had broad signals in the ^1H NMR spectrum. The filtrate residue indicated that some of the desired $[\text{ipropNPNZr}(\text{THF})]_2(\mu\text{-}\eta^2\text{:}\eta^2\text{-N}_2)$ [5.1] complex did form post-reduction, albeit in a mixture with other side-products. Side-reactions may involve reactions of the reduced zirconium species with the solvent or the ancillary ligand. For example, the reduction of $\text{P}_2\text{N}_2\text{ZrCl}_2$ with KC_8 led to activation of the phenyl rings of the ligand.³¹⁷ The C-O cleavage of the THF solvent³¹⁸ could presumably lead to butoxy complexes.

As the outcome from this current reduction reaction procedure is somewhat unreliable and was difficult to scale up, it was problematic to produce a sufficiently large quantity of dinitrogen complex from which a series of reactivity studies could be conducted. It was therefore attempted to perform the reduction in a high pressure vessel with a more efficient mechanical stirrer. The poor solubility of N_2 in hydrocarbon based solvents can be increased with increasing the N_2 pressure³¹⁹⁻³²¹ and better stirring would enhance the solid-liquid-gas interface. A glass lined 600 cm^3 Parr reactor was used with the N_2 pressure regulated at 600 psi. The N_2 was purified through a pre-column packed with activated molecular sieves and a copper catalyst. In

order to ensure that mixing between the solid KC_8 and dissolved precursor zirconium dichloride only occurred after the introduction of N_2 , the KC_8 was sealed in a glass ampoule which would break on the initiation of stirring after the reactor was pressurised to 600 psi N_2 (Figure 131).

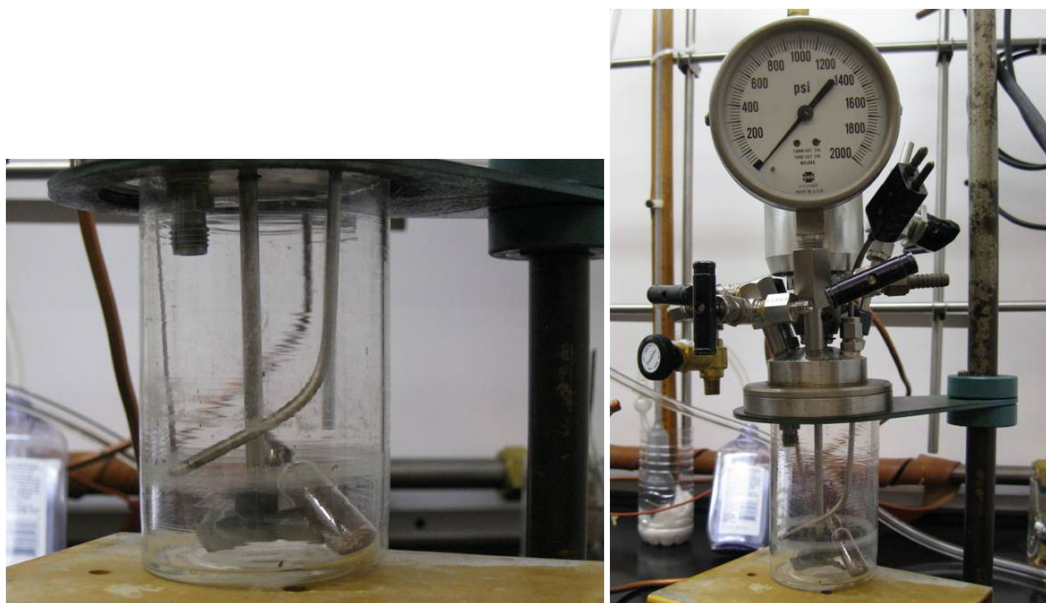


Figure 131: Experimental set-up of the glass liner for the Parr reactor with the KC_8 ampoule

In a controlled experiment with an empty sealed ampoule, a purple solution of $[\text{ipropNPNZr}(\text{THF})_2(\mu\text{-}\eta^2\text{:}\eta^2\text{-N}_2)]$ **[5.1]** was subjected to 600 psi N_2 . The solution exhibited no observable colour change and no ipropNPNH_2 **[2.10]** was detected, further indicating that the experimental conditions were anaerobic. The $^{31}\text{P}\{^1\text{H}\}$ NMR spectrum displayed a single peak at δ 1.56, slightly downfield shifted of what is usually observed for **[5.1]**. The reduction of a zirconium dichloride solution at 600 psi N_2 did not yield the desired dinitrogen complex **[5.1]** (see experimental details). One complication of the high-pressure experimental set-up as described above is that minimum immersion of the liquid in the mechanical stirrer required five times (50 cm^3) the volume THF used in the conventional 4 atm N_2 reductions. The 600 psi N_2 reduction had been performed at a significantly lower concentration (0.2 g in 50 cm^3 THF) and a subsequent control experiment performed with a similar lower concentration at 4 atm N_2 yielded

a complex mixture of products. A reaction with *ca* 1.5 g zirconium dichloride at 600 psi was not attempted.

Single crystals of $[\text{ipropNPNZr(THF)}]_2(\mu\text{-}\eta^2\text{:}\eta^2\text{-N}_2)$ **[5.1]** were obtained to reveal a dizirconium structure with a bridging side-on N_2 unit (Figure 132). The N1-N1a bond length at 1.542(4) Å is longer than the N-N bond length in hydrazine (1.47 Å) and can be considered a N_2^{4-} hydrazido unit (free N_2 is 1.0975(2) Å).¹²⁵ The bond lengths for side-on dinitrogen transition metal complexes range from 1.088(12) Å to 1.635(5) Å.^{125, 144} and complex **[5.1]** can be considered to contain a strongly activated N_2 ligand. The N1-N1a bond length for **[5.1]** is longer than those reported for $[\text{mesNPNZr(THF)}]_2(\mu\text{-}\eta^2\text{:}\eta^2\text{-N}_2)$,^{92, 97} $[\text{CY5NPN}^{\text{DMP}}\text{Zr(THF)}]_2(\mu\text{-}\eta^2\text{:}\eta^2\text{-N}_2)$,^{139, 140} $[\text{SiNPNZr(THF)}]_2(\mu\text{-}\eta^2\text{:}\eta^2\text{-N}_2)$ ^{137, 138} (see Table 23) and $[(\eta^5\text{-C}_5\text{Me}_4\text{H})\text{Zr}]_2(\mu\text{-}\eta^2\text{:}\eta^2\text{-N}_2)$ (1.377(3) Å)⁹³ and corresponds with that reported for $[\text{PNPZrCl}]_2(\mu\text{-}\eta^2\text{:}\eta^2\text{-N}_2)$ at 1.548(7) Å.¹³⁵ Two of the Zr-N bond lengths (Zr-N1 and Zr1a-N1a) for **[5.1]** are longer than the remaining two (Zr-N1a and Zr1a-N1), and all are shorter than those observed for $[\text{mesNPNZr(THF)}]_2(\mu\text{-}\eta^2\text{:}\eta^2\text{-N}_2)$.

The geometry about the zirconium centre can be considered distorted pseudo-trigonal bipyramidal, with the oxygen atom of the THF and the phosphorus atom of the NPN donor set positioned axially and the two N atoms of the NPN donor set and the centroid of the N_2^{4-} unit occupying the equatorial positions. The trigonal angles between the N atoms of the NPN donor set and the N_2^{4-} unit range from 111.37(11)° to 123.30(12)°. The pseudo-axial P-Zr-O angle of one of the zirconium centres is more distorted than the other (136.87(7)° compared to 141.63(7)°). The NPN donor sets are coordinated facially to the zirconium centres, and form a *trans*-dinuclear structure. The N-N axis of the N_2^{4-} unit occupies the same planes that contain the P-Zr-O axes and is perpendicular to the plane containing the N atoms of the NPN donor set.

The two N8-Zr1-N8a and N8b-Zr1a-N8c bite angles for $[\text{ipropNPNZr(THF)}]_2(\mu\text{-}\eta^2\text{:}\eta^2\text{-N}_2)$ **[5.1]** differ ($116.84(11)^\circ$ and $120.97(11)^\circ$) and as expected, both are wider compared to the more bulky $[\text{mesNPNZr(THF)}]_2(\mu\text{-}\eta^2\text{:}\eta^2\text{-N}_2)$ complex ($111.84(12)^\circ$). The smaller of the two angles (N8b-Zr1a-N8c) is comparable those reported for the zirconium N_2 complexes with silyl-methylene and cyclopentenyl bridges (Table 23). The P-Zr-N8 NPN bite angles for **[5.1]** and $[\text{mesNPNZr(THF)}]_2(\mu\text{-}\eta^2\text{:}\eta^2\text{-N}_2)$ have the typical values observed for the *o*-phenylene ligands ($69.91(8)^\circ$ to $73.72(8)^\circ$), are comparable to those for the $[\text{CY}^5\text{NPN}^{\text{DMP}}\text{Zr(THF)}]_2(\mu\text{-}\eta^2\text{:}\eta^2\text{-N}_2)$ complex with a cyclopentenyl bridge ($74.29(5)^\circ$ to $74.63(6)^\circ$) and all are more acute compared to the $[\text{SiNPNZr(THF)}]_2(\mu\text{-}\eta^2\text{:}\eta^2\text{-N}_2)$ complex with a silyl-methylene bridge ($76.62(6)^\circ$ to $77.15(5)^\circ$).

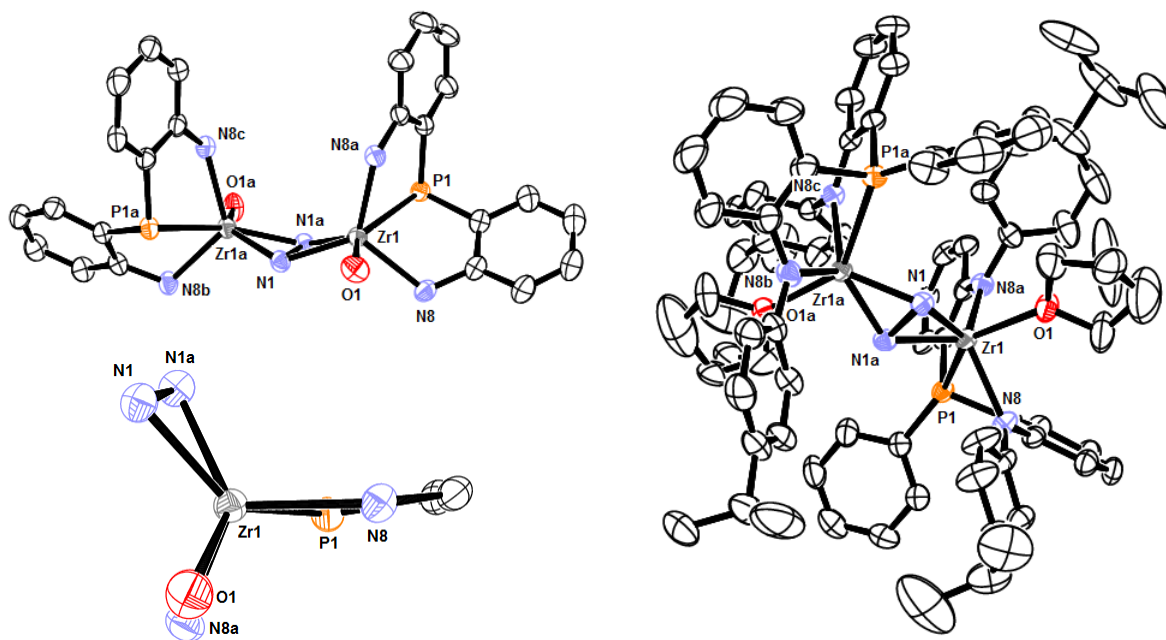


Figure 132: ORTEP representation of the solid state molecular structure of $[\text{ipropNPNZr(THF)}]_2(\mu\text{-}\eta^2\text{:}\eta^2\text{-N}_2)$ **[5.1]**

The Zr-P bond lengths for **[5.1]** are longer than for $[\text{mesNPNZr(THF)}]_2(\mu\text{-}\eta^2\text{:}\eta^2\text{-N}_2)$, which supports the upfield shift observed in the $^{31}\text{P}\{^1\text{H}\}$ NMR spectrum and a weaker Zr-P bond. The Zr-O bond lengths for **[5.1]** are shorter compared to $[\text{mesNPNZr(THF)}]_2(\mu\text{-}\eta^2\text{:}\eta^2\text{-N}_2)$, which corroborates physical observations and ^1H NMR spectroscopic data that the THF is more strongly

bound in the dinitrogen complexes with the less sterically hindered ^{iprop}NPN and ^{tol}NPN donor sets compared to the ^{mes}NPN donor set.

Table 23 : Selected bond lengths (Å) and angles (°) for [^{iprop}NPNZr(THF)]₂(μ-η²:η²-N₂) [5.1] compared to [^{mes}NPNZr(THF)]₂(μ-η²:η²-N₂), [^{Si}NPNZr(THF)]₂(μ-η²:η²-N₂) and [^{CY5}NPN^{DMP}Zr(THF)]₂(μ-η²:η²-N₂)

| | ^{iprop} NPN [5.1] | ^{mes} NPN | ^{Si} NPN | ^{CY5} NPN ^{DMP} |
|--------------|----------------------------|--------------------|-------------------|-----------------------------------|
| N1-N1a | 1.542(4) | 1.505(6) | 1.503(3) | 1.508(4) |
| Zr1-N1 | 2.056(3) | 2.090(3) | 2.069(2) | 2.071(2) |
| Zr1-N1a | 2.015(3) | 2.023(3) | 2.026(2) | 2.020(2) |
| Zr1a-N1 | 2.029(3) | | | |
| Zr1a-N1a | 2.053(3) | | | |
| Zr1-P1 | 2.6852(10) | 2.6776(10) | 2.6685(5) | 2.7133(7) |
| Zr1a-P1a | 2.6859(10) | | | |
| Zr1-O1 | 2.284(3) | 2.370(2) | 2.305(1) | 2.3476(17) |
| Zr1a-O1a | 2.265(3) | | | |
| Zr1-N8 | 2.203(3) | 2.185(3) | 2.175(2) | 2.233(2) |
| Zr1-N8a | 2.202(3) | 2.226(3) | 2.228(2) | 2.190(2) |
| Zr1a-N8b | 2.210(3) | | | |
| Zr1a-N8c | 2.175(3) | | | |
| Zr...Zr | 3.610(4) | 3.800(6) | | |
| N1-Zr1-N1a | 44.52(11) | 42.88(16) | 43.04(8) | 43.25(10) |
| N1-Zr1a-N1a | 44.40(11) | | | |
| Zr1-N1-Zr1a | 124.21(13) | | | |
| Zr1-N1a-Zr1a | 125.07(14) | 134.97(16) | 136.96(8) | 136.75(10) |
| P1-Zr1-O1 | 136.87(7) | 154.12(7) | 149.24(4) | 152.24(5) |
| P1a-Zr1a-O1a | 141.63(7) | | | |
| P1-Zr1-N1a | 93.53(8) | 81.98(9) | 80.73(5) | 82.57(6) |
| P1a-Zr1a-N1 | 89.28(8) | | | |
| P1-Zr1-N1 | 137.66(8) | 124.31(9) | 123.68(4) | 125.31(6) |
| P1a-Zr1a-N1a | 133.29(8) | | | |
| P1-Zr1-N8 | 72.35(8) | 71.85(8) | 76.62(5) | 74.63(6) |
| P1-Zr1-N8a | 69.91(8) | 73.38(8) | 77.15(5) | 74.29(5) |
| P1a-Zr1a-N8b | 73.72(8) | | | |
| P1a-Zr1a-N8c | 71.39(8) | | | |
| O1-Zr1-N1 | 85.45(10) | 80.99(11) | 87.08(5) | 82.05(7) |
| O1a-Zr1a-N1a | 85.08(11) | | | |
| O1a-Zr1a-N1 | 128.86(11) | | | |
| O1-Zr1-N1a | 129.41(10) | 121.99(11) | 129.95(6) | 123.62(7) |
| O1-Zr1-N8 | 86.22(11) | 102.88(10) | 89.88(6) | 99.80(7) |
| O1-Zr1-N8a | 91.72(10) | 85.95(10) | 84.90(5) | 84.39(7) |
| O1a-Zr1a-Nb | 85.55(11) | | | |
| O1a-Zr1a-Nc | 90.86(10) | | | |
| N8-Zr1-N8a | 120.97(11) | 111.84(12) | 116.84(6) | 115.70(8) |
| N8b-Zr1a-N8c | 116.84(11) | | | |
| N8-Zr1-N1 | 121.82(11) | 117.55(12) | 117.75(6) | 116.92(8) |
| N8-Zr1-N1a | 111.37(11) | 114.08(12) | 114.07(6) | 112.90(9) |
| N8a-Zr1-N1 | 116.75(11) | 130.54(12) | 124.70(6) | 129.59(8) |
| N8a-Zr1-N1a | 114.62(11) | 116.59(12) | 116.77(6) | 114.38(9) |
| N8b-Zr1a-N1 | 112.93(11) | | | |
| N8b-Zr1a-N1a | 123.30(12) | | | |
| N8c-Zr1a-N1 | 117.40(11) | | | |
| N8c-Zr1a-N1a | 119.09(11) | | | |

Of the amido-phosphine based zirconium side-on dinitrogen complexes, some of the solid state molecular structures reveal Zr_2N_2 cores that are planar i.e. $[\text{PNPZrCl}]_2(\mu\text{-}\eta^2\text{:}\eta^2\text{-N}_2)$,¹³⁵ $[\text{P}_2\text{N}_2]\text{Zr}(\mu\text{-}\eta^2\text{:}\eta^2\text{-N}_2)$,^{137, 322} $[\text{Si}^\text{NPNZr}(\text{THF})]_2(\mu\text{-}\eta^2\text{:}\eta^2\text{-N}_2)$, $[\text{Si}^\text{NPNZr}(\text{Py})]_2(\mu\text{-}\eta^2\text{:}\eta^2\text{-N}_2)$,^{137, 138} and $[\text{CY}^\text{NPN}^\text{DMP}\text{Zr}(\text{THF})]_2(\mu\text{-}\eta^2\text{:}\eta^2\text{-N}_2)$ ^{139, 140} and some display a butterfly distortion i.e. $[\text{PNPZr}(\text{O-2,6-Me}_2\text{C}_6\text{H}_3)]_2(\mu\text{-}\eta^2\text{:}\eta^2\text{-N}_2)$,¹³⁶ $[\text{mes}^\text{NPNZr}(\text{THF})]_2(\mu\text{-}\eta^2\text{:}\eta^2\text{-N}_2)$, $[\text{mes}^\text{NPNZr}(\text{Py})]_2(\mu\text{-}\eta^2\text{:}\eta^2\text{-N}_2)$ and $[\text{mes}^\text{NPNZr}(\text{PPhMe}_2)](\mu\text{-}\eta^2\text{:}\eta^2\text{-N}_2)[\text{mes}^\text{NPNZr}]^{92, 97}$ with a hinge angle between the ZrN_2 planes determined to be 156.2° , 166.0° , 168° and 165° , respectively. While not observed in the solid state, a DFT calculation for a model compound of $[\text{P}_2\text{N}_2]\text{Zr}(\mu\text{-}\eta^2\text{:}\eta^2\text{-N}_2)$ determined that a butterfly distortion of the Zr_2N_2 core with a hinge angle of 147.8° ($-11.2 \text{ kcal.mol}^{-1}$) is a probable structure for $[\text{P}_2\text{N}_2]\text{Zr}(\mu\text{-}\eta^2\text{:}\eta^2\text{-N}_2)$ and may have been observed in solution with Raman spectroscopy.¹⁴¹ The solid state molecular structure of $[\text{iprop}^\text{NPNZr}(\text{THF})]_2(\mu\text{-}\eta^2\text{:}\eta^2\text{-N}_2)$ **[5.1]** also displays butterfly distortion of the Zr_2N_2 core with a hinge angle between the ZrN_2 planes of 146.9° , which allows for a shorter $\text{Zr}\cdots\text{Zr}$ internuclear distance compared to the more bulky $[\text{mes}^\text{NPNZr}(\text{THF})]_2(\mu\text{-}\eta^2\text{:}\eta^2\text{-N}_2)$ complexes. The N1-Zr-N1a (and N1-Zr1a-N1a) angles for **[5.1]** is also larger compared to $[\text{mes}^\text{NPNZr}(\text{THF})]_2(\mu\text{-}\eta^2\text{:}\eta^2\text{-N}_2)$, in keeping with the longer N-N bond distance.

As only a single peak is observed in the $^{31}\text{P}\{^1\text{H}\}$ NMR spectrum of solvated $[\text{iprop}^\text{NPNZr}(\text{THF})]_2(\mu\text{-}\eta^2\text{:}\eta^2\text{-N}_2)$ **[5.1]**, a C_{2h} symmetry may be present in the solution phase with a mirror plane passing through a “planar” Zr_2N_2 core with perfectly symmetric NPN donor sets on the two different zirconium centres. In solution, the Zr_2N_2 core of complex **[5.1]** thus either no longer displays the butterfly distortion, or is inter-converting rapidly about the $\text{Zr}\cdots\text{Zr}$ axis on a timescale unobservable via NMR spectroscopy. A solution of $[\text{tol}^\text{NPNZr}(\text{THF})]_2(\mu\text{-}\eta^2\text{:}\eta^2\text{-N}_2)$ **[5.3]** in toluene- d_8 was cooled down to -95°C , with no observable change in the singlet in the $^{31}\text{P}\{^1\text{H}\}$ NMR spectrum.

In order to unambiguously verify that the source of the N_2^{4-} unit in **[5.1]** and **[5.3]** was molecular N_2 , a reduction was conducted with $^{15}\text{N}_2$. $[\text{ipropNPNZr}(\text{THF})]_2(\mu-\eta^2:\eta^2-^{15}\text{N}_2)$ **[5.2]** was isolated as a purple solid in 68% yield; no exchange of coordinate $^{15}\text{N}_2$ in **[5.2]** with $^{14}\text{N}_2$ was observed, even after storage in solid form under an N_2 atmosphere for 3 years. A singlet is observed in the $^{31}\text{P}\{^1\text{H}\}$ NMR spectrum at δ -3.07 and in the $^{15}\text{N}\{^1\text{H}\}$ NMR spectrum at δ 88.54 (relative to MeNO_2 at δ 0). The ^{15}N chemical shift values reported for side-on dinitrogen transition metal complexes range from δ -30.6 to δ 689.7¹²⁵ and for $[\text{mesNPNZr}(\text{THF})]_2(\mu-\eta^2:\eta^2-^{15}\text{N}_2)$ at δ 116.6 ($^2J_{\text{PN}} = 6.7$ Hz).^{92, 97} It is unclear why no $^2J_{\text{PN}}$ coupling was observed for **[5.2]**.

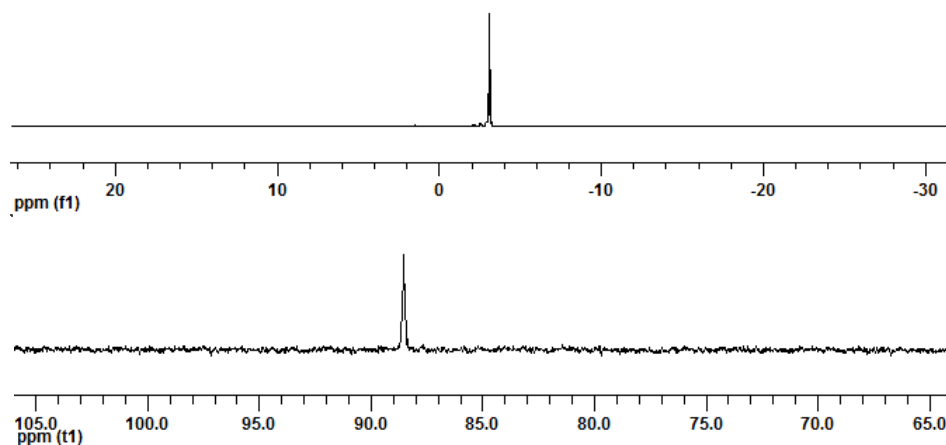


Figure 133: $^{31}\text{P}\{^1\text{H}\}$ and $^{15}\text{N}\{^1\text{H}\}$ NMR spectra for $[\text{ipropNPNZr}(\text{THF})]_2(\mu-\eta^2:\eta^2-^{15}\text{N}_2)$ **[5.2]** in C_6D_6

Inspection of the infrared spectra of $[\text{ipropNPNZr}(\text{THF})]_2(\mu-\eta^2:\eta^2-\text{N}_2)$ **[5.1]** overlaid with the $^{15}\text{N}_2$ isotopomer **[5.2]** reveals a shift in a peak at 625 cm^{-1} for **[5.1]** by -18 cm^{-1} to 607 cm^{-1} for **[5.2]** (Figure 134).

Detailed vibration spectroscopy studies have revealed that five in-plane modes (Figure 135) can be expected for a Zr_2N_2 core, three being Raman-active ($2 \times \text{A}_g$ and B_{1g}) and two being IR-active (B_{2u} and B_{3u}).¹⁴¹ Raman and infrared spectra for $[\text{P}_2\text{N}_2]_2\text{Zr}$ and its $^{15}\text{N}_2$ isotopomer were used to determine the frequencies of the $\text{A}_g(\text{N-N})$, $\text{A}_g(\text{Zr-Zr})$, B_{2u} and B_{3u} stretches to be 775, 295, 441 and 690 cm^{-1} , respectively, and the $\text{B}_{1g}(\text{ZrN})$ stretch was predicted with DFT calculations to occur at $600\text{-}700 \text{ cm}^{-1}$ with an isotope shift of 20 cm^{-1} . The peak observed at 625 cm^{-1} for $[\text{ipropNPNZr}(\text{THF})]_2(\mu\text{-}\eta^2\text{:}\eta^2\text{-N}_2)$ **[5.1]** in the infrared spectrum with an observed 18 cm^{-1} isotopomer shift could tentatively be assigned as the B_{3u} stretch. In a different infrared study of laser-ablated Zr atoms with excess N_2 , a line at 675.2 cm^{-1} for a rhombic $\text{Zr}(\mu\text{-N})_2\text{Zr}$ species was assigned as the b_{2u} stretch.³²³

Detailed vibration spectroscopy studies have revealed that five in-plane modes (Figure 135) can be expected for a Zr_2N_2 core, three being Raman-active ($2 \times \text{A}_g$ and B_{1g}) and two being IR-active (B_{2u} and B_{3u}).¹⁴¹ Raman and infrared spectra for $[\text{P}_2\text{N}_2]_2\text{Zr}$ and its $^{15}\text{N}_2$ isotopomer were used to determine the frequencies of the $\text{A}_g(\text{N-N})$, $\text{A}_g(\text{Zr-Zr})$, B_{2u} and B_{3u} stretches to be 775, 295, 441 and 690 cm^{-1} , respectively, and the $\text{B}_{1g}(\text{ZrN})$ stretch was predicted with DFT calculations to occur at $600\text{-}700 \text{ cm}^{-1}$ with an isotope shift of 20 cm^{-1} . The peak observed at 625 cm^{-1} for $[\text{ipropNPNZr}(\text{THF})]_2(\mu\text{-}\eta^2\text{:}\eta^2\text{-N}_2)$ **[5.1]** in the infrared spectrum with an observed 18 cm^{-1} isotopomer shift could tentatively be assigned as the B_{3u} stretch. In a different infrared study of laser-ablated Zr atoms with excess N_2 , a line at 675.2 cm^{-1} for a rhombic $\text{Zr}(\mu\text{-N})_2\text{Zr}$ species was assigned as the b_{2u} stretch.³²³

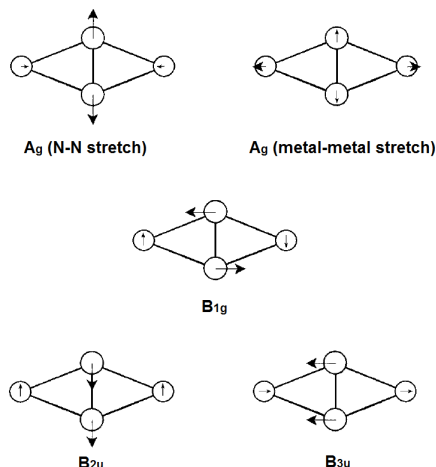


Figure 135: Theoretical vibrational modes for a Zr_2N_2 core¹⁴¹

These d^0 zirconium dinitrogen complexes often form highly coloured complexes. For example $[\text{PNPZrCl}]_2(\mu\text{-}\eta^2\text{:}\eta^2\text{-N}_2)$,¹³⁵ $[\text{PNPZr}(\text{O-2,6-Me}_2\text{C}_6\text{H}_3)]_2(\mu\text{-}\eta^2\text{:}\eta^2\text{-N}_2)$,¹³⁶ $[\text{P}_2\text{N}_2]\text{Zr}(\mu\text{-}\eta^2\text{:}\eta^2\text{-N}_2)$,^{137, 322} and $[\text{CY}^5\text{NPN}^{\text{DMP}}\text{Zr}(\text{THF})]_2(\mu\text{-}\eta^2\text{:}\eta^2\text{-N}_2)$,^{139, 140} forms dark blue complexes, $[\text{PNPZrCp}]_2(\mu\text{-}\eta^2\text{:}\eta^2\text{-N}_2)$ ¹²⁶ forms a dark brown complex, $[\text{SiNPNZr}(\text{THF})]_2(\mu\text{-}\eta^2\text{:}\eta^2\text{-N}_2)$ ^{137, 138} forms a dark purple complex and $[\text{mesNPNZr}(\text{THF})]_2(\mu\text{-}\eta^2\text{:}\eta^2\text{-N}_2)$, $[\text{mesNPNZr}(\text{Py})]_2(\mu\text{-}\eta^2\text{:}\eta^2\text{-N}_2)$ and $[\text{mesNPNZr}(\text{PR}_3)](\mu\text{-}\eta^2\text{:}\eta^2\text{-N}_2)[\text{mesNPNZr}]$ ^{92, 97} form dark blue-green complexes. Similarly, the new zirconium dinitrogen complexes $[\text{ipropNPNZr}(\text{THF})]_2(\mu\text{-}\eta^2\text{:}\eta^2\text{-N}_2)$ **[5.1]** and $[\text{tolNPNZr}(\text{THF})]_2(\mu\text{-}\eta^2\text{:}\eta^2\text{-N}_2)$ **[5.3]** are have an intense purple.

Due to a significant colour difference between the *o*-phenylene bridged NPN zirconium dinitrogen complexes with reduced bulk steric bulk (ipropNPN and tolNPN) compared to those containing mesNPN donor sets, the UV-Vis spectra of $[\text{ipropNPNZr}(\text{THF})]_2(\mu\text{-}\eta^2\text{:}\eta^2\text{-N}_2)$ **[5.1]** were obtained and compared with $\text{mesNPNZr}(\text{THF})]_2(\mu\text{-}\eta^2\text{:}\eta^2\text{-N}_2)$. A ~ 0.074 M toluene solution of $[\text{mesNPNZr}(\text{THF})]_2(\mu\text{-}\eta^2\text{:}\eta^2\text{-N}_2)$ was previously reported to display two bands with λ_{max} at 652 ($\epsilon = 6,100 \text{ dm}^3\cdot\text{mol}^{-1}\cdot\text{cm}^{-1}$) and 358 nm ($\epsilon = 10,000 \text{ dm}^3\cdot\text{mol}^{-1}\cdot\text{cm}^{-1}$).^{92, 97} Two bands with λ_{max} at 530 ($\epsilon = 3,300 \text{ dm}^3\cdot\text{mol}^{-1}\cdot\text{cm}^{-1}$) and 304 nm ($\epsilon = 40,000 \text{ dm}^3\cdot\text{mol}^{-1}\cdot\text{cm}^{-1}$) were obtained for 0.24 mM / 0.024 mM toluene solutions of $[\text{ipropNPNZr}(\text{THF})]_2(\mu\text{-}\eta^2\text{:}\eta^2\text{-N}_2)$ **[5.1]** (Figure 136), which have

significant hypsochromic (or blue) shifts of 122 nm and 54 nm, respectively, relative to $[\text{mesNPNZr(THF)}]_2(\mu\text{-}\eta^2\text{:}\eta^2\text{-N}_2)$.

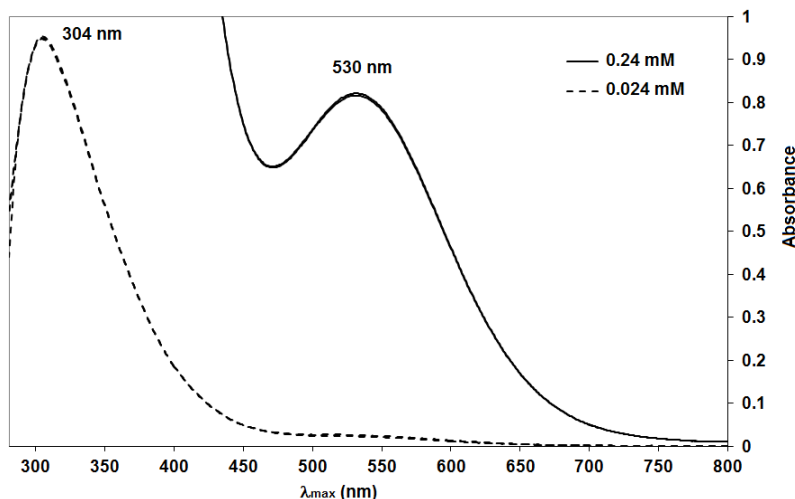


Figure 136: UV-Vis spectra for $[\text{ipropNPNZr(THF)}]_2(\mu\text{-}\eta^2\text{:}\eta^2\text{-N}_2)$ [5.1]

UV-Vis spectra of $[\text{P}_2\text{N}_2]_2(\mu\text{-}\eta^2\text{:}\eta^2\text{-N}_2)$ displayed three bands with λ_{max} at 670 nm, 455 and 390 nm. Being the lowest energy band, λ_{max} at 670 nm was assigned as the HOMO-LUMO transition, which could be considered a $\text{LMCT}_{\text{N}_2 \rightarrow \text{Zr}}$ with the HOMO consisting of a combination of a π_g^* orbital from N_2^{4+} and a zirconium d_{yz} , d_{xy} or d_{xz} orbital (i.e. the Zr- N_2 back-bond) and the LUMO containing an empty d orbital of zirconium. The other two higher energy bands with λ_{max} at 455 and 390 nm would be transitions from the HOMO to higher energy empty zirconium d orbitals.

The blue shifts observed for $[\text{ipropNPNZr(THF)}]_2(\mu\text{-}\eta^2\text{:}\eta^2\text{-N}_2)$ [5.1] may be an indication of larger $\text{LMCT}_{\text{N}_2 \rightarrow \text{Zr}}$ transitions and a stronger back-bond compared to $[\text{mesNPNZr(THF)}]_2(\mu\text{-}\eta^2\text{:}\eta^2\text{-N}_2)$. Such a conclusion would be consistent with a more activated N_2^{4+} unit and correspondingly longer N-N and shorter Zr-N bond lengths (with increased imido character) for [5.1] compared to $[\text{mesNPNZr(THF)}]_2(\mu\text{-}\eta^2\text{:}\eta^2\text{-N}_2)$, as was observed experimentally (see earlier discussion). Such a hypsochromic phenomenon has previously been reported for a hafnocene N_2 complex relative to the zirconocene congener.¹⁰⁵

5.2. Reduction of $^{\text{iprop}}\text{NPNHfCl}_2(\text{THF})$ [3.21] with KC_8 and N_2

The reduction of $^{\text{iprop}}\text{NPNHfCl}_2(\text{THF})$ [3.21] with KC_8 in the presence of N_2 was conducted thrice, yielding a range of yellow to brown solids. For the lighter coloured solids, the $^{31}\text{P}\{^1\text{H}\}$ NMR spectra indicated major peaks at δ -15.12 and δ -3.88 (signals for reduction with $^{\text{mes}}\text{NPNHfI}_2$ reported at δ -10.6, -10.5, -6.9 and -3.1),⁹⁷ with minor peaks at δ -5.67, -5.39, -4.07, 1.05 and 18.52. The presence of only trace quantities of the $^{\text{iprop}}\text{NPNHfCl}_2(\text{THF})$ [3.21] precursor suggests complete reduction occurred. For the brown solid isolated, no signals were observed in $^{31}\text{P}\{^1\text{H}\}$ NMR or EPR spectra.

Mass spectra of these solids contained no peaks indicative of a dinitrogen complex $[\text{ipropNPNHf}(\text{THF})]_2(\text{N}_2)$, expected at 1440 m/z, or an arene bridged $[\text{ipropNPNHf}]_2$ side-product, expected at 1412 m/z. Two prominent peaks at 1416 m/z and 1232 m/z were however observed, which could represent molecular ions for $[\text{ipropNPNHf}]_2(\text{H})_4$ and $[\text{ipropNPN}]_2\text{Hf}$, respectively (Figure 137). No further attempts were made to determine the identity of the major species for this reaction. As the reduction of closely related $^{\text{mes}}\text{NPNHfI}_2$ with Na/Hg amalgam under 1 or 4 atm N_2 had failed to yield a dinitrogen complex, no reduction was attempted with an iodo analogue of [3.21].

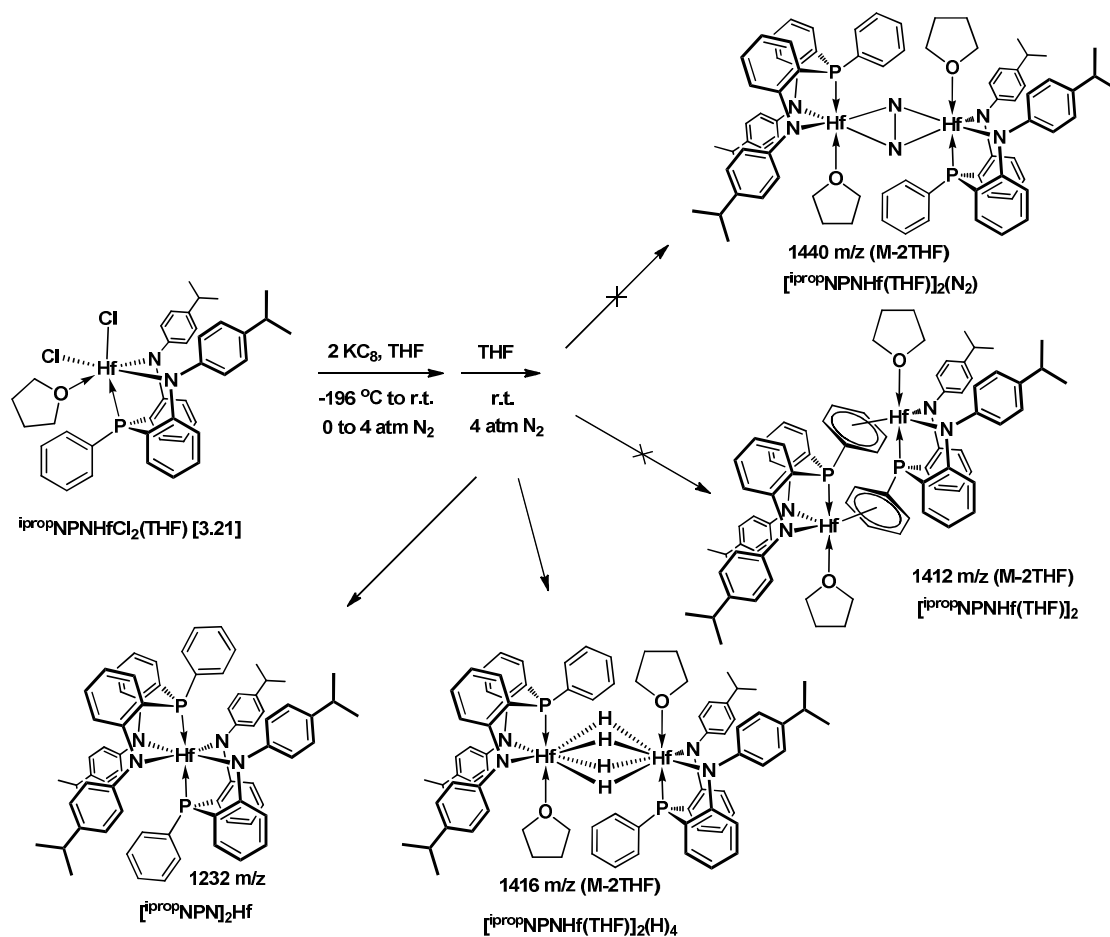


Figure 137: Reduction of $\text{ipropNPNHfCl}_2(\text{THF})$ [3.21] with KC_8 and N_2

5.3. Zirconium Dinitrogen Adducts

An interesting feature of the tridentate diamidophosphine zirconium dinitrogen complexes $[\text{NPNZr}(\text{THF})]_2(\mu\text{-}\eta^2\text{:}\eta^2\text{-N}_2)$ compared to those containing the P_2N_2 donor set (Figure 138) is the ready accessibility of changing the monodentate donor atom from oxygen (THF) to a variety of different donor atoms (such as P, N, S, C), which would alter the electronic structure of the metal atoms, and hence the bonded N_2 unit and reactivity of the dinitrogen complex.

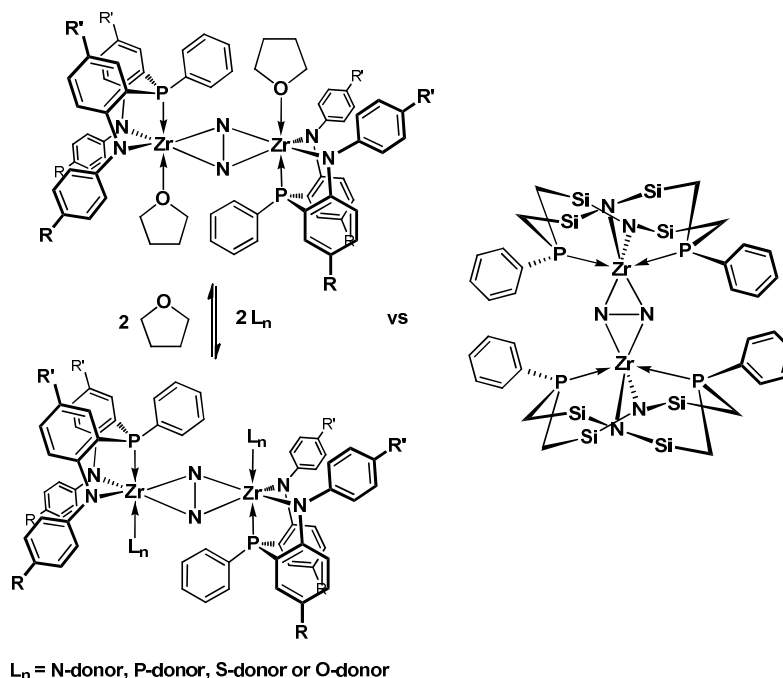


Figure 138: Comparison of zirconium dinitrogen complexes P_2N_2 (silyl methyls omitted for clarity) with $NPN(L_n)$

5.3.1. Nitrogen Atom Donors

5.3.1.1. Pyridine

Pyridine adducts of zirconium dinitrogen complexes with NPN donor sets have previously been prepared, i.e., $[^{Si}NPNZr(Py)]_2(\mu-\eta^2:\eta^2-N_2)^{137}$ and $[^{mes}NPNZr(Py)]_2(\mu-\eta^2:\eta^2-N_2)^{92,97}$. As with their precursor THF adducts, the solid state molecular structures of these pyridine adducts reveal that the former has a planar Zr_2N_2 core and the latter is butterfly distorted (Figure 139). In the case of the ^{Si}NPN containing dinitrogen complexes, the THF was less easily displaced and in solution the THF and pyridine complexes were observed to co-exist, forming a mixed THF /pyridine adduct $[^{Si}NPNZr(Py)](\mu-\eta^2:\eta^2-N_2)[^{Si}NPNZr(THF)]^{137}$

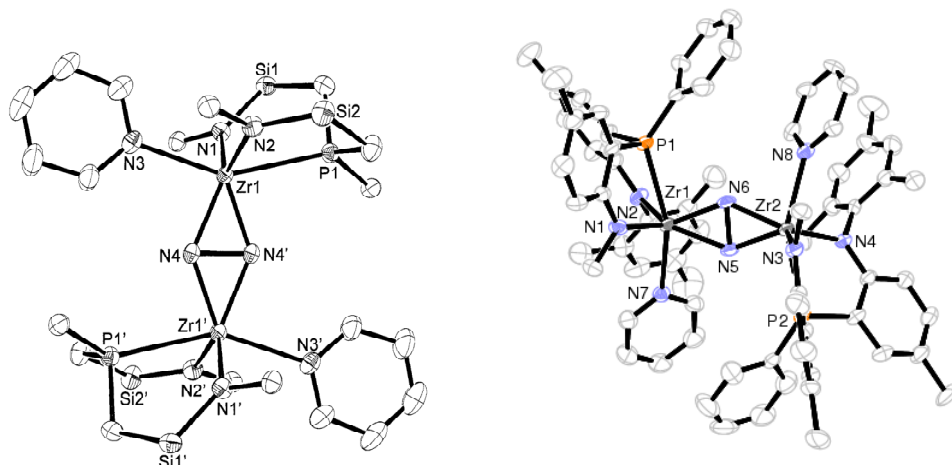


Figure 139: ORTEP representations of the solid state molecular structures of related $[\text{SiNPNZr(Py)}]_2(\mu\text{-}\eta^2\text{:}\eta^2\text{-N}_2)$ ¹³⁷ and $[\text{mesNPNZr(Py)}]_2(\mu\text{-}\eta^2\text{:}\eta^2\text{-N}_2)$ ^{92, 97} complexes

Unlike the pyridine adducts obtained with the ^{Si}NPN and ^{mes}NPN containing zirconium dinitrogen complexes, it was not possible to isolate pyridine adducts of the ^{tol}NPN ligand analogue by adding pyridine to toluene / benzene solutions of the precursor THF adduct $[\text{tolNPNZr(THF)}]_2(\mu\text{-}\eta^2\text{:}\eta^2\text{-N}_2)$ **[5.3]**. In this instance, a colour change from the purple THF adduct to the green pyridine adduct is observed, but complete THF removal was not possible on solvent removal. The green solids $[\text{tolNPNZr(Py)}]_2(\mu\text{-}\eta^2\text{:}\eta^2\text{-N}_2)$ **[5.4]** and $[\text{tolNPNZr(Py-}d_5\text{)}]_2(\mu\text{-}\eta^2\text{:}\eta^2\text{-N}_2)$ **[5.5]** were obtained after dissolution of $[\text{tolNPNZr(THF)}]_2(\mu\text{-}\eta^2\text{:}\eta^2\text{-N}_2)$ **[5.3]** in neat pyridine and pyridine-*d*₅, respectively (Figure 140). Suitable crystals for **[5.4]** and **[5.5]** were not obtained for X-ray crystallographic analysis.

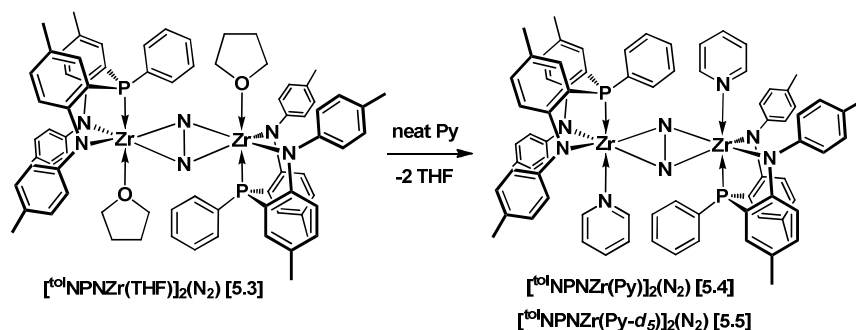


Figure 140: Synthesis of $[\text{tolNPNZr(Py)}]_2(\mu\text{-}\eta^2\text{:}\eta^2\text{-N}_2)$ **[5.4]** and $[\text{tolNPNZr(Py-}d_5\text{)}]_2(\mu\text{-}\eta^2\text{:}\eta^2\text{-N}_2)$ **[5.5]**

The $^{31}\text{P}\{^1\text{H}\}$ NMR spectra of **[5.4]** and **[5.5]** display singlets at δ -4.94 and δ -4.93, respectively (Figure 142). In solution (with excess pyridine), distinct bound and free pyridine signals can be observed in the ^1H NMR spectrum of **[5.4]** which are not visible in the corresponding experiment with pyridine- d_5 **[5.5]** (Figure 142 and Table 24). Representing the bound pyridine are signals at δ 8.81, δ 6.74 and δ 6.33 for *ortho*-H, *para*-H and *meta*-H, respectively. The two broad signals at δ 8.54 and δ 6.65 may represent the *ortho*-H and *meta*-H signals for excess free pyridine (the *para*-H signal may be obscured by ^{101}NPN ligand signals).

Table 24 : ^1H and $^{13}\text{C}\{^1\text{H}\}$ NMR Data for the Py ligand in **[5.4]** and **[5.5]** in C_6D_6

| | <i>ortho</i> -H | <i>meta</i> -H | <i>para</i> -H |
|--|-----------------|----------------|----------------|
| Py (free) | 8.53 | 6.80 | 7.15 |
| $[\text{}^{51}\text{NPNZr}(\text{Py})_2(\mu\text{-}\eta^2\text{:}\eta^2\text{-N}_2)]$ | 8.70 | 5.94 | 6.51 |
| $[\text{}^{101}\text{NPNZr}(\text{Py})_2(\mu\text{-}\eta^2\text{:}\eta^2\text{-N}_2)]$ | 7.12 | 6.00 | 6.55 |
| [5.4] Py (bound) | 8.81(d) | 6.33(t) | 6.74(t) |
| [5.4] Py (free) | 8.54(bs) | 6.65(s) | |
| | <i>ortho</i> -C | <i>meta</i> -C | <i>para</i> -C |
| Py (free) | 150.4 | 123.9 | 135.9 |
| [5.4] Py (bound) | 150.6 | 123.4 | 136.8 |
| [5.4] Py (free) | 150.3 | 123.4 | 135.2 |
| [5.5] Py (bound) | 149.9 | 122.9 | 134.7 |

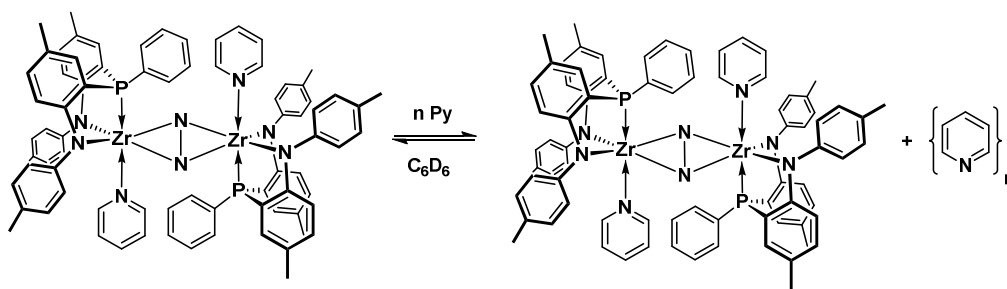


Figure 141: $[\text{}^{101}\text{NPNZr}(\text{Py})_2(\mu\text{-}\eta^2\text{:}\eta^2\text{-N}_2)]$ **[5.4]** with excess pyridine

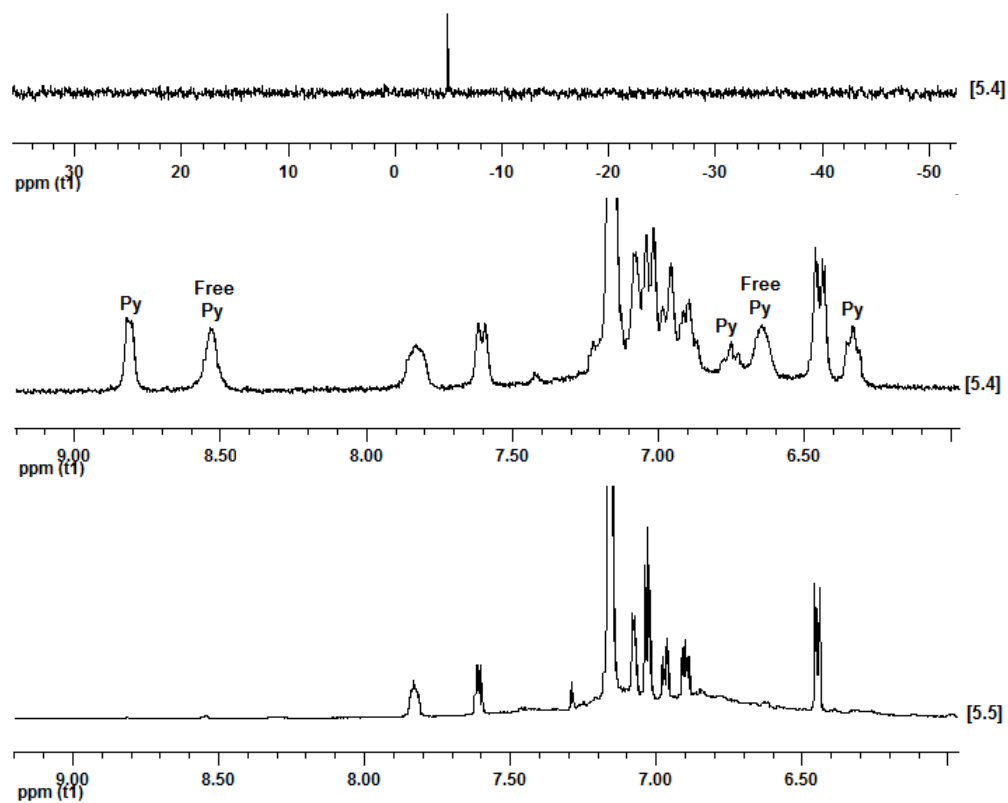


Figure 142: $^{31}\text{P}\{^1\text{H}\}$ NMR (top) spectrum of [5.4] and partial ^1H NMR spectra of [5.4] (middle) and [5.5] (bottom) in C_6D_6

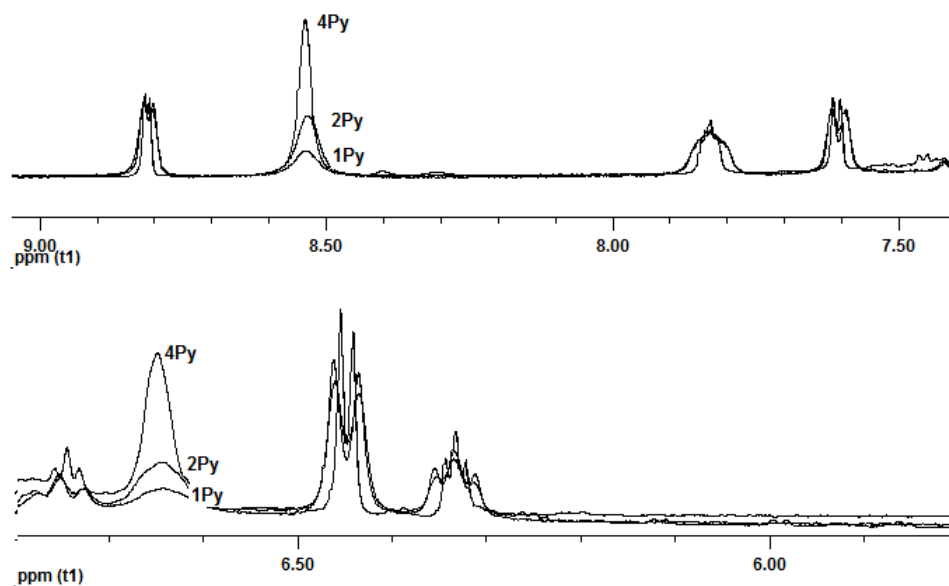


Figure 143: Partial ^1H NMR spectra with variation in free pyridine for $[\text{t}^{01}\text{NPNZr}(\text{Py})_2(\mu\text{-}\eta^2\text{:}\eta^2\text{-N}_2)]$ [5.4] in C_6D_6

Relative integration of the two broad peaks at δ 8.54 and δ 6.65 compared to $[\text{tolNPNZr(Py)}]_2(\mu\text{-}\eta^2\text{:}\eta^2\text{-N}_2)$ **[5.4]** signals varies with the free pyridine content and the *meta*-H signal has shifted upfield compared to a unary solution of pyridine at δ 6.80 (Figure 143 and Figure 141).

5.3.1.2. 4,4'-Bipyridine

In an NMR-scale experiment, addition of *ca* two equiv of 4,4'-bipyridine to $[\text{ipropNPNZr(THF)}]_2(\mu\text{-}\eta^2\text{:}\eta^2\text{-N}_2)$ **[5.1]** in C_6D_6 resulted in a colour change from deep purple (THF adduct) to a dark brown solution, which displayed a single peak in the $^{31}\text{P}\{^1\text{H}\}$ NMR spectrum at δ -4.89 (Figure 144).

A ^1H NMR spectrum (Figure 144) of the solution depicted three peaks for *ortho*-H signals of 4,4'-bipyridine at δ 8.95, 8.63 and 8.57 (free 4,4'-bipyridine at δ 8.59). Each of the former two (δ 8.95 and 8.63) integrate to two protons relative to one $^{\text{iprop}}\text{NPN}$ unit signals, with one of the peaks shifted significantly downfield of free 4,4'-bipyridine. These peaks may represent two inequivalent sets of *ortho*-H signals of 4,4'-bipyridine, one set being bound to zirconium (δ 8.95) and one free (δ 8.63), i.e. $[\text{ipropNPNZr(4,4'-bipy)}]_2(\mu\text{-}\eta^2\text{:}\eta^2\text{-N}_2)$ **[5.6]** (Figure 145). The latter signal (δ 8.57) is indicative of free 4,4'-bipyridine, and this is to be expected as the exact molar ratio was greater than 2 equiv of 4,4'-bipyridine. Signals at δ 1.42 and 3.57 reflect that the THF is free and has been displaced by 4,4'-bipyridine. No further work-up of this experiment was attempted due to the small scale of the test material.

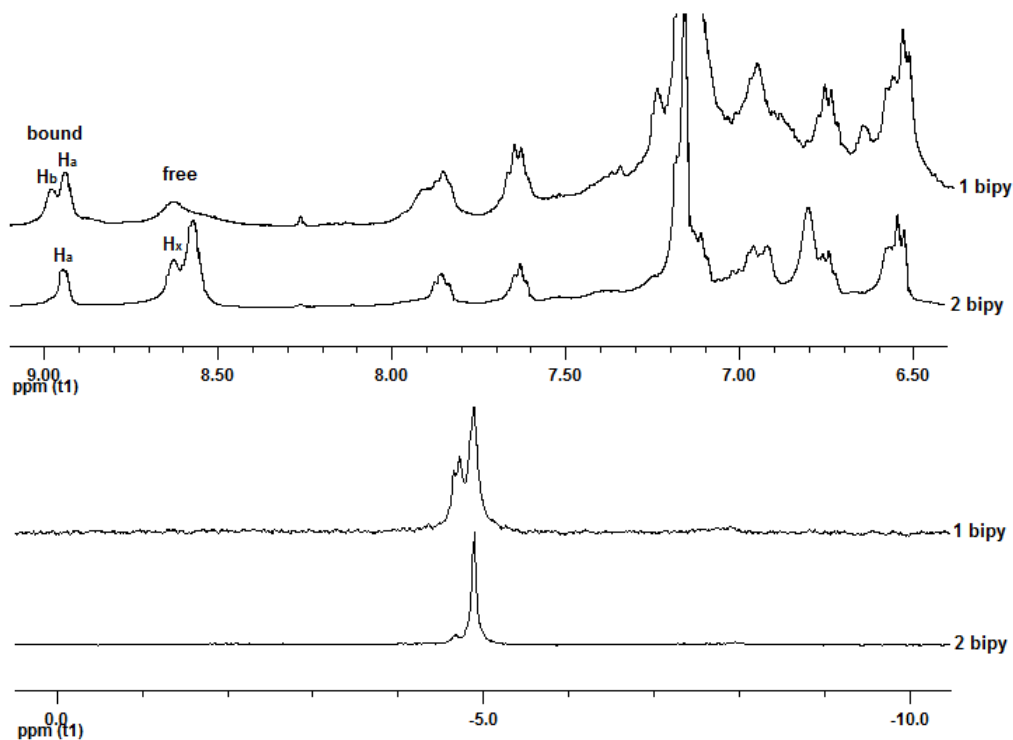


Figure 144: $^{31}\text{P}\{^1\text{H}\}$ NMR (bottom) and partial ^1H NMR (top) spectra of $[\text{ipropNPNZr}(\text{THF})]_2(\mu\text{-}\eta^2\text{-}\eta^2\text{-N}_2)$ [5.1] after 1 and 2 equiv of 4,4'-bipyridine in C_6D_6

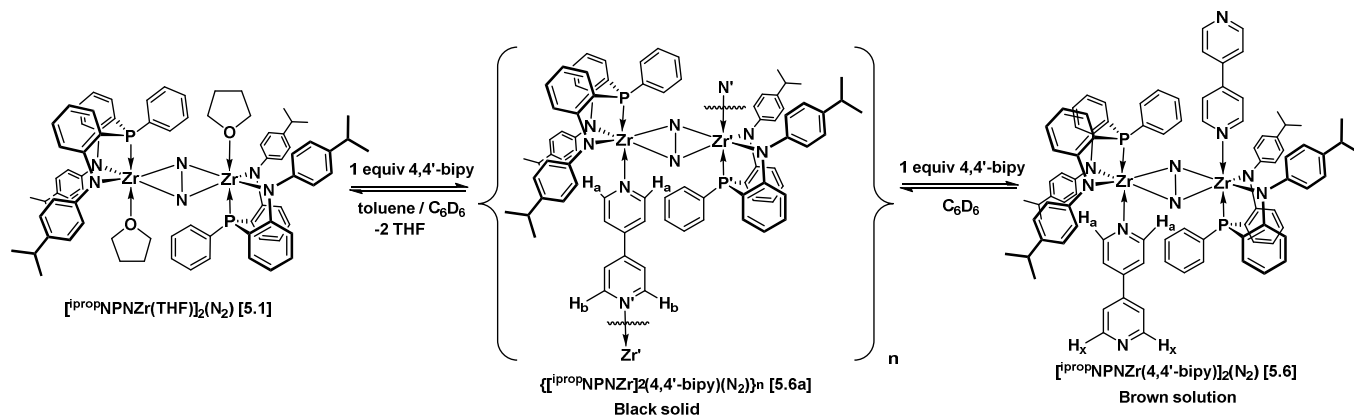


Figure 145: Reaction of $[\text{ipropNPNZr}(\text{THF})]_2(\mu\text{-}\eta^2\text{-}\eta^2\text{-N}_2)$ [5.1] with one and two equiv of 4,4'-bipyridine

A black solid was isolated after addition of one equiv of 4,4'-bipyridine to [5.1] in toluene. The $^{31}\text{P}\{^1\text{H}\}$ NMR spectrum displays a broad signal at δ -4.89 and a doublet at δ -4.68 (Figure 144), suggesting two slightly inequivalent environments for the phosphorus atoms of the

ⁱpropNPN donor sets. The ¹H NMR spectrum displays two downfield shifted signals at δ 8.98 and 8.94 for *ortho*-H signals of bound 4,4'-bipyridine, which may reflect that now both nitrogen atoms are strongly bound to zirconium, albeit one slightly stronger. There was also an absence of THF signals in the ¹H NMR spectrum; hence both THF molecules had been displaced by the one equiv of 4,4'-bipyridine, i.e. $\{[\text{}^{\text{i}}\text{propNPNZr}]_2(4,4'\text{-bipy})(\mu\text{-}\eta^2\text{:}\eta^2\text{-N}_2)\}_n$ [**5.6a**] (Figure 145). Increased steric crowding at the zirconium centre may account for the observed reduced symmetry. A broad peak is also observed at δ 8.63, indicative of the *ortho*-H protons of free 4,4'-bipyridine. It may be that in the absence of excess 4,4'-bipyridine, a small amount of 4,4'-bipyridine partially dissociates in the C₆D₆ solution.

Most notably, the ¹H NMR spectrum of the solid isolated after addition of 1 equiv of 4,4'-bipyridine strongly suggests that both nitrogen atoms are involved in coordination events with zirconium, and by inference these zirconium atoms have to be located on different dinitrogen complexes. While conceivably self-assembly into infinite chains is a possibility, the smallest unit could be a dimer, where the ⁱpropNPN ligands are in a *cis*-arrangement (Figure 146). The solubility of the complex in C₆D₆ is more amenable with a smaller molecular mass. The largest ion observed in the mass spectrum of the black solid is 1444 m/z, which is larger than what would be expected for a single $[\text{}^{\text{i}}\text{propNPNZr}]_2(4,4'\text{-bipy})(\mu\text{-}\eta^2\text{:}\eta^2\text{-N}_2)$ unit (1416 m/z).

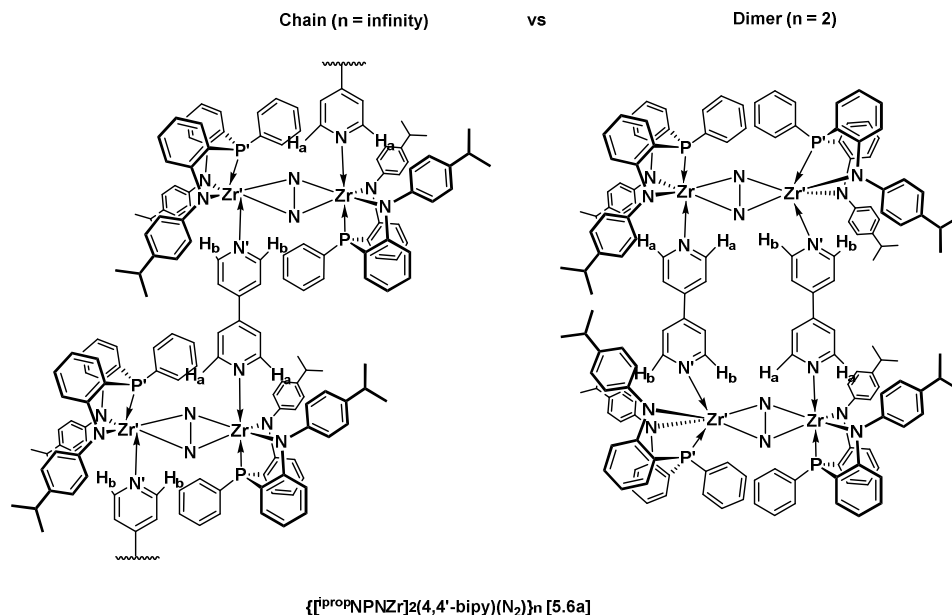


Figure 146: Chain vs. Dimer structure for $[\text{ipropNPNZr}(4,4'\text{-bipy})]_2(\mu\text{-}\eta^2:\eta^2\text{-N}_2)$ [5.6]

5.3.2. Phosphorus Atom Donors

Displacement of THF in the dinitrogen complexes $[\text{NPNZr}(\text{THF})]_2(\mu\text{-}\eta^2:\eta^2\text{-N}_2)$ with monodentate phosphines PRMe_2 ($\text{R} = \text{Me}$ and Ph) could lead to dinitrogen complexes $[\text{NPNZr}(\text{PRMe}_2)]_2(\mu\text{-}\eta^2:\eta^2\text{-N}_2)$. As THF substitution with PRMe_2 is expected at both zirconium centres, it could be considered a 2:2 complex (i.e. 2 Zr: 2 PRMe_2). This NPN(P) donor set would mimic the electronics of the macro-cyclic P_2N_2 dinitrogen complexes (Figure 138), that displayed interesting reactivity with H_2 ⁹⁰ and other carbon-based substrates.¹⁰³

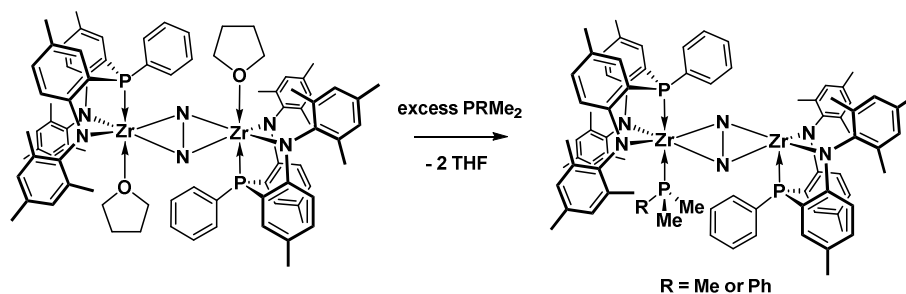


Figure 147: Reaction of $[\text{mesNPNZr}(\text{THF})]_2(\mu\text{-}\eta^2:\eta^2\text{-N}_2)$ with PMe_3 and PPhMe_2

Another possibility is the formation of a 2:1 complex $[\text{NPNZr}(\text{PRMe}_2)](\mu\text{-}\eta^2\text{:}\eta^2\text{-N}_2)[\text{NPNZr}]$ (Figure 147),^{92, 97} where only one phosphine molecule was coordinated to the dinuclear dinitrogen complex, leaving an open coordination site on the other zirconium centre. The steric bulk of the N-mesityl-containing ^{mes}NPN donor set was considered a factor in forming 2:1 rather than the expected 2:2 adducts. In this study, the reaction of phosphines with the sterically less hindered ^{iprop}NPN and ^{tol}NPN zirconium dinitrogen complexes is explored.

5.3.2.1. PMe_3 and PPhMe_3

It was found that, for the purple dinitrogen complexes **[5.1]** and **[5.3]** with less bulky ^{iprop}NPN and ^{tol}NPN donor sets, both THF's were displaced by PRMe_2 ($\text{R} = \text{Me}$ and Ph) to form blue 2:2 complexes $[\text{ipropNPNZr}(\text{PMe}_3)]_2(\mu\text{-}\eta^2\text{:}\eta^2\text{-N}_2)$ **[5.8]** and $[\text{tolNPNZr}(\text{PMe}_3)]_2(\mu\text{-}\eta^2\text{:}\eta^2\text{-N}_2)$ **[5.9]** when $\text{R} = \text{Me}$ and green 2:2 complexes $[\text{ipropNPNZr}(\text{PPhMe}_2)]_2(\mu\text{-}\eta^2\text{:}\eta^2\text{-N}_2)$ **[5.10]** and $[\text{tolNPNZr}(\text{PPhMe}_2)]_2(\mu\text{-}\eta^2\text{:}\eta^2\text{-N}_2)$ **[5.11]** when $\text{R} = \text{Ph}$ (Figure 148). It proved difficult to remove the THF from **[5.1]** and **[5.3]** and a large excess or neat phosphine was required to isolate complexes **[5.8]**, **[5.9]**, **[5.10]** and **[5.11]**. In some cases, it was possible to observe a mixed NPN(O)/NPN(P) species such as $\text{ipropNPNZr}(\text{THF})(\mu\text{-}\eta^2\text{:}\eta^2\text{-N}_2)[\text{ipropNPNZr}(\text{PMe}_3)]$ **[5.7]**, where only one THF was displaced.

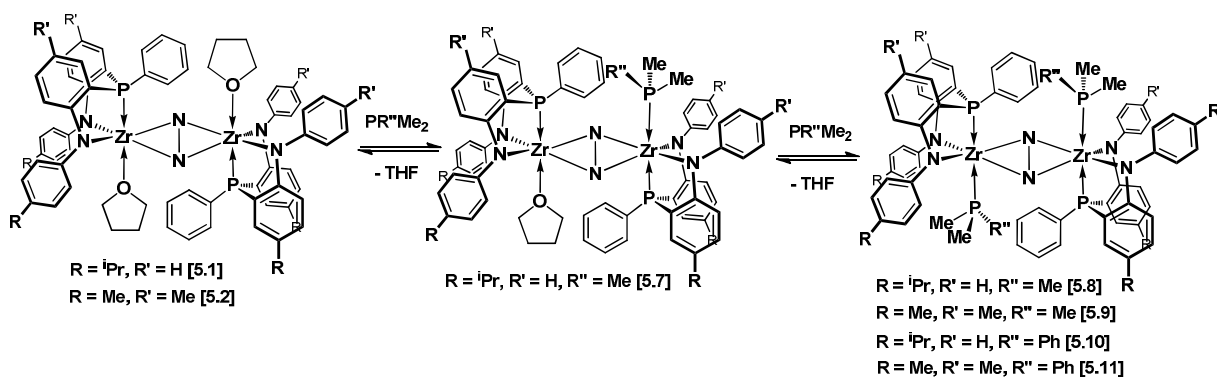
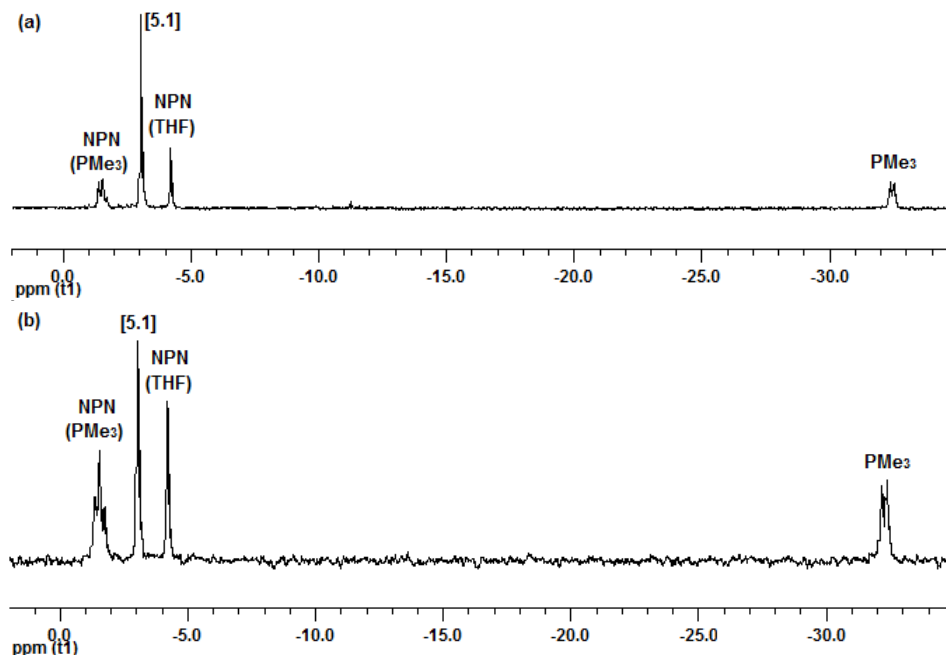


Figure 148: Reaction of the zirconium dinitrogen THF adducts **[5.1]** and **[5.3]** with PMe_3 and PPhMe_2

For example, no colour changes were observed after addition of *ca* 5 equiv of PMe_3 to a C_6D_6 solution of **[5.1]** at room temperature, and the $^{31}\text{P}\{^1\text{H}\}$ NMR spectrum indicated a mixture of **[5.1]** and $^{\text{iprop}}\text{NPNZr}(\text{THF})(\mu\text{-}\eta^2\text{:}\eta^2\text{-N}_2)[^{\text{iprop}}\text{NPNZr}(\text{PMe}_3)]$ **[5.7]** with two doublets at δ -32.30 and δ -1.64 ($^2J_{\text{PP}} = 25$ Hz) and a singlet at δ -4.20 in the $^{31}\text{P}\{^1\text{H}\}$ NMR spectrum (see **(b)** in Figure 149). A blue solution was observed on addition of *ca* 50 equivalents PMe_3 to an Et_2O solution of **[5.1]** at -30 °C, but the blue-green residue obtained after solvent removal dissolved in C_6D_6 to form a purple solution that contained **[5.1]** as the major component (see **(a)** in Figure 149). The green complex $^{\text{iprop}}\text{NPNZr}(\text{THF})(\mu\text{-}\eta^2\text{:}\eta^2\text{-N}_2)[^{\text{iprop}}\text{NPNZr}(\text{PMe}_3)]$ **[5.7]** was isolated as the major component after three successive addition / evacuation cycles with *ca* 5, 16 and 30 equiv of PMe_3 in Et_2O . The $^{31}\text{P}\{^1\text{H}\}$ NMR spectrum (see **(c-1)** in Figure 149) is similar to that observed in **(a)** and **(b)**, but with only a trace of complex **[5.1]**. The ^1H NMR spectrum displays a doublet at δ 0.58 ($^2J_{\text{PH}} = 6$ Hz) for coordinated PMe_3 and singlets at δ 0.46 and δ 3.75 for coordinated THF with some free PMe_3 at δ 0.80 (see **(c-2)** in Figure 149).



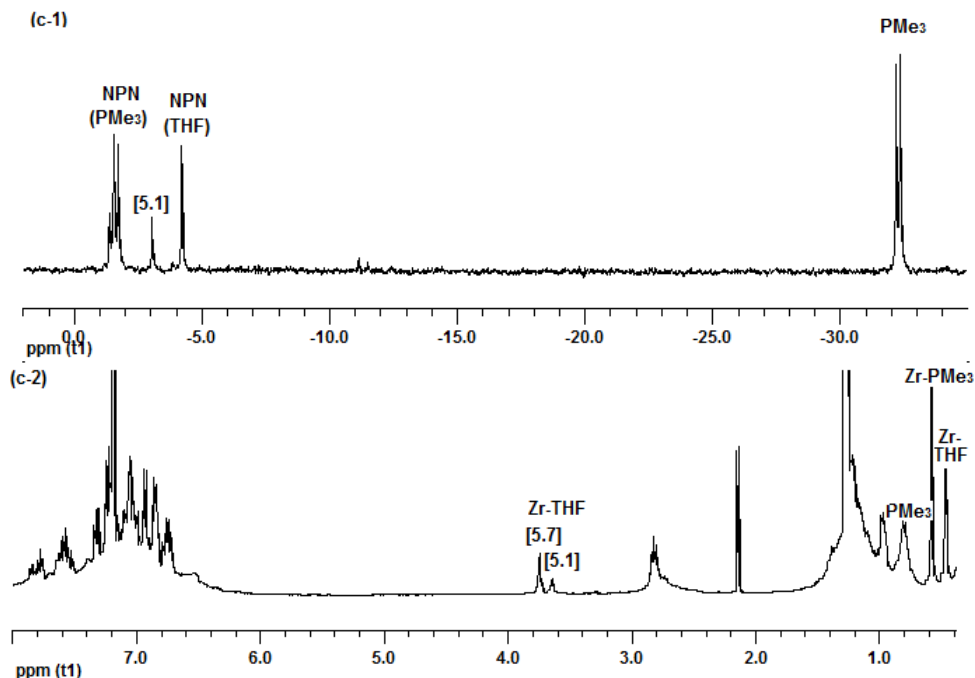


Figure 149: $^{31}\text{P}\{^1\text{H}\}$ (a, b and c-1) and ^1H NMR (c-2) spectra of mixtures of $[\text{ipropNPNZr}(\text{THF})](\mu\text{-}\eta^2\text{:}\eta^2\text{-N}_2)[\text{ipropNPNZr}(\text{PMe}_3)]$ [5.7] and $[\text{ipropNPNZr}(\text{THF})]_2(\mu\text{-}\eta^2\text{:}\eta^2\text{-N}_2)$ [5.1] in C_6D_6

The most successful method for the isolation of the 2:2 PMe_3 dinitrogen complexes required multiple dissolution / evacuation cycles of the precursor THF complexes with Et_2O prior to phosphine addition, with up to two neat phosphine addition cycles for PMe_3 (a large excess of 50-75 equiv of was sufficient for PPhMe_2).

The $^{31}\text{P}\{^1\text{H}\}$ NMR spectra displayed doublets at δ -31.93 and δ -1.41 ($^2J_{\text{PP}} = 23\text{-}25$ Hz) and δ -31.68 and δ -1.09 ($^2J_{\text{PP}} = 26$ Hz), respectively, for $[\text{ipropNPNZr}(\text{PMe}_3)]_2(\mu\text{-}\eta^2\text{:}\eta^2\text{-N}_2)$ [5.8] and $[\text{tolNPNZr}(\text{PMe}_3)]_2(\mu\text{-}\eta^2\text{:}\eta^2\text{-N}_2)$ [5.9] and at δ -18.92 and δ -1.79 ($^2J_{\text{PP}} = 25\text{-}26$ Hz) for $[\text{ipropNPNZr}(\text{PPhMe}_2)]_2(\mu\text{-}\eta^2\text{:}\eta^2\text{-N}_2)$ [5.10] (Figure 150).

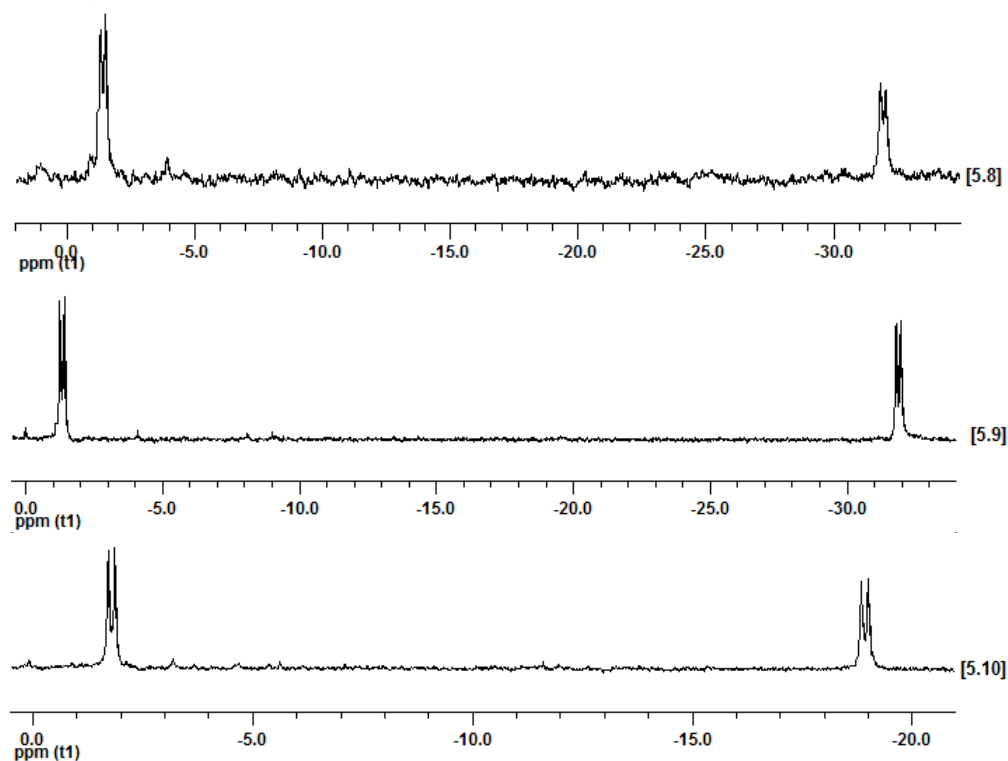


Figure 150: $^{31}\text{P}\{^1\text{H}\}$ spectra of $[\text{ipropNPNZr}(\text{PMe}_3)_2(\mu\text{-}\eta^2\text{:}\eta^2\text{-N}_2)]$ [5.8] (top), $[\text{tolNPNZr}(\text{PMe}_3)_2(\mu\text{-}\eta^2\text{:}\eta^2\text{-N}_2)]$ [5.9] (middle) and $[\text{ipropNPNZr}(\text{PPhMe}_2)_2(\mu\text{-}\eta^2\text{:}\eta^2\text{-N}_2)]$ [5.10] (bottom)

For $[\text{tolNPNZr}(\text{PPhMe}_2)_2(\mu\text{-}\eta^2\text{:}\eta^2\text{-N}_2)]$ [5.11], two broad peaks were observed in the $^{31}\text{P}\{^1\text{H}\}$ NMR spectrum at room temperature, which sharpened into doublets at δ -17.59 and δ -1.04 ($^2J_{\text{PP}} = 26$ Hz) when the sample was cooled down to -25 °C (Figure 151).

It was hard to completely remove the large excess free phosphine and the ^1H NMR spectra displayed doublets at δ 0.55 ($^2J_{\text{PH}} = 9$ Hz) and δ 0.72 ($^2J_{\text{PH}} = 6$ Hz) for the methyls of coordinated PMe_3 for [5.8] and [5.9] (with free PMe_3 at δ 0.81) and doublets at δ 1.01 ($^2J_{\text{PH}} = 5$ Hz) and δ 0.97 ($^2J_{\text{PH}} = 7$ Hz) for the methyls of coordinated PPhMe_2 for [5.10] and [5.11] (with free PPhMe_2 at δ 1.16 ($^2J_{\text{PH}} = 4$ Hz)) (Figure 152).

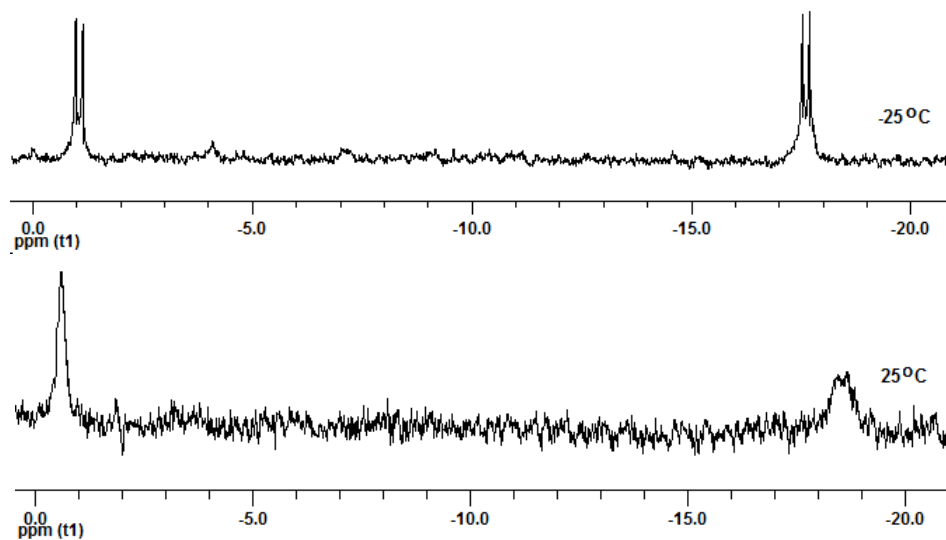


Figure 151: $^{31}\text{P}\{^1\text{H}\}$ NMR spectra of $[\text{}^{10}\text{lNPNZr}(\text{PPhMe}_2)_2(\mu\text{-}\eta^2\text{:}\eta^2\text{-N}_2)]$ [5.11] at 25 and -25°C in C_6D_6

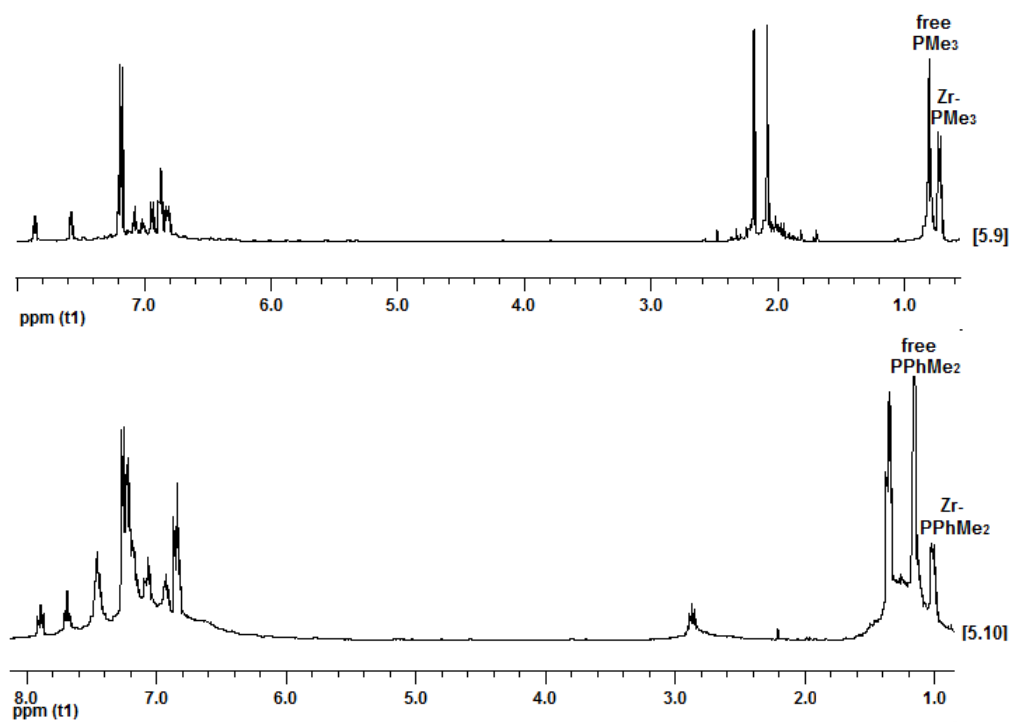


Figure 152: ^1H NMR spectra of $[\text{}^{10}\text{lNPNZr}(\text{PMe}_3)_2(\mu\text{-}\eta^2\text{:}\eta^2\text{-N}_2)]$ [5.9] (top) and $[\text{}^{i10}\text{lNPNZr}(\text{PPhMe}_2)_2(\mu\text{-}\eta^2\text{:}\eta^2\text{-N}_2)]$ [5.10] (bottom), with excess free phosphine in C_6D_6

The steric bulk of the N-aryl amido groups of the NPN donor set is thus a crucial factor in whether 2:1 ($^{\text{mes}}\text{NPN}$) or 2:2 ($^{\text{i}10}\text{lNPN}$ / $^{\text{tol}}\text{NPN}$) dinitrogen complexes are formed. The steric bulk of the monodentate phosphine is another consideration, as no displacement of THF occurred

when $[\text{ipropNPNZr(THF)}]_2(\mu\text{-}\eta^2\text{:}\eta^2\text{-N}_2)$ [**5.1**] was reacted with bulky P^tBu_3 . The $\text{ipropNPN} / \text{tolNPN}$ donor sets also favour a less labile THF ligand, which further inhibits displacement reactions. It was attempted to avoid the intransigent THF adduct by performing a reduction of $\text{ipropNPNZrCl}_2(\text{THF})$ [**3.5**] in Et_2O , followed by phosphine addition, but this route proved unsuccessful.

A probe experiment with one other phosphine (dmpe) was conducted, with the observation of a dark green solution after addition of 10 equiv to $[\text{ipropNPNZr(THF)}]_2(\mu\text{-}\eta^2\text{:}\eta^2\text{-N}_2)$ [**5.1**] in an Et_2O medium. The isolation of a brown solid suggests complications arose during product work-up, but the experiment was not repeated.

5.3.3. Sulphur Atom Donors

In natural systems, the FeMo cofactor ($7\text{Fe-9S-Mo-C-homocitrate}$)^{32, 324} within the MoFe protein of the nitrogenase enzyme contains nine sulphur atoms and is associated with the binding of dinitrogen and the formation of ammonia.^{26, 325, 326} There is a strong interest in obtaining sulphur-containing transition metal dinitrogen complexes,^{83, 327} but few have been reported.³²⁸ This dearth in dinitrogen complexes with sulphur donors is due in part to potential incompatibility between the typical route for the synthesis of dinitrogen complexes (i.e. reduction of transition metal complexes) and the accessibility of numerous sulphur oxidation states, as well as the stability of metal sulphide complexes. The ability to introduce a sulphur donor post-reduction is a promising potential for these strongly activated NPN based dinitrogen complexes.

5.3.3.1. THT

Initially, a reduction of $[\text{tolNPNZrCl}_2]_2$ [**3.10**] was conducted with KC_8 in tetrahydrothiophene (THT) as a solvent instead of THF. A brown solid with no coordinated THT was obtained, and the $^{31}\text{P}\{^1\text{H}\}$ NMR spectrum displayed downfield-shifted signals at δ 3.88 to δ 28.05. It is possible the reduced zirconium species reacted with the large excess THT solvent

instead of N₂ to form zirconium sulphide species, as was observed in the reduction of thiodialkyl substituted zirconocene dichlorides.³²⁹

Addition of neat THT to purple [¹⁰¹NPNZr(THF)₂(μ-η²:η²-N₂)] **[5.3]** led to the isolation of a red-purple solid with a single peak displayed in the ³¹P{¹H} NMR spectrum at δ -3.93 (Figure 153). While this signal is indicative of the THF complex **[5.3]**, the ¹H NMR spectrum displayed signals for coordinated THT at δ 2.50 and δ 1.40 (free THT at δ 2.58 and δ 1.62) in addition to those for coordinated THF at δ 3.58 and δ 0.95 (free THF at δ 3.57 and δ 1.40) of **[5.3]**. As in the preparation of the phosphine adducts, removal of strongly coordinated THF was inhibited.

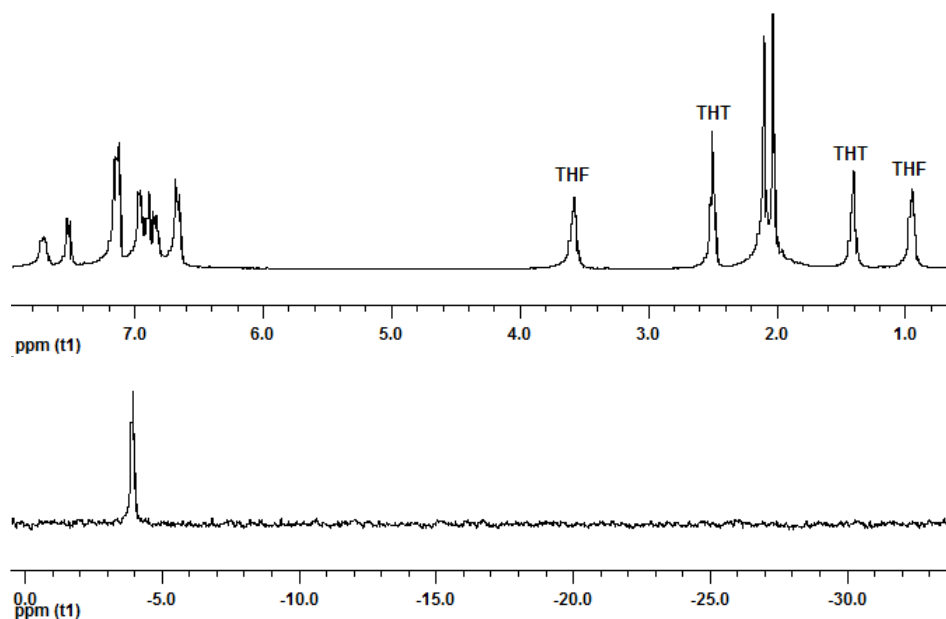


Figure 153: ³¹P{¹H} (bottom) and ¹H NMR (top) spectra of exchanging [¹⁰¹NPNZr(THF)₂(μ-η²:η²-N₂)] **[5.3]** and [¹⁰¹NPNZr(THT)₂(μ-η²:η²-N₂)] **[5.14]** in C₆D₆

Integration relative to ¹⁰¹NPN ligand signals indicated two molecules THF and two molecules THT were coordinated (Figure 153); however, steric considerations would make a seven-coordinated zirconium species unlikely. While the single ³¹P{¹H} NMR spectral signal may suggest exchange between coordinated THF of **[5.3]** and coordinated THT of a [¹⁰¹NPNZr(THT)₂(μ-η²:η²-N₂)] **[5.14]** complex (Figure 154); more simply, it could be interpreted

that the THT did not displace THF and its ^1H NMR signals represent free THT, despite being shifted upfield compared to a unary THT solution.

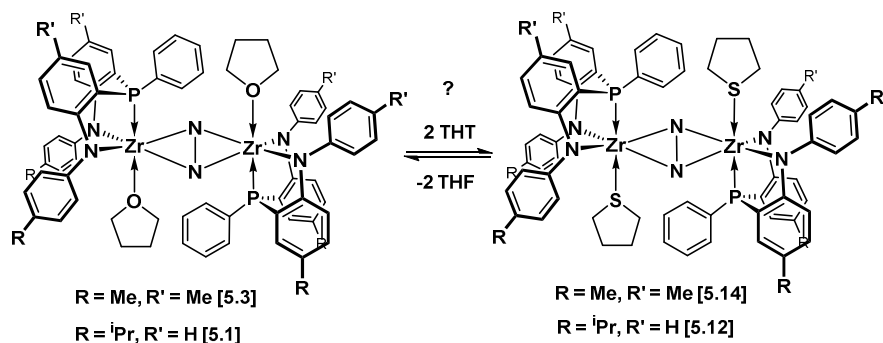


Figure 154: Exchange between THF ([5.3] and [5.1]) and potential THT ([5.14] and [5.12]) adducts

In order to avoid THF, displacement from phosphine adducts were considered. In one case, 30 equiv of THT was added to a solution of $[\text{ipropNPNZr}(\text{PMe}_3)_2(\mu\text{-}\eta^2\text{:}\eta^2\text{-N}_2)]$ [5.8] in C_6D_6 .

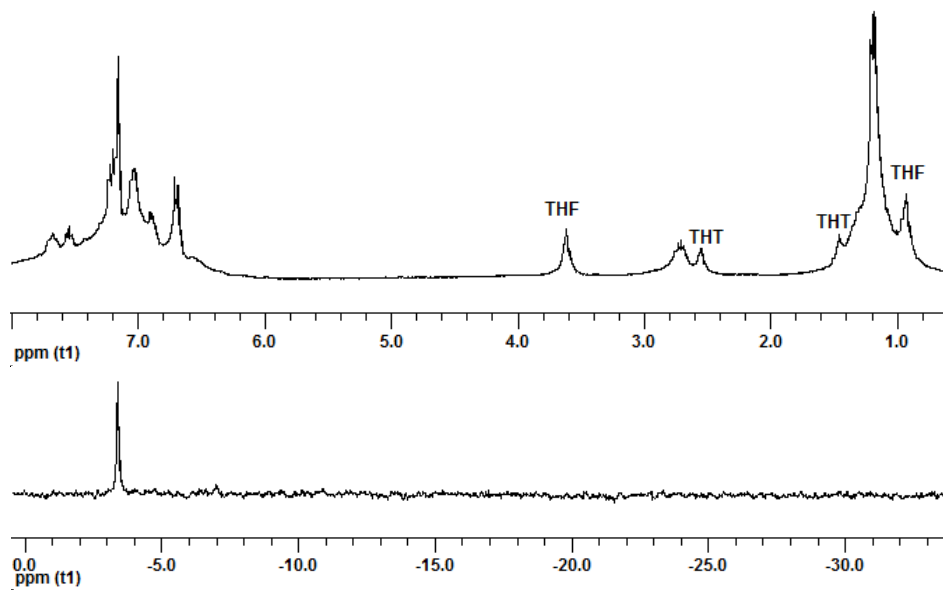


Figure 155: $^{31}\text{P}\{^1\text{H}\}$ (bottom) and ^1H NMR (top) spectra of 30 equiv of THT with $[\text{ipropNPNZr}(\text{PMe}_3)_2(\mu\text{-}\eta^2\text{:}\eta^2\text{-N}_2)]$ [5.8] + trace THF in C_6D_6

While THT did displace PMe_3 , the source [5.8] complex unfortunately contained traces of THF, hence the ^1H NMR spectrum (Figure 155) displayed signals at δ 3.62 and δ 0.93 for complex [5.1] in addition to signals at δ 2.55 and δ 1.46 for “coordinated” THT in the desired

$[\text{ipropNPNZr}(\text{THT})]_2(\mu\text{-}\eta^2\text{:}\eta^2\text{-N}_2)$ **[5.12]** complex. Again, the $^{31}\text{P}\{^1\text{H}\}$ NMR spectrum displays a single signal at δ -3.38, this time upfield of complex **[5.1]** and may, or may not, be due to exchange between the THF and THT complexes.

In a second case, exposure of $[\text{tolNPNZr}(\text{THF})]_2(\mu\text{-}\eta^2\text{:}\eta^2\text{-N}_2)$ **[5.3]** to neat PMe_3 followed by neat THT led to the isolation of a purple solid, where the ^1H NMR spectrum (Figure 156) indicated that “coordinated” THT at δ 2.55 and δ 1.46 was in large excess compared to THF and PMe_3 , which was not completely displaced.

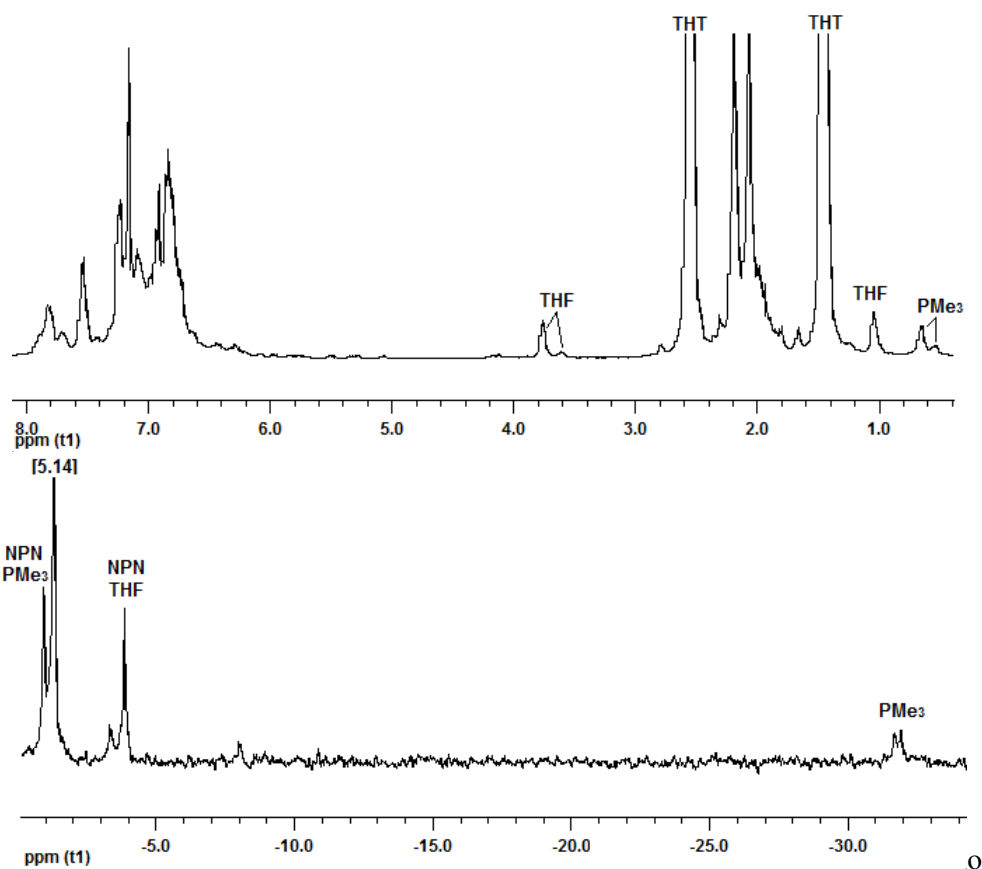


Figure 156: $^{31}\text{P}\{^1\text{H}\}$ (bottom) and ^1H NMR (top) spectra of $[\text{tolNPNZr}(\text{THT})]_2(\mu\text{-}\eta^2\text{:}\eta^2\text{-N}_2)$ **[5.14]** in C_6D_6

In the $^{31}\text{P}\{^1\text{H}\}$ NMR spectrum (Figure 156), the doublets at δ -1.12 and -31.80 and singlet at -3.86 may be indicative of a mixed PMe_3 / THF species (Figure 157), similar to what was postulated for complex **[5.7]**. The larger singlet at δ -1.30 could be interpreted to represent

the THT adduct $[\text{}^{101}\text{NPNZr}(\text{THT})]_2(\mu\text{-}\eta^2\text{:}\eta^2\text{-N}_2)$ [5.14], which is now clearly shifted upfield relative to the precursor THF complex [5.3]. Relative integration of THT signals to the ^{101}NPN ligand signals in the ^1H NMR spectrum implies greater than two equiv of THT is present in the sample, and perhaps exchange between bound and excess free THT may be occurring.

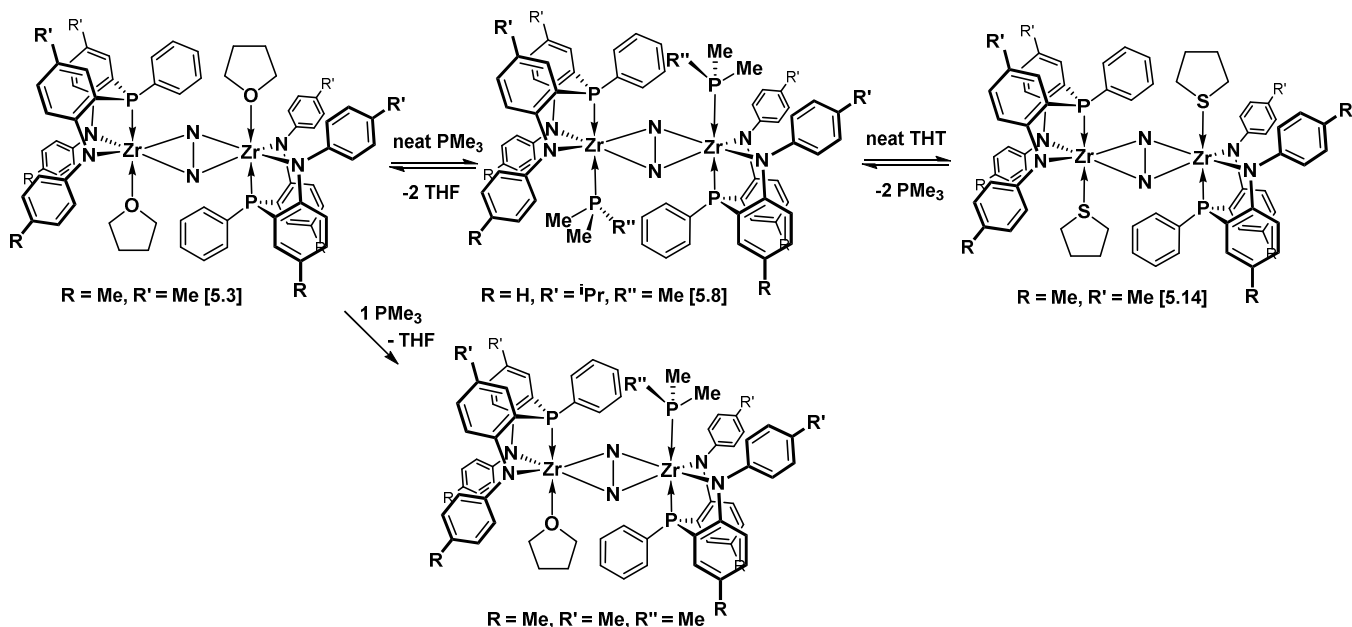


Figure 157: Phosphine displacement with neat THT, *in situ* from $[\text{}^{101}\text{NPNZr}(\text{THF})]_2(\mu\text{-}\eta^2\text{:}\eta^2\text{-N}_2)$ [5.3]

From the above experiments, it is clear that THT does not readily displace THF. An experiment involving multiple dissolution / evacuation cycles of the precursor THF complexes with Et_2O prior to THT addition (which had proved a useful strategy in the isolation of the 2:2 phosphine adducts) was not conducted and should be considered for future work. As *in situ* displacement of THF with either Et_2O or PMe_3 prior to THT addition may not be rigorous enough to ensure complete removal of THF, it may be better to isolate the pure Et_2O or PMe_3 adducts. Displacement with a less volatile S-donor such as 1,3-dihydro-2-benzothiophene instead of THT may promote the formation of more stable Zr-S bonds and potentially lead to the isolation of pure $[\text{NPNZr}(\text{S-donor})]_2(\mu\text{-}\eta^2\text{:}\eta^2\text{-N}_2)$ complexes.

A different approach for the introduction of a sulphur donor atom may be via tridentate NSN donor sets. Perhaps the sulphur in a NSN donor set would be less readily reduced than THT, and it would also only be present in stoichiometric amounts. Phenylene-based NSN donor sets may be prepared via a palladium catalysed Buchwald-Hartwig arylation of commercially available 2,2'-thiodianiline and with a mono-substituted arylhalide³³⁰ and zirconium dichloride NSNZrCl₂ complexes³³¹ have previously been prepared.

5.4. Titanium Dinitrogen Complexes

5.4.1. Synthesis of [ⁱpropNPNTi(THF)]₂N₂ [5.17] and [^{tol}NPNTi(THF)]₂N₂ [5.15]

Unlike phosphinimide formation reported for the reduction of the ^{Si}NPNTiCl₂ complex^{137, 138} (see introduction), the reaction of dark purple ^{tol}NPNTiCl₂ [3.18] with KC₈ in THF under N₂ led to the isolation of the brown dinitrogen complex [^{tol}NPNTi(THF)]₂(μ-η¹:η¹-N₂) [5.15] (Figure 158).³³²

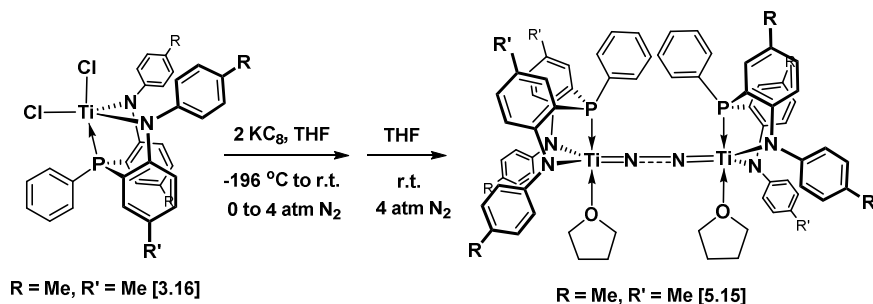


Figure 158: Synthesis of [^{tol}NPNTi(THF)]₂(μ-η¹:η¹-N₂) [5.15]

The ³¹P{¹H} NMR spectrum of [5.15] displays a signal at δ 5.64, with signals for coordinated THF at δ 1.09 and 3.27 in the ¹H NMR spectrum (Figure 159) and at δ 25.7 and δ 72.52 in the ¹³C{¹H} NMR spectrum. A mass spectrum exhibits a THF-free fragment ion [M - 2THF]⁺ at 1121 m/z. The toluene solvent used during product work-up is hard to remove and elemental analysis results reflect its continued presence.

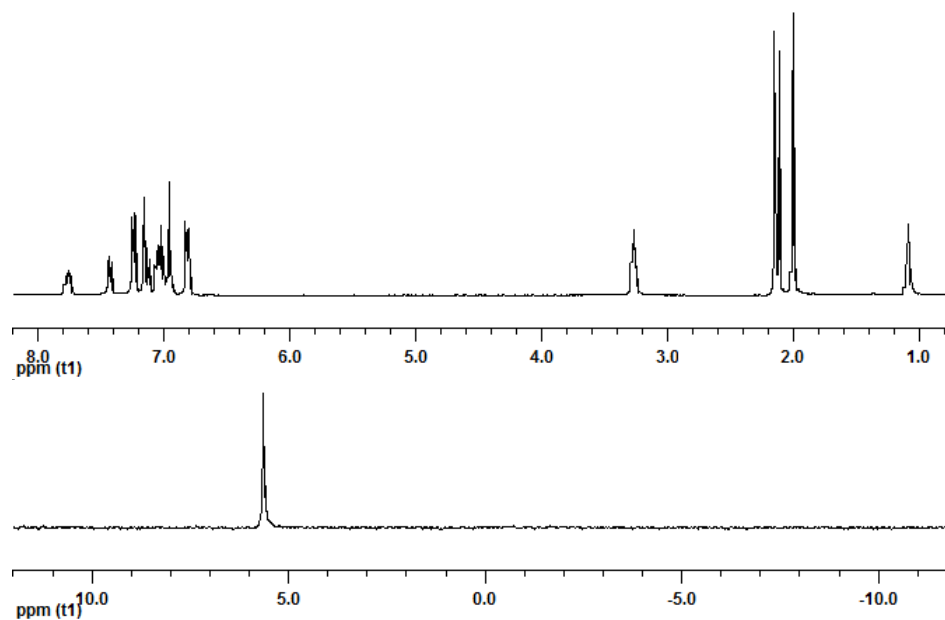


Figure 159: $^{31}\text{P}\{^1\text{H}\}$ (bottom) and ^1H NMR (top) spectra of $[\text{}^{101}\text{NPNTi}(\text{THF})_2(\mu\text{-}\eta^1\text{:}\eta^1\text{-N}_2)]$ **[5.15]** in C_6D_6

During a clean reduction, only a single sharp peak for $[\text{}^{101}\text{NPNTi}(\text{THF})_2(\mu\text{-}\eta^1\text{:}\eta^1\text{-N}_2)]$ **[5.15]** is observed at δ 5.64 in the $^{31}\text{P}\{^1\text{H}\}$ NMR spectrum of the crude reaction mixture. However, in most cases a mixture of **[5.15]** and species with signals at δ -4.02, δ -7.37 and downfield at δ 39.20 are observed, to be referred to respectively as **species a**, **unknown** and **species b** in future discussions, with no signal for protonated $^{101}\text{NPNH}_2$ **[2.11]** ligand. In some cases, the signals for **[5.15]** and **species a** of the brown solid isolated from the crude THF reaction mixture are quite broad, with the corresponding ^1H NMR spectrum exhibiting broad THF signals (Figure 160). Crystallisation from toluene / *n*-pentanes or benzene / *n*-pentanes mixtures in the freezer at -40 °C leads to the isolation of pure $[\text{}^{101}\text{NPNTi}(\text{THF})_2(\mu\text{-}\eta^1\text{:}\eta^1\text{-N}_2)]$ **[5.15]**.

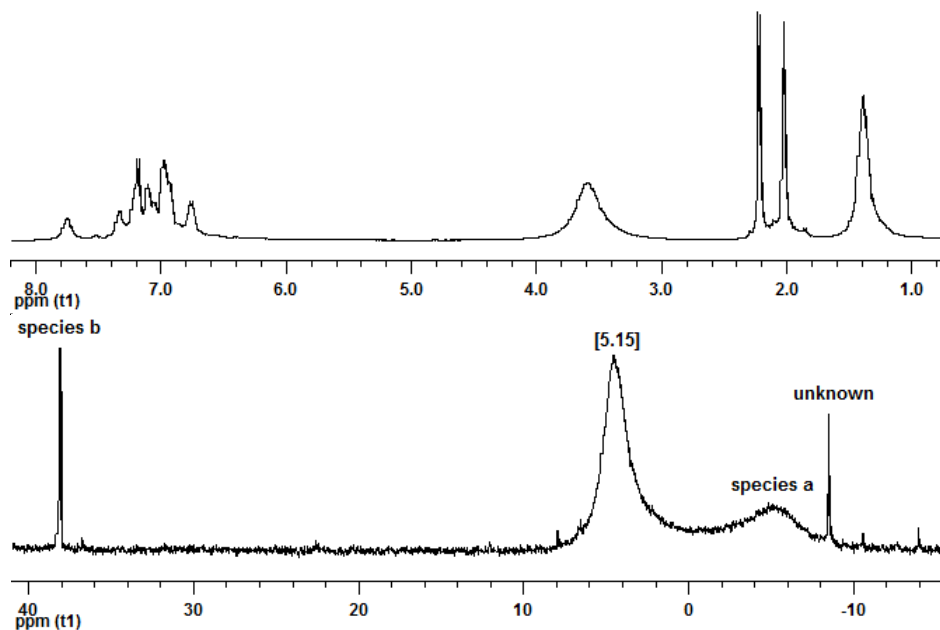


Figure 160: $^{31}\text{P}\{^1\text{H}\}$ (bottom) and ^1H NMR (top) spectra of crude brown solid after THF centrifuge in C_6D_6

Titanium dinitrogen complexes are more likely than zirconium to exhibit end-on bonding, with DFT calculations confirming an end-on mode being more favoured by 11.9 kcalmol^{-1} relative to side-on for titanium dinitrogen complexes (NH_2 and PH_3 ligands), compared to -3.1 kcalmol^{-1} for analogous zirconium calculations.¹⁴¹

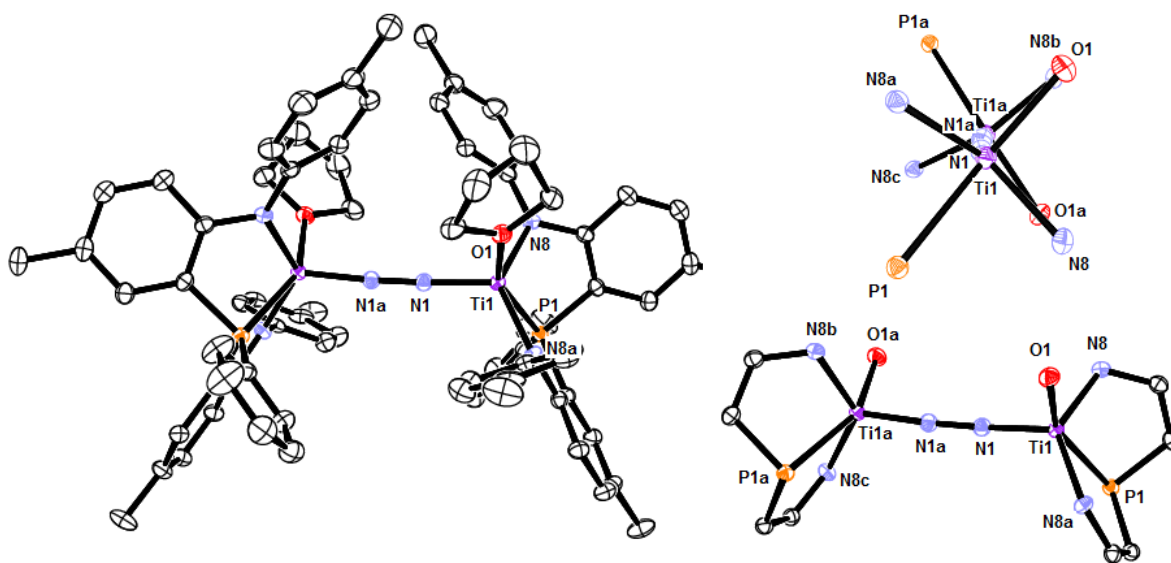


Figure 161: ORTEP representation of solid state molecular structure of $[\text{tolNPNTi}(\text{THF})]_2(\mu\text{-}\eta^1:\eta^1\text{-N}_2)$ [5.15]³³²

The solid state molecular structure obtained for $[\text{}^{101}\text{NPNTi}(\text{THF})]_2(\mu\text{-}\eta^1\text{:}\eta^1\text{-N}_2)$ [**5.15**] (Figure 161) revealed that the dinitrogen is bound end-on with a moderately activated N-N bond length of 1.260(4) Å, which falls within the range of 1.24 - 1.27 Å reported for the $[\text{PNPTiCl}]_2(\mu\text{-}\eta^1\text{:}\eta^1\text{-N}_2)$ ¹⁸² and $[\text{P}_2\text{N}_2\text{Ti}]_2(\mu\text{-}\eta^1\text{:}\eta^1\text{-N}_2)$.¹³⁷ The Ti1-N1 bond lengths are significantly shorter than the Ti1-N8 / Ti1-N8a amido bond lengths of the ^{101}NPN donor set (see Table 25) and indicates some double bond imido character,³³³⁻³³⁵ as is typical for moderately activated side-on dinitrogen.^{137, 174, 182} The titanium is five-coordinate with a square pyramidal geometry for both titanium centres. The Ti-N-N-Ti bond axis is nearly linear with a N1a-N1-Ti1 angle of 172.5(2)°.

Table 25 : Selected bond lengths (Å) and angles (°) for $[\text{}^{101}\text{NPNTi}(\text{THF})]_2(\mu\text{-}\eta^1\text{:}\eta^1\text{-N}_2)$ [5.15**] compared to $[\text{PNPTiCl}]_2(\mu\text{-}\eta^1\text{:}\eta^1\text{-N}_2)$ ¹⁸² and $[\text{P}_2\text{N}_2\text{Ti}]_2(\mu\text{-}\eta^1\text{:}\eta^1\text{-N}_2)$ ¹³⁷**

| | ^{101}NPN [5.15] | | PNP(Cl) | | $\text{P}_2\text{N}_2(1)$ | $\text{P}_2\text{N}_2(2)$ |
|-------------------|------------------------------------|--------------------|----------|--------------------|---------------------------|---------------------------|
| N1-N1a | 1.260(4) | N1-N1a | 1.275(7) | N1-N1a | 1.255(7) | 1.245(7) |
| Ti1-N1 | 1.7719(19) | Ti1-N1 | 1.775(4) | Ti1-N1 | 1.783(4) | |
| Ti1-P1 | 2.5517(8) | Ti1-P1 | 2.630(2) | Ti1-P1 | 2.5669(13) | |
| Ti1-O1 | 2.1021(16) | Ti1-P1a | 2.589(2) | Ti1-P1a | 2.5552(13) | |
| Ti1-N8 | 2.0670(19) | Ti1-N8 | 2.035(5) | Ti1-N8 | 2.076(4) | |
| Ti1-N8a | 2.0427(19) | Ti1-Cl1 | 2.331(2) | Ti1-N8a | 2.049(4) | |
| N1a-N1-Ti | 172.5(2) | N1a-N1-Ti | 173.7(2) | N1a-N1-Ti | 177.7(4) | 179.0(4) |
| N1-Ti1-P1 | 111.42(6) | N1-Ti1-P1 | 104.6(2) | N1-Ti1-P1 | 105.24(11) | |
| N1-Ti1-O1 | 95.60(8) | N1-Ti1-P1a | 91.2(2) | N1-Ti1-P1a | 100.17(11) | |
| N1-Ti1-N8 | 115.43(8) | N1-Ti1-N8 | 115.3(2) | N1-Ti1-N8 | 123.60(15) | |
| N1-Ti1-N8a | 111.60(8) | N1-Ti1-Cl1 | 116.7(2) | N1-Ti1-N8a | 116.91(17) | |
| P1-Ti1-N8 | 74.58(5) | P1-Ti1-N8 | 82.3(1) | P1-Ti1-N8 | 79.30(11) | |
| P1-Ti1-N8a | 76.82(6) | P1-Ti1-Cl1 | 88.91(8) | P1-Ti1-N8a | 87.19(11) | |
| O1-Ti1-N8 | 93.94(7) | P1a-Ti1-N8 | 80.8(1) | P1a-Ti1-N8 | 80.75(11) | |
| O1-Ti1-N8a | 94.02(7) | P1a-Ti1-Cl1 | 93.96(9) | P1a-Ti1-N8a | 87.25(11) | |

NPN donor sets with group 4 metals typically bind in a facial manner and in binuclear complexes the ligands are usually in a *trans* arrangement, with the two P atoms on opposite sides of the bridging bonding axis. In the case of $[\text{}^{101}\text{NPNTi}(\text{THF})]_2(\mu\text{-}\eta^1\text{:}\eta^1\text{-N}_2)$ [**5.15**] in the solid state, the two ^{101}NPN donor sets are facial as expected, but in a *cis* arrangement relative to each other, with the P atoms on the same side of the Ti-N-N-Ti bond axis. From an aspect down the Ti1-N1-N1a-Ti1a bond axis, the N8 and N8a atoms on the ^{101}NPN donor set on the Ti1 atom are slightly staggered relative to the P1a and O1a on Ti1a, such that the oxygen atoms O1 and O1a of the

THF are in a *cis* arrangement (Figure 161). A similar *cis* arrangement was observed for the chloride atoms in the $[\text{PNPTiCl}]_2(\mu\text{-}\eta^I\text{:}\eta^I\text{-N}_2)^{182}$ complex.

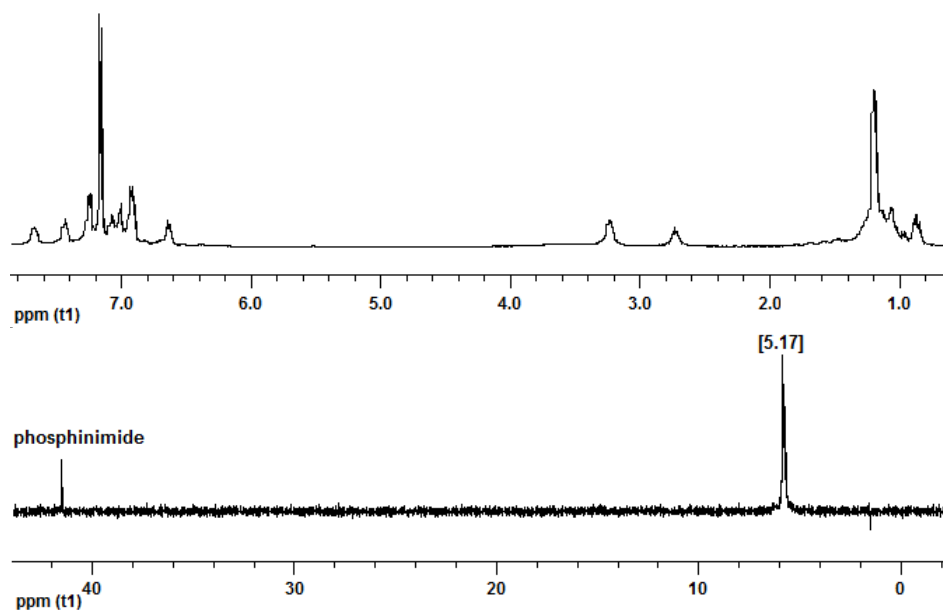


Figure 162: $^{31}\text{P}\{^1\text{H}\}$ (bottom) and ^1H NMR (top) spectra of crude brown solid for $^{\text{iprop}}\text{NPNTiCl}_2$ [3.17] reduction in C_6D_6

Considering the similarity between the value obtained for the olive green intermediate speculated to be $[\text{SiNPNTi}]_2(\text{N}_2)$ at δ 5.6^{137, 138} and $[\text{tolNPNTi}(\text{THF})]_2(\mu\text{-}\eta^I\text{:}\eta^I\text{-N}_2)$ [5.15], coupled with the fact that the signal for **species b** is commensurate with the phosphinimide $\{[\text{SiN}(\text{P}=\text{N})\text{N}]\text{Ti}\}_2$ at δ 39.9,^{137, 138} it is proposed that **species b** may be an analogous $\{[\text{tolN}(\text{P}=\text{N})\text{N}]\text{Ti}\}_2$ phosphinimide side-product (Figure 163). Similarly, the crude of the reduction of $^{\text{iprop}}\text{NPNTiCl}_2$ [3.17] exhibited a major signal at δ 5.80 in its $^{31}\text{P}\{^1\text{H}\}$ NMR spectrum for $[\text{ipropNPNTi}(\text{THF})]_2(\mu\text{-}\eta^I\text{:}\eta^I\text{-N}_2)$ [5.17], with the potential phosphinimide side-product reflected in a signal at δ 41.54 (Figure 162).

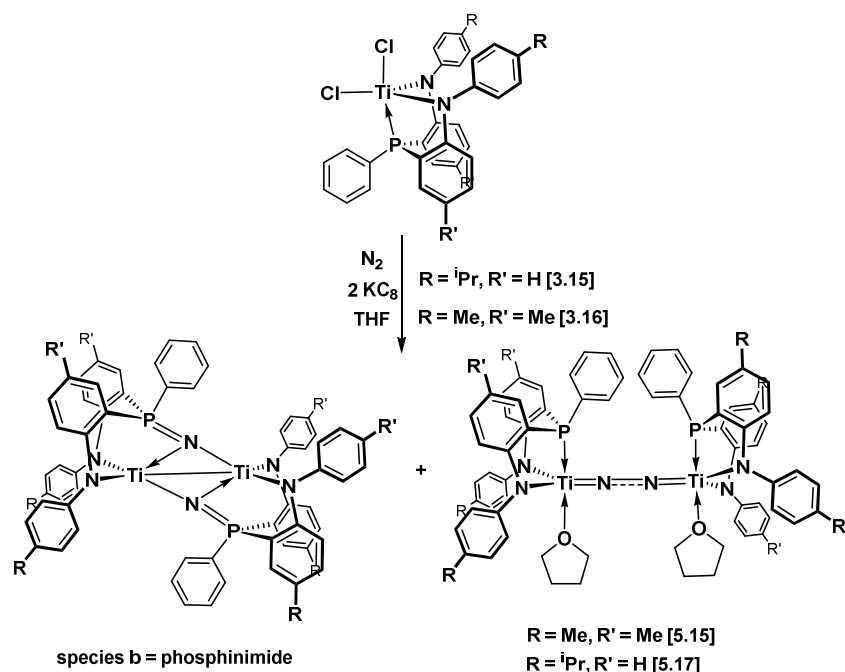


Figure 163: Potential phosphinimide formation during the reduction of NPNTiCl₂ [3.17] and [3.18]

Due to a limited number of reductions conducted with the ^{iprop}NPN donor set, a pure sample of [^{iprop}NPNTi(THF)]₂(μ-η¹:η¹-N₂) [**5.17**] has not been isolated in this study. Signals for coordinated THF of [**5.17**] were observed at δ 1.06 and 3.23 in the ¹H NMR spectrum and a mass spectrum of the crude displayed signals at 1309 m/z and 1297 m/z, which represents fragment ions with loss of one and two N atoms, [M - N]⁺ and [M - 2N]⁺ respectively. A peak was also observed at 1181 m/z, that would represent a fragment ion with loss of 2 THF [M - 2THF]⁺.

When crystallising [^{tol}NPNTi(THF)]₂(μ-η¹:η¹-N₂) [**5.15**] from the crude with toluene / *n*-hexanes mixtures where the THF reaction solvent was not rigorously excluded, the isolated brown solids comprised a mixture of [**5.15**] and **species a**. When a C₆D₆ solution of such a mixture is spiked with THF, **species a** was exclusively observed (Figure 164).

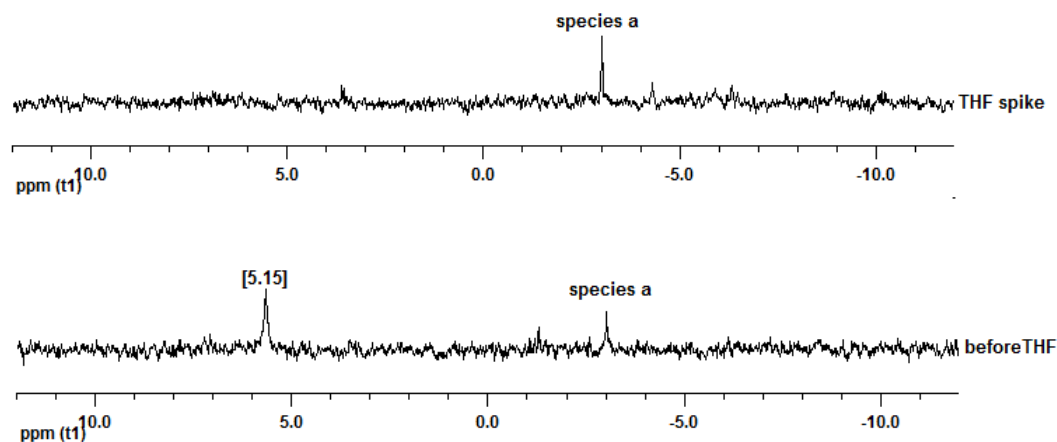


Figure 164: $^{31}\text{P}\{^1\text{H}\}$ NMR spectra of $[\text{tolNPNTi}(\text{THF})_2(\mu\text{-}\eta^1\text{:}\eta^1\text{-N}_2)]$ [5.15] + species a before (bottom) and after THF spike (top) in C_6D_6

Crystallisation is hampered by enhanced solubility in THF, but it was possible to isolate an impure sample of **species a** from a THF / Et_2O / *n*-hexanes mixture. The ^1H NMR spectrum of **species a** differed from complex [5.15] with broad THF signals at δ 1.42 and 3.61 (more similar to free or weakly coordinated THF) and upfield shifted phenyl peaks, most prominently a triplet at δ 6.16 (Figure 165).

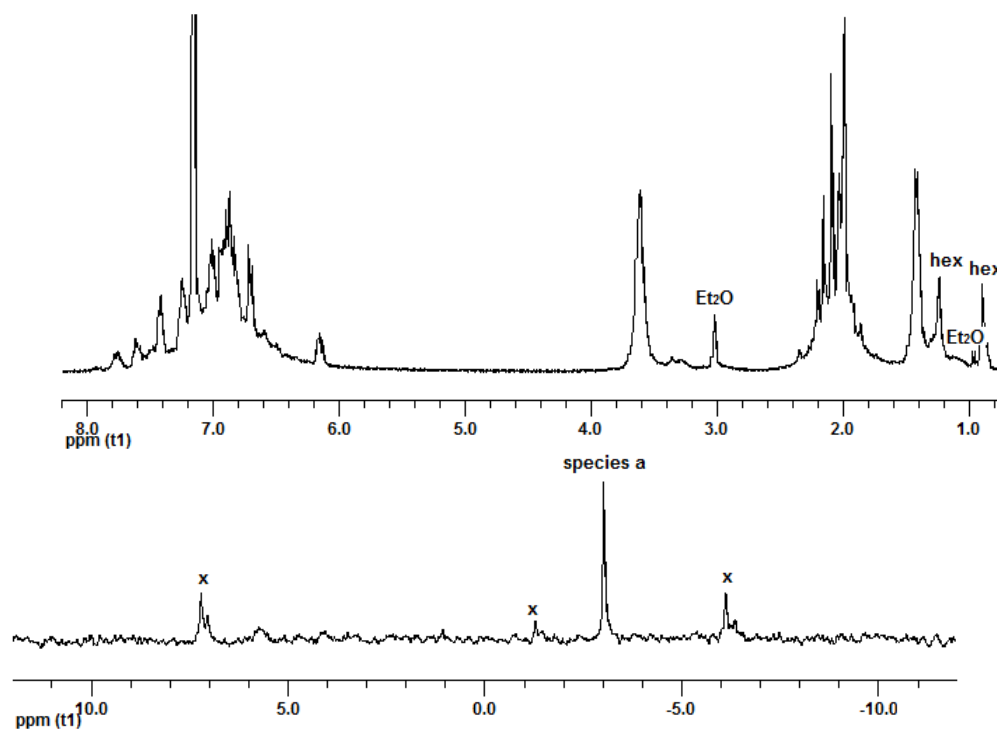


Figure 165: $^{31}\text{P}\{^1\text{H}\}$ (bottom) and ^1H NMR (top) spectra of species a in C_6D_6

It is postulated that **species a** may contain two coordinated THF molecules per titanium centre to form $[\text{}^{\text{tol}}\text{NPNTi}(\text{THF})_2]_2(\mu\text{-}\eta^{\text{I}}:\eta^{\text{I}}\text{-N}_2)$ **[5.16]** (Figure 166) in a structure analogous to that found for *trans*- $[\text{}^{\text{tol}}\text{NPNTi}(\text{Py})_2]_2(\mu\text{-}\eta^{\text{I}}:\eta^{\text{I}}\text{-N}_2)$ **[5.19]** (see later discussion). A mass spectrum of **species a** (i.e. complex **[5.16]**) exhibited a peak at 1410 m/z, which agrees with a parent ion formulation for $[\text{}^{\text{tol}}\text{NPNTi}(\text{THF})_2]_2(\mu\text{-}\eta^{\text{I}}:\eta^{\text{I}}\text{-N}_2)$.

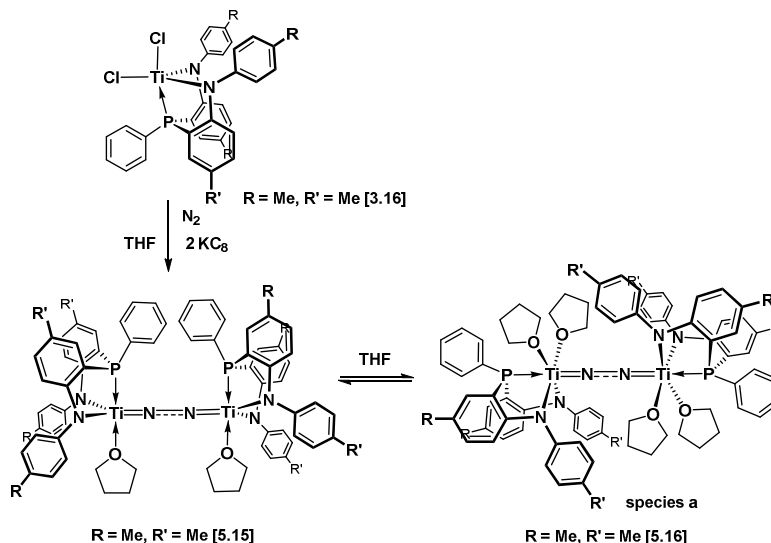


Figure 166: Formation of $[\text{}^{\text{tol}}\text{NPNTi}(\text{THF})_2]_2(\mu\text{-}\eta^{\text{I}}:\eta^{\text{I}}\text{-N}_2)$ **[5.16]**

The reduction of $^{15}\text{N}_2$ with $\text{}^{\text{tol}}\text{NPNTiCl}_2$ **[3.18]** and KC_8 in THF did not lead to isolation of the expected $^{15}\text{N}_2$ isotopologue. While some protonated ligand and additional peaks were observed in the $^{31}\text{P}\{^1\text{H}\}$ NMR spectrum, $[\text{}^{\text{tol}}\text{NPNTi}(\text{THF})]_2(\mu\text{-}\eta^{\text{I}}:\eta^{\text{I}}\text{-N}_2)$ **[5.15]** and $[\text{}^{\text{iprop}}\text{NPNTi}(\text{THF})_2]_2(\mu\text{-}\eta^{\text{I}}:\eta^{\text{I}}\text{-N}_2)$ **[5.16]** nonetheless comprised the bulk of the crude. A mass loss of the $^{15}\text{N}_2$ canister further indicated that $^{15}\text{N}_2$ was consumed during the reaction, however, the lack of signals in a $^{15}\text{N}\{^1\text{H}\}$ NMR spectrum suggests that the major species **[5.16]** and **[5.15]** contained $^{14}\text{N}_2$ and not $^{15}\text{N}_2$. It can be surmised that during product work-up inside the glove-box, exchange between coordinated $^{15}\text{N}_2$ and free $^{14}\text{N}_2$ had occurred. In future, manipulation of the $^{15}\text{N}_2$ isotopologue under an argon atmosphere is recommended.

5.5. Titanium Dinitrogen Adducts

5.5.1. Nitrogen Atom Donors

5.5.1.1. Pyridine

The electronic environment of the metal centres of these NPN based group 4 dinitrogen complexes may be altered by displacing THF with other two-electron donor molecules. The $^{31}\text{P}\{^1\text{H}\}$ NMR spectrum of a C_6D_6 solution after the addition of two equiv of Py to $[\text{tolNPNTi}(\text{THF})]_2(\mu\text{-}\eta^1\text{:}\eta^1\text{-N}_2)$ **[5.15]** displayed four new signals at δ 4.17, δ 3.04, δ -0.29 and δ -0.79, which persisted after addition of a further two equiv of Py, albeit in differing relative proportions. After addition of twenty equiv of Py, only the single species with a peak at δ -0.25 could be observed (Figure 167).

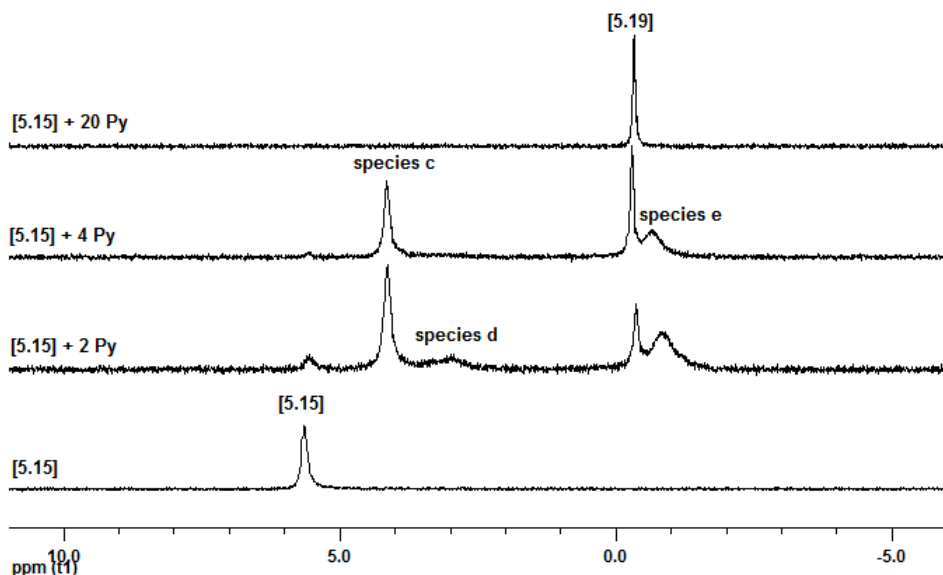


Figure 167: $^{31}\text{P}\{^1\text{H}\}$ NMR spectra after pyridine addition to $[\text{tolNPNTi}(\text{THF})]_2(\mu\text{-}\eta^1\text{:}\eta^1\text{-N}_2)$ **[5.15]** in C_6D_6

Based on the solid state solution structure obtained from crystals grown from this solution (Figure 170), the species with a signal at δ -0.25 contains four pyridine molecules: two per titanium centre, being *cis* relative to each other on the same titanium centre, *cis* relative to the Ti-N-N-Ti bonding axis and *trans* relative to the other titanium centre *trans*- $[\text{tolNPNTi}(\text{Py})_2]_2(\mu\text{-}$

$\eta^1:\eta^1\text{-N}_2$) [5.19]. Considering the *cis* arrangement of the THF adducts on opposing titanium centres in the precursor complex [5.15] (Figure 161), a rotation about the Ti-N-N-Ti bonding axis may be invoked to account for the *trans* arrangement observed for the Py adducts on opposing titanium centres in complex [5.19] (Figure 168).

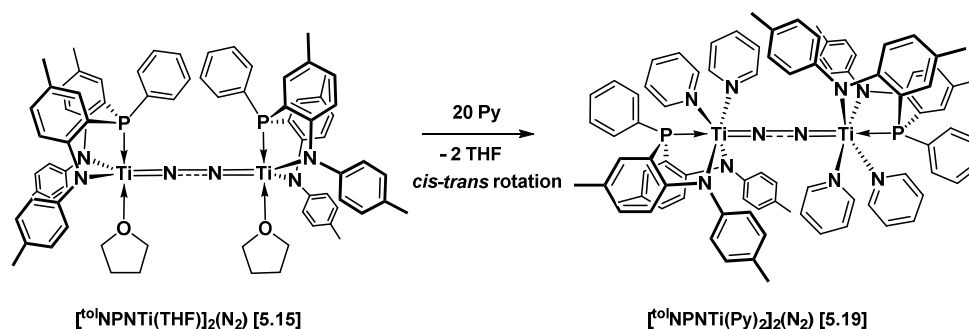


Figure 168: Synthesis of *trans*- $[\text{tolNPNTi(Py)}_2]_2(\mu\text{-}\eta^1:\eta^1\text{-N}_2)$ [5.19] from $[\text{tolNPNTi(THF)}]_2(\mu\text{-}\eta^1:\eta^1\text{-N}_2)$ [5.15]

For further discussions, the $^{31}\text{P}\{^1\text{H}\}$ NMR spectral signals at δ 4.17, δ 3.04 and δ -0.79 would be referred to as **species c**, **d** and **e**, respectively (Figure 167). The corresponding ^1H NMR spectra of these solutions reflect free THF only, thus the formation of mixed THF / Py adducts may be discounted as potential candidates for **species c**, **d** and **e**. It is postulated that **species e**, upfield and adjacent to complex [5.19], may be a less stable *cis* isomer *cis*- $[\text{tolNPNTi(Py)}_2]_2(\mu\text{-}\eta^1:\eta^1\text{-N}_2)$ [5.19a]. **Species c and d**, adjacent and less upfield shifted compared to complexes [5.19] and [5.19a], may represent *cis* and *trans* isomers for the case where each titanium centre only has one Py coordinated. Assuming that *cis* adducts are more preferred when titanium is five-coordinate (solid state solution structure for [5.15]), the more prominent signal for **species c** may be associated with *cis*- $[\text{tolNPNTi(Py)}]_2(\mu\text{-}\eta^1:\eta^1\text{-N}_2)$ [5.18] and the less distinct **species d** with *trans*- $[\text{tolNPNTi(Py)}]_2(\mu\text{-}\eta^1:\eta^1\text{-N}_2)$ [5.18a] (Figure 169). The observation of [5.19] and [5.19a] with [5.18] and [5.18a] after addition of two equivalents of pyridine suggests that the adducts with two Py per titanium centre are more preferred and isolation of *cis/trans*- $[\text{tolNPNTi(Py)}_2]_2(\mu\text{-}\eta^1:\eta^1\text{-N}_2)$ [5.18] / [5.18a] from an isomeric mixture may be difficult to accomplish.

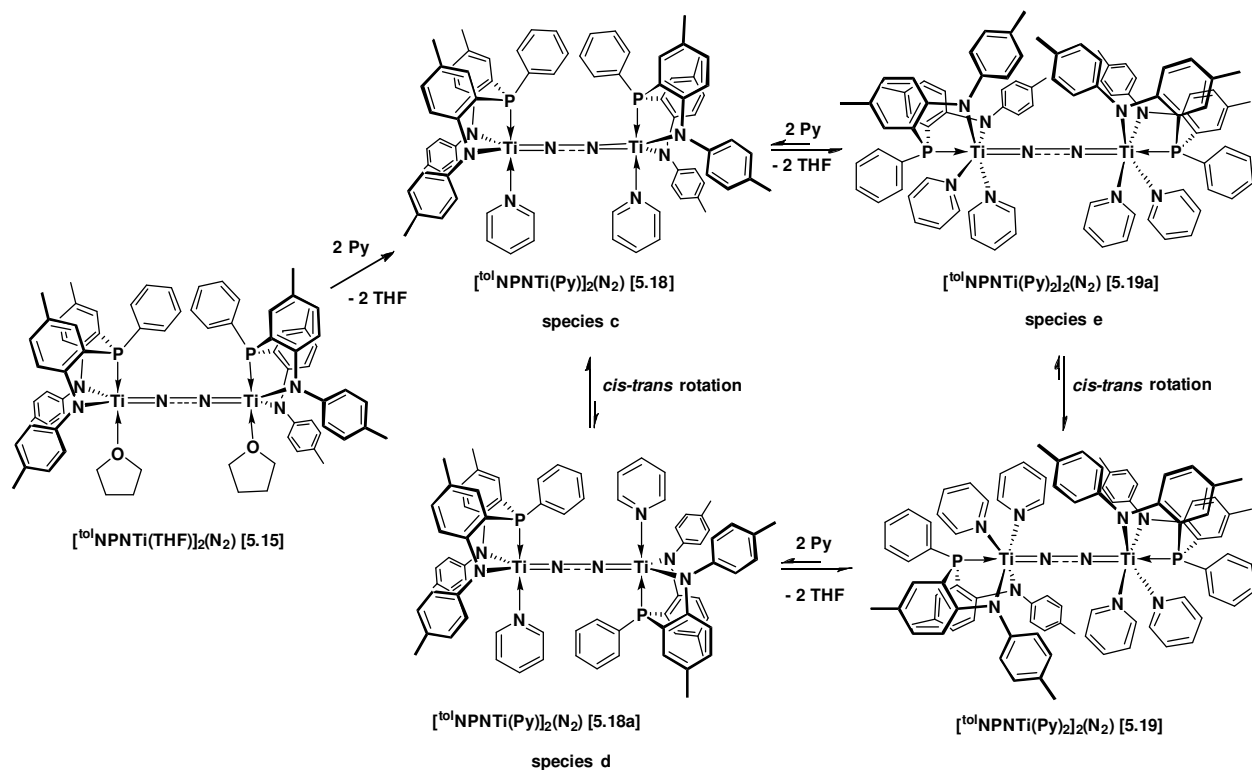


Figure 169: Potential pyridine adducts observed in the C_6D_6 solution with two or four Py per titanium centre

Pure *trans*- $[\text{tolNPNTi(Py)}_2]_2(\mu\text{-}\eta^1\text{:}\eta^1\text{-N}_2)$ [5.19] was isolated as a brown solid from the reaction of twenty equiv of Py with [5.15] in toluene.³³² The pyridine- d_5 isotopomer *trans*- $[\text{tolNPNTi(Py-}d_5)_2]_2(\mu\text{-}\eta^1\text{:}\eta^1\text{-N}_2)$ [5.19b] was obtained by dissolution of [5.15] in neat pyridine- d_5 with crystallisation from pyridine / *n*-pentane layering at -40°C . The solid state molecular structure obtained for *trans*- $[\text{tolNPNTi(Py)}_2]_2(\mu\text{-}\eta^1\text{:}\eta^1\text{-N}_2)$ [5.19] (Figure 170) reveals a bridging end-on bonding for the dinitrogen, with shorter N-N and longer Ti-N bond lengths (Table 26) compared to $[\text{tolNPNTi(THF)}]_2(\mu\text{-}\eta^1\text{:}\eta^1\text{-N}_2)$ [5.15] (Table 25). The pyridine adduct [5.19] thus contains a less activated dinitrogen ligand compared to [5.15] and the N-N-Ti bond angles of $175.5(3)^\circ$ and $169.7(3)^\circ$ are inequivalent and not perfectly linear. The N-N bond length for [5.19] is also shorter than that reported for $[\text{((Me}_3\text{Si)}_2\text{N)TiCl(Py)}_2]_2(\mu\text{-}\eta^1\text{:}\eta^1\text{-N}_2)$ at $1.263(7)$ Å.¹⁷⁵ The pyridine-titanium bond lengths Ti1-N21, Ti1-N27 (and Ti1a-N21a, Ti1a-N27a) are much longer than for the dinitrogen-titanium bond lengths Ti1-N1 (and Ti1a-N1a), as well as the amido-titanium bond lengths Ti1-N8, Ti1-N8a (and Ti1a-N8b, Ti1a-N8c) and not significantly

different to those reported for $[(\text{Me}_3\text{Si})_2\text{N})\text{TiCl}(\text{Py})_2]_2(\mu\text{-}\eta^1\text{:}\eta^1\text{-N}_2)$ at 2.268(4) Å and 2.251(4)

Å.¹⁷⁵

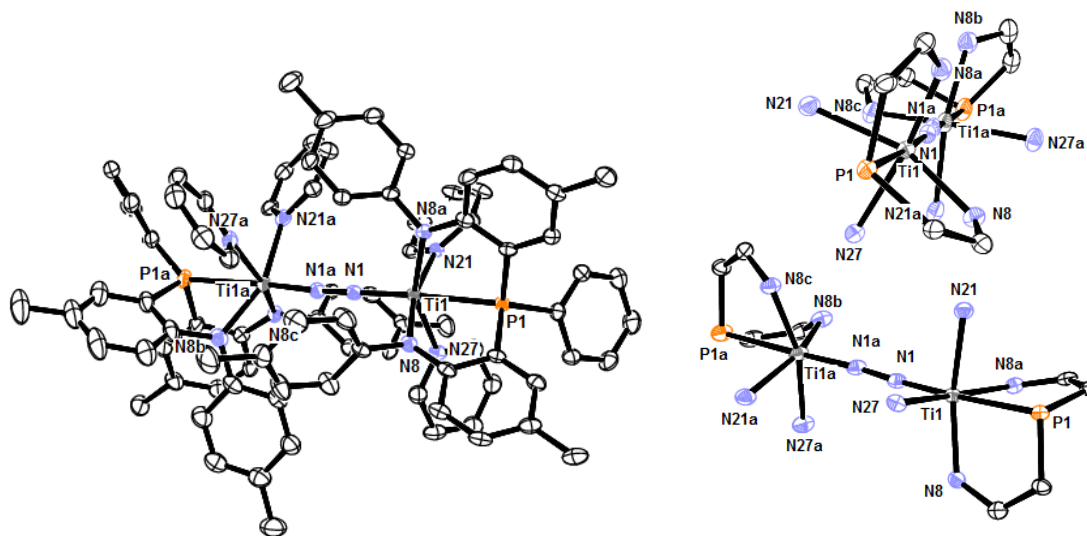


Figure 170: ORTEP representation of solid state molecular structure of $\text{trans-}[\text{tolNPNi}(\text{Py})_2]_2(\mu\text{-}\eta^1\text{:}\eta^1\text{-N}_2)$ [5.19]³³²

Table 26 : Selected bond lengths (Å) and angles (°) for $\text{trans-}[\text{tolNPNi}(\text{Py})_2]_2(\mu\text{-}\eta^1\text{:}\eta^1\text{-N}_2)$ [5.19]

| $\text{trans-}[\text{tolNPNi}(\text{Py})_2]_2(\mu\text{-}\eta^1\text{:}\eta^1\text{-N}_2)$ [5.19] | | | |
|---|------------|----------------|------------|
| N1-N1a | 1.242(5) | | |
| Ti1-N1 | 1.813(3) | Ti1a-N1a | 1.815(3) |
| Ti1-P1 | 2.6125(13) | Ti1a-P1a | 2.6510(13) |
| Ti1-N21 | 2.277(3) | Ti1a-N21a | 2.264(4) |
| Ti1-N27 | 2.259(3) | Ti1a-N27a | 2.247(4) |
| Ti1-N8 | 2.125(3) | Ti1a-N8b | 2.120(4) |
| Ti1-N8a | 2.092(3) | Ti1a-N8c | 2.068(3) |
| N1a-N1-Ti | 169.7(3) | N1-N1a-Ti1a | 175.5(3) |
| N1-Ti1-P1 | 176.74(11) | N1a-Ti1a-P1a | 175.68(12) |
| N8-Ti1-N21 | 154.09(13) | N8b-Ti1a-N21a | 158.02(14) |
| N8a-Ti1-N27 | 166.84(12) | N8c-Ti1a-N27a | 161.42(13) |
| N1-Ti1-N21 | 96.18(13) | N1a-Ti1a-N21a | 94.60(14) |
| N1-Ti1-N27 | 89.41(13) | N1a-Ti1a-N27a | 92.86(14) |
| N1-Ti1-N8 | 106.03(14) | N1a-Ti1a-N8b | 106.21(15) |
| N1-Ti1-N8a | 102.63(14) | N1a-Ti1a-N8c | 105.23(14) |
| P1-Ti1-N21 | 81.54(9) | P1a-Ti1a-N21a | 89.43(9) |
| P1-Ti1-N27 | 92.57(9) | P1a-Ti1a-N27a | 85.86(9) |
| P1-Ti1-N8 | 76.74(9) | P1a-Ti1a-N8b | 69.60(10) |
| P1-Ti1-N8a | 75.17(9) | P1a-Ti1a-N8c | 76.41(10) |
| N8-Ti1-N8a | 96.68(13) | N8b-Ti1a-N8c | 93.07(14) |
| N8-Ti1-N27 | 84.86(12) | N8b-Ti1a-N27a | 85.78(13) |
| N21-Ti1-N8a | 91.18(12) | N21a-Ti1a-N8c | 88.12(13) |
| N21-Ti1-N27 | 82.16(12) | N21a-Ti1a-N27a | 86.19(13) |

Each titanium centre has an octahedral coordination sphere, with the tolNPN donor set in the usual facial coordination mode (Figure 170). Compared to $[\text{tolNPNi}(\text{THF})_2]_2(\mu\text{-}\eta^1\text{:}\eta^1\text{-N}_2)$

[5.15], the P-Ti bonds of [5.19] are aligned (rather than perpendicular) with the Ti-N-N-Ti bond axis. The two N atoms of the ^{101}NPN donor set in the equatorial plane of one of the titanium centres are arranged *cis*, with the N atoms of the two pyridines also *cis* relative to each other. Looking down the P-Ti-N-N-Ti-P axis, the N atoms on Ti1 are slightly staggered compared to the N atoms on Ti1a and the pyridines of the titanium centres occur on opposite sides of the P-Ti-N-N-Ti-P axis in a “*trans*” arrangement. All the bond lengths and angles of the two ^{101}NPN donor set fragments display significant differences.

^1H NMR characterisation of *trans*-[$^{101}\text{NPNTi}(\text{Py})_2(\mu-\eta^1:\eta^1-\text{N}_2)$] [5.19] was confounded by the observation of all four species [5.18], [5.18a], [5.19] and [5.19a] during the dissolution of pure [5.19] in C_6D_6 . Spiking the C_6D_6 solution with a slight excess 20 μL Py (or $\text{Py}-d_5$) is needed to assure the dominance of most preferred *trans*-[$^{101}\text{NPNTi}(\text{Py})_2(\mu-\eta^1:\eta^1-\text{N}_2)$] [5.19] (Figure 171)

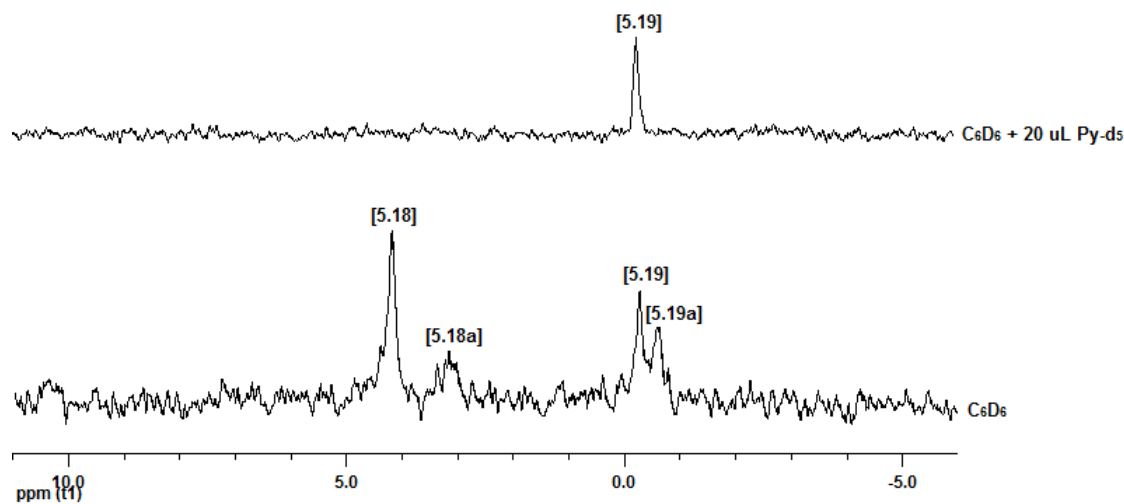


Figure 171: $^{31}\text{P}\{^1\text{H}\}$ NMR spectra of *trans*-[$^{101}\text{NPNTi}(\text{Py})_2(\mu-\eta^1:\eta^1-\text{N}_2)$] [5.19] (bottom) and with a 20 μL $\text{Py}-d_5$ spike (top) in C_6D_6

The ^1H NMR spectrum of the [5.18], [5.18a], [5.19] and [5.19a] mixture containing no excess pyridine (Figure 172) displays three different *ortho*-proton signals for pyridine at δ 8.52, δ 8.06 and δ 7.83 (broad). The major signal at δ 8.52 suggests free or weakly coordinated pyridine

(free pyridine at δ 8.53). As no excess pyridine is present in this sample, it can be assumed that this signal represents *ortho*-protons of weakly coordinated pyridine, as would be expected in **[5.19]** / **[5.19a]**. The other signals at δ 8.06 and δ 7.83 (broad) may represent *ortho*-proton signals for coordinated pyridine in **[5.18]** / **[5.18a]**, though more typically a downfield shift would be expected to reflect coordination, as reported in the case of $[(\text{Me}_3\text{Si})_2\text{N})\text{TiCl}(\text{Py})_2]_2(\mu\text{-}\eta^1\text{:}\eta^1\text{-N}_2)$ with resonances for coordinated pyridine at δ 8.71, δ 7.56 and δ 7.19.¹⁷⁵

While the ^1H NMR spectrum of *trans*- $[\text{}^{\text{tol}}\text{NPN}(\text{Py})_2]_2(\mu\text{-}\eta^1\text{:}\eta^1\text{-N}_2)$ **[5.19]** in C_6D_6 with 20 μL Py ensures that **[5.19]** is the only species present, the free pyridine signals swamp observation of coordinated pyridine and some phenyl signals (Figure 172). The lack of signals at δ 8.06 and δ 7.83 (previously observed in the C_6D_6 only spectrum) further suggests that these may be associated with coordinated pyridine signals of **[5.18]** / **[5.18a]**. Spiking with 20 μL $\text{Py-}d_5$ instead (Figure 172) led to the observation of pyridine resonances at δ 8.53, δ 7.00 and δ 6.69 **[5.19]** (free pyridine at δ 8.53, δ 7.15 and δ 6.80), which further corroborates the suggestion that pyridine may only be weakly coordinated when two molecules are coordinated per titanium centre. The possibility that exchange had occurred between the excess $\text{Py-}d_5$ and coordinated Py is likely, and the observed signals may be a time-averaged mixture. Variable temperature NMR experiments (not conducted in this study) may help to resolve this issue. The *meta*- and *para*-protons of pyridine, however, still inhibited characterisation of some phenyl signals for the $^{\text{tol}}\text{NPN}$ donor set of **[5.19]**. This was overcome by dissolution of the pyridine- d_5 isotopomer **[5.19b]** in C_6D_6 with 20 μL $\text{Py-}d_5$, which allowed elucidation of phenyl signals at δ 6.74, δ 7.02, δ 7.12 and δ 7.47.

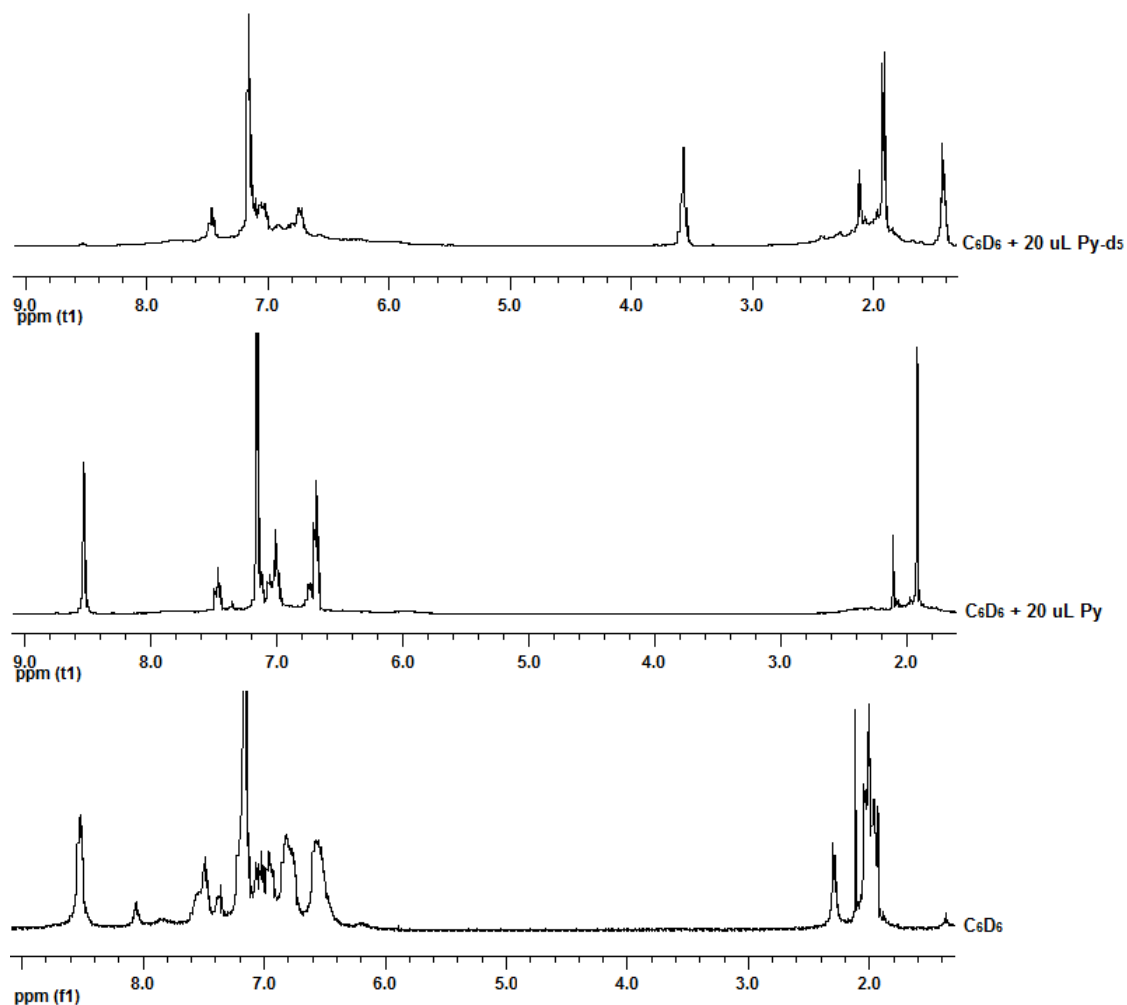


Figure 172: ^1H NMR spectra of $\text{trans-}[\text{}^{101}\text{NPNTi}(\text{Py})_2]_2(\mu\text{-}\eta^1\text{:}\eta^1\text{-N}_2)$ [5.19] (bottom) and with a 20 μL Py-d_5 spike (top) and with a 20 μL Py spike (middle) in C_6D_6

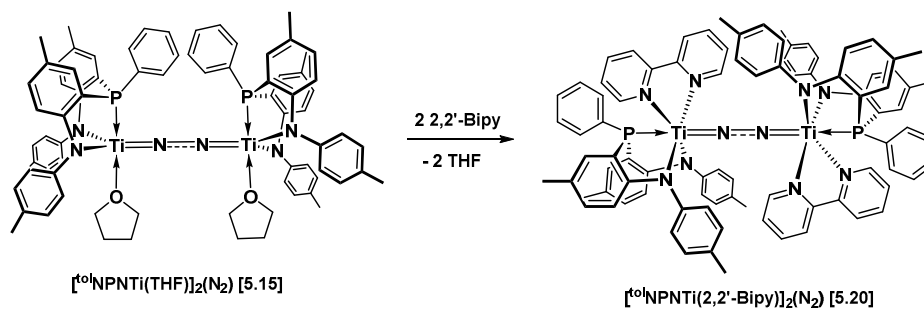


Figure 173: Synthesis of $[\text{}^{101}\text{NPNTi}(2,2'\text{-bipy})]_2(\mu\text{-}\eta^1\text{:}\eta^1\text{-N}_2)$ [5.20]

Reaction of two equivalents of 2,2'-bipyridine with [5.15] led to the isolation of a single brown species with a signal at δ 9.41 in the $^{31}\text{P}\{^1\text{H}\}$ NMR spectrum (Figure 173 and Figure 174).

The ^1H NMR spectrum displays three distinct signals downfield of the ^{101}NPN donor set phenyl signals at δ 9.05, δ 8.72 and δ 8.54 (free 2,2'-bipyridine at δ 8.72, δ 8.54, δ 7.23 and δ 6.71). Most significantly, coordination of 2,2'-bipyridine may be indicated by the downfield shifted signal δ 9.05. A 2,2'-bipyridine adduct may prove to be a more well-behaved model complex compared to *trans*- $[\text{}^{101}\text{NPNTi}(\text{Py})_2]_2(\mu\text{-}\eta^1\text{:}\eta^1\text{-N}_2)$ [5.19] and further work with nitrogen donor atom should focus on the purification and characterisation of this adduct.

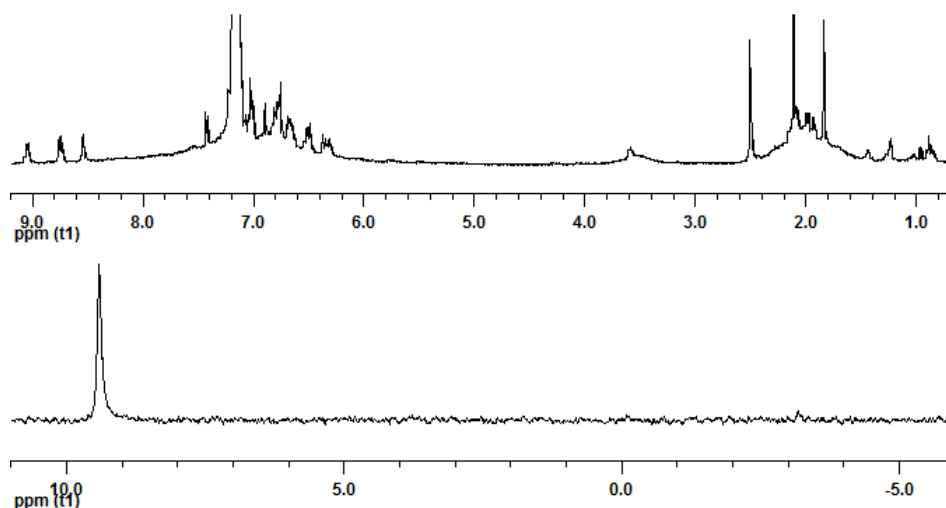


Figure 174: $^{31}\text{P}\{^1\text{H}\}$ (bottom) and ^1H NMR (top) spectra of $[\text{}^{101}\text{NPNTi}(2,2'\text{-bipy})]_2(\mu\text{-}\eta^1\text{:}\eta^1\text{-N}_2)$ [5.20] in C_6D_6

5.6. Titanium Hydrides for Alternative Dinitrogen Activation Route

One of the important considerations for developing a homogeneous catalytic process to transform dinitrogen into higher value nitrogen compounds is the ability to constantly regenerate the transition metal dinitrogen complex during the catalytic cycle. Reduction of metal chlorides in the presence of dinitrogen is the typical way of accessing dinitrogen complexes, but such a reaction tends to be irreversible.

Transition metal hydrides have been identified as the most promising solution to this problem, liberation hydrogen to activate dinitrogen.¹⁹⁰ Tantalum dinitrogen complexes with the diamidophosphine $^{\text{Si}}\text{NPN}$ donor set are formed via this route.^{79, 80} However, attempts at forming

zirconium and hafnium hydrides from precursor alkyl complexes with the ^{mes}NPN donor set failed.⁹⁷ A titanium dinitrogen complex was reported on exposure of a bis(cyclopentadienyl)titanium hydride complex to dinitrogen, with a titanocene (II) complex implicated as an intermediate.³³⁶ A substituted cyclopentadienyl side-on titanium dinitrogen complex was isolated from a precursor hydride complex¹²⁹ and more recently, a trinuclear titanium polyhydride complex was reported to activate and cleave dinitrogen.^{100, 101}

The reaction of purple ^{tol}NPNTiCl₂ [**3.18**] with KHBet₃ at -40 °C led to the isolation of [^{tol}NPNTiH₂]₂ [**5.21**] (Figure 175) as a brown solid with a ³¹P{¹H} NMR spectrum that displays a peak at δ -2.57. The ¹H NMR spectrum displays a triplet downfield 14.45 with ²J_{PH} = 16 Hz, which becomes a singlet in a decoupled ¹H{³¹P} NMR spectrum (Figure 176),

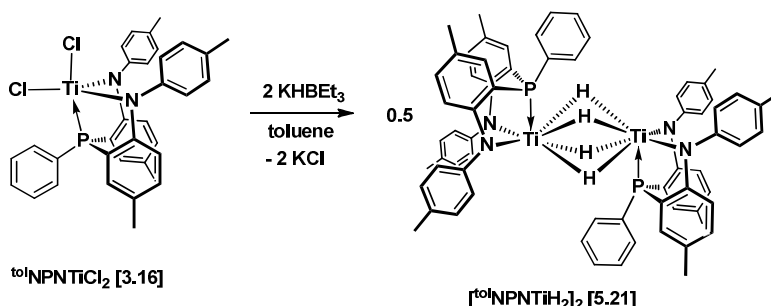


Figure 175: Synthesis of [^{tol}NPNTiH₂]₂ [**5.21**]

The synthesis of [^{tol}NPNTiH₂]₂ [**5.21**] was conducted in a dinitrogen atmosphere, thus complex [**5.21**] does not activate dinitrogen at 1 atm pressure. Transition metal hydrides are, however, implicated in important industrial processes such as hydrogenations, hydrosilylation,³³⁷ carbonylation³³⁸ and ethylene polymerisation^{339, 340} and has potential hydrogen storage materials.³⁴¹ Complex [**5.21**] may thus have potential in areas other than dinitrogen activation.

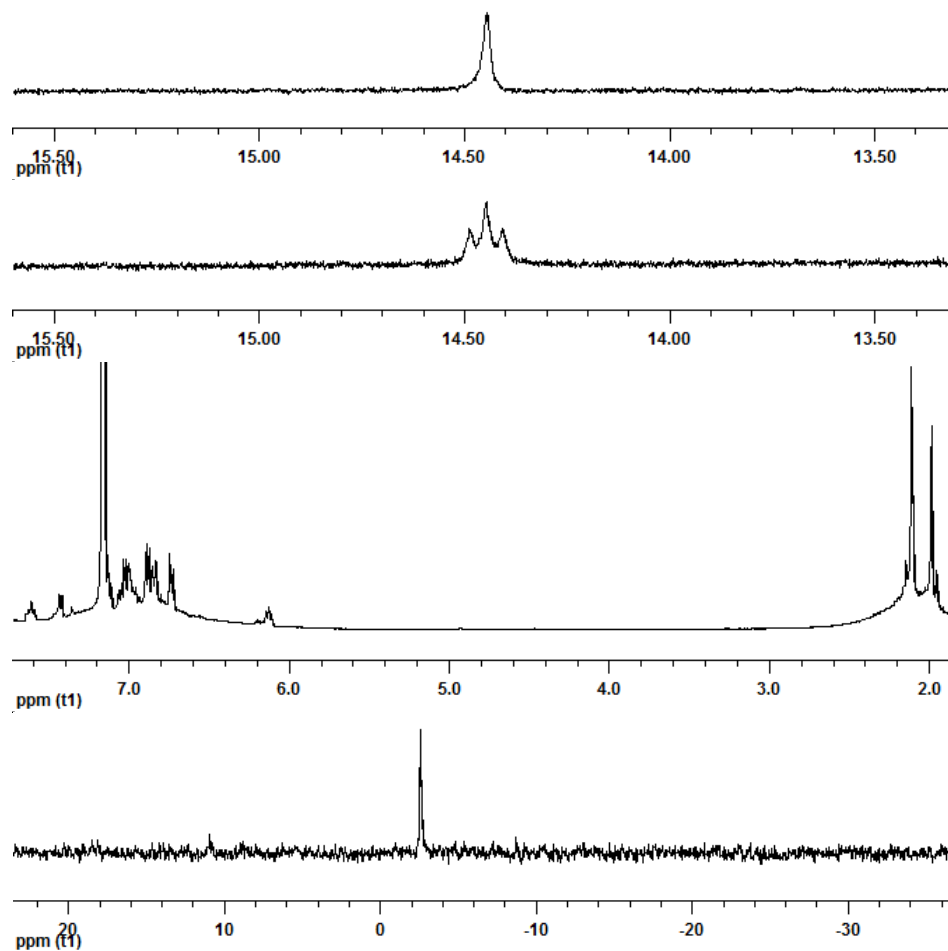


Figure 176: $^{31}\text{P}\{^1\text{H}\}$ (bottom), partial ^1H (middle two) and partial $^1\text{H}\{^{31}\text{P}\}$ NMR (top) spectra of $[\text{tolNPNZr}(\text{THF})_2(\mu\text{-}\eta^2\text{:}\eta^2\text{-N}_2)]$ [5.21] in C_6D_6

5.7. Summary

The purple dinitrogen complexes $[\text{ipropNPNZr}(\text{THF})_2(\mu\text{-}\eta^2\text{:}\eta^2\text{-N}_2)]$ [5.1] and $[\text{tolNPNZr}(\text{THF})_2(\mu\text{-}\eta^2\text{:}\eta^2\text{-N}_2)]$ [5.3] prepared in this study with sterically less hindered ipropNPN and tolNPN ligands contain more strongly activated side-on N_2^{-4} units compared to the blue-green $[\text{mesNPNZr}(\text{THF})_2(\mu\text{-}\eta^2\text{:}\eta^2\text{-N}_2)]$ reported in a previous Fryzuk group study. It was also found that complexes [5.1] and [5.3] had more strongly bound, less labile THF ligands. Reactions involving displacement of THF with other donor atoms consequently required an excess (or neat) amount of the displacing ligand. In the case of the softer THT ligand, it was not possible to completely

displace THF, and experiments suggested that more labile Et₂O or PMe₃ pre-cursor adducts may have better success.

Another significant difference between the zirconium N₂ complexes with ^{iprop}NPN and ^{tol}NPN ligands compared to the ^{mes}NPN analogue can be observed for the PPhMe₂ and PMe₃ phosphine adducts. From the previous study, it was reported that the more bulky ^{mes}NPN ligand impedes coordination of a second phosphine, resulting in an open site at one of the zirconium centres i.e. [NPNZr(PMe₂)](μ - η^2 : η^2 -N₂)[NPNZr]. The same is not true for the ^{iprop}NPN and ^{tol}NPN ligands in this study, and phosphine coordinates to both zirconium centres i.e. [NPNZr(PMe₂)]₂(μ - η^2 : η^2 -N₂) [5.8], [5.9], [5.10] and [5.11].

An attempt at performing the reduction of a dilute zirconium dichloride solution at r.t. and higher N₂ pressure (600 psi) yielded multiple products, with a control experiment at normal reduction temperatures and N₂ pressure suggesting that lower concentrations promotes more reduction side-products. A high pressure reduction of a concentrated solution was not attempted due to the large volume required.

Reduction of hafnium dichlorides with N₂ failed to yield the corresponding hafnium N₂ complexes, which is not unexpected as hafnium is typically harder to reduce than zirconium. The titanium tetrahydride [^{tol}NPNTiH₂]₂ [5.21] also proved unreactive with N₂, however, reduction of titanium dichlorides with N₂ did lead to the formation of medium activated end-on dinitrogen complexes [^{tol}NPNTi(THF)]₂(μ - η^1 : η^1 -N₂) [5.15] and [^{iprop}NPNTi(THF)]₂(μ - η^1 : η^1 -N₂) [5.17].

In previous work with the more flexible ^{Si}NPN ligand, the titanium dinitrogen complex had only been observed in solution as an intermediate during the conversion of the ^{Si}NPN ligand into a phosphinimide. In this study, it is demonstrated that the more rigid o-phenylene ligands ^{iprop}NPN and ^{tol}NPN stabilised the dinitrogen species to allow for isolation and inhibited phosphinimide formation. For the THF adduct, the titanium is five-coordinate with square

pyramidal geometry, however, during displacement with excess pyridine, each THF is replaced with two Py, resulting in octahedral coordination with the two Py *cis* on each titanium atom, but *trans* relative to the other titanium atom of the complex *trans*-[¹⁰¹NPNTi(Py)₂]₂(μ-η^l:η^l-N₂)

[5.19]. Complex **[5.19]** is unstable in solution, but an exploratory displacement reaction with 2,2'-bipyridine appeared to form a single stable species. For THF adducts, there is NMR spectroscopy and mass spectrometry indications that a species with two THF per titanium atom can also be formed i.e. 1410 m/z representative of [¹⁰¹NPNTi(THF)₂]₂(μ-η^l:η^l-N₂).

Chapter 6: Group 4 Dinitrogen Complex Reactivity

6.1. Reactivity of Zirconium Dinitrogen Complexes

In chapter 5, the synthesis of dinitrogen complexes has been discussed. While this has presented many challenges, and the isolation and characterisation of these species are important accomplishments, it is also of interest to try and functionalise the coordinated dinitrogen unit. In this section, exploratory studies are presented with zirconium complexes and dihydrogen, isocyanide, phenylsilane, ethylene, carbon monoxide, 4,4'-dimethylbenzophenone, carbon dioxide and (trimethylsilyl)diazomethane. None of the studies resulted in the full characterisation of the products and no crystals could be obtained to confirm the structures of the transformed N₂ complexes. For this reason, the studies described below present suggested structures on the basis of ¹H and ³¹P{H} NMR data alone.

6.1.1. Reaction with Dihydrogen

The Haber-Bosch process, converting dinitrogen and dihydrogen catalytically into ammonia, is the only viable industrial process utilising N₂ as a feedstock. The process requires high temperatures (400 to 500 °C) and pressures (130 to 300 atm) and involves the formation of surface metal nitride species (usually Fe, Ru, Os). The metal surface also cleaves the dihydrogen homolytically and the nitrogen and hydrogen ions on the surface combine to liberate ammonia. There is a strong incentive to develop a catalyst system that can operate at lower temperatures and pressures, which may be able to challenge the efficiency of the Haber-Bosch process. For example, heterogeneous ruthenium and palladium catalysts were reported to perform the conversion at atmospheric dinitrogen pressure, with protons supplied through a solid electrolyte rather than reaction with dihydrogen.³⁴²⁻³⁴⁴ Ambient conditions are achieved in natural systems with transition metal centres containing coordinated dinitrogen in nitrogenase enzymes, where the hydrogen ions are provided via a protic source rather than molecular hydrogen. For transition

metal dinitrogen complexes, the liberation of ammonia via the addition of protons was first reported for titanium,^{84, 86, 87, 160} followed by tungsten and molybdenum^{345, 346} and the development of model molybdenum complexes in support of the Chatt Cycle.^{30, 55} In a seminal report by Schrock *et al.*,^{51, 347-350} the first transition metal dinitrogen coordination complex was reported to perform this transformation catalytically at ambient conditions with 2,6-lutidinium cations as a protic source. This weak acid, as well as 2-picolinium, proved effective in a subsequent catalyst system reported by Nishibayashi *et al.*⁵⁰ More recently, an iron dinitrogen catalyst was reported by Peters *et al.*,^{88, 89} with protons provided by $\text{HB}(\text{C}_6\text{H}_3(3,5\text{-CF}_3)_2)_4$. Catalytic turnover for the above-mentioned systems are however not yet sufficient for industrial utilisation.

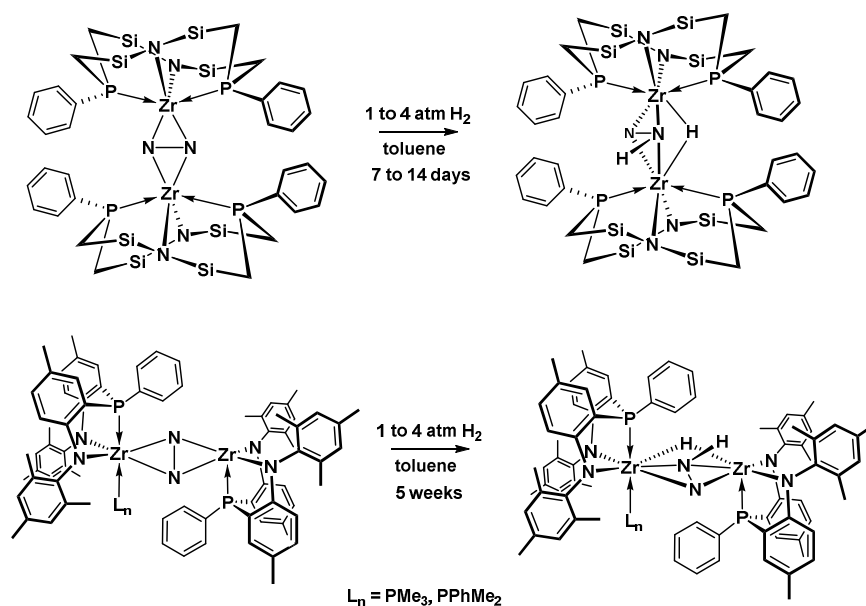


Figure 177: Hydrogenation with P_2N_2 (silyl methyls omitted for clarity) and NPN amido-phosphine N_2 complexes

The discovery of a homogeneous alternative to the solid-state Haber-Bosch catalysts with coordinated transition metal dinitrogen complexes and molecular hydrogen however, remains elusive. Examples of partial hydrogenation of coordinated dinitrogen is limited to zirconium dinitrogen complexes containing amido-phosphine based P_2N_2 ⁹⁰ and NPN^{92, 97} ligands (Figure

177), and cyclopentadienyl^{93, 98} based ligands, with substoichiometric liberation of ammonia reported in the latter case.⁹³ A hafnocene⁹⁹ and a iron-potassium⁶³ dinitrogen complex were able to form ammonia from molecular hydrogen, and ammonia was also liberated by the addition of molecular hydrogen to a cooperative mixture of tungsten dinitrogen and ruthenium dihydrogen complexes.⁹¹ In an unprecedented reaction, a trinuclear titanium polyhydride complex formed *in situ* on exposure to molecular hydrogen simultaneously activates and partially hydrogenates dinitrogen at ambient temperature and pressure conditions.^{100, 101}

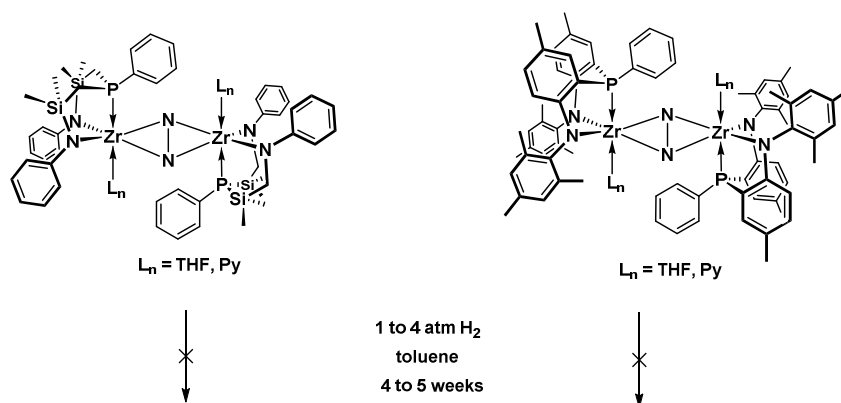


Figure 178: Failed hydrogenations with $\text{NPN}(L_n)$ zirconium N_2 complexes

While complex $[\text{mes-NPNZr}(\text{PRMe}_2)](\mu\text{-}\eta^2\text{:}\eta^2\text{-N}_2)[\text{mes-NPNZr}]$, $\text{R} = \text{Ph, Me}$ (Figure 177), can be hydrogenated with molecular hydrogen,^{92, 97} other diamido-phosphine based dinitrogen complexes $\text{NPN}(L_n)$ such as $[\text{Si-NPNZr}(L_n)]_2(\mu\text{-}\eta^2\text{:}\eta^2\text{-N}_2)$ ¹³⁷ and $[\text{mes-NPNZr}(L_n)]_2(\mu\text{-}\eta^2\text{:}\eta^2\text{-N}_2)$,⁹⁷ $L_n = \text{THF}$ and Py , failed to react with dihydrogen (Figure 178). It may be that for 2:1 complexes (i.e. 2 Zr : 1 L_n), where only one of the zirconium centres is coordinated by an adduct L_n molecule, hydrogenation is favoured at the open coordination site of the other zirconium centre. The zirconium centres of the 2:2 complexes formed when $L_n = \text{THF}$ and Py do not contain an open coordination site and consequently remained unreactive. While an obvious conclusion could be that an open coordination site, as present in the 2:1 $\text{NPN}(L_n)$ complexes, is essential for hydrogenation, it may be argued that having phosphine and amido donors are more important,

with hydrogenation disfavoured when the nitrogen donor is pyridine, or when an oxygen-containing donor such as THF is present. For the closely related P_2N_2 zirconium dinitrogen complex, both zirconium centres display octahedral geometries without an open coordination site, but reaction with dihydrogen proceeded (Figure 177).

To further explore this issue, the 2:2 zirconium dinitrogen complexes $[^{tol}NPNZr(THF)]_2(\mu-\eta^2:\eta^2-N_2)$ **[5.3]** and $[^{tol}NPNZr(PMe_3)]_2(\mu-\eta^2:\eta^2-N_2)$ **[5.9]** of the type $NPN(L_n)$, $L_n = THF$ and PMe_3 , formed in this study were exposed to 1 atm H_2 in toluene- d_8 for four weeks, with no observable reactivity (Figure 179).³¹⁴

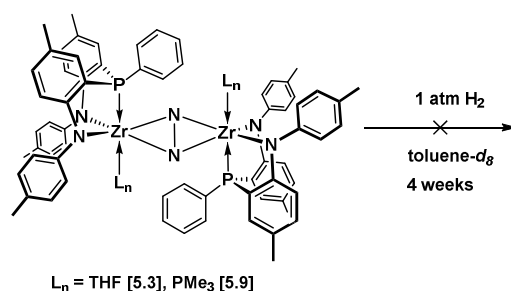


Figure 179: Reaction of 2:2 dinitrogen complexes $NPN(L_n)$, $[^{tol}NPNZr(THF)]_2(\mu-\eta^2:\eta^2-N_2)$ **[5.3] and $[^{tol}NPNZr(PMe_3)]_2(\mu-\eta^2:\eta^2-N_2)$ **[5.9]** with molecular hydrogen**

The lack of reactivity for complex **[5.9]** when L_n was a phosphine donor further confirms the theory that an open coordination site on zirconium for dinitrogen complexes with a $NPN(L_n)$ donor set promotes reaction with dihydrogen and that it is a more important factor than the nature of the L_n donor.³¹⁴ In the case of hydrogenation for the related P_2N_2 zirconium dinitrogen complex, the N and P donor atoms of the macrocyclic P_2N_2 ligand are pulled away from the equatorial plane, exposing the metal centre, which may be enough to compensate for the lack of an open coordination site.

The observation of the green 2:2 complex $[^{iprop}NPNZr(THF)](\mu-\eta^2:\eta^2-N_2)$ **[5.7]** confirms that removal of THF to form a 2:1 complex with an open

site would be impossible for the sterically less hindered dinitrogen complexes with ^{iprop}NPN and ^{tol}NPN donor sets prepared in this study (compared to ^{mes}NPN, where THF was also more weakly bound).

6.1.2. Reaction with Isocyanide

The isocyanide moiety may act as a neutral two-electron donor via the lone pair of the carbon atom³⁵¹⁻³⁵³ or become involved in insertion reactions as reported for metal-carbon,³⁵⁴⁻³⁵⁷ metal-nitrogen³⁵⁸ or metal-phosphorus³⁵⁹ bonds. Dual coordination and insertion modes involving multiple isocyanide molecules at a single metal site can also occur.^{354, 360} In this study, the reaction of two different isocyanides, namely 2,6-dimethylphenylisocyanide (xylylNC) and tert-butylisocyanide (^tBuNC), were investigated with [^{iprop}NPNZr(THF)₂(μ-η²:η²-N₂)] **[5.1]**, [^{iprop}NPNZr(THF)]₂(μ-η²:η²-¹⁵N₂) **[5.2]** or [^{tol}NPNZr(THF)]₂(μ-η²:η²-N₂) **[5.3]**.

Table 27 : ³¹P{¹H} and ¹⁵N{¹H} NMR data for reactions of xylylNC and ^tBuNC with **[5.1]**, **[5.2]** and **[5.3]**

| Complex | 2 RCN | Species | P1 | P1a | ¹⁵ N1 | ¹⁵ N1a |
|-----------------------------------|-------------------|-------------|-------------------------------------|-------|--|-------------------|
| ^{iprop} NPN [5.1] | xylylNC | species a | 1.67 | 11.19 | | |
| ^{tol} NPN [5.3] | xylylNC | species b | 1.25 | 11.89 | | |
| ^{iprop} NPN [5.2] | xylylNC | species a-1 | 2.03 (d) J _{PN} = 20 Hz | 11.54 | -220.91 (d) J _{PN} = 20 Hz | -17.70 |
| ^{iprop} NPN [5.1] | ^t BuNC | species c | 4.40 | 10.84 | | |
| ^{tol} NPN [5.3] | ^t BuNC | species d | 2.25 | 10.50 | | |
| 4 RCN | | | | | | |
| ^{iprop} NPN [5.1] | xylylNC | species e | -0.08 | 0.90 | | |
| ^{iprop} NPN [5.2] | xylylNC | species e-1 | -1.10 (d) J _{PN} = 9 Hz | 0.07 | -152.11 (d) J _{PN} = 5 Hz | -17.67 |

Purple solutions of complexes **[5.1]**, **[5.2]** and **[5.3]** immediately turned dark brown on addition of two equiv of xylylNC or ^tBuNC. For future discussions, the products from reactions of complexes **[5.1]**, **[5.2]** and **[5.3]** with two equiv of xylylNC will be referred to as **species a**, **species a-1** and **species b** and of complexes **[5.1]** and **[5.3]** with two equiv of ^tBuNC as **species c** and **species d** (Table 27). In further reactions of complexes **[5.1]** and **[5.2]** with four equiv of xylylNC, a different product was observed, to be referred to as **species e** and **species e-1** (Table 27). Reactions with four equiv of ^tBuNC did not lead to the observation of any new species.

Reactions with the ^{15}N labelled N_2 complex [5.2] (i.e. species **a-1** and **e-1**) served to verify that N_2 was not displaced, but underwent further reactivity.

Species a (and a-1), b, c and d displays two distinctly different downfield shifted signals in their respective $^{31}\text{P}\{^1\text{H}\}$ NMR spectra (Table 27), as illustrated for **species a** with signals at δ 11.19 and δ 1.67 (Figure 180). This indicates at least two NPN donor sets per molecular structure for **species a-d**, with a unique environment for each phosphorus atom. Furthermore, the mass spectrum obtained for **species a** displayed a parent ion at 1522 m/z , which is consistent with the presence of two xylyl ligands in a dimer structure $[\text{ipropNPNZr}(\text{xylylNC})]_2(\text{N}_2)$.

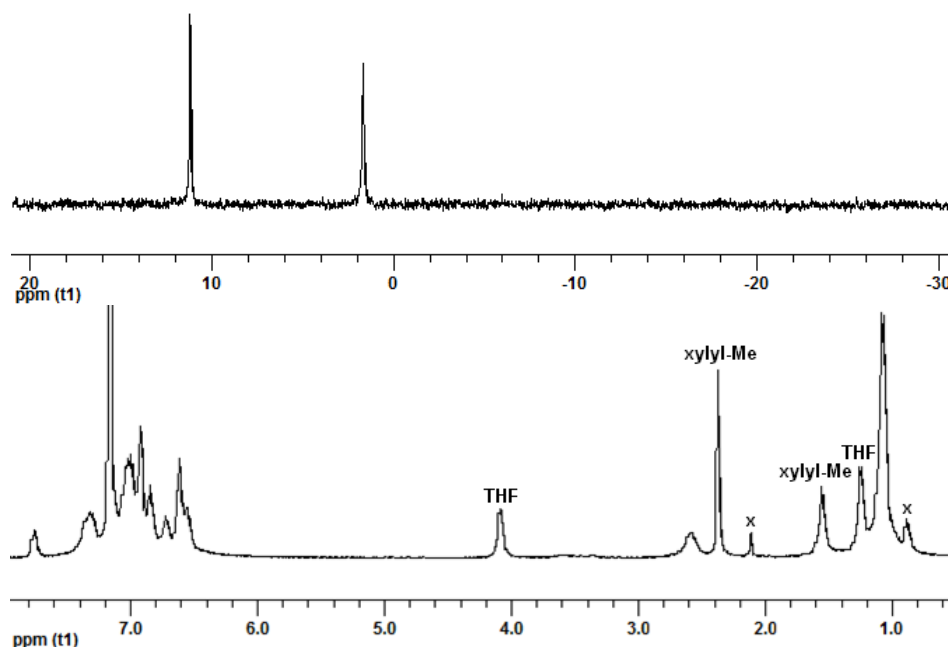


Figure 180: $^{31}\text{P}\{^1\text{H}\}$ (top) and ^1H NMR (bottom) spectra of complex [5.1] + 2 equiv of xylylNC (species a) in C_6D_6 , x denotes residual toluene and *n*-hexane solvents

The corresponding ^1H NMR spectrum for **species a** (Figure 180) indicates one THF remains coordinated with broad signals at δ 4.09 and δ 1.14 (correlation confirmed with ^1H - ^1H COSY NMR spectrum) and two different signals for the methyls of xylylNC at δ 1.56 and δ 2.37 (free xylylNC at δ 2.06).

The ^{15}N isotopologue **species a-1** displays upfield shifted signals in the $^{15}\text{N}\{^1\text{H}\}$ NMR spectrum at δ -220.91 (d, $^2J_{\text{PN}} = 20$ Hz) and δ -17.70 (δ 88.54 for $[\text{ipropNPNZr}(\text{THF})]_2(\mu\text{-}\eta^2\text{:}\eta^2\text{-}^{15}\text{N}_2)$ [**5.2**]) and the corresponding $^{31}\text{P}\{^1\text{H}\}$ NMR spectrum displays signals in at δ 2.03 (d, $J_{\text{PN}} = 20$ Hz) and δ 11.54 (Figure 181). It is unclear why J_{PN} coupling was only observed for one of the nitrogen and phosphorus atoms, but $^2J_{\text{PN}}$ coupling had also not been observed for complex [**5.2**] (see chapter 5). For comparison, $^2J_{\text{PN}}$ coupling was reported for $[\text{mesNPNZr}(\text{THF})]_2(\mu\text{-}\eta^2\text{:}\eta^2\text{-}^{15}\text{N}_2)$ at 6.7 Hz,^{92, 97} and $[\text{SiNPNTaH}]_2(^{15}\text{N}_2)$ at 21.5 Hz⁷⁹ and $^3J_{\text{PN}}$ coupling for $[\text{SiNPNTaH}]_2(^{15}\text{N}_2)$ at 3.5 Hz.⁷⁹

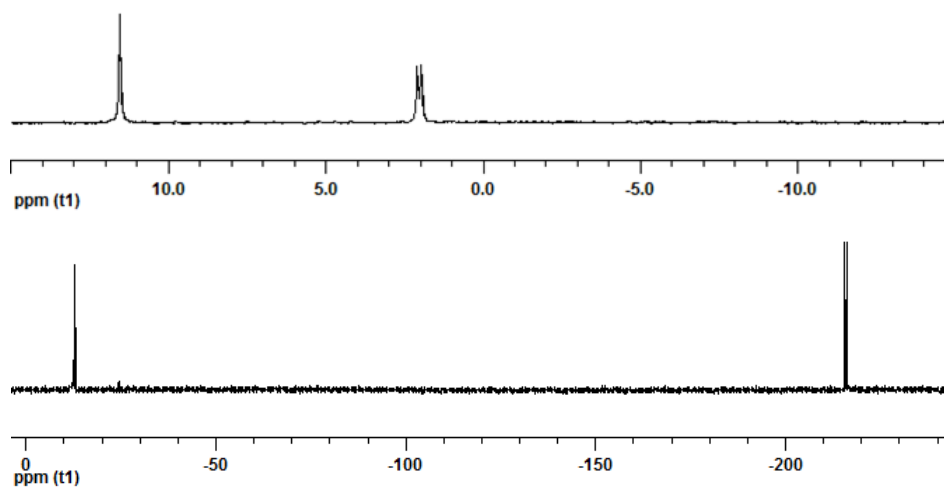


Figure 181: $^{31}\text{P}\{^1\text{H}\}$ (top) and $^{15}\text{N}\{^1\text{H}\}$ NMR (bottom) spectra of complex [**5.2**] + 2 equiv of xylylNC (**species a-1**) in C_6D_6

The significantly upfield shifted location of the doublet for **species a-1** in the $^{15}\text{N}\{^1\text{H}\}$ NMR spectrum at δ -220.91 (reported range for side-on bound N_2 transition metal complexes δ -30.6 to δ 689.7¹²⁵) suggests that at least one of the coordinated dinitrogen atoms had undergone significant transformation. The large variance in relative upfield shift experienced by the two nitrogen atoms of **species a-1** (compared to the nitrogens in complex [**5.2**]) implies unique reactivity at the two nitrogen centres.

The presence of a coordinated THF argues against a simple displacement model of two THF donors by two RNC moieties. Facile insertion of the first isocyanide into one of the Zr-N bonds may have occurred, after initial displacement of one of the THF donors. Preferential coordination of the second isocyanide to the zirconium centre involved with the first isocyanide insertion rather than displacing THF at the other zirconium centre could result in the proposed product structures $[\text{NPNZr}(\text{THF})](\text{RNC-N}_2)[\text{NPNZr}(\text{RNC})]$ [6.1], [6.2], [6.3], [6.4] and [6.5] (Figure 182). Such a dual behavior for two isocyanide ligands at a single metal centre has previously been reported for zirconocene complexes.^{354, 360}

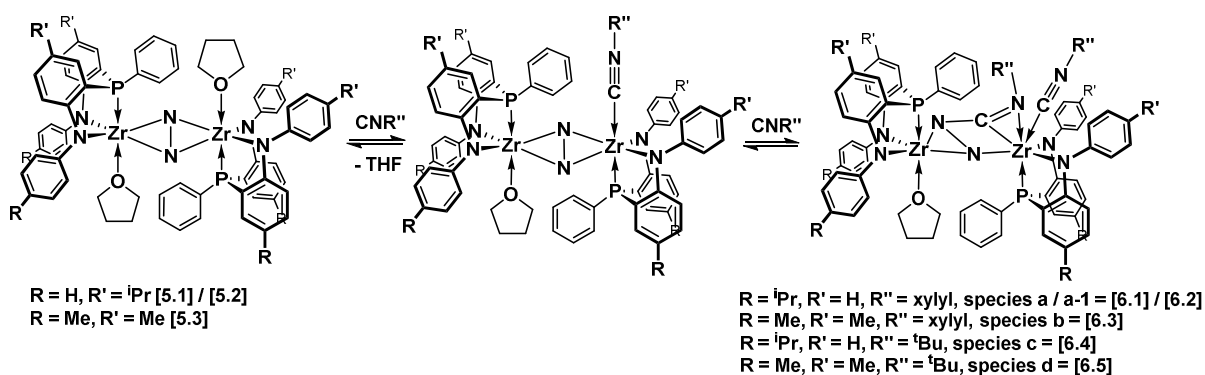


Figure 182: Proposed reaction of complexes [5.1], [5.2] and [5.3] with 2 equiv of xylylNC or ^tBuNC. Note: (i) the N-N bond is depicted intact, as insufficient data to evaluate if N-N cleavage occurred, (ii) isocyanide insertion is depicted as N-inside, but may be N-outside³⁵⁴ and (iii) the P atoms of the ligands are depicted in a *trans* arrangement (as in the precursors), but could be *cis*.

A further intricacy becomes evident on inspection of the reaction of complex [5.1] with 2 equiv of ^tBuNC. The ¹H NMR spectrum for **species c** (proposed complex [6.4]) displays two broad signals at δ 3.48 / 3.74 and δ 1.09 / 1.14 indicating two discreet THF environments and there are also two different methine signals at δ 2.67 / 2.86 (Figure 183).

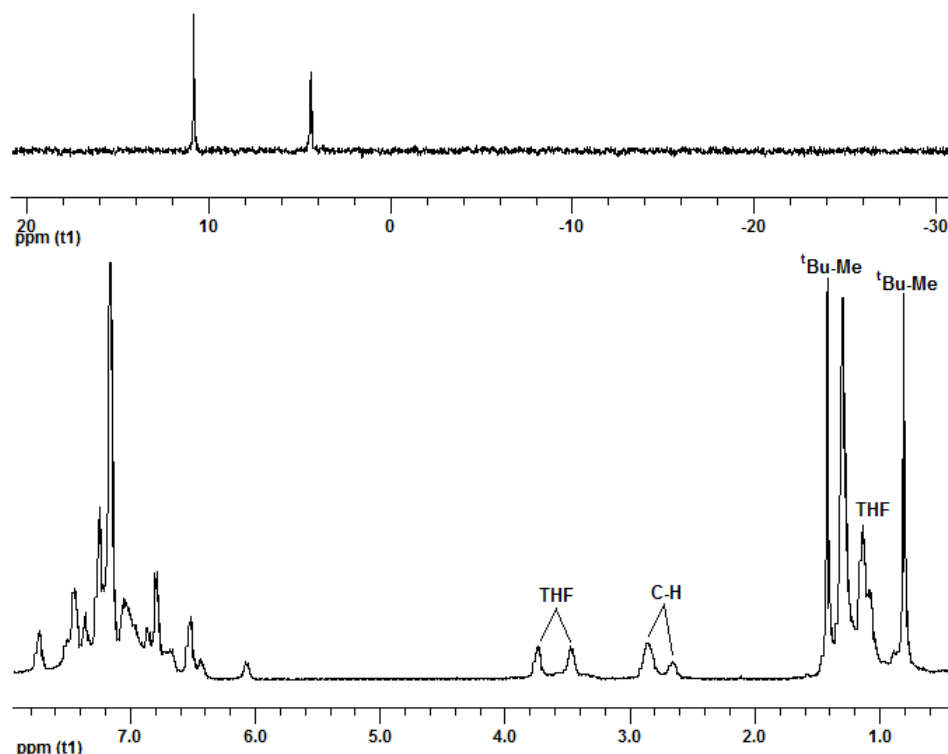


Figure 183: $^{31}\text{P}\{^1\text{H}\}$ (top) and ^1H NMR (bottom) spectra of complex [5.1] + 2 equiv of $t\text{BuNC}$ (species **c**) in C_6D_6

In all of the aforementioned proposed structures for complexes [6.1] to [6.5], the isocyanide was depicted inserting into the Zr-N bond such that the N atom of the inserted isocyanide is next to the carbon of the adjacent coordinated isocyanide i.e. N-inside (Figure 182). It is also possible for the C atom of the inserted isocyanide to be next to the carbon of the adjacent coordinated isocyanide i.e. N-outside.³⁵⁴ In a different scenario, while the P atoms for these types of NPN zirconium dinuclear complexes as proposed for complex [6.4] is usually *trans*, they may also occur in a *cis* arrangement. A mixture of either co-existing N-inside / N-outside or P-*cis* / *trans* isomers may explain the additional signals present in the ^1H NMR spectrum.

The effect of the addition of one to four equiv of xylylNC to $[\text{ipropNPNZr}(\text{THF})_2(\mu-\eta^2:\eta^2-^{15}\text{N}_2)]$ [5.2] was investigated. The $^{31}\text{P}\{^1\text{H}\}$ NMR spectrum after one equiv of xylylNC indicated the presence of **species a-1**, unreacted dinitrogen complex [5.2] and an unidentified intermediate

species x at δ -7.22 (Figure 184), with **species a-1** being observed exclusively after addition of two equiv of xylylNC. On addition of a third equiv of xylylNC, a mixture of **species a-1** and a new **species e-1** was observed, with new signals at δ 0.90 and δ -0.08. Four equiv of xylylNC was required to complete the conversion of **species a-1** to **e-1** (Figure 184).

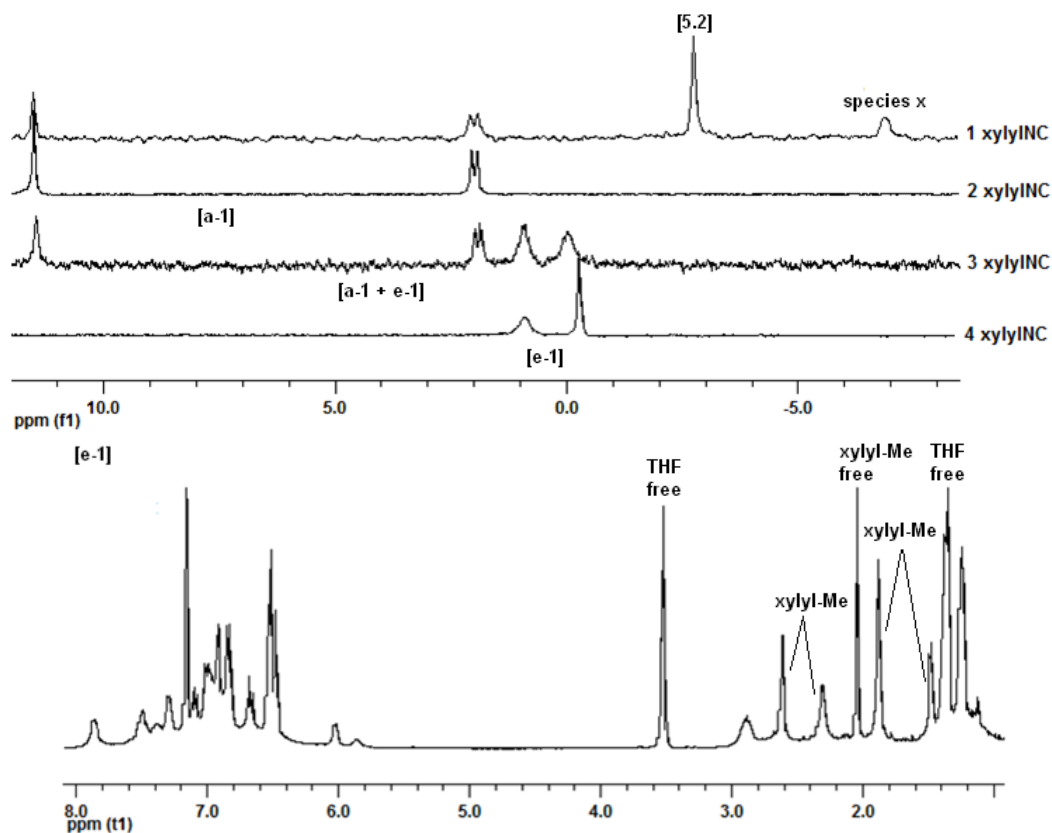


Figure 184: $^{31}\text{P}\{^1\text{H}\}$ NMR spectra of complex [5.2] with 1, 2, 3 and 4 xylylNC (species a-1 and e-1) (top) and ^1H NMR spectrum with 4 xylylNC (species e-1) (bottom) in C_6D_6

The ^1H NMR spectrum of species **e-1** no longer displayed coordinated THF signals at δ 4.09 and δ 1.14, but peaks at δ 3.52 and δ 1.35 representing unbound THF (Figure 184). There are four different signals for the methyls of xylylNC at δ 1.47, δ 1.88, δ 2.31 and δ 2.61, with some excess free xylylNC at δ 2.05. Similar trends were observed for the addition of 1-4 equiv of xylylNC to $[\text{ipropNPNZr}(\text{THF})_2(\mu\text{-}\eta^2\text{:}\eta^2\text{-N}_2)]$ [5.1].

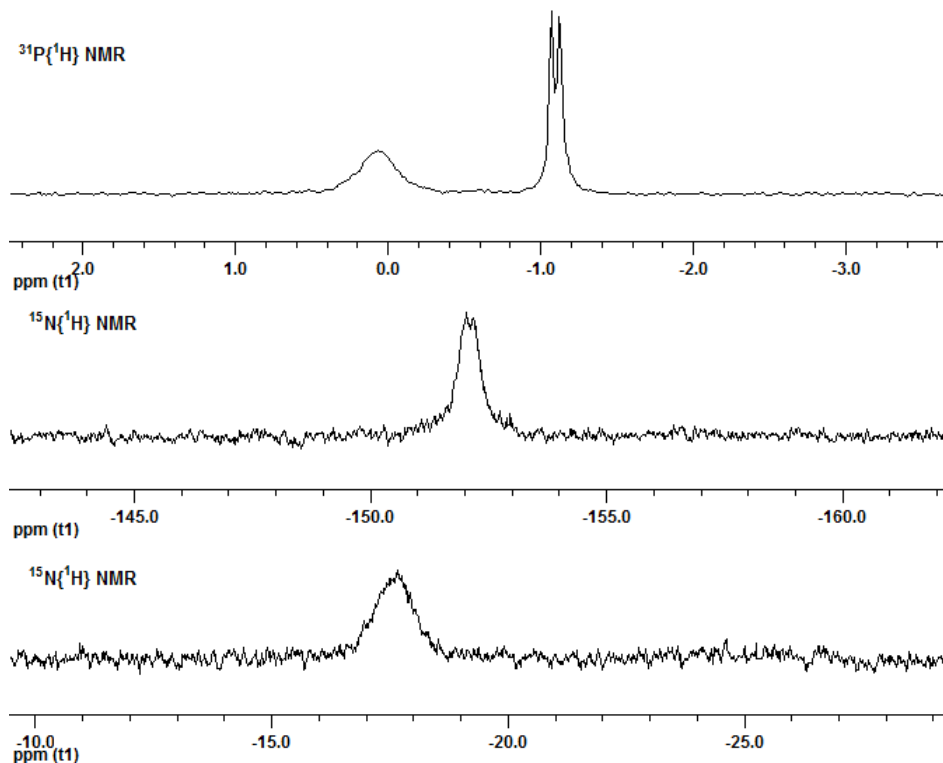


Figure 185: $^{31}\text{P}\{^1\text{H}\}$ and partial $^{15}\text{N}\{^1\text{H}\}$ NMR spectra of complex [5.2] with 4 xylylNC (species e-1) in C_6D_6

The two unique phosphorus environments indicated for **species e** (and **e-1**) via their $^{31}\text{P}\{^1\text{H}\}$ NMR spectra (Figure 184 / Figure 185) are less downfield shifted than **species a** (and **a-1**). The corresponding $^{15}\text{N}\{^1\text{H}\}$ NMR spectrum (Figure 185) for species **e-1** provides evidence that the nitrogen atoms of the precursor N_2 unit are retained and confirms two unique nitrogen environments, where the signal at δ -17.67 remains unchanged compared to **species a-1**, but the doublet is less upfield at δ -152.11 with a smaller P-N coupling constant of 5 Hz (Figure 185). Again, P-N coupling is only observed for one of the nitrogen and phosphorus atoms, with a more clearly defined doublet observed with a coupling constant of 9 Hz in the $^{31}\text{P}\{^1\text{H}\}$ NMR spectrum of **species e-1** (Figure 185).

In the absence of any further experimental data or x-ray crystal structures for any of these RNC species, the most simplest speculation on the identity of **species e** (or **e-1**) could be a repetition of the proposed dual isocyanide insertion / coordination process at the second

zirconium centre for the addition of the third and fourth equiv of xylylNC, with associated liberation of the remaining THF.

Signals for the carbon atom of the RNC ligands in $^{13}\text{C}\{^1\text{H}\}$ NMR spectra could be a useful diagnostic tool, but difficulties were encountered in attaining $^{13}\text{C}\{^1\text{H}\}$ NMR spectra in C_6D_6 at room temperature, even for a prolonged collection period with a 600 MHz instrument. Infrared spectroscopy may potentially prove useful to discriminate between $\nu(\text{C}\equiv\text{N})$ vs. $\nu(\text{C}=\text{N})$ moieties and should be pursued in any further investigations.

6.1.3. Reaction with Phenylsilane

Hydrosilylation of activated dinitrogen was first reported for the reaction of one equivalent $n\text{-BuSiH}_3$ with the side-on dinitrogen zirconium P_2N_2 complex, forming a new N-Si bond and a bridging hydride (Figure 186).⁹⁰ Thereafter, the side-on and end-on bound tantalum $^{\text{Si}}\text{NPN}$ dinitrogen complex was reported to react with two equivalents of $n\text{-BuSiH}_3$, leading to the cleavage of the N-N bond and new N-Si bonds for both nitrogen atoms.¹⁰⁷

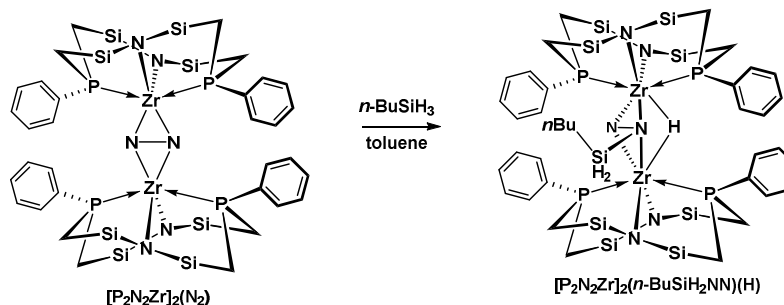


Figure 186: Hydrosilylation with P_2N_2 and $^{\text{Si}}\text{NPN}$ dinitrogen complexes

It was found that the diamidophosphine zirconium $\text{NPN}(\text{N})$ complex $[\text{mesNPNZr}(\text{Py})]_2(\mu\text{-}\eta^2\text{:}\eta^2\text{-N}_2)$ undergoes similar reactivity as the P_2N_2 complex, reacting with one equivalent of PhSiH_3 to form a bridging hydride and one new N-Si bond. During the reaction, one of the pyridine adducts became labilised, with the resulting electron deficient zirconium forming a side-on end-on bond with the N-N unit.⁹⁷

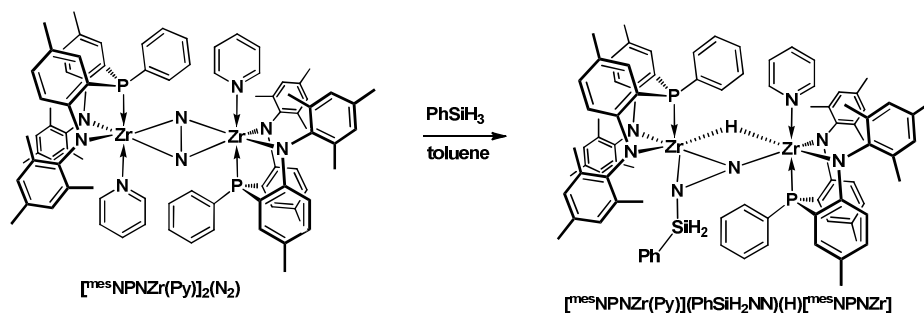


Figure 187: Hydrosilylation with the ^{mes}NPN containing dinitrogen complex

In this study, addition of one, two or twenty equivalents of PhSiH₃ to purple solutions of [ⁱpropNPNZr(THF)]₂(μ-η²:η²-N₂) [**5.1**] in C₆D₆ gave dark brown solutions with identical ³¹P{¹H} NMR spectra containing a sharp singlet at δ -10.09 as the main product (Figure 188). For comparison, peaks are reported at δ 14.9 and δ -4.3 for hydrosilylation of [^{mes}NPNZr(Py)]₂(μ-η²:η²-N₂).⁹⁷ As a single signal is observed irrespective of how much PhSiH₃ was added, only one molecule reacts with complex [**5.1**] and the product should possess C₂ symmetry.

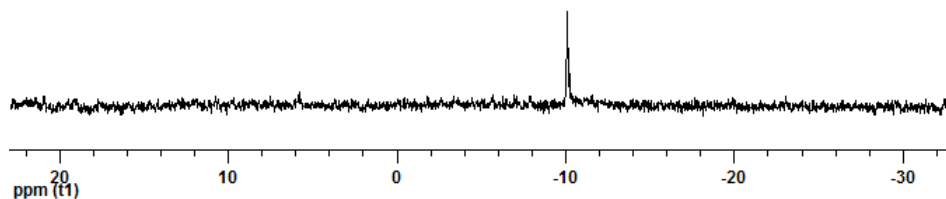


Figure 188: ³¹P{¹H} NMR spectrum of [ⁱpropNPNZr(THF)]₂(μ-η²:η²-N₂) [**5.1**] + PhSiH₃ in C₆D₆

In the associated ¹H NMR spectrum, signals could be observed at δ 4.78 and δ 0.29 in addition to broad signals for phenyl and isopropyl protons, with no signals for THF indicated. Assuming a similar hydrosilylation model for reaction of [ⁱpropNPNZr(THF)]₂(μ-η²:η²-N₂) [**5.1**] with PhSiH₃ as for the P₂N₂ zirconium dinitrogen complex (Figure 189), the signal at δ 4.78 may represent the Si-H signal for an NNSiH₂ group (peaks at δ 5.17 / 3.94 for ^{mes}NPN and δ 5.07 / 4.80 for P₂N₂ zirconium complexes, free PhSiH₃ at δ 4.24). The signal at δ 0.29 may represent a Zr-H-Zr group (peaks at δ 8.25 for ^{mes}NPN and δ 1.53 for P₂N₂ zirconium complexes).

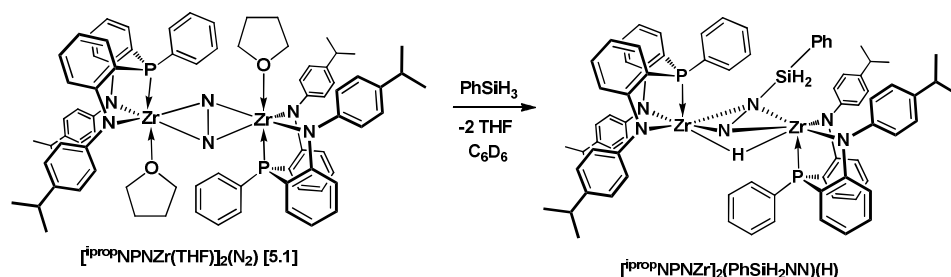


Figure 189: Hydrosilylation with $[\text{ipropNPNZr}(\text{THF})]_2(\mu\text{-}\eta^2\text{:}\eta^2\text{-N}_2)$ [5.1] with PhSiH_3

Attempts had been made to obtain $^{29}\text{Si}\{^1\text{H}\}$ NMR spectra, but no appreciable signals were observed. For future work, as loss of the coordinated THF was indicated in the isolated solid, it may be considered to repeat the reaction with pyridine or phosphine adducts instead.

6.1.4. Reaction with Ethylene

The 2 + 2 cycloaddition of ethylene to a coordinated dinitrogen unit³⁶¹ is an intriguing process that has yet to be observed. Group 4 transition metal complexes^{362, 363} (including dinitrogen complexes)³⁶⁴ are, however, well known to catalyse the polymerisation of ethylene. Coordinated ethylene species have to be accounted for as part of the suite of catalytic intermediates, and while a bis(pentamethyl cyclopentadienyl)-titanium ethylene complex^{365, 366} was isolated, it was found to convert ethylene to polymer at an extremely low rate (without an activator).³⁶⁵ This, coupled with the fact that dinitrogen containing catalysts still require an alkylating cocatalyst to achieve high activity,³⁶⁴ argues against ethylene complexes being a major active catalytic species contributor. The formation of polymer was reported for $[\text{Si}^{\text{iprop}}\text{NPNZr}(\text{THF})]_2(\mu\text{-}\eta^2\text{:}\eta^2\text{-N}_2)$ ¹³⁷ and $[\text{mes}^{\text{NPNZr}}(\text{THF})]_2(\mu\text{-}\eta^2\text{:}\eta^2\text{-N}_2)$,⁹⁷ but in both cases only the unreacted dinitrogen complexes were observed after ethylene exposure. There is the potential that polymer formation was due to other reduced zirconium species present at levels below the detection limits of NMR spectroscopy.

In this study, a purple toluene solution of $[\text{ipropNPNZr}(\text{THF})]_2(\mu\text{-}\eta^2\text{:}\eta^2\text{-N}_2)$ [5.1] was exposed to 1 atm ethylene at room temperature for 3 days. An amount of polymer was formed

and no colour changes were observed. The $^{31}\text{P}\{^1\text{H}\}$ NMR spectrum of the red-brown residue, obtained after removal of the toluene solvent, displayed a major peak with a similar chemical shift to unreacted complex **[5.1]** at δ -3.80, together with a new unidentified peak at δ 0.82 (Figure 190). It should be noted that no ingress of air was incurred during the above manipulations, as evidenced by the lack of a signal for $^{\text{iprop}}\text{NPNH}_2$ **[2.10]**.

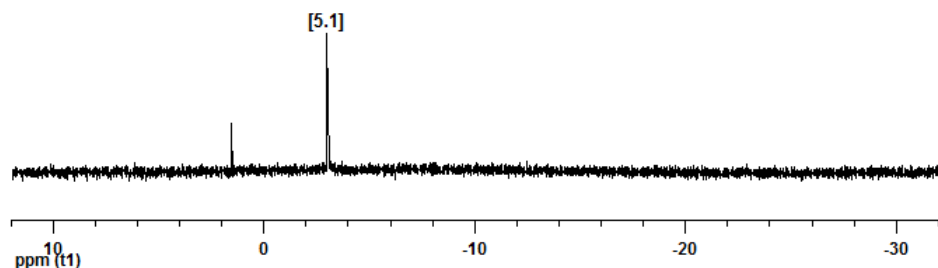


Figure 190: $^{31}\text{P}\{^1\text{H}\}$ (top) and ^1H NMR (bottom) of $[\text{ipropNPNZr}(\text{THF})_2(\mu\text{-}\eta^2\text{:}\eta^2\text{-N}_2)]$ **[5.1]** after 1 atm $\text{H}_2\text{C}=\text{CH}_2$

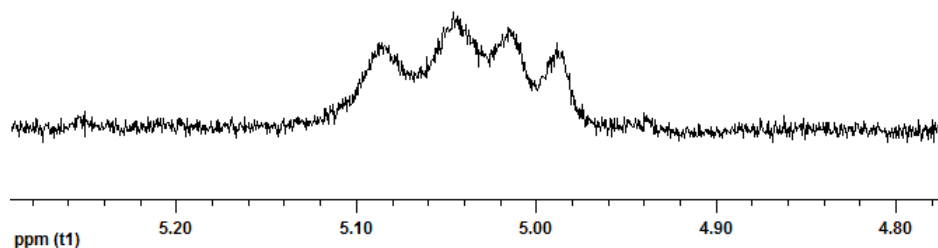


Figure 191: Partial ^1H NMR of $[\text{ipropNPNZr}(\text{THF})_2(\mu\text{-}\eta^2\text{:}\eta^2\text{-N}_2)]$ **[5.1]** after 1atm $\text{H}_2\text{C}=\text{CH}_2$ in C_6D_6

In addition to ligand, coordinated THF and residual toluene solvent, there was a small multiplet with four signals centred at δ 5.04 in the corresponding ^1H NMR spectrum (Figure 191). While this may potentially represent coordinated ethylene, reported chemical shifts for protons of zirconium ethylene complexes range from $\sim \delta$ -0.5 to 1.3^{176, 367-369} and would strongly discount the presence of a zirconium ethylene complex. Like the previous NPN zirconium dinitrogen experiments with ethylene, the strongly activated side-on dinitrogen ligand in **[5.1]** did not react with ethylene and the observed polymer may be catalysed by trace impurities of other reduced zirconium species.

6.1.5. Reaction with Carbon Monoxide

Based on reported reactions for group 4 (Zr, Hf) dinitrogen complexes with CO,^{97, 154, 155} a wide array of products may be theorised for reaction of $[\text{ipropNPNZr}(\text{THF})_2(\mu\text{-}\eta^2\text{:}\eta^2\text{-N}_2)]$ [5.1] (Figure 192), depending on whether exposure to CO was stoichiometric (1 equiv) or in a large excess (1-4 atm).

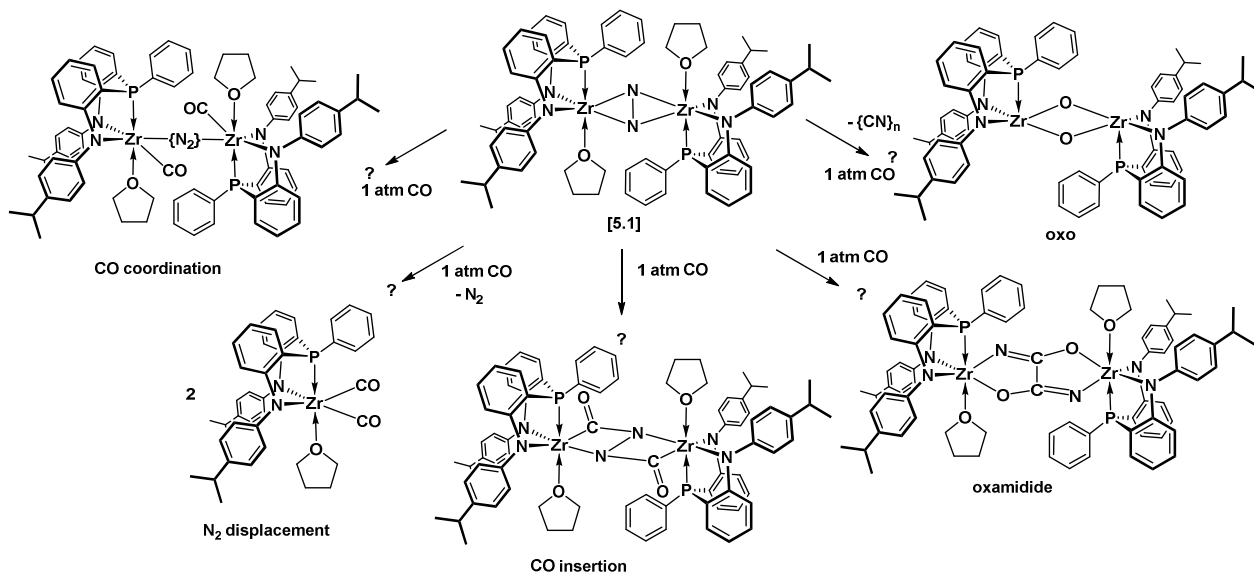


Figure 192: Theoretical products for reaction of $[\text{ipropNPNZr}(\text{THF})_2(\mu\text{-}\eta^2\text{:}\eta^2\text{-N}_2)]$ [5.1] with large excess CO

With a large excess CO, the activated dinitrogen unit may remain intact, with the formation of species with mixed CO and N₂ coordinated units, as was spectroscopically observed for a zirconocene dinitrogen complex.¹⁵⁵ Mixed CO and N₂ species were also reported for osmium and iron atoms.³⁷⁰ The N₂ unit could be completely displaced by CO, forming a zirconium carbonyl species.¹⁵⁵ The zirconium dinitrogen complex may undergo a double insertion into the Zr-N bonds, or commence with further transformation into a bridging oxamidide N₂C₂O₂⁴⁻ moiety.¹⁵⁴⁻¹⁵⁶

The reaction of $[\text{mesNPNZr}(\text{THF})_2(\mu\text{-}\eta^2\text{:}\eta^2\text{-N}_2)]$ and $[\text{mesNPNZr}(\text{PPhMe}_2)](\mu\text{-}\eta^2\text{:}\eta^2\text{-N}_2)$ $[\text{mesNPNZr}(\text{PPhMe}_2)]$ with 1 atm CO was reported to form the bridged di-μ-oxo species

$[\text{mesNPNZr}(\text{THF})_2(\mu\text{-O})_2]$, with a single peak displayed at δ -19.2 in the $^{31}\text{P}\{^1\text{H}\}$ NMR spectrum.

⁹⁷ No mechanism was indicated, and while it is probable that the source of the oxo group may have been molecular oxygen as an impurity in the CO gas, it is also plausible that the CO had reacted with the dinitrogen unit in such a way so as to cleave the $\text{C}\equiv\text{O}$ bond. Unfortunately no attempts had been made in the aforementioned study to identify any associated carbon and / or nitrogen containing side-products. In a different study, a bridged μ -oxo hafnocene species was formed after reaction of a hafnocene dinitrogen complex with CO and *n*-hexylSiH₃. The source of the O atom was in that case confirmed to be from CO, and the observation of *n*-hexylSiH₂CN in the product mixture verified the fate of the carbon and nitrogen atoms.¹⁵⁵

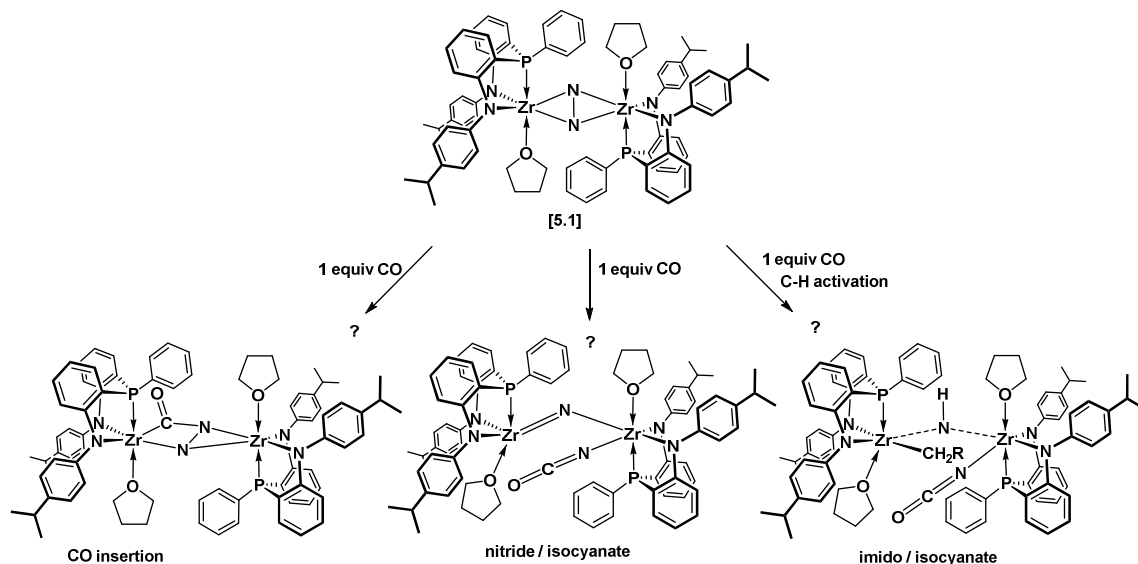


Figure 193: Theoretical products for reaction of $[\text{ipropNPNZr}(\text{THF})_2(\mu\text{-}\eta^2\text{:}\eta^2\text{-N}_2)]$ [5.1] with 1 equiv of CO

With one equivalent of CO (Figure 193), insertion of a single CO into a Zr-N bond may occur, or further transform accompanied by N-N scission to a terminal isocyanate ligand NCO with a bridging nitride, as was postulated for intermediates of the reaction with hafnocene dinitrogen.^{154, 155} Assuming N-N cleavage accompanies the reaction with one equiv of CO, the resulting postulated reactive nitride may engage in C-H activation of alkyl substituents of the ipropNPN ligand, forming a bridging imido Zr-NH-Zr and a new Zr-C bond, as was the case for

the reported product with hafnocene dinitrogen, 1 equiv of CO and methyl substituents of the substituted cyclopentadienyl ligand.^{154, 155}

In this study, the CO reactivity of the less encumbered N₂ complex [^{iprop}NPNZr(THF)]₂(μ-η²:η²-N₂) [**5.1**] was evaluated. Purple solutions of [^{iprop}NPNZr(THF)]₂(μ-η²:η²-N₂) [**5.1**] were exposed 1 equiv and 1 atm of CO, respectively, at room temperature. The solution exposed to 1 atm CO turned cherry red after 1 day, transitioning into an orange solution after 16 days. The ³¹P{¹H} NMR spectrum after 1 day revealed numerous peaks between δ -0.94 to δ 11.53 and a singlet at δ 23.00, together with a significant amount of unreacted complex [**5.1**] (Figure 194). The main change after 16 days is that only traces of complex [**5.1**] remain. This initial result suggests that while reaction of complex [**5.1**] with CO may be sluggish, a complex mixture of reaction products were obtained. Most notably, no signal was observed upfield close to δ -19.2 (as reported for [^{mes}NPNZr(THF)]₂(μ-O)₂),⁹⁷ hence the formation of a μ-oxo bridged product is not indicated to occur for the reaction of complex [**5.1**] with 1 atm CO.

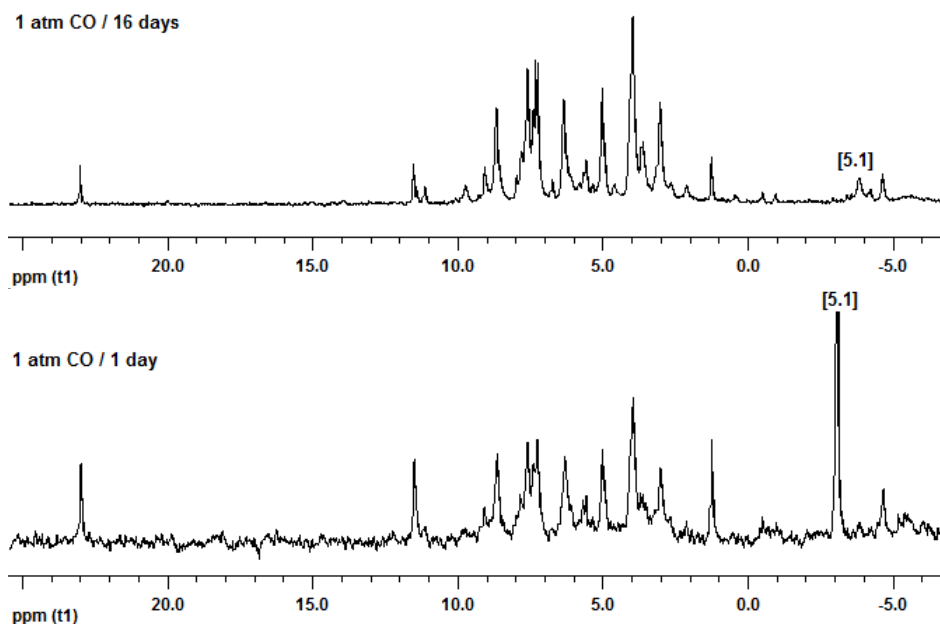


Figure 194: ³¹P{¹H} NMR spectra of [^{iprop}NPNZr(THF)]₂(μ-η²:η²-N₂) [**5.1**] after 1 atm CO in C₆D₆

The solution with 1 equiv of CO also turned cherry red-brown after 1 day, forming a dark brown solution after 15 days. A less complicated $^{31}\text{P}\{^1\text{H}\}$ NMR spectrum was obtained (Figure 195), with only five different signals, three of which also occur in the spectra of the solutions exposed to 1 atm CO (δ at 23.00, 11.53 and 1.25) and two peaks which are unique to the reaction with 1 equiv of CO (δ at -0.90 and -2.23).

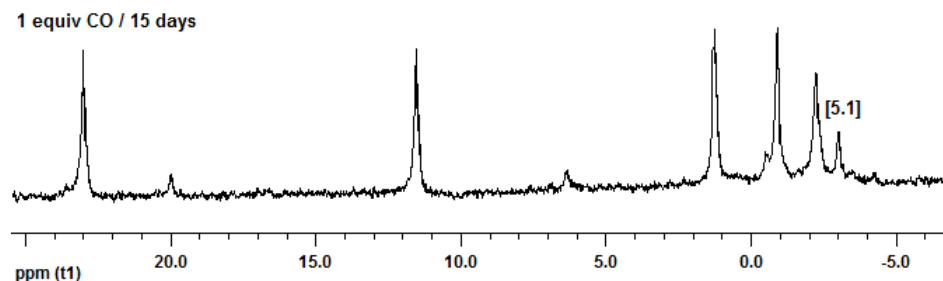


Figure 195: $^{31}\text{P}\{^1\text{H}\}$ spectrum of $[\text{ipropNPNZr}(\text{THF})_2(\mu\text{-}\eta^2\text{:}\eta^2\text{-N}_2)]$ [5.1] after 1 equiv of CO

Unfortunately crystals suitable for X-ray analysis were not obtained. Due to the observed complexity for the reactions of $[\text{ipropNPNZr}(\text{THF})_2(\mu\text{-}\eta^2\text{:}\eta^2\text{-N}_2)]$ [5.1] with CO, future work on this system should focus on increasing the steric bulk of the NPN ligands instead.

6.1.6. Reaction with 4,4'-Dimethylbenzophenone

$[\text{mesNPNZr}(\text{THF})_2(\mu\text{-}\eta^2\text{:}\eta^2\text{-N}_2)]$ was reported to react with one equiv of 4,4'-dimethylbenzophenone to give a dinuclear zirconium complex $[\text{mesNPNZr}]_2(\mu\text{-O})(\mu\text{-}\eta^1\text{:}\eta^2\text{-NN}=\text{C}(\text{C}_6\text{H}_4\text{Me})_2)$ with a side-on end-on bound hydrazonato ligand and a μ -oxo bridge.⁹⁷ Complete scission of the C=O bond was required to effect this transformation and the $^{31}\text{P}\{^1\text{H}\}$ NMR spectrum displayed two inequivalent signals at δ -7.7 and δ -10.4.⁹⁷ In addition to the afore-mentioned oxo / hydrazonato complex⁹⁷ (Figure 196) other theoretical products include an oxy / hydrazinato species or bridged oxo / nitrido / iminato complex (these latter alternatives

modelled on the reactivity of hafnium and zirconium dinitrogen complexes with CO₂ to form carboxyhydrazinato and isocyanate products).^{106, 157}

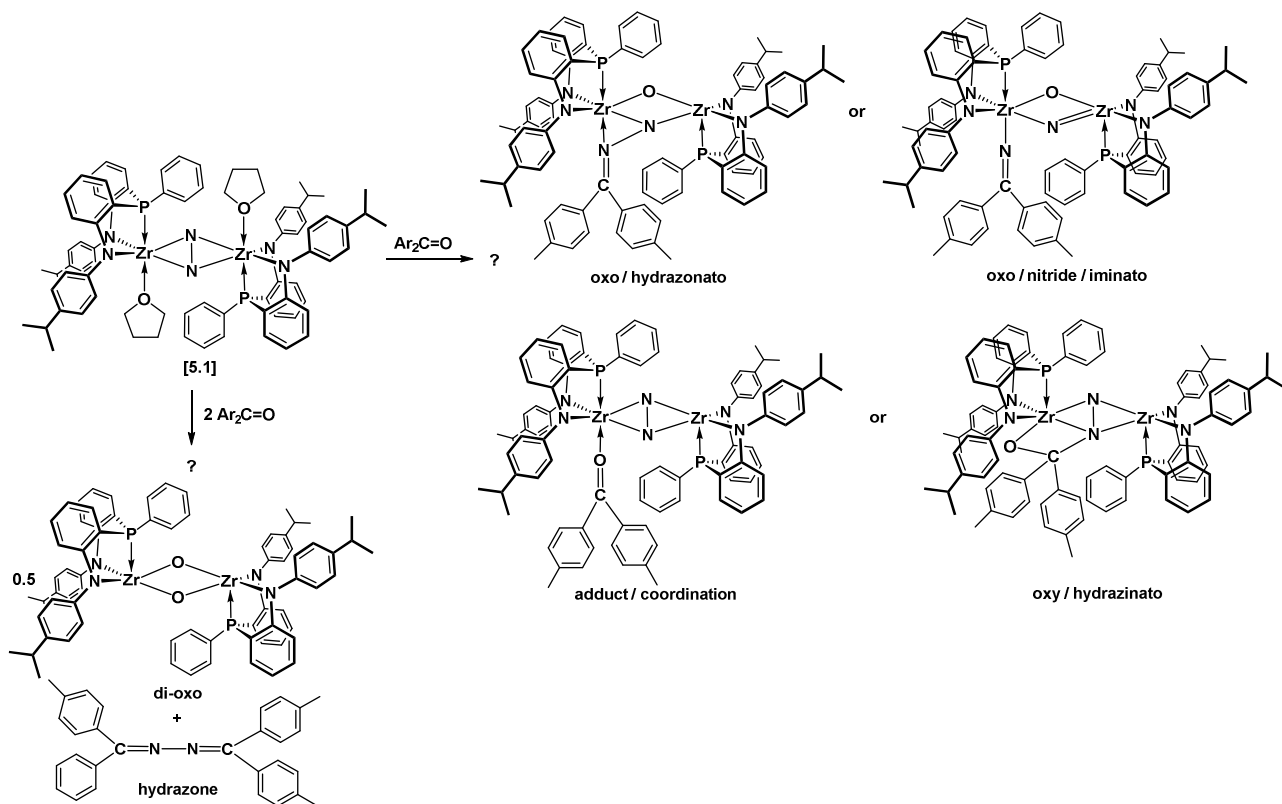


Figure 196: Theoretical products for reaction of $[\text{ipropNPNZr(THF)}]_2(\mu\text{-}\eta^2\text{:}\eta^2\text{-N}_2)$ **[5.1]** with $\text{Ar}_2\text{C}\equiv\text{O}$

In this study, when purple $[\text{ipropNPNZr(THF)}]_2(\mu\text{-}\eta^2\text{:}\eta^2\text{-N}_2)$ **[5.1]** was reacted with one equiv of 4,4'-dimethylbenzophenone, an orange solid was obtained with the $^{31}\text{P}\{^1\text{H}\}$ NMR spectrum displaying broad signals at δ -12.52, δ -10.49, δ -9.52 and δ -21.15, together with a minor signal δ -5.33. The peak at δ -21.15 suggests that one of the product species may be a di- μ -oxo bridged complex (δ -19.2 reported for $[\text{mesNPNZr}]_2(\mu\text{-O})_2$).⁹⁷

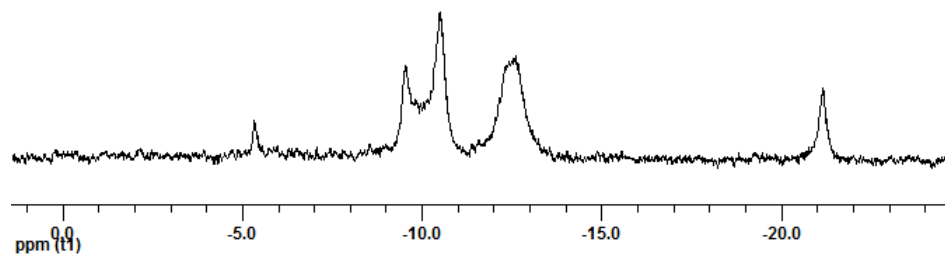


Figure 197: $^{31}\text{P}\{^1\text{H}\}$ NMR spectrum of $[\text{ipropNPNZr}(\text{THF})]_2(\mu\text{-}\eta^2\text{:}\eta^2\text{-N}_2)$ [5.1] after 1 equiv of $\text{Ar}_2\text{C=O}$ in C_6D_6

The associated ^1H NMR spectrum reflects an absence of coordinated THF and the mass spectrum displayed a peak at 1472 m/z, which reflects the presences of an ion composed of complex [5.1] combined with one equiv of 4,4'-dimethylbenzophenone. Fragment ion peaks were also observed at 1264 m/z and 1249 m/z, which could represent $[\text{ipropNPNZr}]_2(\text{N}_2)$ and less one N atom $[\text{ipropNPNZr}]_2(\text{N})$, and implies that at least one of the reaction products contain an intact N-N bond. No x-ray crystals were obtained and no further reactions were attempted. Again, the less bulky ipropNPN ligand introduced more complex reactivity.

6.1.7. Reaction with Carbon Dioxide

The possibility of forming nitrogen-based compounds from dinitrogen and carbon dioxide with transition metal complexes represents numerous challenges, as both molecules are very stable and unreactive. Recently it was reported that hafnocene and zirconocene dinitrogen complexes react with CO_2 to form bridging dicarboxyhydrazinato ligands of the type $\text{NN}(\text{CO}_2)_2$ and $(\text{NCO}_2)_2$, depending on which Zr-N bond is chosen for the second CO_2 insertion.^{106, 157} Further reaction with electrophiles led to the liberation of N,N'-dicarboxylated hydrazines.

In this study, a single reaction was conducted with $[\text{ipropNPNZr}(\text{THF})]_2(\mu\text{-}\eta^2\text{:}\eta^2\text{-N}_2)$ [5.1] and 2 equiv of CO_2 at room temperature. The purple solution immediately turned orange and the $^{31}\text{P}\{^1\text{H}\}$ NMR spectrum was of poor quality, but peaks were discernible at δ -19.92, -12.47, -8.16, -7.09 and 10.54. However, traces of ipropNPNH_2 [2.10] in the crude suggest air

contamination, despite the use of a molecular sieve trap, and future work would involve a repetition of the above-mentioned experiment under more rigorous CO₂ pre-treatment conditions.

6.1.8. Reaction with (Trimethylsilyl)diazomethane

Diazoalkanes have the ability to act either as a 2-electron or 4-electron donor³⁷¹ and theoretical reaction products for the reaction of [ⁱpropNPNZr(THF)]₂(μ-η²:η²-N₂) [**5.1**] with N₂CHSiMe₃ is presented in (Figure 198). In the former case, terminal end-on η¹-N displacement of THF would form a mixed N₂ and N₂CHSiMe₃ coordination complex. In the latter case, the N₂⁴⁺ unit could be displaced by N₂CHSiMe₃ to create mononuclear η¹ or η² coordinated complexes (as in reaction of diphenyldiazomethane with a titanium dinitrogen complex¹⁶⁹) or a dinuclear bridging side-on end-on μ-η²:η²-N₂ complex.

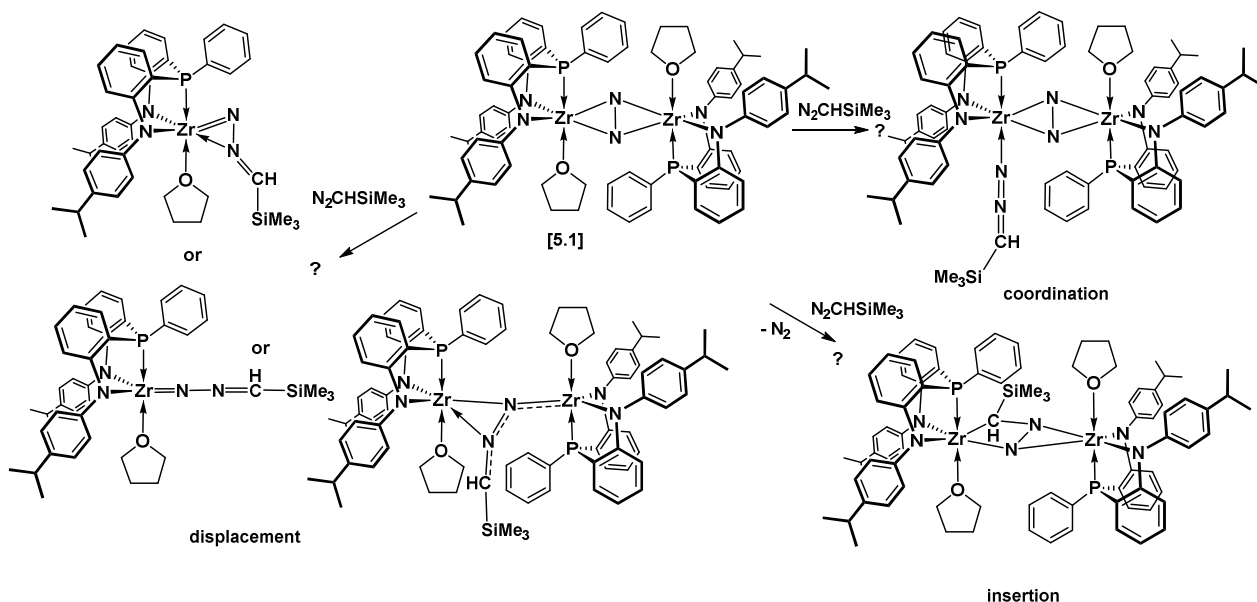


Figure 198: Theoretical products for [ⁱpropNPNZr(THF)]₂(μ-η²:η²-N₂) [**5.1**] with 1 equiv of N₂CHSiMe₃

A third (and more desired) potential reaction outcome relates to the insertion ability of :CH(SiMe₃), the carbene readily generated *in situ* via loss of N₂ from (trimethylsilyl) diazomethane,³⁷²⁻³⁷⁵ which may form a species with new Zr-C and N-C bonds on reaction with complex [**5.1**] (Figure 198). The chemical utility of creating a new N-C bond from activated N₂

by liberating N₂ from a diazo moiety may, however, be self-defeating. Insertion of stable isolable Aduengo-type carbenes³⁷⁶⁻³⁷⁸ may be considered, as well as other related stable dialkylstannylene,³⁷⁹ dialkylgermylenes³⁸⁰ and dialkylsilylene^{381, 382} compounds for the potential generation of new N-Sn, N-Ge or N-Si bonds from activated N₂.

In this study, addition of one equivalent of N₂CHSiMe₃ to a purple solution of [^{iprop}NPNZr(THF)]₂(μ-η²:η²-N₂) [**5.1**] resulted in an orange solution. The ³¹P{¹H} NMR spectrum displayed two peaks in a 1:1 ratio at δ -4.23 and δ -12.03 (Figure 199), suggesting a single dinuclear product with two inequivalent ^{iprop}NPN ligand environments. This reaction would merit further investigation.

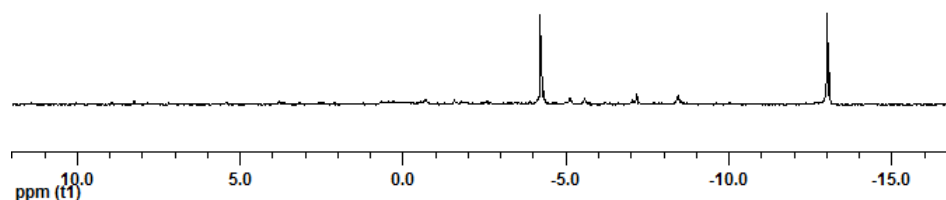


Figure 199: ³¹P{¹H} NMR spectrum of [^{iprop}NPNZr(THF)]₂(μ-η²:η²-N₂) [**5.1**] + 1 equiv of N₂CHSiMe₃ in C₆D₆

6.2. Titanium Dinitrogen Complex Reactivity

Exploratory reactivity studies were conducted for titanium dinitrogen complexes with dihydrogen, carbon monoxide and ethylene.

6.2.1. Reaction with Dihydrogen

While zirconocene and hafnocene dinitrogen complexes^{93, 98, 99} react with molecular hydrogen (see earlier discussion), the corresponding titanocene dinitrogen complex was shown to be unreactive.¹²⁹ Computational DFT studies conducted on the above systems demonstrated that the side-one dinitrogen bonding mode observed in these systems was essential for satisfying all the criteria for the hydrogenation of coordinated nitrogen,³⁸³ however, reactivity was only observed for Zr and Hf as they have singlet electronic ground states, but not for titanium, which

has a triplet electronic ground state.³⁸⁴ Atomic titanium is also able to activate dinitrogen to form Ti_2N_2 dimers^{385, 386} and calculations were done demonstrating a catalytic cycle for the formation of ammonia from dinitrogen and dihydrogen with a C_{60}Ti_2 catalyst.³⁸⁷ Very recently, it has been demonstrated that a trinuclear titanium polyhydride cluster is capable of partial hydrogenation of N_2 at ambient temperature and pressure.^{100, 101}

While the dominance of side-on bound dinitrogen to react with dihydrogen is beyond dispute, there has been at least one report of an end-on bound bis-indenyl zirconium dinitrogen complex reacting with dihydrogen to form a hydrazido ligand.⁹⁸ A toluene solution of the end-on bound titanium complex $[\text{}^{\text{tol}}\text{NPNTi}(\text{THF})]_2(\mu\text{-}\eta^{\text{I}}:\eta^{\text{I}}\text{-N}_2)$ **[5.15]** prepared in this study was exposed to 1 atm H_2 for 24 days, with no evidence of any reaction. The fact that the coordinated dinitrogen was not displaced by dihydrogen to form a titanium hydride (another likely outcome) attests to the stability of $[\text{}^{\text{tol}}\text{NPNTi}(\text{THF})]_2(\mu\text{-}\eta^{\text{I}}:\eta^{\text{I}}\text{-N}_2)$ **[5.15]**, with respect to H_2 addition.

6.2.2. Reaction with Carbon Monoxide

Zirconium and hafnium side-on dinitrogen complexes with substituted cyclopentadienyl ligands have been shown to react with 1 to 4 atm CO at room temperature.¹⁵⁴⁻¹⁵⁶ No reaction products were observed on exposure of a toluene solution of $[\text{}^{\text{tol}}\text{NPNTi}(\text{THF})]_2(\mu\text{-}\eta^{\text{I}}:\eta^{\text{I}}\text{-N}_2)$ **[5.15]** to 1 atm CO for 24 days; only starting material was isolated.

6.2.3. Reaction with Ethylene

A brown toluene solution of $[\text{}^{\text{tol}}\text{NPNTi}(\text{THF})]_2(\mu\text{-}\eta^{\text{I}}:\eta^{\text{I}}\text{-N}_2)$ **[5.15]** was exposed to 1 atm ethylene for 13 days, with no visual observation of polymer formation or colour change.

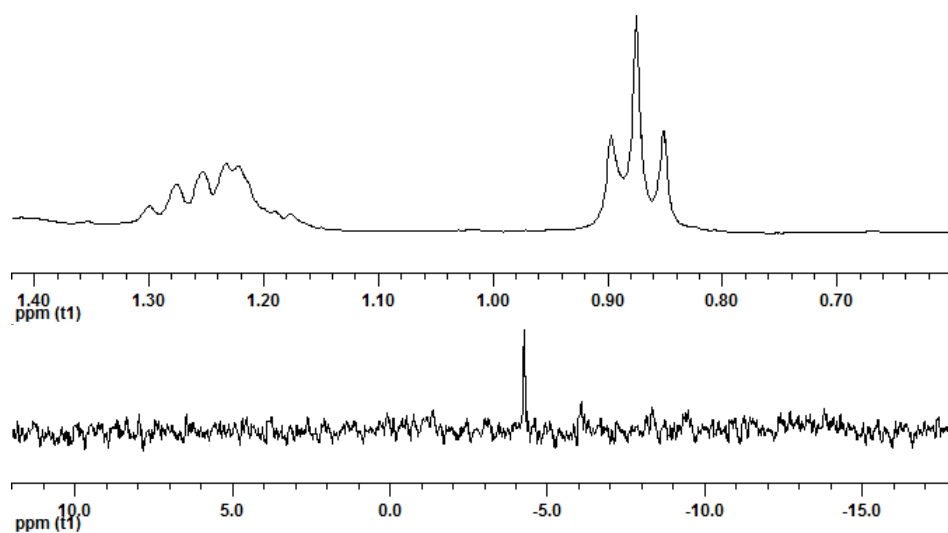


Figure 200: $^{31}\text{P}\{^1\text{H}\}$ (bottom) and partial ^1H NMR (top) spectra for $[\text{}^{101}\text{NPNTi}]_2(\text{H}_2\text{C}=\text{CH}_2)$ [5.22] in C_6D_6 . The $^{31}\text{P}\{^1\text{H}\}$ NMR spectrum of the brown crude displayed numerous signals and washing with *n*-hexanes led to the isolation of a brown solid with a signal at δ -4.78 (Figure 200). The corresponding ^1H NMR spectrum revealed a triplet at δ 0.87 (7 Hz) and a multiplet at δ 1.25 (5 Hz), with no discernible THF resonances. While the triplet and multiplet occurs in a similar region as that reported for coordinated ethylene in $\text{Cp}^*\text{Ti}(\text{H}_2\text{C}=\text{CH}_2)$,³⁶⁵ the fact that CO, which is a better ligand than ethylene, does not displace N_2 (see 6.2.2) argues against ethylene being able to displace the coordinated N_2 . This reaction should be repeated to verify repeatability.

Chapter 7: Conclusions and Future Directions

7.1. Summary

In **Chapter 2**, the preparation of the new ^{iprop}NPN donor set is described. It is a modification of the synthesis reported for the ^{mes}NPN donor set,²¹⁴ whereby the *o*-bromo-diarylamine intermediate is obtained using a Buchwald-Hartwig arylation.^{97, 314}

A new directed *ortho* metalation (DOM) process is employed for the synthesis of the ^{tol}NPN and ^{ph}NPN donor sets,^{261, 314, 332} which allows for commercially available diarylamine precursors. Competitive phosphorus-carbon vs. phosphorous-nitrogen bond formation during the PPhCl₂ quenching stage led to modest overall yields, but the ability to bypass column chromatography associated with the Buchwald-Hartwig arylation allows for the ligand synthesis to be conducted on a larger scale. A drawback of the DOM process is that the arylamine moiety is exempted from having *ortho* substituents.

In **chapter 3**, the synthesis of amido and dichloro complexes of zirconium, titanium and hafnium with ^{iprop}NPN and ^{tol}NPN donor sets is described.^{314, 332} For zirconium, salt metathesis using a ZrCl₄(THF)₂ precursor was found to favour formation of bis-NPN complexes [NPN]₂Zr. In general, protonolysis with Zr(NMe₂)₄, Ti(NMe₂)₄ and Hf(NMe₂)₄ precursors followed by TMSCl mediated chlorination proved consistently to be the most successful route for obtaining dichloro complexes. In the case of zirconium and hafnium, the dichloro species isolated formed dimeric structures, which were easily disrupted by THF into monomeric THF adducts.

When conducting protonolysis with pre-chlorinated precursors, traces of trichloro species may be introduced as impurities during synthesis of the ZrCl₂(NMe₂)₂DME and TiCl₂(NMe₂) precursors. The resultant NPN dichlorides also contained dimethylamine adducts, which required an additional reaction step for removal.

The ability to form bis-(ligand) complexes, dichloro dimers and stable adducts with solvent molecules (HNMe₂, THF) are prominent features of the ⁱpropNPN and ^{tol}NPN donor sets relative to the ^{mes}NPN^{97, 214} donor set. This is likely attributable to the reduced steric bulk afforded by the lack of substituents in the *ortho* position of the amido moieties.

In **chapter 4**, the synthesis of trichloro complexes of tantalum with diamidophosphine donor sets (ⁱpropNPN, ^{tol}NPN and ^{Ph}NPN) were reported for the first time. All previous attempts with the original ^{Si}NPN donor set (and any other intervening variations such as ^{mes}NPN) had proved futile. The trichloro complexes provided new avenues with which to approach the synthesis of tantalum dinitrogen complexes, such as the traditional reduction method. Dinitrogen complexes [ⁱpropNPNTaCl]₂(N₂) [**4.19**] and [^{tol}NPNTaCl]₂(N₂) [**4.20**] were detected during the reduction of the respective trichlorides with 2 equiv of KC₈ under 4 atm N₂, but other side-products hampered isolation and further characterisation.

The standard method for accessing tantalum dinitrogen complexes with the ^{Si}NPN donor set is via exposure of a dinuclear tetrahydride to an atmosphere of nitrogen, obtained from hydrogenation of a trimethyl precursor.^{79, 80} In **chapter 4**, the first synthesis of trimethyl tantalum complexes with an arene bridged modification (^{tol}NPN) is described. For the trimethyl complex with the ^{Si}NPN donor set, salt metathesis was conducted with TaCl₂Me₃ and the anionic form of the ligand. The potassium analogue rather than the lithium salt of the ligand precursor proved central in preparing the trimethyl complex containing the ^{tol}NPN ligand set.

While new reactivity continues to be discovered for tantalum dinitrogen complexes with the ^{Si}NPN ligand,¹⁹² there is a considerable drive to replace the Si-N bond in the backbone due to deleterious ligand rearrangements.^{110, 112} Unfortunately, hydride complexes from the new trimethyl tantalum complexes reported in this study did not yield dinitrogen complexes on exposure to N₂. There was, however, some evidence that hydride complexes generated via

reaction of the trichloro derivatives with KBET_3 , under an N_2 atmosphere, yielded dinitrogen complexes $[\text{ipropNPNTaH}]_2(\text{N}_2)$ [4.17] and $[\text{tolNPNTaH}]_2(\text{N}_2)$ [4.18] and /or BEt_3 adducts $[\text{ipropNPNTaH}]_2(\text{NBET}_3)_2(\text{N}_2)_2$ [4.17a] and $[\text{tolNPNTaH}]_2(\text{NBET}_3)_2(\text{N}_2)_2$ [4.18a]; unfortunately, none of these complexes could be isolated in pure form.

Numerous other alkyl species were observed during the discovery process for the trimethyl tantalum complexes. When salt metathesis was conducted with TaCl_2Me_3 at room temperature or with the lithiated ligand precursors, the major side-product **species** \mathbf{u}_{tol} and **species** \mathbf{u}_{ipr} exhibit data consistent with a tetramethyl dinuclear species. Reaction of tantalum trichlorides with 4 equiv MeLi indicated that the trimethyl species reacted with MeLi , forming in one instance the ionic species $[\text{tolNPNTaMe}_4][\text{Li}(\text{THF})_4]$ [4.14], but in all other cases **species** $\mathbf{tol}_{4\text{MeLi}}$ which exhibited data consistent with an alkyl-bridged lithium-tantalum tetramethyl molecule $\text{tolNPNTaMe}_4\text{Li}(\text{Et}_2\text{O})$ [4.13].

In **chapter 5**, the new side-on zirconium dinitrogen complexes, $[\text{ipropNPNZr}(\text{THF})]_2(\mu-\eta^2:\eta^2-\text{N}_2)$ [5.1] and $[\text{tolNPNZr}(\text{THF})]_2(\mu-\eta^2:\eta^2-\text{N}_2)$ [5.3],³¹⁴ were found to be more stable than sterically encumbered $[\text{mesNPNZr}(\text{THF})]_2(\mu-\eta^2:\eta^2-\text{N}_2)$, with longer N-N and shorter Zr-N bond lengths and the THF was less labile, with shorter Zr-O bonds. It was still possible to displace the THF with pyridine, 4,4'-bipyridine, trimethylphosphine, dimethyl(phenyl)phosphine and tetrahydrothiophene, often requiring a large excess of the displacing ligand. Due to the reduced steric bulk at the *ortho* position for the ipropNPN and tolNPN donor sets, no open site was generated at any of the zirconium centres, as had been reported for the dimethyl(phenyl)phosphine adduct of the dinitrogen complex with the mesNPN donor set.

Although the reduction of hafnium dichlorides under N_2 failed to yield dinitrogen complexes, this reduction approach was successful for the titanium precursors; thus new end-on titanium dinitrogen complexes $[\text{ipropNPNTi}(\text{THF})]_2(\mu-\eta^1:\eta^1-\text{N}_2)$ [5.17] and $[\text{tolNPNTi}(\text{THF})]_2(\mu-$

$\eta^1:\eta^1\text{-N}_2$) [5.15] were obtained.³³² This represents the first example of titanium dinitrogen complexes with the diamidophosphine donor set, as the $^{\text{Si}}\text{NPN}$ donor set had undergone ligand rearrangement to a phosphinimide.¹³⁸ Displacement of THF with pyridine led to four different isomers, from which the new adduct $[\text{}^{\text{tol}}\text{NPNTi(Py)}_2]_2(\mu\text{-}\eta^1:\eta^1\text{-N}_2)$ was obtained when an excess of pyridine was maintained. A single species was observed when the displacement was conducted with 2,2'-bipyridine. In an attempt to avoid the reduction method, the new titanium hydride $[\text{}^{\text{tol}}\text{NPNTiH}_2]_2$ [5.21] was obtained from the dichloro precursor and KHBet_3 ; however, it was found to be too stable to generate a dinitrogen complex on exposure to N_2 .

Previously reported $[\text{}^{\text{mes}}\text{NPNZr(THF)}]_2(\mu\text{-}\eta^2:\eta^2\text{-N}_2)$ does not react with H_2 ,⁹⁷ and the same result was found for $[\text{}^{\text{tol}}\text{NPNZr(THF)}]_2(\mu\text{-}\eta^2:\eta^2\text{-N}_2)$ [5.3] (see **chapter 6**). Also in that previous study, the phosphine adducts with an open site on one of the zirconiums i.e. $[\text{}^{\text{mes}}\text{NPNZr(PMe}_3)](\mu\text{-}\eta^2:\eta^2\text{-N}_2)[\text{}^{\text{mes}}\text{NPNZr}]$ and $[\text{}^{\text{mes}}\text{NPNZr(PPhMe}_2)](\mu\text{-}\eta^2:\eta^2\text{-N}_2)[\text{}^{\text{mes}}\text{NPNZr}]$ did react with H_2 ;⁹⁷ however, $[\text{}^{\text{tol}}\text{NPNZr(PMe}_3)]_2(\mu\text{-}\eta^2:\eta^2\text{-N}_2)$ [5.9] was also found to be unreactive with H_2 , emphasizing the importance of coordinative unsaturation at the zirconium centre for this reaction to proceed. The end-on bonding mode is not amenable to hydrogenolysis and the titanium dinitrogen complexes also do not react with hydrogen. Progress with reactivity studies is hampered by the lack of ability to scale up the reduction process to create a large stock-pile of precursor dinitrogen complexes, coupled with the labour-intensive multi-step NPN ligand synthesis.

Screening tests, predominantly $^{31}\text{P}\{^1\text{H}\}$ NMR experiments, were conducted for zirconium dinitrogen complexes with isocyanide, phenylsilane, ethylene, carbon monoxide, 4,4'-dimethylbenzophenone, carbon dioxide and (trimethylsilyl)diazomethane and for titanium dinitrogen complexes with ethylene and carbon monoxide (Table 28).

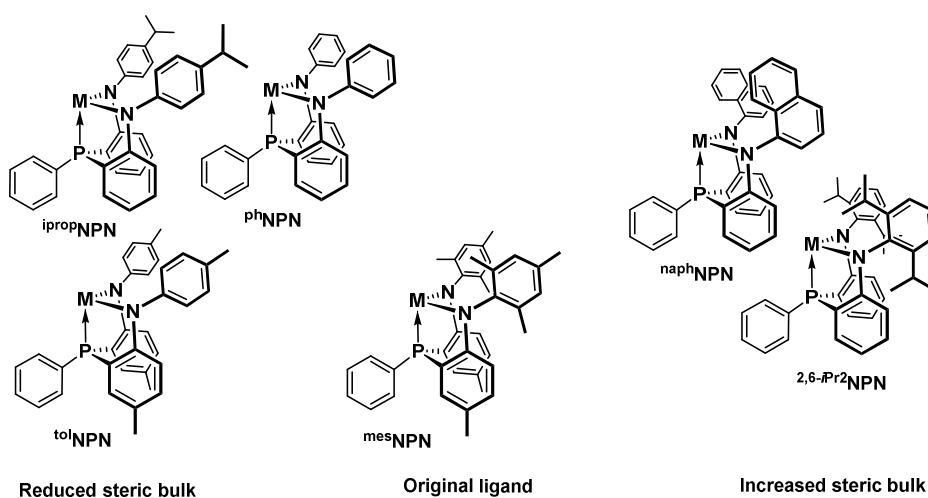
Table 28 : Screening studies with zirconium dinitrogen complexes

| Reagent | Comments |
|---------------------------------------|--|
| Zirconium Dinitrogen Complexes | |
| dihydrogen | no reaction |
| isocyanide | discreet complexes with 2 xylylNC, 2 ^t BuNC and 4 xylylNC |
| phenylsilane | single unidentified brown species |
| ethylene | no reaction and polymer (possibly catalysed by trace Zr impurities) |
| carbon monoxide | multiple product species |
| 4,4'-dimethylbenzophenone | multiple product species |
| carbon dioxide | multiple product species (to repeat as air ingress was indicated) |
| (trimethylsilyl)diazomethane | single unidentified orange species |
| Titanium Dinitrogen Complexes | |
| dihydrogen | no reaction |
| ethylene | no polymer, and single unidentified brown species |
| carbon monoxide | no reaction |

Most promising results were obtained by reaction of the zirconium dinitrogen complexes with isocyanide, phenylsilane and (trimethylsilyl)diazomethane, and these would be an ideal areas for future investigations.

7.2. Future Ligand Designs

A future project may involve investigation of diamidophosphine ligands with increased steric bulk in the *ortho* position of the amido moiety, such as donor sets with a 1-naphthylamide or 2,6-diisopropylamide group (Figure 201).

**Figure 201: NPN donor set variation of arylamido groups**

Decreased steric bulk led to more stable dinitrogen complexes with less labile THF adducts, inhibiting the presence of an open coordination site and subsequent reaction with dihydrogen. A

corollary is that increased steric bulk could promote more labile L_n groups and coordinative unsaturation of the zirconium centres. The potential to generate an open site at both zirconium centres may encourage reaction with two molecules of dihydrogen (Figure 202).

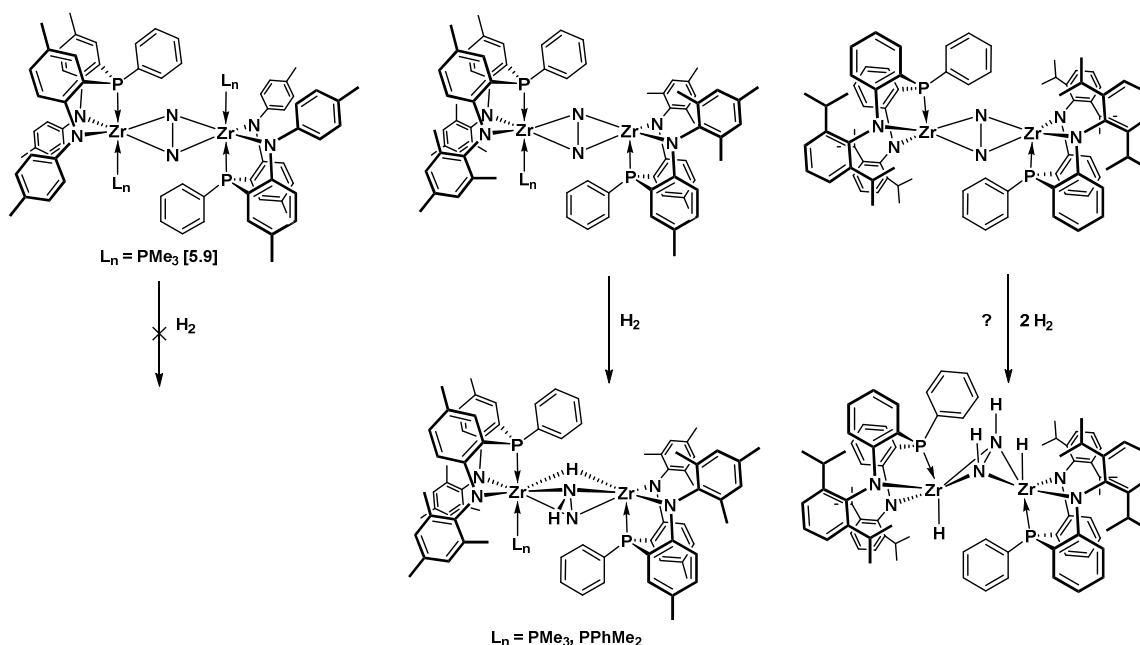


Figure 202: Potential reactivity of bulky NPN zirconium N_2 complexes with dihydrogen

For the end-on titanium dinitrogen complexes, limited reactivity is expected, as it is the nitrogen atom lone pairs in side-on coordination mode that are more accessible for further reactivity.¹²⁵ DFT calculations confirm that titanium dinitrogen complexes are more likely than zirconium to exhibit an end-on bonding.¹⁴¹ Despite this, titanocene dinitrogen chemistry demonstrated that reducing the steric bulk of the substituted cyclopentadienyl ligands can result in the isolation of a side-on dinitrogen complex¹⁸⁰ and side-on titanium dinitrogen complexes with bis(silyl)amide ligands have been reported.¹⁷²

Likewise, future ligand designs for *o*-phenylene bridged NPN titanium dinitrogen complexes could focus on sterically less hindered amido groups with alkyl or silyl substituents i.e. $(\text{RNC}_6\text{H}_4)_2\text{PPh}$, R = alkyl, SiMe_3 (Figure 203).

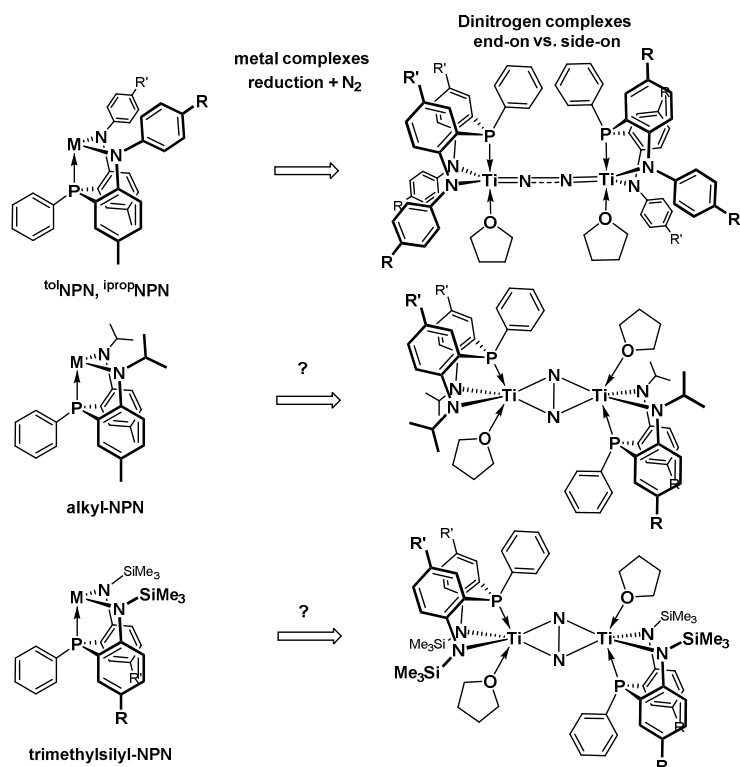


Figure 203: Potential NPN ligand design for side-on titanium N₂ complexes

7.3. ^{naph}NPN and ^{2,6-iPr₂}NPN Donor Sets

The DOM method is unsuitable for the synthesis of ^{naph}NPN and ^{2,6-iPr₂}NPN donor sets due to *ortho* substitution, hence the Buchwald-Hartwig arylamination method was investigated. The *ortho*-halogenated secondary amine precursors with 2-naphthyl or 2,6-diisopropyl substituents can be synthesised from a 1,2-dihaloarene^{224, 228, 388-390} and the respective substituted amine, or from a 2-haloaniline and the respective substituted haloarene.²²⁴ The aforementioned reactions are catalysed by palladium complexes and side reactions to form carbazoles^{223-225, 389, 391} and asymmetric dearomatisation^{388, 389} are known.

7.3.1. Synthesis of ^{naph}Ar^{Br}ArNH [7.1] and ^{2,6-iPr₂}Ar^{Br}ArNH [7.2]

^{naph}Ar^{Br}ArNH [7.1] has previously been isolated by reaction of ^{naph}ArNH₂ with C₆H₄BrI,²²⁴ Ph-^{naph}Ar^{Br}ArNH from Ph-^{naph}ArNH₂ with C₆H₄Br₂³⁸⁸ and ^{naph}Ar^{Cl}ArNH from 2-

chloroaniline with 2-bromonaphthalene.²²⁴ $^{2,6-iPr_2}Ar^{Br}ArNH$ [7.2] was also previously prepared by reaction of $^{2,6-iPr_2}ArNH_2$ with $C_6H_4Br_2$ ²²⁸ or C_6H_4BrI .^[8-10] In this study, $^{naph}Ar^{Br}ArNH$ [7.1] and $^{2,6-iPr_2}Ar^{Br}ArNH$ [7.2] were prepared from their respective primary amines and dibromobenzene in 55% and 62% isolated yields, using a palladium diphosphine catalyst Pd / DPPF (1:3) with a 2.0-2.3 mol% Pd loading at 140-145 °C in 1,4-dioxane (Figure 204). Product losses were incurred during purification by column chromatography, for example, the pre-column yield for $^{2,6-iPr_2}Ar^{Br}ArNH$ [7.2] was 92% (using GC-MS).

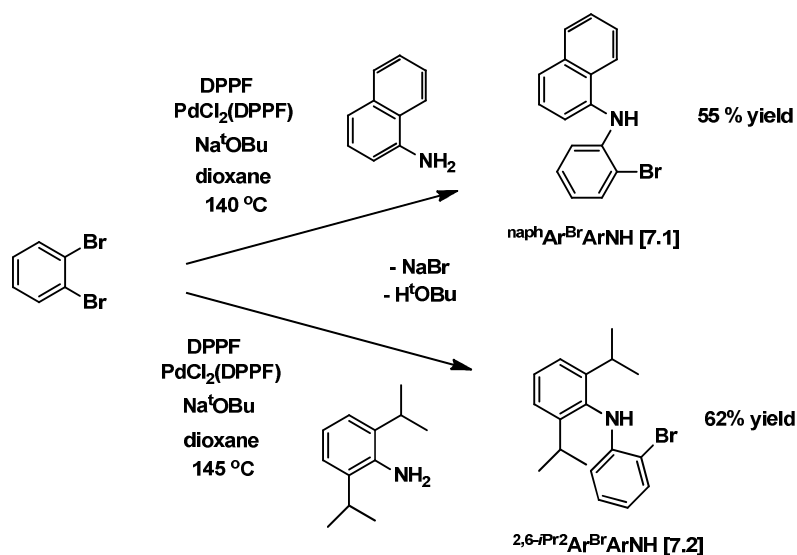


Figure 204: Synthesis of $^{naph}Ar^{Br}ArNH$ [7.1] and $^{2,6-iPr_2}Ar^{Br}ArNH$ [7.2]

The solid state molecular structure of $^{2,6-iPr_2}Ar^{Br}ArNH$ [7.2] and $^{naph}Ar^{Br}ArNH$ [7.1] were obtained (Figure 205) and the Br1-C2, N8-C7, N8-C9 and C7-N8-C9 bond lengths and angles are similar for both [7.2] and [7.1] (Table 29).

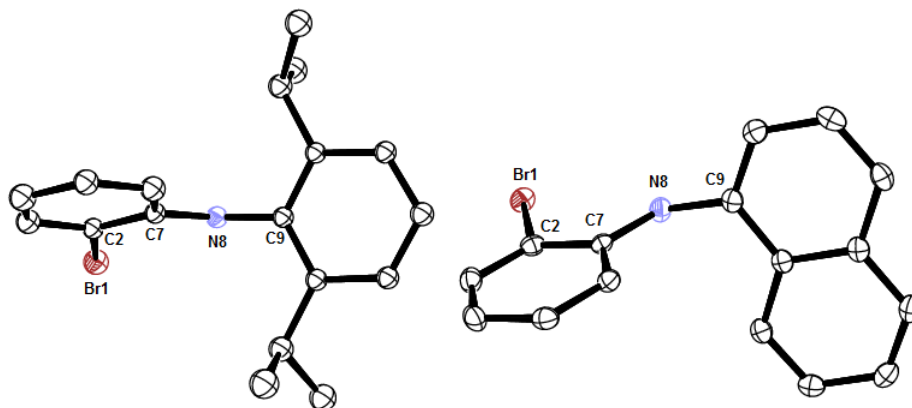


Figure 205: Solid state molecular structures of $^{2,6-i\text{Pr}_2}\text{ArBrArNH}$ [7.2] and $^{\text{naph}}\text{Ar}^{\text{Br}}\text{ArNH}$ [7.1]

Table 29 : Selected bond lengths (Å) and angles (°) for $^{2,6-i\text{Pr}_2}\text{ArBrArNH}$ [7.2] and $^{\text{naph}}\text{Ar}^{\text{Br}}\text{ArNH}$ [7.1]

| | $^{2,6-i\text{Pr}_2}\text{ArBrArNH}$ [7.2] | $^{\text{naph}}\text{Ar}^{\text{Br}}\text{ArNH}$ [7.1] |
|----------|--|--|
| Br1-C2 | 1.913(8) | 1.916 (4) |
| N8-C7 | 1.396(10) | 1.386(5) |
| N8-C9 | 1.432(10) | 1.431(5) |
| C7-N8-C9 | 122.0(7) | 123.2(3) |

7.3.2. Synthesis of $^{2,6-i\text{Pr}_2}\text{Ar}^{\text{Li}}\text{ArNLi}]_n$ [7.3] and $^{2,6-i\text{Pr}_2}\text{Ar}^{\text{Li}}\text{ArNLi}\cdot 2\text{THF}]_2$ [7.3a]

Unlike with the synthesis of $[\text{ipropNPNLi}_2\cdot\text{diox}]_n$ [2.6] or $[\text{Ph}_{\text{mes}}\text{NPNLi}_2\cdot\text{diox}]_n$,⁹⁷ quenching of the *in situ* generated lithium amide with PPhCl_2 did not yield $^{2,6-i\text{Pr}_2}\text{NPNLi}_2\cdot\text{diox}]_n$ [7.7] and it became essential to isolate the lithium amide intermediate. The lithiation of $^{2,6-i\text{Pr}_2}\text{Ar}^{\text{Br}}\text{ArNH}$ [7.2] with *n*-BuLi, *tert*-BuLi and mixtures thereof were monitored via GC-MS after quenching with $\text{NMe}_3\cdot\text{HCl}$ in Et_2O at -30°C (Table 30 and Figure 206). It was found that three equiv of *tert*-BuLi or four equiv of *n*-BuLi were required for complete formation of $^{2,6-i\text{Pr}_2}\text{Ar}^{\text{Li}}\text{ArNLi}]_n$ [7.3]. Hence, while no excess *tert*-BuLi was needed,³⁹² it is apparent that four equiv of *n*-BuLi are essential.

Table 30 : GC-MS data for lithiation of $^{2,6-i\text{Pr}_2}\text{ArBrArNH}$ [7.2]

| equiv <i>n</i> -BuLi | equiv <i>t</i> -BuLi | $^{2,6-i\text{Pr}_2}\text{Ar}^{\text{Br}}\text{ArNH}$ (wt%) | $^{2,6-i\text{Pr}_2}\text{Ar}^{\text{H}}\text{ArNH}$ (wt%) |
|----------------------|----------------------|---|--|
| 1 | | 100 | |
| 2 | | 55-62 | 45-38 |
| 1 | 1 | 62 | 38 |
| | 2 | 12 | 88 |
| 3 | | 10 | 90 |
| | 3 | | 100 |
| 4 | | | 100 |

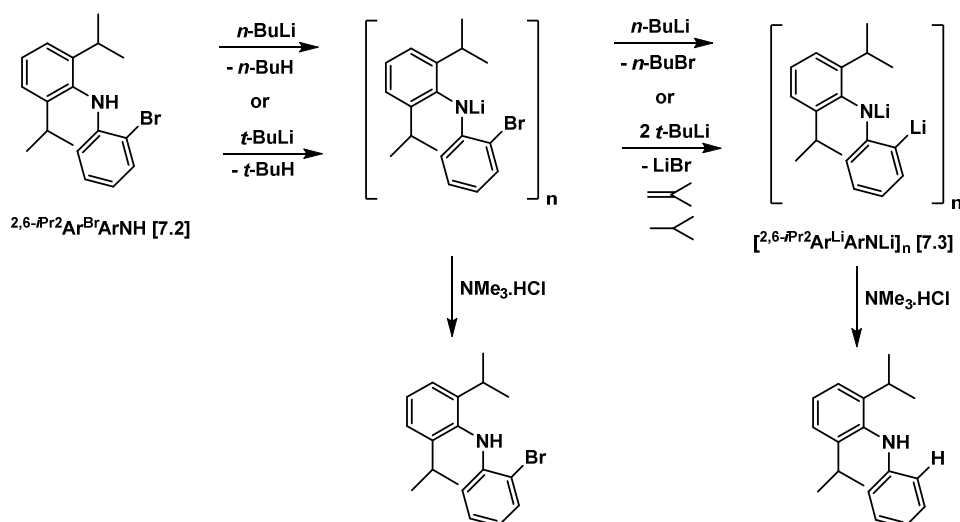


Figure 206: Lithiation of $2,6\text{-iPr}_2\text{Ar}^{\text{Br}}\text{Ar}^{\text{NH}}$ [7.2]

Using $n\text{-BuLi}$, the white solid $\left[2,6\text{-iPr}_2\text{Ar}^{\text{Li}}\text{Ar}^{\text{NLi}} \right]_n$ [7.3] was isolated in 71% yield (Figure 207) and the most efficient method for separating the product from excess $n\text{-BuLi}$ proved to be via centrifugation of the $n\text{-hexane}$ suspension.

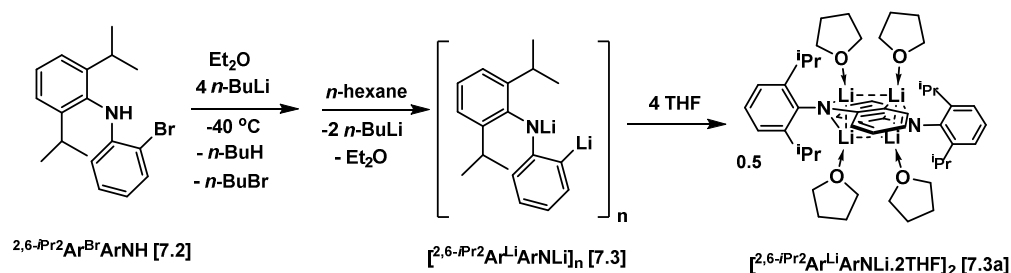


Figure 207: Synthesis of $\left[2,6\text{-iPr}_2\text{Ar}^{\text{Li}}\text{Ar}^{\text{NLi}} \right]_n$ [7.3] and $\left[2,6\text{-iPr}_2\text{Ar}^{\text{Li}}\text{Ar}^{\text{NLi}} \cdot 2\text{THF} \right]_2$ [7.3a]

The ^1H NMR spectrum of $\left[2,6\text{-iPr}_2\text{Ar}^{\text{Li}}\text{Ar}^{\text{NLi}} \right]_n$ [7.3] in C_6D_6 after the $n\text{-hexane}$ work-up reflects two different isopropyl environments and the absence of Et_2O signals attests to the lability of Et_2O as a supporting solvent donor (Figure 208). The $^7\text{Li}\{^1\text{H}\}$ NMR spectrum of $\left[2,6\text{-iPr}_2\text{Ar}^{\text{Li}}\text{Ar}^{\text{NLi}} \right]_n$ [7.3] in C_6D_6 displays two signals at δ 2.97 and δ -5.26, indicating at least two vastly different Li environments within the aggregate structure (Figure 208).

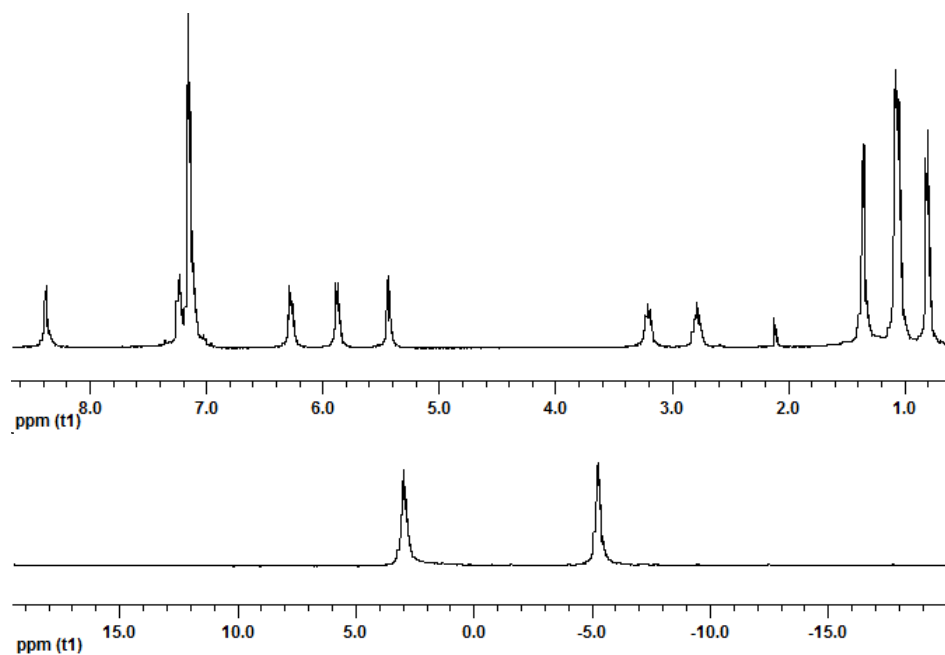


Figure 208: ${}^7\text{Li}\{{}^1\text{H}\}$ (bottom) and ${}^1\text{H}$ NMR (top) of $[\text{}^{2,6-i\text{Pr}_2}\text{Ar}^{\text{Li}}\text{ArNLi}]_n$ **[7.3]** in C_6D_6

In the absence of Et_2O (or THF) solvent, the lithium in the $[\text{}^{2,6-i\text{Pr}_2}\text{Ar}^{\text{Li}}\text{ArNLi}]_n$ **[7.3]** aggregate may potentially coordinate in an η^6 mode to the phenyl group of the 2,6-diisopropyl phenyl moiety, or to the deuterated benzene solvent. Donor-solvent free *m*-terphenyl aryllithium compounds^{254, 257, 258} have been reported with η^6 coordination to the phenyl rings of the bulky ligand or to the benzene solvent and their reported ${}^7\text{Li}\{{}^1\text{H}\}$ NMR values (δ -3.97 to δ -5.16) agrees with the upfield signal at δ -5.26 for compound **[7.3]**. Such structures would presumably fall into the aggregate class Type A as defined by van Koten and workers.³⁹³ By inference, the signal at δ 2.97 for compound **[7.3]** could be attributed to a lithium ion with more amide and limited Li-C bond character.

$[\text{}^{2,6-i\text{Pr}_2}\text{Ar}^{\text{Li}}\text{ArNLi}]_n$ **[7.3]** dissolves in $\text{THF-}d_8$ to form the solvated species $[\text{}^{2,6-i\text{Pr}_2}\text{Ar}^{\text{Li}}\text{ArNLi}\cdot 2\text{THF}]_2$ **[7.3a]** (Figure 207), which could be classified as aggregate class Type B,³⁹³ whereby the core dimer structure is retained with one solvent molecule coordinated to each lithium atom. The ${}^1\text{H}$ NMR spectrum of **[7.3a]** indicates one isopropyl group environment and the THF signals at δ 3.59 and 1.74 correspond to unbound or very weakly coordinated THF

(Figure 209). Based on the solid state molecular structure (Figure 210) obtained for $[\text{}^{2,6}\text{-}i\text{Pr}_2\text{Ar}^{\text{Li}}\text{ArNLi}\cdot 2\text{THF}]_2$ [**7.3a**] it is likely that the lithium atoms are solvated in THF- d_8 , thus exchange between coordinated THF and a large excess free THF can explain why the experimentally observed δ values suggest little to no solvent coordinated.

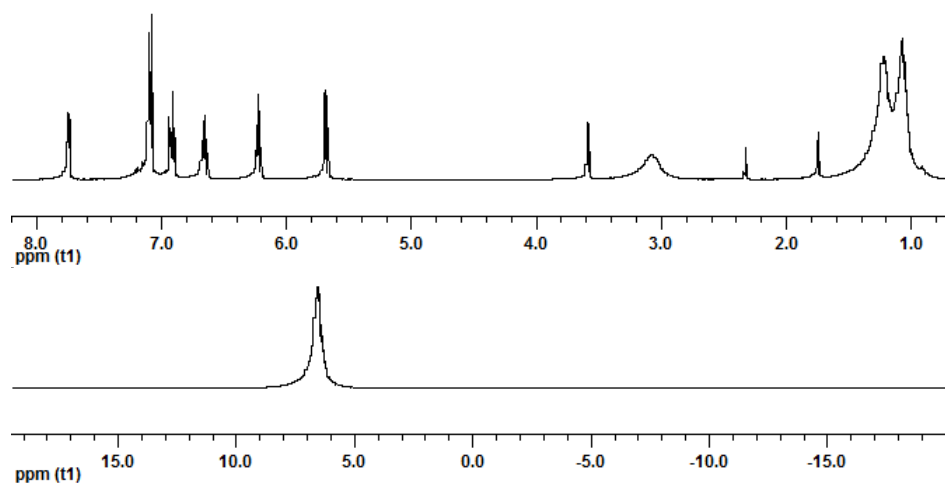


Figure 209: ${}^7\text{Li}\{^1\text{H}\}$ (bottom) and ${}^1\text{H}$ NMR (top) of $[\text{}^{2,6}\text{-}i\text{Pr}_2\text{Ar}^{\text{Li}}\text{ArNLi}\cdot 2\text{THF}]_2$ [**7.3a**] in THF- d_8

Compound [**7.3a**] displays a single downfield shifted peak at δ 6.55 in the ${}^7\text{Li}\{^1\text{H}\}$ NMR spectrum (Figure 209). Chemical shifts values for (solvated) aryllithium compounds in ${}^7\text{Li}\{^1\text{H}\}$ NMR spectra have been reported from δ -5.16 to δ 3.72.^{254, 259, 393} For the THF-solvated compound [**7.3a**], an upfield signal for η^6 coordination to arene groups is absent, but the solid state molecular structure (see later discussion and Figure 210) indicates that compound [**7.3a**] contains two different Li atom environments, with varying bond contributions from nitrogen and carbon atoms. It is possible that these differences cannot be observed on the NMR timescale at room temperature and for future work, a low temperature ${}^7\text{Li}\{^1\text{H}\}$ NMR spectrum should be acquired. Clearly, the Li-C bonds involved with η^6 coordination to phenyl groups (as in compound [**7.3**]) result in more shielded Li atoms than when the carbon atoms only form part of the $\text{Li}_4\text{C}_4\text{N}_2$ core (as in THF solvated compound [**7.3a**]).

The solid state molecular structure of $[\text{}^{2,6-i\text{Pr}_2}\text{Ar}^{\text{Li}}\text{ArNLi}\cdot 2\text{THF}]_2$ [**7.3a**] (Figure 210) was obtained from crystals grown by slow diffusion of hexane into a THF solution of $[\text{}^{2,6-i\text{Pr}_2}\text{Ar}^{\text{Li}}\text{ArNLi}]_n$ [**7.3**]. The dimer has a central core containing two nitrogen (N8, 'N8), four lithium (Li1, Li8, 'Li1, 'Li8) and four carbon (C2, C7, 'C2, 'C7) atoms, with the 4 Li atoms forming a distorted tetrahedron having three shorter Li \cdots Li (av 2.47 Å) and one long Li \cdots Li (3.124(7) Å) non-bonding close contacts (Figure 210). The Li \cdots Li close contacts are all shorter than the sum of the van der Waals radii between two lithium atoms (3.64 Å) and agree with values reported in the literature.^{256, 259, 395}

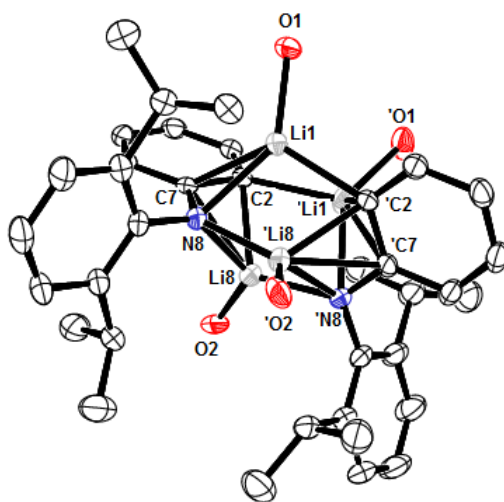


Figure 210: Solid state molecular structure of dimeric $[\text{}^{2,6-i\text{Pr}_2}\text{Ar}^{\text{Li}}\text{ArNLi}\cdot 2\text{THF}]_2$ [**7.3a**] in two different orientations, with the carbon atoms of the THF adducts omitted for clarity

All the lithium atoms are five coordinate with three Li \cdots Li close contacts, but there are two different lithium environments, with Li1 (and Li1') being coordinated to one nitrogen atom and three carbon atoms and Li8 (and Li8') to two nitrogen atoms and two carbon atoms (Figure 210). Each lithium atom is bound to one THF molecule, which are also in a tetrahedral arrangement. The lithium oxygen bond lengths (see chapter 2) are similar to that reported for $[\text{}^{\text{i}pr\text{op}}\text{NPNLi}_2\cdot\text{diox}]_n$ [**2.6**],^{97 mes} $\text{NPN}'\text{Li}_2\cdot\text{diox}$,^{97 mes} $\text{NPNLi}\cdot 2\text{THF}$,^{97, 214} $\text{}^{\text{tol}}\text{NPNLi}_2\cdot 0.5\text{TMEDA}\cdot\text{DME}$ ²⁶¹ and other organolithium adducts.^{256, 259} Each nitrogen atom is coordinated to three lithium atoms (Li1, Li8 and Li8') and the Li-amide bond lengths (see

chapter 2) compare well with those reported for [^{tol}Ar^{Li}ArNLi·TMEDA]₂ [2.2] and other lithium amides.^{245, 246, 253}

Table 31 : Selected bond lengths (Å) and angles (°) for [^{2,6-*i*Pr₂}Ar^{Li}ArNLi·2THF]₂ [7.3a]

| [^{2,6-<i>i</i>Pr₂} Ar ^{Li} ArNLi·2THF] ₂ [7.3a] | | | |
|--|-----------|--------------|-----------|
| N8-C7 | 1.418(4) | Li8···Li1 | 3.124(7) |
| N8-C9 | 1.436(3) | Li8···Li1' | 2.531(7) |
| Li1···Li1' | 2.426(10) | Li8···Li8' | 2.468(10) |
| Li1-N8 | 2.233(5) | Li8-N8 | 2.218(5) |
| Li1-C2 | 2.221(6) | Li8-N8' | 2.067(5) |
| Li1-C2' | 2.236(5) | Li8-C2 | 2.146(5) |
| Li1-C7 | 2.345(5) | Li8-C7 | 2.324(5) |
| Li1-O1 | 1.962(5) | Li8-O2 | 1.941(6) |
| C2-C7 | 1.442(4) | C9-C10 | 1.421(4) |
| C2-C3 | 1.405(4) | C10-C11 | 1.400(4) |
| C3-C4 | 1.414(4) | C11-C12 | 1.390(5) |
| C4-C5 | 1.383(5) | C12-C13 | 1.387(5) |
| C5-C6 | 1.387(4) | C13-C14 | 1.404(4) |
| C6-C7 | 1.424(4) | C14-C9 | 1.418(4) |
| Li1-N8-Li8 | 89.15(19) | Li8-C2-Li1 | 91.3(2) |
| Li1-N8-Li8' | 72.00(19) | Li8-C2-Li1' | 70.51(19) |
| Li8-N8-Li8' | 70.2(2) | Li1-C2-Li1' | 66.0(2) |
| Li8-Li1-Li8' | 50.4(2) | Li1-Li8-Li1' | 49.5(2) |
| Li1-Li8-Li8' | 82.36(19) | Li8-Li1-Li1' | 52.44(15) |
| Li1-Li8'-Li8 | 77.34(18) | Li8-Li1'-Li1 | 78.10(17) |
| N8-C7-Li1 | 67.68(19) | Li1-C7-Li8 | 83.97(19) |
| C7-N8-Li1 | 76.34(19) | C7-Li1-Li8 | 47.73(13) |
| C7-Li1-N8 | 35.98(12) | C7-Li8-Li1 | 48.29(14) |
| N8-C7-Li8 | 67.77(18) | C7-C2-Li1 | 76.3(2) |
| C7-N8-Li8 | 75.95(19) | C2-C7-Li1 | 67.0(2) |
| C7-Li8-N8 | 36.27(12) | C2-Li1-C7 | 36.69(12) |
| | | C7-C2-Li8 | 78.03(19) |
| | | C2-C7-Li8 | 64.60(18) |
| | | C2-Li8-C7 | 37.36(12) |

The phenyl ring containing the carbon atoms involved in the core structure form a plane that is perpendicular to the 2,6-diisopropyl substituted phenyl ring (Figure 210), as was observed in the structure reported for [^{naph}ArPhNLi·TMEDA]₂.²⁴⁶ The C2-C7 bond length is also longer than benzene (1.39 Å) as well as the other aromatic carbon-carbon bonds in [^{2,6-*i*Pr₂}Ar^{Li}ArNLi·2THF]₂ [7.3a].

There are two different carbon environments for the four five-coordinate carbon atoms in the core (Figure 210). Each of the two *ortho* carbons C2 (and C2') are coordinated to three lithium atoms, forming four-centre, two-electron bonds^{393, 395} CLi₃ compared to the two *ipso* C7 (and C7') carbons, which are bound to an amido nitrogen and two lithium atoms, forming three-

centre, two electron bonds²⁵⁶ CLi_2 . The *ortho* carbon-lithium bond lengths are shorter (average 2.33 Å) than the amido carbon-lithium bond lengths (average 2.20 Å) and they both fall within the range reported for $[\text{}^{\text{tol}}\text{Ar}^{\text{Li}}\text{ArNLi}\cdot\text{TMEDA}]_2$ [2.2] and other aryllithium compounds.^{246, 254-259}

7.3.3. Synthesis of $[\text{}^{\text{naph}}\text{Ar}^{\text{Li}}\text{ArNLi}\cdot 2\text{Et}_2\text{O}]_2$ [7.4] and $[\text{}^{\text{naph}}\text{Ar}^{\text{Li}}\text{ArNLi}\cdot 2\text{THF}]_2$ [7.5]

$\text{}^{\text{naph}}\text{Ar}^{\text{Br}}\text{ArNH}$ [7.1] reacts with two equiv of *n*-BuLi at -40 °C in Et_2O to give $[\text{}^{\text{naph}}\text{Ar}^{\text{Li}}\text{ArNLi}\cdot 2\text{Et}_2\text{O}]_2$ [7.4] in 97% yield and in THF to give $[\text{}^{\text{naph}}\text{Ar}^{\text{Li}}\text{ArNLi}\cdot 2\text{THF}]_2$ [7.5] in 52% yield (Figure 211). The yellow solids are stable indefinitely under inert atmosphere at room temperature, but decompose over a period of days when in solution.

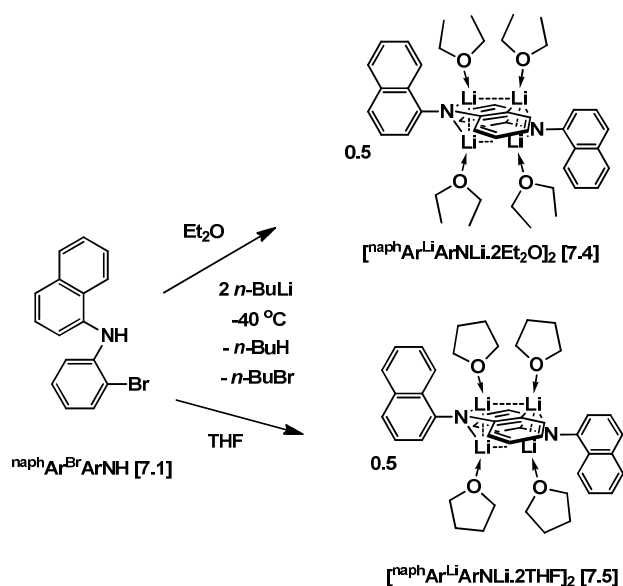


Figure 211: Synthesis of $[\text{}^{\text{naph}}\text{Ar}^{\text{Li}}\text{ArNLi}\cdot 2\text{Et}_2\text{O}]_2$ [7.4] and $[\text{}^{\text{naph}}\text{Ar}^{\text{Li}}\text{ArNLi}\cdot 2\text{THF}]_2$ [7.5]

The solid state molecular structure of $[\text{}^{\text{naph}}\text{Ar}^{\text{Li}}\text{ArNLi}\cdot\text{TMEDA}]_n$ was previously reported as a mixed monomer / dimer species,²⁴⁶ with the dimer displaying intermolecular associations of Li with the phenyl ring of the adjacent $\text{}^{\text{naph}}\text{Ar}^{\text{Li}}\text{ArNLi}$ unit. Based on this, as well as the solid state molecular structure for $[\text{}^{2,6\text{-}i\text{Pr}_2}\text{Ar}^{\text{Li}}\text{ArNLi}\cdot 2\text{THF}]_2$ [7.3a], it is proposed that dimeric structures with two Et_2O (or two THF) molecules per $\text{}^{\text{naph}}\text{Ar}^{\text{Li}}\text{ArNLi}$ unit are formed, i.e. $[\text{}^{\text{naph}}\text{Ar}^{\text{Li}}\text{ArNLi}\cdot 2\text{Et}_2\text{O}]_2$ [7.4] and $[\text{}^{\text{naph}}\text{Ar}^{\text{Li}}\text{ArNLi}\cdot 2\text{THF}]_2$ [7.5]. The ^1H NMR spectrum of [7.4] has Et_2O peaks at δ 2.68 and δ 0.42 (δ 3.26 and δ 1.11 for free Et_2O) and of [7.5] has THF peaks

at δ 3.58 and δ 1.75 (δ 3.57 and δ 1.40 for free THF). The $^7\text{Li}\{^1\text{H}\}$ NMR spectrum of [7.4] exhibits a single broad peak at δ 1.13 in C_6D_6 and for [7.5] in $\text{THF-}d_8$ further upfield to δ 0.43.

7.3.4. Synthesis of $[\text{naph}^{\text{NP}}\text{NLi}_2\cdot\text{diox}]_n$ [7.6]

As with $[\text{iprop}^{\text{NP}}\text{NLi}_2\cdot\text{diox}]_n$ [2.6], the synthesis of $[\text{naph}^{\text{NP}}\text{NLi}_2\cdot\text{diox}]_n$ [7.6] can be effected in a one-pot two-step process directly from $\text{naph}^{\text{Ar}^{\text{Br}}}\text{ArNH}$ [7.1] by quenching the *in situ* formed $[\text{naph}^{\text{Ar}^{\text{Li}}}\text{ArNLi}\cdot 2\text{Et}_2\text{O}]_2$ [7.4] with PPhCl_2 in Et_2O (Figure 212).

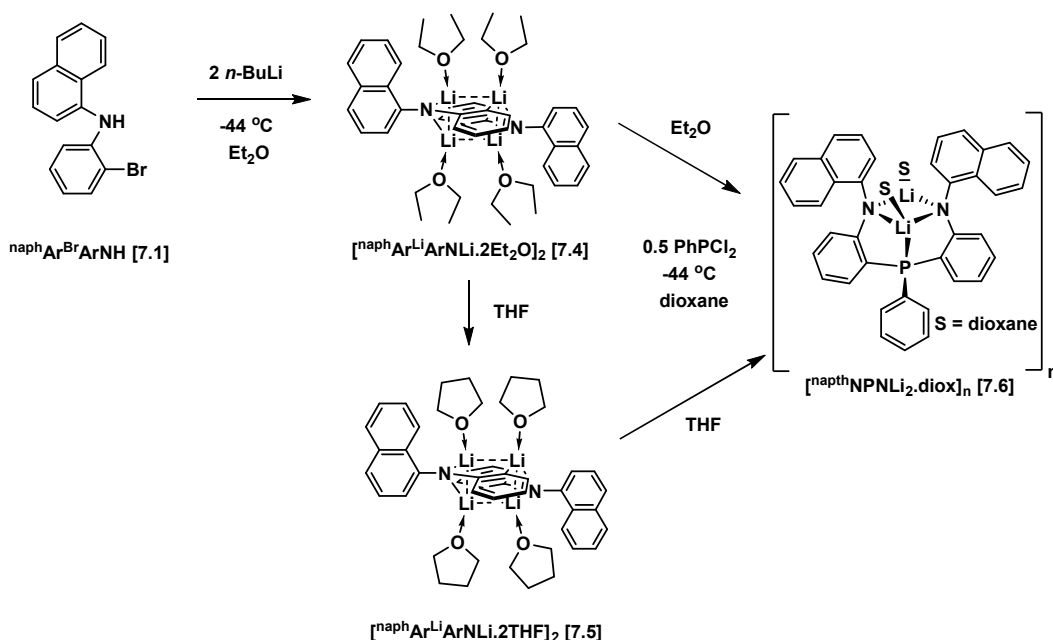


Figure 212: Synthesis of $[\text{naph}^{\text{NP}}\text{NLi}_2\cdot\text{diox}]_n$ [7.6]

The reaction also proceeds in THF, but best results were obtained by isolating the $[\text{naph}^{\text{Ar}^{\text{Li}}}\text{ArNLi}\cdot 2\text{Et}_2\text{O}]_2$ [7.4] intermediate prior to quenching. Temperature control is of utmost importance during the addition of PPhCl_2 , and should be at or below $-40\text{ }^\circ\text{C}$. The yields obtained for compound [7.6] are moderate (46 to 66%), with the $^{31}\text{P}\{^1\text{H}\}$ NMR spectrum displaying prominent side-product signals at δ -21.00, δ 87.44, δ 66.84 and δ 47.17. The signals at δ 87.44 to 47.17 may be indicative of N-P bond formation, as was observed in the formation of the

^{tol}NPNPPh [2.9] side-product (see chapter 2) and PⁱPr₂Cl quenching of the trilithio-diarylamide [(^{tol}-Li Ar)₂NLi·TMEDA]_n.

Purification of compound [7.6] required up to three successive re-crystallisations from an *n*-hexanes/toluene mixtures. The ³¹P{¹H} NMR spectrum of pure [^{naph}NPNLi₂·diox]_n [7.6] in C₆D₆ indicated a mixture of two compounds; a major species (70%) with a quartet at δ -34.47 (¹J_{PLi} = 40 Hz) and a minor species (30%) with a broad peak centred at δ -32.47 (Figure 213).

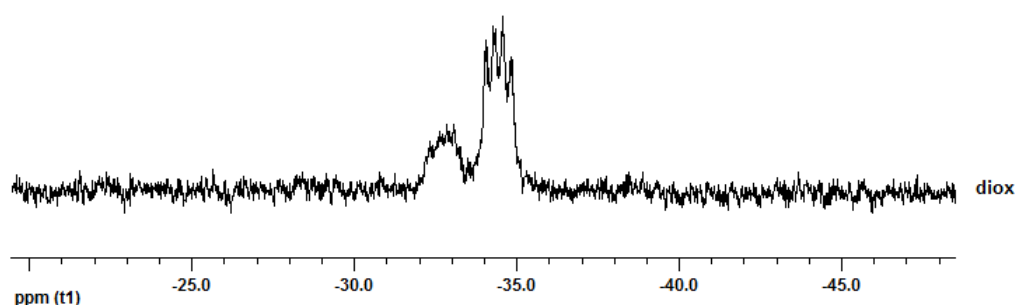


Figure 213: ³¹P{¹H} NMR spectrum of [^{naph}NPNLi₂·diox]_n [7.6] in toluene-*d*₈

The ⁷Li{¹H} NMR spectrum displayed a singlet at δ 0.70 and a doublet at δ 1.85 (¹J_{LiP} = 44 Hz), indicating that the P atom is coupled to one of the Li atoms (Figure 214), with no apparent discrepancy between the major and minor species. A solid state molecular structure was not obtained, but it can be assumed that the structure of [^{naph}NPNLi₂·diox]_n [7.6] is similar to that observed for [^{iprop}NPNLi₂·diox]_n [2.6], with one 1,4-dioxane molecule bridging two ^{naph}NPNLi₂ units, forming a one-dimensional chain structure (Figure 215).

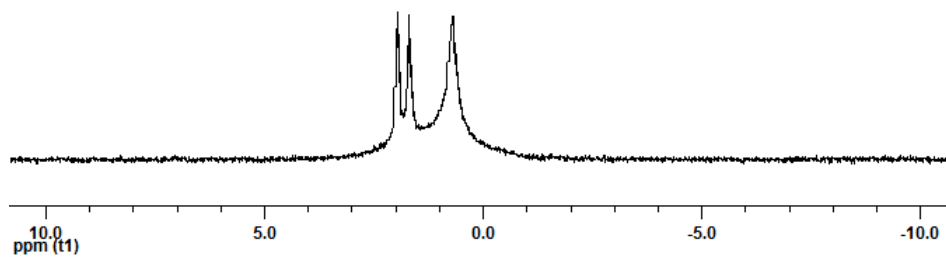


Figure 214: ⁷Li{¹H} NMR spectrum of [^{naph}NPNLi₂·diox]_n [7.6] in toluene-*d*₈

Overlapping signals due to the presence of a mixture of two species, coupled with poor solubility in C_6D_6 or toluene- d_8 , meant that assignments of 1H NMR and $^{13}C\{^1H\}$ NMR spectral signals were only possible for the major species. The 1H NMR spectral signal for coordinated 1,4-dioxane at δ 2.77 (unbound at δ 3.53) was shifted upfield compared to $[^{i\text{prop}}\text{NPnLi}_2\cdot\text{diox}]_n$ [**2.6**] (δ 3.09), indicating that 1,4-dioxane forms stronger bonds with Li in compound [**7.6**], despite the increased steric bulk of the naphthyl group.

If all the excess 1,4-dioxane was not removed on drying compound [**7.6**], the minor signal observed in the $^{31}P\{^1H\}$ NMR spectrum may be indicative of a species such as $[^{\text{naph}}\text{NPnLi}_2\cdot 1.5\text{diox}]_n$ [**7.6a**], whereby the Li atoms not coupled to phosphorus are coordinated to two different bridging 1,4-dioxane molecules (Figure 215).

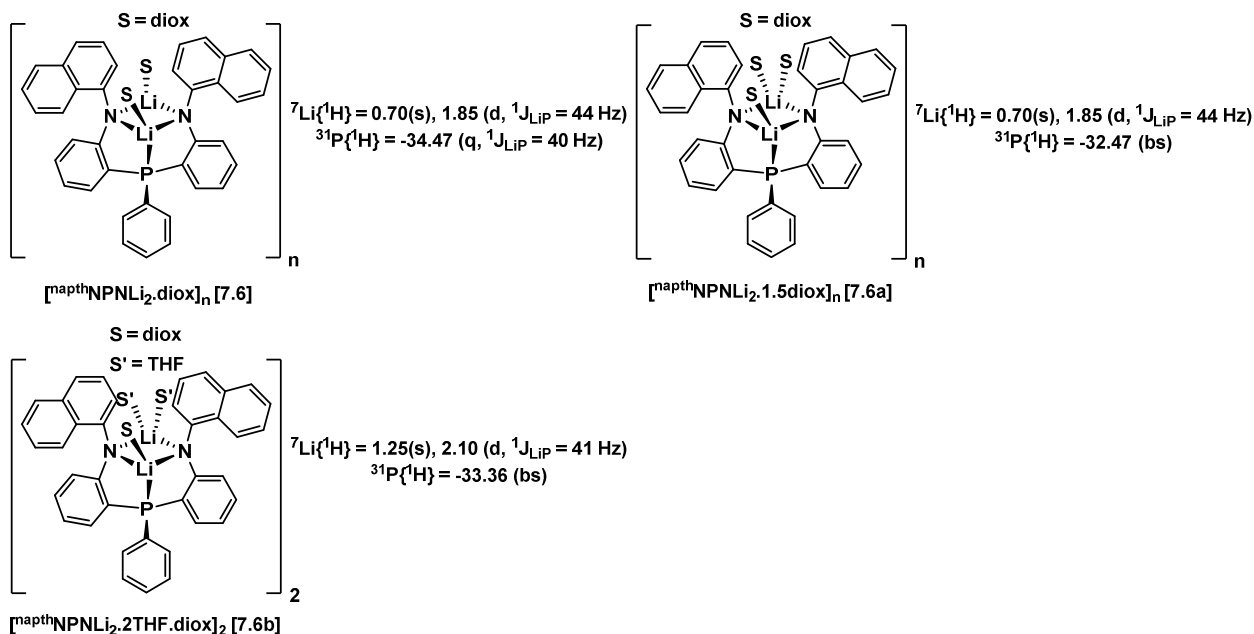


Figure 215: Structural forms for $[^{\text{naph}}\text{NPnLi}_2\cdot\text{diox}]_n$ [**7.6**], $[^{\text{naph}}\text{NPnLi}_2\cdot 1.5\text{diox}]_n$ [**7.6a**] and $[^{\text{naph}}\text{NPnLi}_2\cdot\text{diox}\cdot 2\text{THF}]_n$ [**7.6b**]

On addition of 2 equiv of THF to $[^{\text{naph}}\text{NPnLi}_2\cdot\text{diox}]_n$ [**7.6**] in C_6D_6 , the $^{31}P\{^1H\}$ NMR spectrum displayed a single broad peak at δ -33.36 (Figure 216) and the $^7\text{Li}\{^1H\}$ NMR spectrum confirmed that one of the Li atoms is still coordinated to the P atom, with a singlet at δ 1.25 and a

doublet at δ 2.10 ($^1J_{\text{LiP}} = 41$ Hz). The ^1H NMR spectrum displayed signals for coordinated THF at δ 3.08 and 1.01 and the 1,4-dioxane signal shifted downfield to δ 3.08, indicating that it remained coordinated.

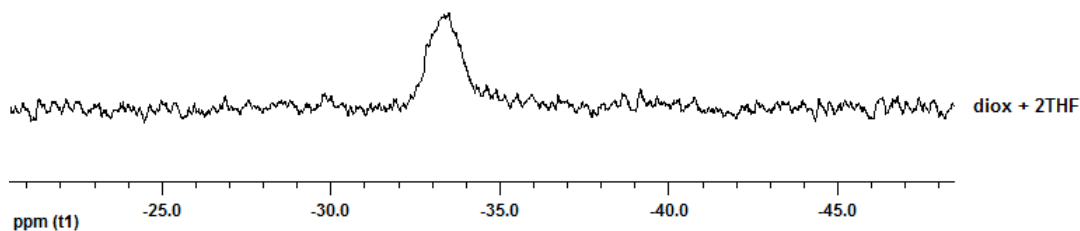


Figure 216: $^{31}\text{P}\{^1\text{H}\}$ NMR spectrum of $[\text{naphNPNLi}_2\cdot\text{diox}\cdot 2\text{THF}]_n$ **[7.6b]** in C_6D_6

Based on the above experimental data, it is proposed that the species formed on addition of 2 equiv of THF to compound **[7.6]** has the structural formulae of $[\text{naphNPNLi}_2\cdot\text{diox}\cdot 2\text{THF}]_n$ **[7.6b]**, whereby 1,4-dioxane bridges the Li atoms still coordinated to a phosphorus atom, and two THF's bind to the other Li atoms to give a dimeric structure (Figure 215), reminiscent of structures reported in chapter two for the $^{\text{iprop}}\text{NPN}$, $^{\text{tol}}\text{NPN}$ and $^{\text{ph}}\text{NPN}$ donor sets.

7.3.5. Synthesis of $[\text{}^{2,6\text{-iPr}_2}\text{NPNLi}_2\cdot\text{diox}]_n$ **[7.7]**

The one-pot synthesis of $[\text{}^{2,6\text{-iPr}_2}\text{NPNLi}_2\cdot\text{diox}]_n$ **[7.7]** from $^{2,6\text{-iPr}_2}\text{Ar}^{\text{Br}}\text{ArNH}$ **[7.2]** using *n*-BuLi is not viable as it had been established an excess *n*-BuLi (though not *t*-BuLi) is required. A one-pot reaction was thus conducted using three equiv of *t*-BuLi in Et_2O . The crude reaction mixture indicated $[\text{}^{2,6\text{-iPr}_2}\text{NPNLi}_2\cdot\text{diox}]_n$ **[7.7]** did not form; instead two prominent broad signal were observed at δ 52.01 and δ -8.11 in the $^{31}\text{P}\{^1\text{H}\}$ NMR spectrum. These signals could be indicative of P-N and P-C bonds, respectively, and their broadness (see (a) in Figure 219) suggests the presence of P-Li coupling, arguing against a $^{2,6\text{-iPr}_2}\text{NPNPPh}$ side-product (see $^{\text{tol}}\text{NPNPPh}$ **[2.9]** in chapter 2). The corresponding $^7\text{Li}\{^1\text{H}\}$ NMR spectrum displays a broad singlet at δ 0.69. Significant disfavouring of P-C relative to P-N bond formation (as observed in $\text{P}^{\text{iPr}_2}\text{Cl}$ quenching of the trilithio-diarylamide $[(^{\text{tol-Li}}\text{Ar})_2\text{NLi}\cdot\text{TMEDA}]_n$) may have resulted in side

products where PPhCl_2 selectively quenches only the two Li-N bonds, or one Li-N and one Li-C bond (see Figure 217).

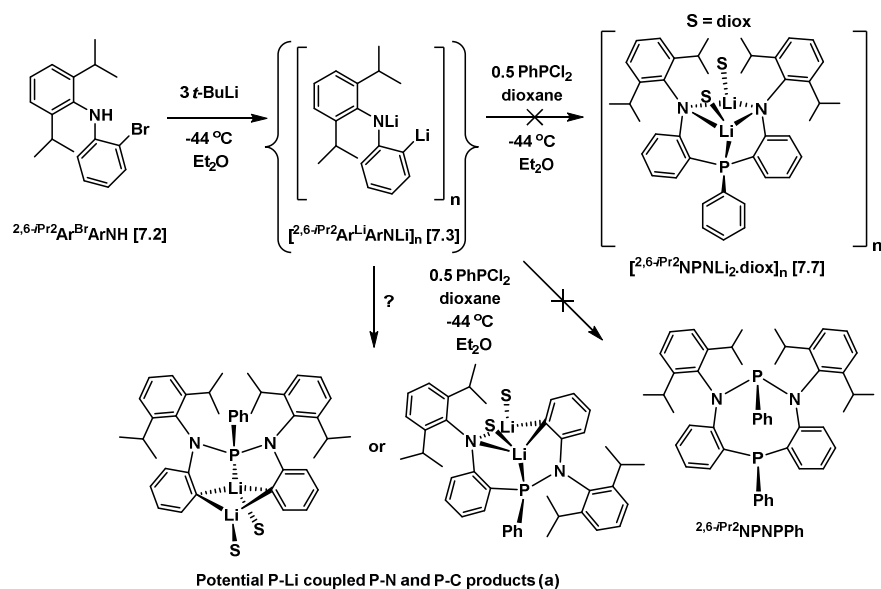


Figure 217: Potential P-Li coupled P-N and P-C side-products for one-pot reaction (a)

Reaction of $[\text{2,6-}i\text{Pr}_2\text{Ar}^{\text{Li}}\text{ArNLi}]_n$ [7.3] with PPhCl_2 in Et_2O was conducted once as an NMR experiment and once on a 1.5 g scale. In the former case, the major product displayed a broad signal at δ -27.95 in the $^{31}\text{P}\{^1\text{H}\}$ NMR spectrum (see (b) in Figure 219) and the $^7\text{Li}\{^1\text{H}\}$ NMR spectrum displayed a singlet at δ 0.69 and a doublet at δ 2.01 ($^1J_{\text{LiP}} = 60$ Hz). In the latter case, the $^{31}\text{P}\{^1\text{H}\}$ NMR spectrum displayed two distinct products; a major species (80%) with a broad signal at δ -31.80 and a minor species (20%) with a broad signal at -33 (see (c) in Figure 219). The $^7\text{Li}\{^1\text{H}\}$ NMR spectrum displayed a singlet at δ -0.14 and a doublet at δ 1.87 ($^1J_{\text{LiP}} = 43$ Hz), with no apparent distinction between the major and minor species. Following on the proposed structures for the $^{\text{naph}}\text{NPN}$ donor set, the two species obtained from the 1.5 g scale reaction may be the desired lithiated $^{2,6-i\text{Pr}_2}\text{NPnLi}_2$ donor set, with slightly different structures due to an excess of 1,4-dioxane i.e. $[\text{2,6-}i\text{Pr}_2\text{NPnLi}_2\cdot\text{diox}]_n$ [7.7] and $[\text{2,6-}i\text{Pr}_2\text{NPnLi}_2\cdot 1.5\text{diox}]_n$ [7.7a] (Figure 218). $[\text{2,6-}i\text{Pr}_2\text{NPnLi}_2\cdot\text{diox}]_n$ [7.7] was not isolated; a single recrystallisation from toluene / *n*-hexanes resulted in 92% purity and further optimisation is required.

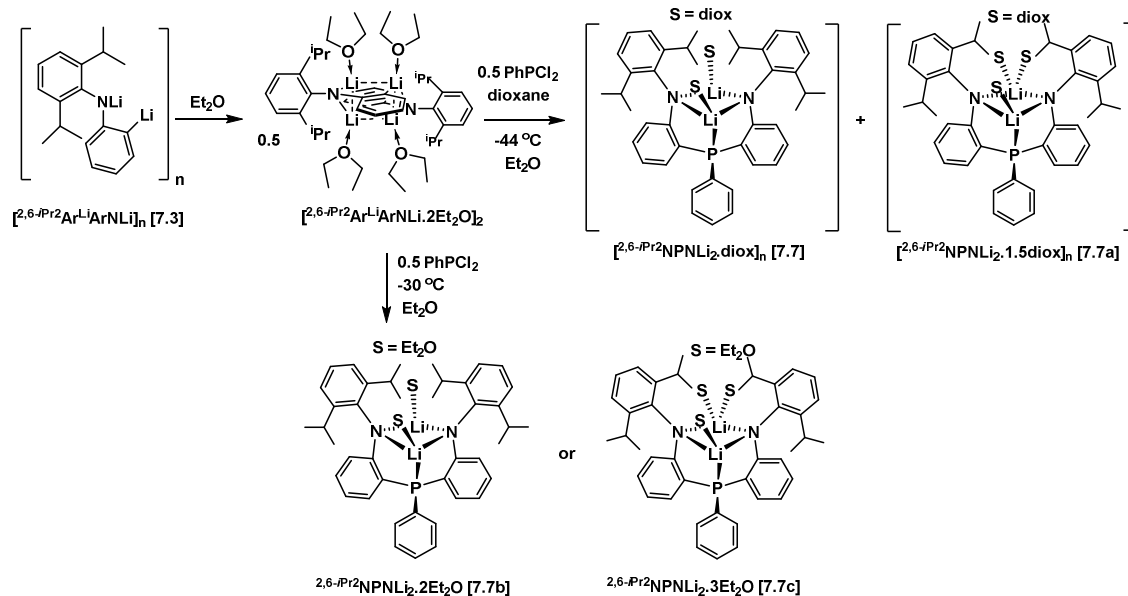


Figure 218: Synthesis of $[^{2,6-iPr_2}NPnLi_2 \cdot diox]_n$ [7.7], $[^{2,6-iPr_2}NPnLi_2 \cdot 1.5diox]_n$ [7.7a], $^{2,6-iPr_2}NPnLi_2 \cdot 2Et_2O$ [7.7b] or $^{2,6-iPr_2}NPnLi_2 \cdot 3Et_2O$ [7.7c]

In the case of the NMR scale experiment, the addition of 1,4-dioxane was omitted; hence the downfield shifted signal at δ -27.95 in the $^{31}P\{^1H\}$ NMR spectrum could be attributed to a monomeric Et_2O adduct wherein the Li-P coupling was retained (Figure 218). The lithium atom not coupled to phosphorus may be coordinated to either one or two Et_2O molecules, i.e. $^{2,6-iPr_2}NPnLi_2 \cdot 2Et_2O$ [7.7b] or $^{2,6-iPr_2}NPnLi_2 \cdot 3Et_2O$ [7.7c]

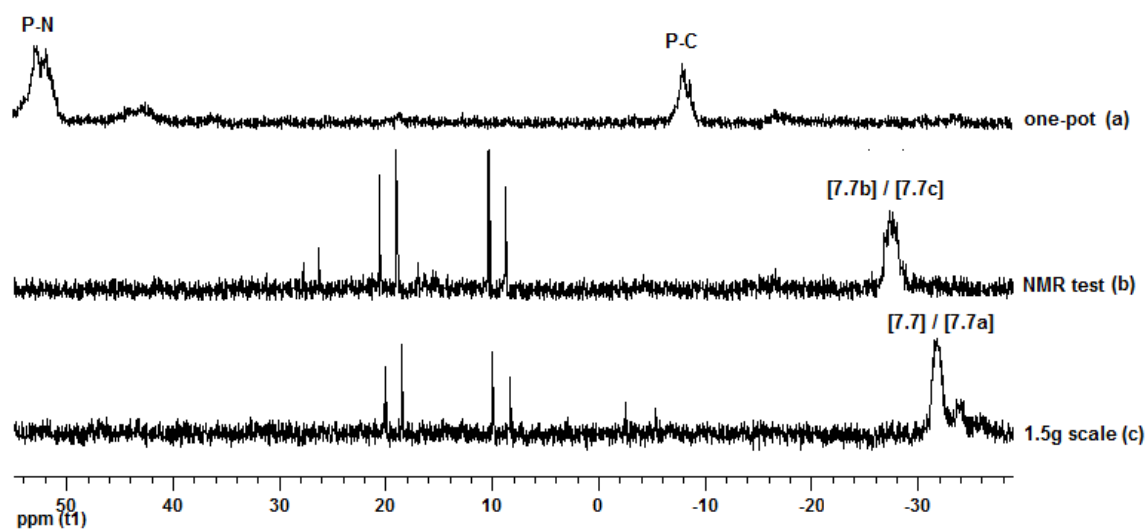


Figure 219: $^{31}P\{^1H\}$ NMR spectra of crude reaction mixtures for $[^{2,6-iPr_2}NPnLi_2 \cdot diox]_n$ [7.7] in C_6D_6

7.3.6. Synthesis of $^{\text{naph}}\text{NPNH}_2$ [7.8] and $^{2,6\text{-}i\text{Pr}_2}\text{NPNH}_2$ [7.9]

Reaction of $[\text{^{\text{naph}}NPNLi}_2 \cdot \text{diox}]_n$ [7.6] with two equiv of $\text{NMe}_3 \cdot \text{HCl}$ formed $^{\text{naph}}\text{NPNH}_2$ [7.8] as an off-white solid in 46% yield (Figure 220). The $^{31}\text{P}\{^1\text{H}\}$ NMR spectrum exhibited a peak at δ -33.34 and the ^1H NMR spectrum displayed the characteristic doublet at δ 6.82 ($^4J_{\text{HP}} = 6$ Hz) for the N-H proton. A parent ion was observed at 544 m/z via mass spectrometry.

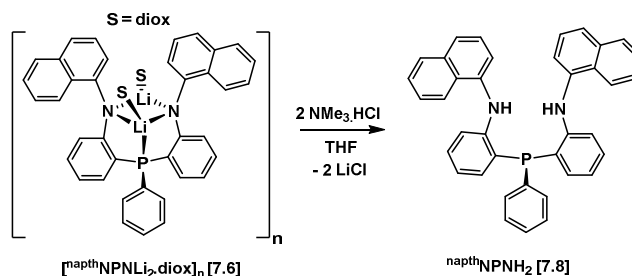


Figure 220: Synthesis of $^{\text{naph}}\text{NPNH}_2$ [7.8]

A single protonolysis conducted with $^{\text{naph}}\text{NPNH}_2$ [7.8] and $\text{Zr}(\text{NMe}_2)_4$, followed by TMSCl addition resulted in the isolation of a species with a $^{31}\text{P}\{^1\text{H}\}$ NMR signal at δ 38.71 and a fragment ion at 704 m/z corresponding to a formulation of $^{\text{naph}}\text{NPNZrCl}_2$. The reduction of this unidentified species with KC_8 and N_2 led to the isolation of a discrete dark brown species which exhibited a single signal at δ 12.29 in a $^{31}\text{P}\{^1\text{H}\}$ NMR spectrum.

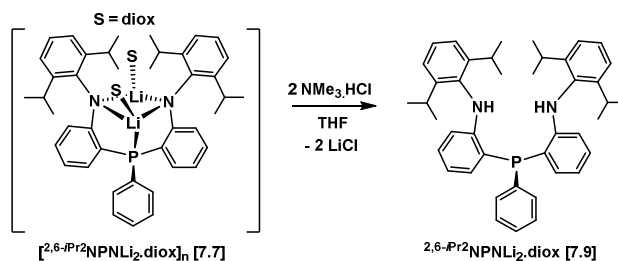


Figure 221: Synthesis of $^{2,6\text{-}i\text{Pr}_2}\text{NPNH}_2$ [7.9]

$[\text{^{2,6-}iPr}_2\text{NPNLi}_2 \cdot \text{diox}]_n$ [7.7] at 92% purity was protonated with excess $\text{NMe}_3 \cdot \text{HCl}$. The $^{31}\text{P}\{^1\text{H}\}$ NMR spectrum indicated a major signal at δ -38.42, with a corresponding mass spectrum

exhibiting a parent ion at 612 m/z. Further purification of $^{2,6-iPr_2}NPNH_2$ [7.9] was not attempted and future work should focus on obtaining the pure $[^{2,6-iPr_2}NPNLi_2 \cdot diox]_n$ [7.7] precursor.

7.4. Final Thoughts

In general for this project, modification of the original N-mesitylene containing first generation o-phenylene bridged ^{mes}NPN ligand system developed by E. MacLachlan with less bulky N-amido groups (^{Ph}NPN , ^{tol}NPN and ^{iPr}NPN) led to complexes that were more coordinately saturated. The zirconium dinitrogen complexes with these ligands were more stable and less reactive, failing to react with hydrogen. Optimal ancillary ligands for the study of dinitrogen complexes have to bridge the divide between providing enough support to stabilise the dinitrogen ligand while at the same time allow for interaction with substrates to promote functionalisation of the activated dinitrogen unit. It would be of interest to investigate how increased steric bulk ($^{2,6-iPr_2}NPN$ and ^{naph}NPN) of the N-amido groups affect this subtle balance between stability and reactivity.

The more rigid and stable o-phenylene backbone led to the isolation of stable titanium and tantalum chloride complexes, which could open up interesting new areas of reactivity. For tantalum, the dinitrogen complexes with reduced steric bulk of the N-amido groups were too unstable or reactive to be isolated, and there may be merit in future studies altering the sterics and/or electronics of the N-amido groups. For titanium, efforts should be focused on ligand design to promote a side-on mode of dinitrogen coordination.

Chapter 8: Experimental

8.1. General Experimental

Unless otherwise stated, all manipulations were performed under a moisture- and oxygen-free N₂ or Ar atmosphere, using standard Schlenk or glovebox techniques (Vacuum Atmospheres HE-553-2 glovebox equipped with a MO-40-2H purification system and a -40 °C freezer). N₂ was dried and deoxygenated by passing through a column packed with 4 Å molecular sieves and a copper catalyst. Toluene, *n*-hexanes, THF and Et₂O were purchased anhydrous from Aldrich, sparged with N₂ and passed through columns containing activated alumina. *n*-Pentanes and benzene were either obtained as aforementioned or distilled over sodium-benzophenone ketyl. 1,4-Dioxane was distilled over sodium-benzophenone ketyl. Petroleum ether and ethyl acetate were purchased from commercial suppliers and used without further purification. CDCl₃, C₆D₆, toluene-*d*₈ and THF-*d*₈ were degassed with N₂ and dried over 4 Å molecular sieves. *n*-BuLi and *t*-BuLi was purchased from Aldrich and titrated with self-indicating diphenylacetic acid or with benzoic acid, using 1,10-phenanthroline as an indicator. Celite was heated to 200 °C and cooled under vacuum overnight. ¹H and ³¹P{¹H} NMR spectra were recorded on a Bruker AV-300, Bruker AV-400 or Bruker DIR-400 spectrometer, operating at 300.1 and 400.0 MHz for ¹H spectra, respectively. ¹³C{¹H} NMR spectra were either recorded on the aforementioned instruments or a Bruker AV-600 spectrometer, operating at 600.0 MHz for ¹H spectra. ⁷Li{¹H} and ²H NMR spectra were recorded on the Bruker AV-400 or Bruker DIR-400. Unless otherwise stated, all spectra were recorded at room temperature. Chemical shifts (δ) are listed in ppm and absolute values of the coupling constants are in hertz (Hz). ¹H NMR spectra were referenced to residual protons in the deuterated solvent: CDCl₃ (δ 7.24), C₆D₆ (δ 7.16), toluene-*d*₈ (δ 2.09) or THF-*d*₈ (δ 3.58). ¹³C{¹H} NMR spectra were referenced to residual carbons in the deuterated solvent: CDCl₃ (δ 77.23), C₆D₆ (δ 128.0), toluene-*d*₈ (δ 20.4) or THF-*d*₈ (δ 67.4). ³¹P{¹H} NMR spectra were referenced to external P(OPh)₃ (δ 128.2 with respect to 85% H₃PO₄ at δ 0.0).

$^7\text{Li}\{^1\text{H}\}$ NMR spectra were referenced to external LiCl in $\text{D}_2\text{O}/\text{H}_2\text{O}$ at δ 0.0. Mass spectrometry (EI-MS) and microanalysis (C, H, N) were performed at the Department of Chemistry at the University of British Columbia. GC-MS spectra were recorded on an Agilent series 6890 GC system with a 5973 mass selective detector. $^{15}\text{N}\{^1\text{H}\}$ NMR spectra were recorded on a Bruker AV-400 direct detect spectrometer operating at 400.1 MHz for ^1H NMR spectra and were referenced externally to MeNO_2 at δ 0 (or NO_3 in NH_4NO_3 at δ -5). ^{15}N -labelled complexes were isolated and handled under unlabelled N_2 . UV-Vis spectra were recorded on a Varian/Cary 5000 UV-Vis spectrometer using a 1 cm cuvette. For UV-Vis spectra, the compound was dissolved in toluene and the solution was transferred to a Teflon-sealed UV-Vis cuvette.

8.2. Starting Materials and Reagents

DBa,^{396, 397} Pd_2dba_2 ,^{398, 399} $\text{PdCl}_2(\text{NCMe})_2$,^{400, 401} $\text{PdCl}_2(\text{DPPF})$,⁴⁰² $\text{ZrCl}_2(\text{NMe}_2)_2(\text{DME})$,²⁶⁶ $\text{ZrCl}_4(\text{THF})_2$,⁴⁰³ $\text{TiCl}_2(\text{NMe}_2)_2$,⁴⁰⁴ mes-NPNH_2 ,^{97, 214} mes-NPNZrCl_2 ,^{97, 214} $\text{TaCl}_3(\text{NMe}_2)_2(\text{THF})$,^{405, 406} $[\text{TaCl}_3(\text{PMe}_3)_2]_2$,²⁸¹ $\text{Si-NPNLi}_2\cdot\text{THF}_2$,⁸⁰ and KC_8 ⁴⁰⁷⁻⁴⁰⁹ were prepared according to literature procedures. CH_3CN was distilled over CaH_2 . Tol_2NH , Ph_2NH , $o\text{-C}_6\text{H}_4\text{BrF}$, $o\text{-C}_6\text{H}_4\text{Br}_2$,^{2,6-} $i\text{Pr}_2\text{ArNH}_2$, pyridine and pyridine- d_5 were purchased from commercial suppliers, degassed with N_2 and stored over activated molecular sieves. PhSiH_3 was purchased from commercial suppliers and stored over activated molecular sieves. PdCl_2 , *rac*-BINAP, DPPF, Na^tOBu , K^tOBu , PPhCl_2 , TMEDA, $^{\text{naph}}\text{ArNH}_2$, $\text{NMe}_3\cdot\text{HCl}$, ZrCl_4 , $\text{Zr}(\text{NMe}_2)_4$, TiCl_4 , $\text{Ti}(\text{NMe}_2)_4$, $\text{Hf}(\text{NMe}_2)_4$, TMSCl , $\text{Ta}(\text{NMe}_2)_5$, $[\text{TaCl}_5]_2$, potassium metal, KH , 4,4'-bipyridine, PMe_3 , PPhMe_2 , P^tBu_3 , *dmpe*, 2,2'-bipyridine, KHBET_3 , *xylylNC*, $^t\text{BuNC}$, 4,4'-dimethylbenzophenone and (trimethylsilyl)diazomethane were purchased from commercial suppliers and used without further purification. THF was distilled over sodium-benzophenone ketyl. Graphite was heated to 200 °C and cooled under reduced pressure. $^{15}\text{N}_2$ gas (isotopic purity 98+ %, 1 or 2 dm^3) was purchased from Cambridge Isotopes Ltd. in a small carbon steel lecture bottle and used as received. Carbon monoxide and carbon dioxide were passed through a column packed with 4 Å

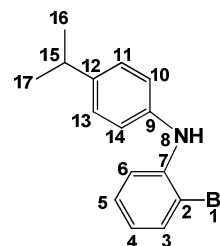
activated molecular sieves. Dihydrogen and ethylene were passed through a column packed with layers of 4 Å activated molecular sieves and copper catalyst.

8.3. Synthetic Methods

^{iprop}Ar^{Br}ArNH [2.1] (a) with Pd₂dba₃ / *rac*-BINAP (80 °C): Pd₂dba₃ (0.61 g, 0.66 mmol) and *rac*-BINAP (1.21 g, 1.95 mmol) were dissolved with stirring in 270 cm³ toluene in the glovebox, forming a wine-red solution. The solution was transferred to the Schlenk line and ^{4-*i*Pr}ArNH₂ (30.34 g, 0.22 mol), Na^tOBu (26.80 g, 0.28 mol) and *o*-C₆H₄Br₂ (47.33 g, 0.20 mol) were added sequentially, forming a dark cherry red mixture that was refluxed for 19 hrs at 80 °C. The resulting tan brown mixture with a brown precipitate turned dark purple on exposure to air. The toluene solvent was removed *in vacuo* and the residue was dissolved in petroleum ether. This mixture was filtered using a Buchner funnel, washing three times with petroleum ether. The petroleum ether was removed *in vacuo* from the filtrate, giving *ca* 25 cm³ of a viscous purple liquid (pre-column GC-MS yield 42%). The product was separated from *o*-C₆H₄Br₂ using column chromatography (silica gel 60-200 µm, 70-230 mesh) with 100% petroleum ether as eluent (19.2 g, 66.2 mmol ^{iprop}Ar^{Br}ArNH [2.1], 33% yield based on *o*-C₆H₄Br₂); **(b) with PdCl₂(DPPF) / DPPF (130 °C):** PdCl₂(DPPF) (2.119 g, 3.96 mmol), DPPF (4.41 g, 7.96 mmol) and K^tOBu (25.13 g, 0.22 mol) were combined with stirring in 200 cm³ 1,4-dioxane in the glovebox, giving in a red-brown mixture with suspended solids. The reaction mixture was transferred to a Schlenk line and *o*-C₆H₄Br₂ (24.00 cm³, 0.20 mol) and ^{4-*i*Pr}ArNH₂ (25.00 cm³, 0.18 mol) were added sequentially, forming a dark brown mixture. The reaction mixture was heated to 80 °C for 20 min and then refluxed for 7 hrs at 130 °C (pre-column GC-MS yield 82%). The 1,4-dioxane solvent was removed *in vacuo* from the dark brown reaction mixture and 200 cm³ ethyl acetate was added to the residue. The resultant mixture was filtered using a Buchner funnel, washing with ethyl acetate. The ethyl acetate was removed *in vacuo* from the filtrate, leaving a viscous dark purple-black oil. The product was separated from *o*-C₆H₄Br₂ using column chromatography

(silica gel 60-200 μm , 70-230 mesh) with 100% petroleum ether as eluent (25.28 g, 87.11 mmol $\text{iprop-Ar}^{\text{Br}}\text{ArNH}$ [**2.1**], 44% yield based on $o\text{-C}_6\text{H}_4\text{Br}_2$)

^1H NMR (C_6D_6 , 300 MHz): δ = 1.15 (d, $^3J_{\text{HH}}$ = 7 Hz, 3 H16 and 3 H17, CH_3), 2.90 (hep, $^3J_{\text{HH}}$ = 7 Hz, 1 H15, CH), 5.94 (bs, 1 H8, NH), 6.42 (d of t, $^3J_{\text{HH}}$ = 8 Hz, $^4J_{\text{HH}}$ = 1 Hz, 1 H4, ArH), 6.84 (d, $^3J_{\text{HH}}$ = 8 Hz, 1 H10 and 1 H14, ArH, overlapping d of t, $^3J_{\text{HH}}$ = 8 Hz, $^4J_{\text{HH}}$ = 1 Hz, 1 H5, ArH), 6.97 (d, $^3J_{\text{HH}}$ = 8 Hz, 1 H11 and 1 H13, ArH), 7.08 (d of d, $^3J_{\text{HH}}$ = 8 Hz, $^4J_{\text{HH}}$ = 1 Hz, 1 H6, ArH), 7.38 (d of d, $^3J_{\text{HH}}$ = 8 Hz, $^4J_{\text{HH}}$ = 1 Hz, 1 H3, ArH). $^{13}\text{C}\{^1\text{H}\}$ NMR (C_6D_6 , 101 MHz): δ = 24.2 (C16 and C17, CH_3), 33.9 (C15, CH), 111.9 (C2, C_{ipso}), 115.5 (C6, ArC), 120.6 (C4, ArC), 121.8 (C10 and C14, ArC), 127.5 (C11 and 13, ArC), 128.4 (C5, ArC), 133.2 (C3, ArC), 139.4 (C9, C_{ipso}), 142.9 (C7, C_{ipso}), 143.9 (C12, C_{ipso}). Anal. Calcd. for $\text{C}_{15}\text{H}_{16}\text{BrN}$: C, 62.08; H, 5.56; N, 4.83; Found: C, 62.100; H, 5.64; N, 5.20. EI-MS (m/z): 289 (75, $[\text{M}]^+$), 274 (100, $[\text{M} - \text{CH}_3]^+$), 194 (20, $[\text{M} - \text{CH}_3 - \text{Br}]^+$).



$[\text{}^{\text{tol}}\text{Ar}^{\text{Li}}\text{ArNLi}\cdot\text{TMEDA}]_2$ [**2.2**] ToI_2NH (49.71 g, 251.98 mmol) was suspended in 950 cm^3 n -hexanes in a 2.0 dm^3 round bottom flask and the mixture was cooled to $-43\text{ }^\circ\text{C}$ (dry ice/ethanol). 1.65 M $n\text{-BuLi}$ in n -hexanes (305.6 cm^3 , 504.2 mmol) was added via syringe over a period of 20 min, forming a thick, white suspension. TMEDA (75.60 cm^3 , 504.2 mmol) was added via syringe to the lithiated reaction mixture, resulting in partial dissolution of the suspended solids. The reaction mixture was allowed to warm slowly to room temperature and stirred overnight for *ca* 16 hrs, resulting in a yellow solution with a cream precipitate. Inside the glovebox, the cream-coloured solid was collected on a sintered glass frit, washed with 3 x 40 cm^3 n -hexanes and dried *in vacuo* (77.93 g, 239.53 mmol $[\text{}^{\text{tol}}\text{Ar}^{\text{Li}}\text{ArNLi}\cdot\text{TMEDA}]_2$ [**2.2**], 95% yield based on tol_2NH). Single crystals of [**2.2**] were grown via vapour diffusion of an $\text{Et}_2\text{O}/\text{THF}$ (1:1) solution with n -hexanes in the freezer.

$[\text{tolAr}^{\text{Li}}\text{ArNLi} \cdot 2\text{THF}]_2$: $^7\text{Li}\{^1\text{H}\}$ NMR (THF- d_8 , 156 MHz):

$\delta = -1.16$ (s, Li1 and Li8). ^1H NMR (THF- d_8 , 600 MHz): δ

$= 1.73$ (s, H19, CH_2), $^{(a)} 2.8$ (s, 3 H16, CH_3), 2.16 (s, 6 H,

TMEDA, CH_3) $^{(b)}$, 2.61 (s, 3 H15, CH_3), 2.101 (s, 2 H,

TMEDA, CH_2) $^{(b)}$, 3.58 (s, H18, CH_2), $^{(a)} 6.54$ (s, 1 H6, ArH),

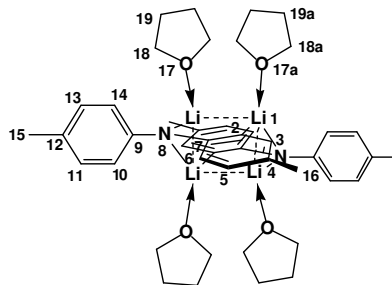
6.63 (s, 1 H3, ArH), 6.86 (s, 1 H10, 1 H11, 1 H13, and 1 H14, ArH), 7.53 (s, 1 H5, ArH).

$^{13}\text{C}\{^1\text{H}\}$ NMR (THF- d_8 , 151 MHz): $\delta = 20.9$ (C15, CH_3), 21.4 (C16, CH_3), 25.3 (C19, CH_2), 46.2

(TMEDA, CH_3), 58.9 (TMEDA, CH_2), 67.4 (C18, CH_2), 109.0 (C6, ArC), 119.3 (C3, ArC),

121.5 (C2, C_{ipso}), 125.9 (C10 and C14, ArC), 128.4 (C4, C_{ipso}), 129.6 (C12, C_{ipso}), 129.9 (C11 and

C13, ArC), 147.2 (C5, ArC), 159.6 (C9, C_{ipso}), 164.9 (C7, C_{ipso}).



$[\text{tolAr}^{\text{Li}}\text{ArNLi} \cdot \text{TMEDA}]_2$ [2.2]: $^7\text{Li}\{^1\text{H}\}$ NMR (C_6D_6 ,

156 MHz): $\delta = 0.73$ (s, Li1,8). ^1H NMR (C_6D_6 , 300

MHz): $\delta = 1.76$ (s, 4 H18, CH_2 and 12 H17, CH_3) $^{(c)}$, 2.68

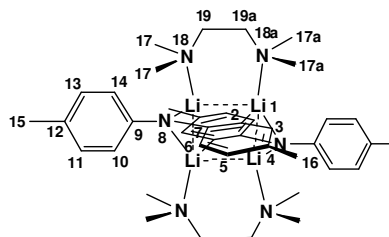
(s, 3 H15 and 3 H16, CH_3), 7.12 (s, 1 H3, 1 H5, 1 H6, 1

H10, and 1 H14 ArH), 7.18 (s, 1 H11 and 1 H13, ArH). $^{13}\text{C}\{^1\text{H}\}$ NMR (C_6D_6 , 75 MHz): $\delta = 20.8$

(C15 and C16, CH_3), 45.7 (C17, CH_3), 57.1 (C19, CH_2), 120.3 (C11 and C13, ArC), 124.1 (C12,

C_{ipso}), 128.0 (C3, C6, C10, C14, ArC and C2, C_{ipso}), 130.5 (C5, ArC and C4, C_{ipso}), 156.1 (C7 and

C9, C_{ipso}). EI-MS (m/z): 197 (100, $[\text{M} - 2\text{Li} - \text{TMEDA} + 2\text{H}]^+$).



$^{(a)}$ δ value indicates exchange between completely solvated (coordinated) THF and large excess THF solvent (free THF at δ 1.73 and δ 3.58).

$^{(b)}$ δ value indicates TMEDA is not coordinated to lithium (free TMEDA at δ 2.04 and δ 2.18 in C_6D_6) and integration indicates 0.5 molecules free TMEDA per $\text{tolAr}^{\text{Li}}\text{ArNLi}$ unit.

^(c) δ value indicates TMEDA is coordinated to lithium (free TMEDA at δ 2.04 and δ 2.18) and integration indicates one molecule TMEDA per $^{101}\text{Ar}^{\text{Li}}\text{ArNLi}$ unit.

$[\text{phAr}^{\text{Li}}\text{ArNLi} \cdot 1.5\text{TMEDA}]_2$ **[2.3]** Ph_2NH (27.87 g, 164.70 mmol) was suspended in 600 cm^3 *n*-hexanes in a 2.0 dm^3 round bottom flask and the mixture was cooled to -50°C (dry ice/ethanol). *n*-BuLi in *n*-hexanes (1.69M, 109 cm^3 , 184.2 mmol + 1.50M, 96 cm^3 , 144.0 mmol = 328.2 mmol) was added via syringe over a period of 6 min, giving a thick, white suspension. TMEDA (49.50 cm^3 , 330.12 mmol) was added via syringe to the lithiated reaction mixture, resulting in partial dissolution of the suspended solids. The reaction mixture was allowed to warm slowly to room temperature and stirred overnight for *ca* 16 hr, resulting in a yellow solution with a cream precipitate. Inside the glovebox, the cream-coloured solid was collected on a sintered glass frit, washed with 2 x 40 cm^3 *n*-hexanes and dried *in vacuo* (43.96 g, 123.70 mmol $[\text{phAr}^{\text{Li}}\text{ArNLi} \cdot 1.5\text{TMEDA}]_2$ **[2.3]**, 75% yield based on Ph_2NH).

$[\text{phAr}^{\text{Li}}\text{ArNLi} \cdot 2\text{THF}]_2$: $^7\text{Li}\{^1\text{H}\}$ NMR ($\text{THF-}d_8$, 156 MHz): δ

= -0.91 (s, Li1 and Li8). ^1H NMR ($\text{THF-}d_8$, 300 MHz): δ =

1.74 (s, H19, CH_2), ^(a) 2.61 (s, 18 H, TMEDA, CH_3), ^(b) 2.106 (s,

6 H, TMEDA, CH_2), ^(b) 3.58 (s, H18, CH_2), ^(a) 6.35 (bs, 1 H4,

ArH), 6.62 (bs, 1 H12, ArH), 6.74 (s, 1 H5 and 1 H6, ArH),

7.02 (d, $^3J_{\text{HH}} = 7.2$ Hz, 1 H10 and 1 H14, ArH), 7.07 (t, $^3J_{\text{HH}} = 7.8$ Hz, 1 H11 and 1 H13, ArH),

7.73 (d, $^3J_{\text{HH}} = 5.7$ Hz, 1 H3, ArH). $^{13}\text{C}\{^1\text{H}\}$ NMR ($\text{THF-}d_8$, 151 MHz): δ = 25.2 (C19, CH_2),

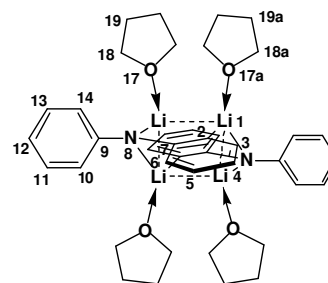
46.2 (TMEDA, CH_3), 58.8 (TMEDA, CH_2), 67.4 (C18, CH_2), 109.6 (C6, ArC), 115.0 (C4, ArC),

117.8 (C12, ArC), 119.5 (C2, C_{ipso}), 125.3 (C10 and C14, ArC), 127.6 (C5, ArC), 129.9 (C11 and

C13, ArC), 146.2 (C3, ArC), 158.3 (C9, C_{ipso}), 166.9 (C7, C_{ipso}). Anal. Calcd. for

$\text{phAr}^{\text{Li}}\text{ArNLi} \cdot 1.5\text{TMEDA}$ ^(c) $\text{C}_{21}\text{H}_{33}\text{Li}_2\text{N}_4$: C, 70.97; H, 9.36; N, 15.76; Found: C, 70.20; H, 9.13;

N, 15.33. EI-MS (m/z): 169 (65, $[\text{M} - 2\text{Li} - \text{TMEDA} + 2\text{H}]^+$).



^(a) δ value indicates exchange between completely solvated (coordinated) THF and large excess THF solvent (free THF at δ 1.73 and δ 3.58).

^(b) δ value indicates TMEDA is not coordinated to lithium (free TMEDA at δ 2.04 and δ 2.18 in C_6D_6) and integration indicates 1.5 molecules free TMEDA per $^{ph}ArLi$ unit.

^(c) Elemental analysis indicates 1.5 TMEDA units per $^{ph}ArLi$ molecule.

$^{tol}Ar^D ArND$ [2.4] $^{tol}ArLi$ $ArNLi$ ·TMEDA (0.05 g, 0.15 mmol) was dissolved in 10 cm³ THF, forming a light yellow solution. D₂O (1.0 cm³, 55.3 mmol) was added and the THF was immediately removed *in vacuo*. The residue was extracted with toluene and filtered through celite with a sintered glass frit, washing with additional toluene. The toluene was removed *in vacuo* from the filtrate, leaving a white residue.

²H NMR (C_6D_6 , ^(a) 61.4 MHz): δ = 4.91 (s, 1 D8, N-D), 6.85 (s, 1 D1, ArD).

¹H NMR (C_6D_6 , 400 MHz): δ = 2.15 (s, 3 H15 and 3 H16, CH₃), 6.84 (d,

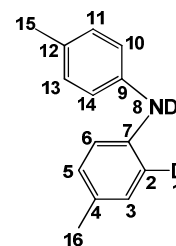
³J_{HH} = 8 Hz, 1 H10 and 1 H14, ArH), 6.85 (s, 1 H3, ArH), 6.95 (d, ³J_{HH} = 7

Hz, 1 H5, 1 H6, 1 H11 and 1 H13, ArH). ¹³C{¹H} NMR (C_6D_6 , 151 MHz): δ

= 20.7 (C15 and C16, CH₃), 118.2 (C10 and C14, ArC), 118.3 (m, C2 and C9, C_{ipso}), 129.9 (d,

²J_{CD} = 5.4 Hz, C3, ArC), 130.0 (C5, C6, C11 and C13, ArC), 141.5, 141.6, 141.7 (C4, C12, and

C7, C_{ipso}). EI-MS (*m/z*): 199 (50, [M]⁺), 198 (100, [M - D + H]⁺) and 197 (82, [M - 2D + 2H]⁺).



^(a) External reference C_6D_6 , with sample dissolved in C_6H_6

$^{ph}Ar^D ArND$ [2.5] [$^{ph}ArLi$ $ArNLi$ ·1.5TMEDA]₂ [2.3] (1.08 g, 3.05 mmol) was partially dissolved in 10 cm³ Et₂O, forming a cream coloured suspension. D₂O (1.60 cm³, 88.43 mmol) was added, forming a clear solution. The Et₂O was immediately removed *in vacuo*, giving a clear oil with a white precipitate. This residue was extracted with toluene and filtered through celite with a sintered glass frit, washing with additional toluene. The toluene was removed *in vacuo* from the

filtrate giving a clear oil that was placed in the freezer to crystallise (0.51 g, 3.01 mmol

$^{\text{ph}}\text{Ar}^{\text{D}}\text{ArND}$ [2.5], 99% yield based on $[\text{phAr}^{\text{Li}}\text{ArNLi} \cdot 1.5\text{TMEDA}]_2$ [2.3]).

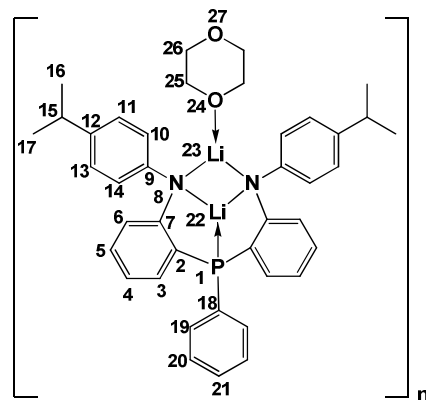
^2H NMR (C_6D_6 , ^(a) 61.4 MHz): δ = 4.97 (s, D8), 6.85 (s, D1). ^1H NMR (C_6D_6 , 400 MHz): δ = 6.84 (m, $^3J_{\text{HH}}$ = 7 Hz, 1 H4, 1 H6, 1 H10, 1 H12, and 1 H14, ArH), 7.10 (m, $^3J_{\text{HH}}$ = 7 Hz, 1 H3, 1 H5, 1 H11, and 1 H13, ArH). $^{13}\text{C}\{^1\text{H}\}$ NMR (C_6D_6 , 101 MHz): δ = 118.07 (C4 and C12, ArC), 118.09 (C9, C_{ipso}), 121.1 (C10, C14 and C6, ArC), 129.3 (C7, C_{ipso}), 129.5 (C3, C5, C11 and C13, ArC), 143.4 (C2, C_{ipso}). EI-MS (m/z): 171 (80, $[\text{M}]^+$), 170 (100, $[\text{M} - \text{D} + \text{H}]^+$) and 169 (60, $[\text{M} - 2\text{D} + 2\text{H}]^+$).

^(a) external reference C_6D_6 , with sample dissolved in C_6H_6

$[\text{ipropNPNLi}_2 \cdot \text{diox}]_n$ [2.6] $^{\text{iprop}}\text{Ar}^{\text{Br}}\text{ArNH}$ [2.1] (6.18 g, 21.30 mmol) was dissolved in 300 cm^3 Et_2O in a 1 dm^3 3-necked round-bottomed flask fitted with a pressure-regulated dropping funnel. The solution was cooled to $-35\text{ }^\circ\text{C}$ (dry ice/ethanol) and 1.61 M $n\text{-BuLi}$ in $n\text{-hexanes}$ (26.45 cm^3 , 42.7 mmol) was added dropwise via syringe, forming a light yellow solution. The cooling bath was removed and the reaction mixture was allowed to equilibrate at room temperature for 1 hr 30 min. Meanwhile 300 cm^3 Et_2O and PPhCl_2 (1.45 cm^3 , 10.6 mmol) were added to the dropping funnel. The reaction flask was re-cooled to $-40\text{ }^\circ\text{C}$ before the PPhCl_2 solution was added slowly over 3hr 10min (approx. dripping rate 16 $\text{cm}^3/10\text{ min}$), resulting in a orange solution. The solution was allowed to warm slowly to room temperature and stirred overnight for *ca* 16 hrs, giving in a yellow solution with yellow and white precipitates. The Et_2O was removed *in vacuo*, leaving a yellow foam. This yellow residue was triturated with 80 cm^3 $n\text{-hexanes}$ and filtered through celite with a sintered glass frit, washing with 3 x 40 cm^3 $n\text{-hexanes}$. To the filtrate was added 1,4-dioxane (3.50 cm^3 , 41.07 mmol), forming a yellow precipitate. The $n\text{-hexanes}$ solvent was reduced and the mixture was placed in the freezer for 10 minutes before the yellow solid was collected on a sintered glass frit and washed with $n\text{-hexanes}$ and dried *in vacuo* (6.18 g, 9.84

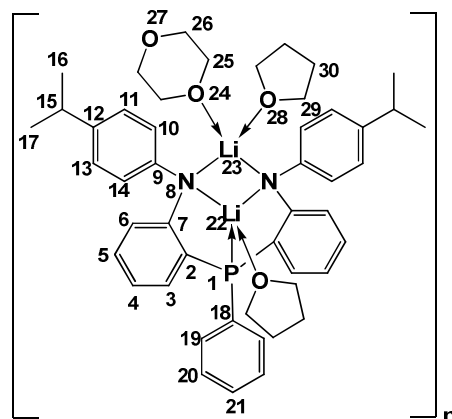
mmol [^{iprop}NPNLi₂·diox]_n [**2.6**], 92% yield based on ^{iprop}Ar^{Br}ArNH [**2.1**]). Single crystals of [**2.6**] were grown by slow evaporation from a C₆H₆ solution, as reported in Erin MacLachlan's PhD thesis.⁹⁷

[^{iprop}NPNLi₂·diox]_n [**2.6**]: ³¹P{¹H} NMR (C₆D₆, 122 MHz): δ = -31.62 (qt, ¹J_{PLi} = 42 Hz, P1). ⁷Li{¹H} NMR (C₆D₆, 156 MHz): δ = 0.93 (s, 1 Li23), 2.62 (d, ¹J_{LiP} = 43 Hz, 1 Li22). ¹H NMR (C₆D₆, 600 MHz): δ = 1.207, 1.214 (d 's, ³J_{HH} = 7 Hz, 6 H16 and 6 H17, CH₃), 2.97 (hep, ³J_{HH} = 7 Hz, 2 H15, CH), 3.09 (s, 4 H25 and 4 H26, CH₂),^(a) 6.62 (t, 1 H21, ArH), 7.02, 7.05 (d 's, ³J_{HH} = 8 Hz, 2 H3



and 2 H19, ArH), 7.10 (d, ³J_{HH} = 8 Hz, 2 H6, ArH), 7.13 (d, ³J_{HH} = 8 Hz, 2 H10 and 2H 14, ArH), 7.30 (d, ³J_{HH} = 8 Hz, 2 H11 and 2H13, ArH), 7.49 (t, ³J_{HH} = 7 Hz, 2 H4, ArH), 7.67 (t, ³J_{HH} = 8 Hz, 2 H5, ArH), 7.75 (t, ³J_{HH} = 6 Hz, 2 H20, ArH). ¹³C{¹H} NMR (C₆D₆, 151 MHz): δ = 24.67, 24.69 (C16 and C17, CH₃), 33.8 (C15, CH), 67.0 (C25 and C26, CH₂), 117.2 (C21, ArC), 118.6 (d, ⁴J_{CP} = 4 Hz, C5, ArC), 120.9 (C11 and C13, ArC), 125.5 (d, ¹J_{CP} = 10 Hz, C2, C_{ipso}), 127.2 (C6, ArC), 128.0 (C10, C14 and C3, ArC, hidden by C₆D₆), 129.3 (C7, C_{ipso}), 130.6 (C19, ArC), 132.4 (d, ³J_{CP} = 14 Hz, C4, ArC), 135.6 (d, ³J_{CP} = 2 Hz, C20, ArC), 138.1 (C9, C_{ipso}), 154.1 (C12, C_{ipso}), 161.2 (d, ¹J_{CP} = 28 Hz, C18, C_{ipso}).

[^{iprop}NPNLi₂·2THF·diox]_n: ³¹P{¹H} NMR (C₆D₆, 122 MHz):^(a) δ = -31.94 (qt, ¹J_{PLi} = 41 Hz, P1). ⁷Li{¹H} NMR (C₆D₆, 156 MHz): δ = 1.19 (s, 1 Li23), 2.27 (d, ¹J_{LiP} = 41 Hz, 1 Li22). ¹H NMR (C₆D₆, 400 MHz): δ = 1.08 (bs, 8H, THF, CH₂),^(b) 1.23 (d, ³J_{HH} = 7 Hz, 6 H16 and 6 H17, CH₃), 2.99 (hep, ³J_{HH} = 7 Hz, 2 H15, CH), 3.08 (s, 4 H25 and 4



H26, CH₂), ^(c) 3.14 (s, 8H, THF, CH₂), ^(b) 6.65 (t, 1 H21, ArH), 7.01 (m, ³J_{HH} = 8 Hz, 2 H3 and 2 H19, ArH), 7.10 (d, ³J_{HH} = 8 Hz, 2 H6, ArH), 7.15 (d, ³J_{HH} = 8 Hz, 2 H10 and 2H 14, ArH), 7.38 (d, ³J_{HH} = 8 Hz, 2 H11 and 2H13, ArH), 7.60 (t, ³J_{HH} = 7 Hz, 2 H4, ArH), 7.71 (t, ³J_{HH} = 7 Hz, 2 H5, ArH), 7.77 (t, ³J_{HH} = 6 Hz, 2 H20, ArH).

ipropNPNLi₂·4THF: ³¹P{¹H} NMR (THF-*d*₈, 122 MHz): ^(b) δ = -33.21 (s, P1). ⁷Li{¹H} NMR (THF-*d*₈, 156 MHz): δ = 3.49 (s, Li22 and Li23). ¹H NMR (THF-*d*₈ + THF, 400 MHz): δ = 1.15 (d, ³J_{HH} = 7 Hz, 6 H16 and 6 H17, CH₃), 1.74 (s, 8 H26, THF, CH₂), ^(d) 2.90 (hep, ³J_{HH} = 7 Hz, 2 H15, CH), 3.52 (s, 16 H, CH₂), ^(e) 3.58 (s, 8 H25, THF, CH₂), ^(d) 6.90 (bm, 2 H5, 2 H10 and 2 H14, ArH), 7.02 (bd, ³J_{HH} = 6 Hz, 2 H11 and 2 H13, ArH), 7.10 (t, ³J_{HH} = 6 Hz, 2 H4, ArH), 7.19 (m, ³J_{HH} = 7 Hz, 2 H3, 2 H19 and H21 ArH), 7.30 (bs, 2 H6, ArH), 7.41 (bs, 2 H20, ArH). ¹³C{¹H} NMR (C₆D₆, 101 MHz): δ = 24.5 (C16 and C17, CH₃ and THF, CH₂), 33.5 (C15, CH), 66.6 (THF, CH₂), 67.1 (C25 and C26, CH₂), 117.5 (C12, C_{ipso}), 118.4 (C11 and C13, ArC), 127.2 (C6, ArC), 126.0 (C4, ArC), 126.6 (C10 and C14, ArC) 127.5 (d, ²J_{CP} = 4 Hz, C3 and C19, ArC), 128.1 (C21, ArC), 129.0 (C5, ArC), 132.1 (d, ¹J_{CP} = 7 Hz, C2, C_{ipso}), 134.5 (d, ³J_{CP} = 8 Hz, C20, ArC), 139.6 (C7, C_{ipso}), 155.4 (C9, C_{ipso}), 162.2 (d, ¹J_{CP} = 31 Hz, C18, C_{ipso}).

Anal. Calcd. for C₄₀H₄₃Li₂N₂O₂P: C, 76.42; H, 6.89; N, 4.46; Found: C, 71.13; H, 6.83; N, 4.84.^(e) EI-MS (*m/z*): 528 (100, [M - 2Li - diox + 2H]⁺), 394 (25, [M - 2Li - diox - C₆H₄C(H)Me₂ - Me + H]⁺), 211 (30, [N-Ph-(C₆H₄-4-C(H)Me₂)NH]⁺), 196 (80, [N-Ph-(C₆H₄-4-C(H)CH₂)NH]⁺).

^(a) δ value indicates 1,4-dioxane is coordinated to lithium (free 1,4-dioxane at δ 3.53) and relative integration indicates one molecule 1,4-dioxane per ^{iprop}NPNLi₂ unit.

^(b) δ value indicates THF is coordinated to lithium (free THF at δ 1.73 and δ 3.58) and relative integration indicates two molecules THF per ^{iprop}NPNLi₂ unit.

^(c) δ value indicates 1,4-dioxane is coordinated to lithium (free 1,4-dioxane at δ 3.53) and relative integration indicates one molecule 1,4-dioxane per ^{iprop}NPNLi₂ unit.

^(d) δ value indicates exchange between completely solvated (coordinated) THF and large excess THF solvent (free THF at δ 1.73 and δ 3.58).

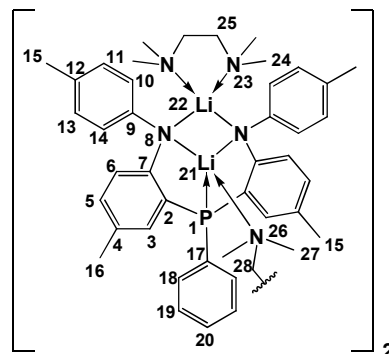
^(e) δ value indicates 1,4-dioxane is not coordinated to lithium (free 1,4-dioxane at δ 3.53).

^(e) Analyst reported discoloration of sample from light yellow to light green during analysis. Repeat analysis failed to yield any better results.

[^{tol}NPNLi₂·1.5TMEDA]₂ [**2.7**] Inside the glovebox, ^{tol}Ar^{Li}ArNLi·TMEDA (34.64 g, 106.46 mmol) was partially dissolved in 500 cm³ THF in a 2.0 dm³ 3-necked round-bottomed flask and 300 cm³ THF was added to a pressure-regulated dropping funnel. The flask and dropping funnel were removed from the box, assembled under a N₂ atmosphere and the suspended mixture cooled to -40 °C (dry ice/ethanol), while PPhCl₂ (7.25 cm³, 53.2 mmol) was added to the dropping funnel. The PPhCl₂ solution was added slowly over 5 hrs (approx. dripping rate 10 cm³/10 min), resulting in a dark orange solution. The reaction mixture was allowed to warm slowly to room temperature and stirred overnight for 17hrs, resulting in a dark orange solution with a suspended yellow solid. The THF was removed *in vacuo*, giving an orange foam. This orange residue was triturated with toluene inside the glovebox and filtered through celite with a sintered glass frit, washing with additional toluene. The toluene solvent was removed *in vacuo* with heating (60 °C), resulting in an orange sticky semi-solid residue, which was triturated with 200 cm³ *n*-hexanes to form a fluffy yellow ppt. The *n*-hexanes solvent was reduced and the mixture placed in the freezer (-40 °C) for 10 min before the yellow solid was collected on a sintered glass frit and washed with 3 x 10 cm³ *n*-hexanes and dried *in vacuo* (21.08 g, 30.69 mmol ^{tol}NPNLi₂·1.5 TMEDA, 58% yield based on ^{tol}Ar^{Li}ArNLi·TMEDA). Single crystals of **2.7** were grown by slow evaporation of a C₆D₆ solution. Single crystals of ^{tol}NPNLi₂·DME + 0.5 TMEDA were grown

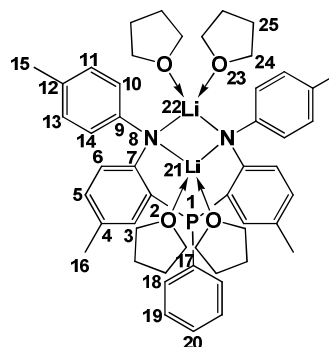
from a toluene / Et₂O / DME (*ca* 10:10:1) solution, as reported in an internal Fryzuk Research Group report by Prof. Y. Ohki.²⁶¹

[^{tol}NPNLi₂·1.5TMEDA]₂: ³¹P{¹H} NMR (C₆D₆, 162 MHz): δ = -31.66 (bs, P1). ⁷Li{¹H} NMR (C₆D₆, 156 MHz): δ = 1.08 (bs, Li21 / Li22). ¹H NMR (C₆D₆, 400 MHz): δ = 1.92 (bs, TMEDA, CH₂ and CH₃),^(a) 2.07, 2.8, 2.14, 2.16, 2.63, 2.66 (s, H15 / H16, CH₃),^(b) 6.93 to 7.86 (m, phenyls, ArH).^(c)



[^{tol}NPNLi₂·0.5TMEDA·2THF]₂: ³¹P{¹H} NMR (C₆D₆ + 4THF, 162 MHz): δ = -32.8 (qt, ¹J_{PLi} = 41 Hz, P1). ⁷Li{¹H} NMR (C₆D₆ + 4THF, 156 MHz): δ = 0.49 (s, 1 Li22), 2.06 (d, ¹J_{LiP} = 41 Hz, 1 Li21). ¹H NMR (C₆D₆ + 4THF, 600 MHz): δ = 1.28 (s, 8 H28, CH₂),^(d) 1.84 (s, 4 H25, CH₂),^(e) 1.87 (s, 12 H24, CH₃)^(e), 2.16 (s, 6 H16, CH₃), 2.69 (s, 6 H15, CH₃), 3.43 (s, 8 H27, CH₂),^(d) 7.00 (d, ³J_{HH} = 8 Hz, 2 H18, ArH), 7.03 (d, ³J_{HH} = 8 Hz, 2 H6, ArH), 7.11 (d, ³J_{HH} = 8 Hz, 4 H10 and 4 H14 ArH), 7.12 (s, 2 H3, ArH), 7.34 (d, ³J_{HH} = 8 Hz, 4 H11 and 4 H13, ArH), 7.68 (t, ³J_{HH} = 7 Hz, 2 H19, ArH), 7.77 (d, ³J_{HH} = 7 Hz, 2 H5, ArH), 7.78 (t, ³J_{HH} = 7 Hz, H20, ArH). ¹³C{¹H} NMR (C₆D₆ + 4THF, 101 MHz): δ = 20.8 (C15 and C16, CH₃), 25.5 (C28, CH₂), 45.9 (C24, CH₃), 57.4 (C25, CH₂), 67.8 (C27, CH₂), 119.3 (C10 and C14, ArC), 120.4 (C19, ArC), 123.8 (C12, C_{ipso}), 125.8 (C4, C_{ipso}), 126.7 (C6, ArC), 130.4 (C11 and C13 and C3, ArC), 131.2 (C18, C), 132.4, 132.7 (C20, ArC and C7, C_{ipso}), 135.1 (C5, ArC), 139.7 (C2, C_{ipso}), 155.2 (C9, C_{ipso}), 159.5 (d, ¹J_{CP} = 28 Hz, C17, C_{ipso}).

^{tol}NPNLi₂·4THF: ³¹P{¹H} NMR (THF-*d*₈ + THF, 121.5 MHz):^(d) δ = -33.21 (s, P1). ⁷Li{¹H} NMR (THF-*d*₈ + THF, 156 MHz): δ = 0.52 (s, Li21 and Li22). ¹H NMR (THF-*d*₈ + THF, 400 MHz): δ = 1.75 (s, H25, CH₂),^(f) 2.14 (s, 6 H16,



CH₃), 2.18 (s, 6 H15 and 18 H, TMEDA, CH₃),^(g) 2.104 (s, 6 H, TMEDA, CH₂),^(g) 3.60 (s, H24, CH₂),^(f) 6.81 (d, ³J_{HH} = 10 Hz, 2 H6, ArH), 6.85 (d, ³J_{HH} = 8 Hz, 4 H10 and 4 H14 ArH), 7.01 (d, ³J_{HH} = 8 Hz, 4 H11 and 4 H13, ArH), 7.16 (t, ³J_{HP} = 7 Hz, 2 H3, ArH), 7.27 (m, ³J_{HH} = 7 Hz, 2 H5, 2 H18 and H20, ArH). 7.47 (t, ³J_{HH} = 7 Hz, 2 H19, ArH). ¹³C{¹H} NMR (C₆D₆ + 4THF, 151 MHz): δ = 17.4 (C15 and C16, CH₃), 23.1 (C25, CH₂), 42.3 (TMEDA, CH₃), 55.6 (TMEDA, CH₂), 64.9 (C24, CH₂), 115.6 (C11 and C13, ArC), 118.5 (d, ²J_{CP} = 5 Hz, C18, C), 119.6 (C12, C_{ipso}), 123.4 (C3, ArC), 125.0 (d, ⁴J_{CP} = 5 Hz, C20, ArC), 126.9 (C10 and C14, ArC), 127.7 (C6, ArC), 129.6 (d, ¹J_{CP} / ³J_{CP} = 14 Hz, C19, ArC and C2, C_{ipso}), 131.0 (d, ²J_{CP} = 16 Hz, C7, C_{ipso}), 131.6 (d, ⁴J_{CP} = 3 Hz, C5, ArC), 137.4 (C4, C_{ipso}), 152.3 (C9, C_{ipso}), 157.4 (d, ¹J_{CP} = 28 Hz, C17, C_{ipso}).

EI-MS (*m/z*): 500 (100, [M - 2Li - TMEDA + 2H]⁺), 394 (35, [M - 2Li - TMEDA - C₆H₄Me - Me + 2H]⁺), 303 (30, [M - 2Li - TMEDA - 2C₆H₄Me - Me + 2H]⁺).

^(a) very broad peak suggests a fluxional process and δ value indicates TMEDA is coordinated to lithium (free TMEDA at δ 2.04 and δ 2.18).

^(b) numerous tolyl methyl environments are indicated

^(c) poor solubility hampered complete characterisation for [^{tol}NPNLi₂·1.5TMEDA]₂ [**2.7**] in C₆D₆.

^(d) δ value indicates THF is coordinated to lithium (free THF at δ 1.73 and δ 3.58) and relative integration indicates two molecules THF per ^{tol}NPNLi₂ unit.

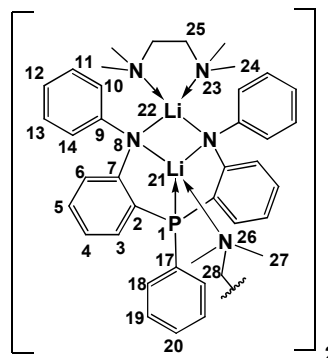
^(e) δ value indicates TMEDA is coordinated to lithium (free TMEDA at δ 2.04 and δ 2.18) and integration indicates one molecule TMEDA per ^{tol}NPNLi₂ unit.

^(f) δ value indicates exchange between completely solvated (coordinated) THF and large excess THF solvent (free THF at δ 1.73 and δ 3.58).

^(g) δ value indicates TMEDA is not coordinated to lithium (free TMEDA at δ 2.04 and δ 2.18 in C_6D_6) and integration indicates 1.5 molecules free TMEDA per $^{101}NPNLi_2$ unit.

[^{ph}NPNLi₂·1.5 TMEDA]₂ [2.8]: Inside the glovebox, [^{ph}Ar^{Li}ArNLi·1.5TMEDA]₂ [**2.3**] (22.01 g, 61.94 mmol) was partially dissolved in 600 cm³ THF in a 2.0 dm³ 3-necked round-bottomed flask and 300 cm³ THF was added to a pressure-regulated dropping funnel. The flask and dropping funnel were removed from the box, assembled under an Ar atmosphere and the suspended mixture cooled to -40 °C (dry ice/ethanol), while PPhCl₂ (5.00 cm³, 36.9 mmol) was added to the dropping funnel. The PPhCl₂ solution was added slowly over 3hr 12min (approx. dripping rate 14 cm³/10 min), resulting in a dark orange solution. The reaction mixture was warmed slowly to room temperature and stirred overnight for 16hr 50 min, resulting in an orange solution with a yellow precipitate. The THF was removed *in vacuo*, giving an orange foam. This orange residue was triturated with 100 cm³ toluene inside the glovebox and filtered through celite with a sintered glass frit, washing with additional 6 x 20 cm³ toluene. The toluene solvent was removed *in vacuo* with heating (60 °C), resulting in a dark orange foam. This was triturated in a *n*-hexanes/toluene (7:1) mixture, with heating (60 °C), to form a fluffy yellow ppt. The mixture placed in the freezer (-40 °C) for 5 min before the crude yellow solid was collected on a sintered glass frit and washed with 3 x 10 cm³ *n*-hexanes and dried *in vacuo*. This crude yellow solid was triturated in 35 cm³ *n*-hexanes, with heating (60 °C). The mixture was placed in the freezer (-40 °C) for 10 min before the pure yellow solid was collected on a sintered glass frit and washed with 3 x 10 cm³ *n*-hexanes and dried *in vacuo* (5.57 g, 8.84 mmol [^{ph}NPNLi₂·1.5 TMEDA]₂, 29% yield based on [^{ph}Ar^{Li}ArNLi·1.5TMEDA]₂ [**2.3**]).

[^{ph}NPNLi₂·1.5TMEDA]₂ [2.8]: ³¹P{¹H} NMR (C_6D_6 , 162 MHz): δ = -31.96 (bs, P1). ⁷Li{¹H} NMR (C_6D_6 , 156 MHz): δ = 0.09 (s, 1 Li22), 1.67 (d, ¹J_{LiP} = 40 Hz, 1 Li21). ¹H NMR (C_6D_6 , 400 MHz): δ



= 1.47, 1.57, 1.63 (s, TMEDA, CH₂ and CH₃),^(a) 6.70 to 7.87 (m, phenyls, ArH).^(b)

[^{ph}NPNLi₂·0.5TMEDA·2THF]₂: ³¹P{¹H} NMR (C₆D₆ + 8THF,

162 MHz):^(b) δ = -32.16 (qt, ¹J_{PLi} = 40 Hz, P1). ⁷Li{¹H} NMR

(C₆D₆ + 8THF, 156 MHz): δ = 0.35 (s, 1 Li22), 2.00 (d, ¹J_{LiP} = 42

Hz, 1 Li21). ¹H NMR (C₆D₆ + 8THF, 400 MHz): δ = 1.35 (s, H28,

CH₂),^(c) 1.85 (s, 18 H24, CH₃),^(d) 1.93 (s, 6 H25, CH₂),^(d) 3.49 (s,

H27, CH₂),^(c) 6.72 (t, ³J_{HH} = 7 Hz, 2 H4 and 2 H12, ArH),^(c) 7.12 (t,

³J_{HH} = 8 Hz, 2 H19, ArH), 7.13 (d, ³J_{HH} = 7 Hz, 2 H6, ArH), 7.26 (d, ³J_{HH} = 8 Hz, 2 H3 ArH),

7.28 (d, ³J_{HH} = 7 Hz, 4 H10 and H14 ArH), 7.36 (d, ³J_{HH} = 8 Hz, 4 H11 and H13, ArH), 7.71 (m,

³J_{HH} = 7 Hz, 2 H18 and 1 H20, ArH), 7.82 (t, ³J_{HH} = 6 Hz, 2 H5, ArH). ¹³C{¹H} NMR (C₆D₆ +

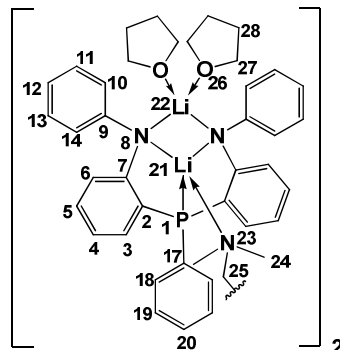
8THF, 101 MHz): δ = 25.7 (C28, CH₂), 45.8 (C24, CH₃), 57.7 (C25, CH₂), 67.8 (C27, CH₂),

115.7 (C12, ArC), 117.8 (C4, ArC), 119.3 (C10 and C14, ArC), 120.7 (⁴J_{PC} = 4Hz, C20, ArC),

126.8 (C2, C_{ipso}), 128.0 (C3, ArC), 129.8 (C11 and C13, ArC), 130.1 (C6, and C19, ArC), 132.4

(d, ²J_{PC} = 14 Hz, C18, ArC), 135.5 (d, ⁴J_{PC} = 3 Hz, C5, ArC), 139.2 (C7, C_{ipso}), 157.3 (C9, C_{ipso}),

161.5 (d, ¹J_{CP} = 29 Hz, C17, C_{ipso}).



^{ph}NPNLi₂·4THF: ³¹P{¹H} NMR (THF-*d*₈, 162 MHz): δ = -32.61

(s, P1). ⁷Li{¹H} NMR (THF-*d*₈, 156 MHz): δ = -1.46 (s, 1 Li22

and 1 Li21). ¹H NMR (THF-*d*₈, 400 MHz): δ = 1.74 (s, H25,

CH₂),^(e) 2.17 (s, 48 H24, CH₃),^(f) 2.103 (s, 16 H25, CH₂),^(f) 3.58 (s,

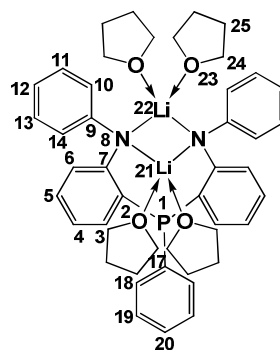
H24, CH₂),^(e) 6.32 (bs, 2 H4 and 2 H19, ArH), 6.58 (bs, 2 H12,

ArH), 6.72 (bs, 2 H5, 2 H18 and 1 H20, ArH), 6.99 (d, ³J_{HH} = 7

Hz, 4 H10 and H14 ArH), 7.06 (bs, 4 H11 and H13, ArH), 7.70 (bs, 2 H3 and 2 H6, ArH).

¹³C{¹H} NMR (THF-*d*₈, 101 MHz): δ = 25.3 (THF, CH₂), 46.2 (C24, CH₃), 58.8 (C25, CH₂),

67.4 (THF, CH₂), 109.7 (C18 and C20, ArC), 115.0 (C4 and C19, ArC), 117.8 (C12, ArC), 119.6



(C2, C_{ipso}), 125.4 (C10 and C14, C_{ipso}), 127.6 (C5, ArC), 129.0 (C11 and C13, ArC), 146.2 (C3 and C6, ArC), 158.3 (C7 and C9, C_{ipso}), 167.1 (C17, C_{ipso}).

EI-MS (*m/z*): 444 (90, [M - 2Li - 1.5TMEDA + 2H]⁺), 352 (40, [M - 2Li - TMEDA - NHC₆H₅ + 2H]⁺).

^(a) broad peaks suggests a fluxional process and δ value indicates TMEDA is coordinated to lithium (free TMEDA at δ 2.04 and δ 2.18).

^(b) poor solubility hampered complete characterisation for [^{ph}NPNLi₂·1.5TMEDA]₂ [**2.8**] in C₆D₆.

^(c) δ value indicates THF is coordinated to lithium (free THF at δ 1.73 and δ 3.58).

^(d) δ value indicates TMEDA is coordinated to lithium (free TMEDA at δ 2.04 and δ 2.18) and integration indicates 1.5 molecules TMEDA per ^{ph}NPNLi₂ unit.

^(e) δ value indicates exchange between completely solvated (coordinated) THF and large excess THF solvent (free THF at δ 1.73 and δ 3.58).

^(f) δ value indicates TMEDA is not coordinated to lithium (free TMEDA at δ 2.04 and δ 2.18 in C₆D₆) and integration indicates 4 molecules free TMEDA per ^{ph}NPNLi₂ unit. The degree of drying to which the sample was exposed dictates the quantity of TMEDA observed.

^{tol}NPNPPh [**2.9**] Inside the glovebox, ^{tol}Ar^{Li}ArNLi·TMEDA (47.95 g, 147.37 mmol) was partially dissolved in 600 cm³ Et₂O in a 2.0 dm³ 3-necked round-bottomed flask and 300 cm³ THF was added to a pressure-regulated dropping funnel. The flask and dropping funnel were removed from the box, assembled under a N₂ atmosphere and the suspended mixture cooled to -54 °C (dry ice/ethanol), while PPhCl₂ (10.00 cm³, 73.7 mmol) was added to the dropping funnel. The PPhCl₂ solution was added slowly over 5hr 25min (approx. dripping rate 9 cm³/10 min), resulting in an orange-yellow solution. The reaction mixture was allowed to warm slowly to

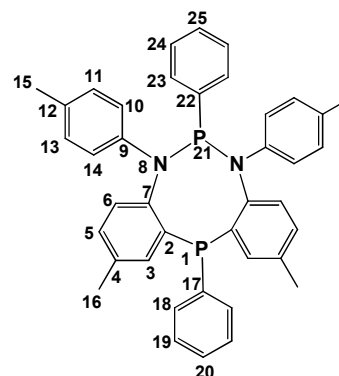
room temperature and stirred overnight for 14hr 45 min, resulting in a yellow solution with a suspended orange solid. The Et₂O was removed *in vacuo*, giving an orange foam. This orange residue was triturated with 100 cm³ toluene inside the glovebox and filtered through celite with a sintered glass frit, washing with additional toluene. The toluene solvent was removed *in vacuo* with heating (60 °C), resulting in an orange sticky semi-solid residue, which was triturated with 40 cm³ *n*-hexanes to form a fluffy yellow ppt. The mixture placed in the freezer (-40 °C) for a short while before the yellow solid was collected on a sintered glass frit and washed with 2 x 20 cm³ *n*-hexanes and dried *in vacuo* (6.17 g, ^(a) 8.99 mmol ^{tol}NPNLi₂·1.5TMEDA, 12% crude yield based on ^{tol}Ar^{Li}ArNLi·TMEDA). The *n*-hexanes filtrate was heated and placed in the freezer (-40 °C) for 20 hr 32 min, giving an orange solid that was collected on a sintered glass frit and washed with cold *n*-hexanes and dried *in vacuo* (18.52 g, 30.53 mmol ^{tol}NPNPPh [**2.9**], ^(b) 41% yield based on ^{tol}Ar^{Li}ArNLi·TMEDA).

³¹P{¹H} NMR (C₆D₆, 162 MHz): δ = -5.7 (s, P1), 93.8 (s, P21).

EI-MS (*m/z*): 606 (10, [M]⁺), 529 (35, [M - C₆H₅]⁺), 500 (35, [M - NC₆H₄Me]⁺).

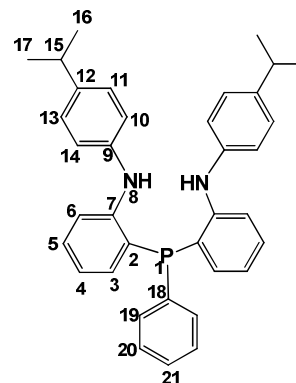
^(a) 6.17 g calculated using 43% relative integration in ³¹P{¹H} NMR spectrum of mixture (14.35 g).

^(b) sample was too soluble to recrystallise pure product



^{iprop}NPNH₂ [**2.10**] In the glove-box, [^{iprop}NPNLi₂·diox]_n [**2.6**] (2.33 g, 4.67 mmol) and NMe₃·HCl (1.23 g, 12.113 mmol) were mixed together as solids and 30 cm³ THF was added. The reaction mixture was stirred for 23 hrs before the THF solvent was removed *in vacuo*. The residue was extracted with 20 cm³ toluene and filtered through celite with a sintered glass frit, washing with 3 x 10 cm³ toluene. The toluene solvent was removed *in vacuo* from the filtrate, leaving a clear oil (2.65 g, 4.26 mmol ^{iprop}NPNH₂ [**2.10**], 91% yield based on [^{iprop}NPNLi₂·diox]_n [**2.6**]).

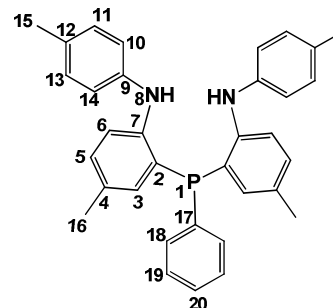
$^{31}\text{P}\{^1\text{H}\}$ NMR (C_6D_6 , 122 MHz): $\delta = -31.35$ (s, P1). ^1H NMR (C_6D_6 , 400 MHz): $\delta = 1.12$ (d, $^3J_{\text{HH}} = 7$ Hz, 6 H16 and 6H17, CH_3), 2.76 (hep, $^3J_{\text{HH}} = 7$ Hz, 2 H15, CH), 6.38 (d, 2 H8, $^4J_{\text{HP}} = 6$ Hz, NH), 6.72 (t, $^3J_{\text{HH}} = 7$ Hz, 1 H21, ArH), 6.82 (d, $^3J_{\text{HH}} = 8$ Hz, 2 H10 and 2 H14, ArH), 6.91 (d, $^3J_{\text{HH}} = 8$ Hz, 2 H11 and 2 H13, ArH), 7.05 (overlapping d's, $^3J_{\text{HH}} = ^3J_{\text{PH}} = 8$ Hz, 2 H3, 2 H6 and 2 H19, ArH), 7.30 (overlapping t's, $^3J_{\text{HH}} = 7$ Hz, 2 H5 and 2 H20, ArH), 7.50 (d of t, $^3J_{\text{HH}} = 8$ Hz, $^4J_{\text{HH}} = 2$ Hz, 2 H4, ArH). $^{13}\text{C}\{^1\text{H}\}$ NMR (C_6D_6 , 75 MHz): $\delta = 24.3$ (C16 and C17, CH_3), 33.8 (C15, CH), 116.6 (C5, ArC), 120.5 (C10 and C14, ArC), 121.2 (C21, ArC), 122.2 (d, $^1J_{\text{CP}} = 5$ Hz, C2, C_{ipso}), 127.4 (C11 and C13, ArC), 129.1 (C6, ArC and overlapping d, $^2J_{\text{CP}} = 11$ Hz, C3, ArC), 130.7 (C19, ArC), 134.2 (d, $^3J_{\text{CP}} = 14$ Hz, C4, C_{ipso}), 134.9 (d, $^3J_{\text{CP}} = 3$ Hz, C20, ArC), 140.7 (C12, C_{ipso}), 142.9 (C9, C_{ipso}), 148.3 (d, $^1J_{\text{CP}} = 13$ Hz, C18, C_{ipso}). Anal. Calcd. for $\text{C}_{36}\text{H}_{37}\text{N}_2\text{P}$: C, 81.79; H, 7.05; N, 5.30; Found: C, 81.48; H, 7.12; N, 4.95. EI-MS (m/z): 528 (100, $[\text{M}]^+$), 394 (20, $[\text{M} - \text{C}_6\text{H}_4\text{C}(\text{H})\text{Me}_2 - \text{CH}_4]^+$), 319 (20, $[\text{M} - \text{C}_6\text{H}_4\text{C}(\text{H})\text{Me}_2 - \text{NC}_6\text{H}_5 + 2\text{H}]^+$), 198 (20, $[\text{M} - \text{C}_6\text{H}_4\text{C}(\text{H})\text{Me}_2 - \text{NC}_6\text{H}_5 - \text{PC}_6\text{H}_5 - \text{CH}_4 + 2\text{H}]^+$).



$^{\text{tol}}\text{NPNH}_2$ [2.11] (a) from $[\text{tolNPNLi}_2 \cdot 1.5\text{TMEDA}]_2$ [2.7]: In glove-box, $[\text{tolNPNLi}_2 \cdot 1.5\text{TMEDA}]_2$ [2.7] (7.07 g, 5.15 mmol) and $\text{NMe}_3 \cdot \text{HCl}$ (2.70 g, 27.21 mmol) were mixed together as solids and 130 cm^3 THF was added. The reaction mixture stirred for 20 hrs before the THF solvent was removed *in vacuo*. The residue was extracted with 40 cm^3 toluene and filtered through celite with a sintered glass frit, washing with $4 \times 10 \text{ cm}^3$ toluene. The toluene solvent was removed *in vacuo* from the filtrate, leaving a white solid (4.59 g, 9.18 mmol $^{\text{tol}}\text{NPNH}_2$ [2.11], 89% yield based on $[\text{tolNPNLi}_2 \cdot 1.5\text{TMEDA}]_2$ [2.7]); (b) from $^{\text{tol}}\text{NPNPPh}$ [2.9]: $^{\text{tol}}\text{NPNPPh}$ [2.9] (0.10 g, 0.16 mmol) was dissolved in 1 cm^3 C_6D_6 and H_2O (0.2 cm^3 , 11.11 mmol) was added, with a colour change from orange to light yellow and the formation of a white precipitate (33% crude yield^(a) $^{\text{tol}}\text{NPNH}_2$

[**2.11**], based on $^{101}\text{NPNPPh}$ [**2.9**]). Single crystals of $^{101}\text{NPNH}_2$ [**2.11**] were grown from a *n*-hexanes solution at $-40\text{ }^\circ\text{C}$.

$^{31}\text{P}\{^1\text{H}\}$ NMR (C_6D_6 , 122 MHz): $\delta = -29.39$ (s, P1). ^1H NMR (C_6D_6 , 600 MHz): $\delta = 1.98$ (s, 6 H16, CH_3), 2.09 (s, 6 H15, CH_3), 6.21 (d, $^4J_{\text{PH}} = 5\text{ Hz}$, 2 H8, NH), 6.78 (d, $^3J_{\text{HH}} = 8\text{ Hz}$, 2 H10 and 2 H14, ArH), 6.84 (d, $^3J_{\text{HH}} = 8\text{ Hz}$, 2 H11 and 2 H13, ArH), 6.90 (d, $^3J_{\text{HH}} = 8\text{ Hz}$, 2 H6, ArH), 7.02 (t, $^3J_{\text{HH}} = ^3J_{\text{PH}} = 7\text{ Hz}$, 2 H18, ArH), 7.06 (t, $^3J_{\text{HH}} = 7\text{ Hz}$, 1 H20, ArH), 7.23 (d, $^3J_{\text{PH}} = 5\text{ Hz}$, 2 H3, ArH), 7.50 (d of d, $^3J_{\text{HH}} = 8\text{ Hz}$, $^5J_{\text{PH}} = 5\text{ Hz}$, 2 H5, ArH), 7.55 (t, $^3J_{\text{HH}} = 8\text{ Hz}$, 2 H19, ArH). $^{13}\text{C}\{^1\text{H}\}$ NMR (C_6D_6 , 151 MHz): $\delta = 20.7$ (C15, 16, CH_3), 118.2 (d, $^4J_{\text{PC}} = 2\text{ Hz}$, C5, ArC), 119.2 (C10,14, ArC), 123.8 (d, $^2J_{\text{PC}} = 8\text{ Hz}$, C7, C_{ipso}), 129.1 (C20, ArC), 129.1 (C18, ArC), 130.0 (C11,13, ArC), 130.5 (C9, C_{ipso}), 130.8 (d, $^3J_{\text{PC}} = 3\text{ Hz}$, C4, C_{ipso}), 131.5 (C6, ArC), 134.0 (d, $^1J_{\text{CP}} = 19\text{ Hz}$, C17, C_{ipso}), 135.1 (d, $^3J_{\text{PC}} = 5\text{ Hz}$, C19, ArC), 135.2 (d, $^2J_{\text{PC}} = 7\text{ Hz}$, C3, ArC), 141.3 (C12, C_{ipso}), 145.7 (d, $^1J_{\text{PC}} = 18\text{ Hz}$, C2, C_{ipso}). Anal. Calcd. for $\text{C}_{34}\text{H}_{33}\text{N}_2\text{P}$: C, 81.57; H, 6.64; N, 5.60; Found: C, 81.36; H, 6.69; N, 5.99. EI-MS (m/z): 500 (100, $[\text{M}]^+$), 484 (20, $[\text{M} - \text{CH}_4]^+$), 408 (20, $[\text{M} - \text{C}_6\text{H}_5\text{Me}]^+$), 394 (30, $[\text{M} - \text{C}_6\text{H}_5\text{Me} - \text{CH}_4]^+$), 303 (30, $[\text{M} - 2\text{C}_6\text{H}_5\text{Me} - \text{CH}_4]^+$).

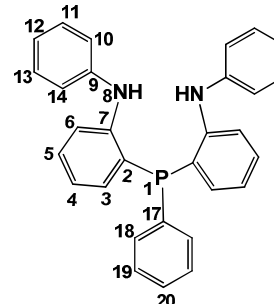


(a) relative integration of $^{31}\text{P}\{^1\text{H}\}$ NMR spectrum of mixture

$^{\text{ph}}\text{NPNH}_2$ [**2.12**] In glove-box, $[\text{phNPNLi}_2 \cdot 1.5\text{TMEDA}]_2$ [**2.8**] (5.15 g, 8.17 mmol) and $\text{NMe}_3 \cdot \text{HCl}$ (2.20 g, 51.64 mmol) were mixed together as solids in a conical flask and 30 cm^3 THF was added. The reaction mixture was stirred for 20 hrs before the THF solvent was removed *in vacuo*. The residue was extracted with 40 cm^3 toluene and filtered through celite with a sintered glass frit, washing with $4 \times 10\text{ cm}^3$ toluene. The toluene solvent was removed *in vacuo* from the combined filtrate and toluene washings, giving a white solid (2.08 g, 4.69 mmol $^{\text{ph}}\text{NPNH}_2$ [**2.12**], 57% yield based on $[\text{phNPNLi}_2 \cdot 1.5\text{TMEDA}]_2$ [**2.8**]). Single crystals of $^{\text{ph}}\text{NPNH}_2$ [**2.12**] were

grown from slow evaporation of a Et₂O solution, as reported in an internal Fryzuk Research Group report by Prof. Y. Ohki.²⁶¹

³¹P{¹H} NMR (C₆D₆, 122 MHz): δ = -30.80 (s, P1). ¹H NMR (C₆D₆, 300 MHz): δ = 6.30 (d, ⁴J_{PH} = 5 Hz, 2 H8, NH), 6.76 (m, ³J_{HH} = 8 Hz, 2 H10, 2 H44, 2 H12 and 2 H19, ArH), 6.99 (m, ³J_{HH} = 9 Hz, 2 H11, 2 H13, 2 H4, 2 H6 and 2 H18, ArH), 7.26 (m, ³J_{HH} = 6 Hz, 2 H3 and 1 H20, ArH), 7.45 (t, ³J_{HH} = 6 Hz, 2 H5, ArH).



¹³C{¹H} NMR (C₆D₆, 151 MHz): δ = 117.8 (d, ⁴J_{PC} = 2 Hz, C20, ArC), 119.2 (C10,14, ArC), 121.8 (C12, ArC and C9, C_{ipso}), 121.9 (d, ³J_{PC} = 2 Hz, C19, ArC), 129.1 (d, ²J_{PC} = 7 Hz, C18, ArC), 129.3 (C6, ArC), 129.5 (C11,13, ArC), 130.7 (C4, ArC), 134.1 (d, ¹J_{PC} = 20 Hz, C2, C_{ipso}), 134.9 (d, ²J_{PC} = ⁴J_{PC} = 3 Hz, C3 and C5, ArC), 143.2 (C7, C_{ipso}), 147.4 (d, ¹J_{PC} = 18 Hz, C17, C_{ipso}). Anal. Calcd. for C₃₀H₂₅N₂P: C, 81.06; H, 5.67; N, 6.30; Found: C, 80.25; H, 6.18; N, 6.40. EI-MS (*m/z*): 444 (100, [M]⁺), 352 (50, [M - NHC₆H₅]⁺).

[^{iprop}NPN]₂Zr [3.1] (a) from [^{iprop}NPNLi₂·diox]_n [2.6] / ZrCl₄(THF)₂: Yellow

[^{iprop}NPNLi₂·diox]_n [2.6] (0.40 g, 0.64 mmol) and white ZrCl₄(THF)₂ (0.12 g, 0.32 mmol) were added to a Schlenk flask in the glove box. 20 cm³ Toluene was added to the solids and the reaction mixture was stirred *ca* 19 hrs^(a) at room temperature. The reaction mixture was filtered through celite with a sintered glass frit, washing the celite with 20 cm³ toluene. The toluene was removed *in vacuo* from the orange filtrate, giving an orange film. This residue was triturated with 5 cm³ *n*-hexanes, resulting in a yellow ppt. This mixture was placed in the freezer overnight and the yellow solid was collected on a chilled sintered glass frit and washed with chilled (-40 °C) *n*-pentanes (0.0445 g, 0.0389 mmol [^{iprop}NPN]₂Zr [3.1]). The solvent was removed *in vacuo* from the orange filtrate and the orange residue was dried (0.12 g, 0.10 mmol [^{iprop}NPN]₂Zr [3.1], combined yield 43% based on ZrCl₄(THF)₂) **(b) from [^{iprop}NPNLi₂·diox]_n [2.6] /**

[^{iprop}NPNZrCl₂]₂ [3.9]: Yellow [^{iprop}NPNZrCl₂]₂ [3.9] (0.05 g, 0.04 mmol) was dissolved in 10

cm³ toluene. Yellow [^{iprop}NPNLi₂·diox]_n [**2.6**] (0.05 g, 0.086 mmol) was dissolved in 14 cm³ toluene and added drop wise via a glass pipette to the stirring solution of [^{iprop}NPNZrCl₂]₂ [**3.9**] at room temperature. The reaction mixture was stirred overnight with no distinctive colour change. The toluene solvent was removed *in vacuo* and the resulting yellow solid was re-dissolved in minimum toluene. *n*-Hexanes was added to ppt the yellow solid and the mixture was placed in the freezer at -40 °C. The yellow solid was collected on a chilled sintered glass frit and washed with 3 x 5 cm³ chilled (-40 °C) *n*-hexanes (18.2 mg, 0.02 mmol, 21% yield based on [^{iprop}NPNZrCl₂]₂ [**3.9**]).^(b)

³¹P{¹H} NMR (C₆D₆, 162 MHz): δ = 19.58 (s, P1). ¹H NMR

(C₆D₆, 400 MHz): δ = 1.17 (d, ³J_{HH} = 7 Hz, 6 H16 and 6

H17, CH₃), 1.26, 1.29 (d's, ³J_{HH} = 7 Hz, 6 H16a and 6

H17a, CH₃), 2.70, 2.80 (hep's, ³J_{HH} = 7 Hz, 2 H15 and 2

H15a, CH), 5.95 (d of d, ³J_{HH} = 8 Hz and ⁴J_{PH} = 5 Hz, 2 H6, ArH), 6.29 (d of dm, ³J_{HH} = 8 Hz and

⁴J_{PH} = 6 Hz, 2 H6a, ArH), 6.38 (t, ³J_{HH} = 7 Hz, 4 H20, ArH), 6.50 (t, ³J_{HH} = 7 Hz, 4 H4, ArH),

6.75 (m, ³J_{HH} = 8 Hz, 2 H21 and 2 H5, ArH), 6.88 (m, ³J_{HH} = 8 Hz, 2 H5a, ArH), 7.04 (d, ³J_{HH} = 8

Hz, 4 H10 and 4 H14, ArH), 7.16 (m, ³J_{HH} = 8 Hz, 4 H11, 4 H13 and 4 H19, ArH), 7.45 (t, ³J_{HH} =

³J_{PH} = 9 Hz, 4 H3, ArH). ¹³C{¹H} NMR (C₆D₆, 101 MHz): δ = 24.3, 24.4, 24.6 (C16, C16a, C17

and C17a, CH₃), 34.0, 34.1 (C15 and C15a, CH), 116.5 (d, ³J_{PC} = 6 Hz, C6a, ArC), 116.9 (d, ³J_{PC}

= 10 Hz, C6, ArC), 117.3 (C20, ArC), 117.4 (C7a, ArC), 120.2 (d, ²J_{PC} = 6 Hz, C7, ArC), 116.7

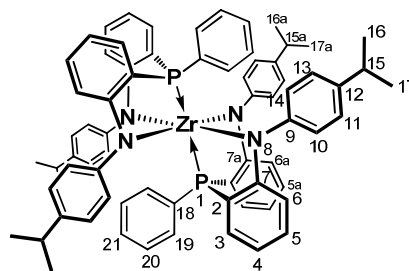
(C4, ArC), 128.00 (C5, C5a, ArC and C12, C_{ipso}), 128.5 (C11 and C13, ArC), 128.9 (d, ¹J_{PC} = 8

Hz, C2, C_{ipso}), 129.5 (C10 and C14, ArC), 132.4 (C21, ArC), 133.2 (d, ²J_{PC} = 11 Hz, C3, ArC),

134.2 (C19, ArC), 146.0 (C9, C_{ipso}), 166.3 (d, ¹J_{PC} = 30 Hz, C18, C_{ipso}). Anal. Calcd. for

C₇₂H₇₀N₄P₂Zr + 4 LiCl^(c): C, 65.81; H, 5.37; N, 4.26; Found: C, 65.21; H, 5.67; N, 5.10. EI-MS

(*m/z*): 1143 (90, [M]⁺), 932 (10, [M - C₆H₄C(H)Me₂ - NC₆H₅]⁺), 528 (100, [M - ^{iprop}NPNZr + 2H]⁺).



(a) after 1hr 40 min an orange solution with some white ppt was already observed.

(b) the high solubility of [^{iprop}NPN]₂Zr [3.1] resulted in low isolated yields.

(c) toluene filtration had been omitted, resulting in LiCl in the product.

[^{tol}NPN]₂Zr [3.2] (a) from ^{tol}NPNH₂ [2.11] / Zr(NMe₂)₄: White ^{tol}NPNH₂ [2.11] (0.10 g, 0.23 mmol) and light yellow Zr(NMe₂)₄ (0.03 g, 0.10 mmol) were added to a scintillation vial inside the glovebox and 5 cm³ toluene was added. The mixture heated to 60 °C for a few minutes until a clear yellow solution was obtained. The toluene was removed *in vacuo*, leaving behind an oily orange film. The residue was re-dissolved in a few drops toluene and 5 cm³ *n*-pentanes was added, leading to the ppt of a yellow solid. This mixture was placed in the freezer overnight and the yellow solid was collected on a chilled sintered glass frit and washed with chilled (-40 °C) *n*-pentanes (0.01 g, 0.01 mmol [^{tol}NPN]₂Zr [3.2], 9% yield based on Zr(NMe₂)₄). Single crystals of [^{tol}NPN]₂Zr [3.2] were grown by slow evaporation of a C₆D₆ solution at room temperature.^(a)

³¹P{¹H} NMR (C₆D₆, 121.5 MHz): δ = 16.03 (s, P1). ¹H

NMR (C₆D₆, 600 MHz): δ = 1.88, 1.91 (s's, 6 H16 and 6

H16a, CH₃), 2.15, 2.19 (s's, 6 H15 and 6 H15a, CH₃), 6.12

(m, ³J_{HH} = 4 Hz, 2 H6, ArH), 6.27 (m, ³J_{HH} = 5 Hz, 2 H6a,

ArH), 6.39 (m, ³J_{HH} = 6 Hz, 2 H20, ArH), 6.70 (m, ³J_{HH} = 8

Hz, 4 H5, ArH), 6.86 (d, ³J_{HH} = 8 Hz, 4 H19, ArH), 6.91 (m,

³J_{HH} = 9 Hz, 2 H10, 2 H11, 2 H13 and 2 H14, ArH), 7.07 (d, ³J_{HH} = 7 Hz, 2 H3, ArH), 7.10 (d,

³J_{HH} = 6 Hz, 2 H3a, ArH), 7.48 (t, ³J_{HH} = 8 Hz, 4 H18, ArH). ¹³C{¹H} NMR (C₆D₆, 151 MHz): δ

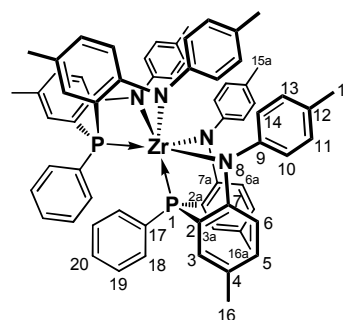
= 20.3 (C16, CH₃), 20.5 (C16a, CH₃), 21.0 (C15, CH₃), 21.1 (C15a, CH₃), 116.5 (C6a, ArC),

117.1 (C6, ArC), 118.7 (d, ¹J_{CP} = 39 Hz, C17, C_{ipso}), 126.3 (C7a, C_{ipso}), 128.0 (C20, ArC), 128.5

(C11 and C13, ArC), 128.9 (C7, C_{ipso}), 130.0 (C10 and C14, ArC), 131.1 (C19, ArC), 131.7 (C3,

ArC), 132.7 (C4, C_{ipso}), 133.2 (C5, ArC), 133.3 (C3a, ArC), 133.6 (t, ²J_{CP} = 8 Hz, C18, ArC),

145.4 (C12, C_{ipso}), 148.5 (C9, C_{ipso}), 160.3 (d, ¹J_{CP} = 30 Hz, C2, C_{ipso}), 164.0 (d, ¹J_{CP} = 27 Hz,



C2a, C_{ipso}). Anal. Calcd. for C₆₈H₆₂N₄P₂Zr: C, 75.04; H, 5.74; N, 5.15; Found: C, 75.27; H, 6.13; N, 5.00. EI-MS (*m/z*): 1088 (90, [M]⁺), 890 (20, [M - 2C₆H₅Me - CH₄]⁺), 782 (20, [M - 3C₆H₅Me - 2CH₄]⁺), 694 (20, [M - 4C₆H₅Me - 2CH₄]⁺), 500 (100, [M - ¹⁰¹NPNZr + 2H]⁺).

^(a) the high solubility of [¹⁰¹NPN]₂Zr [**3.2**] combined with the small scale of the reaction resulted in the low isolated yield.

Attempted synthesis of ^{mes}NPNZrCl₂: White ^{mes}NPNH₂ (0.50 g, 0.91 mmol) was dissolved in 40 cm³ toluene and added to a solution of brown ZrCl₂(NMe₂)₂(DME) (0.31 g, 0.91 mmol) in 20 cm³ toluene. The dark brown solution was stirred for 16hrs at room temperature with no observed ppt. ^(a) The toluene was reduced *in vacuo* to *ca* 20 cm³ and THF was added. The solvent was removed *in vacuo* and the residue was triturated with *n*-hexanes for *ca* 20 hrs, with the *n*-hexanes becoming a yellow solution. This mixture was filtered through celite with a sintered glass frit.

The *n*-hexanes was removed *in vacuo* from the filtrate, leaving a yellow residue. ^(b)

^(a) using ³¹P{¹H} NMR spectroscopy, only a single peak for unreacted ¹⁰¹NPNH₂ [**2.11**]

^(b) using ³¹P{¹H} NMR spectroscopy, 14% conversion to ^{mes}NPNZrCl₂.

^{iprop}NPNZrCl₂(HNMe₂) [3.3**] (a) from [^{iprop}NPNLi₂·diox]_n [**2.6**] / NMe₃·HCl /**

ZrCl₂(NMe₂)₂(DME): Yellow [^{iprop}NPNLi₂·diox]_n [**2.6**] (1.44 g, 2.29 mmol) and NMe₃·HCl (0.49 g, 5.09 mmol) were added to a Schlenk tube and 50 cm³ THF was added. The dark orange solution was placed under reduced pressure and stirred at room temperature for 21.5 hrs, forming a light yellow solution with a white ppt. The THF solvent was removed *in vacuo* and 40 cm³ toluene was added to the residue. This mixture was filtered through celite with a sintered glass frit, washing the celite with 30 cm³ toluene. The toluene solvent was removed *in vacuo* and the yellow semi-solid was dried overnight (1.01 g, 1.91 mmol ^{iprop}NPNH₂ [**2.10**], 83% yield based on [^{iprop}NPNLi₂·diox]_n [**2.6**]). This residue was triturated in 10 cm³ *n*-hexanes and the solvent was removed *in vacuo*, giving a yellow foam. The foam was dissolved in 10 cm³ toluene and brown ZrCl₂(NMe₂)₂(DME) (0.58 g, 1.70 mmol) dissolved in 10 cm³ toluene was added. The dark orange solution was stirring overnight at room temperature, with the formation of an orange ppt.

The toluene was removed *in vacuo*, leaving an orange residue $^{\text{iprop}}\text{NPNZrCl}_2(\text{HNMe}_2)$ [**3.3**].^(a) (**b**)

NMR scale: Orange [$^{\text{iprop}}\text{NPNLi}_2 \cdot \text{diox}$]_n [**2.6**] (0.06 g, 0.09 mmol) and $\text{NMe}_3 \cdot \text{HCl}$ (0.06 g, 0.60 mmol) were added to a scintillation vial inside the glovebox and 5 cm³ toluene was added. The orange solution was stirred until a clear solution with a white ppt was obtained. This mixture was filtered through celite with a sintered glass frit, washing the celite with 5 cm³ toluene. To this ($^{\text{iprop}}\text{NPNH}_2$ [**2.10**]) filtrate was added brown $\text{ZrCl}_2(\text{NMe}_2)_2(\text{DME})$ (0.03 g, 0.09 mmol) dissolved in 10 cm³ toluene. The dark orange solution was stirring overnight at room temperature, with the formation of an orange ppt. The toluene was removed *in vacuo*, leaving an orange residue. The residue was triturated with *ca* 5 cm³ *n*-hexanes to form an orange ppt. The orange solid was collected on a sintered glass frit, washing with 2 x 5 cm³ *n*-hexanes (0.03 g, 0.04 mmol $^{\text{iprop}}\text{NPNZrCl}_2(\text{HNMe}_2)$ [**3.3**], 37% yield based on $\text{ZrCl}_2(\text{NMe}_2)_2(\text{DME})$).

$^{31}\text{P}\{\text{H}\}$ NMR (C_6D_6 , 162 MHz): $\delta = 9.06$ (s, P1). ^1H NMR

(C_6D_6 , 400 MHz): $\delta = 1.13$ (d, $^3J_{\text{HH}} = 7$ Hz, 6 H16 and 6 H17,

CH_3), 2.08 (d, $^3J_{\text{HH}} = 5$ Hz, 6 H23, N- CH_3), 2.57 (bs, 1 H22,

NH), 2.71 (hep, $^3J_{\text{HH}} = 7$ Hz, 2 H15, CH), 6.31 (d of d, $^3J_{\text{HH}} = 8$

Hz, $^4J_{\text{PH}} = 6$ Hz, 2 H6, ArH), 6.59 (t, $^3J_{\text{HH}} = 7$ Hz, 2 H4, ArH),

6.93 (t, $^3J_{\text{HH}} = 8$ Hz, 2 H5, ArH), 7.13 (m, 2 H10, 2 H14, 2H19 and H21, ArH), 7.20 (d, $^3J_{\text{HH}} = 8$

Hz, 2 H11 and 2 H13, ArH), 7.29 (t, $^3J_{\text{HH}} = ^3J_{\text{PH}} = 8$ Hz, 2 H3, ArH), 7.81 (t, $^3J_{\text{HH}} = 8$ Hz, 2 H20,

ArH). $^{13}\text{C}\{^1\text{H}\}$ NMR (C_6D_6 , 101 MHz): $\delta = 24.1$, 24.2 (C16 and C17, CH_3), 34.1 (C15, CH),

41.8 (C23, N- CH_3), 117.2 (d, $^3J_{\text{PC}} = 9$ Hz, C6, ArC), 120.8 (C4, ArC), 122.9 (d, $^2J_{\text{PC}} = 39$ Hz, C7,

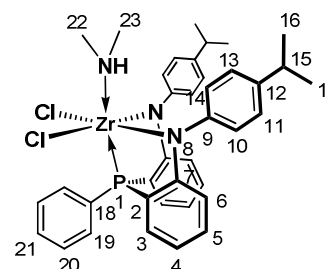
C_{ipso}), 128.9 (C10 and C14, ArC), 128.9 (d, $^2J_{\text{PC}} = 9$ Hz, C19, ArC), 129.9 (C21, ArC), 130.4 (d,

$^1J_{\text{PC}} = 41$ Hz, C18, C_{ipso}), 130.6 (C11 and C13, ArC), 132.6 (C5, ArC), 133.2 (d, $^2J_{\text{PC}} / ^3J_{\text{PC}} = 11$

Hz, C3 and C20, ArC), 141.3 (C9, C_{ipso}), 148.0 (C12, C_{ipso}), 163.5 (d, $^1J_{\text{CP}} = 27$ Hz, C2, C_{ipso}).

Anal. Calcd. for $\text{C}_{38}\text{H}_{42}\text{Cl}_2\text{N}_3\text{PZr} + 6.83 \text{C}_{36}\text{H}_{35}\text{Cl}_2\text{N}_2\text{PZr}^{(\text{b})} + 0.50 \text{C}_2\text{H}_6\text{Cl}_3\text{NZr}^{(\text{c})}$: C, 61.55; H,

5.15; N, 4.32; Found: C, 61.22; H, 5.18; N, 3.93. EI-MS (m/z): 724 (10, $[\text{M} - \text{HNMe}_2 + \text{Cl}]^+$), 688



(100, [M - HNMe₂]⁺), 673 (30, [M - HNMe₂ - Me]⁺), 635 (10, [M - HNMe₂ - Me - Cl]⁺), 528 (80, [M - HNMe₂ - Zr - 2Cl + 2H]⁺).

(a) the solid ^{iprop}NPNZrCl₂(HNMe₂) [**3.3**] was not isolated, but reacted further with THF to form ^{iprop}NPNZrCl₂(THF) [**3.5**] in 45% yield (see synthesis [**3.5**]). A ³¹P{¹H} NMR spectrum of the crude indicated 93% ^{iprop}NPNZrCl₂(HNMe₂) [**3.3**] at δ 8.7 and 7% unknown at δ -7.4.

(b) Loss of HNMe₂ may have occurred while drying the sample for analysis

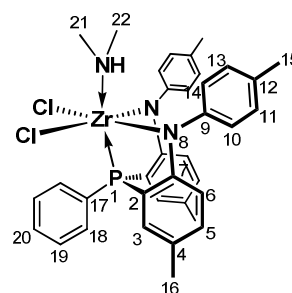
(c) ZrCl₃NMe₂ may be an impurity formed during the reaction of ZrCl₄ with Zr(NMe₂)₄

^{tol}NPNZrCl₂(HNMe₂) [**3.4**] (a) from ^{tol}NPNH₂ [**2.11**] / ZrCl₂(NMe₂)(DME): Brown

ZrCl₂(NMe₂)(DME) (1.35 g, 3.96) was dissolved in 20 cm³ toluene and added to a solution of ^{tol}NPNH₂ [**2.11**] (1.99 g, 3.97 mmol) dissolved in 20 cm³ toluene. The resulting dark orange solution was stirred overnight at room temperature, forming an orange ppt. The toluene solvent was removed *in vacuo*, giving in a crude orange solid ^{tol}NPNZrCl₂(HNMe₂) [**3.4**]. (a) (b) NMR

scale: Brown ZrCl₂(NMe₂)(DME) (0.09 g, 0.28 mmol) and white ^{tol}NPNH₂ [**2.11**] (0.14 g, 0.29 mmol) were placed together in a scintillation vial and 20 cm³ toluene was added. The dark orange solution was stirred overnight at room temperature, with the formation of an orange ppt. The toluene was removed *in vacuo*, leaving an orange solid. This orange residue was triturated with 5 cm³ *n*-hexanes and the orange solid was collected on a sintered glass frit, washing with 3 x 5 cm³ *n*-hexanes (0.15 g, 0.22 mmol ^{tol}NPNZrCl₂(HNMe₂) [**3.4**], 76% yield based on ZrCl₂(NMe₂)(DME)). Single crystals of ^{tol}NPNZrCl₂(HNMe₂) [**3.4**] were grown by slow evaporation of a benzene solution, as reported by Prof. Y. Ohki.²⁶¹

³¹P{¹H} NMR (C₆D₆, 121 MHz): δ = 8.20 (s, P1). ¹H NMR (C₆D₆, 300 MHz): δ = 1.82 (s, 6 H16, CH₃), 1.96 (s, 6 H15, CH₃), 2.01 (bs, 6 H22, N-CH₃), 2.39 (bs, 1 H21, N-H), 6.17 (d of d, ³J_{HH} = 8 Hz, ⁴J_{PH} = 6 Hz, 2 H6, ArH), 6.67 (d, ³J_{HH} = 8 Hz, 2 H5, ArH), 6.91 (d, ³J_{HH} = 8 Hz, 2 H10 and 2 H14, ArH), 7.03 (bs, 2 H18 and



H₂₀, ArH), 7.10 (d, $^3J_{\text{HH}} = 8$ Hz, 2 H₁₁ and 2 H₁₃, ArH), 7.17 (d, $^3J_{\text{HH}} = ^3J_{\text{PH}} = 7$ Hz, 2 H₃, ArH), 7.78 (t, $^3J_{\text{HH}} = 8$ Hz, 2 H₁₉, ArH). $^{13}\text{C}\{^1\text{H}\}$ NMR (C_6D_6 , 75 MHz): $\delta = 20.9$ (C₁₆, CH₃), 21.4 (C₁₅, CH₃), 42.2 (C₂₂, CH₃), 117.9 (d, $^3J_{\text{PC}} = 9$ Hz, C₆, ArC), 123.3 (d, $^2J_{\text{PC}} = 38$ Hz, C₇, C_{ipso}), 129.5 (overlapping d's, $^1J_{\text{PC}} = 22$ Hz, C₁₇, C_{ipso}, $^2J_{\text{PC}} = 9$ Hz, C₁₈, ArC), 130.4 (d, $^4J_{\text{PC}} = 5$ Hz, C₂₀, ArC), 130.7 (C₁₁ and C₁₃, ArC), 131.5 (C₁₀ and C₁₄, ArC), 133.2 (C₃, ArC and C₄, C_{ipso}), 133.6 (d, $^3J_{\text{PC}} = 10$ Hz, C₁₉, ArC), 134.0 (C₅, ArC), 136.9 (C₁₂, C_{ipso}), 142.2 (C₉, C_{ipso}), 161.9 (d, $^1J_{\text{CP}} = 27$ Hz, C₂, C_{ipso}). Anal. Calcd for $\text{C}_{36}\text{H}_{38}\text{N}_3\text{Cl}_2\text{PZr}$: C, 61.26; H, 5.43; N, 5.95. Found: C, 61.49; H, 5.80; N, 5.80. EI-MS (m/z): 704 (2, $[\text{M}]^+$), 660 (100, $[\text{M} - \text{HNMe}_2]^+$), 500 (15, $[\text{M} - \text{HNMe}_2 - \text{Zr} - 2\text{Cl} + 2\text{H}]^+$).

(a) the solid $^{\text{tol}}\text{NPNZrCl}_2(\text{HNMe}_2)$ **[3.4]** was not isolated, but reacted further with THF to form $^{\text{tol}}\text{NPNZrCl}_2(\text{THF})$ **[3.6]** in 91% yield (see synthesis **[3.3]**). A $^{31}\text{P}\{^1\text{H}\}$ NMR spectrum of the crude indicated a single peak for $^{\text{tol}}\text{NPNZrCl}_2(\text{HNMe}_2)$ **[3.4]** at δ 8.2.

$^{\text{iprop}}\text{NPNZrCl}_2(\text{THF})$ **[3.5]** (a) from $[\text{ipropNPN}]_2\text{Zr}$ **[3.1]** / $\text{ZrCl}_4(\text{THF})_2$: White $\text{ZrCl}_4(\text{THF})_2$ (0.02 g, 0.04 mmol) was partially dissolved in 2.5 cm³ toluene- d_8 . Orange $[\text{ipropNPN}]_2\text{Zr}$ **[3.1]** (0.04 g, 0.04 mmol) was dissolved in 2.5 cm³ toluene- d_8 and added to the $\text{ZrCl}_4(\text{THF})_2$ mixture. The reaction mixture was stirred at room temperature for 6 days^(a) and thereafter an additional 12 days.^(b) (b) from $^{\text{iprop}}\text{NPNZrCl}_2(\text{HNMe}_2)$ **[3.3]** / THF: The crude orange solid $^{\text{iprop}}\text{NPNZrCl}_2(\text{HNMe}_2)$ **[3.3]**^(c) was partially dissolved in 10 cm³ THF. The reaction mixture was stirred for 5 minutes at room temperature before the THF was removed *in vacuo*.^(d) The orange residue was re-suspended in THF and the orange slurry was stirred overnight at room temperature before the THF was removed *in vacuo*.^(e) The orange residue was partially dissolved in 20 cm³ toluene / THF (1:1) and stirred for 8 days at room temperature under reduced pressure. The solvent was removed *in vacuo* and the orange residue was triturated with *n*-hexanes. The orange solid was collected on a sintered glass frit and washed with 20 cm³ *n*-hexanes and 10 cm³ *n*-pentanes (0.94 g).^(f) This orange solid was completely dissolved in *ca* 40-50 cm³ THF and

stirred for 7 days at room temperature under reduced pressure. The THF was removed *in vacuo*, leaving an orange oil which was triturated with *ca* 40-60 cm³ *n*-hexanes to form an orange ppt. The orange solid was collected on a sintered glass frit, washing with 2 x 10 cm³ *n*-hexanes (0.59 g, 0.77 mmol ^{iprop}NPNZrCl₂(THF) [3.5], 45% yield based on ZrCl₂(NMe₂)(DME)). (c) from [^{iprop}NPNZrCl₂]₂ [3.9] / THF: Orange [^{iprop}NPNZrCl₂]₂ [3.9] (7.49 g, 10.88 mmol) was dissolved in 60 cm³ THF and the solution was stirred for *ca* 13 hrs at room temperature. The THF was removed *in vacuo* with gentle heating (60 °C), leaving an orange foam. This foam was triturated with 40 cm³ *n*-hexanes to form an orange ppt. The orange solid was collected on a sintered glass frit and washed with 4 x 10 cm³ *n*-hexanes (7.33 g, 9.63 mmol ^{iprop}NPNZrCl₂(THF) [3.5], 89% yield based on [^{iprop}NPNZrCl₂]₂ [3.9]). (d) from [^{iprop}NPNLi₂·diox]_n [2.6] / NMe₃·HCl / Zr(NMe₂)₄ / TMSCl / THF: Yellow [^{iprop}NPNLi₂·diox]_n [2.6] (3.99 g, 6.35 mmol) and NMe₃·HCl (1.82 g, 19.06 mmol) were added together in a conical flask. 60 cm³ THF was added and the yellow solution stirred for *ca* 17 hrs at room temperature under reduced pressure, with the solution gradually becoming lighter in colour. The THF was removed *in vacuo* and 40 cm³ toluene was added to the beige residue ^{iprop}NPNH₂ [2.10]. The mixture was filtered through celite with a sintered glass frit, washing the celite with 3 x 10 cm³ toluene. Light yellow Zr(NMe₂)₄ (1.70 g, 6.36 mol) was dissolved in 20 cm³ toluene and added to the ^{prop}NPNH₂ filtrate, forming a dark yellow solution that was stirred for *ca* 4 days at room temperature. The toluene was removed *in vacuo* and the yellow residue (^{iprop}NPNZr(NMe₂)₂ [3.7]) was dried for 2 hrs. This residue was re-dissolved in 40 cm³ toluene and TMSCl (5.30 cm³, 42.02 mmol) was added via syringe. The resulting orange solution was stirred for 19 hrs at room temperature before it was filtered through celite with a sintered glass frit. The toluene was removed *in vacuo*, leaving an orange residue that was triturated with 30 cm³ *n*-hexanes. The mixture was placed in the freezer for 18 hrs and the orange solid collected on a sintered glass frit ([^{iprop}NPNZrCl₂]₂ [3.9]). This solid was dissolved in 60 cm³ THF and stirred for 10 min at room temperature before THF was removed *in vacuo*. The resulting orange foam was triturated with 40 cm³ *n*-hexanes. This mixture

was placed in the freezer for 1 hr before being collected on a sintered glass frit and washed with 10 cm³ *n*-hexanes and 10 cm³ *n*-pentanes (4.01 g, 5.27 mmol ^{iprop}NPNZrCl₂(THF) [**3.5**], 83% yield based on [^{iprop}NPNLi₂·diox]_n [**2.6**]. Single crystals of ^{iprop}NPNZrCl₂(THF) [**3.5**] were grown via vapour diffusion of *n*-hexanes into a toluene solution at -40 °C.

³¹P{¹H} NMR (C₆D₆, 162 MHz): δ = 6.48 (s, P1). ¹⁵N{¹H} NMR

(toluene-*d*₈, 51 MHz): δ = -160.8 (s, N8).^(g) ¹H NMR (C₆D₆, 400

MHz): δ = 1.03 (bs, 4 H23, CH₂),^(h) 1.14 (d, ³J_{HH} = 7 Hz, 6 H1 6

and 6 H17, CH₃), 2.72 (hep, ³J_{HH} = 7 Hz, 2 H15, CH), 3.87 (bs,

4 H22, CH₂),^(h) 6.37 (d of d, ³J_{HH} = 8 Hz and ⁴J_{PH} = 6 Hz, 2 H6,

ArH), 6.63 (t, ³J_{HH} = 7 Hz, 2 H4, ArH), 6.95 (t, ³J_{HH} = 8 Hz, 2 H5, ArH), 7.15 (d, ³J_{HH} = 8 Hz, 2

H10 and 2 H14 and overlapping 2 H19 and H21, ArH), 7.24 (d, ³J_{HH} = 8 Hz, 2 H11 and 2 H13,

ArH), 7.34 (t, ³J_{HH} = ³J_{PH} = 8 Hz, 2 H3, ArH), 7.85 (s, 2 H20, ArH). ¹³C{¹H} NMR (C₆D₆, 151

MHz): δ = 24.1, 24.2 (C16 and C17, CH₃), 25.1 (C23, CH₂),^(h) 34.0 (C15, CH), 74.4 (C22,

CH₂),^(h) 117.2 (d, ³J_{PC} = 9 Hz, C6, ArC), 120.8 (d, ³J_{PC} = 5 Hz, C4, ArC), 122.9 (d, ²J_{PC} = 38 Hz,

C7, C_{ipso}), 128.9, 129.0 (C10 and C14, ArC), 130.0 (d, ²J_{PC} = 2 Hz, C19 and C21, ArC), 130.3 (d,

¹J_{PC} = 32 Hz, C18, C_{ipso} and C11 and C13, ArC), 132.5 (C5, ArC), 133.1 (d, ²J_{PC} / ³J_{PC} = 11 Hz,

C3 and C20, ArC), 141.6 (C9, C_{ipso}), 147.4 (C12, C_{ipso}), 163.5 (d, ¹J_{CP} = 27 Hz, C2, C_{ipso}). Anal.

Calcd. for C₄₀H₄₃Cl₂N₂OPZr: C, 63.14; H, 5.70; N, 3.68; Found: C, 63.04; H, 5.71; N, 3.76. EI-

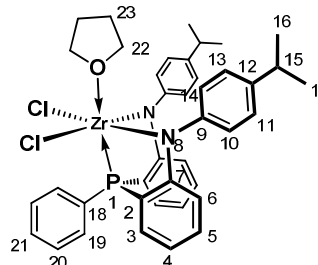
MS (*m/z*): 688 (100, [M - THF]⁺), 673 (30, [M - THF - Me]⁺), 651 (8, [M - THF - Cl]⁺), 635 (12,

[M - THF - Me - Cl]⁺), 528 (80, [M - THF - Zr - 2Cl + 2H]⁺

(a) using ³¹P{¹H} NMR spectroscopy, 14% conversion to ^{iprop}NPNZrCl₂(THF) [**3.5**]

(b) using ³¹P{¹H} NMR spectroscopy, 28% conversion to ^{iprop}NPNZrCl₂(THF) [**3.5**]

(c) the crude ^{iprop}NPNZrCl₂(HNMe₂) [**3.3**] was obtained from 1.44 g [^{iprop}NPNLi₂·diox]_n [**2.6**], 0.49 g NMe₃·HCl and 0.58 g ZrCl₂(NMe₂)₂(DME) (see synthesis [**3.3**])



- (d) using $^{31}\text{P}\{^1\text{H}\}$ NMR spectroscopy, 28% conversion to $^{\text{iprop}}\text{NPNZrCl}_2(\text{THF})$ [3.5], 59% unreacted $^{\text{iprop}}\text{NPNZrCl}_2(\text{HNMe}_2)$ [3.3] and 11% unknown at δ -7.3.
- (e) using $^{31}\text{P}\{^1\text{H}\}$ NMR spectroscopy, 62% conversion to $^{\text{iprop}}\text{NPNZrCl}_2(\text{THF})$ [3.5] and 38% unreacted $^{\text{iprop}}\text{NPNZrCl}_2(\text{HNMe}_2)$ [3.3] with no unknown at δ -7.3.
- (f) using $^{31}\text{P}\{^1\text{H}\}$ NMR spectroscopy, 79% conversion to $^{\text{iprop}}\text{NPNZrCl}_2(\text{THF})$ [3.5] and 21% unreacted $^{\text{iprop}}\text{NPNZrCl}_2(\text{HNMe}_2)$ [3.3]
- (g) using the natural abundance of ^{15}N in a concentrated sample *ca* 400mg in 0.8 cm³ toluene-*d*₈ (0.66 M).
- (h) free THF signals at δ 1.40 and δ 3.57 in ^1H NMR spectrum and at δ 25.72 and δ 67.80 in $^{13}\text{C}\{^1\text{H}\}$ NMR spectrum.

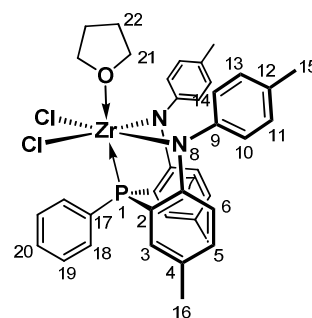
$^{\text{tol}}\text{NPNZrCl}_2(\text{THF})$ [3.6] (a) from $^{\text{tol}}\text{NPNZrCl}_2(\text{HNMe}_2)$ [3.4] / THF (at 60 °C): The crude orange solid $^{\text{tol}}\text{NPNZrCl}_2(\text{HNMe}_2)$ [3.4]^(a) was dissolved in 20 cm³ THF with heating to 60 °C for 2hrs. The THF was removed *in vacuo*, leaving an orange foam. This foam was triturated with 20 cm³ *n*-hexanes, forming a yellow ppt which was placed in the freezer (-40 °C) overnight. The yellow solid was collected on a sintered glass frit, washing with 2 x 10 cm³ *n*-hexanes.^(b) The solid was re-dissolved in 30 cm³ THF with heating to 60 °C for 4hrs. The THF was removed *in vacuo*, giving an orange foam that was triturated in *n*-hexanes, giving a yellow ppt. This mixture was placed in the freezer (-40 °C) overnight and the yellow solid was collected on a sintered glass frit, washing with 2 x 10 cm³ *n*-hexanes (2.65 g, 3.49 mmol $^{\text{tol}}\text{NPNZrCl}_2(\text{THF})$ [3.6], 91% yield based on $\text{ZrCl}_2(\text{NMe}_2)_2(\text{DME})$). **(b) from $^{\text{tol}}\text{NPNH}_2$ [2.11] / $\text{ZrCl}_2(\text{NMe}_2)_2(\text{DME})$ / THF (at 60 °C):** Brown $\text{ZrCl}_2(\text{NMe}_2)_2(\text{DME})$ (1.84 g, 5.41 mmol) and white $^{\text{tol}}\text{NPNH}_2$ [2.11] (2.72 g, 5.43 mmol) were added to a conical flask in the glove box and dissolved in 60 cm³ THF, forming an orange solution. This solution was heated for 17 hrs at 60 °C, with the formation of an orange ppt. The THF was removed *in vacuo* and the orange residue triturated with 40 cm³ *n*-hexanes, forming a yellow ppt. This mixture which was placed in the freezer for 4 days before the yellow

solid was collected on a sintered glass frit, washing with 2 x 10 cm³ *n*-hexanes (4.04 g, 20% purity = 0.81 g, 1.10 mmol ^{tol}NPNZrCl₂(THF) [**3.6**], 20% yield based on ZrCl₂(NMe₂)₂(DME)).^(c)

(c) from ^{tol}NPNZr(NMe₂)₂ [3.8**] / TMSCl / THF:** Yellow ^{tol}NPNZr(NMe₂)₂ [**3.8**] (1.85 g, 2.73 mmol) was dissolved in 20 cm³ toluene and TMSCl (2.00 cm³, 15.76 mmol) was added via syringe. The yellow solution was stirred for 3 days, forming a yellow ppt. The toluene was removed *in vacuo* to leave a yellow residue ([^{tol}NPNZrCl₂]₂ [**3.10**]). This residue was dissolved in 10 cm³ THF and the orange solution was stirred for 20 hrs at room temperature. The THF was removed *in vacuo* and the orange residue was triturated with 20 cm³ *n*-hexanes. The mixture was placed in the freezer (-40 °C) for 7 days before the orange solid was collected on a sintered glass frit, washed with 10 cm³ *n*-hexanes (1.34 g, 7.85 mmol ^{tol}NPNZrCl₂(THF) [**3.6**], 67% yield based on ^{tol}NPNZr(NMe₂)₂ [**3.8**]). Single crystals of ^{tol}NPNZrCl₂(THF) [**3.6**] were grown from a concentrated benzene solution, as reported by Prof. Y. Ohki.²⁶¹

³¹P{¹H} NMR (C₆D₆, 162 MHz): δ = 6.07 (s, P1). ¹H NMR

(C₆D₆, 600 MHz): δ = 1.10 (bs, 4 H22, CH₂),^(d) 1.96 (s, 6 H16, CH₃), 2.10 (s, 6 H15, CH₃), 3.83 (bs, 4 H21, CH₂),^(d) 6.35 (bs, 2 H6, ArH), 6.81 (d, ³J_{HH} = 8 Hz, 2 H5, ArH), 7.05 (d, ³J_{HH} = 7 Hz, 2 H10 and 2 H14, ArH), 7.12 (d, ³J_{HH} = 6 Hz, H20, ArH),



7.16 (bs, 2 H18, ArH), 7.25 (bs, 2 H11 and 2 H13, ArH), 7.34 (d, $^3J_{\text{PH}} = 7$ Hz, 2 H3, ArH), 7.95 (bs, 2 H19, ArH). $^{13}\text{C}\{^1\text{H}\}$ NMR (C_6D_6 , 151 MHz): $\delta = 20.5$ (C16, CH_3), 21.1 (C15, CH_3), 25.2 (C22, CH_2), $^{(d)}$ 72.9 (bs, C21, CH_2), $^{(d)}$ 117.7 (d, $^3J_{\text{PC}} = 9$ Hz, C6, ArC), 123.2 (d, $^2J_{\text{PC}} = 37$ Hz, C7, C_{ipso}), 129.0 (d, $^4J_{\text{PC}} = 9$ Hz, C20, ArC), 130.1 (C11, C13 and C18, ArC), 130.5 (d, $^1J_{\text{PC}} = 31$ Hz, C17, C_{ipso}), 130.8 (C10 and C14, ArC), 132.7 (C3, ArC and C4, C_{ipso}), 133.1 (d, $^3J_{\text{PC}} = 11$ Hz, C19, ArC), 133.5 (C5, ArC), 136.1 (C12, C_{ipso}), 142.1 (C9, C_{ipso}), 161.6 (d, $^1J_{\text{CP}} = 27$ Hz, C2, C_{ipso}). Anal. Calcd. for $\text{C}_{38}\text{H}_{39}\text{Cl}_2\text{N}_2\text{OPZr}$: C, 62.28.14; H, 5.36; N, 3.82; Found: C, 62.66; H,

5.75; N, 4.20. EI-MS (m/z): 660 (70, $[M - \text{THF}]^+$), 528 (100, $[M - \text{THF} - \text{Zr} - 2\text{Cl} + 2\text{H}]^+$).

MALDI-TOF (m/z): 660 ($[M - \text{THF}]^+$)^(e)

^(a) the crude ^{iprop}NPNZrCl₂(HNMe₂) [**3.3**] was obtained from 1.9873 g ^{tol}NPNH₂ [**2.11**] and 1.3482 g ZrCl₂(NMe₂)₂(DME) (see synthesis [**3.4**])

^(b) using ³¹P{¹H} NMR spectroscopy, 88% conversion to ^{tol}NPNZrCl₂(THF) [**3.6**].

^(c) the ³¹P{¹H} NMR spectrum has sharp peaks at δ 6.19 (20% ^{tol}NPNZrCl₂(THF) [**3.6**]), δ -9.10 (23% ^{tol}NPNZr(NMe₂)₂ [**3.8**]) and δ -31.35 (28% ^{tol}NPNH₂ [**2.11**]) and broad peaks at δ 9.68 and δ 4.19 (28% [^{tol}NPNZrCl₂]₂ [**3.10**]). The ¹H NMR spectrum has peaks at δ 3.69 and δ 1.24 (THF), δ 2.75 and δ 2.45 (NMe₂) and δ 6.20, ⁴J_{PH} = 5 Hz for N-H for ^{tol}NPNH₂ [**2.11**].

^(d) free THF signals at δ 1.40 and δ 3.57 in ¹H NMR spectrum and at δ 25.72 and δ 67.80 in ¹³C{¹H} NMR spectrum.

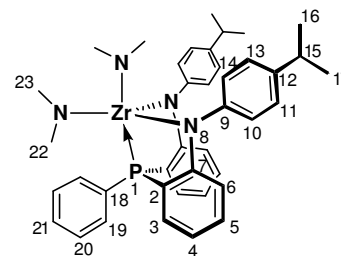
^(e) the matrix used was malonitrile. After analysis the sample was exposed to air and re-analysed, with no peak being observed at 660 m/z .

^{iprop}NPNZr(NMe₂)₂ [**3.7**] Orange [^{iprop}NPNLi₂·diox]_n [**2.6**] (21.70 g, 34.54 mmol) and NMe₃·HCl (10.18 g, 106.47 mmol) were added to a conical flask inside the glovebox and dissolved in 100 cm³ THF, forming an orange solution. This orange solution was stirred overnight at room temperature, gradually becoming lighter in colour to form a creamy light yellow solution. The THF was removed *in vacuo* with heating to 55 °C, leaving behind a mixture of yellow and white solids. To this residue was added 60 cm³ toluene and the mixture was filtered through celite with a sintered glass frit, washing with 5 x 20 cm³ toluene. The toluene was removed *in vacuo* from the light yellow filtrate, giving a light yellow semi-solid (17.54 g, ^{iprop}NPNH₂ [**2.10**]). This semi-solid was dissolved in 80 cm³ toluene and added to a solution of Zr(NMe₂)₄ (7.03 g, 26.28 mmol) in 40 cm³ toluene, forming an orange solution that was stirred for 2 days at room temperature. The toluene was removed *in vacuo* with heating (60 °C), giving a yellow solid that was triturated with 40 cm³ *n*-hexanes. The yellow solid collected on a sintered glass frit, washing with 3 x 20 cm³ *n*-

hexanes (5.05 g, 18.35 mmol $^{i\text{prop}}\text{NPNZr}(\text{NMe}_2)_2$ [**3.7**], 27% yield based on $\text{Zr}(\text{NMe}_2)_4$). The *n*-hexanes was removed *in vacuo* from the filtrate and the yellow residue was triturated with 20 cm³ *n*-hexanes. The *n*-hexanes solvent was removed *in vacuo*, giving a sticky yellow residue. This residue was re-suspended in 20 cm³ *n*-hexanes and the mixture was placed in the freezer (-40 °C) for 1 hr. The yellow solid was collected on a sintered glass frit, washing with 2 x 10 cm³ *n*-hexanes (8.94 g, 12.66 mmol $^{i\text{prop}}\text{NPNZr}(\text{NMe}_2)_2$ [**3.7**], 48% + 27% = 75% cumulative yield based on $\text{Zr}(\text{NMe}_2)_4$). Single crystals of $^{i\text{prop}}\text{NPNZr}(\text{NMe}_2)_2$ [**3.7**] were grown by slow evaporation of a benzene solution, as reported by Dr. E

MacLachlan⁹⁷

$^{31}\text{P}\{\text{H}\}$ NMR (C_6D_6 , 162 MHz): $\delta = -10.16$ (s, P1). ^1H NMR (C_6D_6 , 400 MHz): $\delta = 1.15$ (d, $^3J_{\text{HH}} = 7$ Hz, 6 H16 and 6 H17, CH₃), 2.48 (s, 6 H22, N-CH₃), 2.72 (hep, $^3J_{\text{HH}} = 7$ Hz, 2 H15, CH), 2.80 (s, 6 H23, N-CH₃), 6.61 (t, $^3J_{\text{HH}} = 7$ Hz, 2 H4, ArH), 6.72 (d of d, $^3J_{\text{HH}} = 8$ Hz, $^4J_{\text{PH}} = 6$ Hz, 2 H6, ArH), 7.00 (m, $^3J_{\text{HH}} = 8$ Hz, $^2J_{\text{PH}} = 2$ Hz, 2 H5, 2 H19 and H21, ArH), 7.13 (d, $^3J_{\text{HH}} = 6$ Hz, 2 H10, 2 H14, 2 H11 and 2 H13, ArH), 7.43 (m, $^3J_{\text{HH}} = 8$ Hz, $^4J_{\text{PH}} = 2$ Hz, 2 H3 and 2 H20, ArH). $^{13}\text{C}\{^1\text{H}\}$ NMR (C_6D_6 , 151 MHz): $\delta = 24.2, 24.4$ (C16 and C17, CH₃), 34.0 (C15, CH), 40.7 (C23, N-CH₃), 41.5 (C22, N-CH₃), 116.4 (d, $^2J_{\text{PC}} = 35$ Hz, C7, C_{ipso}), 117.7 (d, $^3J_{\text{PC}} = 8$ Hz, C6, ArC), 119.3 (d, $^3J_{\text{PC}} = 5$ Hz, C4, ArC), 126.1 (C11 and C13, ArC), 128.0 (C10 and C14, ArC), 129.1 (overlapping d's, $^1J_{\text{PC}} = 36$ Hz, C18, C_{ipso}, $^2J_{\text{PC}} = 9$ Hz, C19 and C21, ArC), 132.2 (d, $^2J_{\text{PC}} = 13$ Hz, C3, ArC), 133.2 (C5, ArC), 134.9 (C20, ArC), 142.3 (C12, C_{ipso}), 149.2 (d, $^4J_{\text{PC}} = 3$ Hz, C9, C_{ipso}), 163.7 (d, $^1J_{\text{CP}} = 30$ Hz, C2, C_{ipso}). Anal. Calcd. for $\text{C}_{40}\text{H}_{47}\text{N}_4\text{PZr}$: C, 68.05; H, 6.71; N, 7.94; Found: C, 68.12; H, 6.75; N, 7.71. EI-MS (m/z): 704 (40, $[\text{M}]^+$), 660 (100, $[\text{M} - \text{NMe}_2]^+$), 615 (10, $[\text{M} - 2\text{NMe}_2]^+$), 528 (100, $[\text{M} - \text{Zr} - 2\text{NMe}_2 + 2\text{H}]^+$).



$^{\text{tol}}\text{NPNZr}(\text{NMe}_2)_2$ [**3.8**] White $^{\text{tol}}\text{NPNH}_2$ [**2.11**] (1.83 g, 3.51 mmol) and $\text{Zr}(\text{NMe}_2)_4$ (0.94 g, 3.51 mmol) were added together and dissolved in 40 cm³ toluene, forming a yellow solution that was

stirred for 29 hrs at room temperature. The toluene was removed *in vacuo*, giving a yellow solid which was triturated in 10 cm³ *n*-hexanes. The *n*-hexanes was removed *in vacuo* and the yellow solid was re-suspended in 10 cm³ *n*-hexanes and placed in the freezer (-40 °C) for 2 hrs before the yellow solid was collected on a sintered glass frit, washed with 20 cm³ *n*-hexanes (1.88 g, 2.76 mmol ^{tol}NPNZr(NMe₂)₂ [**3.8**], 79% yield based in Zr(NMe₂)₄). Single crystals

^{tol}NPNZr(NMe₂)₂ [**3.8**] were grown from a concentrated benzene solution, as reported by Prof. Y. Ohki.²⁶¹

³¹P{¹H} NMR (C₆D₆, 162 MHz): δ = -10.60 (s, P1). ¹H NMR

(C₆D₆, 400 MHz): δ = 2.00 (s, 6 H16, CH₃), 2.19 (s, 6 H15,

CH₃), 2.56 (s, 6 H21, N-CH₃), 2.87 (s, 6 H22, N-CH₃), 6.74 (d

of d, ³J_{HH} = 8 Hz, ⁴J_{PH} = 6 Hz, 2 H6, ArH), 6.97 (m, ³J_{HH} = 8

Hz, ⁵J_{PH} = 1 Hz, 2 H5 and H20, ArH), 7.05 (d of d, ³J_{HH} = 8

Hz, ³J_{PH} = 2 Hz, 2 H18, ArH), 7.09 (d, ³J_{HH} = 9 Hz, 2 H10 and 2 H14, ArH), 7.19 (d, ³J_{HH} = 8 Hz,

2 H11 and 2 H13, ArH), 7.51 (m, ³J_{HH} = 9 Hz, ³J_{PH} = 2 Hz, ⁴J_{PH} = 1 Hz, 2 H3 and 2 H19, ArH).

¹³C{¹H} NMR (C₆D₆, 101 MHz): δ = 20.4 (C16, CH₃), 20.9 (C15, CH₃), 40.8 (C22, N-CH₃), 41.6

(C21, N-CH₃), 116.3 (d, ²J_{PC} = 33 Hz, C7, C_{ipso}), 117.9 (d, ³J_{PC} = 9 Hz, C6, ArC), 126.1 (C11 and

C13, ArC), 129.0 (d, ²J_{PC} = 9 Hz, C18, ArC), 129.3 (C20, ArC), 130.4 (C10 and C14, ArC),

131.8 (C12, C_{ipso}), 132.2 (d, ²J_{PC} = 14 Hz, C3, ArC), 133.3 (d, ¹J_{PC} = 25 Hz, C17, C_{ipso}), 134.5 (d,

³J_{CP} = 7 Hz, C4, C_{ipso} and C19 and C5, ArC), 149.2 (d, ⁴J_{PC} = 3 Hz, C9, C_{ipso}), 161.9 (d, ¹J_{CP} = 30

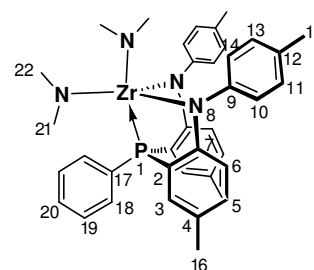
Hz, C2, C_{ipso}). Anal. Calcd. for C₃₈H₄₃N₄PZr: C, 67.32; H, 6.39; N, 8.26; Found: C, 67.33; H,

6.48; N, 8.29. EI-MS (*m/z*): 676 (75, [M]⁺), 632 (100, [M - NMe₂]⁺), 587 (15, [M - 2NMe₂]⁺).

[^{iprop}NPNZrCl₂]₂ [**3.9**] (a) The lemon yellow solid ^{iprop}NPNZr(NMe₂)₂ [**3.7**] (0.94 g, 1.33 mmol)

was dissolved in 40 cm³ toluene and 2.36 equiv of TMSCl (0.40 cm³, 3.15 mmol) was added via syringe and the yellow solution was allowed to stir for 3 days. After ³¹P{¹H} NMR analysis,^(a)

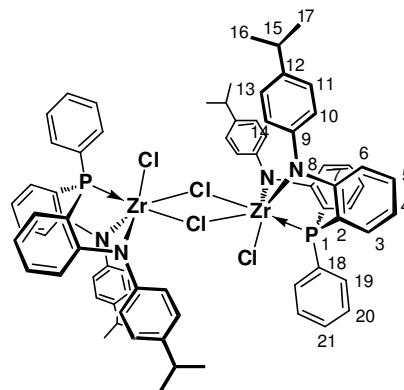
another 2.36 equiv of TMSCl (0.4 cm³, 3.15 mmol) was added via syringe. The solution was



allowed to stir for 1 day before $^{31}\text{P}\{^1\text{H}\}$ NMR analysis;^(b) thereafter another 2.36 equiv of TMSCl (0.4 cm^3 , 3.15 mmol) was added via syringe. After stirring for 1 day the solvent was removed completely and the yellow solid was suspended in 10 cm^3 *n*-hexanes and placed in freezer overnight. The yellow solid was collected on a sintered glass frit and washed $2 \times 5\text{ cm}^3$ *n*-hexanes (0.75 g, 1.08 mmol [$^{\text{iprop}}\text{NPNZrCl}_2$]₂ [3.9], 81% based on $^{\text{iprop}}\text{NPNZr}(\text{NMe}_2)_2$ [3.7]). (b) Lemon yellow $^{\text{iprop}}\text{NPNZr}(\text{NMe}_2)_2$ [3.7] (8.87 g, 12.56 mmol) was dissolved in 80 cm^3 toluene and TMSCl (10.6 cm^3 , 83.52 mmol) was added via syringe. The yellow solution was stirred for 23 hrs at room temperature, forming an orange solution with an orange ppt. The toluene was removed *in vacuo* and the residue was triturated with 60 cm^2 *n*-hexanes, giving a yellow ppt. The *n*-hexanes solvent was removed *in vacuo* and the residue re-suspended in 60 cm^3 *n*-hexanes. The yellow solid was collected on a sintered glass frit, washing with $2 \times 20\text{ cm}^3$ *n*-hexanes (8.44 g, 6.13 mmol [$^{\text{iprop}}\text{NPNZrCl}_2$]₂ [3.9], 98% yield based on $^{\text{iprop}}\text{NPNZr}(\text{NMe}_2)_2$ [3.7]). Single crystals of [$^{\text{iprop}}\text{NPNZrCl}_2$]₂ [3.9] were grown from a concentrated toluene solution at $-40\text{ }^\circ\text{C}$.

$^{31}\text{P}\{\text{H}\}$ NMR (C_6D_6 , 162 MHz, $25\text{ }^\circ\text{C}$): $\delta = 11.23$ (bs, P1).

^1H NMR (C_6D_6 , 400 MHz, $25\text{ }^\circ\text{C}$): $\delta = 1.13$ (d, $^3J_{\text{HH}} = 7$ Hz, 12 H16 and 12 H17, CH_3), 2.69 (s, 4 H15, CH), 6.34 (t, $^3J_{\text{HH}} = ^4J_{\text{PH}} = 6$ Hz, 4 H6, ArH), 6.59 (t, $^3J_{\text{HH}} = 7$ Hz, 4 H4, ArH), 6.91 (t, $^3J_{\text{HH}} = 8$ Hz, 4 H5, ArH), 7.09 (d, $^3J_{\text{HH}} = 8$ Hz, 4 H10 and 4 H14 overlapping 4 H19 and 2 H21, ArH), 7.18 (s, 4 H11 and 4 H13, ArH), 7.30 (t, $^3J_{\text{HH}} = ^3J_{\text{PH}}$



$= 8$ Hz, 4 H3, ArH), 7.73 (s, 4 H20, ArH). $^{13}\text{C}\{^1\text{H}\}$ NMR (C_6D_6 , 151 MHz, $25\text{ }^\circ\text{C}$): $\delta = 24.1$ (C16 and C17, CH_3), 34.3 (C15, CH), 116.8 (d, $^3J_{\text{PC}} = 8$ Hz, C6, ArC), 121.6 (d, $^3J_{\text{PC}} = 3$ Hz, C4, ArC), 124.1 (bs, C7, C_{ipso}), 128.5 (C11 and C13, ArC), 128.6 (d, $^2J_{\text{PC}} = 11$ Hz, C19, ArC), 129.1 (bs, C18, C_{ipso} and C21, ArC), 129.3 (C10 and C14, ArC), 132.8 (C5, ArC), 133.3 (C3, ArC), 134.0

(d, $^3J_{PC} = 9$ Hz, C20, ArC), 141.0 (bs, C9, C_{ipso}), 148.0 (C12, C_{ipso}), 162.3 (d, $^1J_{CP} = 24$ Hz, C2, C_{ipso}).

$^{31}\text{P}\{^1\text{H}\}$ NMR (C_6D_6 , 162 MHz, 90 °C): $\delta = 4.54$ (s, P1, minor isomer 18%), 7.14 (s, P1, major isomer 82%). ^1H NMR (C_6D_6 , 400 MHz, 90 °C): $\delta = 1.12$ (d, $^3J_{HH} = 6$ Hz, 12 H16 and 12 H17, CH₃), 2.71 (bs, 4 H15, CH), 6.38 (bs, 4 H6, ArH), 6.65 (bs, 4 H4, ArH), 6.96 (bs, 4 H5, ArH), 7.08 (bs, 4 H19 and 2 H21, ArH), 7.13 (d, $^3J_{HH} = 8$ Hz, 4 H10 and 4 H14, ArH), 7.26 (bs, 4 H11 and 4 H13, ArH), 7.38 (bs, 4 H3, ArH), 7.57 (bs, 4 H20, ArH). $^{13}\text{C}\{^1\text{H}\}$ NMR (C_6D_6 , 101 MHz, 90 °C): $\delta = 23.9$ (C16 and C17, CH₃), 34.1 (C15, CH), 116.5 (d, $^3J_{PC} = 9$ Hz, C6, ArC), 121.6 (C4, ArC) 122.1 (d, $^2J_{PC} = 42$ Hz, C7, C_{ipso}), 128.8 (C10 and C14, ArC), 128.9 (d, $^2J_{PC} = 10$ Hz, C19, ArC), 129.8 (C11 and C13, ArC), 130.2 (C21, ArC), 133.2 (d, $^1J_{PC} = 11$ Hz, C18, C_{ipso} and C20, ArC), 133.3 (C5, ArC), 133.8 (C3, ArC), 141.0 (d, $^4J_{PC} = 4$ Hz, C9, C_{ipso}), 148.5 (C12, C_{ipso}), 163.1 (d, $^1J_{CP} = 29$ Hz, C2, C_{ipso}).

Anal. Calcd. for $\text{C}_{72}\text{H}_{70}\text{Cl}_4\text{N}_4\text{P}_2\text{Zr}_2$: C, 62.78; H, 5.12; N, 4.07; Found: C, 62.55; H, 5.34; N, 4.23.

EI-MS (m/z): 688 (100, $[\text{M} - \text{ipropNPNZrCl}_2]^+$), 673 (20, $[\text{M} - \text{ipropNPNZrCl}_2 + \text{Me}]^+$), 635 (10, $[\text{M} - \text{ipropNPNZrCl}_2 - \text{Me} - \text{Cl}]^+$), 528 (10, $[\text{M} - \text{ipropNPNZrCl}_2 - \text{Zr} - 2\text{Cl} + 2\text{H}]^+$).

(a) using $^{31}\text{P}\{^1\text{H}\}$ NMR spectroscopy, a single sharp peak of an unidentified intermediate at δ 0.09.

(b) using $^{31}\text{P}\{^1\text{H}\}$ NMR spectroscopy, a broader peak for the unidentified intermediate at δ 0.09 and a very broad peak at δ 10.69 for $[\text{ipropNPNZrCl}_2]_2$ [**3.9**].

$[\text{tolNPNZrCl}_2]_2$ [**3.10**] Lemon yellow $\text{tolNPNZr}(\text{NMe}_2)_2$ [**3.8**] (0.86 g, 1.27 mmol) was dissolved in 20 cm³ toluene and TMSCl (1.13 cm³, 8.92 mmol) was added via syringe, forming an orange solution that was stirred for *ca* 20 hrs at room temperature The toluene was removed *in vacuo* and the orange residue was triturated with 10 cm³ *n*-hexanes, resulting in a yellow ppt. The *n*-hexanes was removed *in vacuo* and the yellow solid was re-suspended in 10 cm³ *n*-hexanes. This mixture was placed in the freezer overnight (-40 °C) and the yellow solid was collected on a

sintered glass frit, washing with 2 x 10 cm³ *n*-hexanes and 1 x 10 cm³ *n*-pentanes (0.79 g, 0.60 mmol [^{tol}NPNZrCl₂]₂ [**3.10**], 94% yield based on ^{tol}NPNZr(NMe₂)₂ [**3.8**]).

¹P{H} NMR (C₆D₆, 162 MHz): δ = 9.95 (bs, P1). ¹H

NMR (C₆D₆, 400 MHz): δ = 1.88 (s, 12 H16, CH₃),

2.06 (s, 12 H15, CH₃), 6.28 (t, ³J_{HH} = ⁴J_{PH} = 6 Hz, 4

H6, ArH), 6.75 (d, ³J_{HH} = 8 Hz, 4 H5, ArH), 6.97 (d,

³J_{HH} = 8 Hz, 4 H10 and 4 H14, ArH), 7.07 (bs, 4 H18

and 2 H20, ArH), 7.23 (d, ³J_{HH} = 6 Hz, 4 H11 and 4

H13, ArH), 7.29 (d, ³J_{HH} = 8 Hz, 4 H3, ArH), 7.78 (bs, 4 H19, ArH). ¹³C{¹H}f NMR (C₆D₆, 101

MHz): δ = 20.4 (C16, CH₃), 21.1 (C15, CH₃), 116.7 (d, ³J_{PC} = 9 Hz, C6, ArC), 123.9 (d, ²J_{PC} = 38

Hz, C7, C_{ipso}), 128.8 (d, ²J_{PC} = 10 Hz, C18, ArC), 129.6 (C11 and C13, ArC), 129.9 (C20, ArC),

130.8 (bs, C17, C_{ipso}), 131.4 (C10 and C14, ArC), 133.1 (C3, ArC and C4, C_{ipso}), 133.8 (C5,

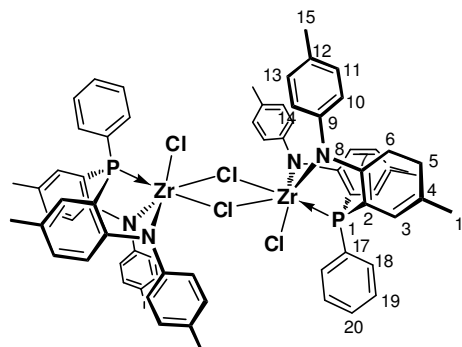
ArC), 133.9 (d, ³J_{PC} = 11 Hz, C19, ArC), 136.8 (C12, C_{ipso}), 141.0 (C9, C_{ipso}), 160.6 (d, ¹J_{CP} = 28

Hz, C2, C_{ipso}). Anal. Calcd. for C₆₈H₆₂Cl₄N₄P₂Zr₂: C, 61.81; H, 4.73; N, 4.24; Found: C, 60.58;

H, 4.91; N, 4.17. EI-MS (*m/z*): 1087 (100, [M - ZrCl₄]⁺), 890 (20, [M - ZrCl₄ - 2C₆H₅Me -

CH₄]⁺), 782 (15, [M - ZrCl₄ - 3C₆H₅Me - 2CH₄]⁺), 660 (100, [M - ^{tol}NPNZrCl₂]⁺), 623 (5, [M -

^{iprop}NPNZrCl₂ - Cl]⁺), 500 (20, [M - ^{iprop}NPNZrCl₂ - Zr - 2Cl + 2H]⁺).



^{iprop}NPNTiCl₂(HNMe₂) [**3.11**] from [^{iprop}NPNLi₂·diox]_n [**2.6**] / NMe₃·HCl / TiCl₂(NMe₂)₂:

Yellow ^{iprop}NPNLi₂·diox (0.50 g, 0.80 mmol) and NMe₃·HCl (0.23 g, 2.45 mmol) were placed in a Schlenk tube and 10 cm³ THF was added. The orange solution that was stirred at room temperature under reduced pressure for 23 hrs, gradually discolouring. The THF was removed *in vacuo* and the residue was dissolved in 10 cm³ toluene. This solution was filtered through celite with a sintered glass frit, washing the celite with 2 x 5 cm³ toluene. Dark brown TiCl₂(NMe₂)₂ (0.63 g, 3.03 mmol) was dissolved in 6 cm³ toluene and added to the pale yellow toluene filtrate (^{iprop}NPNH₂ [**2.10**]). The resulting dark purple solution was stirred for 16 hrs at room

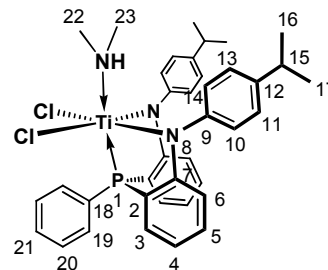
temperature. The toluene was removed *in vacuo* and the purple residue was dissolved in 20 cm³ THF^(a) and stirred for 12 hrs at room temperature, forming a blackish-purple solution. The THF was removed *in vacuo*, leaving a purple residue that was dissolved in 10 cm³ toluene. This solution was filtered through celite with a sintered glass frit, washing with 2 x 5 cm³ toluene. The toluene was removed *in vacuo* and the purple residue was triturated with 10 cm³ *n*-pentanes. The *n*-pentanes was removed *in vacuo* and the purple residue was re-suspended in *n*-pentanes. This mixture was placed in the freezer (-40 °C) overnight and the purple solid was collected on a sintered glass frit (0.10 g, 95% purity^(b) = 0.10 g, 0.14 mmol ^{iprop}NPNTiCl₂(HNMe₂) [**3.11**], 19% yield based on TiCl₂(NMe₂)₂).

³¹P{¹H} NMR (C₆D₆, 162 MHz): δ = 27.83 (bs, P1). ¹H NMR

(C₆D₆, 300 MHz): δ = 1.09 (d, ³J_{HH} = 7 Hz, 6 H16 and 6 H17, CH₃), 2.14 (bs, 2 H23, N-CH₃),^(c) 2.67 (hep, ³J_{HH} = 7 Hz, 2 H15,

CH), 2.91 (bs, 0.33 H22, N-H),^(c) 6.14 (bs, 2 H6, ArH), 6.65 (t, ³J_{HH} = 7 Hz, 2 H4, ArH), 6.83 (t, ³J_{HH} = 7 Hz, 2 H5, ArH), 7.04

(bs, 2H19 and H21, ArH), 7.14 (bs, 2 H10, 2 H14, 2 H11 and 2 H13, ArH), 7.22 (bs, 2 H3, ArH), 7.69 (s, 2 H20, ArH).



^(a) this step may be omitted: the intention was to form ^{iprop}NPNTiCl₂(THF) [**3.13**], however, only the HNMe₂ adduct was obtained.

^(b) using ³¹P{¹H} NMR spectroscopy, an unidentified peak at δ 46.51 (5%).

^(c) relative integration indicates 0.33 equiv of HNMe₂ per ^{iprop}NPNTiCl₂ molecule.

^{tol}NPNTiCl₂(HNMe₂) [**3.12**] White ^{tol}NPNH₂ [**2.11**] (0.24 g, 0.49 mmol) and dark brown TiCl₂(NMe₂)₂ (0.10 g, 0.49 mmol) were dissolved in 5 cm³ toluene. The resulting dark blue-purple solution was stirred overnight at room temperature. The toluene was removed *in vacuo* from the filtrate and the dark blue-purple residue was triturated with 5 cm³ *n*-hexanes. The

blackish-purple solid was collected on a sintered glass frit (0.24 g, 0.36 mmol

$^{101}\text{NPNTiCl}_2(\text{HNMe}_2)$ [**3.12**], 74% yield based on $\text{TiCl}_2(\text{NMe}_2)_2$).

$^{31}\text{P}\{^1\text{H}\}$ NMR (C_6D_6 , 121 MHz): δ = 26.35 (bs, P1). ^1H NMR

(C_6D_6 , 300 MHz): δ = 1.89 (s, 6 H16, CH_3), 2.06 (s, 6 H15,

CH_3), 2.17 (bs, 4 H22, N- CH_3),^(a) 3.09 (bs, 0.67 H21, N-H),^(a)

6.03 (d of d, $^3J_{\text{HH}}$ = 8 Hz and $^4J_{\text{PH}}$ = 6 Hz, 2 H6, ArH), 6.67 (d,

$^3J_{\text{HH}}$ = 8 Hz, 2 H5, ArH), 6.98 (d, $^3J_{\text{HH}}$ = 8 Hz, 2 H10 and 2

H14, ArH), 7.11 (m, $^3J_{\text{HH}}$ = 7 Hz, 2 H18, H20, 2 H11 and 2 H13, ArH), 7.18 (d, $^3J_{\text{PH}}$ = 8 Hz, 2

H3, ArH), 7.94 (t, $^3J_{\text{HH}}$ = 9 Hz, 2 H19, ArH). $^{13}\text{C}\{^1\text{H}\}$ NMR (C_6D_6 , 151 MHz): δ = 20.6 (C16,

CH_3), 21.0 (C15, CH_3), 42.2 (C22, CH_3), 117.7 (d, $^3J_{\text{PC}}$ = 10 Hz, C6, ArC), 127.6 (d, $^2J_{\text{PC}}$ = 19

Hz, C7, C_{ipso}), 128.3 (C11 and C13, ArC), 129.1 (d, $^3J_{\text{PC}}$ = 9 Hz, C4, C_{ipso}), 129.3 (d, $^1J_{\text{PC}}$ = 30

Hz, C17, C_{ipso}), 129.9 (C10 and C14, ArC), 130.6 (d, $^2J_{\text{PC}}$ = 3 Hz, C18 and C20, ArC), 131.5 (C3,

ArC), 133.0 (C5, ArC), 133.3 (d, $^3J_{\text{PC}}$ = 9 Hz, C19, ArC), 135.8 (C12, C_{ipso}), 150.6 (C9, C_{ipso}),

162.7 (d, $^1J_{\text{CP}}$ = 23 Hz, C2, C_{ipso}). Anal. Calcd for $\text{C}_{36}\text{H}_{38}\text{N}_3\text{Cl}_2\text{PTi}$ + 0.1 $\text{C}_2\text{H}_6\text{NCl}_3\text{Ti}$: C, 63.56;

H, 5.69; N, 6.37. Found: C, 63.19; H, 5.80; N, 6.12. EI-MS (m/z): 616 (100, $[\text{M} - \text{HNMe}_2]^+$), 601

(20, $[\text{M} - \text{HNMe}_2 - \text{Me}]^+$), 581 (20, $[\text{M} - \text{HNMe}_2 - \text{Cl}]^+$), 500 (5, $[\text{M} - \text{HNMe}_2 - \text{Ti} - 2\text{Cl} + 2\text{H}]^+$).

^(a) relative integration indicates 0.67 equiv of HNMe_2 per $^{101}\text{NPNTiCl}_2$ molecule.

$^{i\text{prop}}\text{NPNTiCl}_2(\text{THF})$ [**3.13**] from $^{i\text{prop}}\text{NPNTi}(\text{NMe}_2)_2$ [**3.15**] / TMSCl / THF : Brick-red

$^{i\text{prop}}\text{NPNTi}(\text{NMe}_2)_2$ [**3.15**] (0.05 g, 0.08 mmol) was dissolved in 5 cm^3 toluene and TMSCl (0.10

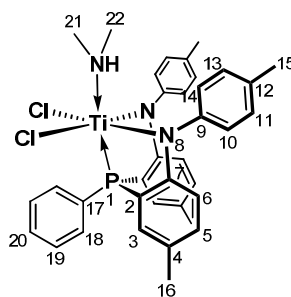
cm^3 , 0.79 mmol) was added via syringe. The resulting purple solution was stirred overnight at

room temperature before the toluene was removed *in vacuo*, with heating to 60 °C. The purple

residue ($^{i\text{prop}}\text{NPNTiCl}_2$ [**3.17**]) was dissolved in 5 cm^3 THF and stirred overnight at room

temperature before THF was removed *in vacuo*. The resulting residue was triturated with 5 cm^3

n-hexanes and the black-purple solid was collected on a sintered glass frit, washing with 2 x 3



cm³ *n*-hexanes (0.03 g, 0.05 mmol ^{iprop}NPNTiCl₂(THF) [3.13], 58% yield based on

^{iprop}NPNTi(NMe₂)₂ [3.15].

³¹P{¹H} NMR (C₆D₆, 162 MHz): δ = 30.34 (s, P1). ¹H NMR

(C₆D₆, 400 MHz): δ = 1.07 (d, ³J_{HH} = 7 Hz, 6 H16 and 6 H17,

CH₃), 1.37 (bs, 1 H23, CH₂),^(a) 2.55, 2.66 (hep's, ³J_{HH} = 7 Hz,

1 H15 and 1 H 15', CH), 3.72 (bs, 1 H22, CH₂),^(a) 5.69 (d of d,

³J_{HH} = 8 Hz, ⁴J_{PH} = 5 Hz, 2 H6, ArH), 6.57 (m, ³J_{HH} = 8 Hz, 2

H4, ArH), 6.80 (m, ³J_{HH} = 8 Hz, 2 H5, ArH), 7.04 (m, 2 H19 and H21, ArH), 7.14 (m, 2 H10, 2

H14, 2 H11, 2 H13 and 2 H3, ArH), 7.91 (t, 2 H20, ArH). ¹³C{¹H} NMR (C₆D₆, 101 MHz): δ =

24.0, 24.1, 24.3 (C16 and C17, CH₃), 25.7 (C23, CH₂),^(a) 33.8, 34.0 (C15, CH), 69.3 (C22,

CH₂),^(a) 114.4 (d, ³J_{PC} = 11 Hz, C6, ArC), 121.1 (d, ²J_{PC} = 48 Hz, C7, C_{ipso}), 123.3 (d, ³J_{PC} = 5 Hz,

C4, ArC), 128.8, 128.9 (C10, C14, C11 and C13, ArC), 131.4 (C19, ArC), 131.8 (C21, ArC),

132.6 (C5, ArC), 133.4 (d, ³J_{PC} = 5 Hz, C20, ArC), 133.52 (C12, C_{ipso}), 134.0 (C3, ArC), 135.0

(d, ¹J_{CP} = 48 Hz, C18, C_{ipso}), 146.2 (d, ⁴J_{PC} = 5 Hz C9, C_{ipso}), 163.5 (d, ¹J_{CP} = 27 Hz, C2, C_{ipso}). EI-

MS (*m/z*): 644 (100, [M]⁺), 629 (10, [M - Me]⁺), 609 (50, [M - Cl]⁺), 593 (5, [M - Me - Cl]⁺), 528

(70, [M - Ti - 2Cl + 2H]⁺).

^(a) Free THF signals at δ 1.40 and δ 3.57 in ¹H NMR spectrum and at δ 25.72 and δ 67.80 in

¹³C{¹H} NMR spectrum. Relative integration indicates 0.25 equiv of THF per ^{iprop}NPNTiCl₂

molecule. When sample was spiked with THF, the THF peaks remained at the same position and

increased in intensity and no changes were observed for the peak in the ³¹P{¹H} NMR spectrum.

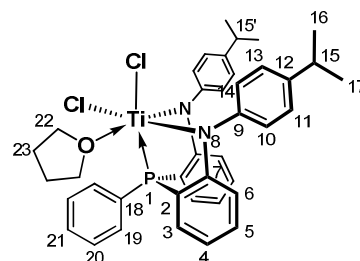
^{tol}NPNTiCl₂(THF) [3.14] (a) from ^{tol}NPNH₂ [2.11] / TiCl₂(NMe₂)₂ / THF at 60 °C: White

^{tol}NPNH₂ [2.11] (1.01 g, 2.02 mmol) was dissolved in 20 cm³ THF and added to a brown

solution of TiCl₂(NMe₂)₂ (0.41 g, 2.00 mmol) in 20 cm³ THF. The green-black solution was

stirred for 1 day at room temperature and then heating to 60 °C for 4 hrs, forming a dark purple

solution with a dark purple ppt. The THF was removed *in vacuo* and the purple residue was



trituated with 20 cm³ *n*-hexanes. The *n*-hexanes volume was reduced *in vacuo* to ca 10 cm³ *n*-hexanes and the mixture placed in freezer (-40 °C) for 4 days. The purple-black solid was collected on a chilled sintered glass frit, washing with 2 x 5 cm⁵ cold (-40 °C) *n*-pentanes (1.33 g, 1.93 mmol ¹⁰¹NPNTiCl₂(THF) [**3.14**], 97% yield based on TiCl₂(NMe₂)₂). **(b) from ¹⁰¹NPNTiCl₂ [3.18] / THF:** Purple ¹⁰¹NPNTiCl₂ [**3.18**] (0.15 g, 0.23 mmol) was dissolved in 5 cm³ THF and the dark blue-purple solution was stirred for 14 hrs at room temperature before the THF was removed in vacuo (100% yield ¹⁰¹NPNTiCl₂(THF) [**3.14**]).^(a)

³¹P{¹H} NMR (C₆D₆, 162 MHz): δ = 24.04 (s, P1). ¹H NMR (C₆D₆,

600 MHz): δ = 1.35 (bs, 4 H22, CH₂),^(b) 1.93 (s, 6 H16, CH₃), 2.06

(s, 6 H15, CH₃), 3.65 (bs, 4 H21, CH₂),^(b) 6.22 (d of d, ³J_{HH} = 8 Hz

and ⁴J_{PH} = 6 Hz, 2 H6, ArH), 6.78 (d, ³J_{HH} = 8 Hz, 2 H5, ArH),

7.04 (m, ³J_{HH} = 8 Hz, 2 H10, 2 H14, 2H18 and H20, ArH), 7.35 (d,

³J_{HH} = 7 Hz, 2 H11, 2 H13 and 2 H3, ArH), 7.72 (d of t, ³J_{HH} = 9 Hz, ⁴J_{PH} = 2 Hz, 2 H19, ArH).

¹³C{¹H} NMR (C₆D₆, 101 MHz): δ = 20.4 (C16, CH₃), 21.0 (C15, CH₃), 25.6 (C22, CH₂),^(b) 68.9

(s, C21, CH₂),^(b) 115.7 (d, ³J_{PC} = 10 Hz, C6, ArC), 122.9 (d, ²J_{PC} = 43 Hz, C7, C_{ipso}), 127.9 (C11

and C13, ArC), 129.2 (d, ²J_{PC} = 10 Hz, C18 and C20, ArC), 130.3 (C10 and C14, ArC), 130.7

(C4, C_{ipso}), 131.6 (d, ¹J_{PC} = 33 Hz, C17, C_{ipso}), 132.3 (d, ³J_{PC} = 29 Hz, C19, ArC), 133.1 (C3,

ArC), 134.4 (C5, ArC), 136.5 (C12, C_{ipso}), 149.8 (C9, d, ⁴J_{CP} = 5 Hz, C_{ipso}), 163.9 (d, ¹J_{CP} = 32

Hz, C2, C_{ipso}). Anal. Calcd. for C₃₈H₃₉Cl₂N₂OPTi + 0.1 C₆H₁₄: C, 66.53; H, 5.71; N, 4.01; Found:

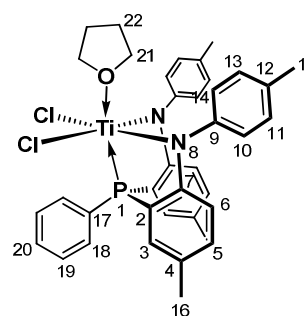
C, 66.13; H, 6.17; N, 3.80. EI-MS (*m/z*): 616 (60, [M - THF]⁺), 601 (10, [M - THF - Me]⁺), 581

(30, [M - THF - Cl]⁺), 500 (100, [M - THF - Ti - 2Cl + 2H]⁺).

^(a) complete conversion determined via ³¹P{¹H} NMR spectroscopy.

^(b) free THF signals at δ 1.40 and δ 3.57 in ¹H NMR spectrum and at δ 25.72 and δ 67.80 in

¹³C{¹H} NMR spectrum.



$\text{iprop}^{\text{NPNTiCl}_2(\text{HNMe}_2)}$ [3.11] / $\text{iprop}^{\text{NPNTiCl}_2(\text{THF})}$ [3.13] from $\text{iprop}^{\text{NPNLi}_2\cdot\text{diox}}$ / $\text{NMe}_3\cdot\text{HCl}$ / $\text{TiCl}_2(\text{NMe}_2)_2$ / **THF**: Yellow $\text{iprop}^{\text{NPNLi}_2\cdot\text{diox}}$ (2.03 g, 3.24 mmol) and $\text{NMe}_3\cdot\text{HCl}$ (0.93 g, 9.78 mmol) were placed in a Schlenk tube and 60 cm³ THF was added. The orange solution that was stirred at room temperature under reduced pressure for 13 hrs, gradually discolouring. The THF was removed *in vacuo* and the residue was dissolved in toluene. This solution was filtered through celite with a sintered glass frit, washing the celite with additional toluene and the filtrate volume was reduced *in vacuo* to 40 cm³. Dark brown $\text{TiCl}_2(\text{NMe}_2)_2^{(a)}$ (0.63 g, 3.03 mmol) was dissolved in 10 cm³ toluene and added to the pale yellow toluene filtrate ($\text{iprop}^{\text{NPNH}_2}$ [2.10]). The resulting dark purple solution was stirred for 4.5 hrs at room temperature before filtering through celite with a sintered glass frit, washing with 2 x 5 cm³ toluene. The toluene was removed *in vacuo* and the purple residue was dissolved in 100 cm³ THF, forming a blackish-purple solution. This solution was stirred under dynamic vacuum for 4.25 hrs, leaving a purple residue^(b) that was dissolved in 15 cm³ THF and stirred for 17 hrs at room temperature. The THF solvent was removed *in vacuo* and the purple residue was triturated with 20 cm³ *n*-hexanes. This mixture was placed in the freezer (-40 °C) overnight and the dark blue-purple solid was collected on a chilled sintered glass frit, washing with 20 cm³ cold *n*-hexanes (1.31 g, 1.86 mmol $\text{iprop}^{\text{NPNTiCl}_2(\text{THF})/(\text{HNMe}_2)}$ [3.13]/[3.11],^(c) 61% yield based on $\text{TiCl}_2(\text{NMe}_2)_2$).

$^{31}\text{P}\{\text{H}\}$ NMR (C_6D_6 , 162 MHz): $\delta =$

25.83 (bs, P1). ^1H NMR (C_6D_6 , 300

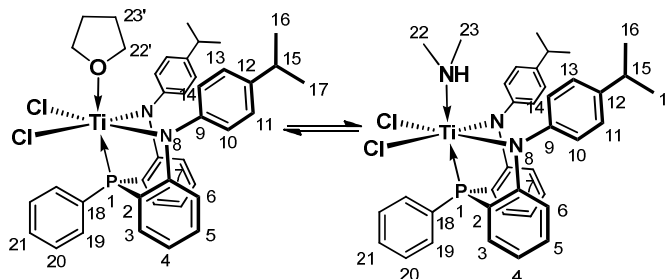
MHz): $\delta = 1.10$ (d, $^3J_{\text{HH}} = 6$ Hz, 6 H16

and 6 H17, CH₃), 1.29 (bs, 3 H23',

CH₂),^(c) 2.14 (bs, 2 H23, N-CH₃),^(d)

2.69 (hep, $^3J_{\text{HH}} = 7$ Hz, 2 H15, CH), 2.91 (bs, 0.33 H22, N-H),^(d) 3.75 (bs, 3 H22', CH₂),^(c) 6.18

(bs, 2 H6, ArH), 6.69 (t, $^3J_{\text{HH}} = 7$ Hz, 2 H4, ArH), 6.86 (t, $^3J_{\text{HH}} = 7$ Hz, 2 H5, ArH), 7.07 (bs,



2H19 and H21, ArH), 7.14 (m, 2 H10, 2 H14, 2 H11 and 2 H13, ArH), 7.27 (bs, 2 H3, ArH), 7.68 (s, 2 H20, ArH).

(a) ^1H NMR (C_6D_6 , 300 MHz): δ = 2.97 (s, N-CH₃). Anal. Calcd. for $\text{C}_4\text{H}_{12}\text{N}_2\text{Cl}_2\text{Ti}$: C, 23.22; H, 5.85; N, 13.54. Found: (a) C, 23.34; H, 5.70; N, 13.32; (b) C, 23.53; H, 5.69; N, 13.24. EI-MS (m/z): 206 (65, $[\text{M}]^+$), 198 (10, $[\text{M} - \text{NMe}_2 + \text{Cl}]^+$).

(b) using $^{31}\text{P}\{^1\text{H}\}$ and ^1H NMR spectroscopy, a mixture of $^{\text{iprop}}\text{NPNTiCl}_2(\text{THF})/(\text{HNMe}_2)$

[3.13]/[3.11] at δ 25.67 (95%) and an unidentified peak at δ 17.33 (5%)

(c) free THF signals at δ 1.40 and δ 3.57 in ^1H NMR spectrum and relative integration indicates 0.75 equiv of THF per $^{\text{iprop}}\text{NPNTiCl}_2$ molecule.

(d) relative integration indicates 0.33 equiv of HNMe_2 per $^{\text{iprop}}\text{NPNTiCl}_2$ molecule.

(e) the average molar mass between the two adducts was used, 704.0333 $\text{g}\cdot\text{mol}^{-1}$.

$^{\text{iprop}}\text{NPNTi}(\text{NMe}_2)_2$ **[3.15]** from $^{\text{iprop}}\text{NPnLi}_2\cdot\text{diox}$ / $\text{NMe}_3\cdot\text{HCl}$ / $\text{Ti}(\text{NMe}_2)_4$: Orange

$[\text{ipropNPnLi}_2\cdot\text{diox}]_n$ **[2.6]** (1.58 g, 2.51 mmol) and $\text{NMe}_3\cdot\text{HCl}$ (0.72 g, 7.54 mmol) were placed in a Schlenk tube and 10 cm^3 THF was added. The orange reaction mixture was stirred for 2.3 days at room temperature, gradually discolouring. The THF was removed *in vacuo* and the residue was extracted with 10 cm^3 toluene and filtered through celite in a sintered glass frit, washing the celite with 3 x 10 cm^3 toluene. This filtrate ($^{\text{iprop}}\text{NPNH}_2$ **[2.10]**) was added to a yellow solution 0.08 M $\text{Ti}(\text{NMe}_2)_4$ in toluene (29.9 cm^3 , 2.40 mmol), forming a darker orange solution that was stirred for 19 hrs at room temperature. The toluene was removed *in vacuo* from the dark red solution, leaving a red oily residue. This red oil was dissolved in 20 cm^3 *n*-hexanes, resulting in the ppt of a red solid. The *n*-hexanes was removed *in vacuo*, leaving a red solid. This solid was re-suspended in 20 cm^3 *n*-hexanes and placed in the freezer (-40 °C) for 27 hrs. The red solid was collected on a sintered glass frit, washing with 10 cm^3 *n*-hexanes (0.84 g, 1.27 mmol

$^{\text{iprop}}\text{NPNTi}(\text{NMe}_2)_2$ **[3.15]**, 53% yield based on $^{\text{iprop}}\text{NPnLi}_2\cdot\text{diox}$). Single crystals of

$^{\text{iprop}}\text{NPNTi}(\text{NMe}_2)_2$ **[3.15]** were grown by slow evaporation of a benzene solution.

$^{31}\text{P}\{\text{H}\}$ NMR (C_6D_6 , 162 MHz): $\delta = -2.05$ (s, P1). ^1H NMR

(C_6D_6 , 400 MHz): $\delta = 1.23$ (d, $^3J_{\text{HH}} = 7$ Hz, 6 H16 and 6 H17,

CH_3), 2.58 (s, 6 H22, N- CH_3), 2.79 (hep, 2 H15, $^3J_{\text{HH}} = 7$ Hz,

CH), 3.14 (s, 6 H23, N- CH_3), 6.68 (m, $^3J_{\text{HH}} = 7$ Hz, 2 H4 and 2

H6, ArH), 7.06 (m, $^3J_{\text{HH}} = 7$ Hz, 2 H5, 2 H19 and H21, ArH), 7.11 (d, $^3J_{\text{HH}} = 8$ Hz, 2 H10 and 2

H14, ArH), 7.17 (d, $^3J_{\text{HH}} = 8$ Hz, 2 H11 and 2 H13, ArH), 7.47 (m, $^3J_{\text{HH}} = 8$ Hz, 2 H3 and 2 H20,

ArH). $^{13}\text{C}\{^1\text{H}\}$ NMR (C_6D_6 , 101 MHz): $\delta = 24.3$, 24.4 (C16 and C17, CH_3), 33.9 (C15, CH),

45.2, 45.3 (C22a/C23a, N- CH_3), 45.8 (C22/C23, N- CH_3), 116.7 (d, $^3J_{\text{PC}} = 9$ Hz, C6, ArC), 117.5

(d, $^2J_{\text{PC}} = 35$ Hz, C7, C_{ipso}), 119.5 (d, $^3J_{\text{PC}} = 5$ Hz, C4, ArC), 125.6 (C11 and C13, ArC), 127.0

(C10 and C14, ArC), 128.8 (d, $^2J_{\text{PC}} = 9$ Hz, C19, ArC), 129.2 (C21, ArC), 132.2 (d, $^3J_{\text{PC}} = 13$ Hz,

C20, ArC), 132.8 (d, $^1J_{\text{PC}} = 26$ Hz, C18, C_{ipso}), 133.0 (C5, ArC), 134.3 (C3, ArC), 142.5 (C12,

C_{ipso}), 152.4 (d, $^4J_{\text{CP}} = 5$ Hz, C9, C_{ipso}), 165.5 (d, $^1J_{\text{CP}} = 33$ Hz, C2, C_{ipso}). Anal. Calcd. for

$\text{C}_{40}\text{H}_{47}\text{N}_4\text{PTi}$: C, 72.50; H, 7.15; N, 8.45; Found: C, 72.32; H, 7.24; N, 8.22. EI-MS (m/z): 662

(20, $[\text{M}]^+$), 618 (100, $[\text{M} - \text{NMe}_2]^+$), 573 (10, $[\text{M} - 2\text{NMe}_2]^+$), 528 (10, $[\text{M} - \text{Ti} - 2\text{NMe}_2 + 2\text{H}]^+$).

$^{101}\text{NPNTi}(\text{NMe}_2)_2$ [3.16] The white solid $^{101}\text{NPNH}_2$ [2.11] (5.81 g, 12.45 mmol) was dissolved in

60 cm^3 toluene and a yellow solution 0.0941 M $\text{Ti}(\text{NMe}_2)_4$ in toluene (130.00 cm^3 , 12.23 mmol)

was added. The dark orange solution was stirred for 27 hrs, forming a dark red solution. The

toluene was removed *in vacuo* with heating (60 $^\circ\text{C}$) and the resulting red foam was triturated with

40 cm^3 *n*-hexanes. The *n*-hexanes was removed *in vacuo* and the brick red residue was re-

suspended in a mixture of 30 cm^3 *n*-pentanes and 20 cm^3 *n*-hexanes. This mixture was placed in

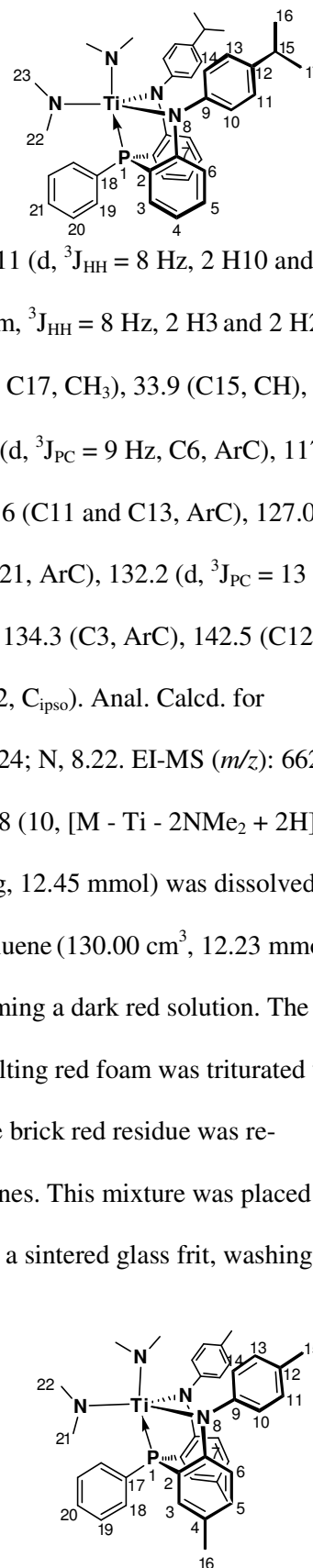
the freezer (-40 $^\circ\text{C}$) overnight and the red solid was collected on a sintered glass frit, washing

with 3 x 5 cm^3 chilled *n*-pentanes (6.00 g, 9.45 mmol

$^{101}\text{NPNTi}(\text{NMe}_2)_2$, 77% yield based on $\text{Ti}(\text{NMe}_2)_4$).

$^{31}\text{P}\{\text{H}\}$ NMR (C_6D_6 , 162 MHz): $\delta = -2.35$ (s, P1). ^1H NMR

(C_6D_6 , 400 MHz): $\delta = 2.00$ (s, 6 H16, CH_3), 2.20 (s, 6 H15,

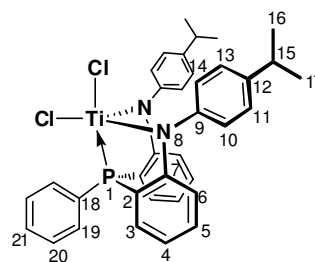


CH₃), 2.62 (s, 6 H₂₁, N-CH₃), 3.14 (s, 6 H₂₂, N-CH₃), 6.62 (d of d, ³J_{HH} = 8 Hz, ⁴J_{PH} = 6 Hz, 2 H₆, ArH), 6.93 (d, ³J_{HH} = 8 Hz, 2 H₅), 7.00 (m, ³J_{HH} = 7 Hz, H₂₀, ArH), 7.05 (bs, 2 H₁₈, ArH), 7.09 (bs, 2 H₁₀, 2 H₁₄, 2 H₁₁ and 2 H₁₃, ArH), 7.46 (d, ³J_{PH} = 7 Hz, 2 H₃, ArH), 7.53 (t, ³J_{HH} = 7 Hz, 2 H₁₉, ArH). ¹³C{¹H NMR (C₆D₆, 151 MHz): δ = 20.3 (C₁₆, CH₃), 20.9 (C₁₅, CH₃), 45.18, 45.20 (C_{21a}/C_{22a}, N-CH₃), 45.8 (C₂₁/C₂₂, N-CH₃), 116.8 (d, ³J_{PC} = 10 Hz, C₆, ArC), 117.4 (d, ²J_{PC} = 34 Hz, C₇, C_{ipso}), 125.6 (C₁₁ and C₁₃, ArC), 128.6 (d, ⁴J_{PC} = 5 Hz C₂₀, ArC), 128.8 (d, ²J_{PC} = 9 Hz, C₁₈, ArC), 129.1 (C₄, C_{ipso}), 129.8 (C₁₀ and C₁₄, ArC), 131.2 (C₁₂, C_{ipso}), 132.1 (d, ³J_{PC} = 13 Hz, C₁₉, ArC), 133.1 (d, ¹J_{PC} = 25 Hz, C₁₇, C_{ipso}), 133.9 (C₃, ArC), 134.2 (C₅, ArC), 152.3 (d, ⁴J_{PC} = 4 Hz, C₉, C_{ipso}), 163.7 (d, ¹J_{CP} = 33 Hz, C₂, C_{ipso}). Anal. Calcd. for C₃₈H₄₃N₄PTi: C, 71.92; H, 6.83; N, 8.83; Found: C, 72.19; H, 6.82; N, 8.80. EI-MS (*m/z*): 634 (40, [M]⁺), 590 (100, [M - NMe₂]⁺), 545 (20, [M - 2NMe₂]⁺).

^{iprop}NPNTiCl₂ [3.17] (a) with 2.2 and 4.4 equiv of TMSCl: Red ^{iprop}NPNTi(NMe₂)₂ [3.15] (0.46 g, 0.70 mmol) was dissolved in 30 cm³ toluene and TMSCl (0.2 cm³, 1.54 mmol) was added via syringe. The dark red solution was stirred for 3 days at room temperature.^(a) A second aliquot TMSCl (0.2 cm³, 1.54 mmol) was added via syringe and the mixture was allowed to stir for 1 day at room temperature.^(b) **(b) with 6.1 equiv of TMSCl:** Red ^{iprop}NPNTi(NMe₂)₂ [3.15] (0.81 g, 1.23 mmol) was dissolved in 20 cm³ toluene and TMSCl (0.95 cm³, 7.49 mmol) was added via syringe. The dark red solution was stirred for 3 days at room temperature. The toluene was removed *in vacuo* and the dark residue was triturated with 20 cm³ *n*-hexanes. The *n*-hexanes was removed *in vacuo* and the residue was re-suspended in 20 cm³ *n*-pentanes and the mixture placed in the freezer (-40 °C) overnight. The purple solid was collected on a chilled sintered glass frit, washing with minimal cold *n*-pentanes (0.64 g, 0.98 mmol ^{iprop}NPNTiCl₂ [3.17], 80% yield based on ^{iprop}NPNTi(NMe₂)₂ [3.15]).

³¹P{¹H} NMR (C₆D₆, 162 MHz, 25 °C): δ = 24.85 (s, P₁). ¹H

NMR (C₆D₆, 400 MHz, 25 °C): δ = 1.07 (d, ³J_{HH} = 7 Hz, 6 H₁₆



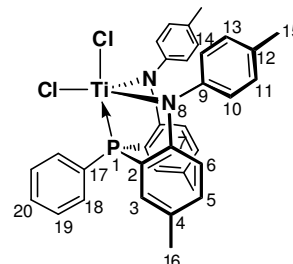
and 6 H17, CH₃), 2.66 (hep, $^3J_{\text{HH}} = 7$ Hz, 2 H15, CH), 6.32 (m, $^3J_{\text{HH}} = 6$ Hz, 2 H6, ArH), 6.70 (t, $^3J_{\text{HH}} = 7$ Hz, 2 H4, ArH), 6.92 (t, $^3J_{\text{HH}} = 8$ Hz, 2 H5, ArH), 6.99 (bs, 2 H19 and H21, ArH), 7.14 (d, $^3J_{\text{HH}} = 8$ Hz, 2 H10 and 2 H14, ArH), 7.36 (m, $^3J_{\text{HH}} = 8$ Hz, 2 H3 and 2 H20, ArH), 7.40 (d, $^3J_{\text{HH}} = 8$ Hz, 2 H11 and 2 H13, ArH). $^{13}\text{C}\{^1\text{H}\}$ NMR (C₆D₆, 151 MHz, 25 °C): $\delta = 23.9, 24.0$ (C16 and C17, CH₃), 34.0 (C15, CH), 114.4 (C6, ArC), 121.4 (d, $^2J_{\text{PC}} = 39$ Hz, C7, C_{ipso}), 123.2 (C4, ArC), 129.05 (C11 and C13, ArC), 129.12 (C10 and C14, ArC), 130.8 (C19 and C21, ArC), 132.0 (C20, ArC), 132.5 (d, $^1J_{\text{PC}} = 43$ Hz, C18, C_{ipso}), 134.2 (C5, C3, ArC), 148.1 (C9, C_{ipso}), 149.4 (C12, C_{ipso}), 166.4 (d, $^1J_{\text{CP}} = 35$ Hz, C2, C_{ipso}). Anal. Calcd. for C₃₆H₃₅Cl₂N₂PTi: C, 66.99; H, 5.47; N, 4.34; Found: C, 67.02; H, 5.76; N, 4.55. EI-MS (m/z): 644 (100, [M]⁺), 629 (10, [M - Me]⁺), 609 (30, [M - Cl]⁺), 593 (10, [M - Me - Cl]⁺), 565 (10, [M - CHMe₂ - Cl]⁺), 528 (70, [M - Zr - 2Cl + 2H]⁺).

(a) using $^{31}\text{P}\{^1\text{H}\}$ NMR spectroscopy, unreacted ^{iprop}NPNTi(NMe₂)₂ [**3.15**] at δ -2.5 (24%), ^{iprop}NPNTiCl₂ [**3.17**] at δ 25.1 (68%) and an unidentified intermediate at δ 17.35 (8%).

(b) using $^{31}\text{P}\{^1\text{H}\}$ NMR spectroscopy, unreacted ^{iprop}NPNTi(NMe₂)₂ [**3.15**] at δ -2.0 (7%), ^{iprop}NPNTiCl₂ [**3.17**] at δ 25.6 (88%) and an unidentified intermediate at δ 17.35 (5%).

^{tol}NPNTiCl₂ [**3.18**] Red ^{tol}NPNTi(NMe₂)₂ [**3.16**] (5.79 g, 9.13 mmol) was dissolved in 143 cm³ toluene and TMSCl (7.30 cm³, 60.23 mmol) was added via syringe. The dark red solution was stirred for 7 days at room temperature. The toluene was removed *in vacuo* with heating (60 °C) and the purple residue was triturated with 45 cm³ *n*-pentanes. The purple solid was collected on a sintered glass frit, washing with 2 x 10 cm³ *n*-pentanes (5.69 g, 9.22 mmol ^{tol}NPNTiCl₂ [**3.18**], 99% yield based on ^{tol}NPNTi(NMe₂)₂). Single crystals of ^{tol}NPNTiCl₂ [**3.18**] were grown by vapour diffusion of *n*-hexanes into a toluene solution at -40 °C.

$^1\text{P}\{^1\text{H}\}$ NMR (C₆D₆, 121 MHz): $\delta = 24.41$ (s, P1). ^1H NMR (C₆D₆, 300 MHz): $\delta = 1.93$ (s, 6 H16, CH₃), 2.03 (s, 6 H15, CH₃), 6.29 (d of d, $^3J_{\text{HH}} = 8$ Hz, $^4J_{\text{PH}} = 6$ Hz, 2 H6, ArH), 6.82 (d, $^3J_{\text{HH}} = 8$ Hz, 2 H5,



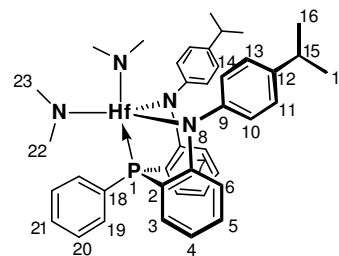
ArH), 7.03 (m, $^3J_{\text{HH}} = 8$ Hz, 2 H10, 2 H14, 2 H18 and H20, ArH), 7.40 (m, $^3J_{\text{HH}} = 8$ Hz, 2 H11, 2 H13 and 2 H3, ArH), 7.51 (bs, 2 H19, ArH). $^{13}\text{C}\{^1\text{H}\}$ NMR (C_6D_6 , 151 MHz): $\delta = 19.6$ (C16, CH_3), 20.4 (C15, CH_3), 113.8 (d, $^3J_{\text{PC}} = 9$ Hz, C6, ArC), 120.9 (d, $^2J_{\text{PC}} = 43$ Hz, C7, C_{ipso}), 128.2 (d, $^1J_{\text{PC}} = 26$ Hz, C17, C_{ipso}), 128.5 (d, $^2J_{\text{PC}} = 10$ Hz, C18 and C20, ArC), 128.6 (C11 and C13, ArC), 130.1 (C10 and C14, ArC), 131.3 (d, $^3J_{\text{PC}} = 11$ Hz, C19, ArC), 132.3 (d, $^3J_{\text{PC}} = 4$ Hz, C4, C_{ipso}), 133.4 (C3, ArC), 134.6 (C5, ArC), 136.5 (C12, C_{ipso}), 148.7 (C9, C_{ipso}), 164.2 (d, $^1J_{\text{CP}} = 35$ Hz, C2, C_{ipso}). Anal. Calcd. for $\text{C}_{34}\text{H}_{31}\text{Cl}_2\text{N}_2\text{PTi} + 0.8 \text{C}_7\text{H}_8$: C, 68.88; H, 5.51; N, 4.39; Found: C, 68.60; H, 5.49; N, 4.15. EI-MS (m/z): 616 (100, $[\text{M}]^+$), 600 (30, $[\text{M} - \text{Me}]^+$), 581 (20, $[\text{M} - \text{Cl}]^+$), 500 (70, $[\text{M} - \text{Ti} - 2\text{Cl} + 2\text{H}]^+$).

$\text{ipropNPNHf}(\text{NMe}_2)_2$ [3.19] from $\text{ipropNPNLi}_2 \cdot \text{diox} / \text{NMe}_3 \cdot \text{HCl} / \text{Hf}(\text{NMe}_2)_4$: Yellow

$\text{ipropNPNLi}_2 \cdot \text{diox}$ (3.28 g, 5.22 mmol) and $\text{NMe}_3 \cdot \text{HCl}$ (1.26 g, 13.21 mmol) were added to a Schlenk tube and 40 cm^3 THF was added. The yellow reaction mixture was stirred overnight at room temperature, gradually discolouring. The THF was removed *in vacuo* and the cream residue was dissolved in 20 cm^3 toluene. This mixture was filtered through celite with a sintered glass frit, washing with 30 cm^3 toluene. White $\text{Hf}(\text{NMe}_2)_4$ (1.76 g, 4.95 mmol) was dissolved in 10 cm^3 toluene and added to the filtrate (ipropNPNH_2 [2.10]), forming a yellow solution that was stirred for 19 hrs at room temperature. The toluene was removed *in vacuo* and the lemon-yellow residue was triturated with 20 cm^3 *n*-hexanes. The *n*-hexanes was removed *in vacuo* and the residue re-suspended in 10 cm^3 *n*-hexanes. The mixture was placed in freezer (-40°C) overnight and the lemon yellow solid was collected on a sintered glass frit, washing with 2 x 5 cm^3 *n*-hexanes (2.24 g, 2.82 mmol $\text{ipropNPNHf}(\text{NMe}_2)_2$, 57% yield based on $\text{Hf}(\text{NMe}_2)_4$). Single crystals of

$\text{ipropNPNHf}(\text{NMe}_2)_2$ [3.19] were grown by vapour diffusion of *n*-hexanes into a toluene solution at -40°C .

$^{31}\text{P}\{\text{H}\}$ NMR (C_6D_6 , 162 MHz): $\delta = -3.12$ (s, P1). ^1H NMR (C_6D_6 , 600 MHz): $\delta = 1.18$ (d, $^3J_{\text{HH}} = 7$ Hz, 6 H16 and 6 H17,



CH₃), 2.56 (s, 6 H₂₂, N-CH₃), 2.75 (hep, ³J_{HH} = 7 Hz, 2 H₁₅, CH), 2.90 (s, 6 H₂₃, N-CH₃), 6.63 (t, ³J_{HH} = 8 Hz, 2 H₄, ArH), 6.73 (d of d, ³J_{HH} = 8 Hz, ⁴J_{PH} = 6 Hz, 2 H₆, ArH), 6.98 (t, ³J_{HH} = 7 Hz, H₂₁, ArH), 7.04 (m, ³J_{HH} = 7 Hz, 2 H₅ and 2 H₁₉, ArH), 7.15 (d, ³J_{HH} = 8 Hz, 2 H₁₀ and 2 H₁₄, ArH), 7.18 (d, ³J_{HH} = 8 Hz, 2 H₁₁ and 2 H₁₃, ArH), 7.44 (m, ³J_{HH} = 8 Hz, 2 H₃ and 2 H₂₀, ArH). ¹³C{¹H}0 NMR (C₆D₆, 101 MHz): δ = 24.2, 24.4 (C₁₆ and C₁₇, CH₃), 34.0 (C₁₅, CH), 40.5 (C₂₃, N-CH₃), 41.1 (C₂₂, N-CH₃), 116.4 (d, ²J_{PC} = 36 Hz, C₇, C_{ipso}), 118.7 (d, ³J_{PC} = 8 Hz, C₆, ArC), 119.5 (d, ³J_{PC} = 5 Hz, C₄, ArC), 126.4 (C₁₁ and C₁₃, ArC), 127.7 (C₁₀ and C₁₄, ArC), 129.0 (d, ²J_{PC} = 9 Hz, C₁₉, ArC), 129.4 (C₂₁, ArC), 132.2 (d, ³J_{PC} = 13 Hz, C₂₀, ArC), 133.3 (d, ¹J_{PC} = 29 Hz, C₁₈, C_{ipso} and C₅, ArC), 134.9 (C₃, ArC), 143.3 (C₁₂, C_{ipso}), 149.1 (d, ⁴J_{PC} = 4 Hz, C₉, C_{ipso}), 164.5 (d, ¹J_{CP} = 29 Hz, C₂, C_{ipso}). Anal. Calcd. for C₄₀H₄₇N₄PHf: C, 60.56; H, 5.97; N, 7.06; Found: C, 60.50; H, 5.83; N, 6.69. EI-MS (*m/z*): 1232 (100, [M - 2NMe₂ + ^{iprop}NPN]⁺), ^(a) 794 (20, [M]⁺), 750 (100, [M - NMe₂]⁺), 705 (10, [M - 2NMe₂]⁺), 528 (100, [M - (Hf + 2NMe₂) + 2H]⁺).

^(a) Sample purity was confirmed via NMR spectroscopy and elemental analysis, thus the [^{iprop}NPN]₂Hf]⁺ ion may have been generated during the EI-MS analysis.

[^{iprop}NPNHfCl₂]₂ [3.20] Lemon yellow ^{iprop}NPNHf(NMe₂)₂ [3.19] (4.72 g, 5.95 mmol) was dissolved in 60 cm³ toluene and TMSCl (5.00 cm³, 39.24 mmol) was added via syringe. The yellow solution was stirred for 2 days at room temperature. The toluene was removed *in vacuo* and the yellow foam was triturated in 20 cm³ *n*-hexanes, forming a crude lime green solid that was collected on a sintered glass frit, washing with 2 x 10 cm³ *n*-hexanes (3.82 g). This crude lime green solid was dissolved in 10 cm³ toluene, with heating to 60 °C and the warm mixture was filtered through celite with a sintered glass frit, washing with warm toluene. The filtrate was placed in the freezer for 3 hrs; then layered with 40 cm³ *n*-hexanes and returned to freezer for 21 hrs. The yellow crystals were collected on a sintered glass frit, washing with 2 x 10 cm³ *n*-pentanes (2.84 g, 1.83 mmol [^{iprop}NPNHfCl₂]₂ [3.20], 62% yield based on ^{iprop}NPNHf(NMe₂)₂). Single crystals of [^{iprop}NPNHfCl₂]₂ [3.20] were grown by from a toluene solution at -40 °C.

$^{31}\text{P}\{\text{H}\}$ NMR (C_6D_6 , 162 MHz, 25 °C): $\delta = 3.80$

(s, P1). ^1H NMR (C_6D_6 , 400 MHz, 25 °C): $\delta =$

1.11 (d, $^3J_{\text{HH}} = 7$ Hz, 12 H16 and 12 H17, CH_3),

2.69 (hep, $^3J_{\text{HH}} = 7$ Hz, 4 H15, CH), 6.24 (t, $^3J_{\text{HH}} = ^4J_{\text{PH}} = 7$ Hz, 4 H6, ArH), 6.50 (t, $^3J_{\text{HH}} = 7$ Hz, 4

H4, ArH), 6.90 (t, $^3J_{\text{HH}} = 8$ Hz, 4 H5, ArH), 7.00 (bs, 4 H19 and 2 H21, ArH), 7.19 (d, $^3J_{\text{HH}} = 8$

Hz, 4 H10 and 4 H14), 7.24 (t, $^3J_{\text{HH}} = ^3J_{\text{PH}} = 8$ Hz, 4 H3, ArH), 7.33 (s, 4 H11 and 4 H13, ArH),

7.50 (bs, 4 H20, ArH). $^{13}\text{C}\{^1\text{H}\}$ NMR (C_6D_6 , 101 MHz, 25 °C): $\delta = 24.0, 24.1$ (C16 and C17,

CH_3), 34.0 (C15, CH), 117.4 (d, $^3J_{\text{PC}} = 9$ Hz, C6, ArC), 121.1 (d, $^3J_{\text{PC}} = 5$ Hz, C4, ArC), 121.5 (d,

$^2J_{\text{PC}} = 42$ Hz, C7, C_{ipso}), 128.4 (C10 and C14, ArC), 128.8 (d, $^1J_{\text{PC}} = 35$ Hz, C18, C_{ipso}), 128.9 (d,

$^2J_{\text{PC}} = 10$ Hz, C19, ArC), 130.0 (C21, ArC), 131.0 (C11 and C13, ArC), 133.2 (C5, ArC), 133.6

(C3, ArC), 133.7 (d, $^3J_{\text{PC}} = 12$ Hz, C20, ArC), 143.5 (C9, C_{ipso}), 147.5 (C12, C_{ipso}), 164.1 (d, $^1J_{\text{CP}}$

$= 24$ Hz, C2, C_{ipso}).

$^{31}\text{P}\{\text{H}\}$ NMR (toluene- d_8 , 162 MHz, -71 °C): $\delta = -0.02$ (s, P1). ^1H NMR (C_7D_9 , 400 MHz, -70

°C): $\delta = 1.13$ (bs, H16 and H17, CH_3), 2.65 (bs, H15, CH), 6.04 (bs, H6, ArH), 6.37 (bs, H4,

ArH), 6.75 (bs, H5, ArH), 6.82 (bs, H19a and H21a), 6.97 (bs, H19 and H21, ArH), 7.05 (bs, H3,

ArH), 7.12 (bs, H10 and H14), 7.23 (bs, H11 and H13, ArH), 7.35 (bs, H20a, ArH), 7.48 (bs,

H20, ArH). $^{13}\text{C}\{^1\text{H}\}$ NMR (C_7D_9 , 101 MHz, -71 °C): $\delta = 24.0, 24.2$ (C16 and C17, CH_3), 34.0

(C15, CH), 116.9 (C6, ArC), 120.4 (C4, ArC), 121.9 (d, $^2J_{\text{PC}} = 38$ Hz, C7, C_{ipso}), 127.6 to 128.9

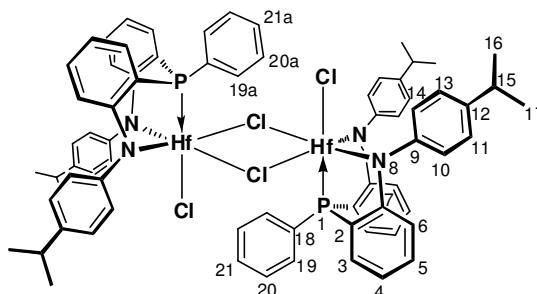
(C10, C14, C11 and C13, ArC, swamped by C_7H_8 solvent), 130.0 (d, $^1J_{\text{PC}} = 38$ Hz, C18, C_{ipso}),

130.2 (C19, ArC), 131.5 (C21, ArC), 132.9 (C5, ArC), 133.4 (C3, ArC), 134.0 (d, $^3J_{\text{PC}} = 10$ Hz,

C20, ArC), 144.1 (C9, C_{ipso}), 146.7 (C12, C_{ipso}), 164.1 (d, $^1J_{\text{CP}} = 22$ Hz, C2, C_{ipso}).

Anal. Calcd. for $\text{C}_{72}\text{H}_{70}\text{Cl}_4\text{N}_4\text{P}_2\text{Hf}_2$: C, 55.72; H, 4.55; N, 3.61; Found: C, 55.83; H, 4.55; N, 3.63.

EI-MS (m/z): 1232 (60, $[\text{M} - \text{HfCl}_4]^+$), 776 (100, $[\text{M} - \text{ipropNPNHfCl}_2]^+$), 761 (50, $[\text{M} -$



$^{\text{iprop}}\text{NPNHfCl}_2 - \text{Me}]^+$, 725 (20, $[\text{M} - ^{\text{iprop}}\text{NPNHfCl}_2 - \text{Me} - \text{Cl}]^+$), 709 (10, $[\text{M} - ^{\text{iprop}}\text{NPNHfCl}_2 - 2\text{Me} - \text{Cl}]^+$), 528 (30, $[\text{M} - ^{\text{iprop}}\text{NPNHfCl}_2 - \text{Hf} - 2\text{Cl} + 2\text{H}]^+$).

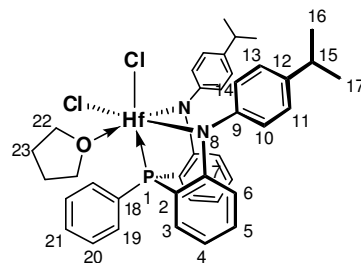
$^{\text{iprop}}\text{NPNHfCl}_2(\text{THF})$ [3.21] from $^{\text{iprop}}\text{NPNHf}(\text{NMe}_2)_2$ [3.19] / TMSCl / THF : Lemon yellow $^{\text{iprop}}\text{NPNHf}(\text{NMe}_2)_2$ [3.19] (0.33 g, 0.42 mmol) was dissolved in 10 cm³ toluene and TMSCl (0.32 cm³, 2.52 mmol) was added via syringe. The yellow solution was stirred for 3 days, forming an orange solution with an orange ppt. The toluene was removed *in vacuo* and the orange residue ($[\text{ipropNPNHfCl}_2]_2$ [3.20]) was dissolved in 5 cm³ THF, stirring for 1 day at room temperature. The THF was removed *in vacuo* and the yellow residue was triturated with 10 cm³ *n*-hexanes. The yellow solid was collected on a sintered glass frit, washing with *n*-hexanes (0.27 g, 0.32 mmol $^{\text{iprop}}\text{NPNHfCl}_2(\text{THF})$ [3.21], 76% based on $^{\text{iprop}}\text{NPNHf}(\text{NMe}_2)_2$). Single crystals of $^{\text{iprop}}\text{NPNHfCl}_2(\text{THF})$ [3.21] were grown by vapour diffusion of *n*-hexanes into a toluene solution at -40 °C.

$^{31}\text{P}\{\text{H}\}$ NMR (C_6D_6 , 162 MHz): $\delta = 5.44$ (s, P1). ^1H NMR

(C_6D_6 , 400 MHz): $\delta = 0.93$ (s, 4 H23, CH₂), 1.13 (d, $^3J_{\text{HH}} =$

7 Hz, 6 H16 and 6 H17, CH₃), 2.72 (hep, $^3J_{\text{HH}} = 7$ Hz, 2

H15, CH), 3.92 (s, 4 H22, CH₂), 6.37 (t, $^3J_{\text{HH}} = ^4J_{\text{PH}} = 6$ Hz,



2 H6, ArH), 6.59 (t, $^3J_{\text{HH}} = 7$ Hz, 2 H4, ArH), 6.94 (t, $^3J_{\text{HH}} = 8$ Hz, 2 H5, ArH), 7.14 (bd, $^3J_{\text{HH}} = 9$ Hz, 2 H10, 2 H14, 2 H11, 2 H13, 2 H19 and H21, ArH), 7.29 (t, $^3J_{\text{HH}} = 7$ Hz, 2 H3, ArH), 7.88 (s,

2 H20, ArH). $^{13}\text{C}\{^1\text{H}\}$ NMR (C_6D_6 , 151 MHz): $\delta = 24.2$, 24.3 (C16 and C17, CH₃), 25.1 (C23,

CH₂), 34.0 (C15, CH), 74.5 (bs, C22, CH₂), 119.3 (d, $^3J_{\text{PC}} = 11$ Hz, C6, ArC), 120.6 (d, $^3J_{\text{PC}} = 5$

Hz, C4, ArC), 122.6 (d, $^2J_{\text{PC}} = 45$ Hz, C7, C_{ipso}), 128.3 (C10 and C14, ArC), 129.1 (d, $^2J_{\text{PC}} = 9$ Hz,

C19 and C21, ArC), 129.4 (d, $^1J_{\text{PC}} = 34$ Hz, C18, C_{ipso}), 130.1 (C11 and C13, ArC), 132.4 (C5,

ArC), 132.7 (C3, ArC), 133.2 (d, $^3J_{\text{PC}} = 11$ Hz, C20, ArC), 144.7 (C9, C_{ipso}), 146.3 (C12, C_{ipso}),

164.4 (d, $^1J_{\text{CP}} = 25$ Hz, C2, C_{ipso}). Anal. Calcd. for $\text{C}_{40}\text{H}_{43}\text{Cl}_2\text{N}_2\text{OPHf}$: C, 56.64; H, 5.11; N, 3.30;

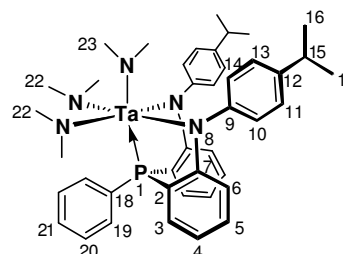
Found: C, 55.97; H, 5.20; N, 3.20. EI-MS (m/z): 776 (100, $[M - \text{THF}]^+$), 761 (40, $[M - \text{THF} - \text{Me}]^+$), 725 (10, $[M - \text{THF} - \text{Me} - \text{Cl}]^+$), 528 (80, $[M - \text{THF} - \text{Hf} - 2\text{Cl} + 2\text{H}]^+$).

^{iprop}NPNTa(NMe₂)₃ [4.1] In the glovebox, 30 cm³ THF was added to the solid mixture of [^{iprop}NPnLi₂·diox]_n [2.6] (2.80 g, 4.46 mmol) and NMe₃·HCl (0.27 g, 13.30 mmol). The orange solution was stirred at room temperature for 19 hrs, gradually discolouring. The THF solvent was removed *in vacuo* and the residue extracted with 20 cm³ toluene. The toluene mixture was filtered through celite with a sintered glass frit, washing with 3 x 10 cm³ toluene. The toluene solvent was removed *in vacuo* from the filtrate and the yellow oil dried (2.32 g, 4.40 mmol ^{iprop}NPNH₂ [2.10], 99% yield based on [^{iprop}NPnLi₂·diox]_n [2.6]). Orange Ta(NMe₂)₅ (1.68 g, 4.18 mmol) dissolved in 20 cm³ toluene was added to the ^{iprop}NPNH₂ [2.10] residue. This mixture was placed in a thick-walled flask under reduced pressure and stirred for 2.4 days at 125 °C, resulting in a dark red solution. The toluene solvent was removed *in vacuo* and the residue was dissolved in 10 cm³ *n*-pentanes. The *n*-pentanes solvent was removed *in vacuo*, giving an orange foam^(a) that was dissolved in a second aliquot 10 cm³ *n*-pentanes and the solution was placed in the freezer (-40 °C). The resulting orange solid was collected on a chilled sintered glass frit (0.27 g) and the *n*-pentanes solvent was removed from the filtrate, leaving an orange foam (2.12 g).^(b) An amount of the orange solid was recrystallised from *n*-pentanes to give pure ^{iprop}NPNTa(NMe₂)₃ [4.1].

³¹P{¹H} NMR (C₆D₆, 162 MHz): δ = 13.00 (s, P1). ¹H NMR

(C₆D₆, 400 MHz): δ = 1.32, 1.33 (d's, ³J_{HH} = 7 Hz, 6 H16 and 6 H17, CH₃), 2.90 (hep, ³J_{HH} = 7 Hz, 2 H15, CH), 3.28 (s, 6 H23, N-CH₃), 3.44 (s, 12 H22, N-CH₃), 6.76 (m, ³J_{HH} = 6 Hz, ⁴J_{PH} = 4 Hz, 2 H4 and 2 H6, ArH), 6.89 (bs, H21, ArH), 7.09

(t, ³J_{HH} = 8 Hz, 2 H5, ArH), 7.19 (d, ³J_{HH} = 8 Hz, 2 H10 and 2 H14, ArH), 7.25 (m, ³J_{HH} = 8 Hz, 2 H11, 2 H13 and 2 H20, ArH), 7.43 (t, ³J_{HH} = ³J_{PH} = 7 Hz, 2 H3, ArH), 7.89 (t, ³J_{HH} = ³J_{PH} = 8 Hz,



2 H19, ArH). $^{13}\text{C}\{^1\text{H}\}$ NMR (C_6D_6 , 151 MHz): δ = 24.5, 24.6 (C16 and C17, CH_3), 33.9 (C15, CH), 47.7 (d, $^3J_{\text{PC}}$ = 1 Hz, C23, N- CH_3), 48.3 (d, $^3J_{\text{PC}}$ = 3 Hz, C22, N- CH_3), 119.9 (d, $^3J_{\text{PC}}$ = 6 Hz, C6, ArC), 121.5 (d, $^3J_{\text{PC}}$ = 6 Hz, C4, ArC), 124.7 (d, $^2J_{\text{PC}}$ = 45 Hz, C7, C_{ipso}), 126.2 (C10 and C14, ArC), 126.9 (C21, ArC), 128.9, 129.0 (C11 and C13, ArC), 129.3 (C20, ArC), 130.7 (C5, ArC), 131.2 (d, $^1J_{\text{PC}}$ = 22 Hz, C18, C_{ipso}), 131.6 (C3, ArC), 133.3 (d, $^2J_{\text{PC}}$ = 11 Hz, C19, ArC), 142.3 (C12, C_{ipso}), 152.6 (C9, C_{ipso}), 165.3 (d, $^1J_{\text{CP}}$ = 23 Hz, C2, C_{ipso}). Anal. Calcd. for $\text{C}_{42}\text{H}_{53}\text{N}_5\text{PTa}$ + 0.43 C_6D_6 ^(c): C, 61.12; H, 6.69; N, 8.00; Found: C, 60.75; H, 6.50; N, 7.17. EI-MS (m/z): 839 (10, $[\text{M}]^+$), 795 (100, $[\text{M} - \text{NMe}_2]^+$), 750 (20, $[\text{M} - 2\text{NMe}_2]^+$), 736 (20, $[\text{M} - 2\text{NMe}_2 - \text{Me}]^+$), 707 (5, $[\text{M} - 3\text{NMe}_2]^+$).

^(a) the orange foam was pure $^{\text{iprop}}\text{NPNTa}(\text{NMe}_2)_3$ **[4.1]** with a single peak at δ 13.00 in the $^{31}\text{P}\{^1\text{H}\}$ NMR spectrum.

^(b) Both the orange solid and foamy residue had 9% and 7%, respectively, of an impurity at δ 1.87, resulting in crude yields of 7% (0.24 g, 0.29 mmol $^{\text{iprop}}\text{NPNTa}(\text{NMe}_2)_3$ **[4.1]**) and 56% (1.97 g, 2.35 mmol $^{\text{iprop}}\text{NPNTa}(\text{NMe}_2)_3$ **[4.1]**), respectively and a cumulative yield of 7 + 56 = 63%, based on $\text{Ta}(\text{NMe}_2)_5$. This was reacted further with TMSCl (see synthesis **[4.4]**), where all impurities were removed from the resulting $^{\text{iprop}}\text{NPNTaCl}_3$ **[4.4]** via recrystallisation from toluene / *n*-hexanes.

^(c) the sample submitted for elemental analysis was sourced from an NMR sample from which the C_6D_6 had been removed *in vacuo*.

$^{\text{tol}}\text{NPNTa}(\text{NMe}_2)_3$ **[4.2]** In the glovebox, $^{\text{tol}}\text{NPNH}_2$ **[2.11]** (1.55g, 3.10 mmol) and $\text{Ta}(\text{NMe}_2)_5$ (1.18 g, 2.94 mmol) were dissolved in 40 cm^3 toluene in a thick-walled flask under reduced pressure. The reaction mixture was stirred for 2 days at 143 °C, resulting in an orange solution with an orange ppt. The toluene solvent was removed *in vacuo* and the orange residue was triturated with 10 cm^3 *n*-hexanes. The *n*-hexanes solvent was removed *in vacuo*, and the residue

was suspended in a second aliquot 20 cm³ *n*-hexanes and placed in the freezer (-40 °C). The resulting yellow-orange solid was collected on a chilled sintered glass frit, washing with 15 cm³ cold *n*-pentanes (1.71 g, 0.40 mmol ¹⁰¹NPNTa(NMe₂)₃ [**4.2**], 72% yield based Ta(NMe₂)₅). Single crystals of ¹⁰¹NPNTa(NMe₂)₃ [**4.2**] were grown by vapour diffusion of *n*-hexanes into a toluene solution in the freezer.

³¹P{¹H} NMR (C₆D₆, 162 MHz): δ = 12.48 (s, P1). ¹H NMR (C₆D₆,

400 MHz): δ = 2.00 (s, 6 H16, CH₃), 2.22 (s, 6 H15, CH₃), 3.22 (s, 6 H22, N-CH₃), 3.32 (s, 12 H21, N-CH₃), 6.65 (d of d, ³J_{HH} = 8 Hz,

⁴J_{PH} = 6 Hz, 2 H6, ArH), 6.77 (bd, ³J_{HH} = 6 Hz, H20, ArH), 6.83 (d,

³J_{HH} = 8 Hz, 2 H5, ArH), 7.01 (d, ³J_{HH} = 8 Hz, 2 H10 and 2 H14,

ArH), 7.13 (m, ³J_{HH} = 8 Hz, 2 H11, 2 H13 and 2 H19, ArH), 7.29 (d, ³J_{PH} = 7 Hz, 2 H3, ArH),

7.86 (t, ³J_{HH} = ³J_{PH} = 8 Hz, 2 H18, ArH). ¹³C{¹H} NMR (C₆D₆, 101 MHz): δ = 20.6 (C16, CH₃),

20.9 (C15, CH₃), 48.0 (d, ³J_{PC} = 1 Hz, C22, N-CH₃), 48.3 (d, ³J_{PC} = 2 Hz, C21, N-CH₃), 122.1 (d,

³J_{PC} = 6 Hz, C6, ArC), 124.9 (d, ²J_{PC} = 44 Hz, C7, C_{ipso}), 126.6 (C20, ArC), 128.3 (C11 and C13,

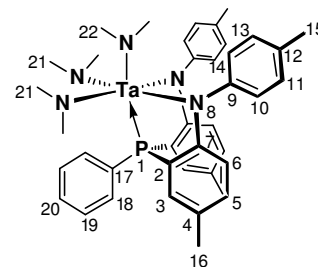
ArC), 128.9 (C10 and C14, ArC), 129.0 (d, ³J_{PC} = 8 Hz, C19, ArC), 129.1 (C12, C_{ipso}), 129.2 (d,

¹J_{PC} = 26 Hz, C17, C_{ipso}), 130.6 (C3, ArC), 131.3 (C4, C_{ipso}), 131.8 (C5, ArC), 133.3 (d, ²J_{PC} = 11

Hz, C18, ArC), 152.7 (C9, C_{ipso}), 163.2 (d, ¹J_{CP} = 23 Hz, C2, C_{ipso}). Anal. Calcd. for

C₄₀H₄₉N₅PTa: C, 59.18; H, 6.08; N, 8.63; Found: C, 59.31; H, 6.30; N, 7.66. EI-MS (*m/z*): 811

(10, [M]⁺), 767 (100, [M - NMe₂]⁺), 723 (20, [M - 2NMe₂]⁺), 708 (20, [M - 2NMe₂ - Me]⁺).



^{Ph}NPNTa(NMe₂)₃ [**4.3**] In the glovebox, ^{Ph}NPNH₂ [**2.12**] (1.95 g, 4.38 mmol) and Ta(NMe₂)₅

(1.67 g, 4.16 mmol) were dissolved in 40 cm³ toluene in a thick-walled flask under reduced

pressure. The reaction mixture was stirred for 18.6 hrs at 142 - 148 °C, resulting in an orange

solution. The toluene solvent was removed *in vacuo* and the orange residue was triturated with 20

cm³ *n*-hexanes. The *n*-hexanes solvent was removed *in vacuo*, and the residue was suspended in

20 cm³ *n*-pentanes and placed in the freezer (-40 °C). The resulting yellow solid was collected on

a chilled sintered glass frit, washing with 3 x 7 cm³ cold *n*-pentanes (2.18 g, 2.89 mmol

^{Ph}NPNTa(NMe₂)₃, 69% yield based Ta(NMe₂)₅).

³¹P{¹H} NMR (C₆D₆, 162 MHz): δ = 13.04 (s, P1). ¹H NMR

(C₆D₆, 600 MHz): δ = 3.14 (s, 6 H₂₀, N-CH₃), 3.29 (s, 12 H₁₉,

N-CH₃), 6.64 (m, ³J_{HH} = ⁴J_{PH} = 7 Hz, 2 H₄ and 2 H₆, ArH), 6.80

(bs, H₁₈, ArH), 6.90 (t, ³J_{HH} = 7 Hz, 2 H₁₂, ArH), 6.97 (t, ³J_{HH} =

8 Hz, 2 H₅, ArH), 7.10 (m, ³J_{HH} = ⁴J_{PH} = 8 Hz, 2 H₁₀, 2 H₁₄, 2 H₁₁, 2 H₁₃ and 2 H₁₇, ArH),

7.30 (t, ³J_{PH} = ³J_{HH} = 7 Hz, 2 H₃, ArH), 7.75 (t, ³J_{HH} = ³J_{PH} = 8 Hz, 2 H₁₆, ArH). ¹³C{¹H}[NMR

(C₆D₆, 101 MHz): δ = 47.8 (d, ³J_{PC} = 2 Hz, C₂₀, N-CH₃), 48.2 (d, ³J_{PC} = 3 Hz, C₁₉, N-CH₃),

120.2 (d, ³J_{PC} = 5 Hz, C₆, ArC), 121.8 (C₁₂, ArC), 121.9 (d, ³J_{PC} = 6 Hz, C₄, ArC), 125.0 (d, ²J_{PC} = 45 Hz, C₇, C_{ipso}), 126.7 (C₁₈, ArC), 128.5 (C₁₁ and C₁₃, ArC), 129.0 (d, ³J_{PC} = 8 Hz, C₁₇,

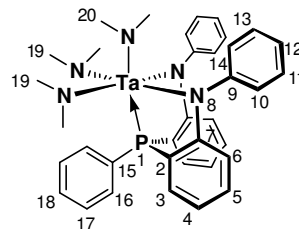
ArC), 129.3 (C₁₀ and C₁₄, ArC), 130.7 (C₅, ArC), 131.0 (d, ¹J_{PC} = 11 Hz, C₁₅, C_{ipso}), 131.5 (C₃,

ArC), 133.2 (d, ²J_{PC} = 11 Hz, C₁₆, ArC), 155.1 (C₉, C_{ipso}), 164.9 (d, ¹J_{CP} = 23 Hz, C₂, C_{ipso}).

Anal. Calcd. for C₃₆H₄₁N₅PTa + 0.54 C₆H₁₄: C, 58.75; H, 6.10; N, 8.73; Found: C, 58.34; H,

5.97; N, 7.61. EI-MS (*m/z*): 755 (0.3, [M]⁺), 711 (100, [M - NMe₂]⁺), 666 (20, [M - 2NMe₂]⁺),

652 (20, [M - 2NMe₂ - Me]⁺).



^{iprop}NPNTaCl₃ [4.4] (a) from ^{iprop}NPNH₂ [2.10]/ TaCl₃(NMe₂)₂(THF): Separate solutions of

light yellow ^{iprop}NPNH₂ [2.10] (0.35 g, 0.66 mmol) and orange TaCl₃(NMe₂)₂(THF) (0.29 g, 0.65

mmol) in 20 cm³ toluene each were placed in the freezer at -30 °C for 5.6 hrs. The solutions were

removed from the freezer and the TaCl₃(NMe₂)₂(THF) solution was quickly added via pipette to

the ^{iprop}NPNH₂ [2.10] solution. After the orange solution was stirred at room temperature for 2

days, the toluene solvent was removed *in vacuo*. The resulting orange residue^(a) was re-dissolved

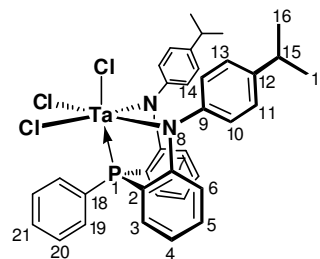
in 10 cm³ toluene in a thick-walled glass reaction flask and stirred at 60 °C for 2.5 days, forming

a darker reddish brown solution. The toluene solvent was removed *in vacuo* and the residue^(a)

was re-dissolved in toluene, placed under reduced pressure and stirred at 95 °C for 2.5 days. The

toluene solvent was removed *in vacuo* and the red-brown residue was triturated with 10 cm³ *n*-hexanes overnight and placed in the freezer. The brown solid was collected on a chilled sintered glass frit and washed with minimal cold *n*-pentanes.^(b) **(b) from** ^{iprop}NPNTa(NMe₂)₃ **[4.1]/**
TMSCl: Orange ^{iprop}NPNTa(NMe₂)₃ **[4.1]** (1.98 g, 2.19 mmol^(c)) was dissolved in 20 cm³ toluene in a thick-walled reaction flask and TMSCl (28 cm³, 221 mmol) was added with no visible colour change. The reaction mixture was placed under reduced pressure and heated to 140-143 °C for 2 days, resulting in a dark brown solution. The toluene solvent was removed *in vacuo* and the residue was triturated with 20 cm³ *n*-hexanes. The *n*-hexanes was removed *in vacuo* and the residue re-suspended in 10 cm³ *n*-hexanes and placed in the freezer for 25 min (-40 °C). The dark solid was collected on a sintered glass frit and washed with 20 cm³ *n*-hexanes (1.72 g)^(d) This solid was dissolved in 20 cm³ toluene, forming a dark purple solution, which was layered with 30 cm³ *n*-pentanes and placed in the freezer. The dark purple-brown crystals were collected on a sintered glass frit and washed with 30 cm³ *n*-pentanes (0.71 g, 1.73 mmol ^{iprop}NPNTaCl₃ **[4.4]**, 40% yield based on ^{iprop}NPNTa(NMe₂)₃ **[4.1]**).

³¹P{¹H} NMR (C₆D₆, 162 MHz, 25 °C): δ = 37.82 (s, P1). ¹H NMR (C₆D₆, 600 MHz, 25 °C): δ = 1.06 (d, ³J_{HH} = 7 Hz, 6 H16 and 6 H17, CH₃), 2.65 (hep, ³J_{HH} = 7 Hz, 2 H15, CH), 6.25 (bs, H21, ArH), 6.62 (bt, ³J_{HH} = ⁴J_{PH} = 7 Hz, 2 H4 and 2 H6, ArH), 6.94 (bs, 2 H5 and 2 H20, ArH), 7.04 (bs, 2 H10 and 2 H14, ArH), 7.06 (d, ³J_{HH} = 8 Hz, 2 H11 and 2 H13, ArH), 7.27 (bs, 2 H3, ArH), 7.68 (bs, 2 H19, ArH). ³¹P{H} NMR (toluene-*d*₈, 162 MHz, -70 °C): δ = 36.16 (s, P1, major isomer 85%), 39.93 (s, P1, minor isomer 15%). ¹H NMR (toluene-*d*₈, 400 MHz, -70 °C): δ = 1.09 (bs, 6 H16 and 6 H17, CH₃), 2.57 (bs, 2 H15, CH), 5.98 (bs, 2 H4, ArH), 6.12 (bs, 2 H6, ArH), 6.55 (bs, H21, ArH), 6.80 (bs, 2 H5, ArH), 7.05 (bm, 2 H10, 2 H14, 2 H11, 2 H13, 2 H3 and 2 H20, ArH), 7.83 (bd, ³J_{HH} = 20 Hz, 2 H19, ArH).^(f) ³¹P{H} NMR (THF-*d*₈, 162 MHz, -70 °C): δ = 37.68 (s, P1, major isomer 89%), 41.66 (s, P1, minor isomer 11%). ¹H NMR (THF-



d_8 , 400 MHz, $-70\text{ }^\circ\text{C}$): $\delta = 1.27$ (bs, 6 H16 and 6 H17, CH_3), 2.94 (bm, $^3J_{\text{HH}} = 6\text{ Hz}$, 2 H15, CH), 5.74 (bd, $^3J_{\text{HH}} = 8\text{ Hz}$, 2 H4, ArH), 5.99 (t, $^3J_{\text{HH}} = ^4J_{\text{PH}} = 6\text{ Hz}$, 2 H6, ArH), 7.08 (m, $^3J_{\text{HH}} = 8\text{ Hz}$, 2 H5, ArH), 7.39 (t, $^3J_{\text{HH}} = ^3J_{\text{PH}} = 8\text{ Hz}$, 2 H3, ArH), 7.44 (d, $^3J_{\text{HH}} = 8\text{ Hz}$, 2 H10 and 2 H14, ArH), 7.52 (d, $^3J_{\text{HH}} = 8\text{ Hz}$, 2 H11 and 2 H13, ArH), 7.57 (t, $^3J_{\text{HH}} = ^3J_{\text{PH}} = 8\text{ Hz}$, 2 H19, ArH), 7.67 (bs, H21, ArH), 7.78 (bt, $^3J_{\text{HH}} = 8\text{ Hz}$, 2 H20, ArH).^(e) $^{13}\text{C}\{^1\text{H}\}$ NMR ($\text{THF-}d_8$, 151 MHz, $-70\text{ }^\circ\text{C}$): $\delta = 24.6$, 24.7 (C16 and C17, CH_3), 35.0 (C15, CH), 121.3 (d, $^3J_{\text{PC}} = 8\text{ Hz}$, C6, ArC), 130.7 (d, $^4J_{\text{PC}} = 6\text{ Hz}$, C5, ArC), 126.8 (d, $^2J_{\text{PC}} = 51\text{ Hz}$, C7, C_{ipso}), 128.2 (C10 and C14, ArC), 129.0 (C11 and C13, ArC), 129.9 (d, $^3J_{\text{PC}} = 11\text{ Hz}$, C4, ArC), 130.3 (C21, ArC), 132.7 (C19 and C20, ArC), 133.5 (d, $^1J_{\text{PC}} = 19\text{ Hz}$, C18, C_{ipso}), 134.1 (d, $^3J_{\text{PC}} = 9\text{ Hz}$, C3, ArC), 143.2 (C9, C_{ipso}), 152.6 (C12, C_{ipso}), 163.0 (d, $^1J_{\text{CP}} = 25\text{ Hz}$, C2, C_{ipso}).^(e) Anal. Calcd. for $\text{C}_{36}\text{H}_{35}\text{Cl}_3\text{N}_2\text{PTa}$: C, 53.12; H, 4.33; N, 3.44; Found: C, 51.87; H, 4.49; N, 3.78. EI-MS (m/z): 814 (100, $[\text{M}]^+$), 777 (40, $[\text{M} - \text{Cl}]^+$), 733 (10, $[\text{M} - \text{Cl} - \text{CH}(\text{Me}_2) + \text{H}]^+$).

(a) $^{31}\text{P}\{^1\text{H}\}$ NMR spectrum reflected unreacted $^{\text{iprop}}\text{NPNH}_2$ [**2.10**] ligand with no product peaks

(b) $^{31}\text{P}\{^1\text{H}\}$ NMR spectroscopy revealed a mixture of broad peaks at δ 37.84 ($^{\text{iprop}}\text{NPNTaCl}_3$ [**4.4**]), 28.46 and 27.63 and sharp peaks at δ 24.66, 20.10, 19.68, 19.34, 18.91 and -1.06 in C_6D_6 .

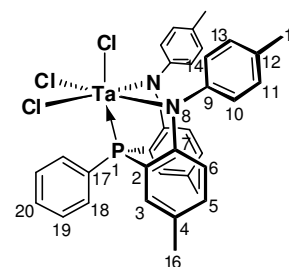
(c) the orange solid $^{\text{iprop}}\text{NPNTa}(\text{NMe}_2)_3$ [**4.1**] had 7% of an impurity at δ 1.87 observed in the $^{31}\text{P}\{^1\text{H}\}$ NMR spectrum, hence 93% of 1.98 g = 1.84 g, 2.19 mmol)

(d) $^{31}\text{P}\{^1\text{H}\}$ NMR spectroscopy revealed 82% $^{\text{iprop}}\text{NPNTaCl}_3$ [**4.4**] with impurities at δ 25.02 (8%) and δ 19.41 (10%).

(e) ^1H and $^{13}\text{C}\{^1\text{H}\}$ NMR data are for major isomer only as concentration of minor isomer was too low for characterisation. After the low temperature measurements, precipitated solids were observed in the solutions.

¹⁰¹NPNTaCl₃ [4.5]: Yellow-orange ¹⁰¹NPNTa(NMe₂)₃ [4.2] (6.98 g, 8.60 mmol) was dissolved in 80 cm³ toluene in a thick-walled reaction flask and TMSCl (110 cm³, 867 mmol) was added with no visible colour change. The reaction mixture was placed under reduced pressure and heated to 135 °C for 2 days, resulting in a dark brown solution. The toluene solvent was removed *in vacuo* with heating and the residue was triturated with a mixture of 10 cm³ toluene / 20 cm³ *n*-hexanes. The solvent was removed *in vacuo* and the brown residue suspended in 40 cm³ *n*-hexanes. The dark brown solid was collected on a sintered glass frit and washed with 30 cm³ *n*-hexanes (5.83 g, 4.32 mmol ¹⁰¹NPNTaCl₃ [4.5], 86% yield based on ¹⁰¹NPNTa(NMe₂)₃ [4.2]).

³¹P{¹H} NMR (C₆D₆, 162 MHz, 25 °C): δ = 36.77 (s, P1). ¹H NMR (C₆D₆, 600 MHz, 25 °C): δ = 1.99 (s, 6 H16, CH₃), 2.04 (s, 6 H15, CH₃), 6.27 (bs, 2 H18, ArH), 6.84 (d, ³J_{HH} = 8 Hz, 2 H6, ArH), 6.99 (d, ³J_{HH} = 7 Hz, 2 H10, 2 H14, 2 H11 and 2 H13, ArH), 7.03 (bs, 2 H19, ArH), 7.06 (bd, ³J_{HH} = 5 Hz, 2 H5, ArH), 7.35 (d, ³J_{PH} = 5 Hz, 2



H3), 7.70 (bs, H20, ArH). ³¹P{¹H} NMR (toluene-*d*₈, 162 MHz, -70 °C): δ = 35.89 (s, P1, major isomer 68%), 40.64 (s, P1, minor isomer 32%). ¹H NMR (toluene-*d*₈, 400 MHz, -70 °C): δ = 1.90 (s, 6 H16, CH₃), 2.03 (s, 6 H15, CH₃), 6.13 (d of d, ³J_{HH} = 8 Hz, ⁴J_{PH} = 5 Hz, 2 H6, ArH), 6.34 (d, ³J_{HH} = 8 Hz, 2 H18, ArH), 6.68 (d, ³J_{HH} = 9 Hz, 2 H5, ArH), 6.91 (m, ³J_{HH} = 9 Hz, 2 H10, 2 H14, 2 H11, 2 H13 and 2 H19, ArH), 7.25 (d, ³J_{PH} = 8 Hz, 2 H3), 7.76 (t, ³J_{HH} = 9 Hz, H20, ArH).***

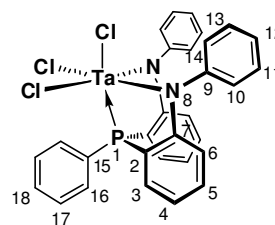
³¹P{¹H} NMR (THF-*d*₈, 162 MHz, -70 °C): δ = 35.82 (s, P1, major isomer 86%), 40.57 (s, P1, minor isomer 14%). ¹H NMR (THF-*d*₈, 400 MHz, -70 °C): δ = 2.38 (s, 6 H16, CH₃), 2.40 (s, 6 H15, CH₃), 5.91 (m, ³J_{HH} = ⁴J_{PH} = 8 Hz, 2 H6, ArH), 7.05 (d, ³J_{PH} = 8 Hz, 2 H3), 7.20 (d, ³J_{HH} = 8 Hz, 2 H5, ArH), 7.34 (d, ³J_{HH} = 5 Hz, 2 H18, ArH), 7.41 (m, ³J_{HH} = 8 Hz, 2 H10, 2 H14, 2 H11 and 2 H13, ArH), 7.67 (bs, H20, ArH), 7.79 (bt, ³J_{HH} = 8 Hz, 2 H19, ArH). ^(a)¹³C{¹H} NMR (THF-*d*₈, 101 MHz, -70 °C): δ = 20.6 (C16, CH₃), 21.3 (C15, CH₃), 121.3 (d, ³J_{PC} = 9 Hz, C6, ArC), 127.1 (d, ²J_{PC} = 50 Hz, C7, C_{ipso}), 129.9 (C20, ArC), 130.1 (d, ²J_{PC} = 5 Hz, C18, ArC),

131.0 (d, $^2J_{PC} = 24$ Hz, C3, ArC), 132.3 (C10 and C14, ArC), 132.6 (C4, C_{ipso}), 133.1 (C11 and C13, ArC), 134.0 (C5, ArC), 134.1 (C19, ArC), 136.4 (d, $^1J_{PC} = 6$ Hz, C17, C_{ipso}), 139.1 (C9, C_{ipso}), 143.4 (C12, C_{ipso}), 160.8 (d, $^1J_{CP} = 25$ Hz, C2, C_{ipso}).^(a) Anal. Calcd. for C₃₄H₃₁Cl₃N₂PTa: C, 51.96; H, 3.98; N, 3.56; Found: C, 51.86; H, 4.02; N, 3.78. EI-MS (m/z): 786 (100, [M]⁺), 768 (20, [M - Me + H]⁺), 749 (40, [M - Cl]⁺), 730 (20, [M - 4Me + 4H]⁺), 713 (10, [M - 2Cl]⁺).

^(a) 1H and $^{13}C\{^1H\}$ NMR data are for major isomer only as concentration of minor isomer was too low for characterisation. After the low temperature measurements, precipitated solids were observed in the solutions.

^{Ph}NPNTaCl₃ [4.6] Yellow **^{Ph}NPNTa(NMe₂)₃ [4.3]** (2.03 g, 2.68 mmol) was dissolved in 20 cm³ toluene in a thick-walled reaction flask and TMSCl (34 cm³, 268 mmol) was added with no visible colour change. The reaction mixture was placed under reduced pressure and heated to 140 °C for 5 days, resulting in a dark brown solution. The toluene solvent was removed *in vacuo* with heating and the residue was triturated with 30 cm³ *n*-hexanes. The dark brown solid was collected on a sintered glass frit and washed with 40 cm³ *n*-hexanes (1.41 g).^(a) This solid was dissolved in 10 cm³ toluene with heating (60 °C), forming a dark solution, which was layered with 7 cm³ *n*-hexanes and placed in the freezer. The brown powder was collected on a sintered glass frit and washed with 15 cm³ *n*-pentanes (1.06 g).^(b) The brown powder was dissolved with heating (60 °C) in 40 cm³ toluene and the solution was filtered hot through celite on a sintered glass frit. The solvent was removed *in vacuo* from the filtrate and the residue dissolved in 10 cm³ toluene, layered with *n*-hexanes and placed in the freezer. The dark brown crystals were collected on a sintered glass frit and washed with *n*-hexanes (0.55 g, 0.75 mmol **^{Ph}NPNTaCl₃ [4.6]**, 28% yield based on **^{tol}NPNTa(NMe₂)₃ [4.2]**). Single crystals of **^{Ph}NPNTaCl₃ [4.6]** were grown by vapour diffusion of *n*-hexanes into a toluene solution in the freezer.

$^{31}\text{P}\{^1\text{H}\}$ NMR (C_6D_6 , 162 MHz, 25 °C): δ = 36.04 (s, P1). ^1H NMR (C_6D_6 , 400 MHz, 25 °C): δ = 6.14 (bt, $^3J_{\text{HH}} = ^3J_{\text{PH}} = 11$ Hz, 2 H16, ArH), 6.60 (t, $^3J_{\text{HH}} = ^4J_{\text{PH}} = 7$ Hz, 2 H6, ArH), 6.93 (m, $^3J_{\text{HH}} = ^4J_{\text{PH}} = 7$ Hz, 2 H4 and 2 H12, ArH), 7.02 (bs, 2 H10, 2 H14 and 2 H17, ArH), 7.08 (bt, $^3J_{\text{HH}} = 7$ Hz, 2 H11, 2 H13 and 2 H5, ArH), 7.24 (t, $^3J_{\text{PH}} = ^3J_{\text{HH}} = 8$ Hz, 2 H3), 7.61 (bs, H18, ArH). $^{31}\text{P}\{^1\text{H}\}$ NMR (toluene- d_8 , 162 MHz, -70 °C): δ = 35.25 (s, P1, major isomer 81%), 40.57 (s, P1, minor isomer 19%). $^{31}\text{P}\{^1\text{H}\}$ NMR (THF- d_8 , 162 MHz, -70 °C): δ = 35.74 (s, P1, major isomer 84%), 41.65 (s, P1, minor isomer 16%). ^1H NMR (THF- d_8 , 400 MHz, -70 °C): δ = 6.00 (bd, $^3J_{\text{HH}} = ^4J_{\text{PH}} = 5$ Hz, 2 H4 and 2 H6, ArH), 7.11 (t, $^3J_{\text{HH}} = 7$ Hz, 2 H12, ArH), 7.24 (t, $^3J_{\text{PH}} = ^3J_{\text{HH}} = 8$ Hz, 2 H3), 7.33 (t, $^3J_{\text{HH}} = ^3J_{\text{PH}} = 7$ Hz, 2 H16, ArH), 7.40 (t, $^3J_{\text{HH}} = 8$ Hz, 2 H5, ArH), 7.57 (m, $^3J_{\text{HH}} = 9$ Hz, 2 H10, 2 H14, 2H11 and 2 H13, ArH), 7.69 (bs, H18, ArH), 7.81 (t, $^3J_{\text{HH}} = 8$ Hz, 2 H17, ArH). $^{(c)}^{13}\text{C}\{^1\text{H}\}$ NMR (THF- d_8 , 101 MHz, -70 °C): δ = 121.4 (d, $^3J_{\text{PC}} = 12$ Hz, C6, ArC), 126.5 (d, $^2J_{\text{PC}} = 13$ Hz, C16, ArC), 126.9 (d, $^2J_{\text{PC}} = 67$ Hz, C7, C_{ipso}), 129.0 (C4, ArC), 129.9 (C10 and C14, ArC), 130.1 (C12, ArC), 130.5 (d, $^2J_{\text{PC}} = 19$ Hz, C3, ArC), 132.3 (C11 and C13, ArC), 132.8 (C18, ArC), 133.3 (C5, ArC), 133.5 (C17, ArC), 133.9 (d, $^1J_{\text{PC}} = 13$ Hz, C15, C_{ipso}), 146.5 (C9, C_{ipso}), 162.9 (d, $^1J_{\text{CP}} = 25$ Hz, C2, C_{ipso}). $^{(c)}$ Anal. Calcd. for $\text{C}_{30}\text{H}_{23}\text{Cl}_3\text{N}_2\text{PTa} + 0.05 \text{C}_7\text{H}_8$: C, 49.65; H, 3.21; N, 3.81; Found: C, 49.90; H, 3.39; N, 3.48. EI-MS (m/z): 730 (90, $[\text{M}]^+$), 693 (50, $[\text{M} - \text{Cl}]^+$), 659 (20, $[\text{M} - 2\text{Cl}]^+$).



$^{(a)} ^{31}\text{P}\{^1\text{H}\}$ NMR spectroscopy revealed peaks at δ 53.35 (4%), 43.68 (4%), 27.87 (28%) and 18.40 (8%) together with 56% $^{\text{Ph}}\text{NPNTaCl}_3$ [**4.6**] at δ 36.13 in C_6D_6 .

$^{(b)} ^{31}\text{P}\{^1\text{H}\}$ NMR spectroscopy revealed peaks at δ 53.32 (9%) and 27.96 (21%) together with 70% $^{\text{Ph}}\text{NPNTaCl}_3$ [**4.6**] at δ 36.11 in C_6D_6 .

(c) ^1H and $^{13}\text{C}\{^1\text{H}\}$ NMR data are for major isomer only as concentration of minor isomer was too low for characterisation. After the low temperature measurements, precipitated solids were observed in the solutions.

$[\text{ipropNPNTaCl}]_x$: Reaction of $[\text{TaCl}_3(\text{PMe}_3)_2]_2$ with $[\text{ipropNPnLi}_2\cdot\text{diox}]_n$: Inside the glovebox, separate solutions of yellow $[\text{ipropNPnLi}_2\cdot\text{diox}]_n$ (0.13 g, 0.20 mmol) in 10 cm^3 toluene and red $[\text{TaCl}_3(\text{PMe}_3)_2]_2$ (0.08 g, 0.10 mmol) in 5 cm^3 toluene were placed inside the freezer at $-40\text{ }^\circ\text{C}$. After 30 min, the two solutions were removed and the $[\text{ipropNPnLi}_2\cdot\text{diox}]_n$ solution was added to the $[\text{TaCl}_3(\text{PMe}_3)_2]_2$ solution and the mixture stirred at room temperature for 16.5 hrs, forming a reddish-brown solution. After NMR analysis, the toluene solution was allowed to stir at room temperature for 39 hrs. The toluene reaction mixture was filtered through celite with a sintered glass frit, washing with additional toluene. The toluene solvent was removed *in vacuo* and the residue was triturated with 2 cm^3 *n*-hexanes. The *n*-hexanes was removed *in vacuo*, and the residue was suspended in *n*-pentanes and placed in the freezer. The brown solid was collected on a sintered frit and combined with the brown residue obtained from the *n*-pentanes filtrate (11.9 mg).^(a) EI-MS (m/z): 1059 (20, unknown), 875(90, $[\text{TaCl}_3(\text{PMe}_3)_2]_2^+$), 742 (20, $[\text{ipropNPNTaCl}]^+$).^(b)

(a) $^{31}\text{P}\{^1\text{H}\}$ NMR spectroscopy revealed that the composition of the brown solid isolated and the brown filtrate residue were identical, with 1:1 doublets at δ 15.01 and -16.38 ($^2J_{\text{PP}} = 4\text{ Hz}$) for $\text{ipropNPNTaCl}(\text{PMe}_3)$, a singlet at δ -3.02 for $[\text{ipropNPNTaCl}]_x$, singlets at δ -30.71 and -51.71 for $[\text{TaCl}_3(\text{PMe}_3)_2]_2$ ^{74, 281} and an unidentified peak at δ -57.14.

(b) which may be a fragment ion of dimeric bridged chlorides $[\text{ipropNPNTaCl}(\text{PMe}_3)]_2$ or $[\text{ipropNPNTaCl}]_2$. Loss of PMe_3 may be possible while drying the solid under reduced pressure.

ipropNPNTaCl_3 [4.4] and $[\text{ipropNPNTaCl}_4][\text{ipropNPNTaCl}_2]$:^(c) **Reaction of $[\text{ipropNPnLi}_2\cdot\text{diox}]_n$ with $[\text{TaCl}_5]_2$:** A yellow solution of $\text{ipropNPnLi}_2\cdot\text{diox}$ (0.41 g, 0.65 mmol) in 20 cm^3 toluene and

a suspension of finely ground white $[\text{TaCl}_5]_2$ (0.22 g, 0.31 mmol) in 10 cm^3 toluene were separately placed in the freezer at -30°C . After 3 hrs the chilled $[\text{TaCl}_5]_2$ suspension was added to the chilled $[\text{ipropNPnLi}_2\cdot\text{diox}]_n$ solution at room temperature, progressively forming a lime-green to darker olive green to dark brown solution within 10 minutes. The reaction mixture was stirred for 16 hrs, filtered through celite with a sintered glass frit, washing with $2 \times 5 \text{ cm}^3$ toluene. The toluene solvent was removed *in vacuo* and the dark brown residue was dissolved in 10 cm^3 THF and stirred for 15.5 hrs. The THF solvent was removed and the brown residue dried was triturated 10 cm^3 *n*-hexanes. The mixture was placed in the freezer for 3.5 hrs. The brown solid was collected and washed with $1 \times 5 \text{ cm}^3$ cold *n*-pentanes (0.2475 g).^(a)

^(a) $^{31}\text{P}\{^1\text{H}\}$ NMR spectroscopy revealed a major product with a broad peak at δ 37.84 for ipropNPNTaCl_3 [4.4] with unidentified sharp peaks at δ 52.78, 29.08 and -53.08 in C_6D_6 . EI-MS (m/z): 850 (20, $[\text{ipropNPNTaCl}_4]$), 814 (100, $[\text{ipropNPNTaCl}_3]$), 777 (30, $[\text{ipropNPNTaCl}_2]$).

$^{\text{tol}}\text{NPNTaCl}_3$ [4.5] and $[\text{tolNPNTaCl}_4][\text{tolNPNTaCl}_2]$:^(c) Reaction of $^{\text{tol}}\text{NPNH}_2$ / KH with $[\text{TaCl}_5]_2$: White $^{\text{tol}}\text{NPNH}_2$ (0.10 g, 0.20 mmol) and KH (0.02 g, 0.45 mmol) were mixed as solids and 3 cm^3 THF was added. The yellow solution was stirred for 17.5 hrs before the THF was removed *in vacuo*. The yellow residue ($^{\text{tol}}\text{NPNK}_2\cdot 2\text{THF}$) was dissolved in 2 cm^3 toluene- d_8 and finely-ground $[\text{TaCl}_5]_2$ (0.07 g, 0.09 mmol) was added at room temperature, immediately forming a dark brown solution. After stirring at room temperature for 24 hrs^(a) the toluene- d_8 solvent was removed *in vacuo* and the brown residue re-dissolved in toluene. The solution was filtered through celite with a sintered glass frit, washing with additional toluene. The toluene solvent was removed from the filtrate and the residue was triturated with *n*-hexanes. The fine brown solid was collected on a sintered glass frit, washing with toluene (37 mg).^(b)

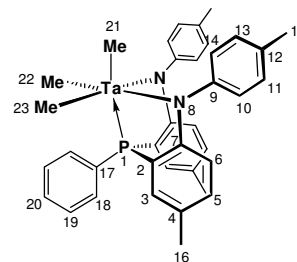
^(a) $^{31}\text{P}\{^1\text{H}\}$ NMR spectroscopy revealed sharp peaks at δ 40.07, -27.69 and -53.22 in toluene- d_8 .

^(b) After trituration with *n*-hexanes, the brown solid was insoluble in toluene-*d*₈ or CDCl₃ and the sample was only analysed with mass spectroscopy. EI-MS (*m/z*): 820 (40, [¹⁰¹NPNTaCl₄]), 786 (100, [¹⁰¹NPNTaCl₃]), 749 (80, [¹⁰¹NPNTaCl₂]).

^(c) Tantalum pentahalides [TaX₅]₂ are known to add a halide to form hexahalotantalates [TaX₆]⁻; for example the reaction of [TaX₅]₂ with a neutral donor L leads to the formation of neutral TaX₅L or ionic [TaX₄L₂]⁺[TaX₆]⁻ complexes.⁴¹⁰⁻⁴¹⁴ In a publication by F. Marchetti and G. Pampaloni, it is put forward that symmetrical breaking of the bridging Ta-X bonds of [TaX₅]₂ leads to formation of TaX₅L, whereas asymmetrical cleavage leads to formation of ionic complexes.⁴¹¹

¹⁰¹NPNTaMe₃ [4.7]: White ¹⁰¹NPNH₂ [2.11] (0.1698 g, 0.3392 mmol) and KH (0.03 g, 0.71 mmol) were mixed with 2 cm³ THF in a scintillation vial protected from light with foil. The reaction mixture was stirred at room temperature for 1.35 hrs before the THF solvent was removed *in vacuo*. To the resulting orange foam (¹⁰¹NPNK₂·2THF) was added TaMe₃Cl₂ (0.11 g, 0.35 mmol) and the solid mixture was chilled in freezer at -40 °C, together with a separate vial of 5 cm³ Et₂O. Thereafter the chilled Et₂O was added to the solids at room temperature, forming an orange solution with a white ppt. The Et₂O solvent was removed *in vacuo* immediately, toluene solvent added and the mixture was filtered through celite on a sintered glass frit, washing with additional toluene and protecting the filtrate from light with foil. The toluene solvent was removed *in vacuo* from the filtrate, leaving in orange oil. This oil was trituated with *n*-hexanes and the *n*-hexanes solvent was removed *in vacuo*. Fresh *n*-hexanes was added to the residue and the mixture was placed in freezer. The orange solid was collected on a chilled sintered glass frit, washing with chilled *n*-hexanes (0.03g, 0.05 mmol ¹⁰¹NPNTaMe₃ [4.7], 14% yield based on ¹⁰¹NPNH₂ [2.11]).

$^{31}\text{P}\{^1\text{H}\}$ NMR (C_6D_6 , 162 MHz): $\delta = 27.88$ (s, P1). ^1H NMR (C_6D_6 , 400 MHz): $\delta = 1.34$ (bs, 3 H21, 3 H22 and 3 H23, Ta-CH₃), 2.04 (s, 6 H16, CH₃), 2.09 (s, 6 H15, CH₃), 6.36 (d of d, $^4J_{\text{PH}} = 5$ Hz, $^3J_{\text{HH}} = 8$ Hz, 2 H6, ArH), 6.86 (d, $^3J_{\text{HH}} = 8$ Hz, 2 H5, ArH), 6.69 (bs, 2 H10 and 2 H14, ArH), 7.19 (bs, 2 H11, 2 H13, 2 H19 and H20, ArH), 7.41 (d, $^3J_{\text{PH}} = 6$ Hz, 2 H3), 7.86 (t, $^3J_{\text{HH}} = ^3J_{\text{PH}} = 8$ Hz, 2 H18, ArH).



$^{101}\text{NPNTaMe}_3$ [4.7] with species \mathbf{u}_{tol} : White $[^{101}\text{NPNLi}_2 \cdot 1.5\text{TMEDA}]_2$ [2.7] (0.35 g, 0.56 mmol) suspended in 2.5 cm³ toluene and TaMe_3Cl_2 (0.15 g, 0.50 mmol) dissolved 2.5 cm³ toluene were placed in the freezer at -40 °C. Immediately on removal from the freezer, the TaMe_3Cl_2 solution was added to the $[^{101}\text{NPNLi}_2 \cdot 1.5\text{TMEDA}]_2$ [2.7] mixture. After 2 min at room temperature the resulting orange reaction mixture was filtered through celite on a chilled sintered glass frit and THF was added to the orange filtrate, which was protected from light with foil. After 2 min, the THF / toluene solvent was removed from the filtrate *in vacuo* and the orange film dried. After 2 days in the freezer the orange film was dissolved in C_6D_6 . After NMR analysis,^(a) the C_6D_6 sample was returned to the flask. Some toluene was added with a few drops 1,4-dioxane and the mixture was placed in the freezer. After 5 days the orange solid was collected on a sintered glass frit, washing with toluene.^(b)

^(a) $^{31}\text{P}\{^1\text{H}\}$ NMR spectroscopy of the crude orange film is similar to that reported for the orange solid isolated in the next step.

^(b) $^{31}\text{P}\{^1\text{H}\}$ NMR spectroscopy revealed peaks at $\delta 27.74$ (41%) $^{101}\text{NPNTaMe}_3$ [4.7] and $\delta 49.67$ (59%) species \mathbf{u}_{tol} . The ^1H NMR spectrum has a doublet at $\delta 1.65$ ($^3J_{\text{PH}} = 10$ Hz) for species \mathbf{u}_{tol} and a broad singlet at $\delta 1.34$ for $^{101}\text{NPNTaMe}_3$ [4.7]. No peaks were observed in the $^7\text{Li}\{^1\text{H}\}$ NMR spectrum.

^{iprop}NPNTaMe₃ [4.8] with species u_{ipr}: Yellow [^{iprop}NPnLi₂·diox]_n [2.6] (0.15 g, 0.25 mmol) and TaMe₃Cl₂ (0.08 g, 0.25 mmol) were added as solids to a NMR tube that was connected via a distillation bridge to a Schlenk flask with 0.8 cm³ toluene-d₈. The NMR tube was covered in foil and placed in a N₂(l) bath. The toluene-d₈ was vacuum-transferred to the NMR tube, which was sealed under vacuum. While the NMR instrument was being cooled down to 193 K (-80 °C), the NMR tube was warmed up to -78 °C with an ethanol / dry ice bath. When the NMR instrument had equilibrated at 193 K (-80 °C) the NMR sample was quickly removed from the ethanol / dry ice bath and the solvent melted with finger warmth before being placed in the NMR instrument. The temperature was increased step-wise up to a maximum of 348 K (75 °C). At each step, the temperature was allowed to equilibrate for 10 min before analysis. Thereafter the sample was removed from the NMR instrument and subjected to the following additional conditions:

- (i) 17.25 hrs in fridge at -5 °C
- (ii) 29 hrs at room temperature i.e. 23 °C
- (iii) 24.33 hrs in NMR heating block at 79 °C
- (iv) 5.81 days at room temperature i.e. 23 °C (no foil)
- (v) 27.25 hrs in NMR heating block at 73 °C (no foil)
- (vi) 14 days at room temperature i.e. 23 °C (no foil)
- (vii) 6 days at 80 °C (no foil)
- (viii) 2 days at 130 °C (no foil)
- (ix) 1.3 years at room temperature i.e. 23 °C (no foil)

Table 32 : $^{31}\text{P}\{^1\text{H}\}$ NMR spectroscopic data for the thermal / light decomposition study of $^{\text{iprop}}\text{NPNTaMe}_3$ [4.8].

| | Temperature (°C) | Equilibration Time | [4.8]: species u_{ipr} $\delta = 29.53:50.95^{(a)}$ | Side-products δ | Side-products % |
|------|---------------------|-----------------------|---|---|--------------------|
| | -80 | 0 min | 88:12 | 31.3, 31.8, 38.3, 39.9, 44.9 | 8 |
| | -80 | 10 min | 88:12 | 31.3, 31.8, 38.3, 39.9, 44.9 | 7 |
| | -70 | 10 min | 88:12 | 31.2, 31.8, 38.1, 40.0, 45.2 | 8 |
| | -45 | 10 min | 88:12 | 31.8, 32.2, 39.0, 43.4 | 9 |
| | -35 | 10 min | 88:12 | 31.9, 39.1 | 6 |
| | -15 | 10 min | 88:12 | 31.7, 32.0, 32.3, 39.4 | 7 |
| | 0 | 10 min | 88:12 | 32.2, 32.4, 39.6 | 8 |
| | 15 | 10 min | 87:13 | 32.4, 39.8 | 7 |
| | 30 | 10 min | 87:13 | 32.5, 40.0 | 9 |
| | 75 | 10 min | 82:18 | 33.1, 40.8 | 8 |
| i | -5 | 17.25 hrs | 80:20 | 32.4, 39.9, 51.8 | 8 |
| ii | 23 | 29.00 hrs | 78:22 | 32.4, 39.9, 51.8 | 9 |
| iii | 79 | 24.33 hrs | 60:40 | 30.2 - 32.4, 42.9, 51.8 | 10 |
| iv | 23 (no foil) | 5.81 days | 54:46 | 30.2 - 32.4, 51.9 | 17 |
| v | 73 (no foil) | 27.25 hrs | 50:50 | 30.2 - 34.4, 42.9, 51.8 | 23 |
| vi | 23 (no foil) | 14 days | 54:46 | 30.2 - 32.4, 51.9 | 17 |
| vii | 80 (no foil) | 6 days | 19:81 | 31.7 - 34.4, 42.9, 45.9, 50.6, 51.6, 51.8 | 45 |
| viii | 130 (no foil) | 2 days | 0:100 | -4.6, 12.5, 20.1, 24.3, 31.4 -34.5, 40.4, 44.8, 95.1 | 73 |
| ix | 23 (no foil) | 1.3 years | 0:0 | -3.8, 13.5, 32.5 -35.3, 45.7, 46.9, 51.5, 51.8, 95.9 | 100 |

^(a) relative integration of methine signal of the *iso*-propyl group with its associated methyl doublet at δ 1.15 ($^3J_{\text{HH}}$)

indicates that the trialkyl methyl signal for $^{\text{iprop}}\text{NPNTaMe}_3$ [4.8] occurs together with the methyl signal of the $^{\text{iprop}}\text{NPN}$ ligand. A doublet is observed to grow at δ 1.44 ($^3J_{\text{PH}} = 10$ Hz) for species u_{ipr} .

Attempted hydrogenation of $^{\text{iprop}}\text{NPNTaMe}_3$ [4.8] (and isolation of species u_{ipr}): (a) Yellow [$^{\text{iprop}}\text{NPNLi}_2\cdot\text{diox}$]_n [2.6] (0.41 g, 0.65 mmol) and TaMe_3Cl_2 (0.19 g, 0.65 mmol) were added as solids to a thick-walled glass flask and cooled to -196 °C with $\text{N}_2(\text{l})$. 20 cm³ Et_2O was vacuum transferred to the solids in the flask, thereafter the $\text{N}_2(\text{l})$ cooling bath was exchanged with an Et_2O /dry ice bath and the reaction mixture to warm up to -41 °C over 3.25 hrs under vacuum, forming an orange solution with a ppt. The Et_2O /dry ice bath was replaced with an ice bath and the reaction mixture was allowed to warm further to 0 °C, with no observable change.^(a) The reaction mixture was re-cooled to -196 °C with a $\text{N}_2(\text{l})$ bath and charged with 4 atm H_2 . The mixture was allowed to warm up slowly to room temperature over 17.2 hrs, resulting in a brown solution. The brown solution was re-cooled down to -196 °C with a $\text{N}_2(\text{l})$ bath and H_2 was evacuated from the frozen mixture. The reaction flask was charged with 4 atm N_2 at -196 °C and

then allowed to warm to room temperature over 3.6 hrs, with no observable change. The Et₂O solvent was removed *in vacuo* and the residue was triturated with 10 cm³ *n*-hexanes. The *n*-hexanes was immediately removed *in vacuo* and the brown residue was extracted with 10 cm³ toluene. The toluene mixture was filtered through celite on a sintered glass frit, washing with 2 x 10 cm³ toluene. The solvent was removed in vacuo from the dark brown filtrate and the dark brown residue was dissolved in 10 cm³ *n*-hexanes. The *n*-hexanes was removed *in vacuo* and the residue was re-dissolved in 10 cm³ *n*-hexanes and placed in the freezer at -35 °C. The brown solid was collected on a chilled sintered frit and washed with 2 x 2 cm³ cold *n*-hexanes (0.14 g)^(b);

(b) with ^{iprop}NPNTaMe₃ [4.8]: Separate solutions of yellow [^{iprop}NPNLi₂·diox]_n (0.40 g, 0.64 mmol) in 10 cm³ Et₂O and TaMe₃Cl₂ (0.25 g, 0.84 mmol) in 2.5 cm³ Et₂O were chilled in freezer at -30 °C for 1hr 35 min. Thereafter the chilled Et₂O solutions were added together at room temperature, forming a dark orange solution. After 14 hrs 45 min, the Et₂O solvent was removed *in vacuo*, toluene solvent added and the mixture filtered through celite on a sintered glass frit, washing with 2 x 5 cm³ toluene. The toluene solvent was removed *in vacuo* from the filtrate, leaving in brown foam. This foam was triturated with *n*-pentanes, forming a dark brown ppt with some lighter brown ppt. The mixture was dissolved in minimal toluene, *n*-pentanes added and placed in freezer. No crystallisation occurred, the solvent was removed in vacuo and the residue dried.^(c)

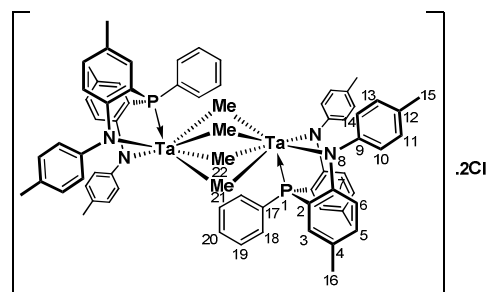
^(a) based on NMR spectroscopy data from previous reaction without H₂ at 0 °C after 10 min, a ratio of 88:12 is assumed for ^{iprop}NPNTaMe₃ [4.8]: **species u_{ipr}**.

^(b) single peak at δ 50.52 for **species u_{ipr}** in the ³¹P{H} NMR spectrum for crude and isolated product.

(c) $^{31}\text{P}\{^1\text{H}\}$ NMR spectroscopy revealed peaks at δ 28.97 (17%) $^{\text{iprop}}\text{NPNTaMe}_3$ [4.8] and δ 50.99 (83%) **species u_{ipr}**. The ^1H NMR spectrum has a doublet at δ 1.67 ($^3J_{\text{PH}} = 10$ Hz) for **species u_{ipr}**. Mass spectrum reveals a parent ion at 1474 m/z for $[\{^{\text{iprop}}\text{NPNTaMe}_2\}_2]^{2+}$ for **species u_{ipr}**.

Isolation of species u_{tol}: White $^{\text{tol}}\text{NPNH}_2$ (0.17 g, 0.34 mmol) and KH (0.02 g, 0.38 mmol) were mixed with 2 cm³ THF in a scintillation vial protected from light with foil. The reaction mixture was stirred at room temperature for 32 min before the THF solvent was removed *in vacuo*. Separate solutions of the resulting orange foam ($^{\text{tol}}\text{NPNK}_2 \cdot 2\text{THF}$) in 2 cm³ Et₂O and TaMe₃Cl₂ (0.10 g, 0.35 mmol) in 2 cm³ Et₂O were chilled in freezer at -40 °C for 32 min. Thereafter the chilled Et₂O solutions were added together at room temperature, forming an orange solution with a white ppt. After 36 min, the Et₂O solvent was removed *in vacuo*, toluene solvent added and the mixture filtered through celite on a sintered glass frit, washing with additional toluene and protecting the filtrate from light with foil. The toluene solvent was removed *in vacuo* from the filtrate, leaving in orange oil. This oil was triturated with *n*-hexanes, forming an orange solid which was collected on a sintered glass frit, washing with *n*-hexanes (0.06g, 0.04 mmol $\{^{\text{tol}}\text{NPNTaMe}_2\}_2\text{Cl}_2^{(\text{a})}$ as **species u_{tol}**, 25% yield based on $^{\text{tol}}\text{NPNH}_2$).

$^{31}\text{P}\{^1\text{H}\}$ NMR (THF-*d*₈, 162 MHz): δ = 49.23 (s, P1). ^1H NMR (THF-*d*₈, 400 MHz): δ = 0.96 (d, $^3J_{\text{PH}} = 10$ Hz, 3 H21 and 3 H22, Ta-CH₃), 2.23 (s, 6 H16, CH₃), 2.37 (s, 6 H15, CH₃), 5.98 (d of d, $^4J_{\text{PH}} = 5$ Hz, $^3J_{\text{HH}} = 8$ Hz, 2 H6, ArH), 6.26 (bs, 2 H5, ArH), 6.95 (d, $^3J_{\text{HH}} = 12$ Hz, 2 H10



and 2 H14, ArH), 7.04 (bs, 2 H19 and H20, ArH), 7.20 (d, $^3J_{\text{HH}} = 8$ Hz, 2 H11 and 2 H13, ArH), 7.54 (bs, 2 H3), 7.69 (t, $^3J_{\text{HH}} = ^3J_{\text{PH}} = 8$ Hz, 2 H18, ArH).

$^{31}\text{P}\{^1\text{H}\}$ NMR (C₆D₆, 162 MHz): δ = 49.67 (s, P1). ^1H NMR (C₆D₆, 400 MHz): δ = 1.67 (d, $^3J_{\text{PH}} = 10$ Hz, 3 H21 and 3 H22, Ta-CH₃), 2.04 (s, 6 H16, CH₃), 2.12 (s, 6 H15, CH₃), 6.31 (d of d,

$^4J_{\text{PH}} = 5$ Hz, $^3J_{\text{HH}} = 8$ Hz, 2 H6, ArH), 6.84 (d, $^3J_{\text{HH}} = 8$ Hz, 2 H5, ArH), 7.00 (bs, 2 H10 and 2 H14, ArH), 7.19 (d, $^3J_{\text{HH}} = 12$ Hz, 2 H11, 2 H13, 2 H19 and H20, ArH), 7.33 (d, $^3J_{\text{PH}} = 8$ Hz, 2 H3), 7.86 (t, $^3J_{\text{HH}} = ^3J_{\text{PH}} = 8$ Hz, 2 H18, ArH). $^{13}\text{C}\{^1\text{H}\}$ NMR (C_6D_6 , 75 MHz): $\delta = 20.4$ (C16, CH_3), 21.0 (C15, CH_3), 50.9 (d, $^2J_{\text{PC}} = 9$ Hz, C21 and C22, Ta- CH_3), 118.4 (d, $^3J_{\text{PC}} = 11$ Hz, C6, ArC), 123.7 (d, $^2J_{\text{PC}} = 40$ Hz, C7, C_{ipso}), 128.6, 128.7 (C11 and C13, ArC), 129.3 (C20, ArC), 130.0 (C17, C_{ipso}), 130.5 (C19, ArC), 131.1, 131.3 (C10 and C14, ArC), 131.6 (d, $^3J_{\text{PC}} = 5$ Hz, C4, C_{ipso}), 132.4 (C3, ArC), 133.5 (C5, ArC), 134.2 (d, $^2J_{\text{PC}} = 9$ Hz, C18, ArC), 137.7 (C12, C_{ipso}), 141.1 (d, $^4J_{\text{PC}} = 4$ Hz, C9, C_{ipso}), 162.2 (d, $^1J_{\text{CP}} = 30$ Hz, C2, C_{ipso}). EI-MS (m/z): 1418 (60, $[\{^{\text{tol}}\text{NPNTaMe}_2\}_2]^+$).

^(a) It is speculated that **species u_{tol}** may be $[\{^{\text{tol}}\text{NPNTaMe}_2\}_2]\text{Cl}_2$ and **species u_{ipr}**

$[\{^{\text{iprop}}\text{NPNTaMe}_2\}_2]\text{Cl}_2$. Established characteristics for **species u_{ipr}** and **species u_{tol}** include:

- contains two methyl groups bonded directly to tantalum per one NPN donor set
- does not contain and lithium (and by inference potassium, depending on source NPN donor set)
- may or may not contain chloride atoms (no diagnostic test conducted)
- parent ion observed at 1418 m/z for **species u_{tol}** and at 1474 m/z for **species u_{ipr}** , which corresponds to an approximate formula of $\text{Ta}_2[^{\text{tol}}\text{NPN}]_2\text{Me}_4$ and $\text{Ta}_2[^{\text{iprop}}\text{NPN}]_2\text{Me}_4$, respectively
- partial solubility in aromatic solvents (C_6D_6) but dissolves fully in more polar solvents such as THF- d_8

Rational for exclusion of certain species identities for **species u_{ipr}** and **species u_{tol}** include:

- the $^31\text{P}\{^1\text{H}\}$ NMR spectral signals for $^{\text{tol}}\text{NPNTaMe}_x\text{Cl}_{x-3}$ species could be expected to be intermediate between $^{\text{tol}}\text{NPNTaCl}_3$ [**4.5**] at δ 36.71 and $^{\text{tol}}\text{NPNTaMe}_3$ [**4.7**] at δ 27.88. It is unlikely the downfield signal at *ca* δ 50 for **species u_{ipr}** and **species u_{tol}** may represent

the molecular dimethyl species $^{101}\text{NPNTaMe}_2\text{Cl}$. A parent ion corresponding to a $^{101}\text{NPNTaMe}_2\text{Cl}$ species was also not observed in mass spectral data.

- the lack of lithium (and by inference potassium) excludes the possibility of any methyl / chloro bridged heterometallic tantalum lithium species

Species v_{tol} with species u_{tol} : White $^{101}\text{NPNH}_2$ (0.32 g, 0.64 mmol) and KH (0.05 g, 1.36 mmol) were mixed with 3 cm³ THF in a scintillation vial protected from light with foil. The reaction mixture was stirred at room temperature for 51 min before the THF solvent was removed *in vacuo*. To the resulting orange foam ($^{101}\text{NPNK}_2 \cdot 2\text{THF}$) was added TaMe_3Cl_2 (0.11 g, 0.35 mmol) and the solid mixture was chilled in freezer at -40 °C, together with a separate vial of 5 cm³ Et₂O. Thereafter the chilled Et₂O was added to the solids at room temperature, forming an orange solution with a white ppt after stirring for 5 min. The Et₂O reaction mixture was placed in the freezer at -40 °C for 20.3 hrs. Thereafter the Et₂O solvent was removed *in vacuo*, toluene solvent added and the mixture was filtered through celite on a sintered glass frit, washing with additional toluene and protecting the filtrate from light with foil. The toluene solvent was removed *in vacuo* from the filtrate, leaving in orange residue. Addition of *n*-pentanes led to the formation of a sticky orange goo. The *n*-pentanes was removed *in vacuo* and the residue dissolved in 1 cm³ toluene, layered with *n*-pentanes and returned to the freezer. The orange solid was collected on a sintered glass frit, which turned gooeey when washing with *n*-pentanes and was dried *in vacuo* (0.11 g).^(a)

^(a) $^{31}\text{P}\{^1\text{H}\}$ NMR spectroscopy revealed a broad peak at δ -0.93 (84%) for species v_{tol} and a sharp peak at δ 49.58 (16%) for species u_{tol} . The ^1H NMR spectrum displays the characteristic doublet at δ 1.65 ($^3J_{\text{PH}} = 10$ Hz) for **species u_{tol}** and broad unassigned singlets at δ 1.43 and δ 2.69. Mass spectrum reveals signals at 784 m/z, which corresponds to $[\text{}^{101}\text{NPNTaMe}_2\text{ClK}]^+$, and 751 m/z (70%), 750 m/z (39%) and 749 (100%), which corresponds to $[\text{}^{101}\text{NPNTaCl}_2]^+$.

[^{tol}NPNTaMe₄][Li(THF)₄] [4.14] from ^{tol}NPNTaMe₄Li(Et₂O) [4.13] (or species **tol**_{4MeLi}):

Sequential addition of 4 equiv of MeLi to ^{tol}NPNTaCl₃ [4.5] at room temperature: Brown

^{tol}NPNTaCl₃ [4.5] (0.10 g, 0.12 mmol) was dissolved with heating (60 °C) in 0.8 cm³ toluene-*d*₈ and transferred to a J-Young NMR tube protected from light with foil. 1.58 M MeLi (80 μL, 0.13 mmol) in Et₂O was added at room temperature, with no significant colour change.^(a) After 40 min the second aliquot 1.58 M MeLi (80 μL, 0.13 mmol) in Et₂O was added, forming a lighter coloured solution.^(b) After 1 hr 10 min the third aliquot 1.58 M MeLi (80 μL, 0.13 mmol) in Et₂O was added, forming a light orange solution.^(c) After 23 hrs 10 min the fourth aliquot 1.58 M MeLi (80 μL, 0.13 mmol) in Et₂O was added.^(d) After 7 days at room temperature the orange solution darkened to a dark brown colour and was transferred to a centrifuge tube. After centrifuging the mixture, the brown supernatant was decanted into a scintillation vial and the toluene-*d*₈ was removed in vacuo. The sticky dark brown residue was triturated with 2 cm³ *n*-hexanes, forming a greenish coloured ppt. The *n*-hexanes solvent was removed *in vacuo* and on addition of 2 cm³ toluene the olive green residue had limited solubility, but completely dissolved after further addition of 0.5 cm³ THF. This solution was placed in the freezer and after 53 days the light green crystals [^{tol}NPNTaMe₄][Li(THF)₄]⁺ [4.14] were collected on a sintered glass frit and were of sufficient quality for x-ray crystallographic analysis. Anal. Calcd. for C₅₄H₇₅LiN₂O₄PTa: C, 62.66; H, 7.30; N, 2.71; Found: C, 62.73; H, 7.07; N, 2.55.

^(a) After 16 min, the ³¹P{¹H} NMR spectrum displayed a signal at δ 27.58 (29%) for ^{tol}NPNTaMe₃ [4.7] and signals at δ 49.40 (13%) and δ 43.42 (58%), suggested to be ^{tol}NPNTaCl_{*x*}Me_{4-*x*}Li(Et₂O) intermediates (assuming final product **species tol**_{4MeLi} is ^{tol}NPNTaMe₄Li(Et₂O) [4.13]). Related chloro-bridged species have been reported for PNPVCl₂Li(TMEDA).¹⁸²

^(b) ³¹P{¹H} NMR spectrum displayed peaks at δ 49.40 (48%) and δ 43.42 (6%) suggested to be ^{tol}NPNTaCl_{*x*}Me_{4-*x*}Li(Et₂O)_{*n*} intermediates and a peak at δ 27.58 (46%) for ^{tol}NPNTaMe₃ [4.7].

(c) $^{31}\text{P}\{^1\text{H}\}$ NMR spectrum displayed a singlet at δ 50.85 (75%) for $^{\text{tol}}\text{NPNTaMe}_4\text{Li}(\text{Et}_2\text{O})$ [**4.13**] (or species $\text{tol}_{4\text{MeLi}}$) and a singlet at δ 27.58 (25%) for $^{\text{tol}}\text{NPNTaMe}_3$ [**4.7**] (still unreacted after 3 equiv of MeLi). Alkyl-bridged lithium-tantalum complexes have been reported for the reaction of tantalum dichloride complexes with $\text{CH}_3\text{SiCH}_2\text{Li}$.⁴¹⁵

(d) $^{31}\text{P}\{^1\text{H}\}$ NMR spectrum displayed one singlet for

$^{\text{tol}}\text{NPNTaMe}_4\text{Li}(\text{Et}_2\text{O})$ [**4.13**] (or species $\text{tol}_{4\text{MeLi}}$). $^{31}\text{P}\{^1\text{H}\}$

NMR (toluene- d_8 , 121.5 MHz): δ = 50.85 (s, P1). ^1H NMR (C₆D₆, 300 MHz): δ = 0.34 (bs, 3 H23/24, Ta-CH₃), 0.84 (d,

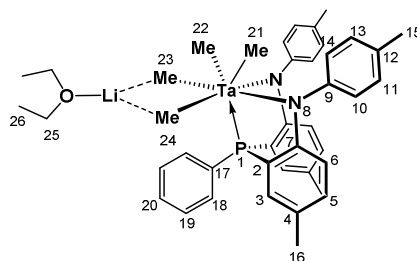
$^3J_{\text{PH}}$ = 11 Hz, 3 H21 and 3 H22, Ta-CH₃), 1.68 (bs, 3

H23/24, Ta-CH₃), 1.11 (m, H26, CH₃), 2.09, 2.21 (s's, 6 H15 and 6 H16, CH₃), 3.30 (m, H25,

CH₂), 6.26 (d of d, $^3J_{\text{HH}}$ = 8 Hz, $^4J_{\text{PH}}$ = 5 Hz, 2 H6, ArH), 6.76 (t, $^3J_{\text{HH}}$ = 6 Hz, 2 H5 and 2

H18/19/20, ArH), 7.09 (m, $^3J_{\text{HH}}$ = 7 Hz, 2 H10, 2 H14, 2 H11 and 2 H13, ArH), and 7.22 (s, 2

H18/19/20, ArH), 7.41 (d, $^3J_{\text{PH}}$ = 8 Hz, 2 H3, ArH), 7.78 (bs, 2 H18/19/20, ArH).



$^{\text{tol}}\text{NPNTaMe}_4\text{Li}(\text{THF})$ [**4.15**] (or species $\text{tol}_{4\text{MeLi}}$): Direct addition of 4 equiv MeLi to

$^{\text{tol}}\text{NPNTaCl}_3$ [**4.5**] at $-40\text{ }^\circ\text{C}$: Brown $^{\text{tol}}\text{NPNTaCl}_3$ (0.33 g, 0.42 mmol) and 10 cm³ toluene were placed in a scintillation vial wrapped in foil and cooled to $-40\text{ }^\circ\text{C}$ inside the glovebox freezer overnight. The solution was removed from the freezer and 1.58 M MeLi (1.06 cm³, 1.68 mmol) in Et₂O was added and the reaction mixture stirred at room temperature for 15 min, forming an orange solution with a white ppt. The mixture was filtered^(a) through celite on a sintered glass frit and the solvent was removed from the orange filtrate *in vacuo* over 56 min to give a light yellow residue. Partway through the evacuation, 1 cm³ THF was added to the toluene concentrate, with a slight cloudiness being observed. The light yellow residue was triturated with *n*-hexanes and the resulting light yellow solid was collected on a sintered glass frit and washed with *n*-hexanes (0.18 g, 0.23 mmol $^{\text{tol}}\text{NPNTaMe}_4\text{Li}(\text{THF})$ [**4.15**], 55% yield based on $^{\text{tol}}\text{NPNTaCl}_3$).

$^{31}\text{P}\{^1\text{H}\}$ NMR (C_6D_6 , 162 MHz): $\delta = 50.38$ (s, P1).^(b)

$^7\text{Li}\{\text{H}\}$ NMR (C_6D_6 , 156 MHz): $\delta = 1.30$ (s, Li1). ^1H

NMR (C_6D_6 , 400 MHz): $\delta = 0.58$ (s, 3 H23/24, Ta-

CH_3),^(b) 0.84 (bs, 4 H26, CH_2),^(c) 1.12 (d, $^3J_{\text{PH}} = 11$ Hz, 3

H21 and 3 H22, Ta- CH_3),^{(b),(d)} 2.03 (s, 3 H23/24, Ta-

CH_3 and 6 H16, CH_3),^(b) 2.16 (s, 6 H15, CH_3), 2.87 (bs, 4 H25, CH_2),^(c) 6.38 (d of d, $^3J_{\text{HH}} = 8$ Hz,

$^4J_{\text{PH}} = 5$ Hz, 2 H6, ArH), 6.78 (m, $^3J_{\text{HH}} = 7$ Hz, H11, H13 and 2 H5, ArH), 7.02 (d, $^3J_{\text{HH}} = 8$ Hz,

H10a and H14a, ArH), 7.16 (m, $^3J_{\text{HH}} = 7$ Hz, H10, H14, 2 H19 and H20, ArH), 7.32 (d, $^3J_{\text{HH}} = 8$

Hz, 2 H11a and 2 H13a, ArH), 7.53 (d, $^3J_{\text{PH}} = 8$ Hz, 2 H3, ArH), 7.88 (t, $^3J_{\text{HH}} = ^3J_{\text{PH}} = 8$ Hz, 2

H18, ArH). $^{13}\text{C}\{^1\text{H}\}$ NMR (C_6D_6 , 101 MHz): $\delta = 20.3$ (C16, CH_3), 20.9 (C15, CH_3), 24.9 (C26,

CH_2), 62.6 (d, $^2J_{\text{PC}} = 15$ Hz, C21 and C22, Ta- CH_3),^(e) 68.4 (C25, CH_3), 81.4 (C23/24, Ta- CH_3),^(e)

82.2 (d, $^2J_{\text{PC}} = 13$ Hz, C23/24, Ta- CH_3),^(e) 119.7 (d, $^3J_{\text{PC}} = 15$ Hz, C6, ArC), 121.4 (d, $^2J_{\text{PC}} = 49$

Hz, C7, C_{ipso}), 128.0 (C19 and C20, ArC), 128.6 (C11 and C13, ArC), 129.2 (C11a and C13a,

ArC and C4, C_{ipso}), 129.4 (C10 and C14, ArC), 129.6 (d, $^1J_{\text{PC}} = 49$ Hz, C17, C_{ipso}), 132.0 (C10a

and C14a, ArC), 132.6 (C5, ArC), 133.6 (d, $^2J_{\text{PC}} = 17$ Hz, C3, ArC and C12, C_{ipso}), 134.7 (d, $^2J_{\text{PC}}$

$= 11$ Hz, C18, ArC), 151.7 (d, $^4J_{\text{PC}} = 6$ Hz, C9, C_{ipso}), 165.3 (d, $^1J_{\text{CP}} = 38$ Hz, C2, C_{ipso}). Anal.

Calcd. for $\text{C}_{41}\text{H}_{48}\text{LiN}_2\text{OPTa}$: C, 61.27; H, 6.02; N, 3.49; Found: C, 61.59; H, 6.08; N, 3.76. EI-

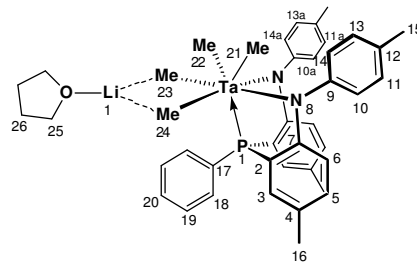
MS (m/z): 725 (5, $[\text{M} - \text{Me} - \text{Li} - \text{THF}]^+$), 709 (60, $[\text{M} - 2\text{Me} - \text{Li} - \text{THF}]^+$), 693 (50, $[\text{M} - 3\text{Me} -$

$\text{Li} - \text{THF}]^+$), 679 (5, $[\text{M} - 4\text{Me} - \text{Li} - \text{THF}]^+$).

^(a) Mass spectral analysis confirmed the presence of chloride in the filtrate residue; hence not all LiCl was removed.

^(b) A ^1H - ^{31}P HMBC spectrum indicated a strong correlation between the phosphorus atom (δ 50.38) and the doublet (δ 1.12) and a weaker correlation for the two singlets (δ 0.58 and δ 2.03) in the corresponding ^1H NMR spectrum.

^(c) One THF molecule per $^{101}\text{NPNTa}$ unit



(d) The doublet at δ 1.12 in the ^1H NMR spectrum collapses to a singlet in a corresponding ^1H $\{^{31}\text{P}\}$ NMR spectrum.

(e) A ^1H - ^{13}C HSQC NMR spectrum confirms the doublet at δ 62.6 ($^2J_{\text{PC}} = 15$ Hz) correlates with the doublet at δ 1.12 in the ^1H NMR spectrum, the doublet at δ 82.2 ($^2J_{\text{PC}} = 13$ Hz) correlates with the singlet at δ 2.03 (overlapped by the methyl signal of ligand tolyl group) and the singlet at δ 81.4 correlates with the singlet at δ 0.58. These values are in agreement with those obtained for the methyl signals in the related $\text{P}_2\text{N}_2\text{TaMe}_3$, $\text{P}_2\text{N}_2\text{TaMe}(\text{=CH}_2)^{293}$ and $^{\text{Si}}\text{NPNTaMe}_3^{79, 80}$ complexes as well as other tantalum alkyl complexes.⁴¹⁶

Reaction of $^{\text{iprop}}\text{NPNTaCl}_3$ [4.4] with KHBet_3 (Ar) + N_2 : $^{\text{iprop}}\text{NPNTaCl}_3$ [4.4] (0.31 g, 0.38 mmol) was dissolved in 10 cm^3 toluene in a Schlenk flask and the dark brown solution was cooled down to $-56\text{ }^\circ\text{C}$ and the degassed 3 times with argon (10 min cycles). The solution was further cooled to $-114.6\text{ }^\circ\text{C}$ before a solution of KHBet_3 (0.16 g, 1.14 mmol) in 1 cm^3 toluene was added via syringe. The cooling bath was removed and the reaction mixture was allowed to warm slowly to room temperature. After 1 hr 20 min, the reddish-brown solution containing a ppt was filtered through celite on a sintered glass frit under argon. The toluene solvent was removed *in vacuo* from the filtrate and the dark brown residue dried for 30 min. The residue was dissolved in 1.5 cm^3 C_6D_6 (degassed 3 times with argon) and after analysis^(a) was placed in the freezer at $-40\text{ }^\circ\text{C}$ for 3 days inside the glovebox. The sample was warmed to room temperature and stirred for 16 min with dynamic exposure to N_2 and for a further 1 day under static N_2 exposure, with no visible colour changes. The C_6D_6 solvent was removed *in vacuo* and the residue triturated with 2 cm^3 *n*-pentanes and in the freezer for 40 min before the dark brown solid was collected and washed with $4 \times 3\text{ cm}^3$ cold *n*-pentanes (40 mg).^(b)

(a) under Ar, $^{31}\text{P}\{^1\text{H}\}$ NMR spectroscopy revealed a mixture of product with singlets at δ 31.48, δ 43.09, δ 43.76, δ 45.09, δ 188.89, δ 191.69 and a doublet δ 49.09 ($^2J_{\text{PH}} = 22$ Hz). The ^1H NMR spectrum has numerous peaks in the hydride region ranging from δ 9.5 to 21.6. A mass spectrum

obtained under Ar contained peaks at 1731 m/z (20), 1612 m/z (20) and 1383 m/z (20), suggesting multi-metal species may have formed, potentially with bridging hydrides, but no signals consistent with a dimeric [$^{\text{iprop}}\text{NPNTaH}_2$]₂ species were observed, by analogy to stable isolated [$^{\text{Si}}\text{NPNTaH}_2$]₂.

^(b) under N₂, $^{31}\text{P}\{^1\text{H}\}$ NMR spectroscopy revealed a mixture of product with singlets at δ 31.48, δ 42.53, δ 43.10, δ 45.10, δ 45.72, δ 47.06, δ 188.89, δ 191.71 and doublets at δ 43.71 ($^2J_{\text{PH}} = 16$ Hz) and δ 49.10 ($^2J_{\text{PH}} = 22$ Hz). Compared to the spectrum obtained under Ar, after exposure to N₂ there are new singlets at δ 42.53, δ 45.72, δ 47.06 and a doublet at δ 43.71 ($^2J_{\text{PH}} = 16$ Hz). The ^1H NMR spectrum has numerous peaks in the hydride region ranging from δ 9.5 to 17.0 (δ 18.5 was downfield spectral limit). EI-MS (m/z): 1697 (20, [$^{\text{iprop}}\text{NPNTaH}$]₂(NBET₃)₂(N₂)₂ [**4.17a**]⁺), 1444 (20, [$^{\text{iprop}}\text{NPNTaH}$]₂(N₂) [**4.17**]⁺).

Reaction of $^{\text{tol}}\text{NPNTaCl}_3$ [4.5**] with KHBET₃ + N₂:** The two solids $^{\text{tol}}\text{NPNTaCl}_3$ [**4.5**] (1.04 g, 1.33 mmol) and KHBET₃ (0.55 g, 4.00 mmol) were added together in a Schlenk flask in the glove box and 40 cm³ toluene pre-cooled to -40 °C was added. The reaction mixture was allowed to warm to room temperature, with stirring. After 3 hrs 22 min, the reaction mixture was filtered through celite on a sintered glass frit, washing with 10 cm³ toluene. The toluene solvent was removed *in vacuo* from the filtrate and the dark brown residue^(a) was triturated with 5 cm³ *n*-pentanes (5 cycles) and *n*-pentanes mixture was placed in the freezer at -40 °C. The dark brown solid was collected and washed with 2 x 5 cm³ cold *n*-pentanes (0.44 g).^(b) The brown solid was dissolved in *n*-hexanes with heating to 60 °C and filtered through celite on a sintered glass frit, washing with 3 x 5 cm³ warm *n*-hexanes. The *n*-hexanes solvent was removed *in vacuo* from the filtrate and the dark brown residue dried (0.43 g).^(c)

^(a) $^{31}\text{P}\{^1\text{H}\}$ NMR spectroscopy revealed a single major product peak at δ 42.83 with minor peaks at δ 41.25, δ 44.64 and δ 46.10.

(b) $^{31}\text{P}\{^1\text{H}\}$ NMR spectroscopy revealed a single major product peak at δ 42.83 with minor peaks at δ 2.43, δ 6.40, δ 33.42, δ 39.73, δ 41.26, δ 44.65 and δ 46.12.

(c) $^{31}\text{P}\{^1\text{H}\}$ NMR spectroscopy was consistent with a single product $[\text{}^{101}\text{NPNTaH}]_2(\text{N}_2)$ [**4.18**] or $[\text{}^{101}\text{NPNTaH}]_2(\text{NBET}_3)_2(\text{N}_2)_2$ [**4.18a**] on the basis of a single peak at δ 42.83. The ^1H NMR spectrum has a broad peak in the hydride region at δ 14.20. EI-MS (m/z): 1585 (20, $[\text{}^{101}\text{NPNTaH}]_2(\text{NBET}_3)_2(\text{N}_2)_2$ [**4.18a**] $^+$), 1389 (20, $[\text{}^{101}\text{NPNTaH}]_2(\text{N}_2)$ [**4.18**] $^+$).

$[\text{}^{\text{iprop}}\text{NPNTaCl}]_2(\text{N}_2)$ [**4.19**] Brown $^{\text{iprop}}\text{NPNTaCl}_3$ [**4.4**] (0.55 g, 0.67 mmol) and bronze KC_8 (0.19 g, 1.40 mmol) were added as solids to a thick-walled reaction flask. After the flask was cooled to -196°C with $\text{N}_2(\text{l})$, 10 cm^3 THF was vacuum-transferred. Thereafter the reaction flask was placed under N_2 flow at -196°C (i.e. 4 atm). The reaction flask was placed behind an explosion shield in an EtOH / N_2 / dry ice cooling bath and the contents were allowed to warm up slowly to room temperature, with vigorous stirring. After 18 hrs 40 min the dark brown solution was slowly depressurizing under N_2 at room temperature. Inside the glovebox, the brown THF mixture was transferred to centrifuge tubes and the solids compacted under centrifugal forces. The brown THF supernatant was decanted into a conical flask and THF solvent was removed *in vacuo* and the brown/purple residue dried and stored in the freezer (0.24 g).^(a)

(a) $^{31}\text{P}\{^1\text{H}\}$ NMR spectroscopy revealed 4 peaks at δ 8.05 $[\text{}^{\text{iprop}}\text{NPNTaCl}]_2(\text{N}_2)$ [**4.19**], δ 19.51, δ 24.07 and δ 28.99. EI-MS (m/z): 1512 (20, $[\text{M}]^+$), 1498 (20, $[\text{M} - \text{N}]^+$), 1484 (30, $[\text{M} - 2\text{N}]^+$)

$[\text{}^{101}\text{NPNTaCl}]_2(\text{N}_2)$ [**4.20**] Brown $^{101}\text{NPNTaCl}_3$ [**4.5**] (0.73 g, 0.93 mmol) and bronze KC_8 (0.28 g, 2.07 mmol) were added as solids to a thick-walled reaction flask. The flask was cooled to -196°C with $\text{N}_2(\text{l})$ and 10 cm^3 THF was vacuum-transferred. Thereafter the reaction flask was placed under N_2 flow at -196°C (i.e. 4 atm). The reaction flask was placed behind an explosion shield in an EtOH / N_2 / dry ice cooling bath and the contents was allowed to warm up slowly to room temperature, with vigorous stirring. After 3 days the dark brown solution was slowly

depressurizing under N₂ at room temperature. Inside the glovebox, the brown THF mixture was filtered through celite on a sintered glass frit, washing with additional THF. The THF solvent was removed *in vacuo* from the filtrate and the reddish-brown residue dissolved in toluene. The toluene solution was filtered through celite on a sintered glass frit, washing with additional toluene. The toluene solvent was removed *in vacuo* from the filtrate and the residue re-dissolved in 5 cm³ toluene with a few drops THF. The volume was reduced to 2 cm³ and placed in the freezer at -40 °C for 7 days with no signs of crystal growth. A *n*-pentanes layer was added and the mixture returned to the freezer for 2 days. The reddish-brown crystals were collected and washed with 3 x 5 cm³ cold *n*-hexanes (0.24 g).^(a)

^(a) ³¹P{¹H} NMR spectroscopy revealed a major peak at δ 10.86 for [¹⁰¹NPNTaCl]₂(N₂) [**4.20**] and three minor peaks at δ 25.11, δ 31.36 and δ 34.40. In other similar reactions, minor peaks were also observed at δ 18.46, δ 33.63 and for unreacted ¹⁰¹NPNTaCl₃ [**4.5**] at δ 36.77. EI-MS (*m/z*): 1456 (20, [M]⁺), 1442 (20, [M - N]⁺), 1428 (40, [M - 2N]⁺) and two other unidentified peaks at 1479 *m/z* and 1423 *m/z*.

¹⁰¹NPNTaCl₃ [**4.5**] + 3.5 KC₈: Brown ¹⁰¹NPNTaCl₃ [**4.5**] (0.81 g, 1.03 mmol) and bronze KC₈ (0.49 g, 3.64 mmol) were added as solids to a thick-walled reaction flask. The flask was cooled to -196 °C with N₂(l) and 10 cm³ THF was vacuum-transferred. Thereafter the reaction flask was placed under N₂ flow at -196 °C (i.e. 4 atm). The reaction flask was placed behind an explosion shield in an EtOH / N₂ / dry ice cooling bath and the contents was allowed to warm up slowly to room temperature, with vigorous stirring. After 22 hrs 34 min the dark brown solution was slowly depressurizing under N₂ at room temperature. Inside the glovebox, the brown THF mixture was filtered through celite on a sintered glass frit, washing with 3 x 10 cm³ THF. The THF solvent was removed *in vacuo* from the filtrate and the brown residue^(a) was triturated with 5 cm³ *n*-hexanes and the mixture placed in the freezer at -40 °C for 19 hrs 47 min. The dark purple-brown solid were collected and washed with 3 x 3 cm³ cold *n*-hexanes (0.63 g).^(b)

(a) $^{31}\text{P}\{^1\text{H}\}$ NMR spectroscopy revealed a single peak at δ 1.49.

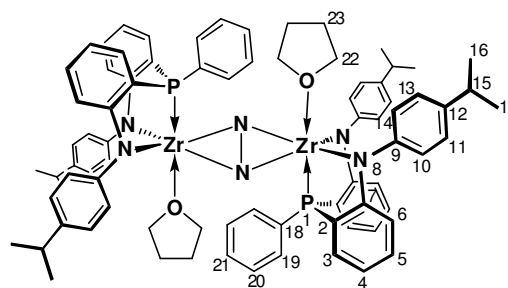
(b) $^{31}\text{P}\{^1\text{H}\}$ NMR spectroscopy revealed three major peaks at δ 11.18, δ 14.19 and δ 17.36, and in a repeat reaction the same major peaks were observed. The highest peak in the mass spectra was observed at 1284 m/z, with no peaks for $[\text{}^{\text{tol}}\text{NPNTaCl}]_2(\text{N}_2)$ [4.20] or unreacted $^{\text{tol}}\text{NPNTaCl}_3$ [4.5].

$[\text{}^{\text{iprop}}\text{NPNZr}(\text{THF})]_2(\mu\text{-}\eta^2\text{:}\eta^2\text{-N}_2)$ [5.1] (a) from $[\text{}^{\text{iprop}}\text{NPNZrCl}_2]_2$ [3.9] with THF filtration: In the glove-box, yellow $[\text{}^{\text{iprop}}\text{NPNZrCl}_2]_2$ [3.9] (0.65 g, 0.47 mmol) and bronze KC_8 (0.28 g, 2.05 mmol) were mixed as solids in a thick-walled flask. The flask was cooling to -196°C with $\text{N}_2(\text{l})$ and 10 cm^3 THF was vacuum-transferred. The frozen solid content of the reaction flask was exposed briefly to a dynamic N_2 flow at -196°C . At this point an olive-green solid and solid white THF was observed. The reaction flask was transferred to an EtOH / N_2 / dry ice slurry bath behind an explosion shield and the reaction mixture was allowed to warm up slowly to room temperature (4 atm N_2) with vigorous stirring, forming a deep purple solution. After 4 days^(a) the reaction flask was cooled down to -196°C with $\text{N}_2(\text{l})$, placed under a dynamic N_2 atmosphere and allowed to warm to room temperature. The reaction flask was sealed and transferred to the glovebox. The reaction mixture was filtered through celite with a sintered glass frit, washing with $3 \times 5\text{ cm}^3$ THF. The THF solvent was removed *in vacuo* and the purple residue dried for 2 hours (0.40 g, 0.28 mmol $[\text{}^{\text{iprop}}\text{NPNZr}(\text{THF})]_2(\mu\text{-}\eta^2\text{:}\eta^2\text{-N}_2)$ [5.1], 60% yield based on $[\text{}^{\text{iprop}}\text{NPNZrCl}_2]_2$ [3.9]. (b) from $^{\text{iprop}}\text{NPNZrCl}_2(\text{THF})$ [3.5] with toluene centrifuge: In the glove-box, yellow $^{\text{iprop}}\text{NPNZrCl}_2(\text{THF})$ [3.5] (0.94 g, 1.23 mmol) and bronze KC_8 (0.37 g, 2.71 mmol) were mixed as solids in a thick-walled flask. The flask was cooling to -196°C with $\text{N}_2(\text{l})$ and 10 cm^3 THF was vacuum-transferred. The frozen solid content of the reaction flask was exposed briefly to a dynamic N_2 flow at -196°C . At this point an olive-green solid and solid white THF was observed. The reaction flask was transferred to an EtOH / N_2 / dry ice slurry bath behind an explosion shield and the reaction mixture was allowed to warm up slowly to room temperature (4

atm N₂) with vigorous stirring, forming a deep purple solution. After 20 hrs the reaction flask was cooled down to -196 °C with N₂(l), placed under a dynamic N₂ atmosphere and allowed to warm to room temperature. The reaction flask was sealed and transferred to the glovebox. The THF solvent was removed *in vacuo* and the residue was suspended in 10 cm³ *n*-hexanes. The *n*-hexanes solvent was removed *in vacuo* and the process repeated with 10 cm³ *n*-hexanes. The residue was suspended in 20 cm³ toluene and transferred to glass centrifuge tubes. After the mixture was centrifuged the purple supernatant was decanted. The residue was suspended in 15 cm³ toluene, centrifuged and the supernatants were combined. The toluene solvent was removed from the supernatant. The purple residue was triturated in 10 cm³ *n*-pentanes and the mixture was placed in the freezer at -40 °C. The purple solid was collected on a sintered glass frit and washed with *n*-pentanes and dried for 50 min (0.63 g, 0.45 mmol [^{iprop}NPNZr(THF)]₂(μ-η²:η²-N₂) [**5.1**], 72% yield based on ^{iprop}NPNZrCl₂(THF) [**3.5**]). Single crystals of [^{iprop}NPNZr(THF)]₂(μ-η²:η²-N₂) [**5.1**] were grown by vapour diffusion of *n*-hexanes into a toluene solution at -40 °C.

³¹P{H} NMR (C₆D₆, 162 MHz): δ = -3.05 (s, P1).

¹H NMR (C₆D₆, 600 MHz): δ = 0.93 (s, 8 H₂₃, CH₂), 1.19 (t^(b), ³J_{HH} = 6 Hz, 12 H₁₆ and 12 H₁₇, CH₃), 2.72 (hep, ³J_{HH} = 7 Hz, 4 H₁₅, CH), 3.62 (s, 8 H₂₂, CH₂), 6.70 (overlapping t and d, ³J_{HH} = 8 Hz, 4



H₄, 4 H₁₀ and 4 H₁₄ ArH), 6.89 (d of d, ³J_{HH} = 6 Hz and ⁴J_{PH} = 6 Hz, 4 H₆, ArH), 7.05 (m, ³J_{HH} = ³J_{PH} = 9 Hz, 4 H₅, 4 H₁₉ and 2 H₂₁, ArH), 7.22 (d, ³J_{HH} = 6 Hz, 4 H₁₁ and 4 H₁₃, ArH), 7.55 (t, ³J_{HH} = ³J_{PH} = 6 Hz, 4 H₃, ArH), 7.68 (t, ³J_{HH} = 6 Hz, 4 H₂₀, ArH). ¹³C{¹H} NMR (C₆D₆, 151 MHz): δ = 24.5, 24.6 (C₁₆ and C₁₇, CH₃), 25.2 (C₂₃, CH₂), 33.9 (C₁₅, CH), 72.1 (C₂₂, CH₂), 118.1 (d, ³J_{PC} = 9 Hz, C₆, ArC), 118.7 (d, ³J_{PC} = 5 Hz, C₄, ArC), 119.1 (d, ²J_{PC} = 32 Hz, C₇, C_{ipso}), 124.1 (C₁₁ and C₁₃, ArC), 127.5 (C₁₀ and C₁₄, ArC), 128.6 (d, ²J_{PC} = 11 Hz, C₁₉, ArC), 129.1 (C₂₁, ArC), 132.4 (C₅, ArC), 132.9 (d, ¹J_{PC} = 32 Hz, C₁₈, C_{ipso}), 133.1 (d, ³J_{PC} = 13 Hz,

C20, ArC), 134.8 (C3, ArC), 141.6 (C12, C_{ipso}), 148.0 (C9, C_{ipso}), 161.9 (d, ¹J_{CP} = 26 Hz, C2, C_{ipso}). Anal. Calcd. for C₈₀H₈₆N₆O₂P₂Zr₂: C, 68.24; H, 6.16; N, 5.97; Found: C, 68.22; H, 6.15; N, 6.01. EI-MS (*m/z*): 1143 (40, [M - 2THF - C₆H₄C(H)Me₂]⁺), MALDI-TOF-MS (*m/z*)^(c): 1264, [M - 2THF]⁺, 1055, [M - 2THF - N(C₆H₄)C₆H₄C(H)Me₂]⁺. UV-Vis (toluene) λ_{max} (ε) = 304 nm (40,000 dm³.mol⁻¹.cm⁻¹),^(d) 530 nm (3,300 dm³.mol⁻¹.cm⁻¹).^(e) IR (KBr, cm⁻¹) = 490 (m), 550 (m), 625 (w), 694 (m), 744 (m), 820 (m), 847 (m), 868 (m), 883 (m), 918 (w), 945 (vw), 1016 (m), 1026 (m), 1034 (m), 1053 (m), 1097 (m), 1128 (m), 1159 (m), 1173 (m), 1200 (m), 1257 (s), 1269 (s), 1292 (s), 1338 (w), 1361 (w), 1381 (w), 1437 (s), 1462 (s), 1500 (s), 1533 (m), 1541 (m), 1562 (m), 1579 (s), 1604 (m), 1614 (m), 1618 (w), 1896 (w), 2065 (w), 2133 (w), 2453 (w), 2544 (w), 2866 (m), 2924 (m), 2951 (m), 3012 (w), 3045 (w), 3454 (bw).

^(a) 1 day is sufficient

^(b) the apparent triplet would be indistinguishable from two doublets for inequivalent protons of C16 and C17 atoms, adjacent to each other with a separation frequency between the doublets equal to the apparent triplet's ³J_{HH} coupling constant of 6 Hz.

^(c) with a 2-amino-4-methyl-5-nitropyridine matrix

^(d) 0.024 mM, identical spectra obtained after 5 and 10 min

^(e) 0.24 mM, identical spectrum obtained after 10 min.

[^{iprop}NPNZr(THF)]₂(μ-η²:η²-¹⁵N₂) [5.2] from ^{iprop}NPNZrCl₂(THF) [3.5] with toluene

filtration: In the glove-box, yellow ^{iprop}NPNZrCl₂(THF) [3.5] (1.26 g, 1.65 mmol) and bronze KC₈ (0.49 g, 3.65 mmol) were mixed as solids in a thick-walled flask. The flask was cooling to -196 °C with N₂(l) and 10 cm³ THF was vacuum-transferred. The reaction flask was connected to a ¹⁵N₂ canister fitted with a pressure regulator (5 psi) and flow meter and the system was placed under reduced pressure. The frozen solid content of the reaction flask was exposed briefly to ¹⁵N₂

while still cooled to $-196\text{ }^{\circ}\text{C}$ with $\text{N}_2(\text{l})$. At this point an olive-green solid and solid white THF was observed. The reaction flask was transferred to an EtOH / N_2 / dry ice slurry bath behind an explosion shield and the reaction mixture was allowed to warm up slowly to room temperature ($4\text{ atm }^{15}\text{N}_2$) with vigorous stirring, forming a deep purple solution. After 15.5 hrs the reaction flask was depressurised under a dynamic $\text{N}_2^{(\text{a})}$ atmosphere at room temperature. The reaction flask was sealed and transferred to the glovebox. The THF solvent was removed *in vacuo* and the residue was suspended in 20 cm^3 toluene. The toluene reaction mixture was filtered through celite with a sintered glass frit, washing with $2 \times 20\text{ cm}^3$ toluene. The deep purple toluene filtrate was re-filtered through celite with a sintered glass frit, washing with 30 cm^3 toluene. The toluene solvent of the filtrate was removed *in vacuo* and the purple / black residue was triturated with 15 cm^3 *n*-hexanes. The *n*-hexanes solvent was removed *in vacuo* and the residue re-triturated with 10 cm^3 *n*-hexanes, resulting in a brown solution with a purple solid. After being placed in the freezer at $-40\text{ }^{\circ}\text{C}$ the purple solid was collected on a sintered glass frit, washed with $2 \times 10\text{ cm}^3$ cold *n*-hexanes and dried for 50 min (0.80 g , $0.56\text{ mmol } [\text{ipropNPNZr}(\text{THF})]_2(\mu\text{-}\eta^2\text{-}^{15}\text{N}_2)$ **[5.2]**, 68% yield based on $\text{ipropNPNZrCl}_2(\text{THF})$ **[3.5]**).

$^{31}\text{P}\{\text{H}\}$ NMR (C_6D_6 , 162 MHz): $\delta = -3.07$ (s, P1).

$^{15}\text{N}\{\text{H}\}$ NMR (C_6D_6 , 40 MHz): $\delta = 88.54$ (s,

$^{15}\text{N}_2$). ^1H NMR (C_6D_6 , 600 MHz): $\delta = 0.94$ (s, 8

H23, CH_2), 1.19, 1.20 (overlapping d's, $^3J_{\text{HH}} = 6$

Hz, 12 H16 and 12 H17, CH_3), 2.71 (hep, $^3J_{\text{HH}} = 7$

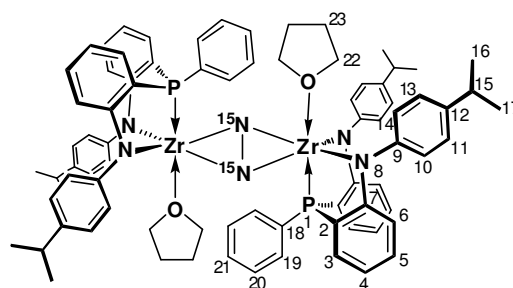
Hz, 4 H15, CH), 3.62 (s, 8 H22, CH_2), 6.70 (overlapping t and d, $^3J_{\text{HH}} = 8\text{ Hz}$, 4 H4, 4 H10 and 4

H14 ArH), 6.89 (t, $^3J_{\text{HH}} = ^4J_{\text{PH}} = 7\text{ Hz}$, 4 H6, ArH), 7.05 (m, $^3J_{\text{HH}} = ^3J_{\text{PH}} = 7\text{ Hz}$, 4 H5, 4 H19 and 2

H21, ArH), 7.22 (d, $^3J_{\text{HH}} = 8\text{ Hz}$, 4 H11 and 4 H13, ArH), 7.55 (t, $^3J_{\text{HH}} = ^3J_{\text{PH}} = 7\text{ Hz}$, 4 H3, ArH),

7.68 (t, $^3J_{\text{HH}} = 5\text{ Hz}$, 4 H20, ArH). $^{13}\text{C}\{\text{H}\}$ NMR (C_6D_6 , 151 MHz): $\delta = 24.5$, 24.6 (C16 and C17,

CH_3), 25.2 (C23, CH_2), 33.9 (C15, CH), 72.1 (C22, CH_2), 118.1 (d, $^3J_{\text{PC}} = 8\text{ Hz}$, C6, ArC), 118.7



(C4, ArC), 119.1 (d, $^2J_{PC} = 30$ Hz, C7, C_{ipso}), 124.1 (C11 and C13, ArC), 127.4 (C10 and C14, ArC), 128.6 (d, $^2J_{PC} = 10$ Hz, C19, ArC), 129.1 (C21, ArC), 132.5 (C5, ArC), 133.0 (d, $^1J_{PC} = 26$ Hz, C18, C_{ipso}), 133.2 (d, $^3J_{PC} = 13$ Hz, C20, ArC), 134.8 (C3, ArC), 141.6 (C12, C_{ipso}), 148.0 (C9, C_{ipso}), 162.0 (d, $^1J_{CP} = 26$ Hz, C2, C_{ipso}). EI-MS (m/z): 1142 (30, [M - 2THF - C₆H₄C(H)Me₂]⁺). IR (KBr, cm⁻¹) = 492 (m), 550 (m), 607 (w), 694 (m), 744 (m), 820 (m), 849 (m), 868 (m), 883 (m), 918 (w), 943 (vw), 1016 (m), 1026 (m), 1038 (m), 1053 (m), 1099 (m), 1128 (m), 1159 (m), 1180 (m), 1190 (m), 1254 (s), 1273 (s), 1292 (s), 1338 (w), 1361 (w), 1381 (w), 1439 (s), 1462 (s), 1500 (s), 1533 (m), 1541 (m), 1558 (m), 1581 (s), 1603 (m), 1616 (m), 1622 (w), 1898 (w), 2069 (w), 2133 (w), 2457 (w), 2546 (w), 2866 (m), 2924 (m), 2954 (m), 3012 (w), 3045 (w), 3452 (bw).

^(a) assuming that the $^{15}\text{N}_2$ ligand does not exchange with unlabelled N_2 .

[^{tol}NPNZr(THF)₂(μ - η^2 : η^2 -N₂)] [5.3] In the glove-box, yellow ^{tol}NPNZrCl₂(THF) [3.6] (1.02 g, 1.39 mmol) and bronze KC₈ (0.41 g, 3.01 mmol) were mixed as solids in a thick-walled flask. The flask was cooling to -196 °C with N₂(l) and 30 cm³ THF was vacuum-transferred. The frozen solid content of the reaction flask was exposed briefly to a dynamic N₂ flow at -196 °C. At this point an olive-green solid and solid white THF was observed. The reaction flask was transferred to an EtOH / N₂ / dry ice slurry bath behind an explosion shield and the reaction mixture was allowed to warm up slowly to room temperature (4 atm N₂) with vigorous stirring, forming a deep purple solution. After 20.33 hrs the reaction flask was cooled down to -196 °C with N₂(l), placed under a dynamic N₂ atmosphere and allowed to warm to room temperature. The reaction flask was sealed and transferred to the glovebox. The reaction mixture was filtered through celite with a sintered glass frit, washing with 2 x 10 cm³ THF. The THF solvent was removed *in vacuo* and the purple residue was triturated in 5 cm³ *n*-hexanes and placed in the freezer at -40 °C for 1.6 hrs. The purple solid was collected on a sintered glass frit, washed with 2 x 5 cm³ *n*-hexanes

and dried for 40 min (0.73 g, 0.54 mmol [tol NPNZr(THF)] $_2(\mu\text{-}\eta^2\text{:}\eta^2\text{-N}_2)$ [**5.3**], 78% yield based on tol NPNZrCl $_2$ (THF) [**3.6**].

$^{31}\text{P}\{\text{H}\}$ NMR (C_6D_6 , 162 MHz): $\delta = -3.93$ (s, P1). ^1H

NMR (C_6D_6 , 600 MHz): $\delta = 0.93$ (s, 8 H22, CH $_2$),

2.04 (s, 12 H16, CH $_3$), 2.10 (s, 12 H15, CH $_3$), 3.58 (s,

8 H21, CH $_2$), 6.67 (d, $^3J_{\text{HH}} = 8$ Hz, 4 H10 and 4 H14,

ArH), 6.84 (t, $^3J_{\text{HH}} = ^4J_{\text{PH}} = 7$ Hz, 4 H6, ArH), 6.91 (d,

$^3J_{\text{HH}} = 8$ Hz, 4 H5, ArH), 6.96 (bs, 2 H20 and 4 H18,

ArH), 7.15 (d, $^3J_{\text{HH}} = 8$ Hz, 4 H11 and 4 H13, ArH), 7.52 (d, $^3J_{\text{PH}} = 7$ Hz, 4 H3, ArH), 7.71 (bm, 4

H19, ArH). $^{13}\text{C}\{\text{H}\}$ NMR (C_6D_6 , 151 MHz): $\delta = 20.5$ (C16, CH $_3$), 20.8 (C15, CH $_3$), 25.3 (C22,

CH $_2$), 71.9 (C21, CH $_2$), 117.9 (d, $^3J_{\text{PC}} = 9$ Hz, C6, ArC), 118.9 (d, $^2J_{\text{PC}} = 31$ Hz, C7, C $_{\text{ipso}}$), 124.2

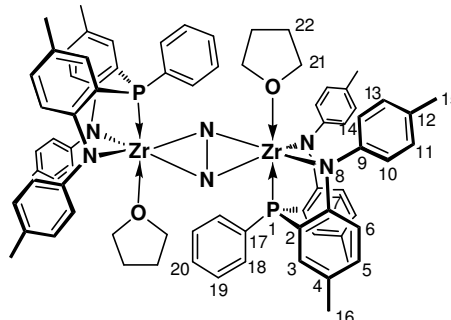
(C11 and C13, ArC), 127.4 (d, $^3J_{\text{PC}} = 4$ Hz, C4, C $_{\text{ipso}}$), 128.5 (d, $^2J_{\text{PC}} = 9$ Hz, C18, ArC), 128.9

(C20, ArC), 129.9 (C12, C $_{\text{ipso}}$), 130.2 (C10 and C14, ArC), 133.2 (d, $^3J_{\text{PC}} = 13$ Hz, C19, ArC),

133.6 (d, $^1J_{\text{PC}} = 41$ Hz, C17, C $_{\text{ipso}}$), 133.7 (C5, ArC), 134.6 (C3, ArC), 148.2 (C9, C $_{\text{ipso}}$), 160.3 (d,

$^1J_{\text{CP}} = 27$ Hz, C2, C $_{\text{ipso}}$). Anal. Calcd. for $\text{C}_{76}\text{H}_{78}\text{N}_6\text{O}_2\text{P}_2\text{Zr}_2$: C, 67.52; H, 5.82; N, 6.22; Found: C,

67.14; H, 6.20; N, 6.60. EI-MS (m/z): 1087 (5, $[\text{M} - 2\text{THF} - 2\text{N} - \text{C}_6\text{H}_4\text{CMe}]^+$).



Variation in reaction conditions for [iprop NPNZr(THF)] $_2(\mu\text{-}\eta^2\text{:}\eta^2\text{-N}_2)$ [**5.1**]

(i) **Scale-up x2** In the glove-box, yellow iprop NPNZrCl $_2$ (THF) [**3.5**] (2.08 g, 2.73 mmol) and bronze KC_8 (0.78 g, 5.80 mmol) were mixed as solids in a thick-walled flask. The flask was cooling to -196°C with $\text{N}_2(\text{l})$ and 20 cm^3 THF was vacuum-transferred. The frozen solid content of the reaction flask was exposed briefly to a dynamic N_2 flow at -196°C . At this point an olive-green solid and solid white THF was observed. The reaction flask was transferred to an EtOH / N_2 / dry ice slurry bath behind an explosion shield and the reaction mixture was allowed to warm up slowly to room temperature (4 atm N_2) with vigorous stirring, forming a dark brown solution.

After 14 hrs the reaction flask was placed under a dynamic N₂ atmosphere at room temperature. The reaction flask was sealed and transferred to the glovebox. The THF mixture was transferred to glass centrifuge tubes. After the mixture was centrifuged the supernatant was decanted. The THF solvent was removed *in vacuo* from the supernatant and the residue dried for 7.45 hrs.^(a) A black / purple solid was obtained from a toluene extraction and washed with *n*-hexanes (0.36 g, 0.25 mmol, [^{iprop}NPNZr(THF)]₂(μ-η²:η²-N₂) [**5.1**], 19% yield based on ^{iprop}NPNZrCl₂(THF) [**3.5**]).

^(a) The ³¹P{¹H} NMR spectrum of the crude residue displays peaks at δ -3.05 (for [**5.1**]) and peaks at δ 7.62 and 32.98.

(ii) Too concentrated In the glove-box, yellow ^{iprop}NPNZrCl₂(THF) [**3.5**] (2.83 g, 3.72 mmol) and bronze KC₈ (1.08 g, 8.02 mmol) were mixed as solids in a thick-walled flask. The flask was cooling to -196 °C with N₂(l) and 10 cm³ THF was vacuum-transferred. The frozen solid content of the reaction flask was exposed briefly to a dynamic N₂ flow at -196 °C. At this point an olive-green solid and solid white THF was observed. The reaction flask was transferred to an EtOH / N₂ / dry ice slurry bath behind an explosion shield and the reaction mixture was allowed to warm up slowly to room temperature (4 atm N₂) with vigorous stirring, forming a dark green solution by 4.2 hrs. After 12.2 hrs, the dark brown mixture in the reaction flask was slowly placed under a dynamic N₂ atmosphere at room temperature. The reaction flask was sealed and transferred to the glovebox. The reaction mixture was filtered through celite with a sintered glass frit, washing with 2 x 10 cm³ THF. The THF solvent was removed *in vacuo* and the residue was suspended in 20 cm³ *n*-hexanes. The *n*-hexanes solvent was removed *in vacuo* and the residue re-triturated with 20 cm³ *n*-hexanes, resulting in a brown solution with a purple solid. After being placed in the freezer at -40 °C the crude purple solid was collected on a sintered glass frit, washed with 90 cm³ *n*-hexanes and dried for 45 min (1.91 g).^(a) A dark brown-purple solid was obtained from a

toluene extraction and washed with *n*-hexanes (0.64 g, 0.46 mmol, [^{iprop}NPNZr(THF)]₂(μ-η²:η²-N₂) [**5.1**], 25% yield based on ^{iprop}NPNZrCl₂(THF) [**3.5**]).

^(a) The ³¹P{¹H} NMR spectrum of the crude solid displays a peak at δ -3.05 (for [**5.1**]) and peaks at δ -8.90, -2.50, 10.22 and 13.48.

(iii) Too dilute: In the glove-box, yellow ^{iprop}NPNZrCl₂(THF) [**3.5**] (0.21 g, 0.27 mmol) and bronze KC₈ (0.08 g, 0.57 mmol) were mixed as solids in a thick-walled flask. The flask was cooling to -196 °C with N₂(l) and 50 cm³ THF was vacuum-transferred. The frozen solid content of the reaction flask was exposed briefly to a dynamic N₂ flow at -196 °C. At this point an olive-green solid and solid white THF was observed. The reaction flask was transferred to an EtOH / N₂ / dry ice slurry bath behind an explosion shield and the reaction mixture was allowed to warm up slowly to room temperature (4 atm N₂) with vigorous stirring, forming a dark green / black solution. After 15.5 hrs, the reaction flask was slowly placed under a dynamic N₂ atmosphere at room temperature. The reaction flask was sealed and transferred to the glovebox. The THF solvent was removed *in vacuo* and the residue was suspended in 20 cm³ toluene. The dark green toluene reaction mixture was filtered through celite with a sintered glass frit, washing with additional toluene. The toluene solvent of the filtrate was removed *in vacuo* and the brown residue dried for 3 hrs.^(a)

^(a) The ³¹P{¹H} NMR spectrum of the crude solid displays numerous peaks between δ -20.22 to 23.73.

(iv) reduction only (no N₂): In the glove-box, yellow ^{iprop}NPNZrCl₂(THF) [**3.5**] (0.50 g, 0.66 mmol) and bronze KC₈ (0.20 g, 1.45 mmol) were mixed as solids in a thick-walled flask. The flask was cooling to -196 °C with N₂(l) and 10 cm³ THF was vacuum-transferred. While still under reduced pressure, the reaction flask was transferred to an EtOH / N₂ / dry ice slurry bath behind an explosion shield and the reaction mixture was allowed to warm up slowly to room

temperature with vigorous stirring, forming a green solution. After 1 day the reaction flask was cooled down to -196 °C with N₂(l), placed under a dynamic N₂ atmosphere and allowed to warm to room temperature. The reaction flask was sealed and transferred to the glovebox. The reaction mixture was filtered through celite with a sintered glass frit, washing with additional THF. The THF solvent was removed *in vacuo*, the residue triturated with 10 cm³ *n*-hexanes and the mixture was placed in the freezer at -40 °C overnight. The solid was collected on a sintered glass frit, washed with 10 cm³ *n*-hexanes and the dark brown / purple solid was dried (0.31 g)^(a). The solvent was removed *in vacuo* from the brown *n*-hexanes filtrate resulting in a brown residue.^(b)

^(a) The ³¹P{¹H} NMR spectrum of the solid showed no signal and the ¹H NMR spectrum displays broad peaks at δ 7.16 (phenyl), δ 3.60 (THF) and δ 2.75 / 1.22 (*i*-propyl).

^(b) The ³¹P{¹H} NMR spectrum of the filtrate residue displays a peak at δ -3.05 (for **[5.1]**) and peaks at δ -9.62, -8.48, -4.57, -0.62, 3.92, 5.83, 6.06, 18.38, 21.04, 33.03, 34.30 and 95.35.

(v) under-reduction (1 equiv of KC₈): In the glove-box, yellow ^{iprop}NPNZrCl₂(THF) **[3.5]** (0.29 g, 0.38 mmol) and bronze KC₈ (0.05 g, 0.40 mmol) were mixed as solids in a thick-walled flask. The flask was cooling to -196 °C with N₂(l) and 10 cm³ THF was vacuum-transferred. The contents of the reaction flask was exposed briefly to a dynamic N₂ flow at -196 °C. At this point an olive-green solid and solid white THF was observed. The reaction flask was transferred to an EtOH / N₂ / dry ice slurry bath behind an explosion shield and the reaction mixture was allowed to warm up slowly to room temperature (4 atm N₂) with vigorous stirring, forming an olive green-brown solution. After 1 day the reaction flask was cooled down to -196 °C with N₂(l), placed under a dynamic N₂ atmosphere and allowed to warm to room temperature. The reaction flask was sealed and transferred to the glovebox. The reaction mixture was filtered through celite with a sintered glass frit, washing with additional THF. The THF solvent was removed *in vacuo*, the residue triturated with 10 cm³ *n*-hexanes and the mixture was placed in the freezer at -40 °C

overnight. The light olive green-brown solid was collected on a sintered glass frit, washed with 10 cm³ *n*-hexanes and the light brown solid dried (0.12 g)^(a). The solvent was removed *in vacuo* from the yellow *n*-hexanes filtrate resulting in a yellow residue.^(b)

^(a) The ³¹P{¹H} NMR spectrum of the solid displayed a peak at δ 6.47 for unreacted ^{iprop}NPNZrCl₂(THF) [3.5].

^(b) The ³¹P{¹H} NMR spectrum of the filtrate residue displays a peak at δ 6.54 (for [3.5]) and peaks at δ -9.68, -4.60, -0.69, 2.86, 5.86 and 95.26.

(vi) no stirring: In the glove-box, yellow ^{iprop}NPNZrCl₂(THF) [3.5] (1.00 g, 1.31 mmol) and bronze KC₈ (0.35 g, 2.63 mmol) were mixed as solids in a thick-walled flask. The flask was cooling to -196 °C with N₂(l) and 50 cm³ THF was vacuum-transferred. The contents of the reaction flask was exposed briefly to a dynamic N₂ flow at -196 °C. At this point an olive-green solid and solid white THF was observed. The reaction flask was transferred to an EtOH / N₂ / dry ice slurry bath behind an explosion shield and the reaction mixture was allowed to warm up slowly to room temperature (4 atm N₂). Initially stagnant, vigorous stirring of the gooey green mixture commenced after 2.75 hrs. After 1 day, the reddish-brown mixture in the reaction flask was cooled down to -196 °C with N₂(l), placed under a dynamic N₂ atmosphere and allowed to warm to room temperature. The reaction flask was sealed and transferred to the glovebox. The THF solvent was removed *in vacuo* and the residue was suspended in 20 cm³ toluene. The toluene reaction mixture was filtered through celite with a sintered glass frit, washing with 2 x 20 cm³ toluene. The toluene solvent of the filtrate was removed *in vacuo* and the residue was triturated with 20 cm³ *n*-hexanes. The *n*-hexanes solvent was removed *in vacuo* and the residue re-triturated with 20 cm³ *n*-hexanes. After being placed in the freezer at -40 °C, an attempt to collect the solid clogged the sintered glass frit and the solid was dissolved with THF. The THF solvent of the filtrate was removed *in vacuo* and the residue triturated with 20 cm³ *n*-hexanes,

resulting in a brown solution with a suspended purple solid. The purple solid was collected on a sintered glass frit, washing copiously with *n*-hexanes in order to remove a *n*-hexanes -soluble brown impurity (0.27 g).^(a)

^(a) The $^{31}\text{P}\{^1\text{H}\}$ NMR spectrum of the solid displayed a peak at δ -9.64 and the ^1H NMR spectrum displays broad peaks at δ 7.16 (phenyl), δ 3.65 (THF) and δ 2.74 / 1.17 (*i*-propyl).

(vii) [$^{\text{iprop}}\text{NPNZr}(\text{THF})_2(\mu\text{-}\eta^2\text{:}\eta^2\text{-N}_2)$] [5.1] at 600 psi (control): Purple [$^{\text{iprop}}\text{NPNZr}(\text{THF})_2(\mu\text{-}\eta^2\text{:}\eta^2\text{-N}_2)$] [5.1] (0.05 g, 0.04 mmol) was dissolved in 50 cm³ THF in the glass lined 600 cm³ Parr 600 ml bench top stirred reactor inside the glove-box, forming a dark purple solution. The reactor was sealed in the glovebox and transferred to a high pressure N₂ line inside the fume hood behind an explosion shield. The high pressure N₂ line was connected to a column packed with alternating layers of molecular sieves and copper catalyst which was pre-activated with H₂ at 200 °C. After purging the line, the reactor was pressurized to 600 psi N₂ and stirred for 35 minutes. The reactor was returned to the glove-box and slowly depressurised. The purple solution was transferred to a conical flask and the THF solvent was removed *in vacuo* and the purple residue with a hint of green was dried for 1.5 hrs.

(viii) Reduction at 600 psi: In the glove-box, yellow $^{\text{iprop}}\text{NPNZrCl}_2(\text{THF})$ [3.5] (0.21 g, 0.27 mmol) was dissolved in 50 cm³ THF in the glass lined Parr reactor and a sealed glass ampoule containing KC₈ (0.08 g, 0.60 mmol) was placed in the yellow solution inside the reactor. The reactor was sealed in the glovebox and transferred to a high pressure N₂ line inside the fume hood behind an explosion shield. After purging the line, the reactor was pressurized to 600 psi N₂ and stirred at 50% for 11.5 hrs. The reactor was returned to the glove-box and slowly depressurised. The dark green solution was transferred to a conical flask and the THF solvent was removed *in vacuo*. The residue was suspended in 10 cm³ toluene and filtered through celite with a sintered glass frit. The toluene solvent of the light yellow filtrate was removed *in vacuo* and the light

yellow residue was triturated with 10 cm³ *n*-pentanes. After being in the freezer at -40 °C a yellow-green solid was collected on a sintered glass frit and dried.^(a) The *n*-pentanes solvent (which may have retained traces of toluene) was removed from the light yellow filtrate and the yellow residue was dried.^(b)

^(a) The ³¹P{¹H} NMR spectrum of the solid showed no signal and the ¹H NMR spectrum displays broad peaks at δ 7.16 (phenyl) and δ 2.76 / 1.20 (*i*-propyl).

^(b) The ³¹P{¹H} NMR spectrum of the filtrate residue displays peaks at δ -13.08, -8.57, -1.05, -0.97, -0.68, -0.57, 0.07, 0.18, 3.17, 3.25, 8.31, 8.35 and 20.30.

Reduction of ^{iprop}NPNHfCl₂(THF) [3.21] with KC₈ in N₂: (a) In the glove-box

^{iprop}NPNHfCl₂(THF) [3.21] (0.19 g, 0.23 mmol) and bronze KC₈ (0.09 g, 0.66 mmol) were mixed as solids in a thick-walled flask. The flask was cooling to -196 °C with N₂(l) and 10 cm³ THF was vacuum-transferred. The frozen solid content of the reaction flask was exposed briefly to a dynamic N₂ flow at -196 °C. The reaction flask was transferred to an EtOH / N₂ / dry ice slurry bath behind an explosion shield and the reaction mixture was allowed to warm up slowly to room temperature (4 atm N₂) with vigorous stirring. After three days, a yellow solution with a black ppt was observed the reaction flask was slowly depressurized to 1 atm N₂ at room temperature under a N₂ flow. The reaction flask was sealed and transferred to the glovebox. THF solvent was removed *in vacuo* and the dark black residue was suspended in 10 cm³ toluene. The reaction mixture was filtered through celite with a sintered glass frit, washing with 5 cm³ toluene. The toluene solvent was removed in vacuo from the orange-brown filtrate, leaving a brown residue.^(a)

(b) In the glove-box ^{iprop}NPNHfCl₂(THF) [3.21] (0.72 g, 0.85 mmol) and bronze KC₈ (0.23 g, 1.68 mmol) were mixed as solids in a thick-walled flask. The flask was cooling to -196 °C with N₂(l) and 10 cm³ THF was vacuum-transferred. The frozen solid content of the reaction flask was exposed briefly to a dynamic N₂ flow at -196 °C. The reaction flask was transferred to an EtOH /

N_2 / dry ice slurry bath behind an explosion shield and the reaction mixture was allowed to warm up slowly to room temperature (4 atm N_2) with vigorous stirring. After a few days the reaction flask was slowly depressurized to 1 atm N_2 at room temperature under a N_2 flow. The reaction flask was sealed and transferred to the glovebox. The reaction mixture was filtered through celite with a sintered glass frit and the THF solvent was removed *in vacuo* from the light brown filtrate, leaving a brown foam.^(b) The foam was dissolved in 0.5 cm³ THF, forming a yellow film which was triturated in 5 cm³ *n*-pentanes, resulting in the ppt of a mustard yellow solid. After the mixture was placed in the freezer, the mustard yellow solid was collected on a sintered glass frit and washed with 3 x 5 cm³ (0.46 g)^(b) (c) In the glove-box ^{iprop}NPNHfCl₂(THF) [3.21] (0.4575 g, 0.5394 mmol) and bronze KC₈ (0.16 g, 1.15 mmol) were mixed as solids in a thick-walled flask. The flask was cooling to -196 °C with $\text{N}_2(\text{l})$ and 10 cm³ THF was vacuum-transferred. The frozen solid content of the reaction flask was exposed briefly to a dynamic N_2 flow at -196 °C. The reaction flask was transferred to an EtOH / N_2 / dry ice slurry bath behind an explosion shield and the reaction mixture was allowed to warm up slowly to room temperature (4 atm N_2) with vigorous stirring. After three days a dark brown mixture with a yellow tinge was obtained and the reaction flask was slowly depressurized to 1 atm N_2 at room temperature under a N_2 flow. The reaction flask was sealed and transferred to the glovebox. The THF solvent was removed *in vacuo* and the residue was triturated with 20 cm³ *n*-hexanes, giving a dark ppt in a yellow solution. The *n*-hexanes solvent was removed *in vacuo* and the residue was suspended in 20 cm³ toluene. The mixture was filtered through celite on a sintered glass frit, washing with 2 x 10 cm³ toluene. The toluene solvent was removed *in vacuo* and the orange residue was dried to give a tan brown solid. This solid was dissolved in 10 cm³ toluene and centrifuged, with some solid observed to settle. The supernatant was removed and the toluene solvent removed *in vacuo*. The orange-brown residue was triturated with twice with *n*-hexanes. After the mixture was placed in the freezer, a brown solid was collected on a sintered glass frit and washed with 2 x 2 cm³ (0.23 g)^(c)

(a) $^{31}\text{P}\{^1\text{H}\}$ NMR spectrum displays peaks at $\delta = -15.12, -5.67, -5.39, -3.88$ (major), $1.05, 5.44$ ($^{\text{iprop}}\text{NPNHfCl}_2(\text{THF})$ [**3.21**]) and 18.52 ($[\text{ipropNPN}]_2\text{Hf}$). EI-MS (m/z): 1232 ($60, [\text{ipropNPN}]_2\text{Hf}^+$).

(b) $^{31}\text{P}\{^1\text{H}\}$ NMR spectrum displays peaks at $\delta = -15.12$ (major), $-5.68, -4.07, -3.39$ (major). EI-MS (m/z): 1416 ($10, [\text{ipropNPNHf}]_2(\text{H})_4^+$), 1232 ($60, [\text{ipropNPN}]_2\text{Hf}^+$).

(c) $^{31}\text{P}\{^1\text{H}\}$ NMR spectrum displays no signals and no signals were observed in the EPR spectrum (apart from a signal for a Zr impurity present in commercially obtained Hf sources).¹⁵² EI-MS (m/z): 1416 ($30, [\text{ipropNPNHf}]_2(\text{H})_4^+$), 1232 ($90, [\text{ipropNPN}]_2\text{Hf}^+$).

$[\text{tolNPNZr}(\text{Py})]_2(\mu\text{-}\eta^2\text{:}\eta^2\text{-N}_2)$ [**5.4**] Purple $[\text{tolNPNZr}(\text{THF})]_2(\mu\text{-}\eta^2\text{:}\eta^2\text{-N}_2)$ [**5.3**] (0.04 g, 0.03 mmol) was dissolved in 1 cm^3 pyridine in a small r/b flask in the glove box, forming a deep green solution. The pyridine solvent was removed in vacuo and the resultant green solid was dried for 1.5 hrs.

$^{31}\text{P}\{\text{H}\}$ NMR (C_6D_6 , 162 MHz): $\delta = -4.94$ (s, P1). ^1H

NMR (C_6D_6 , 600 MHz): $\delta = 1.92$ (s, 12 H16, CH_3), 2.08

(s, 12 H15, CH_3), 6.33 (t, $^3J_{\text{HH}} = 7\text{ Hz}$, 4 H22, ArH), 6.45

(d, $^3J_{\text{HH}} = 8\text{ Hz}$, $4\text{ H10 and }4\text{ H14, ArH}$), 6.65 (bs, H22a

and H23a, ArH), 6.74 (t, $^3J_{\text{HH}} = 8\text{ Hz}$, 2 H23, ArH), 6.91 (d of d, $^3J_{\text{HH}} = 8\text{ Hz}$, $^4J_{\text{PH}} = 5\text{ Hz}$, 4 H6,

ArH), 6.97 (d, $^3J_{\text{HH}} = 8\text{ Hz}$, 4 H5, ArH), 7.03 (d, $^3J_{\text{HH}} = 8\text{ Hz}$, $4\text{ H11 and }4\text{ H13, ArH}$), 7.08 (bs, 2

$\text{H20 and }4\text{ H18, ArH}$), 7.61 (d, $^3J_{\text{PH}} = 7\text{ Hz}$, 4 H3, ArH), 7.83 (bm, 4 H19, ArH), 8.54 (bs, H21a,

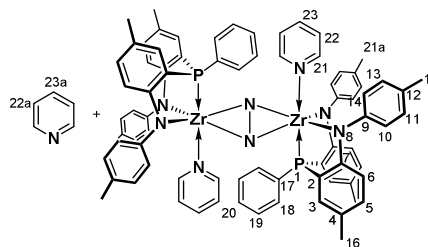
ArH), 8.81 (d, $^3J_{\text{HH}} = 8\text{ Hz}$, 4 H21). $^{13}\text{C}\{^1\text{H}\}$ NMR (C_6D_6 , 151 MHz): $\delta = 20.9$ (C15, CH_3), 21.1

(C16, CH_3), 117.3 (d, $^3J_{\text{PC}} = 9\text{ Hz}$, C6, ArC), 118.9 (d, $^2J_{\text{PC}} = 30\text{ Hz}$, $\text{C7, C}_{\text{ipso}}$), 123.4 (C22 and

C22a, ArC), 125.1 (C11 and C13, ArC), 127.2 (d, $^3J_{\text{PC}} = 4\text{ Hz}$, $\text{C4, C}_{\text{ipso}}$), 128.7 (C20, ArC),

128.8 (d, $^2J_{\text{PC}} = 2\text{ Hz}$, C18, ArC), 129.8 (C10 and C14, ArC), 130.0 ($\text{C12, C}_{\text{ipso}}$), 133.4 (d, $^3J_{\text{PC}} =$

14 Hz , C19, ArC), 133.8 (C5, ArC), 134.4 (d, $^1J_{\text{PC}} = 26\text{ Hz}$, $\text{C17, C}_{\text{ipso}}$), 134.9 (C3, ArC), 135.2



(C23a, ArC), 136.8 (C23, ArC), 147.8 (C9, C_{ipso}), 150.3 (C21a, ArC), 150.6 (C21, ArC), 160.8 (d, ¹J_{CP} = 28 Hz, C2, C_{ipso}).

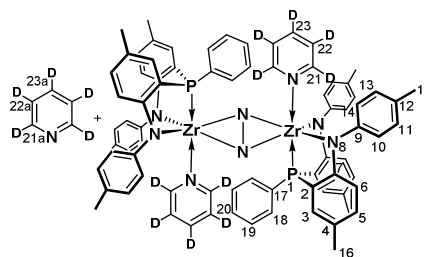
[^{tol}NPNZr(Py-*d*₅)]₂(μ-η²:η²-N₂) [5.5] Purple [^{tol}NPNZr(THF)]₂(μ-η²:η²-N₂) [5.3] (0.04 g, 0.03 mmol) was dissolved in 1 cm³ pyridine-*d*₅ in a small r/b flask in the glove box, forming a deep green solution. The pyridine-*d*₅ solvent was removed in vacuo and the resultant green solid was dried.

³¹P{¹H} NMR (C₆D₆, 162 MHz): δ = -4.93 (s, P1). ¹H

NMR (C₆D₆, 600 MHz): δ = 1.92 (s, 12 H16, CH₃),

2.08 (s, 12 H15, CH₃), 6.45 (d, ³J_{HH} = 8 Hz, 4 H10

and 4 H14, ArH), 6.90 (d of d, ³J_{HH} = 8 Hz, ⁴J_{PH} = 5



Hz, 4 H6, ArH), 6.97 (d, ³J_{HH} = 8 Hz, 4 H5, ArH), 7.03 (d, ³J_{HH} = 8 Hz, 4 H11 and 4 H13, ArH),

7.08 (bs, 2 H20 and 4 H18, ArH), 7.61(d, ³J_{PH} = 7 Hz, 4 H3, ArH), 7.83 (bm, 4 H19, ArH).

¹³C{¹H} NMR (C₆D₆, 151 MHz): δ = 20.5 (C15, CH₃), 20.7 (C16, CH₃), 117.3 (d, ³J_{PC} = 9 Hz,

C6, ArC), 118.9 (d, ²J_{PC} = 30 Hz, C7, C_{ipso}), 122.9 (t, ¹J_{CD} = 25 Hz, C22, ArC), 125.1 (C11 and

C13, ArC), 127.2 (d, ³J_{PC} = 3 Hz, C4, C_{ipso}), 128.7 (C20, ArC), 128.8 (d, ²J_{PC} = 2 Hz, C18, ArC),

129.8 (C10 and C14, ArC), 130.1 (C12, C_{ipso}), 133.4 (d, ³J_{PC} = 14 Hz, C19, ArC), 133.8 (C5,

ArC), 134.4 (d, ¹J_{PC} = 26 Hz, C17, C_{ipso}), 134.7 (d, ¹J_{CD} = 24 Hz, C23, ArC), 135.0 (C3, ArC),

147.8 (C9, C_{ipso}), 149.9 (m, ¹J_{CD} = 26 Hz, C21, ArC), 160.8 (d, ¹J_{CP} = 28 Hz, C2, C_{ipso}).

[^{iprop}NPNZr(4,4'-bipy)]₂(μ-η²:η²-N₂) [5.6] with 2 equiv of 4,4'-bipy: In the glovebox, 2 cm³

C₆D₆ was added to a solid mixture of purple [^{iprop}NPNZrTHF]₂N₂ (0.05 g, 0.04 mmol) and 4,4'-

bipyridine (0.01 g, 0.05 mmol) at room temperature. After NMR spectroscopic analysis, the

solution was placed in the freezer at -40 °C for 3 days. Thereafter, additional 4,4'-bipyridine

(0.01 g, 0.05 mmol) was added at room temperature and the brown solution was re-analysed.

$^{31}\text{P}\{\text{H}\}$ NMR (C_6D_6 , 162 MHz): $\delta = -4.89$ (s, P1 / P1a).^(a)

^1H NMR (C_6D_6 , 400 MHz): $\delta = 0.93$ (m, 6 H16 and 6 H17, CH_3), 1.17 (m, 6 H16a and 6 H17a, CH_3), 1.42 (s, 4 H, THF, CH_2),^(b) 2.47 (hep, $^3J_{\text{HH}} = 7$ Hz, 2 H15, CH), 2.76 (m, $^3J_{\text{HH}} = 7$ Hz, 2 H15a, CH), 3.57 (s, 4 H, THF, CH_2),^(b)

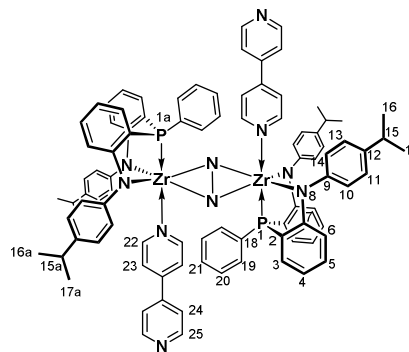
6.55 (overlapping t and d, $^3J_{\text{HH}} = 8$ Hz, 4 H4, 4 H10 and 4

H14 ArH), 6.75 (m, $^3J_{\text{HH}} = ^4J_{\text{PH}} = 7$ Hz, 4 H6, 2 H23 and 2 H24, ArH), 6.80 (s, 4 H, bipy, ArH),^(c)

6.96 (m, $^3J_{\text{HH}} = ^3J_{\text{PH}} = 8$ Hz, 4 H5, 4 H19 and 2 H21, ArH), 7.16 (bs, 4 H11 and 4 H13, ArH

overlapping C_6H_6), 7.63 (t, $^3J_{\text{HH}} = ^3J_{\text{PH}} = 6$ Hz, 4 H3, ArH), 7.86 (t, $^3J_{\text{HH}} = 6$ Hz, 4 H20, ArH),

8.57 (s, 4 H, bipy, ArH),^(c) 8.63 (s, 2 H25, ArH),^(c) 8.95 (s, 2 H22, ArH).



^(a) There are trace impurities from the precursor **[5.1]** complex with peaks at δ 4.32, δ 5.39 and δ 10.49.

^(b) 1 equiv of free THF, signals at δ 0.93 and 3.62 for precursor **[5.1]**.

^(c) 2.5 equiv of 4,4'-bipyridine was added; hence 0.5 equiv of uncoordinated 4,4'-bipyridine + half of 2 equiv of the coordinated 4,4'-bipyridine will give signals expected of free 4,4'-bipyridine. Due to impurities in precursor **[5.1]**, the 4,4'-bipyridine equiv may be greater than 2.5.

$\{[\text{ipropNPNZr}]_2(4,4'\text{-bipy})(\mu\text{-}\eta^2\text{:}\eta^2\text{-N}_2)\}_n$ [5.6a] with 1 equiv 4,4'-bipy: In the glove box, 1 cm^3 toluene was added to a solid mixture of purple $[\text{ipropNPNZr}(\text{THF})_2(\mu\text{-}\eta^2\text{:}\eta^2\text{-N}_2)]$ **[5.1]** (0.27 g, 0.19 mmol) and 4,4'-bipyridine (0.03 g, 0.19 mmol), forming a dark brown solution. The toluene solvent was removed *in vacuo* and the brown residue was dried and triturated twice with 1 cm^3 *n*-pentanes. The *n*-pentanes solvent was removed *in vacuo*, leaving a dark brown-black solid. After NMR analysis, the C_6D_6 solvent was removed *in vacuo* and the brown residue was dried and triturated with *n*-pentanes. The dark purple black solid was collected on a sintered glass frit and washed with 3 x 2 cm^3 *n*-pentanes (0.19 g). After NMR analysis, the sample was returned and the

residue was dissolved in 5 cm³ toluene. The brown solution was filtered through celite with a sintered glass frit, washing with 3 x 5 cm³ toluene. The toluene solvent was removed *in vacuo* from the dark purple filtrate and the dark residue was dried and triturated with 5 cm³ *n*-pentanes. The black solid was collected on a sintered glass frit and washed with *n*-pentanes (0.10 g).

³¹P{¹H} NMR (C₆D₆, 162 MHz): δ = -4.68 (d, ⁴J_{PP} = 11 Hz,

P1), -4.89 (s, P1a).^(a) ¹H NMR (C₆D₆, 400 MHz): δ = 0.83

to 1.37 (m, 6 H16, 6 H16a, 6 H17 and 6 H17a, CH₃), 2.82

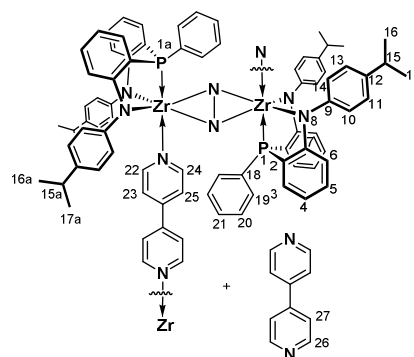
to 2.43 (m, 2 H15 and 2 H15a, CH), 6.55 to 7.25 (m, 4 H4,

4 H10, 4 H14, 4 H6, 2 H23, 2 H25, 2H27, 4 H5, 4 H19 and

2 H21, 4 H11 and 4 H13, ArH), 7.66 (t, ³J_{HH} = ³J_{PH} = 7 Hz,

4 H3, ArH), 7.86 (t, ³J_{HH} = 8 Hz, 4 H20, ArH), 8.63 (bs, 2 H26, ArH), 8.94, 8.98 (s, 2 H22 and

2H24, ArH).



^(a) There are peaks at δ 4.27, δ 5.42 and δ 10.48, which are impurities also present in the precursor THF zirconium N₂ complex [5.1].

[ⁱpropNPNZr(THF)](μ - η^2 : η^2 -N₂)[ⁱpropNPNZr(PMe₃)] [5.7] + [ⁱpropNPNZr(THF)]₂(μ - η^2 : η^2 -N₂)

[5.1] (a) in Et₂O: A purple solution of [ⁱpropNPNZr(THF)]₂(μ - η^2 : η^2 -N₂) [5.1] (0.05 g, 0.04 mmol)

in 2 cm³ Et₂O was cooled down to -30 °C in the freezer in the glovebox. PMe₃ (200 μ L, 1.97 mmol) was added via micro-syringe to the chilled solution and returned to the freezer, forming a blue solution. After 30 min, the Et₂O solvent was removed *in vacuo*, and the blue-green residue

dissolved in C₆D₆, forming a purple solution. (b) in C₆D₆: PMe₃ (6.5 μ L, 0.06 mmol) was added

at room temperature via micro-syringe to a purple solution of [ⁱpropNPNZr(THF)]₂(μ - η^2 : η^2 -N₂)

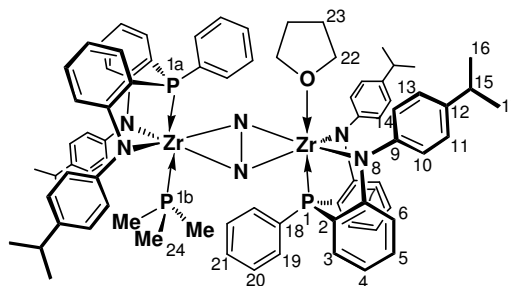
[5.1] (0.04 g, 0.03 mmol) in 1 cm³ C₆D₆ in the glovebox. No colour change was observed, even

after further additions of PMe₃ (2 x 5.0 μ L, 0.0983 mmol) and the resultant purple solution was

analysed using ³¹P{¹H} NMR spectroscopy. (c) excess PMe₃: After NMR analysis of (b), the

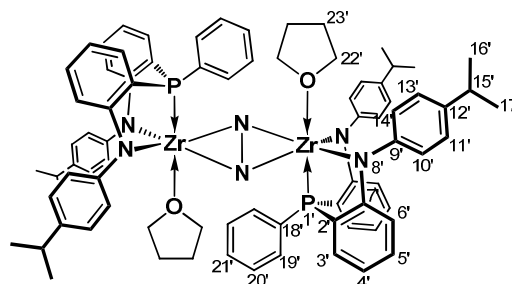
C₆D₆ was removed *in vacuo* and the purple residue was dissolved in 3 cm³ Et₂O. PMe₃ (50 μL, 0.49 mmol) was added via micro-syringe and the solution was placed in the freezer (-30 °C) overnight and the Et₂O solvent was removed *in vacuo*. The green residue was redissolved in Et₂O, forming a purple solution which did not become green when placed in the freezer at -30 °C. Additional PMe₃ was added to the Et₂O solution at room temperature until a colour change to green was observed. The Et₂O solvent was removed *in vacuo* and the green residue was dissolved in toluene-*d*₈ and analysed using ³¹P{¹H} NMR spectroscopy (Figure 149).

³¹P{¹H} NMR (C₆D₆, 162 MHz): δ = -32.30 (d, ²J_{PP} = 25 Hz, P1b), -4.20 (s, P1), -1.64 (d, ²J_{PP} = 25 Hz, P1a). ¹H NMR (C₆D₆, 400 MHz): δ = 0.46 (bd, ³J_{HH} = 4 Hz, H23, CH₂), 0.58 (d, ²J_{PH} = 6 Hz, H24, P-CH₃), 0.81 (bs, P-CH₃), ^(a)1.27 (d, ³J_{HH} = 7 Hz, H16 and H17, CH₃), 2.82 (hep, ³J_{HH} = 7 Hz, H15, CH), 3.75 (s, H22, CH₂), 6.75 (m, ³J_{HH} = 6 Hz, H4, ArH), 6.85 (m, ³J_{HH} = ⁴J_{PH} = 6 Hz, H6, ArH), 6.93 (d, ³J_{HH} = 8 Hz, H10 and H14, ArH), 7.07 (m, ³J_{HH} = ³J_{PH} = 7 Hz, H5, H20 and H21, ArH), 7.24 (d, ³J_{HH} = 8 Hz, H11 and H13, ArH), 7.57 (m, ³J_{HH} = ³J_{PH} = 8 Hz, H3, ArH), 7.78 (t, ³J_{HH} = 9 Hz, H19, ArH).



³¹P{¹H} NMR (C₆D₆, 162 MHz): δ = -3.05 (s, P1').

¹H NMR (C₆D₆, 400 MHz): δ = 0.98 (bd, ³J_{HH} = 6 Hz, H23', CH₂), 1.26 (d, ³J_{HH} = 6 Hz, H16' and H17', CH₃), 2.74 (hep, ³J_{HH} = 7 Hz, H15', CH), 3.64 (s, H22', CH₂), 6.75 (m, ³J_{HH} = 6 Hz, H4', H10' and H14' ArH), 6.85 (m, ³J_{HH} = ⁴J_{PH} = 6 Hz, H6', ArH), 7.07 (m, ³J_{HH} = ³J_{PH} = 7 Hz, H5', H19' and H21', ArH), 7.32 (d, ³J_{HH} = 8 Hz, H11' and H13', ArH), 7.57 (m, ³J_{HH} = ³J_{PH} = 8 Hz, H3', ArH), 7.84 (t, ³J_{HH} = 9 Hz, H20', ArH).



^(a) free PMe₃

[ⁱpropNPNZr(PMe₃)₂(μ-η²:η²-N₂)] [5.8] After NMR analysis of the green [5.7] (c) solution, the toluene-*d*₈ solvent was removed *in vacuo*, with the solution transitioning through a dark blue colour to give a deep blue residue, which became purple when dried. The purple residue was subjected to three cycles of dissolution / evacuation in 2 cm³ Et₂O, resulting in a reddish coloured solution. Addition of PMe₃ (100 μL, 0.98 mmol) led to the formation of a blue-green solution. The Et₂O solvent was removed *in vacuo* and the dark green residue was dissolved in C₆D₆ to form a dark purple to black solution (Figure 152).

³¹P{¹H} NMR (C₆D₆, 162 MHz): δ = -31.93

(d, ²J_{PP} = 25 Hz, P1b), -1.41 (d, ²J_{PP} = 23 Hz,

P1). ¹H NMR (C₆D₆, 300 MHz): δ = 0.55 (d

of d, ²J_{PH} = 9 Hz, ⁴J_{PH} = 2 Hz, H22, P-CH₃),

0.81 (bs, P-CH₃), ^(a) 1.11 (t, ³J_{HH} = 7 Hz, Et₂O,

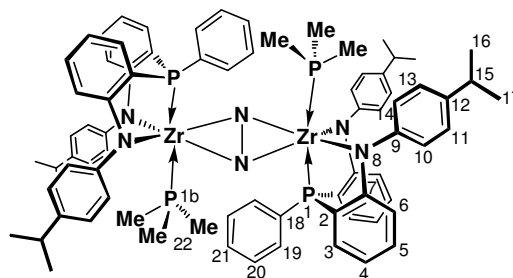
CH₃), ^(b) 1.21 (d, ³J_{HH} = 7 Hz, 12 H16 and 12 H17, CH₃), 1.48 (s, THF, CH₂), ^(c) 2.75 (hep, ³J_{HH} = 7

Hz, 4 H15, CH), 3.28 (q, ³J_{HH} = 7 Hz, Et₂O, CH₂), ^(b) 3.54 (s, THF, CH₂), ^(c) 6.74 (m, ³J_{HH} = ⁴J_{PH} = 7

Hz, 4 H4 and 4 H6, ArH), 6.83 (d, ³J_{HH} = 8 Hz, 4 H10 and 4 H14 ArH), 7.05 (m, ³J_{HH} = ³J_{PH} = 8

Hz, 4 H5, 4 H11, 4 H13, 4 H20 and 2 H21, ArH), 7.47 (t, ³J_{HH} = ³J_{PH} = 7 Hz, 4 H3, ArH), 7.65 (t,

³J_{HH} = 8 Hz, 4 H19, ArH).



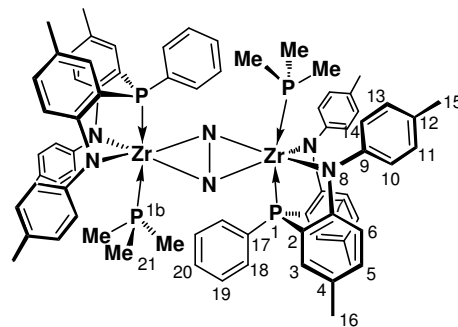
^(a) free PMe₃, ^(b) free Et₂O, ^(c) free THF

[^{tol}NPNZr(PMe₃)₂(μ-η²:η²-N₂)] [5.9] Purple [^{tol}NPNZr(THF)₂(μ-η²:η²-N₂)] [5.3] (0.04 g, 0.03

mmol) was dissolved in neat PMe₃, forming a deep green solution. The PMe₃ solvent was removed *in vacuo*, leaving a green residue. The residue was dissolved in C₆D₆ to form a deep blue solution. After ³¹P{¹H} NMR spectroscopic analysis, the C₆D₆ solvent was removed *in*

vacuo and the residue was re-dissolved in neat PMe_3 , forming a green solution. The PMe_3 solvent was removed in *vacuo* and the residue was re-dissolved in C_6D_6 , forming a deep blue solution.

$^{31}\text{P}\{\text{H}\}$ NMR (C_6D_6 , 162 MHz): $\delta = -31.68$ (d, $^2J_{\text{PP}} = 26$ Hz, P1b), -1.09 (d, $^2J_{\text{PP}} = 26$ Hz, P1). ^1H NMR (C_6D_6 , 600 MHz): $\delta = 0.72$ (d, $^2J_{\text{PH}} = 6$ Hz, H21, P- CH_3), 0.81 (bs, P- CH_3),^(a) 2.01 (s, 12 H16, CH_3), 2.19 (s, 12 H15, CH_3), 6.81 (d of d, $^3J_{\text{HH}} = 8$ Hz, $^4J_{\text{PH}} = 6$ Hz, 4 H6, ArH), 6.87 (d, $^3J_{\text{HH}} = 8$ Hz, 4 H10 and 4 H14, ArH), 6.94 (d, $^3J_{\text{HH}} = 8$ Hz, 4



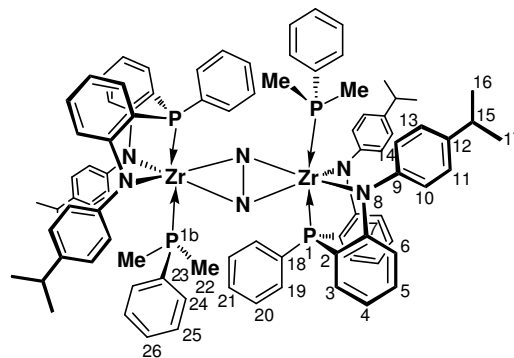
H5, ArH), 7.01 (t, $^3J_{\text{HH}} = 8$ Hz, 2 H20, ArH), 7.08 (t, $^3J_{\text{HH}} = 7$ Hz, 4 H19, ArH), 7.20 (d, $^3J_{\text{HH}} = 8$ Hz, 4 H11 and 4 H13, ArH), 7.58 (d, $^3J_{\text{PH}} = 7$ Hz, 4 H3, ArH), 7.86 (t, $^3J_{\text{HH}} = 9$ Hz, 4 H18, ArH).

$^{13}\text{C}\{\text{H}\}$ NMR (C_6D_6 , 151 MHz): $\delta = 14.0$ (d, $^1J_{\text{PH}} = 13$ Hz, C21, CH_3), 16.2 (P- CH_3),^(a) 20.6 (C16, CH_3), 20.9 (C15, CH_3), 119.3 (d, $^2J_{\text{PC}} = 29$ Hz, C7, C_{ipso}), 120.2 (d, $^3J_{\text{PC}} = 7$ Hz, C6, ArC), 124.1 (C11 and C13, ArC), 128.8 (d, $^3J_{\text{PC}} = 9$ Hz, C19, ArC), 129.5 (C12, C_{ipso}), 129.6 (C20, ArC), 130.3 (C10 and C14, ArC), 131.4 (d, $^1J_{\text{PC}} = 22$ Hz, C17, C_{ipso}), 133.4 (C5 and C4, C_{ipso}), 133.5 (d, $^2J_{\text{PC}} = 3$ Hz, C3, ArC), 133.7 (C18, ArC), 148.6 (C9, C_{ipso}), 157.7 (d, $^1J_{\text{CP}} = 25$ Hz, C2, C_{ipso}).

^(a) free PMe_3

$[\text{ipropNPNZr}(\text{PPMe}_2)_2(\mu\text{-}\eta^2\text{:}\eta^2\text{-N}_2)]$ **[5.10]** PPhMe_2 (320 μL , 2.24 mmol) was added via micro-syringe to a purple solution of $[\text{ipropNPNZr}(\text{THF})_2(\mu\text{-}\eta^2\text{:}\eta^2\text{-N}_2)]$ **[5.1]** (0.04 g, 0.03 mmol) in 3 cm^3 toluene in the glove box, with no visible colour change. The toluene solvent was removed *in vacuo*, with the purple solution transitioning through to a blue-green blue colour to give a deep blue-green residue. The residue was dissolved in C_6D_6 , forming a dark green solution. After analysis, the C_6D_6 solvent was removed *in vacuo* and the green residue dried overnight (Figure 150).

$^{31}\text{P}\{\text{H}\}$ NMR (C_6D_6 , 162 MHz): $\delta = -18.92$ (d, $^2J_{\text{PP}} = 26$ Hz, P1b), -1.79 (d, $^2J_{\text{PP}} = 25$ Hz, P1). ^1H NMR (C_6D_6 , 400 MHz): $\delta = 1.01$ (d, $^2J_{\text{PH}} = 5$ Hz, H22, P-CH₃), 1.16 (bs, P-CH₃), $^{(a)} 1.35$ (d, $^3J_{\text{HH}} = 7$ Hz, 12 H16, CH₃), 1.36 (d, $^3J_{\text{HH}} = 7$ Hz, 12 H17, CH₃), 2.87 (hep, $^3J_{\text{HH}} = 7$ Hz, 4 H15, CH), 6.84

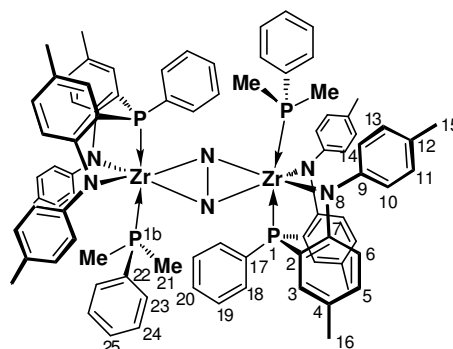


(m, $^3J_{\text{HH}} = 6$ Hz, 4 H4, 4 H10 and 4 H14, ArH), 6.93 (bs, 4 H25, ArH), 7.67 (t, $^3J_{\text{HH}} = ^4J_{\text{PH}} = 7$ Hz, 4 H6, ArH), 7.20 (m, $^3J_{\text{HH}} = ^3J_{\text{PH}} = 9$ Hz, 4 H5, 4 H11, 4 H13, 4 H20 and 2 H21, ArH), 7.46 (bs, 4 H24 and 2 H26, ArH), 7.69 (t, $^3J_{\text{HH}} = ^3J_{\text{PH}} = 7$ Hz, 4 H3, ArH), 7.90 (t, $^3J_{\text{HH}} = 8$ Hz, 4 H19, ArH).

^(a) free PPhMe₂

$[\text{}^{\text{tol}}\text{NPNZr}(\text{PPhMe}_2)]_2(\mu\text{-}\eta^2\text{:}\eta^2\text{-N}_2)$ **[5.11]** Purple $[\text{}^{\text{tol}}\text{NPNZr}(\text{THF})]_2(\mu\text{-}\eta^2\text{:}\eta^2\text{-N}_2)$ **[5.3]** (0.19 g, 0.14 mmol) was subjected to three dissolution / evacuation cycles with 10 cm^3 Et₂O. The resulting reddish-purple solid was re-dissolved in 10 cm^3 Et₂O and PPhMe₂ (1.00 cm^3 , 7.00 mmol) was added via syringe at room temperature, with no colour change being observed. While the Et₂O solvent was being removed *in vacuo*, the solution became black and then blue in colour and eventually a black-purple oil was obtained. On further drying, a green residue was obtained which was triturated in 5 cm^3 *n*-pentanes and placed in the freezer. The olive-green solid was collected on a sintered glass frit and washed with $2 \times 3\text{ cm}^3$ cold *n*-pentanes (0.06 g, 0.04 mmol $[\text{}^{\text{tol}}\text{NPNZr}(\text{PPhMe}_2)]_2(\mu\text{-}\eta^2\text{:}\eta^2\text{-N}_2)$, 27% yield based on $[\text{}^{\text{tol}}\text{NPNZr}(\text{THF})]_2(\mu\text{-}\eta^2\text{:}\eta^2\text{-N}_2)$ **[5.3]**) (Figure 151).

$^{31}\text{P}\{\text{H}\}$ NMR (C_6D_6 , 162 MHz): $\delta = -17.59$ (d, $^2J_{\text{PP}} = 26$ Hz, P1b), -1.04 (d, $^2J_{\text{PP}} = 26$ Hz, P1). ^1H NMR (C_6D_6 , 400 MHz): $\delta = 0.97$ (d, $^2J_{\text{PH}} = 7$ Hz, H21, P-CH₃), 1.16 (bs, P-CH₃), $^{(a)} 2.06$, 2.17 (s, H16, CH₃),



2.09, 2.21 (s, H15, CH₃), 6.79 to 7.41 (m, ³J_{HH} = 8 Hz H5, H6, H10, H11, H13, H14, H19, H20, H23, H24 and H25, ArH), 7.70 (t, ³J_{HH} = ³J_{PH} = 7 Hz, 4 H3, ArH), 7.95 (t, ³J_{HH} = 8 Hz, 4 H18, ArH).

^(a) free PPhMe₂

Reduction of ^{iprop}NPNZrCl₂(THF) [3.5] with KC₈ in Et₂O (+ PPhMe₂): In the glove-box, yellow ^{iprop}NPNZrCl₂(THF) [3.5] (0.35 g, 0.47 mmol) and bronze KC₈ (0.14 g, 1.02 mmol) were mixed as solids in a thick-walled flask. The flask was cooling to -196 °C with N₂(l) and 10 cm³ Et₂O was vacuum-transferred. The frozen solid content of the reaction flask was exposed briefly to a dynamic N₂ flow at -196 °C. At this point an olive-green solid and solid white THT was observed. The reaction flask was transferred to an EtOH / N₂ / dry ice slurry bath behind an explosion shield and the reaction mixture was allowed to warm up slowly to room temperature (4 atm N₂) with vigorous stirring, forming a dark green solution after 2 hrs. After 15.3 hrs the reaction flask containing a dark brown mixture was cooled down to -196 °C with N₂(l), placed under a dynamic N₂ atmosphere and allowed to warm to room temperature. The reaction flask was sealed and transferred to the glovebox. The reaction mixture was filtered through celite with a sintered glass frit, washing with 10 cm³ Et₂O. The Et₂O solvent of the dark brown filtrate was reduced to 2 cm³ and PPhMe₂ (1.40 cm³, 9.80 mmol) was added, with no change in colour observed. The solvent was removed in vacuo to give a brown oil.

Reaction with P^tBu₃: Purple [^{iprop}NPNZr(THF)]₂(μ-η²:η²-N₂) (0.20 g, 0.15 mmol) was subjected to three dissolution / evacuation cycles with 5 cm³ Et₂O. The resulting reddish-purple solid was re-dissolved in 10 cm³ Et₂O and P^tBu₃ (0.29 g, 1.45 mmol) was added via syringe at room temperature, with no colour change being observed. The Et₂O solvent was removed *in vacuo*, leaving a purple oil. On addition of 2 cm³ *n*-hexanes, a purple solid was precipitated and collected on a sintered glass frit (0.11 g, 0.08 mmol [^{iprop}NPNZr(THF)]₂(μ-η²:η²-N₂) [5.1]).

Reaction with dmpe: Purple $[\text{iprop}^{\text{I}}\text{NPNZr}(\text{THF})]_2(\mu\text{-}\eta^2\text{:}\eta^2\text{-N}_2)$ (0.21 g, 0.15 mmol) was subjected to three dissolution / evacuation cycles with 5 cm³ Et₂O. The resulting reddish-purple solid was re-dissolved in 5 cm³ Et₂O and dmpe (0.29 g, 1.45 mmol) was added via micro-syringe at room temperature, forming a dark green solution. The Et₂O solvent was removed *in vacuo*, leaving a dark-brown oil. On addition of 2 cm³ *n*-hexanes, a brown solid was precipitated and collected on a sintered glass frit, washing with 3 x 3 cm³ *n*-hexanes (0.10 g) and a sample dissolved in C₆D₆.

$[\text{tol}^{\text{I}}\text{NPNZr}(\text{THT})]_2(\mu\text{-}\eta^2\text{:}\eta^2\text{-N}_2)$ [5.14] with $[\text{tol}^{\text{I}}\text{NPNZr}(\text{THF})]_2(\mu\text{-}\eta^2\text{:}\eta^2\text{-N}_2)$ [5.3] Purple

$[\text{tol}^{\text{I}}\text{NPNZr}(\text{THF})]_2(\mu\text{-}\eta^2\text{:}\eta^2\text{-N}_2)$ [5.3] (0.05 g, 0.03 mmol) was dissolved in neat tetrahydrothiophene THT, with no colour change being observed. The THT solvent was removed *in vacuo* and the purple residue was dissolved in C₆D₆ (Figure 153).

³¹P{H} NMR (C₆D₆,

162 MHz): $\delta = -3.93^{(a)}$.

¹H NMR (C₆D₆, 600

MHz): $\delta = 0.95$ (s, 8

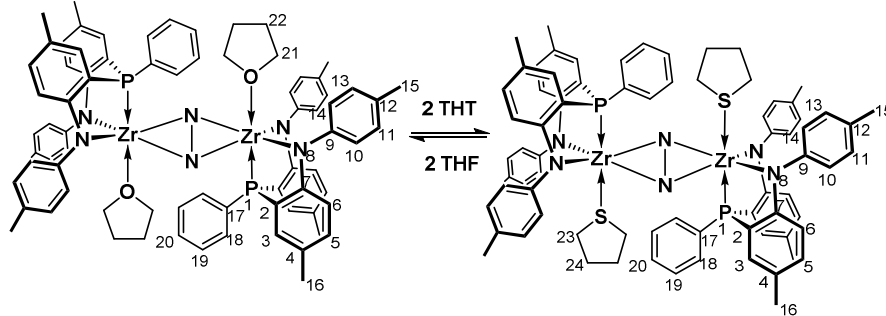
H22, CH₂), 1.40 (s, 8

H24, CH₂), 2.03 (s, 12 H16, CH₃), 2.10 (s, 12 H15, CH₃), 2.50 (s, 8 H23, CH₂), 3.58 (s, 8 H21,

CH₂), 6.67 (d, ³J_{HH} = 8 Hz, 4 H10 and 4 H14, ArH), 6.83 (t, ³J_{HH} = ⁴J_{PH} = 7 Hz, 4 H6, ArH), 6.90

(d, ³J_{HH} = 8 Hz, 4 H5, ArH), 6.96 (bs, 2 H20 and 4 H18, ArH), 7.13 (d, ³J_{HH} = 4 Hz, 4 H11 and 4

H13, ArH), 7.51 (d, ³J_{PH} = 7 Hz, 4 H3, ArH), 7.71 (bm, 4 H19, ArH).



^(a) Singlet may indicate exchange between THF and THT adducts

$[\text{iprop}^{\text{I}}\text{NPNZr}(\text{THT})]_2(\mu\text{-}\eta^2\text{:}\eta^2\text{-N}_2)$ [5.12] with $[\text{iprop}^{\text{I}}\text{NPNZr}(\text{THF})]_2(\mu\text{-}\eta^2\text{:}\eta^2\text{-N}_2)$ [5.1] After the

dark green residue of $[\text{iprop}^{\text{I}}\text{NPNZr}(\text{PMe}_3)]_2(\mu\text{-}\eta^2\text{:}\eta^2\text{-N}_2)$ [5.8] was dissolved in C₆D₆ and

analysed, ^(a) tetrahydrothiophene THT (100 μ L, 1.13 mmol) was added to the dark purple to black solution at room temperature. The solution became less black and more purple in colour. The

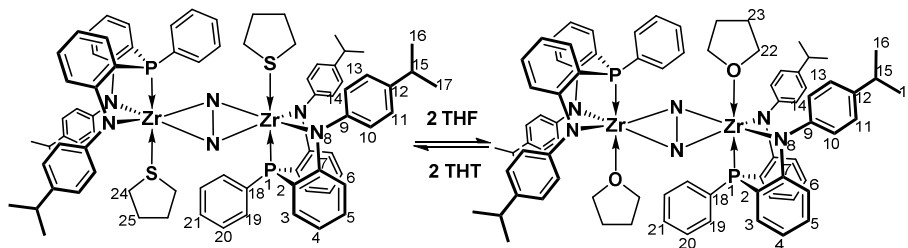
solvent was removed and *vacuo* and the residue was dissolved in C₆D₆, forming a reddish-purple solution (Figure 155).

³¹P{H} NMR

(C₆D₆, 162

MHz): δ = -

3.38^(b). ¹H NMR



(C₆D₆, 300 MHz): δ = 0.93 (s, 4 H23, CH₂), 1.19 (t, ³J_{HH} = 7 Hz, 12 H16 and 12 H17, CH₃), 1.46 (s, 4 H25, CH₂), 2.55 (s, 4 H24, CH₂), 2.71 (hep, ³J_{HH} = 7 Hz, 4 H15, CH), 3.62 (s, 4 H22, CH₂), 6.69 (overlapping t and d, ³J_{HH} = 6 Hz, 4 H4, 4 H10 and 4 H14 ArH), 6.89 (d of d, ³J_{HH} = 8 Hz and ⁴J_{PH} = 6 Hz, 4 H6, ArH), 7.03 (m, 4 H5, 4 H19 and 2 H21, ArH), 7.21 (d, ³J_{HH} = 8 Hz, 4 H11 and 4 H13, ArH), 7.55 (t, ³J_{HH} = ³J_{PH} = 6 Hz, 4 H3, ArH), 7.68 (m, 4 H20, ArH).

^(a) NMR spectroscopic data for [5.8] confirms the sample contained free THF.

^(a) Singlet may indicate exchange between THF and THT adducts

[^{tol}NPNZr(THT)]₂(μ-η²:η²-N₂) [5.14] Purple [^{tol}NPNZr(THF)]₂(μ-η²:η²-N₂) [5.3] (0.02 g, 0.01 mmol) was subjected to two dissolution / evacuation cycles with 1 cm³ PMe₃. The blue residue was dissolved in neat tetrahydrothiophene THT, forming a purple solution. The THT solvent was removed *in vacuo* and the purple residue was dissolved in C₆D₆ (Figure 156).

³¹P{H} NMR (C₆D₆, 162 MHz): δ = -31.80 (d, ²J_{PP} = 29

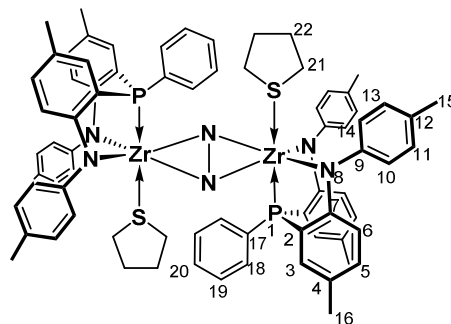
Hz), ^(a) -3.86 (s)^(a), -3.36 (s)^(b), -1.30 (s, P1), -1.12 (d, ²J_{PP}

= 45 Hz). ^(a) ¹H NMR (C₆D₆, 600 MHz): δ = 0.54 and 0.65

(bs, 1.8 H, P-CH₃), ^(c) 1.05 (s, 1.6 H, CH₂), ^(d) 1.46 (s, 46

H22, CH₂), ^(e) 2.07 (s, 12 H16, CH₃), 2.19 (s, 12 H15,

CH₃), 2.55 (s, 46 H21, CH₂), ^(e) 3.61 and 3.76 (s, 1.6 H,



CH₂), ^(d) 6.72 to 7.90 (ArH's for ^{tol}NPN donor set)

^(a) signals for mixed THF / PMe₃ species, similar to complex [5.7].

^(b) unidentified

^(c) bound PMe₃ signals with integration suggesting 0.2 equiv of PMe₃ (δ 0.81 for free PMe₃) for mixed THF / PMe₃ species

^(d) bound THF signals with integration suggesting 0.4 equiv of THF (δ 3.57 for free THF) for mixed THF / PMe₃ species.

^(e) integration suggests 11.5 equiv of bound THT (δ 1.62 and 2.58 for free THT)

Reduction of [^{tol}NPNZrCl₂]₂ [3.10] with KC₈ in THT: In the glove-box, a mixture (0.79 g)^(a) yellow [^{tol}NPNZrCl₂]₂ [3.10] + ^{tol}NPNZrCl₂(Et₂O) (0.72 g, 0.54 mmol [^{tol}NPNZrCl₂]₂ [3.10]) + 0.0710 g, 0.0966 mmol ^{tol}NPNZrCl₂(Et₂O) = 1.18 mmol Zr) and bronze KC₈ (0.36 g, 2.63 mmol) were mixed as solids in a thick-walled flask. The flask was cooling to -196 °C with N₂(l) and 10 cm³ THT was vacuum-transferred. The frozen solid content of the reaction flask was exposed briefly to a dynamic N₂ flow at -196 °C. At this point an olive-green solid and solid white THT was observed. The reaction flask was transferred to an EtOH / N₂ / dry ice slurry bath behind an explosion shield and the reaction mixture was allowed to warm up slowly to room temperature (4 atm N₂) with vigorous stirring, forming a dark green solution after 2 hrs. After 19 hrs the reaction flask containing a dark brown mixture was cooled down to -196 °C with N₂(l), placed under a dynamic N₂ atmosphere and allowed to warm to room temperature. The reaction flask was sealed and transferred to the glovebox. The reaction mixture was diluted with 30 cm³ toluene and filtered through celite with a sintered glass frit, washing with 20 cm³ toluene. The toluene solvent was removed *in vacuo* and the brown residue dried for 2 hours.^(b)

(a) $^{31}\text{P}\{^1\text{H}\}$ and ^1H NMR spectra indicate 9% $^{101}\text{NPnZrCl}_2(\text{Et}_2\text{O})$ impurity in **[3.10]** i.e. $0.7888\text{ g} = 0.7178\text{ g } [^{101}\text{NPnZrCl}_2]_2 \text{ [3.10]} + 0.0710\text{ g } ^{101}\text{NPnZrCl}_2(\text{Et}_2\text{O})$.

(b) $^{31}\text{P}\{^1\text{H}\}$ NMR spectrum displays peaks at δ 3.88 (65%), δ 13.07 (19%), δ 27.69 (8%) and δ 28.05 (8%). ^1H NMR spectrum displays peaks at δ 2.54 and δ 1.48 indicating bound THF.

[$^{101}\text{NPnTi}(\text{THF})_2(\mu\text{-}\eta^1\text{:}\eta^1\text{-N}_2)$ [5.15] (a): In the glove-box, dark purple $^{101}\text{NPnTiCl}_2$ **[3.18]** (0.75 g, 1.21 mmol) and bronze KC_8 (0.32 g, 2.34 mmol) were mixed as solids in a thick-walled flask. The flask was cooling to $-196\text{ }^\circ\text{C}$ with $\text{N}_2(\text{l})$ and 10 cm^3 THF was vacuum-transferred. The frozen solid content of the reaction flask was exposed briefly to a dynamic N_2 flow at $-196\text{ }^\circ\text{C}$. The reaction flask was transferred to an EtOH / N_2 / dry ice slurry bath behind an explosion shield and the reaction mixture was allowed to warm up slowly to room temperature (4 atm N_2) with vigorous stirring, forming a dark brown solution. After 3 days the reaction flask was slowly depressurized to 1 atm N_2 at room temperature under a N_2 flow. The reaction flask was sealed and transferred to the glovebox. The contents of the reaction flask were transferred to glass centrifuge tubes. After the THF mixture was centrifuged the brown supernatant was decanted from a mixture of a black solid + a gelataneous brown solid. The THF solvent was removed *in vacuo* from the supernatant and the brown residue was dissolved in C_6D_6 . After analysis, the C_6D_6 was removed *in vacuo* and the brown residue was triturated twice with 10 cm^3 *n*-pentanes. The brown solid was collected on a sintered glass frit and washed with *n*-pentanes and dried for 1 hr (0.41 g, 0.32 mmol [$^{101}\text{NPnTi}(\text{THF})_2(\mu\text{-}\eta^1\text{:}\eta^1\text{-N}_2)$ **[5.15]**, 53% yield based on $^{101}\text{NPnTiCl}_2$ **[3.18]**). Single crystals of [$^{101}\text{NPnZr}(\text{THF})_2(\mu\text{-}\eta^1\text{:}\eta^1\text{-N}_2)$ were grown from a toluene- d_8 solution in a J-Young NMR tube at room temperature. **(b):** In the glove-box, dark purple $^{101}\text{NPnTiCl}_2$ **[3.18]** (1.21 g, 1.96 mmol) and bronze KC_8 (0.60 g, 4.42 mmol) were mixed as solids in a thick-walled flask. The flask was cooling to $-196\text{ }^\circ\text{C}$ with $\text{N}_2(\text{l})$ and 10 cm^3 THF was vacuum-transferred. The frozen solid content of the reaction flask was exposed briefly to a dynamic N_2 flow at $-196\text{ }^\circ\text{C}$. The reaction flask was transferred to an EtOH / N_2 / dry ice slurry bath behind an

explosion shield and the reaction mixture was allowed to warm up slowly to room temperature (4 atm N₂) with vigorous stirring, forming a dark brown solution. After 4 days the reaction flask was slowly depressurized to 1 atm N₂ at room temperature under a N₂ flow. The reaction flask was sealed and transferred to the glovebox. The contents of the reaction flask were transferred to glass centrifuge tubes. After the THF mixture was centrifuged the brown supernatant was decanted and the THF solution was centrifuged for a second time. The THF solvent was removed *in vacuo* from the supernatant and the brown residue was dried for 7.5 hrs before being triturated with 10 cm³ *n*-hexanes. The brown solid was collected on a sintered glass frit, washed with 3 x 5 cm³ *n*-hexanes and dried for 1.3 hrs (0.82 g, 0.65 mmol [¹⁰¹NPNTi(THF)]₂(μ-η^l:η^l-N₂) [**5.15**], 66% yield based on ¹⁰¹NPNTiCl₂ [**3.18**]).^(b) The solid was dissolved in toluene and centrifuged for a third time. The toluene solvent was removed *in vacuo* and the residue was dissolved in 5 cm³ THF and placed in the freezer at -40 °C. After 1 day no crystals were observed and the THF solvent was removed *in vacuo*. The brown residue dissolved with a few drops THF and 10 cm³ *n*-hexanes was added, leading to the ppt of a brown solid. The mixture was placed in the freezer for 2.8 hrs before the brown solid was collected on a sintered glass frit, washing with 4 x 50 cm³ *n*-hexanes and dried for 20 min (0.45 g).^(c)

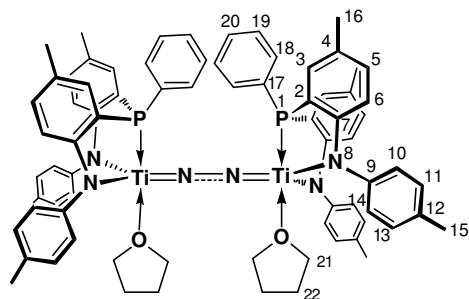
^(a) ³¹P{¹H} spectrum displays two broad peaks at δ -4.02 and δ 5.64 as the major products, with two sharp peaks at δ -7.37 (unknown) and δ 39.20 (phosphinimide analogue)¹³⁸

^(b) ³¹P{¹H} spectrum displayed a single peak at δ 5.63 indicating [¹⁰¹NPNTi(THF)]₂(μ-η^l:η^l-N₂) [**5.15**], but some white precipitate was observed, possibly from trace KCl in THF.

^(c) ³¹P{¹H} spectrum displayed a mixture of 76% [¹⁰¹NPNTi(THF)]₂(μ-η^l:η^l-N₂) [**5.15**] at δ 5.63 and 24% [¹⁰¹NPNTi(THF)]₂(μ-η^l:η^l-N₂) [**5.16**] at δ -3.02 when isolated from toluene / THF / *n*-hexanes mixtures. Spiking the NMR sample with THF leads to the observation of a single peak at δ -3.02 for [¹⁰¹NPNTi(THF)]₂(μ-η^l:η^l-N₂) [**5.16**].

$^{31}\text{P}\{\text{H}\}$ NMR (C_6D_6 , 162 MHz): $\delta = 5.64$ (s, P1).

^1H NMR (C_6D_6 , 600 MHz): $\delta = 1.09$ (s, 8 H22, CH_2), 1.39 (s, 4 H, THF, CH_2), 2.00 (s, 12 H16, CH_3), 2.11 (s, tol, CH_3), 2.15 (s, 12 H15, CH_3), 3.27 (s, 8 H21, CH_2), 3.59 (s, 4 H, THF, CH_2),



6.81 (d, $^3J_{\text{HH}} = 8$ Hz, 4 H10 and 4 H14, ArH), 6.96 (m, $^3J_{\text{HH}} = ^4J_{\text{PH}} = 7$ Hz, 4 H6 and 4 H5, ArH), 7.01 (d, $^3J_{\text{HH}} = 7$ Hz, tol, ArH), 7.05 (d, $^3J_{\text{HH}} = 6$ Hz, 2 H20 and 4 H18, ArH), 7.13 (d, $^3J_{\text{HH}} = 7$ Hz, tol, ArH), 7.25 (d, $^3J_{\text{HH}} = 7$ Hz, 4 H11 and 4 H13, ArH), 7.43 (d, $^3J_{\text{PH}} = 7$ Hz, 4 H3, ArH), 7.75 (t, $^3J_{\text{HH}} = 9$ Hz, 4 H19, ArH). $^{13}\text{C}\{\text{H}\}$ NMR (C_6D_6 , 151 MHz): $\delta = 20.5$ (C16, CH_3), 20.9 (C15, CH_3), 21.4 (tol, CH_3), 25.7 (THF and C22, CH_2), 68.3 (THF, CH_2), 72.52 (C21, CH_2), 116.0 (d, $^3J_{\text{PC}} = 7$ Hz, C6, ArC), 119.3 (d, $^2J_{\text{PC}} = 34$ Hz, C7, C_{ipso}), 125.0 (C11 and C13, ArC), 129.1 (d, $^2J_{\text{PC}} = 9$ Hz, C18, ArC), 129.2 (C20, ArC), 129.2 (d, $^3J_{\text{PC}} = 8$ Hz, C4, C_{ipso}), 129.8 (C10 and C14, ArC), 130.0 (tol, ArC), 133.0 (d, $^3J_{\text{PC}} = 13$ Hz, C19, ArC), 133.3 (C5, ArC), 134.4 (C3, ArC), 134.7 (d, $^1J_{\text{PC}} = 28$ Hz, C17, C_{ipso}), 137.5 (tol, ArC), 137.9 (C12, C_{ipso}), 151.1 (C9, C_{ipso}), 161.1 (d, $^1J_{\text{CP}} = 29$ Hz, C2, C_{ipso}). Anal. Calcd. for $\text{C}_{76}\text{H}_{78}\text{N}_6\text{O}_2\text{P}_2\text{Ti}_2 + 1.86 \text{ C}_7\text{H}_8$: C, 75.30; H, 6.53; N, 6.54; Found: C, 74.91; H, 6.44; N, 6.28. ^(d) EI-MS (m/z): 1410 (10, $[\text{M} + 2\text{THF}]^+$), 1121 (60, $[\text{M} - 2\text{THF}]^+$), 1044 (90, $[(^{\text{tol}}\text{NPN})_2\text{Ti}]^+$). ^(e)

^(d) pure crystals were obtained by toluene / *n*-pentanes layering in the freezer at -40°C .

^(e) the ^1H NMR spectrum displayed signals at 3.57 and 1.39 for free excess THF, which may explain the observation of $[(^{\text{tol}}\text{NPNTi}(\text{THF})_2)_2(\mu\text{-}\eta^1\text{:}\eta^1\text{-N}_2)]$ **[5.16]** in the mass spectrum.

Additional unidentified higher mass peaks observed at 1213 m/z (60%), 1318 m/z (20%), 1379 m/z (5%), 1423 m/z (20%), 1483 m/z (5%), 1515 m/z (5%), 1574 m/z (30%), 1591 m/z (10%)

$[(^{\text{iprop}}\text{NPNTi}(\text{THF}))_2(\mu\text{-}\eta^1\text{:}\eta^1\text{-N}_2)]$ [5.17]: In the glove-box, dark purple $^{\text{iprop}}\text{NPNTiCl}_2$ **[3.17]** (0.41 g, 0.64 mmol) and bronze KC_8 (0.17 g, 1.29 mmol) were mixed as solids in a thick-walled flask.

The flask was cooling to $-196\text{ }^{\circ}\text{C}$ with $\text{N}_2(\text{l})$ and 10 cm^3 THF was vacuum-transferred. The frozen solid content of the reaction flask was exposed briefly to a dynamic N_2 flow at $-196\text{ }^{\circ}\text{C}$. The reaction flask was transferred to an EtOH / N_2 / dry ice slurry bath behind an explosion shield and the reaction mixture was allowed to warm up slowly to room temperature (4 atm N_2) with vigorous stirring, forming an olive-green to dark brown solution. After 16.25 hrs the reaction flask was slowly depressurized to 1 atm N_2 at room temperature under a N_2 flow. The reaction flask was sealed and transferred to the glovebox. The THF mixture was filtered through celite on a sintered glass frit, washing with additional 30 cm^3 THF. The THF solvent was removed *in vacuo* and the brown residue was dried for 3.67 hrs and dissolved in C_6D_6 (Figure 160).^(a) After analysis, the C_6D_6 was removed *in vacuo* and the brown residue was triturated with 10 cm^3 *n*-pentanes. After being in the freezer for 7 hrs, the brown solid was collected on a sintered glass frit and washed with $2 \times 10\text{ cm}^3$ chilled *n*-pentanes and dried for 1 hr (0.28 g).^(b)

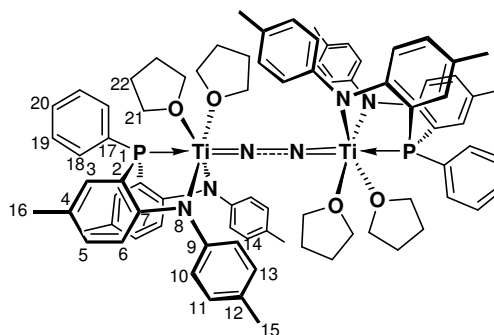
$^{31}\text{P}\{\text{H}\}$ NMR (C_6D_6 , 162 MHz): $\delta = 5.80$ (s, P1). ^1H NMR (C_6D_6 , 400 MHz): $\delta = 1.06$ (s, 8 H23, CH_2), 1.19 (d, $^3J_{\text{HH}} = 4\text{ Hz}$, 12 H16 and 12 H17, CH_3), 2.73 (hep, $^3J_{\text{HH}} = 7\text{ Hz}$, 4 H15, CH), 3.23 (s, 8 H22, CH_2), 6.63 (t, $^3J_{\text{HH}} = ^4J_{\text{PH}} = 7\text{ Hz}$, 4 H6, ArH), 6.91 (overlapping t and d, $^3J_{\text{HH}} = 7\text{ Hz}$, 4 H4, 4 H10 and 4 H14 ArH), 7.00 (m, $^3J_{\text{HH}} = 6\text{ Hz}$, 4 H5, ArH), 7.07 (t, $^3J_{\text{HH}} = ^3J_{\text{PH}} = 7\text{ Hz}$, 4 H19 and 2 H21, ArH), 7.24 (d, $^3J_{\text{HH}} = 8\text{ Hz}$, 4 H11 and 4 H13, ArH), 7.43 (t, $^3J_{\text{HH}} = ^3J_{\text{PH}} = 6\text{ Hz}$, 4 H3, ArH), 7.67 (t, $^3J_{\text{HH}} = 5\text{ Hz}$, 4 H20, ArH). EI-MS (m/z): 1309 (5, $[\text{M} - \text{N} + 2\text{H}]^+$), 1297 (40, $[\text{M} - 2\text{N} + 4\text{H}]^+$), 1255 (15, $[\text{M} - 2\text{N} + 4\text{H} - \text{THF}]^+$), 1181 (5, $[\text{M} + 4\text{H} - 2\text{THF}]^+$), 1100 (100, $[(^{\text{iprop}}\text{NPN})_2\text{Ti}]^+$).

^(a) $^{31}\text{P}\{\text{H}\}$ spectrum of the crude displayed a major product peak at $\delta 5.80$ (85%) for $[(^{\text{iprop}}\text{NPNTi}(\text{THF}))_2(\mu\text{-}\eta^1\text{:}\eta^1\text{-N}_2)]$ **[5.17]** and a peak at $\delta 41.54$ (8%) for the associated phosphinimide complex.¹³⁸ Some protonated ligand $^{\text{iprop}}\text{NPNH}_2$ **[2.10]** was also observed.

(b) $^{31}\text{P}\{^1\text{H}\}$ spectrum of the isolated solid was similar to the crude, with an increase in $[\text{ipropNPNTi}(\text{THF})]_2(\mu\text{-}\eta^I\text{:}\eta^I\text{-N}_2)$ [**5.17**] to 92%.

$[\text{tolNPNTi}(\text{THF})_2]_2(\mu\text{-}\eta^I\text{:}\eta^I\text{-N}_2)$ [5.16**]:** In the glove-box, dark purple $\text{tolNPNTiCl}_2(\text{THF})$ [**3.14**] (0.80 g, 1.16 mmol) and bronze KC_8 (0.35 g, 2.58 mmol) were mixed as solids in a thick-walled flask. The flask was cooling to $-196\text{ }^\circ\text{C}$ with $\text{N}_2(\text{l})$ and 15 cm^3 THF was vacuum-transferred. The frozen solid content of the reaction flask was exposed briefly to a dynamic N_2 flow at $-196\text{ }^\circ\text{C}$. The reaction flask was transferred to an $\text{EtOH} / \text{N}_2 /$ dry ice slurry bath behind an explosion shield and the reaction mixture was allowed to warm up slowly to room temperature (4 atm N_2) with vigorous stirring, forming a green brown solution. After 18 hrs the reaction flask was cooled down to $-196\text{ }^\circ\text{C}$ with $\text{N}_2(\text{l})$, placed under a dynamic N_2 atmosphere and allowed to warm to room temperature. The reaction flask was sealed and transferred to the glovebox. The THF mixture was filtered through celite on a sintered glass frit, washing with additional $3 \times 10\text{ cm}^3$ Et_2O . The THF / Et_2O solvent was removed *in vacuo* and the brown residue was triturated with 5 cm^3 *n*-hexanes and placed in the freezer overnight. The brown solid was collected on a sintered glass frit, washed with $3 \times 2\text{ cm}^3$ *n*-hexanes and dried for 1.5 hrs (0.49 g).^(a)

$^{31}\text{P}\{\text{H}\}$ NMR (C_6D_6 , 162 MHz): $\delta = -3.02$ (s, P1). ^1H NMR (C_6D_6 , 600 MHz): $\delta = 1.42$ (s, H22, CH_2), 1.99, 2.00, 2.03, 2.09, 2.16, 2.20 (s, H16 and H15, CH_3), 3.61 (s, H21, CH_2), 6.16 (t, $^3J_{\text{HH}} = ^4J_{\text{PH}} = 7\text{ Hz}$, H6, ArH), 6.69 to 7.78 (ArH's for tolNPN donor set)



^(a) ^1H NMR spectrum indicates 10% Et_2O in sample. $^{31}\text{P}\{^1\text{H}\}$ NMR spectrum indicates three unidentified peaks at $\delta 7.21$, $\delta -1.29$ and $\delta -6.12$.

Attempted synthesis of [$^{101}\text{NPNTi}(\text{THF})_2(\mu\text{-}\eta^1\text{:}\eta^1\text{-}^{15}\text{N}_2)$]: In the glove-box, dark purple $^{101}\text{NPNTiCl}_2$ [**3.18**] (0.9353 g, 1.5149 mmol) and bronze KC_8 (0.43 g, 3.20 mmol) were mixed as solids in a thick-walled flask. The flask was cooling to $-196\text{ }^\circ\text{C}$ with $\text{N}_2(\text{l})$ and 10 cm^3 THF was vacuum-transferred. The reaction flask was connected to a $^{15}\text{N}_2$ canister fitted with a pressure regulator (5 psi) and flow meter and the system was placed under reduced pressure. The frozen solid content of the reaction flask was exposed briefly to a static $^{15}\text{N}_2$ flow while still cooled to $-196\text{ }^\circ\text{C}$ with $\text{N}_2(\text{l})$.^(a) The reaction flask was transferred to an EtOH / N_2 / dry ice slurry bath behind an explosion shield and the reaction mixture was allowed to warm up slowly to room temperature (4 atm $^{15}\text{N}_2$) with vigorous stirring, forming a dark brown reaction mixture. After 3 days the reaction flask was depressurised under a dynamic N_2 ^(b) atmosphere at room temperature. The reaction flask was sealed and transferred to the glovebox. The content of the reaction flask (green-brown solution + black ppt) was transferred to a conical flask and the THF solvent was removed *in vacu*. The brown residue was dried for 2 hrs before being dissolved in toluene and transferred to centrifuge tubes. The brown solution was subjected to two centrifuge cycles and the resultant supernatant was filtered through celite with a sintered glass frit. The toluene solvent was removed *in vacuo* from the filtrate and the brown residue was dried for 2.5 hrs before being triturated with 10 cm^3 *n*-pentanes. After 2 hrs in the freezer at $-40\text{ }^\circ\text{C}$ the brown solid was collected on a sintered glass frit and washed with 10 cm^3 *n*-pentanes and dried for 1 hr (0.5071 g). The solid was suspended in 8 cm^3 *n*-pentanes with 10 drops THF and returned to the freezer for 1.5 hrs. Thereafter, the brown solid was collected on a sintered glass frit and washed with 4 cm^3 *n*-pentanes and dried for 1.2 hrs (0.35 g).^(c)

^(a) mass loss of $^{15}\text{N}_2$ canister after transfer = $1043.25 - 1041.85 = 1.4\text{ g}$.

^(b) assuming that the $^{15}\text{N}_2$ ligand does not exchange with unlabelled N_2 .

^(c) ³¹P{¹H} spectrum displays two major peaks at δ -3.10 and δ 5.59 for [^{tol}NPNTi(THF)₂]₂(μ - η^1 : η^1 -N₂) [**5.16**] and [^{tol}NPNTi(THF)]₂(μ - η^1 : η^1 -N₂) [**5.15**]. ¹⁵N{¹H} spectrum of the same sample displays no signals, with control spectrum for urea displaying a peak at δ -300.13. This result suggests that the ¹⁵N₂ ligand may exchange with the surrounding unlabelled N₂.

cis-[^{tol}NPNTi(Py)]₂(μ - η^1 : η^1 -N₂) [**5.18**] and **trans**-[^{tol}NPNTi(Py)]₂(μ - η^1 : η^1 -N₂) [**5.19**]: Pyridine (10 μ L, 0.12 mmol) was added to a dark brown solution of [^{tol}NPNTi(THF)]₂(μ - η^1 : η^1 -N₂) [**5.15**] (0.07 g, 0.06 mmol) in 0.8 cm³ C₆D₆ in a J-Young tube, with no significant colour change. ^(a) After 46 min, a second aliquot pyridine (10 μ L, 0.12 mmol) was added. ^(b) Thereafter, an additional amount of [^{tol}NPNTi(THF)]₂(μ - η^1 : η^1 -N₂) [**5.15**] (0.03 g, 0.03 mmol) in 0.6 cm³ C₆D₆ was added to the J-Young tube and a third aliquot pyridine (120 μ L, 1.48 mmol), with no colour change and the ppt of a brown solid observed. ^(c) Single crystals of **trans**-[^{tol}NPNTi(Py)]₂(μ - η^1 : η^1 -N₂) [**5.19**] where grown from the C₆D₆ solution in the J-Young NMR tube at room temperature.

^(a) [**5.15**] + 2 Py: ³¹P{¹H} NMR spectrum displays 5 peaks at δ 5.58 (4%) for [**5.15**], δ 4.17 (36%) for [**5.18**], δ 3.04 (13%) for [**5.18a**], δ -0.29 (15%) for [**5.19**] and δ -0.79 (33%) for [**5.19a**]. ¹H NMR (C₆ D₆, 400 MHz): δ = 1.42, 3.58 (THF), 2.01, 2.28 (tolyl), 6.30, 6.57, 6.78, 6.95, 7.06 (Py, H22, H23 and phenyls), 7.38, 7.46, 7.59 (phenyls), 8.0, 8.52 (Py, H21).

^(b) [**5.15**] + 4 Py: ³¹P{¹H} NMR spectrum displays 4 peaks at δ 5.57 (2%) for [**5.15**], δ 4.16 (37%) for [**5.18**], δ -0.29 (35%) for [**5.19**] and δ -0.65 (26%) for [**5.19a**]. ¹H NMR (C₆ D₆, 400 MHz): δ = 1.42, 3.57 (THF, CH₂), 1.92, 1.95, 2.00, 2.04, 2.28 (tolyl, CH₃), 6.37, 6.58, 6.79, 6.95, 7.06 (Py, H22, H23 and phenyls, ArH), 7.37, 7.46, 7.55 (phenyls, ArH), 8.05, 8.55 (Py, H21, ArH).

^(c) [**5.15**] + 20 Py: ³¹P{¹H} NMR spectrum displays a single peak at δ -0.25 for [**5.19**]. ¹H NMR (C₆ D₆, 400 MHz): δ = 1.44, 3.56 (THF, CH₂), 1.90 (tolyl, CH₃), 6.72 (Py, H22 and phenyls, ArH), 7.03 (Py, H23 and phenyls, ArH), 7.45 (t, phenyls, ArH), 8.51 (Py, H21, ArH).

***trans*-[^{tol}NPNTi(Py)₂]₂(μ-η^l:η^l-N₂)[**5.19**]:** Pyridine (70 μL, 0.86 mmol) was added to a dark brown solution of [^{tol}NPNTi(THF)]₂(μ-η^l:η^l-N₂) [**5.15**] (0.05 g, 0.04 mmol) in 5 cm³ toluene in a scintillation vial inside the glove box, with no significant colour change. After 1.2 hrs, the toluene solvent was removed *in vacuo*. The residue was triturated with *n*-hexanes and the brown solid was collected on a sintered glass frit, washing thrice with *n*-hexanes and drying for 2 hrs (0.04 g, 0.03 mmol [^{tol}NPNTi(Py)₂]₂(μ-η^l:η^l-N₂), 72% yield based on [^{tol}NPNTi(THF)]₂(μ-η^l:η^l-N₂) [**5.15**]).^(a)

³¹P{¹H} NMR (C₆D₆ + 20 μL Py-*d*₅, 162 MHz):

δ = -0.25 (s, P1). ¹H NMR (C₆D₆ + 20 μL Py-*d*₅,

600 MHz): δ = 1.92 (s, H16 and H15, tolyl-

CH₃), 6.69 (t, ³J_{HH} = 6 Hz, H22, Py-ArH), 6.74

(d, ³J_{HH} = 8 Hz, phenyls, ArH), 7.00 (t, ³J_{HH} = 7

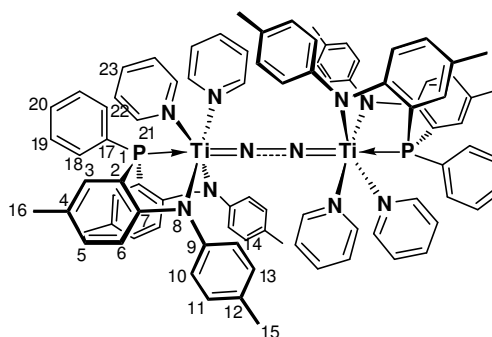
Hz, H23, Py-ArH and phenyls, ArH), 7.12 (d,

³J_{HH} = 8 Hz, phenyls, ArH), 7.06 (d, ³J_{HH} = 8 Hz, phenyls, ArH), 7.47 (t, ³J_{HH} = 7 Hz, phenyls,

ArH), 8.53 (d, ³J_{HH} = 4 Hz, H21, Py-ArH). Anal. Calcd. for C₈₈H₈₂N₁₀P₂Ti₂: C, 73.53; H, 5.75; N,

9.74; Found: C, 72.53; H, 5.95; N, 9.35. EI-MS (*m/z*): 1121 (30, [M - 4Py]⁺), 1044 (50,

[(^{tol}NPN)₂Ti]⁺).^(b)



^(a) ³¹P{¹H} NMR spectrum of [**5.19**] in C₆D₆ displays 4 peaks at δ 4.16 (46%) for [**5.18**], δ 3.15

(17%) for [**5.18a**], δ -0.27 (20%) for [**5.19**] and δ -0.59 (17%) for [**5.19a**]. After spiking the

sample with 20 μL pyridine-*d*₅, a single peak was observed at δ -0.25 for [^{tol}NPNTi(Py)₂]₂(μ-

η^l:η^l-N₂) [**5.19**]. Before spiking with pyridine-*d*₅, ¹H NMR (C₆D₆, 400 MHz): δ = 1.93, 1.96,

2.01, 2.04, 2.29 (tolyl-CH₃), 6.19, 6.56, 6.82, 6.96, (Py, H22, H23 and phenyls, ArH), 7.01 (d,

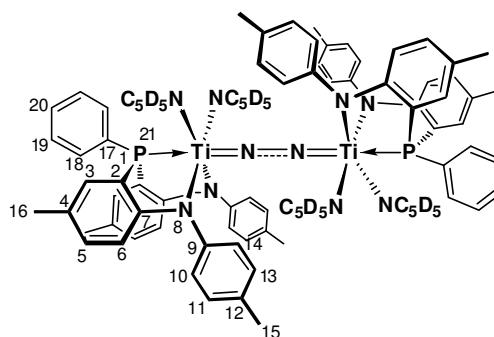
³J_{HH} = 8 Hz, phenyls, ArH), 7.06 (d, ³J_{HH} = 8 Hz, phenyls, ArH), 7.12 (d, ³J_{HH} = 8 Hz, phenyls,

ArH), 7.37, 7.51 (phenyls, ArH), 7.83, 8.06, 8.52 (Py, H21, ArH).

^(b) an unidentified peak is observed at 1211 m/z (a fragment ion for $[M - 3\text{Py}]^+$ would be expected at 1200 m/z)

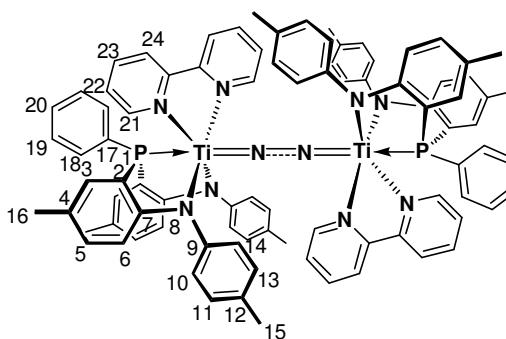
***trans*-[^{tol}NPNTi(Py-*d*₅)₂](μ-η^l:η^l-N₂) [5.19b]:** Crystals of [^{tol}NPNTi(THF)]₂(μ-η^l:η^l-N₂) [5.15] (0.08 g, 0.06 mmol) were dissolved with heating to 60 °C in pyridine-*d*₅ in a scintillation vial inside the glove box, with no significant colour change. A *n*-pentanes layer was carefully added to the brown solution and the mixture was placed in the freezer at -40 °C. After 13.5 hrs, the brown powder was collected on a sintered glass frit, washing with *n*-hexanes and drying for 30 min (0.049 g, 0.034 mmol [^{tol}NPNTi(Py-*d*₅)₂](μ-η^l:η^l-N₂), 69% yield based on [^{tol}NPNTi(THF)]₂(μ-η^l:η^l-N₂) [5.15]).

³¹P{¹H} NMR (C₆D₆ + 20 μL Py-*d*₅, 162 MHz): δ = -0.25 (s, P1). ¹H NMR (C₆D₆ + 20 μL Py-*d*₅, 400 MHz): δ = 1.91 (s, H16 and H15, tolyl-CH₃), 6.74 (d, ³J_{HH} = 9 Hz, phenyls, ArH), 7.02 (m, ³J_{HH} = 8 Hz, phenyls, ArH), 7.12 (d, ³J_{HH} = 10 Hz, phenyls, ArH), 7.47 (t, ³J_{HH} = 10 Hz, phenyls, ArH).



[^{tol}NPNTi(2,2'-bipy)]₂(μ-η^l:η^l-N₂) [5.20]: 2,2-Bipyridine (0.01 g, 0.07 mmol) dissolved in toluene was added to a dark brown solution of [^{tol}NPNTi(THF)]₂(μ-η^l:η^l-N₂) [5.15] (0.04 g, 0.03 mmol) in toluene in a scintillation vial inside the glove box, with no significant colour change. After 10 min, the toluene solvent was removed *in vacuo* and the brown residue was triturated twice with *n*-hexanes. The dark brown solid was collected on a sintered glass frit, washing with *n*-hexanes (0.02 g).^(a)

^(a) ³¹P{¹H} NMR spectrum displays a single peak at δ 9.41 for [5.20]. ¹H NMR (C₆D₆, 400

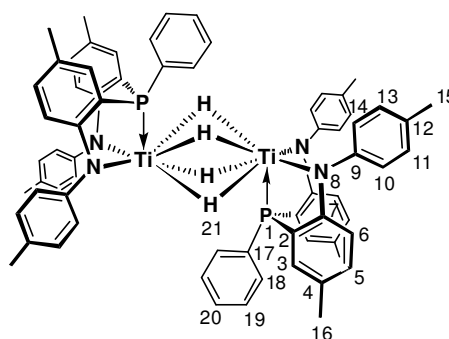


MHz): δ = 1.84, 2.50 (tolyl, CH₃), 6.34 (m), 6.49 (m), 6.67 (m), 6.79 (m), 6.89, 7.03 (t), 7.07, 7.42 (phenyls and bipy, ArH), 8.54 (d, $^3J_{\text{HH}}$ = 4 Hz, bipy), 8.74 (d, $^3J_{\text{HH}}$ = 8 Hz, bipy), 9.05 (d, $^3J_{\text{HH}}$ = 5 Hz, bipy). Free 2,2'-bipyridine displays signals at δ 8.72 (t of d, $^3J_{\text{HH}}$ = 8 Hz, 1 Hz), 8.54 (q of d, $^3J_{\text{HH}}$ = 5 Hz, 1 Hz), 7.23 (d of t, $^3J_{\text{HH}}$ = 8 Hz, 2 Hz), 6.71 (d of d of d, $^3J_{\text{HH}}$ = 8 Hz, 5 Hz, 1 Hz).

[^{tol}NPNTiH₂]₂ [5.21]: In the glove-box, dark purple ^{tol}NPNTiCl₂ [3.18] (0.28 g, 0.45 mmol) and KHBet₃ (0.1459 g, 1.0565 mmol) were mixed as solids in a scintillation vial and cooled to -40 °C in the freezer. In a separate vial 2 cm³ toluene-*d*₈ was also chilled to -40 °C in the freezer. The solid mixture was removed from the freezer and the chilled toluene-*d*₈ was added, immediately forming a dark brown solution, which was allowed to stir at room temperature for 3.5 hrs.^(a) The reaction mixture was filtered through celite with a sintered glass frit, washing with additional toluene. The toluene solvent was removed *in vacuo* and the brown residue was triturated with *n*-hexanes. The hexane solvent was removed *in vacuo* and the brown solid was dried for 5 hr (0.17 g, 0.16 mmol [^{tol}NPNTiH₂]₂ [5.21], 70% yield based on ^{tol}NPNTiCl₂ [3.18]).

³¹P{¹H} NMR (C₆D₆, 162 MHz): δ = -2.57 (s, P1).

¹H NMR (C₆D₆, 400 MHz): δ = 1.99 (s, 12 H16, CH₃), 2.11 (s, 12 H15, CH₃), 6.13 (t, $^3J_{\text{HH}}$ = $^4J_{\text{PH}}$ = 7 Hz, 4 H6, ArH), 6.74 (d, $^3J_{\text{HH}}$ = 8 Hz, 4 H10 and 4 H14, ArH), 6.84 (d, $^3J_{\text{HH}}$ = 8 Hz, 4 H5, ArH), 6.89 (d, $^3J_{\text{HH}}$ = 8 Hz, 4 H11 and 4 H13, ArH), 7.01 (m, $^3J_{\text{HH}}$ = 8 Hz, 2 H20 and 4 H18, ArH), 7.43 (d, $^3J_{\text{PH}}$ = 7 Hz, 4 H3, ArH), 7.61 (d, $^3J_{\text{HH}}$ = 8 Hz, 4 H19, ArH), 14.45 (t, $^2J_{\text{PH}}$ = 16 Hz, 4 H21, Ti-H-Ti).



^(a) crude reaction mixture displayed a single peak in the ³¹P{¹H} NMR spectrum at δ -2.57.

$[\text{}^{\text{tol}}\text{NPNZr}(\text{THF})]_2(\mu\text{-}\eta^2\text{:}\eta^2\text{-N}_2)$ [5.3] + 1 atm H₂: A purple solution of $[\text{}^{\text{tol}}\text{NPNZr}(\text{THF})]_2(\mu\text{-}\eta^2\text{:}\eta^2\text{-N}_2)$ [5.3] (0.15 g, 0.11 mmol) in toluene-*d*₈ was placed in a thick-walled flask and connected to a column filled with activated molecular sieves. The solution was degassed twice and then placed under reduced pressure. 1 atm H₂ was introduced to the solution at room temperature and after two weeks the reddish-brown solution was transferred to a J-Young NMR tube and analysed. The solution was returned to the flask and placed under 1 atm H₂. No colour changes were observed and the solution was analysed after two more weeks.^(a)

^(a) ³¹P{¹H} NMR spectrum indicate unreacted $[\text{}^{\text{tol}}\text{NPNZr}(\text{THF})]_2(\mu\text{-}\eta^2\text{:}\eta^2\text{-N}_2)$ [5.3] and ¹H NMR spectrum display a peak at δ 4.46 indicating dissolved H₂.

$[\text{}^{\text{tol}}\text{NPNZr}(\text{PMe}_3)]_2(\mu\text{-}\eta^2\text{:}\eta^2\text{-N}_2)$ [5.9] + 1 atm H₂: A blue solution of $[\text{}^{\text{tol}}\text{NPNZr}(\text{PMe}_3)]_2(\mu\text{-}\eta^2\text{:}\eta^2\text{-N}_2)$ [5.9] (0.06 g, 0.04 mmol) in toluene-*d*₈ was placed in a thick-walled flask and connected to a column filled with activated molecular sieves. The solution was degassed twice and then placed under reduced pressure. 1 atm H₂ was introduced to the solution at room temperature and after two weeks the blue solution was transferred to a J-Young NMR tube and analysed. The solution was returned to the flask and placed under 1 atm H₂. No colour changes were observed and the solution was analysed after two more weeks.^(a)

^(a) ³¹P{¹H} NMR spectrum indicate unreacted $[\text{}^{\text{tol}}\text{NPNZr}(\text{PMe}_3)]_2(\mu\text{-}\eta^2\text{:}\eta^2\text{-N}_2)$ [5.9] and ¹H NMR spectrum display a peak at δ 4.46 indicating dissolved H₂.

$[\text{}^{\text{iprop}}\text{NPNZr}(\text{THF})](\text{xylylNC-N}_2)[\text{}^{\text{iprop}}\text{NPNZr}(\text{xylylNC})]$ [6.1]: In the glove box, a solution of xylylNC (0.04 g, 0.34 mmol) in 0.5 cm³ toluene was added a purple solution of $[\text{}^{\text{iprop}}\text{NPNZr}(\text{THF})]_2(\mu\text{-}\eta^2\text{:}\eta^2\text{-N}_2)$ [5.1] (0.23 g, 0.16 mmol) in 5 cm³ toluene at room temperature. A brown solution formed immediately, with the presence of a ppt after stirring for 24 hrs. The toluene solvent was removed *in vacuo* and the mustard yellow residue was triturated twice with 5 cm³ *n*-pentanes and once with 5 cm³ *n*-hexanes. The mustard yellow solid was collected on a

sintered glass frit and dried (0.15 g, 0.10 mmol [ⁱpropNPNZr(THF)](CNxylyl)-N₂)[ⁱpropNPNZr(CNxylyl)], 59% yield based on [ⁱpropNPNZr(THF)]₂(μ-η²:η²-N₂) [5.1].

³¹P{¹H} NMR (C₆D₆, 162 MHz): δ = 1.67 (s,

P1), 11.19 (s, P1a).^(a) ¹H NMR (C₆D₆, 600

MHz): δ = 1.08 (bs, 12 H16 and 12 H17, CH₃),

1.14 (s, 4 H23, CH₂),^(b) 1.56 (s, 6 H29a, CH₂),^(c)

2.37 (s, 6 H29, CH₃),^(c) 2.57 (bs, 4 H15, CH),

4.09 (s, 4 H22, CH₂), 6.55 (t, ³J_{HH} = ⁴J_{PH} = 6 Hz,

4 H6, ArH), 6.61 (overlapping t and d, ³J_{HH} = 7 Hz, 4 H19 and 2 H21, ArH), 6.72 (s, 2 H27a and

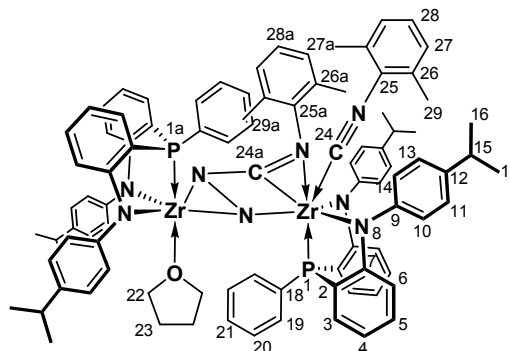
H28a, ArH),^(c) 6.84 (m, ³J_{HH} = 6 Hz, 4 H4, 4 H10 and 4 H14, ArH), 6.92 (bm, ³J_{HH} = 6 Hz, 2 H27

and H28, ArH),^(c) 7.00 (d, ³J_{HH} = 13 Hz, 4 H11 and 4 H13, ArH), 7.04 (t, ³J_{HH} = 8 Hz, 4 H5, ArH),

7.5531 (d of d, ³J_{HH} = 11 Hz, ³J_{PH} = 8 Hz, 4 H3, ArH), 7.76 (t, ³J_{HH} = 8 Hz, 4 H20, ArH). Anal.

Calcd. for C₈₅H₈₇N₇OP₂Zr₂: C, 69.59; H, 5.98; N, 6.68; Found: C, 69.67; H, 6.39; N, 6.65.^(d) EI-

MS (*m/z*): 1522 (60, [M - THF]⁺), 1497 (15, [M - THF - 2Me]⁺).



^(a) P1 and P1a assignments based on complex [6.2].

^(b) ¹H-¹H COSY NMR spectrum of [6.2] confirms that this signal represents coordinated THF

^(c) two different xylylNC environments are indicated (free xylylNC at δ 2.06 (s, CH₃), 6.58 (d,

³J_{HH} = 14 Hz, ArH) and 6.73 (t, ³J_{HH} = 8 Hz, ArH)) and arbitrary assignment of H26 / H26a, H27

/ H27a, H28 / H28a and H29 / H29a.

^(d) Elemental analysis matches one equiv each of xylylNC and THF, with WO:MgO 1:1 added to compensate zirconium carbide formation. This is in conflict with ¹H NMR and mass spectrometry data, which suggests two equiv of xylylNC (Anal. Calcd. for C₉₄H₉₇N₈OP₂Zr₂: C, 70.60; H, 6.11; N, 7.01).

$[\text{ipropNPNZr(THF)}](\text{xylylNC-}^{15}\text{N}_2)[\text{ipropNPNZr(xylylNC)}]$ **[6.2]**: (a) with 1 equiv of xylylNC:

In the glove box, a solid mixture of xylylNC (0.004 g, 0.03 mmol) and purple

$[\text{ipropNPNZr(THF)}]_2(\mu\text{-}\eta^2\text{:}\eta^2\text{-}^{15}\text{N}_2)$ **[5.2]** (0.04 g, 0.03 mmol) was dissolved into $0.6\text{ cm}^3\text{ C}_6\text{D}_6$,

forming a brown solution that was analysed using NMR spectroscopy.^(a) (b) with 2 equiv of

xylylNC: In the glove box, a solid mixture of xylylNC (0.01 g, 0.06 mmol) and purple

$[\text{ipropNPNZr(THF)}]_2(\mu\text{-}\eta^2\text{:}\eta^2\text{-}^{15}\text{N}_2)$ **[5.2]** (0.04 g, 0.03 mmol) was dissolved into $0.6\text{ cm}^3\text{ C}_6\text{D}_6$,

forming a brown solution that was placed in a sealed NMR tube.

$^{31}\text{P}\{^1\text{H}\}$ NMR (C_6D_6 , 162 MHz): $\delta = 2.03$ (d, $^3J_{\text{PN}}$

$= 20\text{ Hz}$, P1), 11.54 (s, P1a).^(b) $^{15}\text{N}\{^1\text{H}\}$ NMR

(C_6D_6 , 40 MHz): $\delta = -215.91$ (d, $J_{\text{PN}} = 20\text{ Hz}$,

$^{15}\text{N1a}$), -12.70 (s, $^{15}\text{N1}$).^(c) ^1H NMR (C_6D_6 , 600

MHz): $\delta = 1.07$ (bs, 12 H16 and 12 H17, CH_3),

1.24 (s, 4 H23, CH_2),^(d) 1.40 (s, THF, CH_2),^(e) 1.55

(s, 6 H29a, CH_2),^(f) 2.37 (s, 6 H29, CH_3),^(f) 2.56 (bs, 4 H15, CH), 3.56 (s, THF, CH_2),^(e) 4.08 (s, 4

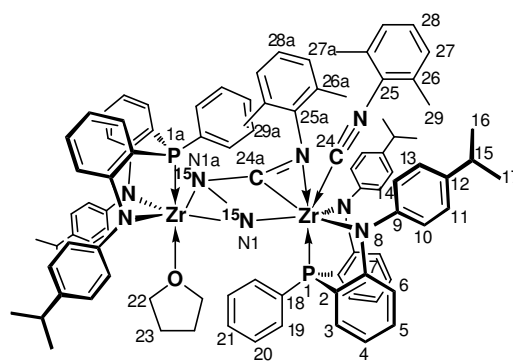
H22, CH_2), 6.55 (t, $^3J_{\text{HH}} = ^4J_{\text{PH}} = 6\text{ Hz}$, 4 H6, ArH), 6.61 (overlapping t and d, $^3J_{\text{HH}} = 7\text{ Hz}$, 4 H19

and 2 H21, ArH), 6.84 (m, $^3J_{\text{HH}} = 7\text{ Hz}$, 4 H4, 4 H10 and 4 H14 ArH), 6.72 (s, 2 H27a and H28a,

ArH),^(f) 6.92 (bm, $^3J_{\text{HH}} = 6\text{ Hz}$, 2 H27 and H28, ArH),^(f) 6.99 (d, $^3J_{\text{HH}} = 8\text{ Hz}$, 4 H11 and 4 H13,

ArH), 7.04 (t, $^3J_{\text{HH}} = 7\text{ Hz}$, 4 H5, ArH), 7.30 (d of d, $^3J_{\text{HH}} = 11\text{ Hz}$, $^3J_{\text{PH}} = 8\text{ Hz}$, 4 H3, ArH), 7.76

(t, $^3J_{\text{HH}} = 8\text{ Hz}$, 4 H20, ArH).



^(a) In addition to the peaks for $[\text{ipropNPNZr(THF)}](\text{xylylNC-}^{15}\text{N}_2)[\text{ipropNPNZr(xylylNC)}]$ **[6.2]**, the $^{31}\text{P}\{^1\text{H}\}$ NMR spectrum displayed signals for unreacted $[\text{ipropNPNZr(THF)}]_2(\mu\text{-}\eta^2\text{:}\eta^2\text{-}^{15}\text{N}_2)$ **[5.2]** at $\delta -3.05$ and an unidentified intermediate **species x** at $\delta -7.22$.

^(b) As no $^2J_{\text{PN}}$ coupling was observed for complex $[\text{ipropNPNZr(THF)}]_2(\mu\text{-}\eta^2\text{:}\eta^2\text{-}^{15}\text{N}_2)$ **[5.2]**, it is assumed that it is the P atom of the zirconium centre which exhibits the PN coupling, and that it

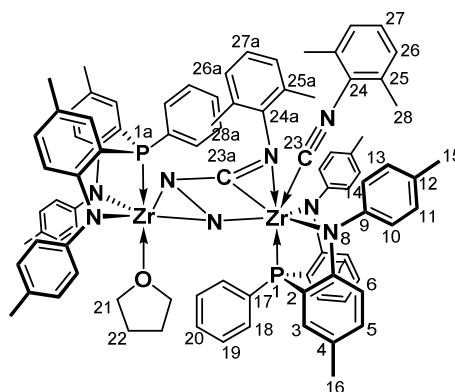
couples with the N atom which experienced the isocyanide insertion, hence three-bond PN coupling is proposed.

(c) $^{15}\text{N}\{^1\text{H}\}$ NMR spectrum obtained using NO_3 in NH_4NO_3 set to δ 0, which converts signals to δ -220.91 (d, $^2J_{\text{PN}} = 20$ Hz, $^{15}\text{N1a}$) and δ -17.70 (s, $^{15}\text{N1}$) if relative to MeNO_2 set to δ 0 ($\Delta\delta$ -5 between MeNO_2 and NO_3 in NH_4NO_3).⁴¹⁷ N1 assignment based on assumption that the signal at δ -17.70 is common to both complexes **[6.2]** and **species e-1** and refers to a Zr-N-Zr moiety.

(d) ^1H - ^1H COSY NMR spectrum of **[6.2]** confirms that this signal represents coordinated THF; (e) unbound THF; (f) two different xylylNC environments are indicated

[$^{101}\text{NPNZr}(\text{THF})$](xylylNC- N_2)[$^{101}\text{NPNZr}(\text{xylylNCN})$] **[6.3] with 2 equiv of xylylNC: In the glove box, a solution of xylylNC (0.04 g, 0.31 mmol) in 3 cm^3 toluene was added a purple solution of [$^{101}\text{NPNZr}(\text{THF})$] $_{2}(\mu\text{-}\eta^2\text{:}\eta^2\text{-N}_2)$ **[5.3]** (0.20 g, 0.15 mmol) in 6 cm^3 toluene at room temperature, immediately forming a brown solution. After stirring for 24 hrs, the toluene solvent was removed *in vacuo* and the tan brown residue was triturated with *n*-pentanes. The brown solid was collected on a sintered glass frit, washed with 4 cm^3 *n*-pentanes and dried. The brown solid was re-suspended and triturated twice in 5 cm^3 *n*-hexanes. The brown solid was collected on a sintered glass frit and washed with 4 cm^3 *n*-pentanes (0.02 g, 0.01 mmol [$^{101}\text{NPNZr}(\text{THF})$](xylylNC- N_2)[$^{101}\text{NPNZr}(\text{xylylNCN})$], 9% yield based on [$^{101}\text{NPNZr}(\text{THF})$] $_{2}(\mu\text{-}\eta^2\text{:}\eta^2\text{-N}_2)$ **[5.3]**.**

$^{31}\text{P}\{^1\text{H}\}$ NMR (C_6D_6 , 162 MHz): δ = 1.25 (s, P1), 11.89 (s, P1a). (a) ^1H NMR (C_6D_6 , 400 MHz): δ = 1.19 (s, 4 H22, CH_2), 1.66 (s, 6 H28a, CH_3), (c) 1.98, 2.03, 2.05 and 2.11 (s, 12 H16 and 12 H15, CH_3), (b) 2.28 (s, 6 H28, CH_3), (c) 4.09 (s, 4 H21, CH_2), 6.45 to 7.40



(H10, H14, H6, H5, H20, H18, H11 and H13, H3, H26, H27, H26a and H27a, ArH), 7.85 (t, 4 H19, ArH).

^(a) P1 and P1a assignments based on complex **[6.2]**.

^(b) Two sets of tolyl signals indicated for the ^{tol}NPN ligand, though possible interference with traces of toluene reaction solvent.

^(c) two different xylylNC environments are indicated and arbitrary assignment of H28 / H28a (free xylylNCN at δ 2.06 (s, CH₃), 6.58 (d, ³J_{HH} = 14 Hz, ArH) and 6.73 (t, ³J_{HH} = 8 Hz, ArH)).

[^{iprop}NPNZr(THF)](^tBuNC-N₂)[^{iprop}NPNZr(^tBuNC)] **[6.4] (a) with 2 equiv of ^tBuNC:** In the glove box, ^tBuNC (40 μ L, 0.35 mmol) was added a purple solution of [^{iprop}NPNZr(THF)]₂(μ - η^2 : η^2 -N₂) **[5.1]** (0.24 g, 0.17 mmol) in 5 cm³ toluene at room temperature, immediately forming a brown solution. After stirring for 2 days, the toluene solvent was removed *in vacuo* and the dark brown residue was triturated twice in *n*-pentanes and once in *n*-hexanes and the resulting mustard solid was dried (0.24 g, 0.17 mmol [^{iprop}NPNZr(THF)](^tBuNC-N₂)[^{iprop}NPNZr(^tBuNC)] **[6.4]**, 97% yield based on [^{iprop}NPNZr(THF)]₂(μ - η^2 : η^2 -N₂) **[5.1]** ^(a) (b) with 4 equiv of ^tBuNC: In the glove box, ^tBuNC (87.4 μ L, 0.77 mmol) was added a purple solution of [^{iprop}NPNZr(THF)]₂(μ - η^2 : η^2 -N₂) **[5.1]** (0.27 g, 0.19 mmol) in 5 cm³ toluene at room temperature, immediately forming a brown solution. After stirring for 2 days, the toluene solvent was removed *in vacuo* and the dark brown residue was triturated thrice in *n*-pentanes. The resulting solid was dissolved in toluene and the brown solution filtered through a sintered glass frit. The toluene solvent was removed *in vacuo* and the residue was triturated once in *n*-hexanes and once in *n*-pentanes before the tan solid was collected on a sintered glass frit and dried (0.03 g). ^(b)

^(a) ³¹P{¹H} NMR (C₆D₆, 162 MHz): δ = 4.40 (s, P1), 10.84 (s, P1a). ^(c) ¹H NMR (C₆D₆, 400

MHz): δ = 0.81 (s, 9 H26a, CH₂), ^(d) 1.09, 1.14 (bs, 4 H23, CH₂), ^(e) 1.30 (bs, 12 H16 and 12 H17,

CH₃), 1.42 (s, 9 H₂₆, CH₃), ^(d) 2.66, 2.86 (bs, 4 H₁₅, CH), ^(f) 3.48, 3.74 (s, 4 H₂₂, CH₂), 6.07 to 7.73 (H₁₀, H₁₄, H₆, H₅, H₂₀, H₁₈, H₁₁, H₁₃, H₃ and H₁₉, ArH).

^(b) same ³¹P{¹H} NMR spectrum as reaction with 2 equiv of ^tBuNC

^(c) P1 and P1a assignments based on complex [6.2].

^(d) two different ^tBuNC environments are indicated and arbitrary assignment of H₂₆ / H_{26a} (free ^tBuNC at δ 1.06).

^(e) two different THF signals, possibly mixture of *cis* / *trans* isomers or N-inside / N-inside insertion.

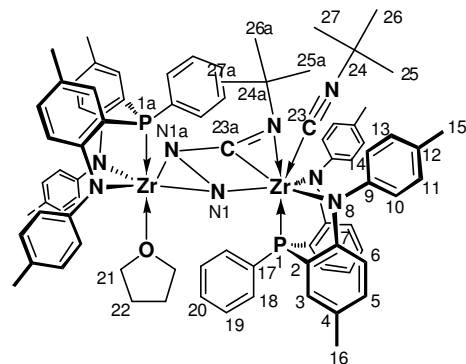
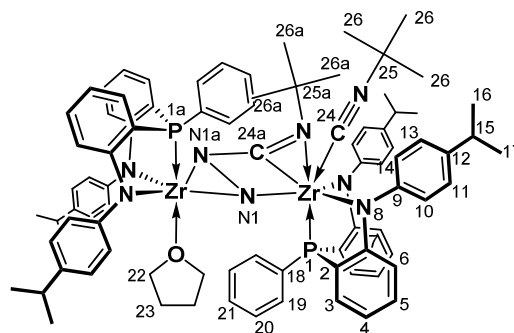
^(f) two different C-H signals for the ^{iprop}NPN ligand, possibly mixture of *cis* and *trans* isomers.

[^{tol}NPNZr(THF)](^tBuNC-N₂)[^{tol}NPNZr(^tBuNC)] [6.5] with 2 equiv of ^tBuNC: In the glove box, ^tBuNC (20 μL, 0.18 mmol) ^(a) was added a purple solution of [^{tol}NPNZr(THF)]₂(μ-η²:η²-N₂) [5.3] (0.08 g, 0.06 mmol) in 2 cm³ toluene-*d*₈ at room temperature, immediately forming a brown solution which was sealed in an NMR tube. ^(b)

^(a) reaction with ^tBuNC in greater than 2 equiv excess

^(b) ³¹P{¹H} NMR (C₆D₆, 162 MHz): δ = 2.25 (s, P1), 10.50 (s, P1a), ^(c) with traces of signals at δ 6.58, and δ -2.29

^(c) P1 and P1a assignments based on complex [6.2]



Species e with successive 1 to 4 equiv of xylylNC: In the glove box, to a purple solution of $[\text{ipropNPNZr}(\text{THF})]_2(\mu\text{-}\eta^2\text{:}\eta^2\text{-N}_2)$ [**5.1**] (0.20 g, 0.14 mmol) in 2 cm³ toluene-*d*₈ was added a 0.5 cm³ toluene-*d*₈ solution of xylylNC (0.02 g, 0.14 mmol) at room temperature, immediately forming a brown solution. After stirring for 14 min, the sample was analysed using NMR spectroscopy.^(a) After 39 min a 0.5 cm³ toluene-*d*₈ solution of xylylNC (0.02 g, 0.15 mmol) was added and the mixture analysed after 49 min.^(b) After 1 hr a 0.5 cm³ toluene-*d*₈ solution of xylylNC (0.02 g, 0.14 mmol) and the mixture was analysed after 1.2 hrs.^(c) After 1.4 hrs a 0.5 cm³ toluene-*d*₈ solution of xylylNC (0.02 g, 0.16 mmol) was added and the mixture was analysed after 1.6 hrs.^(d) The toluene-*d*₈ solvent was removed *in vacuo* and the brown residue dissolved in *n*-hexanes and placed in the freezer (-40 °C) overnight, with no ppt formation. The *n*-hexanes solvent was removed *in vacuo* and the residue triturated with *n*-hexanes, forming a brown ppt. After 4 hrs in the freezer the brown solid was collected on a sintered glass frit and dried (0.07 g).

^(a) $^{31}\text{P}\{^1\text{H}\}$ NMR spectrum indicated mostly unreacted $[\text{ipropNPNZr}(\text{THF})]_2(\mu\text{-}\eta^2\text{:}\eta^2\text{-N}_2)$ [**5.1**] at δ - 3.06;

^(b) $^{31}\text{P}\{^1\text{H}\}$ NMR (C_6D_6 , 162 MHz): δ = 11.19, 2.03 (complex [**6.1**]);

^(c) $^{31}\text{P}\{^1\text{H}\}$ NMR (C_6D_6 , 162 MHz): δ = 11.19, 2.03 (complex [**6.1**]), 0.90, -0.08 (**species e**);

^(d) $^{31}\text{P}\{^1\text{H}\}$ NMR (C_6D_6 , 162 MHz): δ = 0.90, -0.08 (P1, P1a for **species e**).

Species e-1: (a) with 3 equiv of xylylNC: In the glove box, a solid mixture of xylylNC (0.01 g, 0.10 mmol) and purple $[\text{ipropNPNZr}(\text{THF})]_2(\mu\text{-}\eta^2\text{:}\eta^2\text{-}^{15}\text{N}_2)$ [**5.2**] (0.03 g, 0.02 mmol) was dissolved into 0.6 cm³ C_6D_6 , forming a brown solution in a J-young NMR tube;^(a) **(b) with 4 equiv of xylylNC:** Additional solid xylylNC (0.01 g, 0.10 mmol)^(b) was added to the NMR tube.

$^1\text{P}\{\text{H}\}$ NMR (C_6D_6 , 162 MHz): $\delta = -1.10$ (d,

$^3J_{\text{PN}} = 9$ Hz,^(c) P1 or P1a), 0.07 (s, P1 or

P1a).^(d) $^{15}\text{N}\{^1\text{H}\}$ NMR (C_6D_6 , 40 MHz): $\delta = -$

152.11 (d, $^3J_{\text{PN}} = 5$ Hz, N1a), -17.67 (s, N1).^(c)

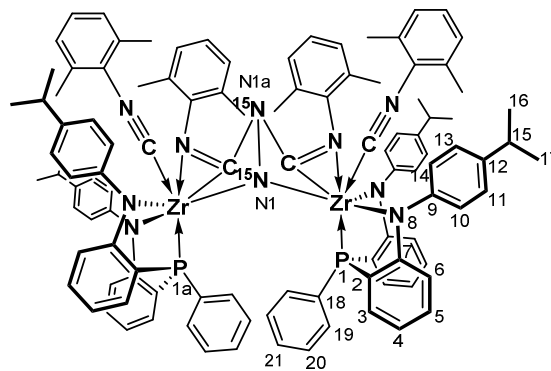
^1H NMR (C_6D_6 , 600 MHz): $\delta = 1.24$ (d, H16

and H17, CH_3), 1.35 (s, CH_2 , free THF), 1.47

(s, xylyl-Me, CH_3), 1.88 (s, xylyl-Me, CH_3), 2.05 (s, free xylyl-Me, CH_3), 2.31 (s, xylyl-Me,

CH_3), 2.61 (s, xylyl-Me, CH_3), 2.88 (bs, 4 H15, CH), 3.52 (s, free THF, CH_2), 5.85-7.87

(phenyl's, ArH)



^(a) some uncertainty in exact equiv, due to small amounts of material used, but spectra very similar to **species e** and 3 equiv of xylylNC

^(b) excess free xylylNC observed with a signal at δ 2.05 for xylyl-Me in the ^1H NMR spectrum.

^(c) arbitrary assignment of P1 and P1a, increased steric crowding may have resulted in increased asymmetry for P1 and P1a, not clear why coupling only observed for one of the P atoms.

^(d) with MeNO_2 at δ 0; assuming Zr-N-Zr is associated with δ -17.67 in $^{15}\text{N}\{^1\text{H}\}$ NMR for both **[6.2]** and **species e-1** and as two bond P-N coupling was also not observed for complex

$[\text{ipropNPNZr}(\text{THF})]_2(\mu\text{-}\eta^2\text{:}\eta^2\text{-N}_2)$ **[5.2]**, three bond P-N coupling is proposed

$[\text{ipropNPNZr}(\text{THF})]_2(\mu\text{-}\eta^2\text{:}\eta^2\text{-N}_2)$ **[5.1]** + **PhSiH₃**: **(a) 1 equiv**: PhSiH_3 (20.0 μL , 0.16 mmol) was added to a purple solution of $[\text{ipropNPNZr}(\text{THF})]_2(\mu\text{-}\eta^2\text{:}\eta^2\text{-N}_2)$ **[5.1]** (0.23 g, 0.16 mmol) in 5 cm_3 C_6D_6 at room temperature, immediately forming a dark brown solution that was transferred to a J-Young NMR tube after 1.75 hrs.^(a) **(a) 2 and 20 equiv**: PhSiH_3 (35.0 μL , 0.28 mmol) was added to a purple solution of $[\text{ipropNPNZr}(\text{THF})]_2(\mu\text{-}\eta^2\text{:}\eta^2\text{-N}_2)$ **[5.1]** (0.20 g, 0.14 mmol) in 5 cm_3 C_6D_6 at room temperature, immediately forming a dark brown solution that was transferred to a

J-Young NMR tube after 1.75 hrs.^(a) After 2 days additional PhSiH₃ (350.0 μ L, 2.84 mmol) was added, with no change in solution colour.^(a) The contents of both J-Young NMR tubes **(a)** and **(b)** were combined into a conical flask inside the glove box.^(b) The C₆D₆ solvent was removed *in vacuo* and the dark brown residue was triturated with 10 cm³ *n*-hexanes. The dark brown solid was collected on a sintered glass frit, washed with 4 x 3 cm³ *n*-hexanes and dried to give an olive green-brown solid (0.10 g).^(c) The *n*-hexanes solvent was removed *in vacuo* from the dark brown filtrate and the residue was combined with the olive green-brown solid.^(d) The combined solids were dissolved in 15 cm³ toluene and centrifuged. The supernatant was decanted and the residue discarded. The toluene solvent was removed *in vacuo* and the residue triturated thrice with 10 cm³ *n*-pentanes. The brown solid was collected on a sintered glass frit, washing with *n*-pentanes (0.08 g).^(e)

³¹P{¹H} NMR (C₆D₆, 162 MHz): δ = -10.09. ¹H NMR (C₆D₆, 400 MHz): δ = 0.29 (Zr-H-Zr?), 1.10 (*iprop*-Me), 2.70 (*iprop*-CH), 4.78 (Si-H?), 6.50-7.80 (phenyls).

^(a) The ³¹P{¹H} NMR spectra after 1, 2 and 20 equiv all displayed a major peak at δ -10.64, with minor peaks at δ -1.78 and δ -3.42 (may have been impurities carried over from the precursor complex **[5.1]**).

^(b) The contents after 1 and 20 equiv were indistinguishable and combined for product work-up.

^(c) The brown solid was observed to be partially soluble in *n*-hexanes. The ³¹P{¹H} NMR spectrum displayed a single peak at δ -10.10. The ¹H NMR spectrum was poorly shimmed, but the absence of coordinated THF is clearly evident.

^(d) as a large part of the product was still present in the filtrate, a second work-up was attempted

^(e) Low recovery due to partial solubility in *n*-pentanes.

$[\text{ipropNPNZr(THF)}]_2(\mu\text{-}\eta^2\text{:}\eta^2\text{-N}_2)$ **[5.1] + H₂C=CH₂ at 1 atm:** A purple solution of $[\text{ipropNPNZr(THF)}]_2(\mu\text{-}\eta^2\text{:}\eta^2\text{-N}_2)$ **[5.1]** (0.09 g, 0.06 mmol) in 20 cm³ toluene was placed in a thick-walled flask and connected to an ethylene cylinder with an intervening column filled with activated molecular sieves / copper catalyst. The solution was subjected to three purge / refill cycles with 1 atm H₂C=CH₂ and then allowed to stir at room temperature. No colour changes were observed, however, some polymer was observed to form after 2 days. After 3 days, the flask was transferred to the glovebox and the purple solution filtered through a celite pipette. The toluene solvent was removed in vacuo, leaving a red-brown residue.^(a)

^(a) ³¹P{¹H} NMR (C₆D₆, 162 MHz): δ = -3.80 (87%), 0.82 (13%). ¹H NMR (C₆D₆, 400 MHz): δ = 0.91-1.36, 2.72, 3.62. 5.00(d, ²J_{HH} = 12 Hz), 5.07(d, ²J_{HH} = 16 Hz), 6.70-7.70.

$[\text{ipropNPNZr(THF)}]_2(\mu\text{-}\eta^2\text{:}\eta^2\text{-N}_2)$ **[5.1] + 1 equiv of CO:** A purple solution of $[\text{ipropNPNZr(THF)}]_2(\mu\text{-}\eta^2\text{:}\eta^2\text{-N}_2)$ **[5.1]** (0.13 g, 0.09 mmol) in 1 cm³ toluene-*d*₈ was placed in a thick-walled flask and connected to a CO cylinder (15 psi) with an intervening column filled with activated molecular sieves. The solution was subjected to three freeze / pump / thaw cycles before 1 equiv of CO was added at room temperature (2.2 μ L, 9 x 10⁻⁵ mol). After 4 days, the solution had changed to a cherry brown colour. After 15 days, the dark brown purple solution was transferred to a J-Young NMR tube.^(a)

^(a) ³¹P{¹H} NMR (C₆D₆, 162 MHz): δ = -3.01 (9%), -2.23 (19%), -0.90 (20%), 1.25 (19%), 11.53 (16%) and 23.00 (17%).

$[\text{ipropNPNZr(THF)}]_2(\mu\text{-}\eta^2\text{:}\eta^2\text{-N}_2)$ **[5.1] + 1 atm CO (a) 1 day:** A purple solution of $[\text{ipropNPNZr(THF)}]_2(\mu\text{-}\eta^2\text{:}\eta^2\text{-N}_2)$ **[5.1]** (0.05 g, 0.04 mmol) in 1.5 cm³ toluene-*d*₈ was placed in a thick-walled flask and connected to a CO cylinder with an intervening column filled with activated molecular sieves. The solution was subjected to three freeze / pump / thaw cycles before 1 atm CO was added at room temperature. After 1 day, the solution had changed to a

cherry red-brown colour and was transferred to a J-Young NMR tube.^(a) **(b) 16 days:** A purple solution of $[\text{ipropNPNZr}(\text{THF})]_2(\mu\text{-}\eta^2\text{:}\eta^2\text{-N}_2)$ [**5.1**] (0.26 g, 0.19 mmol) in 10 cm³ toluene was placed in a thick-walled flask and connected to a CO cylinder with an intervening column filled with activated molecular sieves. The solution was subjected to three freeze / pump / thaw cycles before 1 atm CO was added at room temperature. After 1 day, the solution had changed to a cherry red colour and after 5 days the solution was brown with a hint of yellow. After 16 days the orange solution was transferred to a J-Young NMR tube.^(b)

^(a) $^{31}\text{P}\{\text{H}\}$ NMR (C_6D_6 , 162 MHz): $\delta = -4.67, -3.01$ (major), 1.24, 3.02, 3.97, 5.01, 5.57, 5.70, 6.31, 7.26, 7.60, 8.64, 11.50 and 23.00.

^(b) $^{31}\text{P}\{\text{H}\}$ NMR (C_6D_6 , 162 MHz): $\delta = -4.63, -3.81, -0.94$ to 11.53 and 23.00.

$[\text{ipropNPNZr}(\text{THF})]_2(\mu\text{-}\eta^2\text{:}\eta^2\text{-N}_2)$ [**5.1**] + 1 equiv of **4,4'-dimethylbenzophenone**: A purple solution of $[\text{ipropNPNZr}(\text{THF})]_2(\mu\text{-}\eta^2\text{:}\eta^2\text{-N}_2)$ [**5.1**] (0.20 g, 0.14 mmol) in 5 cm³ toluene and a clear solution of 4,4'-dimethylbenzophenone (0.03 g, 0.15 mmol) in 1.5 cm³ toluene were placed in the glovebox freezer (-40 °C). After 1 hr, the 4,4'-dimethylbenzophenone solution was added to the $[\text{ipropNPNZr}(\text{THF})]_2(\mu\text{-}\eta^2\text{:}\eta^2\text{-N}_2)$ [**5.1**] solution, which turned brown after one minute. After stirring for 5 hrs at room temperature the toluene solvent was removed *in vacuo* and the oily brown residue was triturated in 5 cm³ *n*-hexanes and placed in the freezer for 22 hrs. The light brown / orange solid was collected on a sintered glass frit and washed with 3 x 2 cm³ *n*-hexanes (0.07 g).^(a)

^(a) $^{31}\text{P}\{\text{H}\}$ NMR (C_6D_6 , 101 MHz): $\delta = -21.15, -12.52, -10.49, -9.52, -5.33, 15.70$ and 43.25. EI-MS (m/z): 1472 (50, $[\text{ipropNPNZr}]_2(\mu\text{-O})(\mu\text{-}\eta^1\text{:}\eta^2\text{-NN}=\text{C}(\text{C}_6\text{H}_4\text{Me})_2)^+$)

$[\text{ipropNPNZr}(\text{THF})]_2(\mu\text{-}\eta^2\text{:}\eta^2\text{-N}_2)$ [**5.1**] + 2 equiv of **CO₂**: A purple solution of $[\text{ipropNPNZr}(\text{THF})]_2(\mu\text{-}\eta^2\text{:}\eta^2\text{-N}_2)$ [**5.1**] (0.07 g, 0.05 mmol) in 5 cm³ Et₂O was placed in a thick-

walled flask and connected to a CO₂ cylinder (15 psi) with an intervening column filled with activated molecular sieves. The solution was subjected to two freeze / pump / thaw cycles before 2 equiv of CO₂ was added at room temperature (2.2 μ L, 9×10^{-5} mol), immediately forming an orange solution. After 20 hrs, the solution was filtered through a glass pipette packed with celite into a scintillation vial inside the glovebox. The Et₂O solvent was removed *in vacuo* and the orange residue was dissolved in C₆D₆. The orange solution was transferred to a J-Young NMR tube.^(a)

^(a) ³¹P{H} NMR (C₆D₆, 101 MHz): δ = -31.35, -19.92, -12.47, -8.16, -7.09 and 10.54.

[^{iprop}NPNZr(THF)]₂(μ - η^2 : η^2 -N₂) [5.1] + 1 equiv of (trimethylsilyl)diazomethane: To a purple solution of [^{iprop}NPNZr(THF)]₂(μ - η^2 : η^2 -N₂) [5.1] (0.14 g, 0.10 mmol) in 2 cm³ C₆D₆ at room temperature was added a solution of (trimethylsilyl)diazomethane in Et₂O (2 M, 50 μ L, 0.10 mmol) was added, immediately forming a brown-orange solution.^(a) After 28 min, a second aliquot (trimethylsilyl)diazomethane in Et₂O (2 M, 50 μ L, 0.10 mmol) was added.^(b)

^(a) ³¹P{H} NMR (C₆D₆, 101 MHz): δ = -4.23, -13.05.

^(b) ³¹P{H} NMR (C₆D₆, 101 MHz): δ = -4.23, -13.05 and trace signals at -5.57, -5.12, -2.67 and 10.01.

[^{tol}NPNTi(THF)]₂(μ - η^1 : η^1 -N₂) [5.15] + H₂ at 1 atm: A brown solution of [^{tol}NPNTi(THF)]₂(μ - η^1 : η^1 -N₂) [5.15] (0.07 g, 0.06 mmol) in 1.75 cm³ toluene-*d*₈ was placed in a thick-walled flask and connected to a column filled with activated molecular sieves. The solution was degassed twice and then placed under reduced pressure. 1 atm H₂ was introduced to the solution at room temperature. After 24 days no colour changes were observed and the dark brown solution was transferred to a J-Young NMR tube and analysed.^(a)

(a) $^{31}\text{P}\{^1\text{H}\}$ NMR spectrum indicate unreacted $[\text{}^{101}\text{NPNTi}(\text{THF})]_2(\mu\text{-}\eta^1\text{:}\eta^1\text{-N}_2)$ **[5.15]** and ^1H NMR spectrum display a peak at δ 4.57 indicating dissolved H_2 .

$[\text{}^{101}\text{NPNTi}(\text{THF})]_2(\mu\text{-}\eta^1\text{:}\eta^1\text{-N}_2)$ [5.15] + CO at 1 atm: A brown solution of $[\text{}^{101}\text{NPNZr}(\text{THF})]_2(\mu\text{-}\eta^1\text{:}\eta^1\text{-N}_2)$ (0.06 g, 0.05 mmol) in 1.75 cm^3 toluene- d_8 was placed in a thick-walled flask and connected to a CO cylinder with an intervening column filled with activated molecular sieves. The solution was degassed twice and then placed under reduced pressure. 1 atm CO was introduced to the solution at room temperature. After 24 days no colour changes were observed and the dark brown solution was transferred to a J-Young NMR tube and analysed.^(a)

(a) $^{31}\text{P}\{^1\text{H}\}$ NMR spectrum indicate unreacted $[\text{}^{101}\text{NPNTi}(\text{THF})]_2(\mu\text{-}\eta^1\text{:}\eta^1\text{-N}_2)$ **[5.15]**.

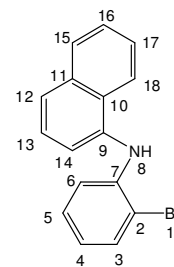
$[\text{}^{101}\text{NPNTi}(\text{THF})]_2(\mu\text{-}\eta^1\text{:}\eta^1\text{-N}_2)$ [5.15] + $\text{H}_2\text{C}=\text{CH}_2$ at 1 atm: A dark brown solution of $[\text{}^{101}\text{NPNTi}(\text{THF})]_2(\mu\text{-}\eta^1\text{:}\eta^1\text{-N}_2)$ **[5.15]** (0.14 g, 0.11 mmol) in 2 cm^3 toluene- d_8 was placed in a thick-walled flask and connected to an ethylene cylinder with an intervening column filled with activated molecular sieves / copper catalyst. The solution was subjected to three purge / refill cycles with 1 atm $\text{H}_2\text{C}=\text{CH}_2$ and then allowed to stir at room temperature. No colour changes or polymer formation was observed. After 13 days, the flask was transferred to the glovebox and the brown solution was transferred to a J-Young tube.^(a) The solution was transferred to a scintillation vial, rinsing with *n*-hexanes. The toluene / *n*-hexanes solvent was removed in vacuo and the brown residue was triturated once with 5 cm^3 *n*-hexanes and once with 3 cm^3 *n*-pentanes. The *n*-pentanes suspension was placed in the freezer and after 2 hrs the solid was collected on a sintered glass frit, washing with $2 \times 3\text{ cm}^3$ *n*-pentanes (0.05 g).^(b)

(a) $^{31}\text{P}\{\text{H}\}$ NMR (C_6D_6 , 101 MHz): $\delta = -4.78$ (major) with numerous side-products within the range of δ 38.06 to δ -18.93 and some $^{101}\text{NPNH}_2$ **[2.11]**

^(b) All the impurities were *n*-hexanes soluble and the major species was isolated as a single peak at δ -4.78 (¹P{¹H} NMR). The ¹H NMR spectrum (C₆D₆, 300 MHz): δ = 0.87 (t, ³J_{PH} = 7 Hz, Ti(H₂C=CH₂)), 1.25 (m, ³J_{PH} / ²J_{HH} / ³J_{HH} = 5 Hz, Ti(H₂C=CH₂)), 1.62 to 2.52 (tolyl, CH₃), 6.12 to 8.23 (phenyls, ArH).

^{naph}Ar^{Br}ArNH [7.1]: PdCl₂(DPPF) (2.84 g, 3.88 mmol), DPPF (4.25 g, 7.66), Na^tOBu (20.45 g, 212.78 mmol) and ^{naph}ArNH₂ (24.00 g, 167.64 mmol) were added to 200 cm³ 1,4-dioxane in the glovebox, forming a dark brown mixture. The reaction flask was transferred to a Schlenk line and *o*-C₆H₄Br₂ (23.00 cm³, 190.71 mmol) was added. The reaction mixture was refluxed for 3 days^(a) at 140 °C. The 1,4-dioxane solvent was removed *in vacuo*, toluene was added to the dark brown residue and the mixture was filtered through a Buchner funnel, washing with toluene. The toluene was removed *in vacuo* from the filtrate, leaving a viscous dark brown oil. The product was separated from *o*-C₆H₄Br₂ using column chromatography (silica gel 60-200 μ m, 70-230 mesh) with 100% petroleum ether as eluent, gradually increasing polarity to petroleum ether/ethyl acetate (4:1) (27.58 g, 92.49 mmol ^{naph}Ar^{Br}ArNH [7.1], 55% yield based on ^{naph}ArNH₂). Single crystals of ^{naph}Ar^{Br}ArNH [7.1] were grown from a toluene solution at -40 °C.

¹H NMR (CDCl₃, 300 MHz): δ = 6.39 (bs, 1 H8, NH), 6.73 (t, ³J_{HH} = 8 Hz, 1 H5, ArH), 6.87 (d, ³J_{HH} = 8 Hz, 1 H3, ArH), 7.09 (t, ³J_{HH} = 8 Hz, 1 H4, ArH), 7.45 (overlapping t, ³J_{HH} = 6 Hz, 1 H13 and d, ³J_{HH} = 6 Hz, 1 H12, ArH), 7.52 (m, 1 H16 and 1 H17, ArH), 7.59 (d of d, ³J_{HH} = 8 Hz, ⁴J_{HH} = 1 Hz, 1 H6, ArH), 7.72 (d of d, ³J_{HH} = 6 Hz, ⁴J_{HH} = 2 Hz, 1 H12, ArH), 7.91 (d of d, ³J_{HH} = 8 Hz, ⁴J_{HH} = 2 Hz, 1 H15, ArH), 8.05 (d of d, ³J_{HH} = 8 Hz, ⁴J_{HH} = 2 Hz, 2 H18, ArH). ¹³C{¹H} NMR (CDCl₃, 75 MHz): δ = 111.4 (C2, C_{ipso}), 115.6 (C3, ArC), 119.9 (C13, ArC), 120.4 (C4, ArC), 122.5 (C18, ArC), 125.1 (C12, ArC), 126.1 (C14, ArC), 126.4, 126.5 (C16 and C17, ArC), 128.4 (C5, ArC), 128.7 (C15, ArC), 129.3 (C11, C_{ipso}), 132.9 (C6, ArC), 134.9 (C10, C_{ipso}), 137.4 (C9,

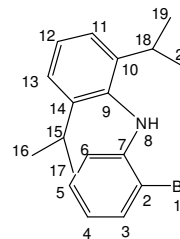


C_{ipso}), 143.3 (C_7 , C_{ipso}) . Anal. Calcd. for $C_{16}H_{12}BrN$: C, 64.45; H, 4.06; N, 4.70; Found: C, 64.30; H, 4.06; N, 4.79. EI-MS (m/z): 299 (75, $[M + H]^+$), 217 (100, $[M - Br + H]^+$).

^(a) GC-MS monitoring showed that reaction is complete after *ca* 20 hrs and $^{\text{naph}}\text{Ar}^{\text{H}}\text{ArNH}$ was observed as a side-product

$^{2,6-i\text{Pr}_2}\text{Ar}^{\text{Br}}\text{ArNH}$ [7.2]: $\text{PdCl}_2(\text{DPPF})$ (2.75 g, 3.77 mmol), DPPF (4.17 g, 7.52 mmol) and Na^tOBu (19.98 g, 207.93 mmol) were combined with 230 cm^3 1,4-dioxane in the glovebox, forming an orange mixture. The reaction flask was transferred to a Schlenk line and $o\text{-C}_6\text{H}_4\text{Br}_2$ (22.70 cm^3 , 188.22 mmol) and $^{2,6-i\text{Pr}_2}\text{ArNH}_2$ (35.60 cm^3 , 188.55 mmol) were added sequentially, forming a dark brown mixture. The reaction mixture was refluxed for 5 days at 145 °C. The 1,4-dioxane solvent was removed *in vacuo* from the brown residue, 60 cm^3 toluene was added to the residue and this mixture was filtered using a Buchner funnel, washing with 2 x 30 cm^3 toluene. The toluene was removed *in vacuo* from the filtrate leaving a viscous dark brown oil. The product was separated from $o\text{-C}_6\text{H}_4\text{Br}_2$ using (i) column chromatography (silica gel 60-200 μm , 70-230 mesh) with 100% petroleum ether as eluent, gradually increasing polarity to petroleum ether/ethyl acetate (19:1) followed by (ii) recrystallisation from *n*-pentanes at -40 °C^(a) (38.73 g, 116.56 mmol $^{2,6-i\text{Pr}_2}\text{Ar}^{\text{Br}}\text{ArNH}$ [7.2], 62% yield based on $o\text{-C}_6\text{H}_4\text{Br}_2$).^(b) Single crystals of $^{2,6-i\text{Pr}_2}\text{Ar}^{\text{Br}}\text{ArNH}$ [7.2] were grown by slow diffusion of *n*-hexanes into a THF solution.

^1H NMR (C_6D_6 , 300 MHz): δ = 1.03 (d, $^3J_{\text{HH}}$ = 7 Hz, 3 H16 and 3 H19, CH_3), 1.10 (d, $^3J_{\text{HH}}$ = 7 Hz, 3 H17 and 3 H20, CH_3)^(c), 3.17 (hep, $^3J_{\text{HH}}$ = 7 Hz, 1 H15 and 1 H18, CH), 5.82 (bs, 1 H8, NH), 6.22 (d of d, $^3J_{\text{HH}}$ = 8 Hz, $^4J_{\text{HH}}$ = 1 Hz, 1 H3, ArH), 6.36 (d of t, $^3J_{\text{HH}}$ = 8 Hz, $^4J_{\text{HH}}$ = 1 Hz, 1 H5, ArH), 6.78 (t, $^3J_{\text{HH}}$ = 8 Hz, 1 H4, ArH), 7.15 (d, $^3J_{\text{HH}}$ = 7 Hz, 1 H11 and 1 H13), 7.23 (m, $^3J_{\text{HH}}$ = 6 Hz, 1 H12, ArH), 7.40 (d of d, $^3J_{\text{HH}}$ = 8 Hz, $^4J_{\text{HH}}$ = 1 Hz, 1 H6, ArH). $^{13}\text{C}\{^1\text{H}\}$ NMR (C_6D_6 , 75 MHz): δ = 23.1 (C16,19, CH_3),



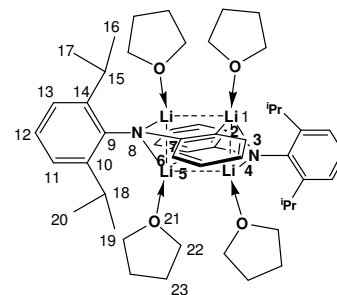
24.6 (C17,20, CH₃), 28.7 (C15/18, CH), 109.3 (C2, C_{ipso}), 113.1 (C3, ArC), 118.9 (C5, ArC), 124.3 (C11, C12, and C13, ArC), 128.6 (C4, ArC), 132.8 (C6, ArC), 135.1 (C9, C_{ipso}), 145.4 (C7, C_{ipso}), 147.9 (C10 and C14, C_{ipso}). Anal. Calcd. for C₁₈H₂₂BrN: C, 65.06; H, 6.67; N, 4.22; Found: C, 65.10; H, 6.64; N, 4.30. EI-MS (*m/z*): 331 (30, [M]⁺), 252 (100, [M - Br]⁺), 236 (40, [M - Br - CH₄]⁺), 222 (35, [M - Br - 2CH₃]⁺), 210 (30, [M - Br - CH(CH₃)₂ + H]⁺), 194 (30, [M - Br - CH(CH₃)₂ - CH₃]⁺).

(a) as ^{2,6-*i*Pr₂Ar^{Br}ArNH [7.2]} is soluble in *n*-pentanes at room temperature, the crystals were collected on a sintered glass frit that had been cooled in the freezer.

(b) Product losses were incurred during purification by column chromatography, and a pre-column GC-MS yield of 92% was observed for ^{2,6-*i*Pr₂Ar^{Br}ArNH [7.2]}.

(c) it was not possible to distinguish between the two distinct sets of methyls on the *i*-propyl moiety, thus one set was arbitrarily designated H16 / H19 and the other H17 / H20 (same for the corresponding carbon atoms).

[^{2,6-*i*Pr₂Ar^{Li}ArNLi]_n [7.3]: ^{2,6-*i*Pr₂Ar^{Br}ArNH [7.2]} (3.44 g, 10.36 mmol) was dissolved in 75cm³ Et₂O in a 500 cm³ round bottom flask and the mixture was cooled to -49 °C (dry ice/ethanol). *n*-BuLi in *n*-hexanes (1.67M, 15 cm³, 25.1 mmol + 1.65M, 10 cm³, 16.5 mmol = 41.6 mmol) was added via syringe over a period of 2 min, giving an orange solution. The reaction mixture was allowed to warm slowly to room temperature and stirred for *ca* 65 min before the solvent was removed *in vacuo*, resulting in an orange solid. Inside the glovebox, orange solid was suspended in 40 cm³ *n*-hexanes, forming an orange solution with a pale yellow suspension. This mixture was subjected to centrifugal forces, the resultant supernatant liquid decanted and the solid re-suspended in 40 cm³ *n*-hexanes. This procedure was conducted 4 times until the supernatant was clear and a white precipitate was obtained. The *n*-hexanes solvent was removed *in vacuo* and the white solid dried (1.94 g, 7.32 mmol [^{2,6-*i*Pr₂Ar^{Li}ArNLi]_n, 71% yield based on ^{2,6-*i*Pr₂Ar^{Br}ArNH}}}



7.18; N, 4.67.^(b) EI-MS (m/z): 253 (85, $[M - Br + H]^+$), 238 (100, $[M - Br - CH_4 + 2H]^+$), 222 (20, $[M - Br - 2CH_3]^+$), 196 (30, $[M - Br - CH(CH_3)_2 - CH_3 + 2H]^+$).

^(a) note that it was not possible to distinguish between the two distinct *i*-propyl moieties, thus the H's of one *i*-propyl group was arbitrarily designated H15 for methine and H16 / H17 for methyl and the other H18 for methine and H19 / H20 for methyl as well as for the analogous carbon atoms.

^(b) Elemental analysis suggests 0.45 LiBr is present in the isolated white solid (even after introduction of an additional toluene filtration step). The LiBr could have become incorporated into the solid state molecular structure, as was reported of LiCl for the PNP lithium amide ligand.⁴¹⁸

$[^{naph}Ar^{Li}ArNLi \cdot 2Et_2O]_2$ [7.4] $^{naph}Ar^{Br}ArNH$ [7.1] (20 g, 67.1 mmol) was dissolved in 300 cm³ Et₂O in a 500 cm³ round bottom flask and the mixture was cooled to -40 °C (dry ice/ethanol). *n*-BuLi in *n*-hexanes (1.64 M, 82.5 cm³, 135.3 mmol) was added via syringe over a period of 5 min. The reaction mixture was allowed to warm slowly to room temperature and stirred for 30 min before the Et₂O solvent was removed *in vacuo*, resulting in a yellow powder. Inside the glovebox, the yellow solid was collected on a sintered frit, washed with *n*-hexanes and dried (19.8 g, 64.9 mmol $^{naph}Ar^{Li}ArNLi \cdot Et_2O$, 97% yield based on $^{naph}Ar^{Br}ArNH$ [7.1]).

$^7Li\{^1H\}$ NMR (C₆D₆, 156 MHz): δ = 1.13 (s, Li1,8). 1H

NMR (C₆D₆, 400 MHz): δ = 0.42 (s, 6 H21, CH₃),^(a) 2.68 (s,

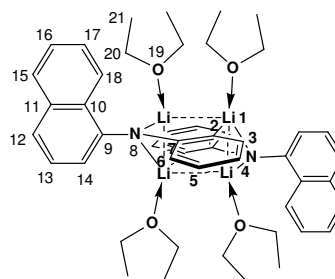
4 H20, CH₂),^(a) 6.22 (t, $^3J_{HH}$ = 7 Hz, 1 H5, ArH), 6.31 (d,

$^3J_{HH}$ = 7 Hz, 1 H3, ArH), 6.70 (t, $^3J_{HH}$ = 7 Hz, 1 H4), 7.03

(m, $^3J_{HH}$ = 7 Hz, 1 H16 and 1 H17, ArH), 7.24 (t, $^3J_{HH}$ = 8

Hz, 1 H13, ArH), 7.34 (d, $^3J_{HH}$ = 7 Hz, 1 H6 and 1 H14, ArH), 7.77 (d, $^3J_{HH}$ = 8 Hz, 1H₁₂), 7.95

(bs, 1 H15), 8.18 (d, $^3J_{HH}$ = 7 Hz, 1 H18). $^{13}C\{^1H\}$ NMR (C₆D₆, 101 MHz): δ = 23.0 (C21, CH₃),



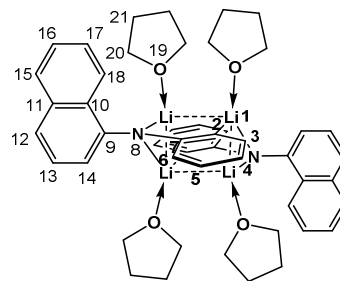
31.9 (C20, CH₂), 114.0 (C5, ArC), 114.3 (C2, C_{ipso}), 118.7 (C3, ArC), 125.5 (C17 and C16, ArC), 125.6, 125.7, 126.0 (C13, C14, C15 and C18, ArC), 129.1 (C4 and C12, ArC and C11, C_{ipso}), 136.5 (C10, C_{ipso}), 154.5 (C9, C_{ipso}), 159.6 (C7, C_{ipso}). Anal. Calcd. for C₂₀H₂₁Br_{0.45}Li_{2.45}NO: C, 69.76; H, 6.15; N, 4.07; Found: C, 69.82; H, 6.04; N, 4.04.^(b) EI-MS (*m/z*): 219 (50, [M - 2Li - Et₂O + 2H]⁺).

^(a) Based on solid state molecular structure of **[7.3a]**, two solvent molecules per ^{naph}Ar^{Li}ArNLi unit are expected, but ¹H NMR integration indicates one Et₂O molecules per ^{naph}Ar^{Li}ArNLi unit.

^(b) Elemental analysis suggest 0.45 LiBr is present in the isolated yellow solid, that may have become incorporated into the aryllithiumamide aggregate.⁴¹⁸

[^{naph}Ar^{Li}ArNLi·2THF]₂ **[7.5]** ^{naph}Ar^{Br}ArNH **[7.1]** (2.31 g, 7.75 mmol) was dissolved in 10 cm³ THF in a conical flask and the mixture was cooled to -40 °C (glovebox freezer). *n*-BuLi in *n*-hexanes (1.60 M, 9.7 cm³, 15.5 mmol) was added via syringe, forming a orange solution with a orange ppt. The reaction mixture was allowed to warm to room temperature and stirred for 1hr 19 min before the THF solvent was removed *in vacuo*, resulting in an orange foam. This orange residue was dissolved in 10 cm³ toluene. This orange residue was triturated with 10 cm³ toluene inside the glovebox and filtered through celite with a sintered glass frit, washing with 2 x 5 cm³ toluene. The toluene solvent was removed *in vacuo* with heating (60 °C), resulting in an orange sticky semi-solid residue, which was triturated with *n*-hexanes to form a fluffy yellow ppt. The yellow solid was collected on a sintered glass frit and washed with 3 x 3 cm³ *n*-hexanes and dried *in vacuo* (1.23 g, 4.07 mmol ^{naph}Ar^{Li}ArNLi·THF, 52% yield based on ^{naph}Ar^{Br}ArNH **[7.1]**).

⁷Li{¹H} NMR (THF-*d*₈, 156 MHz): δ = 0.43 (s, Li1,8). ¹H NMR (THF-*d*₈, 300 MHz): δ = 1.75 (m, 4 H21, CH₂),^(a) 3.58 (t, 4 H20,



CH₂), ^(a) 5.91 (t, ³J_{HH} = 7 Hz, 1 H4, ArH), 6.44 (d, ³J_{HH} = 8 Hz, 1 H6, ArH), 6.67 (overlapping t, ³J_{HH} = 8 Hz, 1 H5 and d, ³J_{HH} = 8 Hz, 1 H3, ArH), 6.87, 7.01, 7.10, 7.17 (m, 1 H13, 1 H17, 1 H14, and 1 H16, ArH), 7.53 (d, ³J_{HH} = 8 Hz, 1H₁₅), 7.81 (d, ³J_{HH} = 5 Hz, 1 H12), 8.27 (d, ³J_{HH} = 8 Hz, 1 H18). ¹³C{¹H} NMR (C₆D₆, 75 MHz): δ = 26.4 (C21, CH₂), 68.2 (C20, CH₂), 109.8 (C4, ArC), 115.4 (C2, C_{ipso}), 116.2 (C6, ArC), 117.2 (C17, ArC), 122.4 (C16, ArC), 123.7 (C14, ArC), 124.0 (C13, ArC), 125.1 (C18, ArC), 128.0 (C15, ArC), 129.0 (C3 and C5, ArC), 133.2 (C11, C_{ipso}), 137.1 (C10, C_{ipso}), 138.2 (C12, ArC), 157.4 (C9, C_{ipso}), 160.6 (C7, C_{ipso}). Anal. Calcd. for C₂₀H₂₁Br_{0.38}Li_{2.38}NO: C, 71.44; H, 5.70; N, 4.17; Found: C, 71.42; H, 6.07; N, 4.05. ^(b) EI-MS (*m/z*): 219 (100, [M - (2Li + THF) + 2H]⁺).

^(a) Based on solid state molecular structure of **[7.3a]**, two solvent molecules per ^{naph}Ar^{Li}ArN^{Li} unit are expected, but ¹H NMR integration indicates one THF molecules per ^{naph}Ar^{Li}ArN^{Li} unit.

^(b) Elemental analysis suggest 0.38 LiBr is present in the isolated yellow solid, that may have become incorporated into the aryllithiumamide aggregate.⁴¹⁸

[^{naph}NPNLi₂·diox]_n [7.6] (a) from ^{naph}Ar^{Br}ArNH [7.1]: ^{naph}Ar^{Br}ArNH [7.1] (5.00 g, 16.76 mmol) was dissolved in 120 cm³ Et₂O in a 300 cm³ 3-necked round-bottomed flask fitted with a pressure-regulated dropping funnel. The solution was cooled to -44 °C (dry ice/ethanol) and 1.68 M *n*-BuLi in *n*-hexanes (20.0 cm³, 33.6 mmol) was added dropwise via syringe, forming a light yellow solution. The cooling bath was removed and the reaction mixture was allowed to warm to room temperature. Meanwhile 60 cm³ Et₂O and PPhCl₂ (1.15 cm³, 8.38 mmol) was added to the dropping funnel. The reaction flask was then cooled to -44 °C before the PPhCl₂ solution was added slowly over 3hr 10min (approx. dripping rate 11 cm³/10 min), resulting in a orange-brown solution with a suspended orange solid. The reaction mixture was allowed to warm slowly to room temperature and stirred overnight for *ca* 41.5 hr. The Et₂O was removed *in vacuo*, giving an orange foam. This orange residue was triturated with a mixture of 20 cm³ *n*-hexanes and 25 cm³

toluene inside the glovebox and filtered through celite with a sintered glass frit, washing with 5 cm³ toluene. To the dark orange filtrate was added 1,4-dioxane (2.90 cm³, 34.03 mmol). As no ppt. was observed, the *n*-hexanes / toluene solvent was removed *in vacuo* with heating (60 °C), giving a viscous orange oil. A mixture of 30 cm³ *n*-hexanes and 10 cm³ toluene was added to this tarry substance with heating until complete dissolution was observed. The solution was placed in the freezer (-40 °C) for 5 min, forming a orange ppt. that was collected on a sintered glass frit and washed with 2 x 6 cm³ *n*-hexanes/toluene (5:1) solvent mixture and dried *in vacuo*. This first crude solid was dissolved with heating in a mixture of 23 cm³ *n*-hexanes and 12 cm³ toluene, forming a dark orange solution with a fluffy orange ppt. The solution was placed in the freezer for 5 min before the second orange solid was collected on a sintered glass frit and washed with 3 x 5 cm³ *n*-hexanes:toluene (5:3) solvent mixture and dried *in vacuo*. This second isolated solid was dissolved with heating in a mixture of 23 cm³ *n*-hexanes and 5 cm³ toluene, forming a dark orange solution with a fluffy orange ppt. The solution was placed in the freezer for 7 min before the third orange solid was collected on a sintered glass frit and washed with 2 x 7 cm³ *n*-hexanes:toluene (5:2) solvent mixture and dried *in vacuo* (2.49 g, 3.87 mmol ^{naph}NPNLi₂.diox, 46% yield based on ^{naph}Ar^{Br}ArNH [7.1]); (b) from [^{naph}Ar^{Li}ArNLi·2Et₂O]₂ [7.4]: Inside the glovebox, [^{naph}Ar^{Li}ArNLi·2Et₂O]₂ [7.4] (15.26 g, 49.99 mmol) was dissolved in 300 cm³ THF in a 1.0 dm³ 3-necked round-bottomed flask and 300 cm³ THF was added to a pressure-regulated dropping funnel. The flask and dropping funnel were removed from the box, assembled under an N₂ atmosphere and the solution cooled to -40 °C (dry ice/ethanol), while PPhCl₂ (3.4 cm³, 25.1 mmol) was added to the dropping funnel. The PPhCl₂ solution was added slowly over 3hr (approx. dripping rate 12 cm³/10 min). The reaction mixture was allowed to warm slowly to room temperature and stirred overnight for 16hr. The THF was removed *in vacuo* and the residue was triturated with 100 cm³ toluene inside the glovebox and filtered through celite with a sintered glass frit, washing with additional toluene. To the filtrate was added 1,4-dioxane (8.7 cm³, 102.1 mmol) and the toluene solvent was removed *in vacuo*, resulting in a viscous dark red oil. The oil

was partially redissolved in 100 cm³ toluene and the undissolved solids were filtered through a sintered glass frit. The toluene solvent was removed *in vacuo* from the filtrate and the residue was triturated in a mixture of 150 cm³ *n*-hexanes and 50 cm³ toluene, forming an orange ppt. This first crude solid was collected on a sintered glass frit and dried *in vacuo* (14.3 g). An amount of this first crude solid (5.0 g) was dissolved with heating in a mixture of 20 cm³ *n*-hexanes and 5 cm³ toluene, forming a dark orange solution with a fluffy orange ppt. The solution was placed in the freezer for 50 min before the second orange solid was collected on a sintered glass frit and dried *in vacuo* (3.7 g, 5.7 mmol [^{naph}NPNLi₂.diox]_n).

[^{naph}NPNLi₂.diox]_n [7.6] major species (70%): ³¹P{¹H} NMR

(toluene-*d*₈, 162 MHz): δ = -34.47 (qt, ¹J_{PLi} = 40 Hz, P1).

⁷Li{¹H} NMR (toluene-*d*₈, 156 MHz): δ = 0.70 (s, 1 Li23),

1.85 (d, ¹J_{LiP} = 44 Hz, 1 Li22). ¹H NMR (toluene-*d*₈, 600

MHz): δ = 2.77 (bs, 8 H26/27, CH₂), 6.37 (t, ³J_{HH} = 8 Hz, 2

H5, ArH), 6.59 (d, ³J_{HH} = 8 Hz, 2 H3, ArH), 6.69 (t, ³J_{HH} = 8

Hz, 2 H4, ArH), 7.07 (m, 2 H14 and 2 H21 ArH), 7.11 (t, ³J_{HH} = 7 Hz, 2 H16 and 2 H17, ArH),

7.19 (t, ³J_{HH} = 8 Hz, 2 H13, ArH), 7.23 (t, ³J_{HH} = 7 Hz, 1 H22, ArH), 7.33 (d, ³J_{HH} = 8 Hz, 2 H6,

ArH), 7.40 (d, ³J_{HH} = 8 Hz, 2 H15, ArH), 7.53 (d, ³J_{HH} = 9 Hz, 2 H20, ArH), 7.58 (d, ³J_{HH} = 8 Hz,

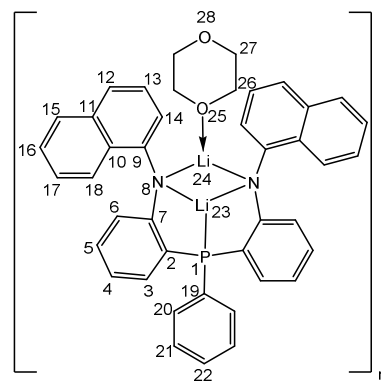
2 H12, ArH), 7.84 (d, ³J_{HH} = 9 Hz, 2 H18, ArH). ¹³C{¹H} NMR (toluene-*d*₈, 151 MHz): δ = 66.8

(C26,27, CH₂), 111.3, (C2, C_{ipso}), 115.7 (C3, ArC), 120.3 (C5, ArC), 122.8 (C18, ArC), 125.4

(C15, C16, C17, ArC and C11, C_{ipso}), 126.3 (C22, ArC), 128.2 (C13, C14, and C21, ArC), 128.5

(C4, ArC), 128.8, (C12 and C20, ArC), 132.4 (d, ¹J_{CP} = 14 Hz, C19, C_{ipso}), 133.0 (C6, ArC),

135.2 (C10, C_{ipso}), 137.8 (C9, C_{ipso}), 143.8 (C7, C_{ipso}).

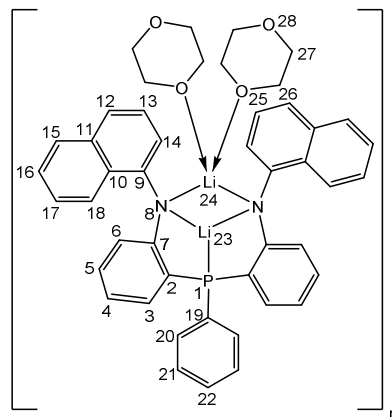


$[\text{}^{\text{naph}}\text{NPnLi}_2 \cdot 1.5\text{diox}]_n$ [7.6a] minor species (30%): $^{31}\text{P}\{^1\text{H}\}$

NMR (toluene- d_8 , 162 MHz): $\delta = -33.36$ (bs). $^7\text{Li}\{^1\text{H}\}$ NMR

(toluene- d_8 , 156 MHz): $\delta = 1.25$ (s, 1 Li23), 2.10 (d, $^1J_{\text{LiP}} =$

41 Hz, 1 Li22).



$[\text{}^{\text{naph}}\text{NPnLi}_2 \cdot \text{diox} \cdot 2\text{THF}]_n$ [7.6b] Two equiv of THF is added to a solution of $[\text{}^{\text{naph}}\text{NPnLi}_2 \cdot \text{diox}]_n$

[7.6] in C_6D_6 .

$^{31}\text{P}\{^1\text{H}\}$ NMR ($\text{C}_6\text{D}_6 + 2\text{THF}$, 162 MHz): $\delta = -33.36$ (bs, P1).

$^7\text{Li}\{^1\text{H}\}$ NMR $\text{C}_6\text{D}_6 + 2\text{THF}$, 156 MHz): $\delta = 1.25$ (s, 1 Li23),

2.10 (d, $^1J_{\text{LiP}} = 41$ Hz, 1 Li22). ^1H NMR ($\text{C}_6\text{D}_6 + 2\text{THF}$, 600

MHz): $\delta = 1.011$ (bs, 8 H31, CH_2 , THF),^(a) 3.076 (bs, 8 H30,

CH_2 , THF and 8 H26/27, CH_2 , diox),^(a) 6.35 (t, $^3J_{\text{HH}} = 7$ Hz, 2

H5, ArH), 6.95 (bs, 1 H22, ArH), 7.01 (d, $^3J_{\text{HH}} = 7$ Hz, 2 H6,

ArH), 7.08 (t, $^3J_{\text{HH}} = 5$ Hz, 2 H17, ArH), 7.20 (m, $^3J_{\text{HH}} = 7$ Hz, 2

H3, 2 H13, 2 H16, and 2 H21 ArH), 7.47 (d, $^3J_{\text{HH}} = 8$ Hz, 2 H14, ArH), 7.70 (bs, 2 H4, 2 H12 and

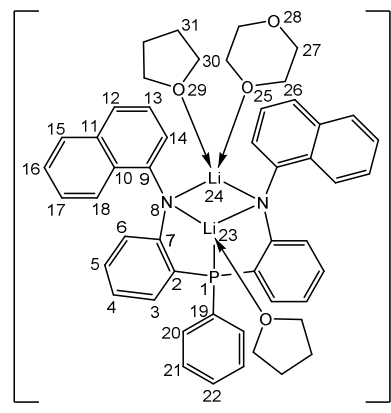
2 H20, ArH), 7.90 (bs, 2 H15, ArH), 8.47 (bs, 2 H18, ArH). $^{13}\text{C}\{^1\text{H}\}$ NMR ($\text{C}_6\text{D}_6 + 2\text{THF}$, 151

MHz): $\delta = 25.2$ (C31, CH_2), 66.9, 68.0 (C30/C26/C27, CH_2), 112.7, (C5, ArC), 122.9 (C10,

C_{ipso}), 124.6 (C19, C_{ipso}), 125.6 (C18 and C21, ArC), 128.0 (C6 and C22, ArC), 128.3 (C3, C13,

C14, and C16, ArC), 129.3 (C4 and C20, ArC), 132.6 (C15, ArC), 132.7 (C12, ArC), 132.9 (C7,

C_{ipso}), 135.2 (C11, C_{ipso}), 138.5 (d, $^1J_{\text{CP}} = 3$ Hz, C2, C_{ipso}), 153.5 (C9, C_{ipso}).



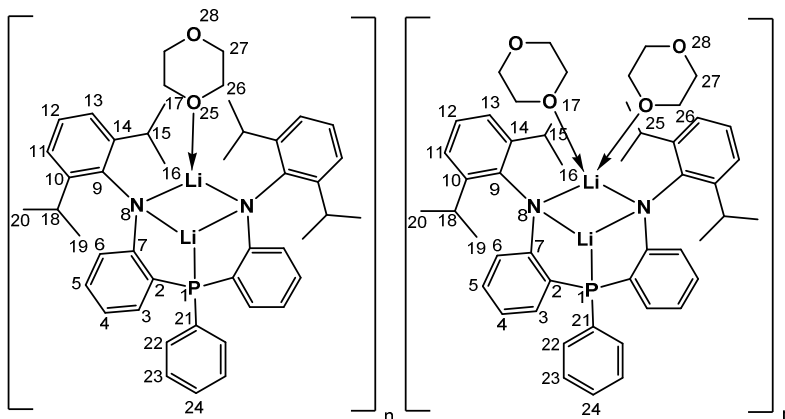
Anal. Calcd. for $C_{40}H_{43}ClLi_3N_2O_2P$: C, 73.43; H, 5.14; N, 4.08; Found: C, 73.35; H, 5.57; N, 3.77.^(b) EI-MS (m/z): 544 (50, $[M - 2Li - diox + 2H]^+$), 415 (20, $[M - 2Li - diox - C_{10}H_7]^+$), 402 (20, $[M - 2Li - diox - NC_{10}H_7 + 2H]^+$), 325 (20, $[M - 2Li - diox - NC_{10}H_7(C_6H_4) + 3H]^+$).

^(a) 1H NMR integration indicates one 1,4-dioxane + two THF molecules per $^{naph}NPnLi_2$ unit

^(b) Elemental analysis suggests one equivalent of LiCl is present in the isolated orange solid.

[$^{2,6-iPr_2}NPnLi_2 \cdot diox$]_n [7.7]: $^{2,6-diiprop}Ar^{Li}ArNLi$ (1.51 g, 5.70 mmol) was partially dissolved in 50 cm³ Et₂O in a 250 cm³ 3-necked round-bottomed flask fitted with a pressure-regulated dropping funnel. The solution was cooled to -44 °C (dry ice/ethanol) while 30 cm³ Et₂O and PPhCl₂ (0.40 cm³, 2.95 mmol) was added to the dropping funnel. The PPhCl₂ solution was added slowly over 54min (approx. dripping rate 6 cm³/10 min), resulting in a orange-brown solution with a suspended yellow solid. The reaction mixture was allowed to warm slowly to room temperature and stirred overnight for *ca* 41.5 hr. The Et₂O was removed *in vacuo*, giving an orange foam. This orange residue was triturated with 10 cm³ toluene inside the glovebox and filtered through celite with a sintered glass frit, washing with 25 cm³ toluene. To the dark orange filtrate was added 1,4-dioxane (0.98 cm³, 11.50 mmol) and the toluene was removed *in vacuo*, giving an orange residue. The residue was suspended in 10 cm³ hexanes, with heating to 60 °C, to give a orange solution with a fluffy yellow ppt. The mixture was placed in the freezer for 10 minutes before the yellow solid was collected on a sintered glass frit and washed with 4 x 5 cm³ *n*-hexanes and dried *in vacuo* (1.01g, 92% purity^(a) = 0.93 g, 1.30 mmol $^{2,6-iPr_2}NPnLi_2 \cdot diox$, 46% yield based on $^{2,6-diiprop}Ar^{Li}ArNLi$).

$^{31}\text{P}\{^1\text{H}\}$ NMR (C_6D_6 , 162 MHz): $\delta = -31.80$ (bs, P1),^(b) - 33.93 (bs, P1).^(c) $^7\text{Li}\{^1\text{H}\}$ NMR (C_6D_6 , 156 MHz): $\delta = -0.14$ (s, 1 Li23), 0.99 (bs, Li23/Li22), 1.87 (d, $^1J_{\text{LiP}} = 60$ Hz, 1 Li22). EI-MS (m/z): 612 (20, $[\text{M}]^+$), 569 (100, $[\text{M} - \text{CH}(\text{CH}_3)_2]^+$).



(a) $^{31}\text{P}\{^1\text{H}\}$ NMR spectrum displays unidentified doublets at δ 8.93 ($^1J_{\text{PP}} = 260.1$ Hz), 19.13 ($^1J_{\text{PP}} = 260.1$ Hz) and 26.43 ($^1J_{\text{PP}} = 228.6$ Hz).

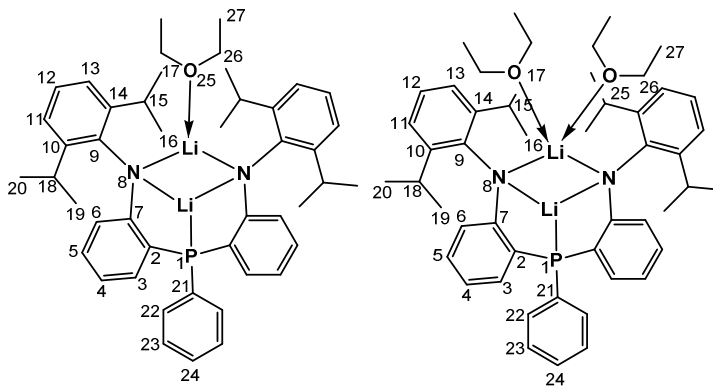
(b) $[\text{}^{2,6-i\text{Pr}_2}\text{NPNLi}_2 \cdot \text{diox}]_n$ **[7.7]** Major species (80%)

(c) $[\text{}^{2,6-i\text{Pr}_2}\text{NPNLi}_2 \cdot 1.5\text{diox}]_n$ **[7.7a]** Major species (20%)

$\text{}^{2,6-i\text{Pr}_2}\text{NPNLi}_2 \cdot 2\text{Et}_2\text{O}$ **[7.7b]**/ $\text{}^{2,6-i\text{Pr}_2}\text{NPNLi}_2 \cdot 3\text{Et}_2\text{O}$ **[7.7c]**: $\text{}^{2,6-i\text{Pr}_2}\text{Ar}^{\text{Li}}\text{ArNLi}$ (0.08 g, 0.03 mmol)

was dissolved in 2 cm³ Et₂O and cooled to - 30 °C before PPhCl₂ (2.1 μL, 0.02 mmol) was added, immediate forming an orange solution that was stir at r. t. for *ca* 16 hrs. The Et₂O was removed *in vacuo*, giving an orange residue, which was dissolved in C₆D₆.

$^{31}\text{P}\{^1\text{H}\}$ NMR (C_6D_6 , 162 MHz): $\delta = -27.95$ (bs). $^7\text{Li}\{^1\text{H}\}$ NMR (C_6D_6 , 156 MHz): $\delta = 0.69$ (s), 2.01 (d, $^1J_{\text{LiP}} = 60$ Hz).



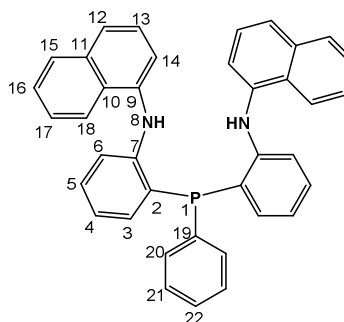
Fail one-pot synthesis of $[^{2,6-i\text{Pr}_2}\text{NPNLi}_2\cdot\text{diox}]_n$ [7.7] with P-N and P-C side-products: ^{2,6-}

$i\text{Pr}_2\text{Ar}^{\text{Br}}\text{ArNH}$ [7.2] (0.1014 g, 0.31 mmol) was dissolved in 5 cm³ Et₂O. The solution was cooled to -74.2 °C and 1.65 M *t*-BuLi in hexanes (0.55 cm³, 0.91 mmol) was added, forming a deep yellow solution with yellow ppt. The reaction mixture was warm to r. t., forming a clear yellow solution that was stirred for *ca* 16 hrs. The solution was cooled to -35 °C and PPhCl₂ (20 μL, 0.15 mmol) was added, immediate forming an orange solution that was stir at r. t. for 3 days. The Et₂O was removed *in vacuo*, giving an orange residue, which was dissolved in C₆D₆.^(a)

^(a) ³¹P{¹H} NMR (C₆D₆, 162 MHz): δ = 52.01 (bs), -8.11 (bs). ⁷Li{¹H} NMR (C₆D₆, 156 MHz): δ = 0.69 (bs).

^{naph}NPNH₂ [7.8] In glove-box, ^{naph}NPNLi₂·diox (2.32 g, 3.60 mmol) and NMe₃·HCl (1.09 g, 11.41 mmol) were mixed together as solids in a conical flask and 30 cm³ THF was added. The reaction mixture was allowed to stir for 17 hrs 6 min before the THF solvent was removed *in vacuo*. The residue was extracted with 20 cm³ toluene and filtered through celite with a sintered glass frit, washing with 3 x 10 cm³ toluene. The toluene solvent was removed *in vacuo* from the combined filtrate and toluene washings with heating to 60 °C, giving a clear oil. Trituration with 10 cm³ *n*-hexanes resulted in the ppt. of a light yellow solid, which was collected on a sintered glass frit and dried *in vacuo* (0.97 g, 93% purity^(a) = 0.90 g, 1.65 mmol ^{naph}NPNH₂ [7.8], 46% yield based on ^{naph}NPNLi₂·diox).

³¹P{¹H} NMR (C₆D₆, 122 MHz): δ = -33.34 (s, P1). ¹H NMR (C₆D₆, 400 MHz): δ = 6.73 (m, ³J_{HH} = 4 Hz, 2 H4), 6.82 (d, ⁴J_{PH} = 6 Hz, 2 H8, NH), 6.99 (m, ³J_{HH} = 7 Hz, 2 H3 and 2 H17, ArH), 7.10 (m, 2 H6, 2 H14, 2 H16, and 2 H21, ArH), 7.16 (m, ³J_{HH} = 6 Hz, 2 H13, ArH), 7.38 (m, ³J_{HH} = 8 Hz, 2 H5, 2 H15 and 1 H22, ArH), 7.61 (m, ³J_{HH} = 8 Hz, 2 H12, 2 H18 and 2 H20). ¹³C{¹H}



NMR (C_6D_6 , 101 MHz): δ = 116.8 (C3, ArC), 118.2 (C6, ArC), 121.0 (C4, ArC), 122.4 (C20, ArC), 124.0 (C15, ArC), 126.1 (d, $^1J_{\text{PC}}$ = 19 Hz, C19, C_{ipso}), 126.2 (C11, C_{ipso}), 128.0^(b) (C13, C14 and C16, ArC and C10, C_{ipso}), 128.6 (C18, ArC), 129.3 (d, $^3J_{\text{PC}}$ = 7 Hz, C21, ArC), 130.9 (C17, ArC), 134.5 (C12, ArC), 134.7 (m, $^4J_{\text{PC}}$ = 4 Hz, C5 and C22, ArC), 135.2 (C9, C_{ipso}), 138.6 (C7, C_{ipso}) 149.1 (C2, C_{ipso}). EI-MS (m/z): 544 (100, $[\text{M}]^+$), 402 (30, $[\text{M} - \text{NHC}_{10}\text{H}_7]^+$).^(c)

(a) $^{31}\text{P}\{^1\text{H}\}$ NMR spectrum displays 7% of an unidentified species at δ 44.12.

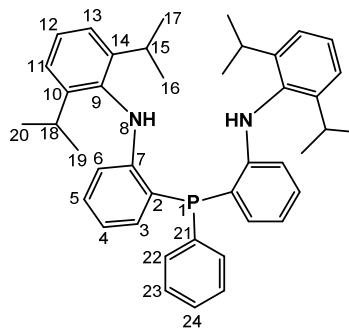
(b) signal masked by residual C_6H_6 in C_6D_6 .

(c) higher mass peaks observed at 650, 640 and 622 m/z

2,6-*i*Pr²NPNH₂ [7.9] 2,6-*i*Pr²NPNLi₂·diox (0.22 g, 0.30 mmol) and NMe₃·HCl (0.12 g, 1.29 mmol) were dissolved in 10 cm³ THF and the yellow solution was stirred overnight for 21 hrs 50 min. The THF solvent was removed *in vacuo* and the residue was dissolved in 10 cm³ toluene and filtered through celite with a sintered glass frit, washing with 2 x 5 cm³ toluene. The toluene solvent removed *in vacuo* and the oily residue was triturated with 2 cm³ hexanes. The hexanes solvent was removed *in vacuo* to give a white foam (0.13 g).^(a)

$^{31}\text{P}\{^1\text{H}\}$ NMR (C_6D_6 , 162 MHz): δ = -38.68 (s, P_1). EI-MS (m/z): 612 (30, $[\text{M}]^+$), 569 (100, $[\text{M} - \text{CH}(\text{CH}_3)_2]^+$).

(a) Impurities: $^{31}\text{P}\{^1\text{H}\}$ NMR spectrum displays three multiplets at δ -8.76, -24.14 and -40.11 and two singlets at δ 45.10 and 41.07.



References

1. Smil, V., *Enriching the Earth: Fritz Haber, Carl Bosch, and the Transformation of World Food Production*. The MIT Press: Cambridge, Massachusetts, 2001; p 338.
2. Fryzuk, M. D., *Angew. Chem., Int. Ed.* **2006**, *45*, 2658-2659.
3. Newton, W. E., Nitrogen Fixation. In *Kirk-Othmer Encyclopedia of Chemical Technology*, John Wiley & Sons, Inc.: 2000.
4. Appl, M., Ammonia, 2. Production Processes. In *Ullmann's Encyclopedia of Industrial Chemistry*, Wiley-VCH Verlag GmbH & Co. KGaA: 2000.
5. Leigh, G. J., *The World's Greatest Fix: A History of Nitrogen and Agriculture*. Oxford University Press: New York, 2004; p 240.
6. Haber, F.; van Oordt, G., *Z. Anorg. Chem.* **1905**, *44* (1), 341-378.
7. Haber, F.; Van Oordt, G., *Z. Anorg. Chem.* **1905**, *43* (1), 111-115.
8. Haber, F. Ammonia from the elements. DE 238450, 1909.
9. Schlögl, R., *Angew Chem Int Ed Engl* **2003**, *42* (18), 2004-8.
10. Howard, J. B.; Rees, D. C., *Chem. Rev.* **1996**, *96* (7), 2965-2982.
11. Forni, L., *Chimica e l'Industria (Milan, Italy)* **2009**, *91* (8), 108-112.
12. Travis, T., *Chem. Ind.* **1993**, (15), 581-585.
13. Eggeman, T., Ammonia. In *Kirk-Othmer Encyclopedia of Chemical Technology*, John Wiley & Sons, Inc.: 2000.
14. Worrell, E.; Phylipsen, D.; Einstein, D.; Martin, N. *Energy Use and Energy Intensity of the U.S. Chemical Industry*; LBNL-44314; University of California: Berkeley, California, 2000; p 40.
15. Apodaca, L. E., Mineral Commodity Summaries 2011: U. S. Geological Survey. Department of the Interior, U. S., Ed. Washington, DC, 2011; pp 112-113.
16. Ostwald, W. Nitric acid. US 858904, 1907.
17. Clarke, S. I.; Mazzafro, W. J., Nitric Acid. In *Kirk-Othmer Encyclopedia of Chemical Technology*, John Wiley & Sons, Inc.: 2000.
18. Oxley, J. C., *Explosive Effects and Applications* **1998**, 137-172.
19. Akhavan, J., Explosives and Propellants. In *Kirk-Othmer Encyclopedia of Chemical Technology*, John Wiley & Sons, Inc.: 2000.
20. Pollak, P., Fine Chemicals. In *Kirk-Othmer Encyclopedia of Chemical Technology*, John Wiley & Sons, Inc.: 2000.
21. Hatten, J. L.; Nauck, K. R., Jr. Continuous manufacturing of adiponitrile from adipic acid and ammonia. US 793044, 1969.

22. Chan, M. K.; Kim, J.; Rees, D. C., *Science (Washington, DC, United States)* **1993**, 260 (5109), 792-4.
23. Carnahan, J. E.; Mortenson, L. E.; Mower, H. F.; Castle, J. E., *Biochim. Biophys. Acta* **1960**, 44, 520-35.
24. Georgiadis, M. M.; Komiya, H.; Chakrabarti, P.; Woo, D.; Kornuc, J. J.; Rees, D. C., *Science (Washington, DC, United States)* **1992**, 257 (5077), 1653-9.
25. Einsle, O.; Tezcan, F. A.; Andrade, S. L. A.; Schmid, B.; Yoshida, M.; Howard, J. B.; Rees, D. C., *Science (Washington, DC, United States)* **2002**, 297 (5587), 1696-1700.
26. Barney, B. M.; Lee, H.-I.; Dos Santos, P. C.; Hoffman, B. M.; Dean, D. R.; Seefeldt, L. C., *Dalton Trans.* **2006**, (19), 2277-2284.
27. Richards, R. L., Chemistry at the unit of nitrogen fixation. In *Modern Coordination Chemistry*, Leigh, G. J.; Winterton, N., Eds. The Royal Society of Chemistry: Cambridge, 2002; pp 171-186.
28. Kurnikov, I. V.; Charnley, A. K.; Beratan, D. N., *J. Phys. Chem. B* **2001**, 105 (23), 5359-5367.
29. Postgate, J., Biological nitrogen fixation. In *Modern Coordination Chemistry*, Leigh, G. J.; Winterton, N., Eds. The Royal Society of Chemistry: Cambridge, 2002; pp 233-251.
30. Pickett, C. J., *J. Biol. Inorg. Chem.* **1996**, 1 (6), 601-606.
31. Evans, D. J.; Henderson, R. A.; Smith, B. E., *Bioinorganic Catalysis (2nd Edition, Revised and Expanded)* **1999**, 153-207.
32. Spatzal, T.; Aksoyoglu, M.; Zhang, L.; Andrade, S. L. A.; Schleicher, E.; Weber, S.; Rees, D. C.; Einsle, O., *Science (Washington, DC, United States)* **2011**, 334 (6058), 940.
33. Lancaster, K. M.; Roemelt, M.; Ettenhuber, P.; Hu, Y.; Ribbe, M. W.; Neese, F.; Bergmann, U.; DeBeer, S., *Science (Washington, DC, United States)* **2011**, 334 (6058), 974-977.
34. Hu, Y.; Lee, C. C.; Ribbe, M. W., *Dalton Trans.* **2012**, 41 (4), 1118-1127.
35. Lovell, T.; Torres, R. A.; Han, W.-G.; Liu, T.; Case, D. A.; Noodleman, L., *Inorg. Chem.* **2002**, 41 (22), 5744-5753.
36. Zhao, Y.; Bian, S.-M.; Zhou, H.-N.; Huang, J.-F., *Journal of Integrative Plant Biology* **2006**, 48 (7), 745-755.
37. Danyal, K.; Mayweather, D.; Dean, D. R.; Seefeldt, L. C.; Hoffman, B. M., *J. Am. Chem. Soc.* **2010**, 132 (20), 6894-6895.
38. Wang, Y.-P.; Houlton, B. Z., *Geophys. Res. Lett.* **2009**, 36 (24), L24403.

39. Hoffman, B. M.; Lukoyanov, D.; Dean, D. R.; Seefeldt, L. C., *Acc. Chem. Res.* **2013**, *46* (2), 587-595.
40. Newton, W. E.; Dilworth, M. J., *Methods in Molecular Biology (New York, NY, United States)* **2011**, 766 (Nitrogen Fixation), 105-127.
41. Lee, C.-C.; Fay, A. W.; Wiig, J. A.; Ribbe, M. W.; Hu, Y., *Methods in Molecular Biology (New York, NY, United States)* **2011**, 766 (Nitrogen Fixation), 31-47.
42. Hu, Y.; Fay, A. W.; Lee, C. C.; Yoshizawa, J.; Ribbe, M. W., *Biochemistry* **2008**, *47* (13), 3973-81.
43. Lee, S. C., Iron-imide clusters and nitrogenase: Abiological chemistry of biological relevance. In *Modern Coordination Chemistry*, Leigh, G. J.; Winterton, N., Eds. The Royal Society of Chemistry: Cambridge, 2002; pp 278-287.
44. Zhang, Y.; Zuo, J.-L.; Zhou, H.-C.; Holm, R. H., *J. Am. Chem. Soc.* **2002**, *124* (48), 14292-14293.
45. Weterings, J., *Chemisch Magazine (Den Haag)* **1983**, (July-Aug.), 330-3.
46. Leigh, G. J., *Can. J. Chem.* **2005**, *83* (4), 277-278.
47. Allen, A. D.; Senoff, C. W., *Chem. Commun.* **1965**, (24), 621-2.
48. Bottomley, F.; Nyburg, S. C., *Acta Crystallogr., Sect. B: Struct. Sci* **1968**, *24* (10), 1289-93.
49. Floriani, C., Metal-Dinitrogen Chemistry After Chatt. In *Modern Coordination Chemistry*, 1st ed.; Leigh, G. J.; Winterton, N., Eds. The Royal Society of Chemistry: Cambridge, 2002; pp 198-207.
50. Arashiba, K.; Miyake, Y.; Nishibayashi, Y., *Nature Chemistry* **2011**, *3* (2), 120-125.
51. Yandulov, D. V.; Schrock, R. R., *Science* **2003**, *301* (5629), 76.
52. Laplaza, C. E.; Cummins, C. C., *Science (Washington, D. C.)* **1995**, *268* (5212), 861-3.
53. Hidai, M.; Mizobe, Y., *Can. J. Chem.* **2005**, *83* (4), 358-374.
54. Hidai, M.; Mizobe, Y., *Chem. Rev.* **1995**, *95* (4), 1115-33.
55. Pickett, C. J.; Talarmin, J., *Nature (London)* **1985**, *317* (6038), 652-3.
56. Ishino, H.; Ishii, Y.; Hidai, M., *Chem. Lett.* **1998**, (7), 677-678.
57. Bell, B.; Chatt, J.; Leigh, G. J., *J. Chem. Soc., Dalton Trans.* **1972**, (22), 2492-6.
58. Komori, K.; Kodama, T.; Jin, D. M.; Takahashi, T.; Uchida, Y.; Hidai, M., *Chem. Lett.* **1983**, (4), 465-6.
59. Holland, P. L., *Can. J. Chem.* **2005**, *83* (4), 296-301.
60. MacBeth, C. E.; Harkins, S. B.; Peters, J. C., *Can. J. Chem.* **2005**, *83* (4), 332-340.

61. Li, Y.; Li, Y.; Wang, B.; Luo, Y.; Yang, D.; Tong, P.; Zhao, J.; Luo, L.; Zhou, Y.; Chen, S.; Cheng, F.; Qu, J., *Nature Chemistry* **2013**, 5 (4), 320-326.
62. Luo, Y.; Li, Y.; Yu, H.; Zhao, J.; Chen, Y.; Hou, Z.; Qu, J., *Organometallics* **2012**, 31 (1), 335-344.
63. Rodriguez, M. M.; Bill, E.; Brennessel, W. W.; Holland, P. L., *Science (Washington, DC, United States)* **2011**, 334 (6057), 780-783.
64. Vidyaratne, I.; Crewdson, P.; Lefebvre, E.; Gambarotta, S., *Inorg. Chem.* **2007**, 46 (21), 8836-8842.
65. Clentsmith, G. K. B.; Bates, V. M. E.; Hitchcock, P. B.; Cloke, F. G. N., *J. Am. Chem. Soc.* **1999**, 121 (44), 10444-10445.
66. Vidyaratne, I.; Gambarotta, S.; Korobkov, I.; Budzelaar, P. H. M., *Inorg. Chem.* **2005**, 44 (5), 1187-1189.
67. Caselli, A.; Solari, E.; Scopelliti, R.; Floriani, C.; Re, N.; Rizzoli, C.; Chiesi-Villa, A., *J. Am. Chem. Soc.* **2000**, 122 (15), 3652-3670.
68. Akagi, F.; Matsuo, T.; Kawaguchi, H., *Angew. Chem., Int. Ed.* **2007**, 46 (46), 8778-8781.
69. Kilgore, U. J.; Yang, X.; Tomaszewski, J.; Huffman, J. C.; Mindiola, D. J., *Inorg. Chem.* **2006**, 45 (26), 10712-10721.
70. Kawaguchi, H.; Matsuo, T., *Angew. Chem., Int. Ed.* **2002**, 41 (15), 2792-2794.
71. Rocklage, S. M.; Schrock, R. R., *J. Am. Chem. Soc.* **1982**, 104 (11), 3077-81.
72. Churchill, M. R.; Wasserman, H. J., *Inorg. Chem.* **1981**, 20 (9), 2899-904.
73. Turner, H. W.; Fellmann, J. D.; Rocklage, S. M.; Schrock, R. R.; Churchill, M. R.; Wasserman, H. J., *J. Am. Chem. Soc.* **1980**, 102 (26), 7809-11.
74. Rocklage, S. M.; Turner, H. W.; Fellmann, J. D.; Schrock, R. R., *Organometallics* **1982**, 1 (5), 703-7.
75. Fryzuk, M. D.; Haddad, T. S.; Mylvaganam, M.; McConville, D. H.; Rettig, S. J., *J. Am. Chem. Soc.* **1993**, 115 (7), 2782-92.
76. Lee, T.-Y.; Wooten, A. J.; Luci, J. J.; Swenson, D. C.; Messerle, L., *Chem. Commun.* **2005**, (43), 5444-5446.
77. Bregel, D. C.; Oldham, S. M.; Lachicotte, R. J.; Eisenberg, R., *Inorg. Chem.* **2002**, 41 (17), 4371-4377.
78. Hirotsu, M.; Fontaine, P. P.; Epshteyn, A.; Zavalij, P. Y.; Sita, L. R., *J. Am. Chem. Soc.* **2007**, 129 (30), 9284-9285.
79. Fryzuk, M. D.; Johnson, S. A.; Patrick, B. O.; Albinati, A.; Mason, S. A.; Koetzle, T. F., *J. Am. Chem. Soc.* **2001**, 123 (17), 3960-3973.

80. Fryzuk, M. D.; Johnson, S. A.; Rettig, S. J., *J. Am. Chem. Soc.* **1998**, *120* (42), 11024-11025.
81. Studt, F.; MacKay, B. A.; Fryzuk, M. D.; Tuczek, F., *J. Am. Chem. Soc.* **2004**, *126* (1), 280-290.
82. Sanders, J. R., Vanadium, molybdenum and iron complexes based on a trithiolate ligand. In *Modern Coordination Chemistry*, Leigh, G. J.; Winterton, N., Eds. The Royal Society of Chemistry: Cambridge, 2002; pp 252-262.
83. Dilworth, J. R.; Arnold, P.; Morales, D.; Wong, Y.-L.; Zheng, Y., The chemistry and applications of complexes with sulfur ligands. In *Modern Coordination Chemistry*, Leigh, G. J.; Winterton, N., Eds. The Royal Society of Chemistry: Cambridge, 2002; pp 217-230.
84. Newton, W. E., *Philos. Trans. R. Soc. London, Ser. B* **1987**, *317* (1184), 259-77.
85. Vol'pin, M. E.; Shur, V. B., *Dokl. Akad. Nauk* **1964**, *156* (5), 1102-4.
86. Vol'pin, M. E.; Shur, V. B.; Ilatovskaya, M. A., *Izv. Akad. Nauk SSSR, Ser. Khim.* **1964**, (9), 1728-9.
87. Volpin, M. E.; Ilatovskaya, M. A.; Kosyakova, L. V.; Shur, V. B., *Chem. Commun.* **1968**, (18), 1074-5.
88. Anderson, J. S.; Rittle, J.; Peters, J. C., *Nature (London, United Kingdom)* **2013**, *501* (7465), 84-87.
89. Anderson, J. S.; Moret, M.-E.; Peters, J. C., *J. Am. Chem. Soc.* **2013**, *135* (2), 534-537.
90. Fryzuk, M. D.; Love, J. B.; Rettig, S. J.; Young, V. G., *Science (Washington, D. C.)* **1997**, *275* (5305), 1445-1447.
91. Nishibayashi, Y.; Iwai, S.; Hidai, M., *Science (Washington, D. C.)* **1998**, *279* (5350), 540-542.
92. MacLachlan, E. A.; Hess, F. M.; Patrick, B. O.; Fryzuk, M. D., *J. Am. Chem. Soc.* **2007**, *129* (35), 10895-10905.
93. Pool, J. A.; Lobkovsky, E.; Chirik, P. J., *Nature* **2004**, *427* (6974), 527-530.
94. Fryzuk, M. D., *Nature (London, United Kingdom)* **2004**, *427* (6974), 498-499.
95. Bobadova-Parvanova, P.; Wang, Q.; Quinonero-Santiago, D.; Morokuma, K.; Musaev, D. G., *J. Am. Chem. Soc.* **2006**, *128* (35), 11391-11403.
96. Bernskoetter, W. H.; Lobkovsky, E.; Chirik, P. J., *J. Am. Chem. Soc.* **2005**, *127* (40), 14051-14061.
97. MacLachlan, E. A. Group 4 Complexes of an Arene-Bridged Diamidophosphine Ligand for Nitrogen Activation. PhD Thesis, University of British Columbia, Vancouver, 2006.

98. Pun, D.; Bradley, C. A.; Lobkovsky, E.; Keresztes, I.; Chirik, P. J., *J. Am. Chem. Soc.* **2008**, *130* (43), 14046-14047.
99. Bernskoetter, W. H.; Olmos, A. V.; Lobkovsky, E.; Chirik, P. J., *Organometallics* **2006**, *25* (4), 1021-1027.
100. Shima, T.; Hu, S.; Luo, G.; Kang, X.; Luo, Y.; Hou, Z., *Science (Washington, DC, United States)* **2013**, *340* (6140), 1549-1552.
101. Fryzuk Michael, D., *Science (New York, N.Y.)* **2013**, *340* (6140), 1530-1.
102. Sacco, A.; Rossi, M., *Chem. Commun.* **1967**, (7), 316.
103. Morello, L.; Love, J. B.; Patrick, B. O.; Fryzuk, M. D., *J. Am. Chem. Soc.* **2004**, *126* (31), 9480-9481.
104. Figueroa, J. S.; Piro, N. A.; Clough, C. R.; Cummins, C. C., *J. Am. Chem. Soc.* **2006**, *128* (3), 940-950.
105. Bernskoetter, W. H.; Olmos, A. V.; Pool, J. A.; Lobkovsky, E.; Chirik, P. J., *J. Am. Chem. Soc.* **2006**, *128* (33), 10696-10697.
106. Bernskoetter, W. H.; Lohkovsky, E.; Chirik, P. J., *Angew. Chem., Int. Ed.* **2007**, *46* (16), 2858-2861.
107. Fryzuk, M. D.; MacKay, B. A.; Patrick, B. O., *J. Am. Chem. Soc.* **2003**, *125* (11), 3234-3235.
108. MacKay, B. A.; Munha, R. F.; Fryzuk, M. D., *J. Am. Chem. Soc.* **2006**, *128* (29), 9472-9483.
109. Studt, F.; MacKay, B. A.; Fryzuk, M. D.; Tuzcek, F., *Dalton Trans.* **2006**, (9), 1137-1140.
110. Fryzuk, M. D.; MacKay, B. A.; Johnson, S. A.; Patrick, B. O., *Angew. Chem., Int. Ed.* **2002**, *41* (19), 3709-3712.
111. MacKay, B. A.; Johnson, S. A.; Patrick, B. O.; Fryzuk, M. D., *Can. J. Chem.* **2005**, *83* (4), 315-323.
112. MacKay, B. A.; Patrick, B. O.; Fryzuk, M. D., *Organometallics* **2005**, *24* (16), 3836-3841.
113. Laplaza, C. E.; Johnson, M. J. A.; Peters, J.; Odom, A. L.; Kim, E.; Cummins, C. C.; George, G. N.; Pickering, I. J., *J. Am. Chem. Soc.* **1996**, *118* (36), 8623-8638.
114. Shaver, M. P.; Thomson, R. K.; Patrick, B. O.; Fryzuk, M. D., *Can. J. Chem.* **2003**, *81* (12), 1431-1437.
115. Spencer, L. P.; MacKay, B. A.; Patrick, B. O.; Fryzuk, M. D., *Proc. Natl. Acad. Sci. U. S. A.* **2006**, *103* (46), 17094-17098.

116. Fryzuk, M. D.; Kozak, C. M.; Patrick, B. O., *Inorg. Chim. Acta* **2003**, 345, 53-62.
117. Fryzuk, M. D.; Kozak, C. M.; Bowdridge, M. R.; Patrick, B. O.; Rettig, S. J., *J. Am. Chem. Soc.* **2002**, 124 (28), 8389-8397.
118. Shiina, K., *J. Amer. Chem. Soc.* **1972**, 94 (26), 9266-7.
119. Komori, K.; Oshita, H.; Mizobe, Y.; Hidai, M., *J. Am. Chem. Soc.* **1989**, 111 (5), 1939-40.
120. Tanaka, H.; Sasada, A.; Kouno, T.; Yuki, M.; Miyake, Y.; Nakanishi, H.; Nishibayashi, Y.; Yoshizawa, K., *J. Am. Chem. Soc.* **2011**, 133 (10), 3498-3506.
121. Yuki, M.; Tanaka, H.; Sasaki, K.; Miyake, Y.; Yoshizawa, K.; Nishibayashi, Y., *Nature Communications* **2012**, 3 (Dec.), 2264/1-2264/6.
122. Mori, M., *J. Organomet. Chem.* **2004**, 689 (24), 4210-4227.
123. Winterton, N., Some notes on the early development of models of bonding in olefin-metal complexes. In *Modern Coordination Chemistry*, Leigh, G. J.; Winterton, N., Eds. The Royal Society of Chemistry: Cambridge, 2002; pp 103-110.
124. Frenking, G., The Dewar-Chatt-Duncanson bonding model of transition metal-olefin complexes examined by modern quantum chemical methods. In *Modern Coordination Chemistry*, Leigh, G. J.; Winterton, N., Eds. The Royal Society of Chemistry: Cambridge, 2002; pp 111-122.
125. MacLachlan, E. A.; Fryzuk, M. D., *Organometallics* **2006**, 25 (7), 1530-1543.
126. Cohen, J. D.; Mylvaganam, M.; Fryzuk, M. D.; Loehr, T. M., *J. Am. Chem. Soc.* **1994**, 116 (21), 9529-34.
127. de Wolf, J. M.; Blaauw, R.; Meetsma, A.; Teuben, J. H.; Gyepes, R.; Varga, V.; Mach, K.; Veldman, N.; Spek, A. L., *Organometallics* **1996**, 15 (23), 4977-4983.
128. Hanna, T. E.; Lobkovsky, E.; Chirik, P. J., *J. Am. Chem. Soc.* **2004**, 126 (45), 14688-14689.
129. Hanna, T. E.; Bernskoetter, W. H.; Bouwkamp, M. W.; Lobkovsky, E.; Chirik, P. J., *Organometallics* **2007**, 26 (9), 2431-2438.
130. Manriquez, J. M.; Bercaw, J. E., *J. Am. Chem. Soc.* **1974**, 96 (19), 6229-30.
131. Manriquez, J. M.; Sanner, R. D.; Marsh, R. E.; Bercaw, J. E., *J. Am. Chem. Soc.* **1976**, 98 (10), 3042-4.
132. Sanner, R. D.; Manriquez, J. M.; Marsh, R. E.; Bercaw, J. E., *J. Am. Chem. Soc.* **1976**, 98 (26), 8351-7.
133. Ishino, H.; Nagano, T.; Kuwata, S.; Yokobayashi, Y.; Ishii, Y.; Hidai, M.; Mizobe, Y., *Organometallics* **2000**, 20 (1), 188-198.

134. Mizobe, Y.; Yokobayashi, Y.; Oshita, H.; Takahashi, T.; Hidai, M., *Organometallics* **1994**, *13* (10), 3764-6.
135. Fryzuk, M. D.; Haddad, T. S.; Rettig, S. J., *J. Am. Chem. Soc.* **1990**, *112* (22), 8185-6.
136. Cohen, J. D.; Fryzuk, M. D.; Loehr, T. M.; Mylvaganam, M.; Rettig, S. J., *Inorg. Chem.* **1998**, *37* (1), 112-119.
137. Morello, L. Amidophosphine complexes of zirconium and titanium for dinitrogen activation. PhD Thesis, University of British Columbia, Vancouver, 2005.
138. Morello, L.; Yu, P.; Carmichael, C. D.; Patrick, B. O.; Fryzuk, M. D., *J. Am. Chem. Soc.* **2005**, *127* (37), 12796-12797.
139. Zhu, T.; Wambach, T. C.; Fryzuk, M. D., *Inorg. Chem.* **2011**, *50* (21), 11212-11221.
140. Zhu, T. Zirconium Complexes of Cyclopentene-Bridged Diamidophosphine Ligands for Dinitrogen Activation. MSc. Thesis, University of British Columbia, Vancouver, 2010.
141. Studt, F.; Morello, L.; Lehnert, N.; Fryzuk, M. D.; Tuczek, F., *Chem. Eur. J.* **2003**, *9* (2), 520-530.
142. Hanna, T. E.; Keresztes, I.; Lobkovsky, E.; Chirik, P. J., *Inorg. Chem.* **2007**, *46* (5), 1675-1683.
143. Chirik, P. J.; Henling, L. M.; Bercaw, J. E., *Organometallics* **2001**, *20* (3), 534-544.
144. Hirotsu, M.; Fontaine, P. P.; Zavalij, P. Y.; Sita, L. R., *J. Am. Chem. Soc.* **2007**, *129* (42), 12690-12692.
145. Pun, D.; Lobkovsky, E.; Chirik, P. J., *J. Am. Chem. Soc.* **2008**, *130* (18), 6047-6054.
146. Hillhouse, G. L.; Bercaw, J. E., *J. Am. Chem. Soc.* **1984**, *106* (19), 5472-8.
147. Jeffery, J.; Lappert, M. F.; Riley, P. I., *J. Organomet. Chem.* **1979**, *181* (1), 25-36.
148. Zeinstra, J. D.; Teuben, J. H.; Jellinek, F., *J. Organomet. Chem.* **1979**, *170* (1), 39-50.
149. Chomitz, W. A.; Sutton, A. D.; Krinsky, J. L.; Arnold, J., *Organometallics* **2009**, *28* (12), 3338-3349.
150. Morello, L.; Joao Ferreira, M.; Patrick, B. O.; Fryzuk, M. D., *Inorg. Chem.* **2008**, *47* (4), 1319-1323.
151. Pyykko, P.; Desclaux, J. P., *Chem. Phys. Lett.* **1977**, *50* (3), 503-7.
152. Lappert, M. F.; Pickett, C. J.; Riley, P. I.; Yarrow, P. I. W., *J. Chem. Soc., Dalton Trans.* **1981**, (3), 805-13.
153. Roddick, D. M.; Fryzuk, M. D.; Seidler, P. F.; Hillhouse, G. L.; Bercaw, J. E., *Organometallics* **1985**, *4* (1), 97-104.
154. Knobloch, D. J.; Lobkovsky, E.; Chirik, P. J., *Nature Chemistry* **2010**, *2* (1), 30-35.

155. Knobloch, D. J.; Lobkovsky, E.; Chirik, P. J., *J. Am. Chem. Soc.* **2010**, *132* (30), 10553-10564.
156. Zhang, X.; Butschke, B.; Schwarz, H., *Chem. Eur. J.* **2010**, *16* (42), 12564-12569.
157. Knobloch, D. J.; Toomey, H. E.; Chirik, P. J., *J. Am. Chem. Soc.* **2008**, *130* (13), 4248-4249.
158. Knobloch, D. J.; Benito-Garagorri, D.; Bernskoetter, W. H.; Keresztes, I.; Lobkovsky, E.; Toomey, H.; Chirik, P. J., *J. Am. Chem. Soc.* **2009**, *131* (41), 14903-14912.
159. Fryzuk, M. D.; Corkin, J. R.; Patrick, B. O., *Can. J. Chem.* **2003**, *81* (11), 1376-1387.
160. Vol'pin, M. E.; Shur, V. B., *Nature (London, United Kingdom)* **1966**, *209* (5029), 1236.
161. Allen, A. D.; Stevens, J. R., *Chem. Comm.* **1967**, (21), 1147.
162. Shilov, A. E.; Shilova, A. K.; Kvashina, E. F., *Kinet. Katal.* **1969**, *10* (6), 1402.
163. Van Tamelen, E. E.; Fechter, R. B.; Schneller, S. W.; Boche, G.; Greeley, R. H.; Akermark, B., *J. Am. Chem. Soc.* **1969**, *91* (6), 1551-2.
164. Bercaw, J. E.; Marvich, R. H.; Bell, L. G.; Brintzinger, H. H., *J. Am. Chem. Soc.* **1972**, *94* (4), 1219-38.
165. Sanner, R. D.; Duggan, D. M.; McKenzie, T. C.; Marsh, R. E.; Bercaw, J. E., *J. Am. Chem. Soc.* **1976**, *98* (26), 8358-65.
166. Pez, G. P., *J. Am. Chem. Soc.* **1976**, *98* (25), 8072-8.
167. Pez, G. P.; Kwan, S. C., *J. Am. Chem. Soc.* **1976**, *98* (25), 8079-83.
168. Pez, G. P.; Apgar, P.; Crissey, R. K., *J. Am. Chem. Soc.* **1982**, *104* (2), 482-90.
169. Hanna, T. E.; Keresztes, I.; Lobkovsky, E.; Bernskoetter, W. H.; Chirik, P. J., *Organometallics* **2004**, *23* (14), 3448-3458.
170. Berry, D. H.; Procopio, L. J.; Carroll, P. J., *Organometallics* **1988**, *7* (2), 570-2.
171. Scherer, A.; Haase, D.; Saak, W.; Beckhaus, R.; Meetsma, A.; Bouwkamp, M. W., *Organometallics* **2009**, *28* (24), 6969-6974.
172. Duchateau, R.; Gambarotta, S.; Beydoun, N.; Bensimon, C., *J. Am. Chem. Soc.* **1991**, *113* (23), 8986-8.
173. Mullins, S. M.; Duncan, A. P.; Bergman, R. G.; Arnold, J., *Inorg. Chem.* **2001**, *40* (27), 6952-6963.
174. Hagadorn, J. R.; Arnold, J., *J. Am. Chem. Soc.* **1996**, *118* (4), 893-4.
175. Beydoun, N.; Duchateau, R.; Gambarotta, S., *J. Chem. Soc., Chem. Commun.* **1992**, (3), 244-6.
176. Baumann, R.; Stumpf, R.; Davis, W. M.; Liang, L.-C.; Schrock, R. R., *J. Am. Chem. Soc.* **1999**, *121* (34), 7822-7836.

177. Studt, F.; Lehnert, N.; Weisler, B. E.; Scherer, A.; Beckhaus, R.; Tuczek, F., *Eur. J. Inorg. Chem.* **2006**, (2), 291-297.
178. Nikiforov, G. B.; Vidyaratne, I.; Gambarotta, S.; Korobkov, I., *Angew. Chem., Int. Ed.* **2009**, 48 (40), 7415-7419.
179. Chirik, P. J., *Organometallics* **2010**, 29 (7), 1500-1517.
180. Hanna, T. E.; Lobkovsky, E.; Chirik, P. J., *Organometallics* **2009**, 28 (14), 4079-4088.
181. Hanna, T. E.; Lobkovsky, E.; Chirik, P. J., *J. Am. Chem. Soc.* **2006**, 128 (18), 6018-9.
182. Chow, P. C. Dinitrogen Complexes of Titanium and Vanadium Stabilized by Phosphine Ligands MSc. Thesis, University of British Columbia, Vancouver, 1993.
183. Horrillo-Martinez, P.; Patrick, B. O.; Schafer, L. L.; Fryzuk, M. D., *Dalton Trans.* **2012**, 41 (5), 1609-1616.
184. Ting, C.; Baenziger, N. C.; Messerle, L., *J. Chem. Soc., Chem. Commun.* **1988**, (16), 1133-5.
185. Denisov, N. T.; Shuvalova, N. I.; Shilov, A. E., *Kinet. Katal.* **1985**, 26 (6), 1493-4.
186. Dilworth, J. R.; Harrison, S. J.; Henderson, R. A.; Walton, D. R. M., *J. Chem. Soc., Chem. Commun.* **1984**, (3), 176-7.
187. Dilworth, J. R.; Henderson, R. A.; Hills, A.; Hughes, D. L.; Macdonald, C.; Stephens, A. N.; Walton, D. R. M., *J. Chem. Soc., Dalton Trans.* **1990**, (3), 1077-85.
188. Schrock, R. R.; Wesolek, M.; Liu, A. H.; Wallace, K. C.; Dewan, J. C., *Inorg. Chem.* **1988**, 27 (12), 2050-4.
189. Churchill, M. R.; Wasserman, H. J., *Inorg. Chem.* **1982**, 21 (1), 218-22.
190. Ballmann, J.; Munha, R. F.; Fryzuk, M. D., *Chem. Commun.* **2010**, 46 (7), 1013-1025.
191. Li, J.; Li, S., *Angew. Chem., Int. Ed.* **2008**, 47 (42), 8040-8043.
192. Ballmann, J.; Yeo, A.; Patrick, B. O.; Fryzuk, M. D., *Angew. Chem., Int. Ed.* **2011**, 50 (2), 507-510.
193. Studt, F.; MacKay, B. A.; Johnson, S. A.; Patrick, B. O.; Fryzuk, M. D.; Tuczek, F., *Chem. Eur. J.* **2005**, 11 (2), 604-618.
194. Fryzuk, M. D.; Johnson, S. A.; Patrick, B. O.; Albinati, A.; Mason, S. A.; Koetzle, T. F., *Journal of the American Chemical Society* **2001**, 123 (17), 3960-3973.
195. Shaver, M. P.; Johnson, S. A.; Fryzuk, M. D., *Can. J. Chem.* **2005**, 83 (6-7), 652-660.
196. Ballmann, J.; Yeo, A.; MacKay, B. A.; van Rijt, S.; Patrick, B. O.; Fryzuk, M. D., *Chem. Commun.* **2010**, 46, 8794-8796.
197. Liang, L.-C., *Coord. Chem. Rev.* **2006**, 250 (9-10), 1152-1177.
198. Fryzuk, M. D.; Mao, S. S. H.; Duval, P. B.; Rettig, S. J., *Polyhedron* **1995**, 14 (1), 11-23.

199. Steinke, T.; Shaw, B. K.; Jong, H.; Patrick, B. O.; Fryzuk, M. D., *Organometallics* **2009**, 28 (9), 2830-2836.
200. Shaw, B. K.; Patrick, B. O.; Fryzuk, M. D., *Organometallics* **2012**, 31 (3), 783-786.
201. Carmichael, C. D.; Fryzuk, M. D., *Can. J. Chem.* **2010**, 88 (7), 667-675.
202. Munha, R. F.; Antunes, M. A.; Alves, L. G.; Veiros, L. F.; Fryzuk, M. D.; Martins, A. M., *Organometallics* **2010**, 29 (17), 3753-3764.
203. Munha, R. F.; Veiros, L. F.; Duarte, M. T.; Fryzuk, M. D.; Martins, A. M., *Dalton Trans.* **2009**, (36), 7494-7508.
204. Fryzuk, M. D.; Hoffman, V.; Kickham, J. E.; Rettig, S. J.; Gambarotta, S., *Inorg. Chem.* **1997**, 36 (16), 3480-3484.
205. Carmichael, C. D.; Shaver, M. P.; Fryzuk, M. D., *Can. J. Chem.* **2006**, 84 (12), 1667-1678.
206. Carmichael, C. D.; Fryzuk, M. D., *Dalton Trans.* **2005**, (3), 452-459.
207. Spencer, L. P.; Fryzuk, M. D., *Journal of Organometallic Chemistry* **2005**, 690 (24-25), 5788-5803.
208. Fryzuk, M. D.; Williams, H. D.; Rettig, S. J., *Inorg. Chem.* **1983**, 22 (6), 863-8.
209. Fryzuk, M. D.; Carter, A.; Westerhaus, A., *Inorg. Chem.* **1985**, 24 (5), 642-8.
210. Fryzuk, M. D.; Kozak, C. M.; Bowdridge, M. R.; Patrick, B. O., *Organometallics* **2002**, 21 (23), 5047-5054.
211. Fryzuk, M. D.; MacNeil, P. A., *J. Am. Chem. Soc.* **1981**, 103 (12), 3592-3.
212. Fryzuk, M. D.; Love, J. B.; Rettig, S. J., *Chem. Comm.* **1996**, (24), 2783-2784.
213. Menard, G.; Jong, H.; Fryzuk, M. D., *Organometallics* **2009**, 28 (17), 5253-5260.
214. MacLachlan, E. A.; Fryzuk, M. D., *Organometallics* **2005**, 24 (6), 1112-1118.
215. Bordwell, F. G., *Acc. Chem. Res.* **1988**, 21 (12), 456-63.
216. Fraser, R. R.; Mansour, T. S.; Savard, S., *J. Org. Chem.* **1985**, 50 (17), 3232-4.
217. Schlummer, B.; Scholz, U., *Adv. Synth. Catal.* **2004**, 346 (13-15), 1599-1626.
218. Hartwig, J. F., *Angew. Chem., Int. Ed.* **1998**, 37 (15), 2046-2067.
219. Buden, M. E.; Vaillard, V. A.; Martin, S. E.; Rossi, R. A., *J. Org. Chem.* **2009**, 74 (12), 4490-8.
220. Tietze, M.; Iglesias, A.; Merisor, E.; Conrad, J.; Klaiber, I.; Beifuss, U., *Org. Lett.* **2005**, 7 (8), 1549-52.
221. Berlin, J. M.; Campbell, K.; Ritter, T.; Funk, T. W.; Chlenov, A.; Grubbs, R. H., *Org. Lett.* **2007**, 9 (7), 1339-1342.

222. Wenderski, T.; Light, K. M.; Ogrin, D.; Bott, S. G.; Harlan, C. J., *Tetrahedron Lett.* **2004**, 45 (37), 6851-6853.
223. Ackermann, L.; Althammer, A., *Angew. Chem., Int. Ed.* **2007**, 46 (10), 1627-1629.
224. Buden Maria, E.; Vaillard Victoria, A.; Martin Sandra, E.; Rossi Roberto, A., *J. Org. Chem.* **2009**, 74 (12), 4490-8.
225. Bedford, R. B.; Betham, M.; Charmant, J. P. H.; Weeks, A. L., *Tetrahedron* **2008**, 64 (26), 6038-6050.
226. Fitton, P.; Rick, E. A., *J. Organometal. Chem.* **1971**, 28 (2), 287-91.
227. Liang, L.-C.; Chien, P.-S.; Lin, J.-M.; Huang, M.-H.; Huang, Y.-L.; Liao, J.-H., *Organometallics* **2006**, 25 (6), 1399-1411.
228. Aluri, B. R.; Kindermann, M. K.; Jones, P. G.; Dix, I.; Heinicke, J., *Inorg. Chem.* **2008**, 47 (15), 6900-6912.
229. Stegmann, H. B.; Kuehne, H. M.; Wax, G.; Scheffler, K., *Phosphorus and Sulfur and the Related Elements* **1982**, 13 (3), 331-6.
230. Wittig, G.; Pieper, G.; Fuhrmann, G., *Ber. Dtsch. Chem. Ges. B* **1940**, 73B, 1193-7.
231. Figuly, G. D.; Loop, C. K.; Martin, J. C., *J. Am. Chem. Soc.* **1989**, 111 (2), 654-8.
232. Gilman, H.; Morton, J. W., Jr., *Org. React.* **1954**, 258-304, and references within.
233. Gschwend, H. W.; Rodriguez, H. R., *Org. React.* **1979**, 26, 1-360.
234. Snieckus, V., *Chem. Rev.* **1990**, 90 (6), 879-933.
235. Gilman, H.; Brown, G. E.; Webb, F. J.; Spatz, S. M., *J. Am. Chem. Soc.* **1940**, 62, 977-9.
236. Posner, G. H.; Canella, K. A., *J. Am. Chem. Soc.* **1985**, 107 (8), 2571-3.
237. Block, E.; Eswarakrishnan, V.; Gernon, M.; Ofori-Okai, G.; Saha, C.; Tang, K.; Zubieta, J., *J. Am. Chem. Soc.* **1989**, 111 (2), 658-65.
238. Gilman, H.; Bebb, R. L., *J. Am. Chem. Soc.* **1939**, 61, 109-12.
239. Wittig, G.; Fuhrmann, G., *Ber. Dtsch. Chem. Ges. B* **1940**, 73B, 1197-1218.
240. Gilman, H.; Brown, G. E., *J. Am. Chem. Soc.* **1940**, 62, 3208-10.
241. Armstrong, D. R.; Clegg, W.; Dale, S. H.; Hevia, E.; Hogg, L. M.; Honeyman, G. W.; Mulvey, R. E., *Angew. Chem., Int. Ed.* **2006**, 45 (23), 3775-3778.
242. Fuhrer, W.; Gschwend, H. W., *J. Org. Chem.* **1979**, 44 (7), 1133-6.
243. Muchowski, J. M.; Venuti, M. C., *J. Org. Chem.* **1980**, 45 (23), 4798-801.
244. Armstrong, D. R.; Barr, D.; Clegg, W.; Hodgson, S. M.; Mulvey, R. E.; Reed, D.; Snaith, R.; Wright, D. S., *J. Am. Chem. Soc.* **1989**, 111 (13), 4719-27.
245. von Buelow, R.; Gornitzka, H.; Kottke, T.; Stalke, D., *Chem. Commun.* **1996**, (14), 1639-1640.

246. Barr, D.; Clegg, W.; Mulvey, R. E.; Snaith, R.; Wright, D. S., *J. Chem. Soc., Chem. Commun.* **1987**, (10), 716-18.
247. Clegg, W.; Horsburgh, L.; Mackenzie, F. M.; Mulvey, R. E., *J. Chem. Soc., Chem. Commun.* **1995**, (19), 2011-12.
248. Fan, L.; Foxman, B. M.; Ozerov, O. V., *Organometallics* **2004**, 23 (3), 326-328.
249. Liang, L.-C. Ligands for metals as catalysts for carbon-carbon bond formation. US 20090163740, 2009.
250. Liang, L.-C. Preparation of aminophosphine ligands for metals as catalysts for carbon-carbon bond formation. US 20050288504, 2005.
251. Yamamoto, Y.; Yamazaki, H., *Bull. Chem. Soc. Jpn.* **1970**, 43 (11), 3634.
252. Shekhar, S.; Ryberg, P.; Hartwig, J. F.; Mathew, J. S.; Blackmond, D. G.; Strieter, E. R.; Buchwald, S. L., *J. Am. Chem. Soc.* **2006**, 128 (11), 3584-91.
253. Fjeldberg, T.; Hitchcock, P. B.; Lappert, M. F.; Thorne, A. J., *J. Chem. Soc., Chem. Commun.* **1984**, (13), 822-4.
254. Ruhlandt-Senge, K.; Ellison, J. J.; Wehmschulte, R. J.; Pauer, F.; Power, P. P., *J. Am. Chem. Soc.* **1993**, 115 (24), 11353-7.
255. Butler, I. R.; Cullen, W. R.; Reglinski, J.; Rettig, S. J., *J. Organomet. Chem.* **1983**, 249 (1), 183-94.
256. Harder, S.; Boersma, J.; Brandsma, L.; Kanters, J. A., *J. Organomet. Chem.* **1988**, 339 (1-2), 7-15.
257. Clyburne, J. A. C.; McMullen, N., *Coord. Chem. Rev.* **2000**, 210, 73-99.
258. Schiemenz, B.; Power, P. P., *Angew. Chem., Int. Ed.* **1996**, 35 (18), 2150-2152.
259. Wehman, E.; Jastrzebski, J. T. B. H.; Ernsting, J. M.; Grove, D. M.; Van Koten, G., *J. Organomet. Chem.* **1988**, 353 (2), 145-55.
260. Hacker, R.; Kaufmann, E.; Schleyer, P. v. R.; Mahdi, W.; Dietrich, H., *Chem. Ber.* **1987**, 120 (9), 1533-8.
261. Ohki, Y., Synthesis of Diamidophosphine Ligands via Direct ortho-Deprotonation of Diarylamine and its Zirconium Complexes and A New Dinitrogen Complex of Zirconium with an Arene-Bridged Diamidophosphine Ligand and its Reaction Chemistry. Internal report to Fryzuk Reserach Group. 2006.
262. Daly, J. J., *J. Chem. Soc.* **1964**, (Oct.), 3799-810.
263. Mornon, J. P.; Bally, R.; Brassy, C., *C. R. Hebd. Seances Acad. Sci., Ser. C* **1977**, 284 (19), 779-81.
264. Ohki, Y.; Fryzuk, M. D., *Angew. Chem., Int. Ed.* **2007**, 46 (18), 3180-3183.

265. Warren, T. H.; Erker, G.; Froehlich, R.; Wibbeling, B., *Organometallics* **2000**, *19* (2), 127-134.
266. Brenner, S.; Kempe, R.; Arndt, P., *Z. Anorg. Allg. Chem.* **1995**, *621* (12), 2121-4.
267. Schrock, R. R.; Seidel, S. W.; Schrodi, Y.; Davis, W. M., *Organometallics* **1999**, *18* (3), 428-437.
268. Yu, X.; Cai, H.; Guzei, I. A.; Xue, Z., *J. Am. Chem. Soc.* **2004**, *126* (14), 4472-4473.
269. Mountford, A. J.; Clegg, W.; Harrington, R. W.; Humphrey, S. M.; Lancaster, S. J., *Chem. Commun.* **2005**, (15), 2044-2046.
270. Wengrovius, J. H.; Schrock, R. R.; Day, C. S., *Inorg. Chem.* **1981**, *20* (6), 1844-9.
271. Lehn, J.-S. M.; Hoffman, D. M., *Inorg. Chem.* **2002**, *41* (15), 4063-4067.
272. Johnson, C. S., Jr., *Prog. Nucl. Magn. Reson. Spectrosc.* **1999**, *34* (3,4), 203-256.
273. Morris, K. F.; Johnson, C. S., *J. Am. Chem. Soc.* **1992**, *114* (8), 3139-3141.
274. Ketterer, N. A.; Ziller, J. W.; Rheingold, A. L.; Heyduk, A. F., *Organometallics* **2007**, *26* (22), 5330-5338.
275. Han, H.; Johnson, S. A., *Eur. J. Inorg. Chem.* **2008**, (3), 471-482.
276. Davie, M. E.; Foerster, T.; Parsons, S.; Pulham, C.; Rankin, D. W. H.; Smart, B. A., *Polyhedron* **2006**, *25* (4), 923-929.
277. Guenther, B.; Noth, H., *Z. Anorg. Allg. Chem.* **2008**, *634* (2), 234-236.
278. Cordero, B.; Gomez, V.; Platero-Prats, A. E.; Reves, M.; Echeverria, J.; Cremades, E.; Barragan, F.; Alvarez, S., *Dalton Trans.* **2008**, (21), 2832-2838.
279. Duraj, S. A.; Towns, R. L. R.; Baker, R. J.; Schupp, J., *Acta Crystallogr., Sect. C: Cryst. Struct. Commun.* **1990**, *C46* (5), 890-2.
280. Blackmore, K. J.; Sly, M. B.; Haneline, M. R.; Ziller, J. W.; Heyduk, A. F., *Inorg. Chem.* **2008**, *47* (22), 10522-32.
281. Sattelberger, A. P.; Wilson, R. B., Jr.; Huffman, J. C., *Inorg. Chem.* **1982**, *21* (6), 2392-6.
282. Noor, A.; Kretschmer, W.; Kempe, R., *Eur. J. Inorg. Chem.* **2006**, (13), 2683-2689.
283. mf 833 (Fryzuk Group) in UBC X-ray Crystallography Database.
<https://wapps.chem.ubc.ca/xrdb/launch.php> (accessed 17/08/2014).
284. Batsanov, A. S.; Churakov, A. V.; Howard, J. A. K.; Hughes, A. K.; Johnson, A. L.; Kingsley, A. J.; Neretin, I. S.; Wade, K., *J. Chem. Soc., Dalton Trans.* **1999**, (21), 3867-3875.
285. Hagen, K.; Holwill, C. J.; Rice, D. A.; Runnacles, J. D., *Inorg. Chem.* **1992**, *31* (23), 4733-6.

286. Davies, H. O.; Jones, A. C.; McKinnell, E. A.; Raftery, J.; Muryn, C. A.; Afzaal, M.; O'Brien, P., *J. Mater. Chem.* **2006**, *16* (23), 2226-2228.
287. Chisholm, M. H.; Tan, L. S.; Huffman, J. C., *J. Am. Chem. Soc.* **1982**, *104* (18), 4879-84.
288. Chisholm, M. H.; Huffman, J. C.; Tan, L.-S., *Inorg. Chem.* **1981**, *20* (6), 1859-66.
289. Chisholm, M. H.; Cotton, F. A.; Extine, M. W., *Inorg. Chem.* **1978**, *17* (7), 2000-3.
290. Chen, S. J.; Yap, G. P. A.; Xue, Z. L., *Sci. China, Ser. B: Chem.* **2009**, *52* (10), 1583-1589.
291. Chen, S.-J.; Cai, H.; Xue, Z.-L., *Organometallics* **2009**, *28* (1), 167-171.
292. Sharma, B.; Chen, S.-J.; Abbott, J. K. C.; Chen, X.-T.; Xue, Z.-L., *Inorg. Chem.* **2012**, *51* (1), 25-27.
293. Fryzuk, M. D.; Johnson, S. A.; Rettig, S. J., *Organometallics* **1999**, *18* (20), 4059-4067.
294. Rabe, S.; Muller, U., *Z. Kristallogr. - New Cryst. Struct.* **2000**, *215* (1), 1-2.
295. Davies, H. O.; Jones, A. C.; Motevalli, M. A.; McKinnell, E. A.; O'Brien, P., *Inorg. Chem. Commun.* **2005**, *8* (7), 585-587.
296. Zhou, C.-C.; Huang, J.-H.; Wang, M.-H.; Lee, T.-Y.; Lee, G.-H.; Peng, S.-M., *Inorg. Chim. Acta* **2003**, *342*, 59-63.
297. Cotton, F. A.; Falvello, L. R.; Najjar, R. C., *Inorg. Chem.* **1983**, *22* (5), 770-4.
298. Sattler, A.; Ruccolo, S.; Parkin, G., *Dalton Trans.* **2011**, *40* (30), 7777-7782.
299. Liang, L.-C.; Cheng, L.-C.; Tsai, T.-L.; Hu, C.-H.; Guo, W.-H., *Inorg. Chem.* **2009**, *48* (13), 5697-5703.
300. Friesse, J. C.; Krol, A.; Puke, C.; Kirschbaum, K.; Giolando, D. M., *Inorg. Chem.* **2000**, *39* (7), 1496-1500.
301. Vaid, T. P.; Veige, A. S.; Lobkovsky, E. B.; Glassey, W. V.; Wolczanski, P. T.; Liable-Sands, L. M.; Rheingold, A. L.; Cundari, T. R., *J. Am. Chem. Soc.* **1998**, *120* (39), 10067-10079.
302. Kaupp, M., *Chem. Eur. J.* **1998**, *4* (9), 1678-1686.
303. Desroches, C.; Pilet, G.; Borshch, S. A.; Parola, S.; Luneau, D., *Inorg. Chem.* **2005**, *44* (24), 9112-9120.
304. van Gorkum, R.; Buda, F.; Kooijman, H.; Spek, A. L.; Bouwman, E.; Reedijk, J., *Eur. J. Inorg. Chem.* **2005**, (11), 2255-2261.
305. Hubert-Pfalzgraf, L. G.; Zaki, A.; Toupet, L., *Polyhedron* **1993**, *12* (11), 1411-13.
306. Tatsumi, K.; Matsubara, I.; Inoue, Y.; Nakamura, A.; Miki, K.; Kasai, N., *J. Am. Chem. Soc.* **1989**, *111* (20), 7766-77.
307. Fryzuk, M. D.; Carter, A.; Rettig, S. J., *Organometallics* **1992**, *11* (1), 469-72.

308. Groysman, S.; Goldberg, I.; Kol, M.; Goldschmidt, Z., *Organometallics* **2003**, 22 (19), 3793-3795.
309. Sattler, A.; Ruccolo, S.; Parkin, G., *Dalton Transactions* **2011**, 40 (30), 7777-7782.
310. Dewan, J. C.; Mialki, W. S.; Walton, R. A.; Lippard, S. J., *J. Am. Chem. Soc.* **1982**, 104 (1), 133-6.
311. Horrillo-Martinez, P.; Patrick, B. O.; Schafer, L. L.; Fryzuk, M. D., *Dalton Transactions* **2012**, 41 (5), 1609-1616.
312. Dunogues, J.; N'Gabe, D.; Laguerre, M.; Duffaut, N.; Calas, R., *Organometallics* **1982**, 1 (11), 1525-8.
313. Arteaga-Muller, R.; Tsurugi, H.; Saito, T.; Yanagawa, M.; Oda, S.; Mashima, K., *J. Am. Chem. Soc.* **2009**, 131 (15), 5370-5371.
314. Hess, F. M.; Fryzuk, M. D., *Abstracts of Papers, 236th ACS National Meeting, Philadelphia, PA, United States, August 17-21 2008*, INOR-004.
315. Fryzuk, M. D.; Mylvaganam, M.; Zaworotko, M. J.; MacGillivray, L. R., *J. Am. Chem. Soc.* **1993**, 115 (22), 10360-1.
316. Fryzuk, M. D.; Mylvaganam, M.; Zaworotko, M. J.; MacGillivray, L. R., *Polyhedron* **1996**, 15 (4), 689-703.
317. Fryzuk, M. D.; Kozak, C. M.; Mehrkhodavandi, P.; Morello, L.; Patrick, B. O.; Rettig, S. J., *J. Am. Chem. Soc.* **2002**, 124 (4), 516-517.
318. Grobelny, Z., *Eur. J. Org. Chem.* **2004**, (14), 2973-2982.
319. Fischer, K.; Wilken, M., *J. Chem. Thermodyn.* **2001**, 33 (10), 1285-1308.
320. Gibanel, F.; Lopez, M. C.; Royo, F. M.; Santafe, J.; Urieta, J. S., *J. Solution Chem.* **1993**, 22 (3), 211-17.
321. Gibanel, F.; Lopez, M. C.; Royo, F. M.; Pardo, J.; Urieta, J. S., *Fluid Phase Equilib.* **1993**, 87 (2), 285-94.
322. Fryzuk, M. D.; Love, J. B.; Rettig, S. J., *Organometallics* **1998**, 17 (5), 846-853.
323. Kushto, G. P.; Souter, P. F.; Chertihin, G. V.; Andrews, L., *J. Chem. Phys.* **1999**, 110 (18), 9020-9031.
324. Dance, I., *Dalton Trans.* **2012**, 41 (16), 4859-4865.
325. Dance, I., *Dalton Trans.* **2008**, (43), 5977-5991.
326. Dance, I., *Dalton Trans.* **2008**, (43), 5992-5998.
327. Dilworth, J. R.; Henderson, R. A.; Hughes, D. L.; Leigh, G. J.; Pickett, C. J.; Richards, R. L., From phosphorus towards sulfur: the development of new dinitrogen binding sites. In *Nitrogen Fixation Res. Prog., Proc. Int. Symp., 6th*, 1985; pp 639-44.

328. Adachi, T.; Sasaki, N.; Ueda, T.; Kaminaka, M.; Yoshida, T., *J. Chem. Soc., Chem. Commun.* **1989**, (18), 1320-2.
329. Krut'ko, D. P.; Borzov, M. V.; Kuz'mina, L. G.; Churakov, A. V.; Lemenovskii, D. A.; Reutov, O. A., *Inorg. Chim. Acta* **1998**, 280 (1-2), 257-263.
330. Takemoto, S.; Kawamura, H.; Yamada, Y.; Okada, T.; Ono, A.; Yoshikawa, E.; Mizobe, Y.; Hidai, M., *Organometallics* **2002**, 21 (19), 3897-3904.
331. Graf, D. D.; Schrock, R. R.; Davis, W. M.; Stumpf, R., *Organometallics* **1999**, 18 (5), 843-852.
332. Hess, F. M.; Fryzuk, M. D., *Abstracts of Papers, 239th ACS National Meeting, San Francisco, CA, United States, March 21-25 2010*, INOR-1366.
333. Bolton, P. D.; Feliz, M.; Cowley, A. R.; Clot, E.; Mountford, P., *Organometallics* **2008**, 27 (23), 6096-6110.
334. Beck, J. F.; Baiz, T. I.; Neshat, A.; Schmidt, J. A. R., *Dalton Trans.* **2009**, (25), 5001-5008.
335. Hayday, G. J.; Wang, C.; Rees, N. H.; Mountford, P., *Dalton Trans.* **2008**, (25), 3301-3310.
336. Bercaw, J. E., *J. Am. Chem. Soc.* **1974**, 96 (16), 5087-95.
337. Kaesz, H. D.; Saillant, R. B., *Chem. Rev.* **1972**, 72 (3), 231-81.
338. Erker, G., *Acc. Chem. Res.* **1984**, 17 (3), 103-9.
339. Bi, S.; Kong, X.; Zhao, Y.; Zhao, X.; Xie, Q., *J. Organomet. Chem.* **2008**, 693 (11), 2052-2060.
340. Schaverien, C. J., *J. Mol. Catal.* **1994**, 90 (1-2), 177-84.
341. Ihm, J.; Lee, H.; Jeon, H. J.; Kim, J. S.; Kim, D. O.; Yoon, H. B.; Park, J.; Oh, S.-G.; Oh, C. Organometallic complexes as hydrogen storage materials and a method of preparing the same. WO 2008032985, 2008.
342. Amar, I. A.; Lan, R.; Petit, C. T. G.; Tao, S., *J. Solid State Electrochem.* **2011**, 15 (9), 1845-1860.
343. Skodra, A.; Stoukides, M., *Solid State Ionics* **2009**, 180 (23-25), 1332-1336.
344. Vogelsang, H., An alternative to the Haber-Bosch process. The solid state ammonia synthesis (SSAS) process. In *NPT Procestechologie*, 2011; Vol. 18, pp 18-19.
345. Chatt, J.; Pearman, A. J.; Richards, R. L., *Nature (London)* **1975**, 253 (5486), 39-40.
346. Hidai, M.; Takahashi, T.; Yokotake, I.; Uchida, Y., *Chem. Lett.* **1980**, (6), 645-6.
347. Schrock, R. R., *Angew. Chem., Int. Ed.* **2008**, 47 (30), 5512-5522.
348. Schrock, R. R., *Acc. Chem. Res.* **2005**, 38 (12), 955-962.

349. Ritleng, V.; Yandulov, D. V.; Weare, W. W.; Schrock, R. R.; Hock, A. S.; Davis, W. M., *J. Am. Chem. Soc.* **2004**, *126* (19), 6150-6163.
350. Neese, F., *Angew. Chem., Int. Ed.* **2006**, *45* (2), 196-199.
351. Bosch, B.; Erker, G.; Froehlich, R.; Meyer, O., *Organometallics* **1997**, *16* (25), 5449-5456.
352. Pflug, J.; Bertuleit, A.; Kehr, G.; Froehlich, R.; Erker, G., *Organometallics* **1999**, *18* (19), 3818-3826.
353. Kool, L. B.; Rausch, M. D.; Herberhold, M.; Alt, H. G.; Thewalt, U.; Honold, B., *Organometallics* **1986**, *5* (12), 2465-8.
354. Ahlers, W.; Erker, G.; Froehlich, R., *Eur. J. Inorg. Chem.* **1998**, (7), 889-895.
355. Fryzuk, M. D.; Duval, P. B.; Mao, S. S. S. H.; Rettig, S. J.; Zaworotko, M. J.; MacGillivray, L. R., *J. Am. Chem. Soc.* **1999**, *121* (8), 1707-1716.
356. Chamberlain, L. R.; Durfee, L. D.; Fanwick, P. E.; Kobriger, L.; Latesky, S. L.; McMullen, A. K.; Rothwell, I. P.; Folting, K.; Huffman, J. C.; et al., *J. Am. Chem. Soc.* **1987**, *109* (2), 390-402.
357. Prashar, S.; Fajardo, M.; Garces, A.; Dorado, I.; Antinolo, A.; Otero, A.; Lopez-Solera, I.; Lopez-Mardomingo, C., *J. Organomet. Chem.* **2004**, *689* (7), 1304-1314.
358. Wu, Z.; Diminnie, J. B.; Xue, Z., *Organometallics* **1999**, *18* (6), 1002-1010.
359. MacMillan, S. N.; Tanski, J. M.; Waterman, R., *Chem. Commun.* **2007**, (40), 4172-4174.
360. Ahlers, W.; Erker, G.; Froehlich, R., *J. Organomet. Chem.* **1998**, *571* (1), 83-89.
361. Fryzuk, M. D., *Chemical Record* **2003**, *3* (1), 2-11.
362. Matsugi, T.; Fujita, T., *Chem. Soc. Rev.* **2008**, *37* (6), 1264-1277.
363. Bochmann, M., *Organometallics* **2010**, *29* (21), 4711-4740.
364. Ishino, H.; Takemoto, S.; Hirata, K.; Kanaizuka, Y.; Hidai, M.; Nabika, M.; Seki, Y.; Miyatake, T.; Suzuki, N., *Organometallics* **2004**, *23* (20), 4544-4546.
365. Cohen, S. A.; Auburn, P. R.; Bercaw, J. E., *J. Am. Chem. Soc.* **1983**, *105* (5), 1136-43.
366. McDermott, J. X.; Wilson, M. E.; Whitesides, G. M., *J. Am. Chem. Soc.* **1976**, *98* (21), 6529-36.
367. Fryzuk, M. D.; Duval, P. B.; Rettig, S. J., *Can. J. Chem.* **2001**, *79* (5/6), 536-545.
368. Takahashi, T.; Kasai, K.; Suzuki, N.; Nakajima, K.; Negishi, E., *Organometallics* **1994**, *13* (9), 3413-14.
369. Alt, H. G.; Denner, C. E.; Thewalt, U.; Rausch, M. D., *J. Organomet. Chem.* **1988**, *356* (3), C83-C85.
370. Lu, Z.-H.; Xu, Q., *J. Phys. Chem. A* **2011**, *115* (39), 10783-10788.

371. Dartiguenave, M.; Menu, J. M.; Dyedier, E.; Dartiguenave, Y.; Siebald, H., *Coord. Chem. Rev.* **1998**, 178-180 (Pt. 1), 623-663.
372. Presser, A.; Huefner, A., *Monatsh. Chem.* **2004**, 135 (8), 1015-1022.
373. Barton, T. J.; Hoekman, S. K., *Synth. React. Inorg. Met.-Org. Chem.* **1979**, 9 (4), 297-300.
374. Bourissou, D.; Guerret, O.; Gabbaie, F. P.; Bertrand, G., *Chem. Rev. (Washington, D. C.)* **2000**, 100 (1), 39-91.
375. Mieusset, J.-L.; Brinker Udo, H., *J. Org. Chem.* **2008**, 73 (4), 1553-8.
376. Arduengo, A. J., III; Harlow, R. L.; Kline, M., *J. Am. Chem. Soc.* **1991**, 113 (1), 361-3.
377. Herrmann, W. A., *Angew. Chem., Int. Ed.* **2002**, 41 (8), 1290-1309.
378. Lloyd-Jones, G. C.; Alder, R. W.; Owen-Smith, G. J. J., *Chem. Eur. J.* **2006**, 12 (20), 5361-5375.
379. Kira, M.; Yauchibara, R.; Hirano, R.; Kabuto, C.; Sakurai, H., *J. Am. Chem. Soc.* **1991**, 113 (20), 7785-7.
380. Kira, M.; Ishida, S.; Iwamoto, T.; Ichinohe, M.; Kabuto, C.; Ignatovich, L.; Sakurai, H., *Chem. Lett.* **1999**, (3), 263-264.
381. Kira, M., *Chem. Commun.* **2010**, 46 (17), 2893-2903.
382. Kira, M.; Ishida, S.; Iwamoto, T.; Kabuto, C., *J. Am. Chem. Soc.* **1999**, 121 (41), 9722-9723.
383. Martinez, S.; Morokuma, K.; Musaev, D. G., *Organometallics* **2007**, 26 (24), 5978-5986.
384. Musaev, D. G.; Bobadova-Parvanova, P.; Morokuma, K., *Inorg. Chem.* **2007**, 46 (7), 2709-2715.
385. Himmel, H.-J.; Huebner, O.; Bischoff, F. A.; Kloppe, W.; Manceron, L., *PCCP* **2006**, 8 (17), 2000-2011.
386. Himmel, H.-J.; Hubner, O.; Kloppe, W.; Manceron, L., *Angew. Chem., Int. Ed.* **2006**, 45 (17), 2799-2802.
387. Kuganathan, N.; Green, J. C.; Himmel, H.-J., *New J. Chem.* **2006**, 30 (9), 1253-1262.
388. Garcia-Fortanet, J.; Kessler, F.; Buchwald, S. L., *J. Am. Chem. Soc.* **2009**, 131 (19), 6676-6677.
389. Chianese, A. R.; Rogers, S. L.; Al-Gattas, H., *Tetrahedron Lett.* **2010**, 51 (17), 2241-2243.
390. Liang, L.-C.; Lee, W.-Y.; Hung, C.-H., *Inorg. Chem.* **2003**, 42 (18), 5471-5473.
391. Iwaki, T.; Yasuhara, A.; Sakamoto, T., *J. Chem. Soc., Perkin Trans. I* **1999**, (11), 1505-1510.

392. Bailey, W. F.; Longstaff, S. C., *Chim. Oggi* **2001**, 19 (3/4), 28-32.
393. Wehman, E.; Jastrzebski, J. T. B. H.; Ernsting, J. M.; Grove, D. M.; Van Koten, G., *J. Organomet. Chem.* **1988**, 353 (2), 133-43.
394. Fripiat, J. G.; Chow, K. T.; Boudart, M.; Diamond, J. B.; Johnson, K. H., *J. Mol. Catal.* **1975**, 1 (1), 59-72.
395. Armstrong, D. R.; Barr, D.; Snaith, R.; Clegg, W.; Mulvey, R. E.; Wade, K.; Reed, D., *J. Chem. Soc., Dalton Trans.* **1987**, (5), 1071-81.
396. Fairlamb, I. J. S.; Kapdi, A. R.; Lee, A. F., *Org. Lett.* **2004**, 6 (24), 4435-4438.
397. Weber, W. M.; Hunsaker, L. A.; Abcouwer, S. F.; Deck, L. M.; Vander Jagt, D. L., *Bioorg. Med. Chem.* **2005**, 13 (11), 3811-3820.
398. Moseley, K.; Maitlis, P. M., *J. Chem. Soc., Dalton Trans.* **1974**, (2), 169-75.
399. Takahashi, Y.; Ito, T.; Sakai, S.; Ishii, Y., *J. Chem. Soc., Chem. Commun.* **1970**, (17), 1065-6.
400. Noskowska, M.; Sliwinska, E.; Duczmal, W., *Transition Met. Chem.* **2003**, 28 (7), 756-759.
401. Wayland, B. B.; Schramm, R. F., *Inorg. Chem.* **1969**, 8 (4), 971-6.
402. Hayashi, T.; Konishi, M.; Kobori, Y.; Kumada, M.; Higuchi, T.; Hirotsu, K., *J. Am. Chem. Soc.* **1984**, 106 (1), 158-63.
403. Manzer, L. E., *Inorg. Synth.* **1982**, 21, 135-40.
404. Benzing, E.; Kornicker, W., *Chem. Ber.* **1961**, 94, 2263-7.
405. Chao, Y. W.; Polson, S.; Wigley, D. E., *Polyhedron* **1990**, 9 (22), 2709-16.
406. Chao, Y. W.; Wexler, P. A.; Wigley, D. E., *Inorg. Chem.* **1989**, 28 (20), 3860-8.
407. Weitz, I. S.; Rabinovitz, M., *J. Chem. Soc., Perkin Trans. 1* **1993**, (1), 117-20.
408. Lalancette, J. M.; Rollin, G.; Dumas, P., *Can. J. Chem.* **1972**, 50 (18), 3058-62.
409. Bergbreiter, D. E.; Killough, J. M., *J. Am. Chem. Soc.* **1978**, 100 (7), 2126-34.
410. Fairbrother, F.; Grundy, K. H.; Thompson, A., *J. Less-Common Met.* **1966**, 10 (1), 38-41.
411. Marchetti, F.; Pampaloni, G., *Chem. Commun.* **2012**, 48 (5), 635-653.
412. Fairbrother, F.; Grundy, K. H.; Thompson, A., *J. Chem. Soc.* **1965**, (Jan.), 765-70.
413. Fuggle, J. C.; Sharp, D. W. A.; Winfield, J. M., *J. Fluorine Chem.* **1972**, 1 (4), 427-31.
414. Moss, K. C., *J. Chem. Soc. A* **1970**, (8), 1224-6.
415. Schmidt, J. A. R.; Chmura, S. A.; Arnold, J., *Organometallics* **2001**, 20 (6), 1062-1064.
416. Mayer, J. M.; Curtis, C. J.; Bercaw, J. E., *J. Am. Chem. Soc.* **1983**, 105 (9), 2651-60.
417. Mason, J., *Chem. Rev.* **1981**, 81 (3), 205-27.
418. Fryzuk, M. D.; Giesbrecht, G. R.; Rettig, S. J., *Organometallics* **1997**, 16 (4), 725-736.

Appendix A: Supporting NMR Spectroscopic Information

A. DOSY $^{31}\text{P}\{^1\text{H}\}$ NMR Data for $[\text{ipropNPNZrCl}_2]_2$ [3.9] at $-40\text{ }^\circ\text{C}$

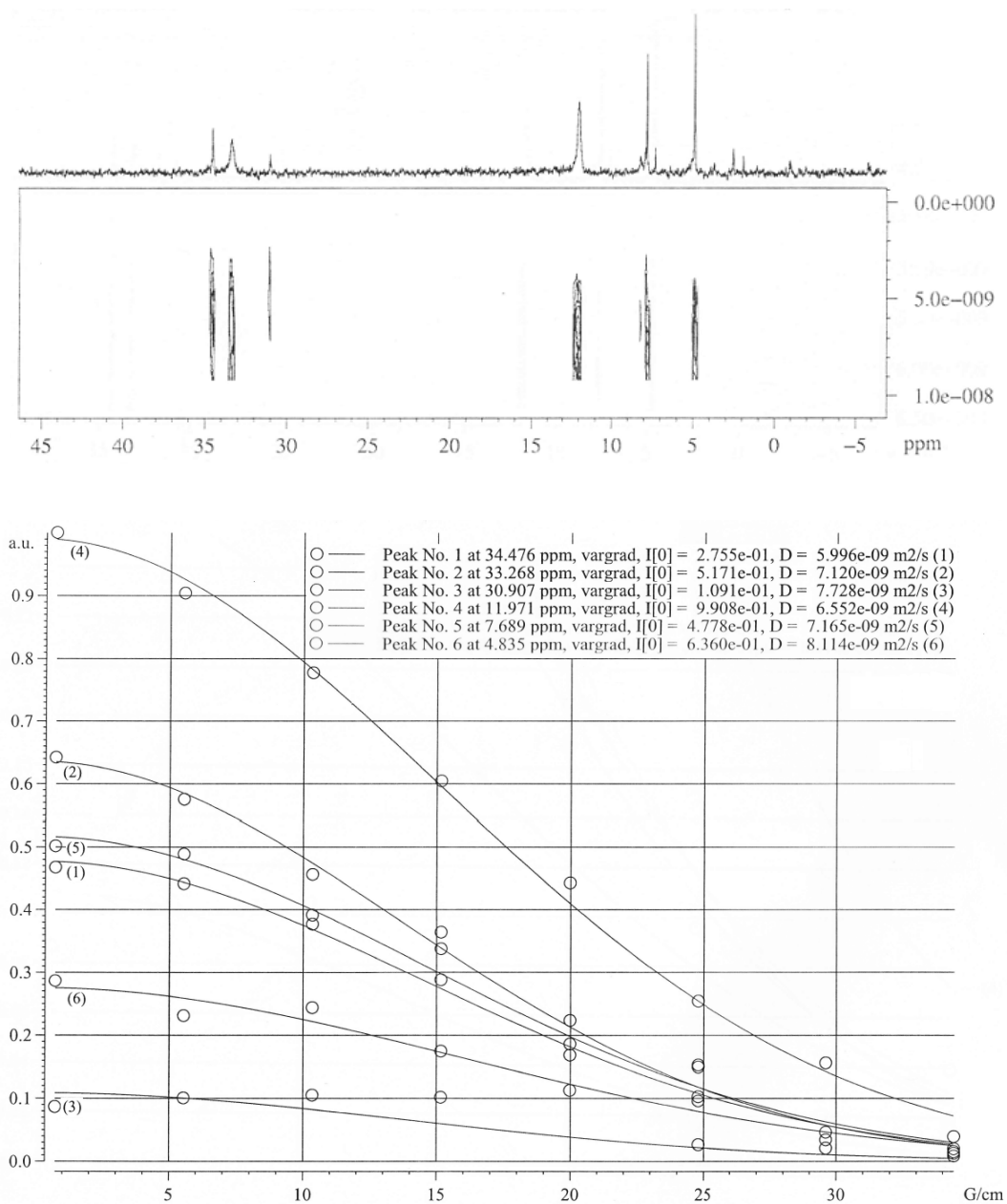


Figure 222: DOSY $^{31}\text{P}\{^1\text{H}\}$ NMR spectrum and diffusion coefficients (D) for $[\text{ipropNPNZrCl}_2]_2$ [3.9] in toluene-d_8 at $-40\text{ }^\circ\text{C}$

C:/Bruker/XWIN-NMR/data/maria/nmr/fi380/101/pdata/1/simfit.txt

Wed Feb 17 11:

SIMFIT RESULTS
=====

Dataset : C:/Bruker/XWIN-NMR/data/maria/nmr/fi380/101/pdata/1/simfit.txt

AREA fit : Diffusion : Variable Gradient :

$$I = I[0] * \exp(-D * \text{SQR}(2 * \text{PI} * \text{gamma} * \text{Gi} * \text{LD}) * (\text{BD} - \text{LD} / 3) * 1e4)$$

8 points for Peak 1, Cursor Point = 12032, 5584.28 Hz, 34.476 ppm

Converged after 64 iterations!

Results Comp. 1

I[0] = 2.755e-01
 Diff Con. = 5.996e-09 m2/s
 Gamma = 1.724e+03 Hz/G
 Little Delta = 1.200m
 Big Delta = 200.000m

RSS = 2.651e-03
 SD = 1.820e-02

| Point | Gradient | Expt | Calc | Difference |
|-------|-----------|-----------|-----------|------------|
| 1 | 7.250e-01 | 2.862e-01 | 2.752e-01 | -1.099e-02 |
| 2 | 5.539e+00 | 2.307e-01 | 2.589e-01 | 2.823e-02 |
| 3 | 1.035e+01 | 2.437e-01 | 2.218e-01 | -2.184e-02 |
| 4 | 1.517e+01 | 1.746e-01 | 1.730e-01 | -1.587e-03 |
| 5 | 1.998e+01 | 1.126e-01 | 1.229e-01 | 1.024e-02 |
| 6 | 2.480e+01 | 9.575e-02 | 7.946e-02 | -1.628e-02 |
| 7 | 2.961e+01 | 2.063e-02 | 4.679e-02 | 2.616e-02 |
| 8 | 3.442e+01 | 3.923e-02 | 2.508e-02 | -1.414e-02 |

=====

8 points for Peak 2, Cursor Point = 12427, 5388.59 Hz, 33.268 ppm

Converged after 55 iterations!

Results Comp. 1

I[0] = 5.171e-01
 Diff Con. = 7.120e-09 m2/s
 Gamma = 1.724e+03 Hz/G
 Little Delta = 1.200m
 Big Delta = 200.000m

RSS = 5.130e-03
 SD = 2.532e-02

| Point | Gradient | Expt | Calc | Difference |
|-------|-----------|-----------|-----------|------------|
| 1 | 7.250e-01 | 5.015e-01 | 5.165e-01 | 1.497e-02 |
| 2 | 5.539e+00 | 4.888e-01 | 4.804e-01 | -8.397e-03 |
| 3 | 1.035e+01 | 3.912e-01 | 3.998e-01 | 8.535e-03 |
| 4 | 1.517e+01 | 3.373e-01 | 2.976e-01 | -3.966e-02 |
| 5 | 1.998e+01 | 1.684e-01 | 1.982e-01 | 2.986e-02 |
| 6 | 2.480e+01 | 1.494e-01 | 1.181e-01 | -3.131e-02 |
| 7 | 2.961e+01 | 3.379e-02 | 6.298e-02 | 2.920e-02 |
| 8 | 3.442e+01 | 8.470e-03 | 3.004e-02 | 2.157e-02 |

=====

8 points for Peak 3, Cursor Point = 13199, 5006.13 Hz, 30.907 ppm

Converged after 75 iterations!

Results Comp. 1

I[0] = 1.091e-01
 Diff Con. = 7.728e-09 m2/s
 Gamma = 1.724e+03 Hz/G
 Little Delta = 1.200m
 Big Delta = 200.000m

RSS = 5.545e-03

SD = 2.633e-02

| Point | Gradient | Expt | Calc | Difference |
|-------|-----------|------------|-----------|------------|
| 1 | 7.250e-01 | 8.680e-02 | 1.090e-01 | 2.218e-02 |
| 2 | 5.539e+00 | 1.004e-01 | 1.007e-01 | 3.485e-04 |
| 3 | 1.035e+01 | 1.048e-01 | 8.253e-02 | -2.225e-02 |
| 4 | 1.517e+01 | 1.014e-01 | 5.992e-02 | -4.150e-02 |
| 5 | 1.998e+01 | -9.024e-03 | 3.855e-02 | 4.757e-02 |
| 6 | 2.480e+01 | 2.622e-02 | 2.198e-02 | -4.235e-03 |
| 7 | 2.961e+01 | -7.240e-03 | 1.111e-02 | 1.835e-02 |
| 8 | 3.442e+01 | 1.974e-02 | 4.973e-03 | -1.476e-02 |

8 points for Peak 4, Cursor Point = 19390, 1939.01 Hz, 11.971 ppm

Converged after 50 iterations!

Results Comp. 1

I[0] = 9.908e-01
 Diff Con. = 6.552e-09 m2/s
 Gamma = 1.724e+03 Hz/G
 Little Delta = 1.200m
 Big Delta = 200.000m

RSS = 8.546e-03

SD = 3.268e-02

| Point | Gradient | Expt | Calc | Difference |
|-------|-----------|------------|-----------|------------|
| 1 | 7.250e-01 | 1.000e+00 | 9.896e-01 | -1.036e-02 |
| 2 | 5.539e+00 | 9.036e-01 | 9.259e-01 | 2.228e-02 |
| 3 | 1.035e+01 | 7.771e-01 | 7.819e-01 | 4.801e-03 |
| 4 | 1.517e+01 | 6.043e-01 | 5.960e-01 | -8.331e-03 |
| 5 | 1.998e+01 | 4.426e-01 | 4.101e-01 | -3.255e-02 |
| 6 | 2.480e+01 | 2.539e-01 | 2.547e-01 | 7.935e-04 |
| 7 | 2.961e+01 | 1.559e-01 | 1.428e-01 | -1.315e-02 |
| 8 | 3.442e+01 | -9.102e-03 | 7.224e-02 | 8.134e-02 |

8 points for Peak 5, Cursor Point = 20790, 1245.43 Hz, 7.689 ppm

Converged after 50 iterations!

Results Comp. 1

I[0] = 4.778e-01

Diff Con. = 7.165e-09 m2/s
 Gamma = 1.724e+03 Hz/G
 Little Delta = 1.200m
 Big Delta = 200.000m

RSS = 7.545e-04
 SD = 9.712e-03

| Point | Gradient | Expt | Calc | Difference |
|-------|-----------|-----------|-----------|------------|
| 1 | 7.250e-01 | 4.675e-01 | 4.772e-01 | 9.726e-03 |
| 2 | 5.539e+00 | 4.412e-01 | 4.437e-01 | 2.460e-03 |
| 3 | 1.035e+01 | 3.767e-01 | 3.688e-01 | -7.876e-03 |
| 4 | 1.517e+01 | 2.878e-01 | 2.740e-01 | -1.376e-02 |
| 5 | 1.998e+01 | 1.860e-01 | 1.821e-01 | -3.978e-03 |
| 6 | 2.480e+01 | 1.026e-01 | 1.081e-01 | 5.520e-03 |
| 7 | 2.961e+01 | 4.586e-02 | 5.743e-02 | 1.157e-02 |
| 8 | 3.442e+01 | 1.236e-02 | 2.726e-02 | 1.491e-02 |

8 points for Peak 6, Cursor Point = 21723, 783.21 Hz, 4.835 ppm

Converged after 60 iterations!

Results Comp. 1

I[0] = 6.360e-01
 Diff Con. = 8.114e-09 m2/s
 Gamma = 1.724e+03 Hz/G
 Little Delta = 1.200m
 Big Delta = 200.000m

RSS = 8.559e-03
 SD = 3.271e-02

| Point | Gradient | Expt | Calc | Difference |
|-------|-----------|------------|-----------|------------|
| 1 | 7.250e-01 | 6.419e-01 | 6.351e-01 | -6.815e-03 |
| 2 | 5.539e+00 | 5.752e-01 | 5.848e-01 | 9.671e-03 |
| 3 | 1.035e+01 | 4.561e-01 | 4.744e-01 | 1.821e-02 |
| 4 | 1.517e+01 | 3.638e-01 | 3.389e-01 | -2.494e-02 |
| 5 | 1.998e+01 | 2.234e-01 | 2.133e-01 | -1.007e-02 |
| 6 | 2.480e+01 | 1.529e-01 | 1.182e-01 | -3.463e-02 |
| 7 | 2.961e+01 | -2.021e-02 | 5.774e-02 | 7.795e-02 |
| 8 | 3.442e+01 | 1.544e-02 | 2.483e-02 | 9.394e-03 |

A.1. DOSY $^{31}\text{P}\{^1\text{H}\}$ NMR Data for $^{\text{tol}}\text{NPNTaCl}_3$ [4.5] at -60°C

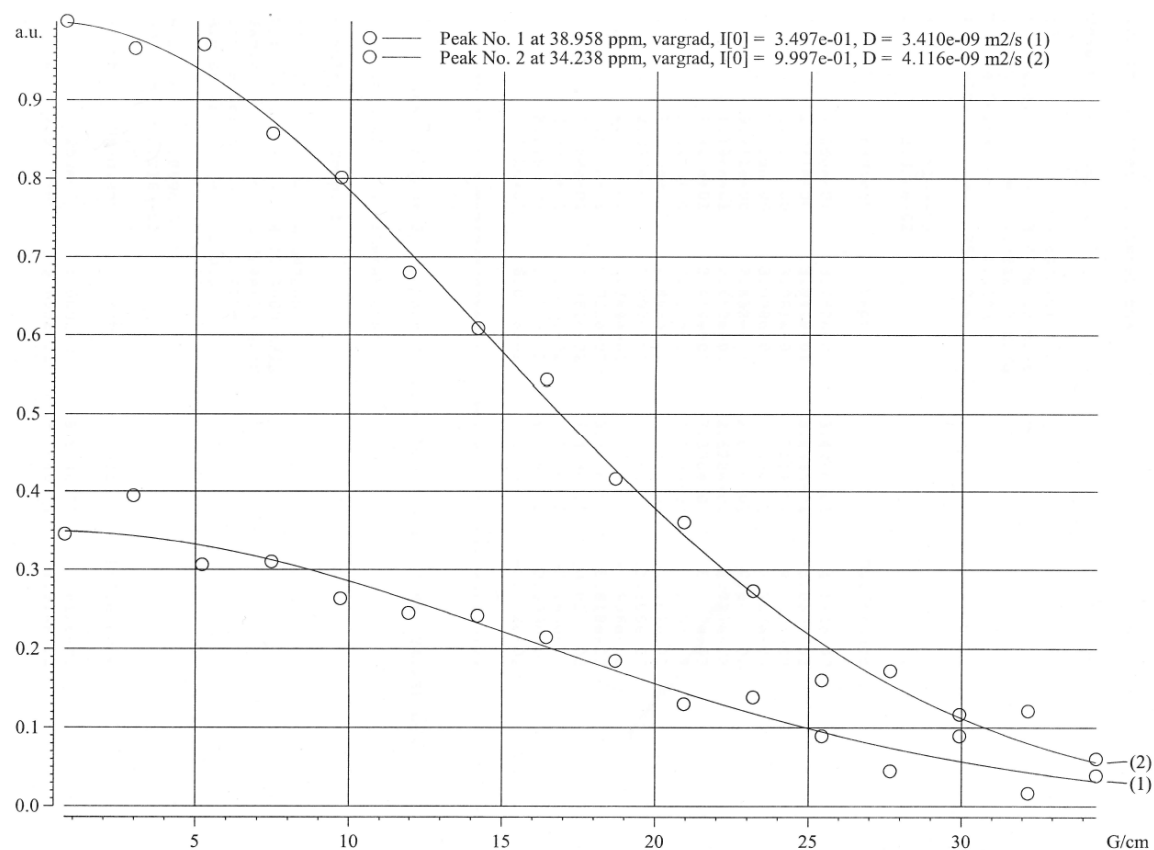


Figure 223: Diffusion coefficients (D) from DOSY $^{31}\text{P}\{^1\text{H}\}$ NMR spectrum of $^{\text{tol}}\text{NPNTaCl}_3$ [4.5] in toluene- d_8 at -60°C

C:/Bruker/XWIN-NMR/data/maria/nmr/fi387/121/pdata/1/simfit.txt

Thu Feb 18 10:

SIMFIT RESULTS

=====

Dataset : C:/Bruker/XWIN-NMR/data/maria/nmr/fi387/121/pdata/1/simfit.txt

AREA fit : Diffusion : Variable Gradient :

 $I = I[0] * \exp(-D * \text{SQR}(2 * \text{PI} * \text{gamma} * \text{Gi} * \text{LD}) * (\text{BD} - \text{LD} / 3) * 1e4)$

16 points for Peak 1, Cursor Point = 15662, 6310.17 Hz, 38.958 ppm

Converged after 52 iterations!

Results Comp. 1

$I[0]$ = 3.497e-01
 Diff Con. = 3.410e-09 m2/s
 Gamma = 1.724e+03 Hz/G
 Little Delta = 1.420m
 Big Delta = 250.000m

RSS = 8.610e-03
 SD = 2.320e-02

| Point | Gradient | Expt | Calc | Difference |
|-------|-----------|-----------|-----------|------------|
| 1 | 7.250e-01 | 3.452e-01 | 3.494e-01 | 4.144e-03 |
| 2 | 2.971e+00 | 3.941e-01 | 3.436e-01 | -5.050e-02 |
| 3 | 5.218e+00 | 3.061e-01 | 3.311e-01 | 2.500e-02 |
| 4 | 7.465e+00 | 3.098e-01 | 3.126e-01 | 2.757e-03 |
| 5 | 9.711e+00 | 2.632e-01 | 2.892e-01 | 2.605e-02 |
| 6 | 1.196e+01 | 2.450e-01 | 2.622e-01 | 1.727e-02 |
| 7 | 1.420e+01 | 2.414e-01 | 2.330e-01 | -8.426e-03 |
| 8 | 1.645e+01 | 2.145e-01 | 2.028e-01 | -1.165e-02 |
| 9 | 1.870e+01 | 1.846e-01 | 1.730e-01 | -1.161e-02 |
| 10 | 2.094e+01 | 1.297e-01 | 1.446e-01 | 1.485e-02 |
| 11 | 2.319e+01 | 1.384e-01 | 1.184e-01 | -1.996e-02 |
| 12 | 2.544e+01 | 8.922e-02 | 9.504e-02 | 5.818e-03 |
| 13 | 2.768e+01 | 4.461e-02 | 7.473e-02 | 3.012e-02 |
| 14 | 2.993e+01 | 8.922e-02 | 5.759e-02 | -3.163e-02 |
| 15 | 3.218e+01 | 1.650e-02 | 4.348e-02 | 2.698e-02 |
| 16 | 3.442e+01 | 6.049e-02 | 3.217e-02 | -2.832e-02 |

=====

16 points for Peak 2, Cursor Point = 17205, 5545.74 Hz, 34.238 ppm

Converged after 48 iterations!

Results Comp. 1

$I[0]$ = 9.997e-01
 Diff Con. = 4.116e-09 m2/s
 Gamma = 1.724e+03 Hz/G
 Little Delta = 1.420m
 Big Delta = 250.000m

RSS = 7.859e-03
 SD = 2.216e-02

| Point | Gradient | Expt | Calc | Difference |
|-------|-----------|-----------|-----------|------------|
| 1 | 7.250e-01 | 1.000e+00 | 9.984e-01 | -1.612e-03 |
| 2 | 2.971e+00 | 9.653e-01 | 9.784e-01 | 1.314e-02 |

| | | | | |
|----|-----------|-----------|-----------|------------|
| 3 | 5.218e+00 | 9.702e-01 | 9.357e-01 | -3.456e-02 |
| 4 | 7.465e+00 | 8.568e-01 | 8.731e-01 | 1.625e-02 |
| 5 | 9.711e+00 | 8.010e-01 | 7.949e-01 | -6.110e-03 |
| 6 | 1.196e+01 | 6.796e-01 | 7.062e-01 | 2.666e-02 |
| 7 | 1.420e+01 | 6.082e-01 | 6.122e-01 | 4.007e-03 |
| 8 | 1.645e+01 | 5.430e-01 | 5.179e-01 | -2.514e-02 |
| 9 | 1.870e+01 | 4.155e-01 | 4.274e-01 | 1.195e-02 |
| 10 | 2.094e+01 | 3.602e-01 | 3.442e-01 | -1.599e-02 |
| 11 | 2.319e+01 | 2.732e-01 | 2.706e-01 | -2.623e-03 |
| 12 | 2.544e+01 | 1.604e-01 | 2.075e-01 | 4.711e-02 |
| 13 | 2.768e+01 | 1.720e-01 | 1.552e-01 | -1.673e-02 |
| 14 | 2.993e+01 | 1.165e-01 | 1.133e-01 | -3.158e-03 |
| 15 | 3.218e+01 | 1.210e-01 | 8.074e-02 | -4.027e-02 |
| 16 | 3.442e+01 | 3.900e-02 | 5.613e-02 | 1.713e-02 |

=====

A.2. Variable Temperature $^{31}\text{P}\{^1\text{H}\}$ NMR Data for NPNTaCl₃ Complexes

Stacked plots of $^{31}\text{P}\{^1\text{H}\}$ NMR spectra for $^{\text{iprop}}$ NPNTaCl₃ [4.4], $^{\text{tol}}$ NPNTaCl₃ [4.5] and $^{\text{Ph}}$ NPNTaCl₃ [4.6] in C₇D₈ at 162 MHz were acquired at regular intervals from room temperature to -70 °C. The coalescence temperatures T_c and the maximum separation $\Delta\nu$ between the two peaks at -70 °C (well below the T_c 's) were obtained. The rate constants k_c at T_c were calculated, using the equation below:

$$k_c = \frac{\pi\Delta\nu}{\sqrt{2}} = 2.22 \Delta\nu$$

The free energy of inter-conversion ΔG^\ddagger between the two isomers was determined for each of the three complexes [4.4], [4.5] and [4.6], using the Eyring equation given below:

$$\Delta G^\ddagger = -R T_c \ln(k_c h / k_B T_c)$$

where R is the gas constant, T_c is the coalescence temperature, k_c is the rate constant at T_c , h is Planck's constant and k_B is the Boltzmann constant, which can be re-written as

$$\Delta G^\ddagger = 4.58 T_c (10.32 + \log(T_c / k_c)) \text{ cal.mol}^{-1}$$

In order to compare the three complexes [4.4], [4.5] and [4.6] directly with each other, the free energy ΔG^\ddagger was also calculated at the same temperature i.e. 20 °C (293 K)

A.2.1. ^{iprop}NPNTaCl₃ [4.4]

For ^{iprop}NPNTaCl₃ [4.4] (Figure 224), the T_c temperature was determined to be 10 ± 5 °C (or 283 ± 5 K) and the $\Delta\nu$ value at -70 °C to be δ 3.77 (or 611 Hz). A k_c value of 1360 ± 2 s⁻¹ was obtained, which gave a ΔG^\ddagger value of 12.5 ± 0.3 kcal.mol⁻¹. At room temperature 20 °C ± 5 °C (or 293 ± 5 K), ΔG^\ddagger is recalculated to be 13.0 ± 0.3 kcal.mol⁻¹.

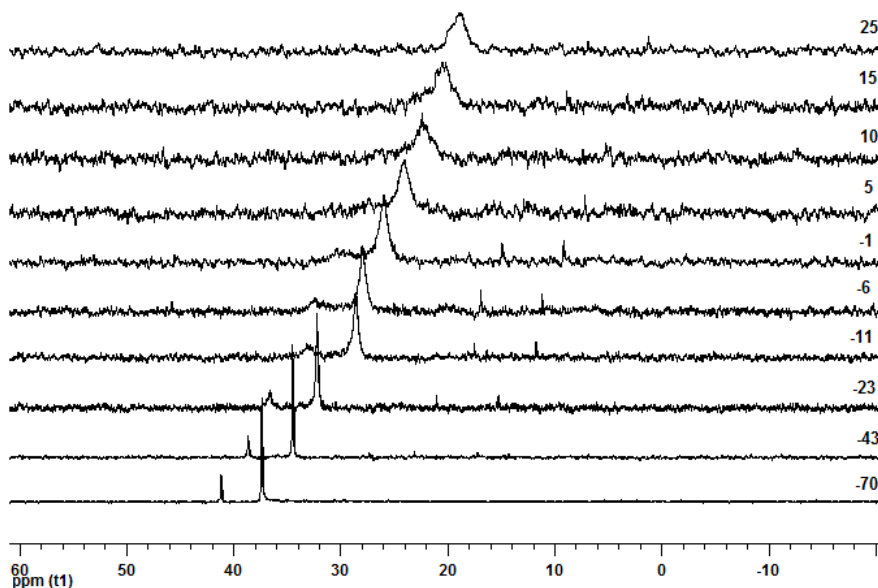


Figure 224: Variable temperature ³¹P{¹H} NMR spectra for ^{iprop}NPNTaCl₃ [4.4] in C₇D₈ from 25 °C to -70 °C

A.2.2. ^{tol}NPNTaCl₃ [4.5]

For ^{tol}NPNTaCl₃ [4.5] (Figure 225), the T_c temperature was determined to be 5 ± 5 °C (or 278 ± 5 K) and the $\Delta\nu$ value at -69 °C to be δ 4.64 (or 752 Hz). A k_c value of 1670 ± 2 s⁻¹ was obtained, which gave a ΔG^\ddagger value of 12.1 ± 0.3 kcal.mol⁻¹. At room temperature 20 °C ± 5 °C (or 293 ± 5 K), ΔG^\ddagger is recalculated to be 12.8 ± 0.3 kcal.mol⁻¹.

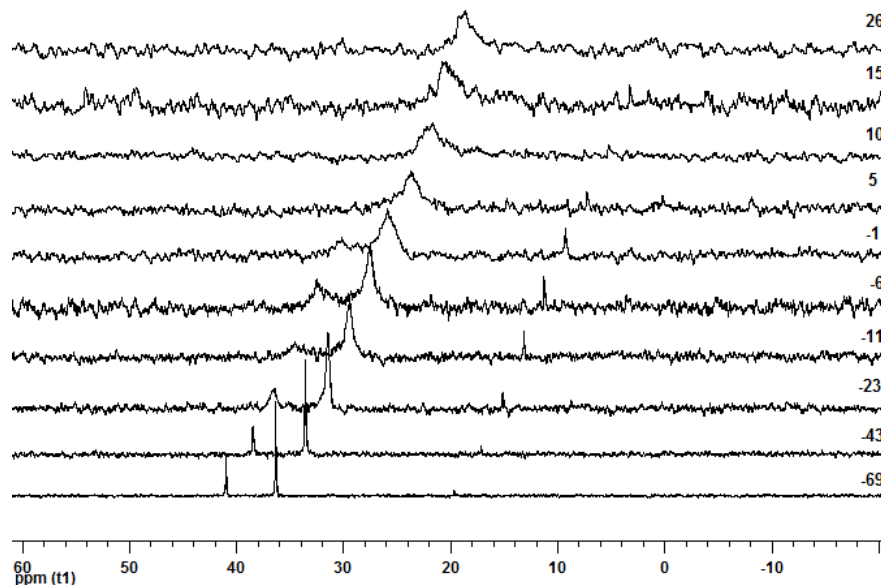


Figure 225: Variable temperature $^{31}\text{P}\{^1\text{H}\}$ NMR spectra for $^{10l}\text{NPNTaCl}_3$ [4.5] in C_7D_8 from 25 °C to -69 °C

A.2.3. $^{\text{Ph}}\text{NPNTaCl}_3$ [4.6]

For $^{\text{Ph}}\text{NPNTaCl}_3$ [4.6] (Figure 226), the T_c temperature was determined to be -6 ± 5 °C (or 267 ± 5 K) and the $\Delta\nu$ value at -69 °C to be δ 5.32 (or 861 Hz). A k_c value of 1910 ± 2 s $^{-1}$ was obtained, which gave a ΔG^\ddagger value of 11.6 ± 0.3 kcal.mol $^{-1}$. At room temperature 20 °C \pm 5 °C (or 293 \pm 5 K), ΔG^\ddagger is recalculated to be 12.8 ± 0.3 kcal.mol $^{-1}$.

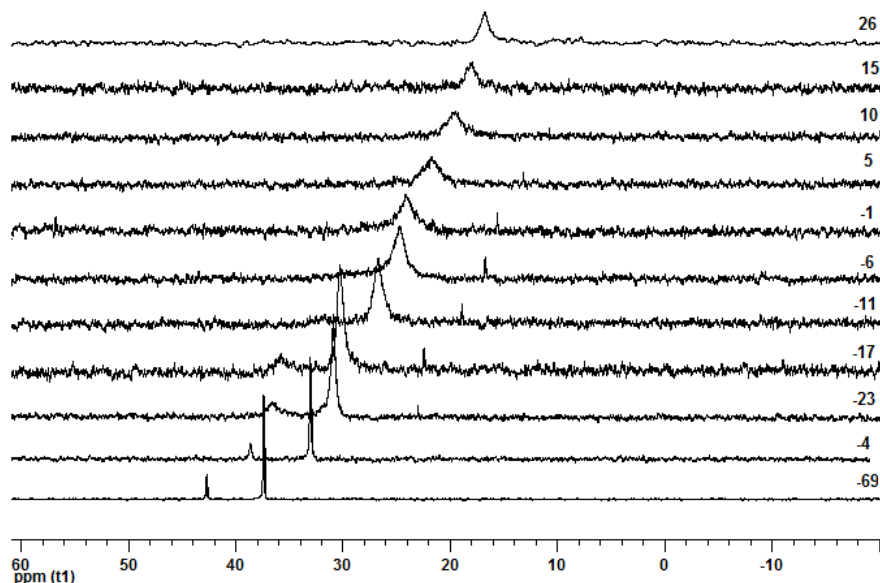


Figure 226: Variable temperature $^{31}\text{P}\{^1\text{H}\}$ NMR spectra for $^{\text{Ph}}\text{NPNTaCl}_3$ [4.6] in C_7D_8 from 25 °C to -69 °C

Appendix B: X-ray Crystal Structure Data

B.1. X-ray Crystal Structure Analysis

Selected crystals were coated in oil, mounted on a glass fiber, and placed under an N₂ stream. Measurements for compounds were made on a Bruker X8 Apex diffractometer or a Rigaku AFC-7 diffractometer, both with graphite-monochromated Mo K α radiation ($\lambda = 0.71073$ Å). The data were collected at a temperature of -100 ± 1 °C. Data were collected and integrated using the Bruker SAINT software package.¹ Data were corrected for absorption effects using the multiscan technique (SADABS)² and for Lorentz and polarization effects. Neutral atom scattering factors were taken from Cromer and Waber.³ Anomalous dispersion effects were included in F_{calc} ;⁴ the values for $\Delta f''$ and $\Delta f'''$ were those of Creagh and McAuley.⁵ The values for the mass attenuation coefficients are those of Creagh and Hubbell.⁶ All refinements were performed using the SHELXTL crystallographic software package of Bruker-AXS. The structure was solved by direct methods. All non-hydrogen atoms were refined anisotropically using SHELXL-97. Except where noted, hydrogen atoms were included in fixed positions. Structures were solved and refined using the WinGX software package version 1.64.05.

¹ SAINT. Version 6.02. Bruker AXS Inc., Madison, Wisconsin, USA. (1999).

² SADABS. Bruker Nonius area detector scaling and absorption correction - V2.05, Bruker AXS Inc., Madison, Wisconsin, USA.

³ Cromer, D. T.; Waber, J. T. *International Tables for X-ray Crystallography, Vol. IV*; The Kynoch Press: Birmingham, England, 1974, Table 2.2 A.

⁴ Ibers, J. A.; Hamilton, W. C. *Acta Crystallogr.*, **1964**, 17, 781.

⁵ Creagh, D. C.; McAuley, W.J. *International Tables for Crystallography, Vol C*; Wilson, A. J. C., ed., Kluwer Academic Publishers: Boston, 1992, Table 4.2.6.8, pp. 219-222.

⁶ Creagh, D. C.; Hubbell, J.H. *International Tables for Crystallography, Vol C*; Wilson, A.J.C., ed., Kluwer Academic Publishers: Boston, 1992, Table 4.2.4.3, pp. 200-206.

B.2. X-ray Crystal Structures

Table 33 lists the mf # reference code for the x-ray crystal structure data for the compounds prepared in this study and related compounds from previous studies.

Table 33: Fryzuk Research Group x-ray data processing code (mf#)

| Compound | mf # | Source |
|---|------|----------------------------------|
| [^{tol} Ar ^{Li} ArNLi·TMEDA] ₂ [2.2] | 813 | Current Thesis |
| ^{mes} NPNLi ₂ ·2THF | 592 | Erin MacLachlan's Thesis |
| [^{Ph,mes} NPNLi ₂ ·diox] _n | 646 | Erin MacLachlan's Thesis |
| [^{iprop} NPNLi ₂ ·diox] _n [2.6] | 629 | Erin MacLachlan's Thesis |
| [^{tol} NPNLi ₂ ·1.5TMEDA] ₂ [2.7] | 799 | Current Thesis |
| [^{tol} NPNLi ₂ ·0.5TMEDA·DME] ₂ | 683 | Dr. Y. Ohki (visiting professor) |
| ^{tol} NPNH ₂ [2.11] | 835 | Current Thesis |
| ^{ph} NPNH ₂ [2.12] | 689 | Current Thesis |
| [^{tol} NPN] ₂ Zr [3.2] | 870 | Current Thesis |
| ^{tol} NPNZrCl ₂ (HNMe ₂) [3.4] | 681 | Dr. Y. Ohki (visiting professor) |
| ^{iprop} NPNZrCl ₂ (THF) [3.5] | 724 | Current Thesis |
| ^{tol} NPNZrCl ₂ (THF) [3.6] | 679 | Current Thesis |
| ^{iprop} NPNZr(NMe ₂) ₂ [3.7] | 627 | Erin MacLachlan's Thesis |
| ^{tol} NPNZr(NMe ₂) ₂ [3.8] | 678 | Dr. Y. Ohki (visiting professor) |
| [^{iprop} NPNZrCl ₂] ₂ [3.9] | 816 | Current Thesis |
| ^{mes} NPNZrCl ₂ (Py) | 599 | Erin MacLachlan's Thesis |
| ^{mes} NPNZrCl ₂ | 590 | Erin MacLachlan's Thesis |
| ^{iprop} NPNTi(NMe ₂) ₂ [3.15] | 685 | Current Thesis |
| ^{tol} NPNTiCl ₂ [3.18] | 819 | Current Thesis |
| ^{iprop} NPNHf(NMe ₂) ₂ [3.19] | 781 | Current Thesis |
| ^{mes} NPNHf(NMe ₂) ₂ | 612 | Erin MacLachlan's Thesis |
| [^{iprop} NPNHfCl ₂] ₂ [3.20] | 818 | Current Thesis |
| ^{mes} NPNHfCl ₂ | 608 | Erin MacLachlan's Thesis |
| ^{iprop} NPNHfCl ₂ (THF) [3.21] | 783 | Current Thesis |
| ^{tol} NPNTa(NMe ₂) ₃ [4.2] | 784 | Current Thesis |
| ^{Ph} NPNTaCl ₃ [4.6] | 766 | Current Thesis |
| ^{iprop-P} NPNTaMe ₃ | 888 | Dr. D. Nied (post-doctoral) |
| [^{tol} NPNTaMe ₄][Li(THF) ₄] [4.14] | 809 | Current Thesis |
| [^{iprop} NPNZr(THF)] ₂ (μ-η ² :η ² -N ₂) [5.1] | 693 | Current Thesis |
| [^{tol} NPNTi(THF)] ₂ (μ-η ¹ :η ¹ -N ₂) [5.15] | 803 | Current Thesis |
| <i>trans</i> -[^{tol} NPNTi(Py)] ₂ (μ-η ¹ :η ¹ -N ₂) [5.19] | 806 | Current Thesis |
| ^{naph} Ar ^{Br} ArNH [7.1] | 841 | Current Thesis |
| ^{2,6-iPr₂} ArBrArNH [7.2] | 829 | Current Thesis |
| [^{2,6-iPr₂} ArLiArNLi·2THF] ₂ [7.3a] | 825 | Current Thesis |

Table 34: Crystal Data and Structure Refinement for $[\text{}^{\text{tol}}\text{Ar}^{\text{Li}}\text{ArNLi} \cdot \text{TMEDA}]_2$ [2.2], $[\text{}^{\text{tol}}\text{NPNLi}_2 \cdot 1.5\text{TMEDA}]_2$ [2.7] and $[\text{}^{\text{tol}}\text{NPNLi}_2 \cdot 0.5\text{TMEDA} \cdot \text{DME}]_2$

| Compound | $[\text{}^{\text{tol}}\text{Ar}^{\text{Li}}\text{ArNLi} \cdot \text{TMEDA}]_2$ [2.2] | $[\text{}^{\text{tol}}\text{NPNLi}_2 \cdot 1.5\text{TMEDA}]_2$ [2.7] | $[\text{}^{\text{tol}}\text{NPNLi}_2 \cdot 0.5\text{TMEDA} \cdot \text{DME}]_2$ |
|---|--|--|---|
| formula | $\text{C}_{20}\text{H}_{30}\text{Li}_2\text{N}_3$ | $\text{C}_{49}\text{H}_{61}\text{Li}_2\text{N}_5\text{P}$ | $\text{C}_{56.5}\text{H}_{58}\text{Li}_2\text{N}_3\text{O}_2\text{P}$ |
| fw | 326.35 | 764.88 | 855.91 |
| colour, habit | colourless, tablet | colourless, prism | Yellow, irregular |
| crystal size, mm | 0.22 x 0.20 x 0.16 | 0.12 x 0.08 x 0.06 | 0.44 x 0.31 x 0.08 |
| cryst syst | monoclinic | triclinic | Triclinic |
| space group | $P2_1/C$ | P-1 | P-1 |
| a, Å | 10.254(5) | 11.377(5) | 13.4900(18) |
| b, Å | 12.152(5) | 12.356(5) | 13.7200(16) |
| c, Å | 15.238(5) | 17.038(5) | 15.510(2) |
| α , deg | 90 | 77.341(5) | 93.550(3) |
| β , deg | 92.598(5) | 75.391(5) | 107.950(3) |
| γ , deg | 90 | 77.921(5) | 103.830(3) |
| V, Å ³ | 1896.8(14) | 2231.1(15) | 2623.0(6) |
| Z | 4 | 2 | 2 |
| T, K | 173 | 293 | 173 |
| ρ_{calc} , g/cm ³ | 1.143 | 1.139 | 1.084 |
| F(000) | 708 | 822 | 910 |
| radiation | Mo | Mo | Mo |
| μ , cm ⁻¹ | 0.66 | 1.0 | 0.93 |
| Trans. factors | 0.986-0.989 | 0.990-0.994 | 0.966-0.993 |
| $2\theta_{\text{max}}$, deg | 50.06 | 44.68 | 50.74 |
| total no. of reflns | 18363 | 19324 | 23826 |
| no. of unique reflns | 3352 | 5631 | 9269 |
| R_{merge} | 0.035 | 0.053 | 0.041 |
| no. with $I \geq n\theta(I)$ | 2839 | 3797 | 5964 |
| no. of parameters | 314 | 758 | 474 |
| R | 0.0474 | 0.0514 | 0.1599 |
| R_w | 0.1314 | 0.1872 | 0.5221 |
| gof | 1.069 | 0.575 | 2.026 |
| residual dens, e/Å ³ | 0.38, -0.68 | 0.69, -0.34 | 1.42, -0.71 |
| $R_1 (F^2, I > 2\sigma(I)) = \Sigma F_o - F_c / \Sigma F_o ; R_w (\text{all data}) = (\Sigma w(F_o ^2 - F_c ^2)^2 / \Sigma w F_o ^2)^{1/2}$ | | | |

Table 35: Crystal Data and Structure Refinement for ^{tol}NPNH₂ [2.11], ^{ph}NPNH₂ [2.12] and [^{tol}NPN]₂Zr [3.2]

| Compound | ^{tol} NPNH ₂ [2.11] | ^{ph} NPNH ₂ [2.12] | [^{tol} NPN] ₂ Zr [3.2] |
|---|--|--|---|
| formula | C ₃₄ H ₃₃ N ₂ P | C ₃₀ H ₂₅ N ₂ P | C ₇₁ H ₆₅ P ₂ Zr |
| fw | 500.59 | 444.49 | 1127.43 |
| colour, habit | colourless, plate | colourless, platelet | Orange, cube |
| crystal size, mm | 0.20 x 0.18 x 0.10 | 0.30 x 0.20 x 0.08 | 0.30 x 0.30 x 0.20 |
| cryst syst | monoclinic | triclinic | Monoclinic |
| space group | C2/c | P-1 | P2 ₁ /c |
| a, Å | 55.115(19) | 9.570(1) | 17.6080(9) |
| b, Å | 6.0682(19) | 11.070(1) | 16.6290(8) |
| c, Å | 16.161(5) | 12.7500(13) | 20.3270(11) |
| α, deg | 90 | 109.640(3) | 90 |
| β, deg | 100.702(9) | 107.360(3) | 93.829(2) |
| γ, deg | 90 | 94.750(3) | 90 |
| V, Å ³ | 5311(3) | 1188.7(2) | 5938.5(5) |
| Z | 8 | 2 | 4 |
| T, K | 173 | 173 | 173 |
| P _{calc} , g/cm ³ | 1.216 | 1.256 | 1.253 |
| F(000) | 2128 | 468 | 2356 |
| radiation | Mo | Mo | Mo |
| μ, cm ⁻¹ | 1.3 | 1.4 | 2.8 |
| Trans. factors | 0.975-0.987 | 0.967-0.989 | 0.919-0.945 |
| 2θ _{max} , deg | 47 | 45.12 | 58.08 |
| total no. of reflns | 4861 | 8589 | 40550 |
| no. of unique reflns | 3608 | 3002 | 10447 |
| R _{merge} | 0.405 | 0.030 | 0.036 |
| no. with I ≥ nθ(I) | 1556 | 2273 | 8922 |
| no. of parameters | 386 | 296 | 711 |
| R | 0.1377 | 0.0371 | 0.0608 |
| R _w | 0.3902 | 0.0876 | 0.2071 |
| gof | 1.103 | 1.034 | 1.140 |
| residual dens, e/Å ³ | 0.56, -0.59 | 0.25, -0.26 | 3.57, -0.61 |
| $R_1 (F^2, I > 2\sigma(I)) = \Sigma F_o - F_c / \Sigma F_o ; R_w (\text{all data}) = (\Sigma w(F_o ^2 - F_c ^2)^2 / \Sigma w F_o ^2)^{1/2}$ | | | |

Table 36: Crystal Data and Structure Refinement for ^{tol}NPNZrCl₂(HNMe₂) [3.4], ^{iprop}NPNZrCl₂(THF) [3.5] and ^{tol}NPNZrCl₂(THF) [3.6]

| Compound | ^{tol} NPNZrCl ₂ (HNMe ₂) [3.4] | ^{iprop} NPNZrCl ₂ (THF) [3.5] | ^{tol} NPNZrCl ₂ (THF) [3.6] |
|---|--|--|--|
| formula | C ₄₅ H ₄₇ Cl ₂ N ₃ PZr | C _{37.60} H _{45.60} C _{11.60} N _{1.60} O _{0.80} P _{0.80} Zr _{0.80} | C ₉₄ H ₉₆ Cl ₄ N ₄ O ₂ P ₂ Zr ₂ |
| fw | 822.95 | 687.23 | 1699.93 |
| colour, habit | yellow, prism | yellow, prism | yellow, rod |
| crystal size, mm | 0.36 x 0.28 x 0.12 | 0.26 x 0.21 x 0.08 | 0.20 x 0.10 x 0.05 |
| cryst syst | triclinic | monoclinic | triclinic |
| space group | P-1 | P2 ₁ /a | P-1 |
| a, Å | 8.7700(5) | 15.546(2) | 8.846(5) |
| b, Å | 16.3600(11) | 10.8820(16) | 17.294(5) |
| c, Å | 16.6500(11) | 25.017(4) | 28.782(5) |
| α, deg | 112.530(2) | 90 | 90 |
| β, deg | 100.280(2) | 101.889(6) | 90.578(5) |
| γ, deg | 91.970(2) | 90 | 90 |
| V, Å ³ | 2157.2(2) | 4141.4(11) | 4255(3) |
| Z | 2 | 5 | 2 |
| T, K | 173 | 173 | 173 |
| P _{calc} , g/cm ³ | 1.301 | 1.378 | 1.327 |
| F(000) | 854 | 1800 | 1764 |
| radiation | Mo | Mo | Mo |
| μ, cm ⁻¹ | 4.6 | 4.7 | 4.6 |
| Trans. factors | 0.857-0.946 | 0.888-0.963 | 0.946-0.977 |
| 2θ _{max} , deg | 55.86 | 55.1 | 50.08 |
| total no. of reflns | 31994 | 67948 | 29976 |
| no. of unique reflns | 9166 | 9475 | 14988 |
| R _{merge} | 0.055 | 0.041 | 0.000 |
| no. with I ≥ nθ(I) | 5873 | 7649 | 13224 |
| no. of parameters | 491 | 505 | 1229 |
| R | 0.0446 | 0.0332 | 0.0449 |
| R _w | 0.0951 | 0.0918 | 0.1358 |
| gof | 0.999 | 1.051 | 0.862 |
| residual dens, e/Å ³ | 0.55, -0.57 | 0.49, -0.62 | 1.01, -0.65 |
| $R_1 (F^2, I > 2\sigma(I)) = \sum F_o - F_c / \sum F_o ; R_w (\text{all data}) = (\sum w(F_o ^2 - F_c ^2)^2 / \sum w F_o ^2)^{1/2}$ | | | |

Table 37: Crystal Data and Structure Refinement for ^{iprop}NPNZr(NMe₂)₂ [3.7], ^{tol}NPNZr(NMe₂)₂ [3.8] and [^{iprop}NPNZrCl₂]₂ [3.9]

| Compound | ^{iprop} NPNZr(NMe ₂) ₂ [3.7] | ^{tol} NPNZr(NMe ₂) ₂ [3.8] | [^{iprop} NPNZrCl ₂] ₂ [3.9] |
|---|---|---|--|
| formula | C ₄₀ H ₄₇ N ₄ PZr | C ₄₄ H ₄₉ N ₄ PZr | C ₄₃ H ₄₃ Cl ₂ N ₂ PZr |
| fw | 706.01 | 756.06 | 780.88 |
| colour, habit | yellow, irregular | yellow, prism | yellow, prism |
| crystal size, mm | 0.50 x 0.20 x 0.15 | 0.20 x 0.20 x 0.10 | 0.24 x 0.22 x 0.14 |
| cryst syst | monoclinic | monoclinic | triclinic |
| space group | P2 ₁ /a | P12 ₁ /c1 | P-1 |
| a, Å | 17.3982(5) | 18.5939(18) | 11.264(5) |
| b, Å | 11.7356(3) | 10.8325(12) | 13.284(5) |
| c, Å | 19.7201(5) | 20.224(2) | 14.358(5) |
| α, deg | 90 | 90 | 105.751(5) |
| β, deg | 113.670(1) | 103.367(6) | 92.409(5) |
| γ, deg | 90 | 90 | 110.055(5) |
| V, Å ³ | 3687.68(17) | 3963.1(7) | 1920.5(13) |
| Z | 4 | 4 | 2 |
| T, K | 173 | 173 | 173 |
| P _{calc} , g/cm ³ | 1.272 | 1.267 | 1.350 |
| F(000) | 1480 | 1584 | 808 |
| radiation | Mo | Mo | Mo |
| μ, cm ⁻¹ | 3.7 | 3.5 | 5.0 |
| Trans. factors | 0.914-0.945 | 0.932-0.965 | 0.887-0.933 |
| 2θ _{max} , deg | 55.78 | 55.28 | 50.08 |
| total no. of reflns | 60432 | 46825 | 23228 |
| no. of unique reflns | 8808 | 9165 | 6716 |
| R _{merge} | 0.057 | 0.047 | 0.027 |
| no. with I ≥ nθ(I) | 6212 | 6989 | 5944 |
| no. of parameters | 423 | 451 | 451 |
| R | 0.0408 | 0.0363 | 0.0250 |
| R _w | 0.1525 | 0.0938 | 0.0653 |
| gof | 0.773 | 1.018 | 1.033 |
| residual dens, e/Å ³ | 1.49, -0.35 | 0.57, -0.38 | 0.51, -0.28 |
| $R_1 (F^2, I > 2\sigma(I)) = \Sigma F_o - F_c / \Sigma F_o ; R_w (\text{all data}) = (\Sigma w(F_o ^2 - F_c ^2)^2 / \Sigma w F_o ^2)^{1/2}$ | | | |

Table 38: Crystal Data and Structure Refinement for ^{iprop}NPNTi(NMe₂)₂ [3.15], ^{tol}NPNTiCl₂ [3.18] and ^{iprop}NPNHf(NMe₂)₂ [3.19]

| Compound | ^{iprop} NPNTi(NMe ₂) ₂ [3.15] | ^{tol} NPNTiCl ₂ [3.18] | ^{iprop} NPNHf(NMe ₂) ₂ [3.19] |
|---|--|--|--|
| formula | C ₄₀ H ₄₇ N ₄ PTi | C ₄₁ H ₃₉ Cl ₂ N ₂ PTi | C ₄₀ H ₄₇ HfN ₄ P |
| fw | 662.69 | 709.51 | 793.28 |
| colour, habit | red, irregular | red, tablet | yellow, irregular |
| crystal size, mm | 0.25 x 0.10 x 0.03 | 0.22 x 0.20 x 0.20 | 0.60 x 0.30 x 0.15 |
| cryst syst | monoclinic | monoclinic | monoclinic |
| space group | P2 ₁ /a | P2 ₁ /c | P2 ₁ /a |
| a, Å | 17.4671(10) | 14.8576(8) | 17.2680(9) |
| b, Å | 11.5564(6) | 12.2640(6) | 11.6630(6) |
| c, Å | 19.6104(9) | 19.6893(11) | 19.6540(9) |
| α, deg | 90 | 90 | 90 |
| β, deg | 114.004(2) | 94.797(3) | 113.832(1) |
| γ, deg | 90 | 90 | 90 |
| V, Å ³ | 3616.1(3) | 3575.1(3) | 3620.7(3) |
| Z | 4 | 4 | 4 |
| T, K | 173 | 173 | 173 |
| P _{calc} , g/cm ³ | 1.217 | 1.434 | 1.455 |
| F(000) | 1408 | 1600 | 1608 |
| radiation | Mo | Mo | Mo |
| μ, cm ⁻¹ | 3.1 | 5.7 | 29.6 |
| Trans. factors | 0.963-0.991 | 0.882-0.892 | |
| 2θ _{max} , deg | 44.98 | 50.14 | 56.2 |
| total no. of reflns | 15259 | 24048 | 34363 |
| no. of unique reflns | 4565 | 6338 | 8770 |
| R _{merge} | 0.064 | 0.029 | 0.036 |
| no. with I ≥ nθ(I) | 3092 | 5375 | 6901 |
| no. of parameters | 415 | 429 | 193 |
| R | 0.0471 | 0.0299 | 0.035 |
| R _w | 0.1046 | 0.0846 | 0.087 |
| gof | 0.999 | 1.028 | 1.02 |
| residual dens, e/Å ³ | 0.28, -0.30 | 0.38, -0.30 | 1.81, -3.60 |
| $R_1 (F^2, I > 2\sigma(I)) = \Sigma F_o - F_c / \Sigma F_o ; R_w (\text{all data}) = (\Sigma w(F_o ^2 - F_c ^2)^2 / \Sigma w F_o ^2)^{1/2}$ | | | |

**Table 39: Crystal Data and Structure Refinement for [^{iprop}NPNHfCl₂]₂ [3.20],
^{iprop}NPNHfCl₂(THF) [3.21] and ^{tol}NPNTa(NMe₂)₃ [4.2]**

| Compound | [^{iprop} NPNHfCl ₂] ₂ [3.20] | ^{iprop} NPNHfCl ₂ (THF) [3.21] | ^{tol} NPNTa(NMe ₂) ₃ [4.2] |
|---|--|---|---|
| formula | C ₃₆ H ₃₅ Cl ₂ HfN ₂ P | C ₄₀ H ₄₃ Cl ₂ HfN ₂ OP | C ₄₅ H ₆₁ N ₅ PTa |
| fw | 776.02 | 848.12 | 883.91 |
| colour, habit | yellow, tablet | yellow, tablet | orange, irregular |
| crystal size, mm | 0.22 x 0.20 x 0.16 | 0.45 x 0.25 x 0.25 | 0.32 x 0.30 x 0.18 |
| cryst syst | triclinic | tetragonal | triclinic |
| space group | P-1 | P4/n | P-1 |
| a, Å | 10.8215(7) | 25.767(5) | 11.109(5) |
| b, Å | 12.9087(9) | 25.767(5) | 12.160(5) |
| c, Å | 16.1543(11) | 11.545(5) | 16.654(5) |
| α, deg | 91.793(3) | 90 | 89.406(5) |
| β, deg | 99.046(3) | 90 | 84.131(5) |
| γ, deg | 96.906(3) | 90 | 85.037(5) |
| V, Å ³ | 2209.5(3) | 7665(4) | 2229.5(15) |
| Z | 4 | 8 | 2 |
| T, K | 173 | 173 | 173 |
| P _{calc} , g/cm ³ | 2.333 | 1.470 | 1.317 |
| F(000) | 1544 | 3408 | 908 |
| radiation | Mo | Mo | Mo |
| μ, cm ⁻¹ | 50.8 | 29.4 | 25.4 |
| Trans. factors | 0.359-0.642 | 0.419-0.480 | 0.462-0.634 |
| 2θ _{max} , deg | 56.12 | 56.02 | 55.96 |
| total no. of reflns | 28288 | 66805 | 10679 |
| no. of unique reflns | 7618 | 9273 | 10679 |
| R _{merge} | 0.028 | 0.04 | 0.0000 |
| no. with I ≥ nθ(I) | 6981 | 6854 | 9944 |
| no. of parameters | 193 | 429 | 481 |
| R | 0.0346 | 0.0505 | 0.0492 |
| R _w | 0.0870 | 0.1840 | 0.1509 |
| gof | 1.024 | 1.275 | 1.192 |
| residual dens, e/Å ³ | 1.89, -0.84 | 3.80, -1.40 | 4.86, -1.77 |
| $R_1 (F^2, I > 2\sigma(I)) = \Sigma F_o - F_c / \Sigma F_o ; R_w (\text{all data}) = (\Sigma w(F_o ^2 - F_c ^2)^2 / \Sigma w F_o ^2)^{1/2}$ | | | |

Table 40: Crystal Data and Structure Refinement for $^{\text{Ph}}\text{NPNTaCl}_3$ [4.6], $^{\text{iprop-P}}\text{NPNTaMe}_3$ and $[\text{}^{\text{tol}}\text{NPNTaMe}_4][\text{Li}(\text{THF})_4]$ [4.14]

| Compound | $^{\text{Ph}}\text{NPNTaCl}_3$ [4.6] | $^{\text{iprop-P}}\text{NPNTaMe}_3$ | $[\text{}^{\text{tol}}\text{NPNTaMe}_4][\text{Li}(\text{THF})_4]$ [4.14] |
|---|---|--|--|
| formula | $\text{C}_{42}\text{H}_{35}\text{Cl}_3\text{N}_2\text{PTa}$ | $\text{C}_{34}\text{H}_{42}\text{N}_2\text{PTa}$ | $\text{C}_{62}\text{H}_{85}\text{LiN}_2\text{O}_4\text{PTa}$ |
| fw | 885.99 | 690.62 | 1141.18 |
| colour, habit | black, irregular | red, prism | yellow, plate |
| crystal size, mm | 0.24 x 0.16 x 0.08 | 0.14 x 0.10 x 0.10 | 0.20 x 0.16 x 0.08 |
| cryst syst | monoclinic | monoclinic | monoclinic |
| space group | $\text{P2}_1/\text{c}$ | $\text{P2}_1/\text{c}$ | $\text{P2}_1/\text{n}$ |
| a, Å | 10.3002(8) | 9.3445(2) | 15.271(5) |
| b, Å | 10.5841(9) | 20.7492(5) | 16.524(5) |
| c, Å | 34.975(3) | 16.0408(3) | 22.264(5) |
| α , deg | 90 | 90 | 90 |
| β , deg | 97.476(3) | 103.869(1) | 100.566(5) |
| γ , deg | 90 | 90 | 90 |
| V, Å ³ | 3780.5(5) | 3019.49(11) | 5523(3) |
| Z | 4 | 4 | 4 |
| T, K | 173 | 173 | 173 |
| ρ_{calc} , g/cm ³ | 1.557 | 1.519 | 1.372 |
| F(000) | 1760 | 1392 | 2376 |
| radiation | Mo | Mo | Mo |
| μ , cm ⁻¹ | 31.9 | 37.2 | 20.7 |
| Trans. factors | 0.547-0.775 | 0.646-0.689 | 0.679-0.848 |
| $2\theta_{\text{max}}$, deg | 56.74 | 50.06 | 50.18 |
| total no. of reflns | 56934 | 19280 | 9767 |
| no. of unique reflns | 9313 | 5341 | 9767 |
| R_{merge} | 0.073 | 0.036 | 0.0000 |
| no. with $I \geq n\theta(I)$ | 7874 | 4233 | 7789 |
| no. of parameters | 348 | 352 | 540 |
| R | 0.1166 | 0.0252 | 0.0697 |
| R_w | 0.2742 | 0.0551 | 0.2092 |
| gof | 1.316 | 1.017 | 1.002 |
| residual dens, e/Å ³ | 3.86, -6.81 | 0.66, -0.38 | 2.35, -1.20 |
| $R_1 (F^2, I > 2\sigma(I)) = \Sigma F_o - F_c / \Sigma F_o ; R_w (\text{all data}) = (\Sigma w(F_o ^2 - F_c ^2)^2 / \Sigma w F_o ^2)^{1/2}$ | | | |

Table 41: Crystal Data and Structure Refinement for $[\text{ipropNPNZr(THF)}]_2(\mu\text{-}\eta^2\text{:}\eta^2\text{-N}_2)$ [5.1], $[\text{tolNPNTi(THF)}]_2(\mu\text{-}\eta^1\text{:}\eta^1\text{-N}_2)$ [5.15] and *trans*- $[\text{tolNPNTi(Py)}]_2(\mu\text{-}\eta^1\text{:}\eta^1\text{-N}_2)$ [5.19]

| Compound | $[\text{ipropNPNZr(THF)}]_2(\mu\text{-}\eta^2\text{:}\eta^2\text{-N}_2)$ [5.1] | $[\text{tolNPNTi(THF)}]_2(\mu\text{-}\eta^1\text{:}\eta^1\text{-N}_2)$ [5.15] | $[\text{tolNPNTi(Py)}]_2(\mu\text{-}\eta^1\text{:}\eta^1\text{-N}_2)$ |
|---|--|---|---|
| formula | $\text{C}_{87}\text{H}_{103}\text{N}_6\text{O}_3\text{P}_2\text{Zr}_2$ | $\text{C}_{106}\text{H}_{94}\text{N}_6\text{O}_2\text{P}_2\text{Ti}_2$ | $\text{C}_{56}\text{H}_{50}\text{N}_5\text{PTi}$ |
| fw | 1525.13 | 1641.61 | 871.88 |
| colour, habit | black, platelet | black, prism | |
| crystal size, mm | 0.54 x 0.35 x 0.16 | 0.12 x 0.08 x 0.06 | |
| cryst syst | monoclinic | monoclinic | triclinic |
| space group | $\text{P2}_1/\text{c}$ | $\text{C2}/\text{c}$ | P-1 |
| a, Å | 17.5738(8) | 27.293(5) | 13.4688(12) |
| b, Å | 33.3965(13) | 15.065(5) | 18.7537(17) |
| c, Å | 14.6997(6) | 21.814(5) | 21.2672(19) |
| α , deg | 90 | 90 | 112.586(2) |
| β , deg | 113.258(2) | 95.322(5) | 90.817(2) |
| γ , deg | 90 | 90 | 106.588(2) |
| V, Å ³ | 7926.2(6) | 8931(4) | 4706.6(7) |
| Z | 4 | 4 | 4 |
| T, K | 173 | 293 | 173 |
| ρ_{calc} , g/cm ³ | 1.278 | 1.221 | 1.230 |
| F(000) | 3204 | 3448 | 1832 |
| radiation | Mo | Mo | Mo |
| μ , cm ⁻¹ | 3.6 | 2.7 | 2.6 |
| Trans. factors | 0.861-0.945 | 0.975-0.984 | |
| $2\theta_{\text{max}}$, deg | 55.14 | 50.14 | 51.16 |
| total no. of reflns | 86978 | 37100 | 53020 |
| no. of unique reflns | 18272 | 7921 | 17431 |
| R_{merge} | 0.057 | 0.026 | 0.071 |
| no. with $I \geq n\theta(I)$ | 12975 | 6775 | 10335 |
| no. of parameters | 929 | 537 | 1133 |
| R | 0.0570 | 0.0482 | 0.0673 |
| R_w | 0.1443 | 0.1285 | 0.2080 |
| gof | 1.066 | 1.042 | 1.015 |
| residual dens, e/Å ³ | 1.73, -0.71 | 1.02, -0.93 | 1.59, -0.96 |
| $R_1 (F^2, I > 2\sigma(I)) = \Sigma F_o - F_c / \Sigma F_o ; R_w (\text{all data}) = (\Sigma w(F_o ^2 - F_c ^2)^2 / \Sigma w F_o ^2)^{1/2}$ | | | |

Table 42: Crystal Data and Structure Refinement for ^{naph}Ar^{Br}ArNH [7.1], ^{2,6-iPr2}ArBrArNH [7.2] and [^{2,6-iPr2}ArLiArNLi·2THF]₂ [7.3a]

| Compound | ^{naph} Ar ^{Br} ArNH [7.1] | ^{2,6-iPr2} ArBrArNH [7.2] | [^{2,6-iPr2} ArLiArNLi·2THF] ₂ [7.3a] |
|---|---|-------------------------------------|--|
| formula | C ₁₆ H ₁₂ BrN | C ₁₈ H ₂₂ BrN | C _{27.75} H ₃₇ Li ₂ NO ₂ |
| fw | 298.18 | 332.28 | 430.46 |
| colour, habit | colourless, tablet | colourless, prism | Colourless, prism |
| crystal size, mm | 0.12 x 0.16 x 0.24 | 0.24 x 0.24 x 0.20 | 0.20 x 0.18 x 0.18 |
| cryst syst | orthorhombic | monoclinic | orthorhombic |
| space group | Pccn | P2 ₁ /n | Fddd |
| a, Å | 14.464(5) | 10.281(5) | 21.952(5) |
| b, Å | 22.027(5) | 8.509(5) | 29.089(5) |
| c, Å | 7.826(5) | 18.464(5) | 31.906(5) |
| α, deg | 90 | 90 | 90 |
| β, deg | 90 | 97.340(5) | 90 |
| γ, deg | 90 | 90 | 90 |
| V, Å ³ | 2493.4(19) | 1602.0(13) | 20374(7) |
| Z | 8 | 4 | 32 |
| T, K | 293 | 173 | 173 |
| P _{calc} , g/cm ³ | 1.59 | 1.378 | 1.116 |
| F(000) | 1200 | 688 | 7392 |
| radiation | Mo | Mo | Mo |
| μ, cm ⁻¹ | 3.28 | 25.6 | 0.7 |
| Trans. factors | | 0.547-0.600 | 0.987-0.988 |
| 2θ _{max} , deg | 50.04 | 49.98 | 50.02 |
| total no. of reflns | 16211 | 18788 | 33011 |
| no. of unique reflns | 2205 | 2763 | 4510 |
| R _{merge} | 0.037 | 0.026 | 0.067 |
| no. with I ≥ nθ(I) | 1921 | 2564 | 3315 |
| no. of parameters | 167 | 169 | 424 |
| R | 0.0193 | 0.0998 | 0.0728 |
| R _w | 0.0500 | 0.3792 | 0.2704 |
| gof | 1.032 | 3.708 | 1.099 |
| residual dens, e/Å ³ | 0.34, -0.19 | 5.59, -4.29 | 0.73, -0.51 |
| $R_1 (F^2, I > 2\sigma(I)) = \Sigma F_o - F_c / \Sigma F_o ; R_w (\text{all data}) = (\Sigma w(F_o ^2 - F_c ^2)^2 / \Sigma w F_o ^2)^{1/2}$ | | | |